VOL. 591 NOS. 1 + 2 FEBRUARY 7, 1992

COMPLETE IN ONE ISSUE

JOURNAL OF CHROMATOGRAPHY

INCLUDING ELECTROPHORESIS AND OTHER SEPARATION METHODS

ELSEVIER

JOURNAL OF CHROMATOGRAPHY

INCLUDING ELECTROPHORESIS AND OTHER SEPARATION METHODS

Scope. The *Journal of Chromatography* publishes papers on all aspects of chromatography, electrophoresis and related methods. Contributions consist mainly of research papers dealing with chromatographic theory, instrumental development and their applications. The section *Biomedical Applications*, which is under separate editorship, deals with the following aspects: developments in and applications of chromatographic and electrophoretic techniques related to clinical diagnosis or alterations during medical treatment; screening and profiling of body fluids or tissues with special reference to metabolic disorders; results from basic medical research with direct consequences in clinical practice; drug level monitoring and pharmacokinetic studies; clinical toxicology; analytical studies in occupational medicine.

Submission of Papers. Manuscripts (in English; *four* copies are required) should be submitted to: Editorial Office of *Journal of Chromatography*, P.O. Box 681, 1000 AR Amsterdam, Netherlands, Telefax (+31-20) 5862 304, or to: The Editor of *Journal of Chromatography, Biomedical Applications*, P.O. Box 681, 1000 AR Amsterdam, Netherlands. Review articles are invited or proposed by letter to the Editors. An outline of the proposed review should first be forwarded to the Editors for preliminary discussion prior to preparation. Submission of an article is understood to imply that the article is original and unpublished and is not being considered for publication elsewhere. For copyright regulations, see below.

Publication. The *Journal of Chromatography* (incl. *Biomedical Applications*) has 39 volumes in 1992. The subscription prices for 1992 are:

J. Chromatogr. (incl. *Cum. Indexes, Vols. 551–600*) + *Biomed. Appl.* (Vols. 573–611):
Dfl. 7722.00 plus Dfl. 1209.00 (p.p.h.) (total *ca.* US$ 4880.25)

J. Chromatogr. (incl. *Cum. Indexes, Vols. 551–600*) only (Vols. 585–611):
Dfl. 6210.00 plus Dfl. 837.00 (p.p.h.) (total *ca.* US$ 3850.75)

Biomed. Appl. only (Vols. 573–584):
Dfl. 2760.00 plus Dfl. 372.00 (p.p.h.) (total *ca.* US$ 1711.50).

Subscription Orders. The Dutch guilder price is definitive. The US$ price is subject to exchange-rate fluctuations and is given as a guide. Subscriptions are accepted on a prepaid basis only, unless different terms have been previously agreed upon. Subscriptions orders can be entered only by calender year (Jan.–Dec.) and should be sent to Elsevier Science Publishers, Journal Department, P.O. Box 211, 1000 AE Amsterdam, Netherlands, Tel. (+31-20) 5803 642, Telefax (+31-20) 5803 598, or to your usual subscription agent. Postage and handling charges include surface delivery except to the following countries where air delivery via SAL (Surface Air Lift) mail is ensured: Argentina, Australia, Brazil, Canada, China, Hong Kong, India, Israel, Japan*, Malaysia, Mexico, New Zealand, Pakistan, Singapore, South Africa, South Korea, Taiwan, Thailand, USA. *For Japan air delivery (SAL) requires 25% additional charge of the normal postage and handling charge. For all other countries airmail rates are available upon request. Claims for missing issues must be made within three months of our publication (mailing) date, otherwise such claims cannot be honoured free of charge. Back volumes of the *Journal of Chromatography* (Vols. 1–572) are available at Dfl. 217.00 (plus postage). Customers in the USA and Canada wishing information on this and other Elsevier journals, please contact Journal Information Center, Elsevier Science Publishing Co. Inc., 655 Avenue of the Americas, New York, NY 10010, USA, Tel. (+1-212) 633 3750, Telefax (+1-212) 633 3990.

Abstracts/Contents Lists published in Analytical Abstracts, Biochemical Abstracts, Biological Abstracts, Chemical Abstracts, Chemical Titles, Chromatography Abstracts, Clinical Chemistry Lookout, Current Contents/Life Sciences, Current Contents/Physical, Chemical & Earth Sciences, Deep-Sea Research/Part B: Oceanographic Literature Review, Excerpta Medica, Index Medicus, Mass Spectrometry Bulletin, PASCAL-CNRS, Pharmaceutical Abstracts, Referativnyi Zhurnal, Research Alert, Science Citation Index and Trends in Biotechnology.

See inside back cover for Publication Schedule, Information for Authors and information on Advertisements.

0021-9673/92/$05.00

This issue is printed on acid-free paper.

Printed in the Netherlands

CONTENTS

(Abstracts/Contents Lists published in Analytical Abstracts, Biochemical Abstracts, Biological Abstracts, Chemical Abstracts, Chemical Titles, Chromatography Abstracts, Current Contents/Life Sciences, Current Contents/Physical, Chemical & Earth Sciences, Deep-Sea Research/Part B: Oceanographic Literature Review, Excerpta Medica, Index Medicus, Mass Spectrometry Bulletin, PASCAL-CRNS, Referativnyi Zhurnal, Research Alert and Science Citation Index)

REGULAR PAPERS

General

Column Liquid Chromatography

(Continued overleaf)

Contents (continued)

Gas Chromatography

In articles with more than one author, the name of the author to whom correspondence should be addressed is indicated in the article heading by a 6-pointed asterisk (*).

FOR ADVERTISING INFORMATION PLEASE CONTACT OUR ADVERTISING REPRESENTATIVES

USA/CANADA

Weston Media Associates

Mr. Daniel S. Lipner
P.O. Box 1110, GREENS FARMS, CT 06436-1110
Tel: (203) 261-2500, Fax: (203) 261-0101

GREAT BRITAIN

T.G. Scott & Son Ltd.

Tim Blake
Portland House, 21 Narborough Road
COSBY, Leicestershire LE9 5TA
Tel: (0533) 753-333, Fax: (0533) 750-522
Mr. M. White or Mrs. A. Curtis
30-32 Southampton Street, LONDON WC2E 7HR
Tel: (071) 240 2032, Fax: (071) 379 7155,
Telex: 299181 adsale/g

JAPAN

ESP - Tokyo Branch

Mr. S. Onoda
20-12 Yushima, 3 chome, Bunkyo-Ku
TOKYO 113
Tel: (03) 3836 0810, Fax: (03) 3839-4344
Telex: 02657617

REST OF WORLD

ELSEVIER SCIENCE PUBLISHERS

Ms. W. van Cattenburch
P.O. Box 211, 1000 AE AMSTERDAM,
The Netherlands
Tel: (20) 515.3220/21/22, Telex: 16479 els vi nl
Fax: (20) 683.3041

Fundamentals and Applications of Chromatography and Related Differential Migration Methods

edited by **E. Heftmann**, *Orinda, CA, USA*

These are completely new books, organized according to the successful plan of the previous four editions. While avoiding repetition of material covered in the previous editions, the authors have succeeded in presenting a coherent and comprehensive picture of the state of each topic. The books provide beginners as well as experienced researchers with a key to understanding current activities in various separation methods. They will also serve as textbooks for graduate courses in technical, medical and engineering schools as well as all universities offering science courses.

Part A: Fundamentals and Techniques

Journal of Chromatography Library Volume 51A

Part A covers the theory and fundamentals of such methods as column and planar chromatography, countercurrent chromatography, field-flow fractionation, and electrophoresis. Affinity chromatography and supercritical-fluid chromatography are covered for the first time. Each topic is treated by one of the most eminent authorities in the field.

Contents Part A: 1. Theory of chromatography *(L.R. Snyder)*. 2. Countercurrent chromatography *(Y. Ito)*. 3. Planar chromatography *(S. Nyiredy)*. 4. Column liquid chromatography *(H. Poppe)*. 5. Ion-exchange chromatography *(H.F. Walton)*. 6. Size-exclusion chromatography *(L. Hagel and J.-C. Janson)*. 7. Affinity chromatography *(T.M. Phillips)*. 8. Supercritical-fluid chromatography *(P.J. Schoenmakers and L.G.M. Uunk)*. 9. Gas chromatography *(C.F. Poole and S.K. Poole)*. 10. Field-flow fractionation *(J. Janca)*. 11. Electrophoresis *(P.G. Righetti)*. Manufacturers and dealers of chromatography and electrophoresis supplies. Subject Index.

1992 xxxvi + 552 pages
Price: US $ 179.50 / Dfl. 350.00
ISBN 0-444-88236-7

Parts A & B Set
Set price: US $ 333.50 / Dfl. 650.00
ISBN 0-444-88404-1

Part B: Applications

Journal of Chromatography Library Volume 51B

Part B presents various applications of these methods. New developments are reviewed and summarized. Important topics such as environmental analysis and the determination of synthetic polymers and fossil fuels, are covered for the first time.

Contents Part B: 12. Inorganic species *(P.R. Haddad and E. Patsalides)*. 13. Amino acids and peptides *(C.T. Mant, N.E. Zhou and R.S. Hodges)*. 14. Proteins *(F.E. Regnier and K.M. Gooding)*. 15. Lipids *(A. Kuksis)*. 16. Carbohydrates *(S.C. Churms)*. 17. Nucleic acids, their constituents and analogs *(N-I Jang and P.R. Brown)*. 18. Porphyrins *(K. Jacob)*. 19. Phenolic compounds *(J.B. Harborne)*. 20. Drugs *(K. Macek and J. Macek)*. 21. Fossil fuels *(R.P. Philp and F.X. de las Heras)*. 22. Synthetic polymers *(T.H. Moury and T.C. Schunk)*. 23. Pesticides *(J. Sherma)*. 24. Environmental analysis *(K.P. Naikwadi and F.W. Karasek)*. 25. Amines from environmental sources *(H.A.H. Billiet)*. Manufacturers and dealers of chromatography and electrophoresis supplies. Subject Index.

1992 xxxii + 630 pages
Price: US $ 189.50 / Dfl. 370.00
ISBN 0-444-88237-5

Elsevier Science Publishers

P.O. Box 211, 1000 AE Amsterdam, The Netherlands
P.O. Box 882, Madison Square Station, New York, NY 10159, USA

JOURNAL OF CHROMATOGRAPHY

VOL. 591 (1992)

JOURNAL of CHROMATOGRAPHY

INCLUDING ELECTROPHORESIS AND OTHER SEPARATION METHODS

ELSEVIER

AMSTERDAM — LONDON — NEW YORK — TOKYO

0021-9673/92/$05.00

Printed in the Netherlands

Journal of Chromatography, 591 (1992) 1–18
Elsevier Science Publishers B.V., Amsterdam

CHROM. 23 800

Comparison of statistical theories of spot overlap in two-dimensional separations and verification of means for estimating the number of zones

Frances J. Oros and Joe M. Davis*

Department of Chemistry and Biochemistry, Southern Illinois University at Carbondale, Carbondale, IL 62901 (USA)

(Received July 29th, 1991)

ABSTRACT

Several theories appropriate to the modeling of zone overlap in two-dimensional (2D) separations are reviewed. One of these, with specific applications to chromatography, was recently proposed by one of the authors. The others are summarized in a book published over two decades ago. These latter theories addressed various problems of overlap (none of which was chromatographic), which were once of interest in the biological and hygienic sciences. Several hundred computer simulations of 2D beds containing various numbers of randomly distributed zones were generated to evaluate these theories. One theory shows exceptional promise in correctly predicting the numbers of singlet and multiplet spots expected in 2D beds over a wide range of chromatographic saturations. This theory predicts that only one sixth of the spot capacity in a 2D bed can be used to resolve spots. A procedure based on this theory is proposed, by which one can estimate the number of detectable zones in a 2D bed from the distribution of distances between the observed spots. The procedure was tested and verified by its application to about 200 computer simulations of 2D beds containing various numbers of randomly distributed zones.

INTRODUCTION

Recently, one of us (J.M.D.) reported equations for the numbers of singlet, doublet and triplet spots expected in two-dimensional (2D) separation beds containing randomly distributed zones [1]. The separations carried out in these beds are of the sequential type [2] and commonly are implemented in a rectangular bed, through which zones migrate at right-angles in two discrete stages. Such beds are used routinely in thin-layer/thin-layer chromatography and sodium dodecyl sulfate (SDS) electrophoresis/isoelectric focusing. The elution profiles of some recently developed coupled columns, *e.g.*, capillary zone electrophoresis–liquid chromatography [3] and gas chromatography–gas chromatography [4], also closely resemble the distribution of zones in such beds. This work was the logical extension of earlier work on the surprisingly profound statistical limitations of one-dimensional (1D) separations [5–22].

The equations for these spot numbers were tested by the interpretation of computer simulations of 2D beds containing randomly distributed zones [1]. When the space available for separation, as measured by the spot capacity of the bed, exceeded the number of zones by a factor of five or more, the equations' predictions agreed fairly well with the results of the simulations. At higher saturations, the numbers of singlet spots continued to agree well with the predictions of theory, but the numbers of doublet and triplet spots exceeded those predicted by theory.

Perhaps the most surprising conclusion drawn from this study was that the spot capacity of a 2D bed is utilized for separation less efficiently than is the peak capacity of a 1D chromatogram, at least when statistical considerations apply [1]. In other

0021-9673/92/$05.00

words, per unit capacity, 2D separations actually are worse than their 1D analogues. This conclusion also was reached by Martin [23]. In essence, the only reason that 2D separations are better than their 1D analogues is that one typically has so much more capacity in two dimensions than in one dimension that one can afford to "waste" a substantial fraction of it by ineffective utilization [1].

A specific example is cited to illustrate this point [1]. If a 100-component mixture were partially resolved on a 2D bed with a spot capacity of 2000 (a realistic value), then approximately 82 singlet spots, 7 doublet spots and 1 triplet spot would be expected (these spots account for 99% of the components). In contrast, if the same mixture were partially resolved on a 1D column having a peak capacity equal to 2000 (an unrealistic value, even in capillary electrophoresis), then 90 singlet peaks, 4 doublet peaks and no triplet peaks would be expected (these peaks account for 98% of the components). For equal capacities, the number of singlets (multiplets) is smaller (larger) in a 2D separation than in a 1D separation. Perhaps the reason why this phenomenon has not been observed experimentally is that unrealistically large 1D peak capacities are required to make the comparison.

After the submission of this work [1], one of us (F.J.O.) found a short but enlightening book by Roach [24], which details several studies during the 1940s–1960s in the biological and hygienic sciences of phenomena closely related to the overlap of spots in 2D beds. This book summarizes the results of several studies on counting errors, including those due to the underestimation of the numbers of bacterial colonies grown on culture plates, the numbers of dust particles collected on sampling plates and the numbers of coal particulates (to which miners were exposed) collected on thermal precipitators. These counting errors arose from the overlap of colonies or particulates by one another, which obscured some from detection. This obscuration is identical with that faced by the separation scientist. Several theories were proposed to account quantitatively for these overlaps. As will be shown below, most of these theories are inferior to that proposed by Davis. A theory proposed by Roach, however, accounts for overlap more correctly at higher saturations (*i.e.*, smaller spot capacities) than does the theory of Davis. In fact, in terms of its completeness and utility, the theory of Roach is perhaps the best theory considered to date by which to describe overlap in 2D beds.

This paper is divided into three parts. Because the studies addressed by Roach's book are probably unknown to most chromatographers, the first part of the paper summarizes these works and contrasts them with the recent results of Davis. In the second part, the theory of Roach is extensively tested by computer simulations of 2D beds containing various numbers of randomly distributed elliptical or circular zones. In the final part, a regressional procedure based on the theory of Roach is proposed, by which one can estimate the total number of detectable zones in a single 2D bed from the distribution of distances among the observed spots.

THEORY

Comparison of theories of spot overlap in two dimensions

According to Davis [1], the numbers of singlet spots s, doublet spots d, straight-chain triplet spots t_s and interlocking triplet spots t_i expected in a 2D bed of area A, which contains m randomly distributed detectable circular zones of diameter d_0, are

$$s = \bar{m}e^{-4\alpha} \tag{1a}$$

$$d = 8\bar{m} \cdot \frac{\alpha^2 e^{-8\alpha}}{1 - e^{-4\alpha}} \tag{1b}$$

$$t_s \approx \frac{256}{5} \cdot \bar{m} \cdot \frac{\alpha^4 e^{-12\alpha}}{(1 - e^{-4\alpha})^2} \tag{1c}$$

$$\lim_{\alpha \to 0} t_i \approx \frac{512}{5} \cdot \bar{m} \cdot \frac{\alpha^6 e^{-12\alpha}}{[1 - (1 + 4\alpha)e^{-4\alpha}]^2} \tag{1d}$$

where $\bar{m}$ is a statistical approximation to m and α, the saturation of the bed, is the ratio of $\bar{m}$ to the spot capacity n_c. The spot capacity is defined as

$$n_c = A/A_0 = 4A/\pi(\beta d_0)^2 \tag{2}$$

where β is a scalar, which allows one to adjust for the degree of overlap that is acceptable in a given application (*e.g.*, zones are considered to be overlapped if they touch or overlay one another, when $\beta = 1$), and A_0 is the scaled area of a zone. This definition of spot capacity is different from that traditionally used in 2D separations [2] but is appropriate for this theory [1]. A straight-chain

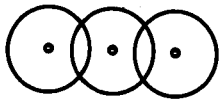

a) straight-chain triplet t_s

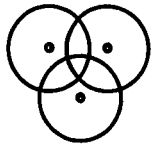

b) interlocking triplet t_i

Fig. 1. Triplet spots (a) t_s and (b) t_i.

triplet t_s is defined by the overlap of a central zone by two other zones, which themselves do not overlap; an interlocking triplet t_i is defined by the overlap of a central zone by two other zones, which themselves overlap. These two types of triplets are illustrated in Fig. 1. The total number t of triplets is the arithmetic sum, $t_s + t_i$. Eqns. 1a–d were derived from selective interpretations of the radial distribution functions governing a 2D Poisson process.

The Taylor-series expansions of eqns. 1b–d will be useful below and are

$$d \approx \bar{m}\left(2\alpha - 12\alpha^2 + \frac{104}{3}\cdot\alpha^3 - 64\alpha^4 + \ldots\right) \quad (3a)$$

$$t_s \approx \bar{m}\left(\frac{16}{5}\cdot\alpha^2 - \frac{128}{5}\cdot\alpha^3 + \frac{1472}{15}\cdot\alpha^4 - \ldots\right) \quad (3b)$$

$$\underset{\lim\alpha\to 0}{t_i} \approx \bar{m}\left(\frac{8}{5}\cdot\alpha^2 - \frac{32}{3}\cdot\alpha^3 + \frac{608}{15}\cdot\alpha^4 - \ldots\right) \quad (3c)$$

The analysis of 500 computer simulations of 2D beds containing $m = 1000$ components showed that the number s of singlets predicted by eqn. 1a is correct to within 7%, as long as α is less than 0.50. The same analysis indicated some errors at modest levels of saturations in the equations for d, t_s and t_i; more specifically, these equations are correct to within 10% as long as α is less than about 0.20, 0.12 and 0.24, respectively. For α values less than 0.10, the simulations indicated that multiplets other than doublets and triplets are unlikely and that the number of observable spots p could be approximated by the arithmetic sum of eqns. 1a–d [1]:

$$p \approx s + d + t_s + t_i \quad \alpha \leqslant 0.10 \quad (4)$$

The other estimates of p summarized in Roach's book are reported below. The original notation has been changed to be compatible with that introduced above. For the sake of consistency, the number p in these theories is interpreted as the number of spots, although the overlapping zones in these theories actually corresponded to other phenomena, *e.g.*, bacterial colonies, dust, and coal particulates. (In passing, we note that the probabilities of forming singlet and multiplet 1D peaks from randomly distributed zones also are reported in this book, as is the mean number of 1D peaks. These results were not derived in terms of chromatography, however, but in terms of overlapping line segments.)

Bourdillon *et al.* [25], who were interested in the effects of the overcrowding of colonies on culture plates, approximated the total number p of spots on these plates as the solution to the differential equation

$$\mathrm{d}p/\mathrm{d}\bar{m} = 1 - p/n_c \quad (5a)$$

i.e.,

$$p = \bar{m}[1 - \exp(-\alpha)]/\alpha \quad (5b)$$

Experimental evidence was presented which confirmed the equation over a small range of α values.

Shortly thereafter, Irwin *et al.* [26], who were interested in the overlapping of dust particles on sampling plates, developed an alternative theory, in which the probability p_n that a zone forms part of a spot containing n overlapping zones was calculated from Poisson statistics as

$$p_n = \frac{(4\alpha)^{n-1}\mathrm{e}^{-4\alpha}}{(n-1)!} \quad (6a)$$

The total number p of spots then was estimated as

$$p = \bar{m}\sum_{n=1}^{\infty} p_n/n = \bar{m}[1 - \exp(-4\alpha)]/4\alpha \quad (6b)$$

The result is identical with that of Bourdillon *et al.*, except that α is replaced by 4α. The authors recognized the existence of shortcomings in their theory, especially when α was sufficiently large that triplets and higher order multiplets would be observed.

Armitage [27], in a detailed subsequent study, approximated the number of singlet spots by eqn. 1a

and the numbers d, t_s and t_i of multiplet spots by the series

$$d \approx \bar{m}\left[2\alpha - \frac{2(4\pi + 3\sqrt{3})}{\pi}\alpha^2\right] = \bar{m}(2\alpha - 11.3080\alpha^2) \tag{7a}$$

$$t_s \approx \bar{m} \cdot \frac{6\sqrt{3}}{\pi} \cdot \alpha^2 = \bar{m}(3.3080)\alpha^2 \tag{7b}$$

$$t_i \approx \bar{m} \cdot \frac{2(4\pi - 3\sqrt{3})}{3\pi} \cdot \alpha^2 = \bar{m}(1.5640)\alpha^2 \tag{7c}$$

He further recognized that the derivation of higher order multiplets was prohibitively difficult by his approach; Roach commented on this difficulty [24]. By expanding eqn. 1a as a three-term Taylor series in α and combining this expansion with eqns. 4 and 7a–c, Armitage concluded that

$$p \approx \bar{m}\left(1 - 2\alpha + \left\{8 - \pi^{-1}\left[2(4\pi + 3\sqrt{3}) - 6\sqrt{3} - 2(4\pi - 3\sqrt{3})/3\right]\right\}\alpha^2\right) = \bar{m}(1 - 2\alpha + 1.564\alpha^2) \tag{8}$$

The theory of Roach [24] is described in some detail because, as will be shown below, its predictions closely agree with the numbers of spots found in extensive computer simulations carried out in this laboratory. Further, an understanding of Roach's theory is essential to the development of the regression procedure (see below) by which $\bar{m}$ can be estimated from the observed distribution of spots in a bed.

In his theory, Roach assumed that the centers of circular zones of diameter d_0 are randomly distributed throughout an unbounded bed (he observed that these zones could represent many phenomena, including dust particles, metal fumes, acid mists, air pollutants and airborne organisms [24]). Any zone in the bed is considered to be overlapped if its center lies within the distance d_0 of the center of an adjacent zone. In this work, for reasons that will be apparent shortly, this critical distance will be equated instead to βd_0, where β is the scaling factor previously introduced. In Roach's theory, $\beta = 1$.

The number of spots is determined in accordance with the following scheme. One arbitrarily selects any zone in the bed and finds its nearest neighbor. If the distance between these two zone centers is greater than βd_0, then the arbitrarily selected zone is a singlet spot. If the distance is less than βd_0, however, then the two zones overlap. In this latter instance, the overlapping pair forms either a doublet spot or a higher order multiplet (*e.g.*, triplet, quartet). One next finds the zone whose center lies closest to either of the centers of the two overlapping zones. In other words, if zones A and B are overlapped and lie in a bed containing zones A, B, C, D, etc., then one determines the distances between zones A and C, between zones A and D, between zones B and C, between zones B and D, etc., and then selects the shortest distance. If this distance is greater than βd_0, then the overlapping pair forms a doublet spot. If the distance is less than βd_0, however, then the selected zone overlaps with at least one of the two overlapping zones. In this latter instance, the overlapping trio forms either a triplet spot or a higher order multiplet (*e.g.*, quartet, quintet). One continues to repeat this sequence of nearest neighbor searching (exclusive of the neighbors comprising the spot) and distance comparison, until the distances between all n zones in the spot and their neighbors not in the spot are greater than βd_0. One then has isolated a spot consisting of n overlapping zones, or an n-tet spot, as shown in Fig. 2 for $n = 5$. One then repeats the above procedure by beginning with another zone and continues until all zones are addressed.

Roach recognized that the probability of these outcomes could be modeled closely (but not exactly) by the binomial distribution. The probability p_1 that the distance between a zone center and the center of its nearest neighbor is greater than βd_0 is [28]

$$p_1 = e^{-4\alpha} \tag{9}$$

The probability that the distance between a zone center and the center of its nearest neighbor is less than βd_0 is the complementary probability, $1 - p_1$. In an n-tet spot, one has $n-1$ sequences in which nearest neighbor distances are less than βd_0 and one sequence, that which breaks the spot away from other zones in the bed, in which a nearest neighbor distance is greater than βd_0. In the quintet in Fig. 2, for example, the four distances a, b, c and d are less

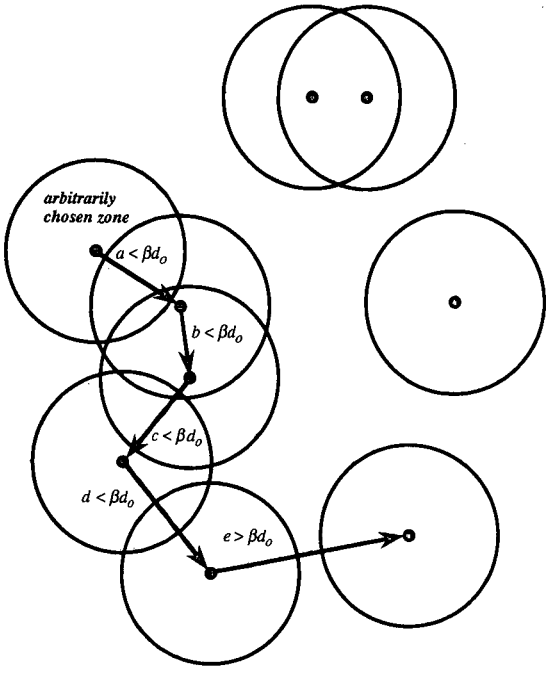

Fig. 2. Illustration of Roach's spot counting procedure. The five central zones overlap to form a quintet spot. The distance between any zone center in the spot and at least one other zone center in the spot is less than βd_0. The distances between all zone centers in the spot and all zone centers not in the spot are greater than βd_0.

than βd_0 and the one distance e is greater than βd_0. Roach recognized that these distances were *approximately* independent of each other, and it was this insight that reduced the 2D overlap problem to a tractable form. He concluded that the probability p_n that a zone forms part of a spot containing n overlapping zones is [24]

$$p_n = e^{-4\alpha}(1 - e^{-4\alpha})^{n-1} \tag{10}$$

Because each of $\bar{m}$ zones has this probability of forming an n-tet spot, the number of zones contributing to the formation of n-tet spots is $\bar{m}p_n$. But since n zones are required to form each spot, the expected number P_n of n-tet spots is $\bar{m}p_n/n$, or

$$P_n = \bar{m}e^{-4\alpha}(1 - e^{-4\alpha})^{n-1}/n \tag{11}$$

Roach then calculated the total number p of spots as the algebraic sum of all n-tet spots:

$$p = \sum_{n=1}^{\infty} P_n = \bar{m} \cdot \frac{4\alpha e^{-4\alpha}}{1 - e^{-4\alpha}} \tag{12}$$

The remainder of this paper principally will focus on the testing and use of this theory, although the other theories are also characterized.

Detailed testing of Roach's theory

To our knowledge, the only test of Roach's theory is presented in his book and is limited. In this test, Roach determined the coordinates of hundreds of points with a random number generator having six significant figures, plotted these points on graph paper, drew with a compass circles of fixed diameter about these points and manually counted the number of overlaps so generated ($\beta = 1$). More specifically, he determined the numbers of singlets and multiplets (up to septets) for m values of 100, 150, 200, 250, 300, 350, 400, 500, 600, 800, 1100, 1500 and 2220 [24]. The spot numbers so determined agreed fairly well with his theory, as will be shown below.

We have augmented substantially this testing of Roach's theory for two reasons. First, for each value of m cited above, the singlet and multiplet numbers reported by Roach were determined from only one simulation and consequently are not statistically robust. Second, and more important, zones in 2D separations actually are elliptical [2], instead of circular. In Roach's theory (indeed, in all of the theories outlined above), however, zones are assumed to be circular. The error introduced by this assumption has not been quantified, except in a cursory way [1], and is investigated here.

In general, a theory for the overlap of elliptical zones is considerably more difficult to develop than that for circular zones, because one no longer can assume that nearest neighbors overlap [1]. The overlap of randomly distributed convex laminae of arbitrary shape has been addressed by Mack [29,30] and can be adapted to elliptical zones, as shown by Roach [24]. Unfortunately, this theory is not applicable to 2D separation beds, because Mack assumed that the laminae were randomly ordered in the bed (he was interested in the random deposition of dust particles). Davis addressed the problem in a prelimi-

nary way by calculating the probability $p_1(e)$ that an elliptical zone of aspect ratio γ (*i.e.*, the ratio of the ellipse's semi-major axis to its semi-minor axis) is a singlet, which is [1]

$$p_1(e) = (2\pi)^{-1} \int_0^{2\pi} \exp\left(-4\alpha \cdot \frac{\gamma}{\cos^2\theta + \gamma^2 \sin^2\theta}\right) d\theta \tag{13}$$

He concluded that the probability of forming elliptical singlets is greater than the probability of forming circular singlets at any saturation α and that this probability increases with both α and γ.

The applicability of Roach's theory to elliptical zones, and the further testing of this theory by the overlap of circular zones, were characterized here by computer simulation. Spots p, singlets s and various multiplets were counted by visual inspection. For completeness, these simulation results also were compared with the predictions of Davis.

Procedure by which $\overline{m}$ can be estimated from a single bed

As was suggested by Davis [1], the number p of spots in a 2D bed can be counted and the spot capacity n_c of the bed can be estimated. One then can fit these data to eqn. 4 and estimate the number $\overline{m}$ of detectable components in the bed. The principal motive for this estimation is determining the extent of separation [15], the square of which equals the ratio, $s/\overline{m}$. This ratio, in turn, is a measure of the quality of the separation. The calculation of this ratio is straightforward, because once $\overline{m}$ has been determined, α can be estimated from the definition, $\overline{m}/n_c$, and s can be estimated from eqn. 1a, $\overline{m}$ and α.

An alternative procedure, by which one can estimate $\overline{m}$ from the distribution of spots in a 2D bed, is suggested here. This procedure is analogous to the "single-chromatogram method" based on the statistical model of overlap (SMO) [13], by which one can estimate the number of components in a 1D chromatogram from the distribution of distances (or times) between adjacent maxima. In essence, one determines by this procedure a series of spot numbers p, in accordance with the theory of Roach. The numbers p differ for each determination, however, because one sets the span βd_0 to different values by arbitrarily changing the scalar, β. In other words, different values of βd_0 (*i.e.*, different values of n_c^{-1}) correspond to different values of p, in accordance with eqns. 2 and 12 and the definition, $\alpha = \overline{m}/n_c$. With this scaling, one can generate a set of coordinates pairs, (n_c^{-1}, p) and then fit them to eqn. 12 with $\overline{m}$ as a least-squares parameter. One would expect this fitting usually to provide a better estimate of $\overline{m}$ than that determined from a single datum, simply because one has more information on which to draw.

It should be emphasized that the numbers p and n_c so generated have little, if any, physico-chemical meaning. They are to be distinguished from the physically meaningful spot number p, which corre-

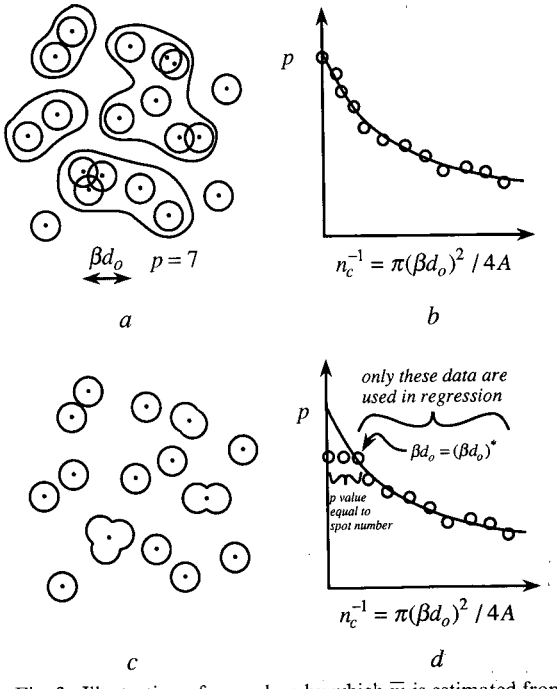

Fig. 3. Illustration of procedure by which $\overline{m}$ is estimated from a single bed. (a) Hypothetical bed in which all zone centers are visible, even when overlapped. The number $p = 7$ for the indicated value of βd_0. The groups of encircled zones each correspond to a "spot". (b) Graph of number p *vs.* reciprocal capacity n_c^{-1} constructed from the distribution of distances among zone centers in (a). Solid curve represents least-squares fit of data to eqn. 12. (c) More realistic bed in which some zone centers are obscured by overlap and spot positions are represented by a single coordinate. (d) Graph of number p *vs.* reciprocal capacity n_c^{-1} constructed from the distribution of distances among spot coordinates in (c). For βd_0 values less than $(\beta d_0)^*$, p equals the total number of spots. Solid curve represents least-squares fit of indicated data to eqn. 12.

sponds to the number of distinct clusters in the bed, and from the physically meaningful spot capacity n_c, which corresponds to the number of spots resolvable by the bed. However, we shall use the same variable to describe both quantities, because they are indistinguishable in a mathematical sense. The distinction should be apparent from context.

The generation and interpretation of these data is illustrated in Fig. 3. Fig. 3a is part of a hypothetical 2D bed in which the centers of all zones are observable, even when the zones overlap. For the βd_0 value in the figure, p equals seven and corresponds to the three singlets and the four groups of zones, which are encircled. Lest any misunderstanding arise, each zone center in an encircled group is within distance βd_0 of some other zone center in the group, and all zones in an encircled group are separated from all zones not in the group by distances greater than βd_0. A different value of βd_0 (or n_c^{-1}) would correspond to a different value of p, in accordance with the above discussion. The data are plotted in Fig. 3b as p *vs.* n_c^{-1}, the latter of which is directly proportional to βd_0. The curve represents a non-linear least-squares fitting of the data so generated to eqn. 12. Because all the zone centers in the bed are observable, the value of p at $\beta d_0 = n_c^{-1} = 0$ corresponds to the total number of zones.

In an actual bed, however, overlap obscures the positions of some zone centers, as shown in Fig. 3c. To apply the procedure to such a bed, one must approximate the positions of these centers by other easily measurable positions, such as the positions of maximum concentration or the first moments of spots. In general, the centers of closely overlapping zones are obliterated completely by overlap, and the remaining measurable positions (however they are determined) are somewhat removed from each other. Because of this obliteration, the distances between measurable positions are all greater than a critical value of βd_0, which is designated here as $(\beta d_0)^*$. For values of βd_0 less than or equal to $(\beta d_0)^*$, the number p is independent of βd_0 and equals the number of spot centers in the bed. As βd_0 is increased beyond $(\beta d_0)^*$, however, the number p decreases, as shown in Fig. 3d. Only the data for which $\beta d_0 \geqslant (\beta d_0)^*$ are fitted to theory.

At low saturations, only a few multiplets exist, and the positions of only a few zone centers are distorted by overlap. In this instance, the data plotted as p *vs.* n_c^{-1} in Fig. 3d differ little from those in Fig. 3b [except when $\beta d_0 < (\beta d_0)^*$], and a fitting of the appropriate data to eqn. 12 provides a good approximation to $\bar{m}$. As the saturation increases, however, the numbers of multiplets increase, and eventually the measurable positions of spots have little correlation with the positions of the underlying zone centers. In this instance, the least-squares fitting of the appropriate data provides a poor estimate of $\bar{m}$.

We should emphasize that this procedure will work well only if the theory to which the coordinates, (n_c^{-1}, p), are fitted correctly describes the numbers p at large values of α. This limitation arises because large α values are determined by selecting arbitrarily large values of β. As is shown below, only the theory of Roach correctly describes the number p at high saturations. Hence, only his theory was used to test the procedure proposed here. Computer simulations were analyzed to determine the saturation below which reliable estimates of $\bar{m}$ can be calculated.

The reader may find a complete 1D analogy to this procedure in ref. 13.

Methods of spot counting

One can envision at least three ways by which spots in a 2D bed can be counted. The first way, in which some degree of physical overlap is tolerated among resolved zones, corresponds to a β value of less than one [1]. The second way, in which zones that overlay one another by any amount are considered to be overlapped, corresponds to a β value equal to one. This method of counting previously was employed by both Roach [24] and Davis [1]. The final way, in which clusters of spatially resolved zones are grouped together and identified as "spots", as discussed above, corresponds to a β value greater than one. The latter two ways of counting, but not the first, are used here. More specifically, the values of p, s and multiplet numbers determined by visual inspection of 2D beds correspond to $\beta = 1$, and the values of p determined by applying the regression procedure correspond to $\beta \geqslant 1$. In a similar manner, peaks in 1D chromatograms have been counted in applications of the SMO by using various values of the resolution factor R_s^* (which is analogous to β), such as 0.5 [10–12], 1.0 [16] and 1.5 [10,11].

PROCEDURES

As observed in the second part of the Theory section, computer simulations of 2D beds were produced to augment the testing of the theory of Roach. These beds contained various numbers m of circular or elliptical zones; more specifically, m was varied among the values, 25, 50, 150, 300, 500, 750 and 1000. The coordinates of each zone center were computed by two sequential subroutine calls on an in-house random number generator adapted from ref. 31. The zones then were plotted as circles or as ellipses with aspect ratios equal to two with the Macintosh application, KaleidaGraph 2.0.2 (Synergy Software, Reading, PA, USA). These graphs then were plotted by either a dot matrix (ImageWriter II, Apple Computer, Cupertino, CA, USA) or laser printer (LaserWriter II). The various singlet and multiplet spots in these plots were counted, such that zones which touched or overlaid one another were considered to be overlapped ($\beta = 1$). A total of 240 simulations of beds containing circular zones and of 170 simulations of beds containing elliptical zones were interpreted.

The choice of an elliptical aspect ratio equal to two was completely arbitrary. Indeed, a study based on widely varying aspect ratios would be desirable. Such a study is postponed to a later date, however, to limit the data here to an amount that can be assessed in detail.

For both the circular and elliptical zones, a minimum of three and a maximum of five simulations were generated for each value of m at a particular α. The sizes of the circular and elliptical zones were limited to those available in KaleidaGraph 2.0.2. Various saturations were obtained for each m by combining various zone sizes with various square and rectangular bed shapes. The values of the bed perimeters were set in KaleidaGraph 2.0.2 (and confirmed by measuring them with a ruler), and the areas of several singlet zones were measured with calipers to three significant figures. From the measured areas, the spot capacity n_c was calculated in accordance with eqn. 2 ($\beta = 1$) and α was approximated as m/n_c. The various α values corresponding to the simulations are reported in Table I. The α values for the circular and elliptical zones typically are not equal, because of the constraints imposed by KaleidaGraph 2.0.2. Further, the α values do not form a simple numerical progression (*e.g.*, $\alpha = 0.05$, 0.10, 0.15, etc.), because of constraints on the sizes of zones and beds.

TABLE I

VALUES OF α CORRESPONDING TO COMPUTER SIMULATIONS OF 2D BEDS CONTAINING CIRCULAR AND ELLIPTICAL ZONES

m	α ($\beta = 1$)	
	Circular zones	Elliptical zones ($\gamma = 2$)
25	0.0287, 0.0470, 0.0696, 0.100, 0.130, 0.164, 0.202, 0.260, 0.298, 0.347	0.0466, 0.0976, 0.122, 0.163, 0.204, 0.248, 0.292, 0.350
50	0.0124, 0.0291, 0.0558, 0.0950, 0.139, 0.195, 0.258, 0.332, 0.403, 0.505	0.0302, 0.0573, 0.137, 0.193, 0.252, 0.331, 0.407, 0.497
150	0.0372, 0.0874, 0.172, 0.282, 0.418, 0.595	0.0325, 0.0906, 0.175, 0.294, 0.416, 0.560
300	0.0688, 0.131, 0.175, 0.259, 0.345, 0.423, 0.563	0.0651, 0.181, 0.350, 0.577
500	0.0896, 0.119, 0.219, 0.291, 0.431, 0.574	0.108, 0.137, 0.302, 0.584
750	0.134, 0.169, 0.328, 0.437, 0.647	0.163, 0.206, 0.453, 0.539
1000	0.172, 0.239, 0.438, 0.583	0.217, 0.275, 0.604, 0.719

We briefly observe that the α values calculated as described above for ellipses (but not for circles) varied with the output device. In other words, the identical graph, when plotted on the dot matrix and laser printers, resulted in slightly different α values (on average, the values varied by about 3%). Some of the slight variations reported in Table I can be attributed to this behavior. Also, some of the beds of elliptical zones, when plotted with the laser printer, contained ellipses with γ values lying between 1.9 and 2.0, instead of γs which exactly equalled 2.0. We tolerated this small error (5% or less), instead of rejecting the graph.

Fig. 4 reports five simulations of square beds containing $m = 50$ zones of different size. The sequence of random numbers defining the zone centers is the same in each simulation. The various beds span the range $0.056 \leqslant \alpha \leqslant 0.258$ ($\beta = 1$). As

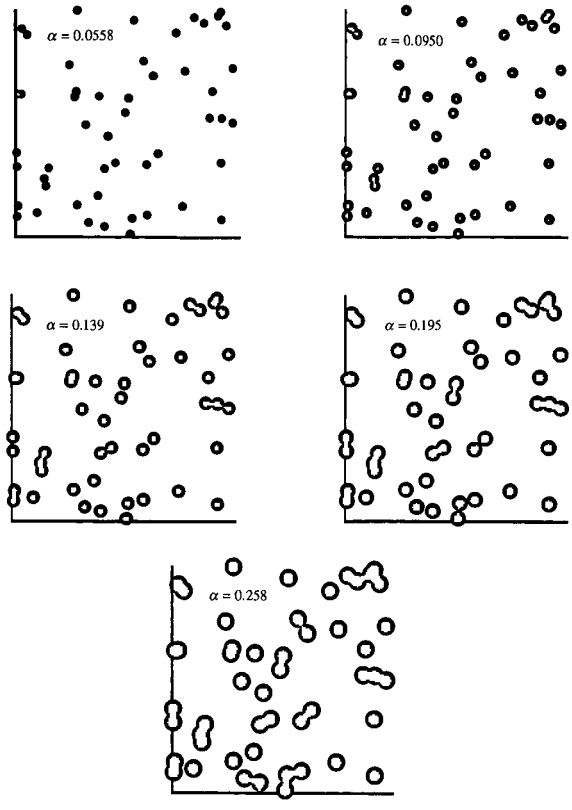

Fig. 4. Computer-simulated beds containing $m = 50$ components at various saturations α ($\beta = 1$). Coordinates of zones centers in each bed are identical.

observed above, the larger α values are not simple multiples of the smallest α, because of constraints on the generation of these plots. These beds should prove useful in gauging the severity of overlap at different saturations.

A preliminary testing of the regression procedure outlined in the third part of the Theory section was implemented by generating several computer simulations of square 2D beds containing $m = 100$, 200 and 300 zones. For each m, ten simulations were produced at each of the α values, 0, 0.05, 0.10, 0.15, 0.20 and 0.25 ($\beta = 1$). In contrast to the study described above, α could be assigned regularly spaced values here, because KaleidaGraph 2.0.2 was not used to generate beds for visual inspection. Rather, all necessary computations were implemented with a computer algorithm. In total, 180 simulations (ten simulations per α times six α values times three m values) were generated. The regression procedure was applied to each simulation.

The coordinates of the zone centers in these beds were computed by the in-house random number generator described above. For each m, a different sequence of coordinates was generated for each of the ten simulations. For each m, however, the same ten sequences of coordinates were used to generate simulations at different α values. This usage made the beds for any one value of m identical, except for the value assigned to α.

We recognized that our $\bar{m}$ estimates would not equal m exactly, even under the best of circumstances, because only a limited number of beds were sampled and because small systematic errors existed in the random number generator. Consequently, we decided to use the $\bar{m}$ estimates determined from beds for which $\alpha = 0$ as a basis by which to evaluate the quality of other $\bar{m}$ estimates. For $\alpha = 0$, the zone diameter d_0 was equated to zero. In other words, these beds contained only zone centers, *i.e.*, a sequence of randomly spaced points. (The resultant beds are analogous to the "line chromatograms" of the 1D "single-chromatogram method" [13].) The distances between each point and its neighbors were calculated. From these distances the coordinates (n_c^{-1}, p) were determined as detailed in the Theory section (here, the various non-zero spans βd_0 were interpreted as a series of arbitrary distances, as $d_0 = 0$). These coordinates then were fitted to eqn. 12, except for the coordinate $(n_c^{-1} = 0, p)$. This coordinate was specifically excluded, because its inclusion forced the $\bar{m}$ estimate to equal m. Approximately 30 to 40 data points were generated for purposes of regression. No value of p less than 20 was included in a fit to minimize the effect of small-number statistics [13].

In the other simulations, the zone diameter d_0 was determined in accordance with assigned values of $\alpha \approx m/n_c$, the spot capacity, n_c, as defined by eqn. 2 and the criterion $\beta = 1$ (no elliptical zones were considered in this part of the study). The spot number was counted in accordance with the criterion $\beta = 1$; zones separated by spans less than d_0 were considered to overlap. Once the number of spots in a given simulation had been determined, then a single representative coordinate was assigned to each spot. The representative coordinate of a singlet spot was the coordinate of the zone center, and the representative coordinate of a multiplet spot

was the arithmetic average of the coordinates of the zone centers comprising the multiplet spot. In general, the representative coordinates of multiplets determined by these means do not correspond to any physically measurable positions. They are simple to determine, however, and are sufficient for our purpose here, which is simply to verify the regression procedure (the optimization of the procedure is addressed later). The distances between these coordinates were then calculated to determine the data

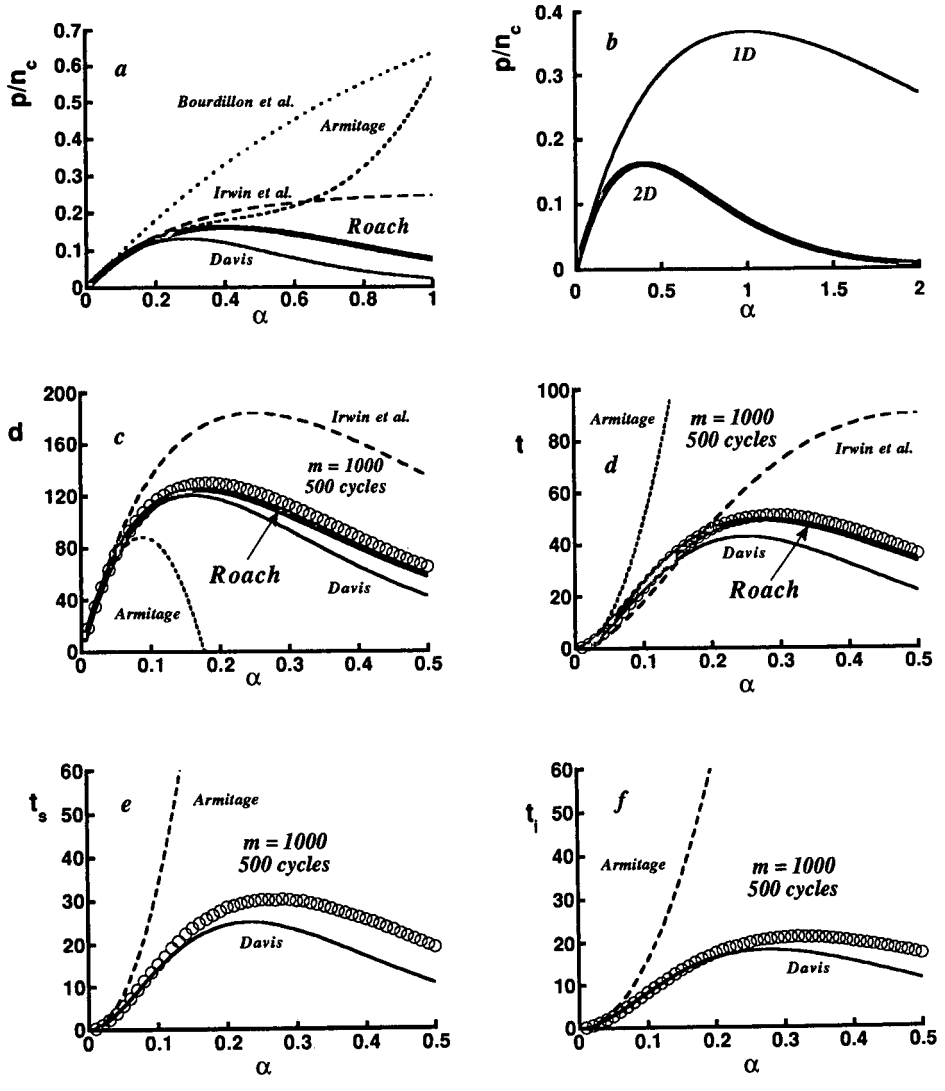

Fig. 5. (a) Graphs of p/n_c *vs.* α predicted by Davis (eqns. 1 and 4), Bourdillon *et al.* (eqn. 5b), Irwin *et al.* (eqn. 6b), Armitage (eqn. 8) and Roach (eqn. 14). All equations but the last were divided by n_c. (b) Graphs of p/n_c *vs.* α for 1D and 2D separations. The former graph is defined by $\alpha \exp(-\alpha)$ and the latter by eqn. 14. (c) Graphs of doublet number d *vs.* α ($\beta = 1$) predicted by Davis (eqn. 1b), Irwin *et al.* (eqn. 6a, with $n = 2$, multiplied by $\overline{m}$), Armitage (eqn. 7a) and Roach (eqn. 11, with $n = 2$) for $m = \overline{m} = 1000$ zones distributed randomly in a square bed. Circles represent the average numbers of doublets determined from 500 computer simulations. (d) Graphs of triplet number t *vs.* α ($\beta = 1$) predicted by Davis (sum of eqns. 1c and d), Irwin *et al.* (eqn. 6a, with $n = 3$, multiplied by $\overline{m}$), Armitage (sum of eqns. 7b and c) and Roach (eqn. 11, with $n = 3$) for $m = \overline{m} = 1000$ zones distributed randomly in a square bed. Circles represent the results of simulations, as detailed above. (e) Graphs of straight-chain triplet number t_s *vs.* α ($\beta = 1$) predicted by Davis (eqn. 1c) and Armitage (eqn. 7b). Circles represent the results of simulations, as detailed above. (f) Graphs of interlocking triplet number t_i *vs.* α ($\beta = 1$) predicted by Davis (eqn. 1d) and Armitage (eqn. 7c). Circles represent the results of simulations, as detailed above.

pairs (n_c^{-1}, p), as detailed above. Approximately 30–40 data pairs were generated for each regression. As before, no values of p less than 20 were used.

For each simulation, these coordinates were plotted in KaleidaGraph 2.0.2 and examined. The data for which $\beta d_0 < (\beta d_0)^*$ were excluded from the non-linear regression. Some subjective judgment was required in the inclusion or elimination of some of these data, as is also required in the application of the SMO.

The algorithm necessary for these computations was written in FORTRAN 77 and executed on the GX-3081 computer at Southern Illinois University. The least-squares regressions were carried out in KaleidaGraph 2.0.2.

RESULTS AND DISCUSSION

Fig. 5a is a graph of the various theoretical estimates of the ratio p/n_c *vs.* α. These ratios are obtained by dividing both sides of eqns. 1a–d and 4, 5b, 6b, 8 and 12 by n_c and then substituting the identity $\alpha = \bar{m}/n_c$. The specific result for the theory of Roach, which will be examined in more detail below, is

$$p/n_c = \frac{4\alpha^2 \exp(-4\alpha)}{1 - \exp(-4\alpha)} \tag{14}$$

and is plotted in bold. All of the theories predict essentially identical results for sufficiently small values of α (*e.g.*, $\alpha < 0.10$). Relative to the results predicted by Roach, the p/n_c estimates predicted by Bourdillon *et al.*, Irwin *et al.* and Armitage are unduly large at high saturations. Further, at large saturations, the theory of Irwin *et al.* unrealistically predicts that p/n_c approaches the constant value 1/4 (for similar reasons, Bourdillon *et al.*'s theory approaches $p/n_c = 1$ at α values larger than shown here). These findings are indicative of errors in these theories. One observes that the theory of Davis underestimates p/n_c at α values greater than *ca.* 0.20 relative to the results of Roach. This underestimation is expected, however, in part because multiplets larger than triplets are neglected in this theory.

By differentiating eqn. 14 with respect to α, equating the derivative to zero and solving the resultant equation numerically, one can show that the maximum value of p/n_c, as predicted by Roach, is 0.162 and is found at $\alpha = 0.398$. In other words, only about one sixth of the entire spot capacity of a bed can be used to resolve spots under the best of circumstances, when statistical considerations apply (as observed elsewhere [1], less than one tenth of the bed can be used to resolve singlet spots). This fraction is considerably smaller than the maximum number of peaks resolvable per unit peak capacity in 1D chromatograms, which is $e^{-1} = 0.368$ [7]. Fig. 5b is a graph of p/n_c *vs.* α, in which the ratios p/n_c for 1D and 2D separations are compared (the theoretical relationship for the 1D separation is $\alpha \exp(-\alpha)$ [7]). At all saturations, the available capacity is utilized less effectively in two dimensions than in one dimension. This graph supports the conclusion asserted in previous works [1,23] and reported in the Introduction that per unit capacity, 2D separations are actually worse than their 1D analogues.

The theories of Irwin *et al.*, Armitage, Roach and Davis all predict that the number of singlets is given by eqn. 1a. However, their predictions of the numbers of multiplet spots differ substantially. Fig. 5c is a graph of the number of doublets d *vs.* α predicted by these four theories for $\bar{m} = 1000$. The circles represent the average numbers of doublets found in 500 computer simulations of 2D beds, each of which contained $m = 1000$ zones distributed randomly in a square area (these data have been reported elsewhere [1]). The number d is correctly predicted by all four theories, when $\alpha < ca.\ 0.05$. The theories of Irwin *et al.* and Armitage, however, clearly break down at levels of saturation greater than this. For values of $\alpha > ca.\ 0.15$, the theory of Davis underestimates d, although the theoretical prediction more or less parallels the results of the computer simulations. The theory of Roach also slightly underestimates these results at higher saturations but agrees with them more closely than that of Davis. Similar trends are indicated in Fig. 5d, which is a graph of the total number $t = t_s + t_i$ of triplets *vs.* α predicted by all four theories and also determined by computer simulation. In particular, the theories of Irwin *et al.* and Armitage agree with the simulation results only for very small values of α.

Only the theories of Armitage and Davis distinguish between the two triplet types, t_s and t_i. Fig. 5e and f are graphs of t_s and t_i *vs.* α predicted by these theories and also determined by computer simulation. The theory of Davis has some shortcomings at large saturations but correctly describes both t_s

and t_i at modest saturations. The predictions of Armitage, however, agree with simulation only for extremely small values of α and depart drastically from these simulations at higher saturations.

It is instructive to compare the Taylor-series expansions of the equations derived by Davis to the series approximations derived by Armitage. A comparison of eqns. 3a and 7a shows that the terms linear in α are identical and that the quadratic terms in α differ by -5.76% if one arbitrarily normalizes the difference by the prediction of Davis. This difference is not unduly large, but because the theory of Armitage predicts d only to quadratic powers of α, it breaks down at even small α values. The comparisons of eqns. 3b and 7b and of eqns. 3c and 7c show that the quadratic terms in α of t_s and t_i are also close (for t_s the difference is 3.38% and for t_i it is -2.25%, if one again normalizes the differences by the predictions of Davis). In his derivation, Davis analytically determined the functional forms of t_s and t_i but had to determine the coefficients by which to multiply these forms by empirical means [1]. He suggested that someone probably would theoretically account for the values of these coefficients someday [1]. Little did he realize the work had already been done (at least for the α^2 term) some 42 years earlier!

The simulations described above were determined with a large m value (1000) to ensure that enough events were included for the statistics to be meaningful [1]. Fig. 6 is a plot of the dimensionless functions p/n_c, s/n_c and d/n_c *vs.* α ($\beta = 1$) as determined from the visual inspection of several hundred simulations of 2D beds containing a wide range of m values ($25 \leqslant m \leqslant 1000$). The various solid (dashed) curves in these figures represent the predictions of Roach (Davis), unless noted otherwise. The solid curves in Fig. 6a and b are graphs of eqn. 14, whereas the dashed curves are graphs of eqn. 4, divided by n_c, with s, d, t_s and t_i expressed by eqns. 1a–d. The solid curves in Fig. 6c and d are graphs of eqn. 1a, divided by n_c (here, the predictions of Roach and Davis are identical), whereas the dashed curve in Fig. 6d is a graph of eqn. 13, multiplied by α. The solid curves in Fig. 6e and f are graphs of eqn. 11, divided by n_c, with $n = 2$, whereas the dashed curves are graphs of eqn. 1b, divided by n_c. The numbers m of zones corresponding to the various symbols are identified in the figure caption. Not all of the available data are plotted in order to minimize the overlap of various symbols. The open diamonds in Fig. 6a, c and e represent the single determinations of Roach.

The division of the indicated equations by n_c allows one to make the substitution $\alpha = \bar{m}/n_c$, such that these functions depend only on α. Further, because eqn. 13 equals the probability $p_1(e)$ of forming elliptical singlets, one must multiply it by $\alpha = \bar{m}/n_c$ to obtain the number $s = \bar{m}p_1(e)$ of elliptical singlets per capacity n_c. For a specified value of γ, this expression also depends only on α. These various functions are represented in dimensionless form to enable us to represent spot numbers corresponding to widely varying m values in the same figure.

Except for the open diamonds, the symbols in Fig. 6 represent the means of spot numbers determined in this laboratory, and the error bars represent the standard deviations of these numbers (the standard deviations are not shown when they are smaller than the symbols). In 6a, c and e, the spots were formed from circular zones and in Fig. 6b, d and f from elliptical zones ($\gamma = 2$). For both zone shapes, the largest deviations at any α are associated with the smallest values of m. This finding, which also was observed in the 1D analogue to this study [32], is unsurprising and simply indicates that the relative standard deviation for Poisson processes increases with decreasing values of $\bar{m}$. Also, for any m, the largest deviations are associated with large α values. This observation again is unsurprising, because spot numbers decrease with increasing α and the relative deviation of any spot number from its small mean value consequently increases. This trend was also observed in the 1D analogue to this study [32]. Because of the large deviations associated with small spot numbers, no values of p, s or d less than 15 are represented in the figure.

The values of p/n_c shown in Fig. 6a agree closely with Roach's theory for αs less than *ca.* 0.30 ($\beta = 1$). At higher saturations, the values of p/n_c are slightly larger than expected, although this difference probably is not statistically significant (the theory typically lies within one standard deviation of the data). The results also agree well with the theory of Davis for α values less than *ca.* 0.20. This finding may be surprising, as Davis's theory for triplet number t_s underestimates this multiplet at α values larger than *ca.* 0.12 (see Theory section). The reason why the

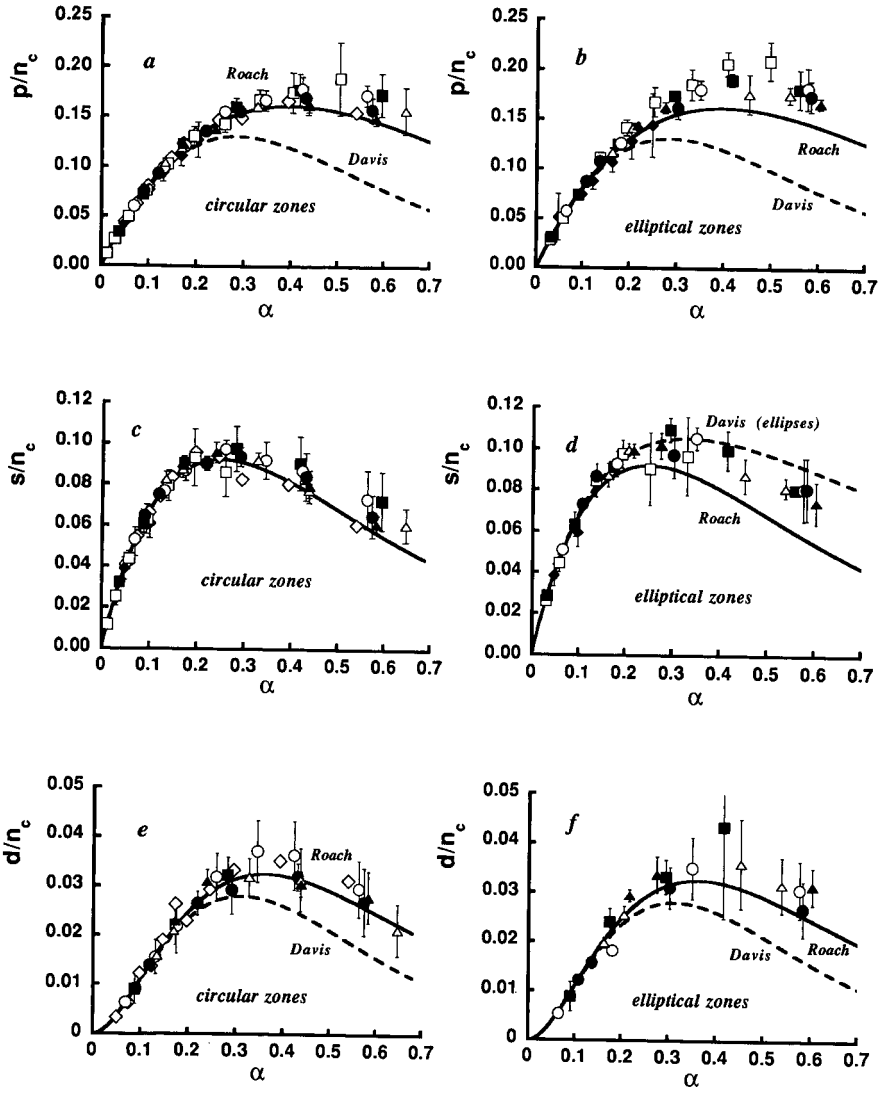

Fig. 6. Graphs of p/n_c *vs.* α ($\beta = 1$) for (a) circular and (b) elliptical zones, as determined by visual inspection. Solid curves are graphs of eqn. 14; dashed curves are graphs of eqn. 4, divided by n_c, with s, d, t_s and t_i expressed by eqns. 1a–d. Graphs of s/n_c *vs.* α ($\beta = 1$) for (c) circular and (d) elliptical zones, as determined by visual inspection. Solid curves are graphs of eqn. 1a, divided by n_c; dashed curve in Fig. 6d is a graph of eqn. 13, multiplied by α. Graphs of d/n_c *vs.* α ($\beta = 1$) for (e) circular and (f) elliptical zones, as determined by visual inspection. Solid curves are graphs of eqn. 11, divided by n_c, with $n = 2$; dashed curves are graphs of eqn. 1b, divided by n_c. Symbols corresponding to different m values are: ◆ = 25; □ = 50; ■ = 150; ○ = 300; ● = 500; △ = 750; ▲ = 1000; ◇ = Roach's data.

numbers p (or p/n_c) do not appear to be erroneous over the α range $0.12 \leqslant \alpha \leqslant 0.20$ is that the "excess" t_s triplets actually found partially compensate for the neglect of quartets and other multiplets, which become increasingly prevalent at saturations above 0.10. (A similar trend is found in the work of Armitage, whose theory severely underestimates doublets and overestimates triplets at even low α values but correctly estimates p up to $\alpha \approx 0.30$ [27], as shown in Fig. 5a.) At saturations greater than *ca.* 0.20, however, the theory of Davis underestimates p/n_c.

As shown in Fig. 6b, Roach's theory also correctly predicts the numbers p/n_c determined by counting elliptical spots ($\gamma = 2$), when α is less than *ca.* 0.25 or so. At larger α values, the numbers p/n_c (and consequently p) are greater than predicted by Roach. Unlike in Fig. 6a, this difference is statistically significant; the differences between theory and simulation are greater than one standard deviation (except for one datum) when α is greater than *ca.* 0.30. The theory of Davis adequately predicts p/n_c for α values less than *ca.* 0.20 but underestimates p/n_c at larger α values.

Fig. 6c is a plot of s/n_c *vs.* α, as determined by counting circular spots. The agreement between simulation and theory is good over the full α range, although it is best at low α values. At larger α values,

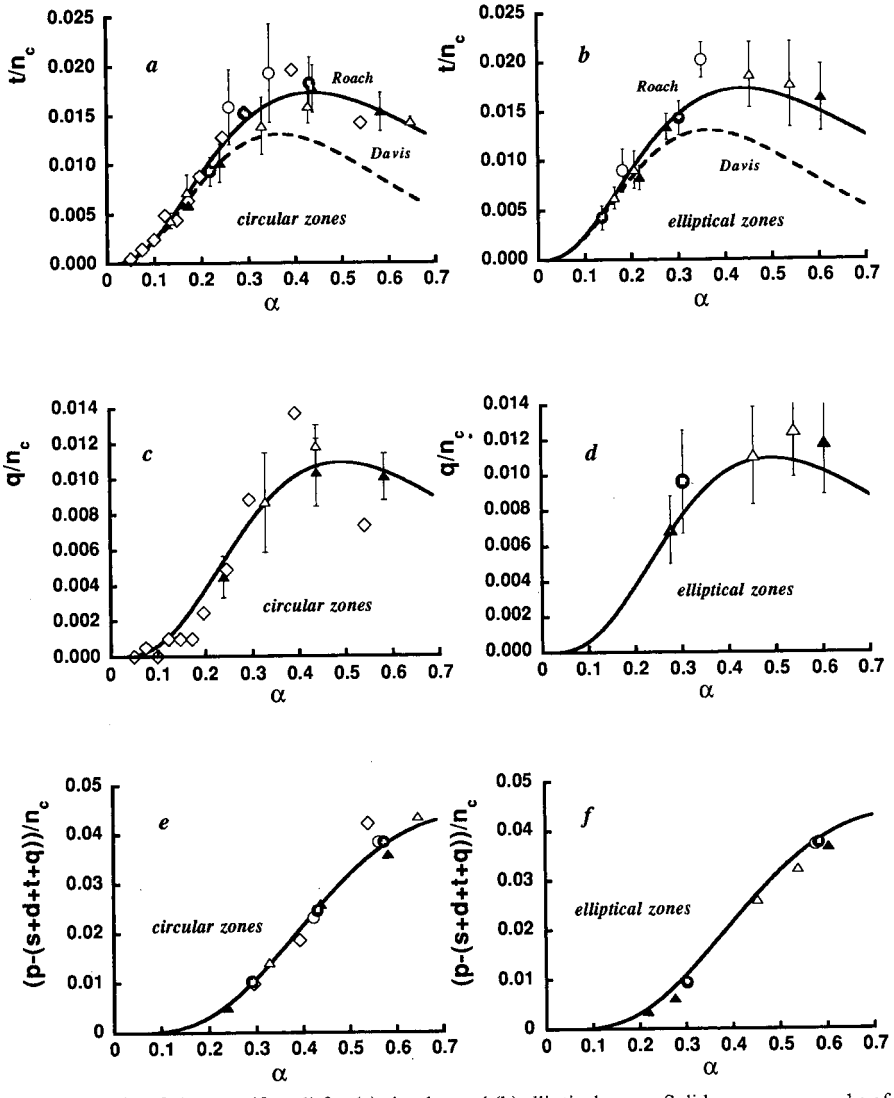

Fig. 7. Graphs of t/n_c *vs.* α ($\beta = 1$) for (a) circular and (b) elliptical zones. Solid curves are graphs of eqn. 11, divided by n_c, with $n = 3$; dashed curves are graphs of the algebraic sum of eqns. 1c and d, divided by n_c. Graphs of q/n_c *vs.* α ($\beta = 1$) for (c) circular and (d) elliptical zones. Solid curves are graphs of eqn. 11, divided by n_c, with $n = 4$. Graphs of $[p - (s + d + t + q)]/n_c$ *vs.* α ($\beta = 1$) for (e) circular and (f) elliptical zones. Solid curves are graphs of eqn. 14, less the algebraic sum of four different expressions of eqn. 11, all divided by n_c. These four expressions are defined by $n = 1, 2, 3$ and 4. Symbols corresponding to different m values are ○ = 300; ● = 500; △ = 750; ▲ = 1000; ◇ = Roach's data.

values of s/n_c slightly exceed theory but not significantly so. In part, these small discrepancies are due to "edge effects", in which zones near the border of the 2D bed are partially shielded from overlap by the absence of zones outside the bed [1]. As shown in Fig. 6d, the theory for circular singlets correctly predicts the number of elliptical singlets ($\gamma = 2$) when α is smaller than *ca.* 0.20. In contrast, this theory predicts results that are statistically smaller than the simulation results when α is larger than *ca.* 0.20. This finding is in qualitative agreement with the prediction of Davis, who argued that singlet formation is more probable for ellipses than for circles [1]. The dashed curve is the quantitative prediction of Davis ($\gamma = 2$). For α values less than *ca.* 0.40, the agreement between this prediction and simulation is good. The theory, however, does overestimate values of s/n_c at higher α values, for unknown reasons.

Fig. 6e and f are plots of d/n_c *vs.* α for circular and elliptical zones, respectively. Here, we observe trends similar to those found in previous figures. More specifically, Roach's theory correctly predicts values of d/n_c for overlapping circular zones over the full range of α values (see Fig. 6e), although the agreement is best for small α values. Roach's theory somewhat underestimates the numbers of doublets formed from overlapping elliptical zones at large α values (see Fig. 6f), but unlike in Fig. 6b and d, this underestimation does not appear to be statistically significant. At least a part of this insignificance may be attributed to the larger standard deviations of d/n_c, which result from the small numbers of doublets found at the larger α values. The theory of Davis agrees well with the simulation results for α values less than *ca.* 0.20.

Fig. 7 is a plot of the dimensionless functions t/n_c, q/n_c and $[p - (s + d + t + q)]/n_c$, *vs.* α ($\beta = 1$). Here, variable q represents the number of quartet spots, and $p - (s + d + t + q)$ represents the algebraic sum of quintets, hextets and all other higher order multiplets. The solid curves in Fig. 7a and b are graphs of eqn. 11, divided by n_c, with $n = 3$, whereas the dashed curves in these figures are the algebraic sums of eqns. 1c and d, divided by n_c. The solid curves in Fig. 7c and d are graphs of eqn. 11, divided by n_c, with $n = 4$. The solid curves in Fig. 7e and f are graphs of eqn. 14, less the algebraic sum of four different expressions of eqn. 11, all of which are divided by n_c. These four expressions are defined by the n values, 1, 2, 3 and 4. The substitution $\alpha = \bar{m}/n_c$ was used as before to scale the theoretical predictions and simulations to fit in the same graph. The numbers m of zones corresponding to the various symbols are identified in the figure caption. The open diamonds in Fig. 7a, c and e represent the single determinations of Roach. Fewer data are plotted in Fig. 7 than in Fig. 6 because spot numbers less than 15 again were excluded and this exclusion restricts the data to large m values only ($m \geqslant 300$).

The values of t/n_c plotted in Fig. 7a and b show that Roach's theory accurately predicts the number of triplets formed from either circular or elliptical ($\gamma = 2$) zones over the examined α range. The standard deviations are somewhat larger than those in Fig. 6a–d because only a few triplets were found, even for large m. Davis's theory adequately predicts t/n_c for α values less than *ca.* 0.20. Roach's theory also adequately describes q/n_c for both zone shapes, although the scatter in the data is so large that a statistical agreement between simulation and theory is hardly surprising. This scatter results from the limited number of quartets observed. Interestingly, the results of Roach's simulations are scattered about his theory for quartets (see Fig. 7c), again because so few quartets were observed in his study. This scatter reflects the lack of statistical robustness in his simulations.

Because so few multiplets for which $n \geqslant 5$ were observed, we chose to plot their algebraic sum in Fig. 7e and f. The ordinates of these plots, therefore, are the sums of the numbers of quintets, hextets, heptets, octets, *etc.*, divided by n_c. No standard deviations are reported here, because they would be meaningless; these deviations would reflect not only variations about the mean of a given multiplet but also variations among the means of different multiplets. The close agreement between simulation and theory further confirms the theory of Roach.

We now turn our attention to evaluating the utility of the regression procedure proposed in the third part of the Theory section. Table II reports the statistical component numbers $\bar{m}$ estimated by fitting the data derived from 180 simulations of 2D square beds to eqn. 12. These estimates of $\bar{m}$ are accurate to within *ca.* 10% as long as $\alpha \leqslant 0.15$ ($\beta = 1$). In particular, for α values less than or equal to 0.10, the $\bar{m}$ estimates differ from the estimates

TABLE II

MEAN AND STANDARD DEVIATION OF NUMBERS $\bar{m}$ OF COMPONENTS ESTIMATED FROM TEN COMPUTER SIMULATIONS OF SQUARE BEDS CONTAINING m = 100, 200 AND 300 ZONES

Numbers p of spots were counted in accordance with the criterion $\beta = 1$. Results in parentheses in the last column are percentage errors in $\bar{m}$, as calculated with respect to the $\bar{m}$ predictions at $\alpha = 0$.

m	α ($\beta = 1$)	p	$\bar{m}$ estimates
100	0.00	100.0 ± 0.0	100.1 ± 5.0
	0.05	91.0 ± 3.3	100.8 ± 5.6 (0.73)
	0.10	82.8 ± 3.7	98.0 ± 7.0 (−2.1)
	0.15	74.3 ± 3.1	90.6 ± 7.5 (−9.6)
	0.20	67.1 ± 4.3	83.0 ± 5.9 (−17.1)
	0.25	59.4 ± 3.5	72.0 ± 3.9 (−28.1)
200	0.00	200.0 ± 0.0	195.6 ± 8.6
	0.05	182.1 ± 5.0	196.7 ± 7.6 (0.58)
	0.10	164.7 ± 2.6	192.9 ± 6.8 (−1.4)
	0.15	148.2 ± 4.6	179.1 ± 10.6 (−8.4)
	0.20	134.1 ± 5.4	162.7 ± 10.4 (−16.8)
	0.25	118.2 ± 3.3	137.2 ± 6.5 (−29.9)
300	0.00	300.0 ± 0.0	294.4 ± 10.7
	0.05	271.8 ± 4.8	295.8 ± 10.4 (0.49)
	0.10	245.3 ± 5.7	288.3 ± 13.3 (−2.1)
	0.15	219.0 ± 7.0	267.5 ± 14.7 (−9.1)
	0.20	198.9 ± 7.4	242.4 ± 8.8 (−17.7)
	0.25	179.8 ± 6.9	211.9 ± 8.9 (−28.0)

determined at $\alpha = 0$ by only 1–2%. These are remarkably accurate estimates, given that only *ca.* 80% of the zones can be detected under these circumstances (eqn. 12 predicts that $p/\bar{m} = 0.813$ at $\alpha = 0.10$). The accuracy of these $\bar{m}$s confirms the validity of the regression procedure, although its application is probably not optimized (see below). At larger α values, the estimates of $\bar{m}$ are too small, and their accuracy decreases substantially with increasing α. By and large, the percentage errors in $\bar{m}$ are independent of m and depend only on α. For example, at $\alpha = 0.20$, the percentage errors in $\bar{m}$ are −17.1, −16.8 and −17.7 for m = 100, 200 and 300, respectively. A similar trend was found when the "single-chromatogram method" was applied to 1D chromatograms [13].

Fig. 8 is a series of superimposed plots of p *vs.* n_c^{-1} generated from six 2D beds containing m = 100 zones. The zone coordinates in these beds were identical; only zone diameter d_0 (and hence α) was varied. The symbols corresponding to various α values are identified in the figure caption. If one examines the data for which p is independent of n_c^{-1} (*i.e.*, the data on the extreme left-hand side of the plot), one sees that the position of the first usable datum in the regression is increasingly shifted to larger values of n_c^{-1} as α increases. If one now examines the data which are fitted to theory (*i.e.*, the data on the right-hand side of the plot), one sees that values of p at any n_c^{-1} are nearly identical when α is small but that these values increase with increasing α. For example, the values of p at the n_c^{-1} coordinate represented in the figure by an arrow, n_c^{-1} = 0.00565, are 31, 35 and 42 for α values of 0.05, 0.15 and 0.25, respectively. This increase in p with increasing α is similar to that observed in the computer simulations by which the "single-chromatogram method" was tested [13]. These increases lead to the loss of curvature in the data representing function p (*i.e.*, eqn. 12) at large αs; indeed, the variation of p with n_c^{-1} is almost linear for $\alpha = 0.20$ and 0.25. This linear variation is a warning sign that the estimates of $\bar{m}$ will be unreliable.

This warning is insufficient, however; criteria other than the qualitative shape of the p *vs.* n_c^{-1} plot are necessary to evaluate the accuracy of the estimated $\bar{m}$ values. Perhaps the most important criterion is the value of α, which can be calculated by numerical means (*e.g.*, bisection method) from the estimated $\bar{m}$, the number p of spots in the bed and eqn. 12. For example, the numerical solution to this equation for the results of one simulation, p = 92

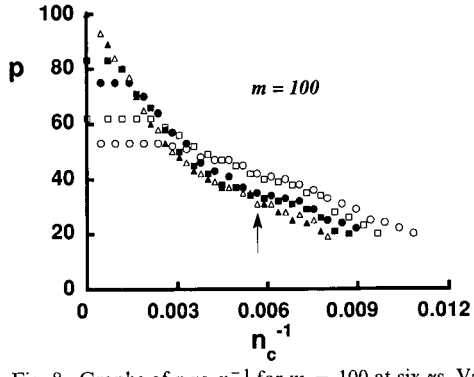

Fig. 8. Graphs of p *vs.* n_c^{-1} for m = 100 at six αs. Values of p at n_c^{-1} value represented by the arrow are discussed in the text. Symbols corresponding to different α values are ▲ = 0; △ = 0.05; ■ = 0.10; ● = 0.15; □ = 0.20; ○ = 0.25.

and $\bar{m} = 100.7$, is $\alpha = 0.044$, which agrees closely with the α value, 0.05, from which the simulation was generated. Because this estimate of α is less than 0.15, one has some confidence in the $\bar{m}$ estimate, which in fact is in error by only 0.7%. This criterion by itself is insufficient, however, because the estimates of $\bar{m}$ tend to decrease with increasing α (see Table II), leading to deceptive underestimations of α itself. Hence, one must also compare the overall appearance of the spot density in the bed to that in computer simulations, such as those reported in Fig. 4. Similar criteria are employed in evaluating the accuracy of $\bar{m}$ estimates determined by applying the "single-chromatogram method" to 1D chromatograms [13,22].

CONCLUSIONS

The theories of Roach and Davis are superior to the theories of Bourdillon *et al.*, Irwin *et al.* and Armitage in describing overlap in 2D beds. Of these two, the theory of Roach more correctly predicts the number of doublet and triplet spots over a wider range of α values than does the theory of Davis, which is correct only for α values less than *ca.* 0.20 ($\beta = 1$). Roach's theory also correctly predicts the number of higher order multiplets. When zones are elliptical, however, both Roach's and Davis's theories exhibit shortcomings in correctly predicting the total number of spots and the number of singlet spots at α values greater than *ca.* 0.25 ($\beta = 1; \gamma = 2$). This shortcoming is of practical concern, as zones in 2D separations are more elliptical than circular. In general, however, Roach's theory should be the basis of future studies of statistical limitations on 2D separations of modest saturation (*e.g.*, $\alpha < 0.25$), at least until an adequate theory for the overlap of elliptical zones is developed. Along these lines, Davis's theory for elliptical singlets shows some promise.

The regression procedure proposed here has been validated by analyses of dozens of computer simulations of 2D beds. The estimates of $\bar{m}$ so calculated are correct to within *ca.* 10% as long as α is less than *ca.* 0.15 ($\beta = 1$). This study is preliminary, however, and merely validates the proposed procedure; it does not determine the limits on it. Indeed, the findings presented here are based on the interpretation of somewhat hypothetical 2D beds, in that the representative coordinates of multiplet spots as determined here do not correspond to any physically measurable positions. By considering more realistic means for counting spots, it should be possible to extend the α range over which this procedure applies, as is now argued.

Based on the demonstrated success of the "single-chromatogram method" as a means for estimating $\bar{m}$ from the relative positions of maxima in single chromatograms [19,20,22], one anticipates that several advantages may accrue by identifying the maxima of measurable concentration pulses in a 2D bed with the representative coordinates of spots. These coordinates physically could be measured by a variety of means, *e.g.*, densitometry or fluorimetry, and experimental data could be gathered easily for purposes of regression. Because an isolated multiplet could contain several such maxima, the identification of spot coordinates with maxima would correspond to a counting procedure in which $\beta < 1$. This counting procedure could have distinct advantages. For example, if two zones slightly overlapped, it is possible that both zone centers would be observable as maxima. The distances between these centers and other similarly determined centers in the 2D bed would more accurately represent the underlying zone structure than do the distances calculated as detailed in the Procedures section. Hence it is possible (moreover, it is probable) that the range of α over which the regression is applicable can be extended by using such a counting procedure.

The reason why we did not interpret maxima as spot centers here is simple. In essence, we were not willing to delay communication of Roach's theory, particularly in the light of the increased interest in the statistical limitations on 2D separations [23], while the necessary but intricate details of this counting procedure were worked out. First, modestly sophisticated software will be required to determine from computer simulations the positions of maxima without the simultaneous detection of false maxima (we found several false maxima in our preliminary efforts in this direction). Further, we do not know yet the appropriate value to assign to β for use with such a counting procedure. This value will have to be determined empirically by counting the numbers of maxima in a series of simulations and adjusting β until simulation and theory agree, as was

done to determine the empirical resolution factor, $R_s^* \approx 0.5$, for the SMO [10–12]. These activities are best deferred to another study.

REFERENCES

1 J. M. Davis, *Anal. Chem.*, 63 (1991) 2141.
2 J. C. Giddings, *Unified Separation Science*, Wiley-Interscience, New York, 1991.
3 M. M. Bushey and J. W. Jorgenson, *Anal. Chem.*, 62 (1990) 978.
4 Z. Liu and J. Phillips, *J. Chromatogr. Sci.*, 29 (1991) 227.
5 D. Rosenthal, *Anal. Chem.*, 54 (1982) 63.
6 L. J. Nagels, W. L. Creten and P. M. Vanpeperstraete, *Anal. Chem.*, 55 (1983) 216.
7 J. M. Davis and J. C. Giddings, *Anal. Chem.*, 55 (1983) 418.
8 M. Martin, D. P. Herman and G. Guiochon, *Anal. Chem.*, 58 (1986) 2200.
9 A. Felinger, L. Pasti and F. Dondi, *Anal. Chem.*, 62 (1990) 1846.
10 J. C. Giddings, J. M. Davis and M. R. Schure, in S. Ahuja (Editor), *Ultrahigh Resolution Chromatography (ACS Symposium Series,* No. 250) American Chemical Society, Washington, DC, 1984, p. 9.
11 J. M. Davis and J. C. Giddings, *J. Chromatogr.*, 289 (1984) 277.
12 D. P. Herman, M. F. Gonnard and G. Guiochon, *Anal. Chem.*, 56 (1984) 995.
13 J. M. Davis and J. C. Giddings, *Anal. Chem.*, 57 (1985) 2168.
14 J. M. Davis and J. C. Giddings, *Anal. Chem.*, 57 (1985) 2178.
15 M. Martin and G. Guiochon, *Anal. Chem.*, 57 (1985) 289.
16 F. Dondi, Y. D. Kahie, G. Lodi, M. Remelli, P. Reschiglian and C. Bighi, *Anal. Chim. Acta*, 191 (1986) 261.
17 W. L. Creten and L. J. Nagels, *Anal. Chem.*, 59 (1987) 822.
18 S. Coppi, A. Betti and F. Dondi, *Anal. Chim. Acta*, 212 (1988) 165.
19 J. M. Davis, *J. Chromatogr.*, 449 (1988) 41.
20 S. L. Delinger and J. M. Davis, *Anal. Chem.*, 62 (1990) 436.
21 M. R. Schure, *J. Chromatogr.*, 550 (1991) 51.
22 F. J. Oros and J. M. Davis, *J. Chromatogr.*, 550 (1991) 135.
23 M. Martin, presented at the *18th International Symposium on Chromatography, Amsterdam, September 23–28, 1990.*
24 S. A. Roach, *The Theory of Random Clumping*, Methuen, London, 1968.
25 R. B. Bourdillon, O. M. Lidwell and J. E. Lovelock, *Studies in Air Hygiene (Medical Research Council Special Report Series,* No. 262), H.M. Stationery Office, London, 1948.
26 J. O. Irwin, P. Armitage and C. N. Davies, *Nature (London)*, 61 (1949) 809.
27 P. Armitage, *Biometrika*, 36 (1949) 257.
28 H. C. Tuckwell, *Elementary Applications of Probability Theory,* Chapman & Hall, London, 1988.
29 C. Mack, *Proc. Cambridge Philos. Soc.*, 50 (1954) 581.
30 C. Mack, *Proc. Cambridge Philos. Soc.*, 52 (1956) 246.
31 L. Nyhoff and S. Leestma, *FORTRAN 77 for Engineers and Scientists*, Macmillan, New York, 1985.
32 J. M. Davis, *Ph.D. Thesis*, University of Utah, Salt Lake City, UT, 1985.

Journal of Chromatography, 591 (1992) 19–29
Elsevier Science Publishers B.V., Amsterdam

CHROM. 23 763

Improved algorithm for resolution of overlapped asymmetric chromatographic peaks

Dae Young Youn, Sun Jin Yun and Kyung-Hoon Jung*

Centre for Molecular Science and Department of Chemistry, Korea Advanced Institute of Science and Technology, P.O. Box 150 Chongyangni, Seoul 130-650 (South Korea)

(First received May 14th, 1991; revised manuscript received September 23rd, 1991)

ABSTRACT

A simple and improved procedure to resolve an overlapped asymmetric chromatogram into its component peaks is proposed. The overlapped asymmetric peak profile was assumed to be a convolution of its component peaks, which were characterized by an exponentially modified Gaussian, and further simplified by the use of its derivative chromatogram. A new technique is suggested for initial guessing of peak parameters. The simulation study showed that peak parameters were able to be recovered within 5% deviations when the reduced resolution (*RR*), the ratio of the resolution to the critical resolution, was larger than 1.0 and were sufficient for recovery process. For RR values from 1.0 to 0.6, however, the recovery was not so efficient with the initial guessed values alone and was achieved with a non-linear least-squares routine within 3% deviations in most instances utilizing these values as initial guesses of iterations. The lower limit of *RR* for this technique was found to be 0.6. The validity of this algorithm for recovered parameters was confirmed by comparison with experimental observations and its recovery ability was found to show no more than a 1.6% deviation from true values and a 2.2% standard deviation throughout the study.

INTRODUCTION

There is growing interest in the deconvolution of an overlapped peak into its components for quantitative analysis of chromatograms. For this purpose, numerical treatments of chromatograms are commonly used in conjunction with optimization of the experimental conditions. These include geometrical methods, principal component analysis and least-squares methods.

Geometrical methods [1–4] such as perpendicular drop at the valley, tangent skimming and triangulation have been the most widely used in commercial integration systems. These methods suffer, however, from relatively low resolution and often give progressively lower resolutions for peaks with a high degree of overlapping or tailing [4]. Considerable improvement has been obtained by using more sophisticated numerical resolution techniques such as principal component and factor analysis [5] in multi-channel detector systems, *e.g.*, gas chromatography–mass spectrometry, gas chromatography–Fourier transform IR spectrometry and high-performance liquid chromatography–UV spectrophotometry. In spite of considerable improvements, these techniques are impractical for single-dimension detector systems. Least-squares methods, *i.e.*, non-linear [6–10] and linear methods [11], on the other hand, assume a fitting function to describe a real chromatogram in terms of peak shape parameters, *i.e.*, area, retention time, broadness and skewness. The iterative method, then, attempts to improve upon an initial set of peak-shape parameters by direct minimization in error space. Therefore, the success of these methods is strongly dependent on the model function, how well it represents real chromatograms, and the method for initial parameterization.

An ideal individual chromatographic peak may well be characterized by a Gaussian function provided that there are no instrumental distortions. In practice, however, the output profile has been better described by a skewed Gaussian form [12] owing to the non-equilibrium mass transfer [13], non-unifor-

0021-9673/92/$05.00

mity of solute–stationary phase interactions [14], dead volume [15], non-homogeneity of tube connection [16] and time lag of the detector response [17–19]. Some modelling techniques to describe these asymmetric distortions have been reported by many workers, including bi-Gaussian [20,21], Poisson [20,21], Gram–Charlier [22] and the exponentially modified Gaussian peak model (EMG) [4,9,20–26]. The EMG model has been found to represent a real chromatogram reasonably well through extensive tests both experimentally and theoretically in the authors' laboratory [9,26].

In this paper we present an improved method to describe an overlapped asymmetric peak profile as a convolution of its component peaks, described by the EMG model, and simplified further by use of its derivative as an extension of our previous work on the characterization of peak parameters of a skewed Gaussian chromatogram [26]. We also propose a simplified and rapid technique to extract initial peak parameters for practical implementation on a microcomputer.

COMPUTATION

Fitting function

The EMG for a single peak can be expressed as the convolution of a normal Gaussian with an exponential decay function:

$$h(t) = \frac{A}{\tau\sigma\,(2\,\pi)^{1/2}} \cdot \int_0^\infty \exp\left[-\frac{(t - t_G - t')^2}{2\,\sigma^2}\right] \exp\left(-\frac{t'}{\tau}\right) dt' \quad (1)$$

where A, σ, t_G and τ represent the peak area, the standard deviation of a Gaussian component, the retention time of the Gaussian component and the time constant of the exponential modifier, respectively. Eqn. 1 is then resolved into a Gaussian and a tailing component by differentiating and applying Leibniz's theorem:

$$h(t) = g(t) - \tau h'(t) \quad (2)$$

and

$$g(t) = \frac{A}{\sigma\,(2\,\pi)^{1/2}} \exp\left[-\frac{(t - t_G)^2}{2\,\sigma^2}\right]$$

where $g(t)$ and $h'(t)$ are the Gaussian and the derivative peak heights, respectively.

An overlapped peak profile $H(t)$ of an n-co-eluted component system at a given time t can be expressed as a sum of component peaks, $h_i(t)$. Now, as A, σ, t_G and τ are different from component to component, these values also have to be included as variables in a multi-component system:

$$H(t) = \sum_{i=1}^{n} [h_i(t;A_i,t_{G_i},\sigma_i,\tau_i)] \quad (3)$$

where the subscript i denotes the ith component. Although eqn. 3 is a general function which accommodates an n-component overlapped system, the deconvolution procedure requires lengthy iterative calculations if it is used as a fitting function. This difficulty can be overcome in most real systems that we encounter by simplifying the equation further by assuming a constant τ value for all component peaks.

The tailing parameter for overlapped pairs, τ, may be expressed as a sum of the extra, τ_e, and the intrinsic, τ_{in}, column effects. The intrinsic column effect can then be broken down further into the non-equilibrium mass transfer, τ_m, and the non-uniform solute–stationary phase interaction terms, τ_{int}:

$$\tau = \tau_e + \tau_{in} = \tau_e + (\tau_m + \tau_{int}) \quad (4)$$

In eqn. 4, as the first term is due to the instrumental geometry and does not vary from component to component, it should be same for all overlapped component peaks for a given instrumental condition. The second term is caused by the non-uniform mass transfer in the linear velocity of mobile phase components. The term will be the same for all component peaks owing to equal peak broadening under given column conditions. On the other hand, as the third term is governed by the retention mechanism of solute–stationary phase interactions, the term may be studied for two different cases of elution patterns depending on either a linear chromatogram caused by physically and chemically similar pairs or a non-linear chromatogram due to the different components. As the first and second terms in eqn. 4 are dominant over the third term in a linear chromatogram, the total τ can be considered as a constant for the convolution. However, as the third term in the case of a non-linear chromatogram,

e.g., with mass overloading of a component [14], is predominant over the sum of the first and second terms, the total τ of overlapping pairs is no longer a constant.

Eqn. 3 for a linear chromatogram is then reduced further to eqn. 5 as a sum of a pure Gaussian and a product of a tailing parameter τ and derivative components of the overlapped peak:

$$H(t) = \sum_{i=1}^{n} [g_i(t;A_i,t_{G_i},\sigma_i)] - \tau H'(t) \quad (5)$$

where

$$H'(t) = \sum_{i=1}^{n} [h_i'(t;A_i,t_{G_i},\sigma_i)]$$

The derivative component, $H'(t)$, can be obtained by electronic [27] or numerical differentiation [28,29]. The distorted asymmetric overlapped peak can then be described by an n Gaussian and a tailing parameter and their parameters can easily be extracted utilizing a non-linear least-squares algorithm with fast convergence. In this study the Levenberg–Marguardt algorithm [30,31] was used for these purposes and the validity of the procedure was confirmed by checking against experimental observations.

Initial parameterization

If a reasonable estimate of the peak parameters of a component peak in the overlapped profile is attainable, the remaining portion can easily be obtained by subtracting the estimated peak contribution from the overall profile.

This procedure was performed in conjunction with our previously proposed chromatographic peak parameter characterization technique for estimation of the component peak [26]. In brief, EMG parameters for a single peak were extracted by use of four or five points of the normal and derivative peak heights by solving a cubic or quartic equation of τ. These require one to choose a starting component peak, either the early or later eluted component, and a time pocket, characterized by four or five equally spaced points depending on a cubic or quartic equation. For these purposes, we chose the later eluted component as a starting peak and its tailing portion for a time pocket[a] and then subtracted the parameters from the whole peak to obtain the parameters for the remaining portion. The peak parameters obtained by solving the equation were normally very sensitive to both noise and the position of the time pocket. The different five-point time average method [26], was used to reduce the noise effect and the partial root mean square error method (PRMSE), a root mean square error for each candidate of the time pocket, to obtain the best position of the time pocket. The initial parameterization procedure was sufficient to recover whole peak parameters when a valley was present. Whereas a valley could not be seen owing to a higher degree of overlapping, the recovered peak parameters showed larger errors and had to be refined with non-linear regression using these values as initial guesses for iteration.

Data acquisition

Simulation and data acquisition of experimental observations were performed using a PC. The computation procedures are illustrated stepwise in Fig. 1.

For the simulation study, the noise-added overlapped peak, $O(t)$, was obtained from a noise-free peak and by adding normal noise to each corresponding intensity point[b]. The normal noise was generated by multiplying 1.0% of the maximum peak height by a normal random number in the range -0.5 to $+0.5$, a possible worst value in a commercial gas chromatograph, using the subroutine GASDEV, Numerical Recipes [33]. The experimental chromatogram was obtained using a home-made GC and an HP 5880A equipped with flame ionization detectors.

---

[a] For deconvolution of an overlapped peak, the best accuracy and resolution are attainable by performing the procedure at the least overlapped portion of the peak. These portions of overlapped pairs are the head part of early-eluted and the tail part of later-eluted component peaks. As the peak shape parameters are heavily dependent on the tail part compared with the head part of an asymmetric peak, the late-eluted component peak was chosen as the starting component peak and the tail part of the peak as a time pocket to extract the peak shape parameters in this study (see also ref. 32).

[b] The noise added overlapped peak, $O(t_i)$, is given by

$$O(t_i) = H(t_i) + \mathrm{Max}[H(t)]/100NRN_i$$

(i = 1 to total data points), where $O(t_i)$ and $H(t_i)$ are ith noise added and noise-free intensity points, respectively, and NRN_i are the normal random numbers in the range $-0.5 \leqslant NRN_i \leqslant +0.5$.

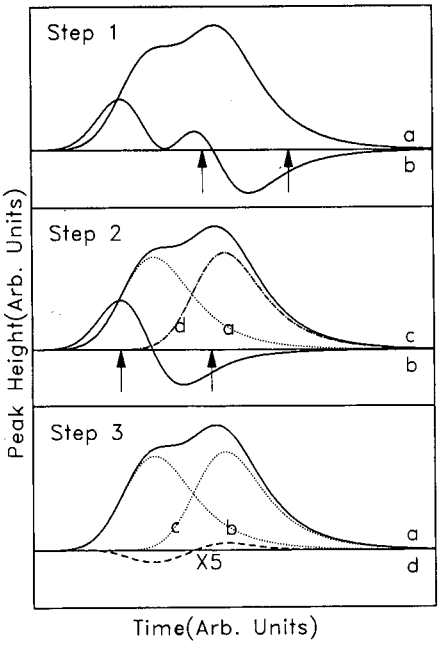

Fig. 1. Graphical representation of each step in the initial guessing routine. Step 1: the later-eluted peak parameters are extracted from the optimized time pocket of the tailing part of the overlapped peak. Solid lines represent the (a) normal and (b) derivative peaks. Arrows indicate the optimized time pocket for the later-eluted peak. Step 2: the early-eluted peak parameters are extracted from the remainder of Step 1, obtained by subtracting calculated peak contributions from the original peak. The subtracted normal, derivative, original and calculated later-eluted peaks are shown as dotted (a) and (b), solid (c), and dashed–dotted (d) lines, respectively. Arrows indicate the optimized time pocket of the early-eluted peak. Step 3: the non-linear least-squares routine is executed to meet the condition of NRMSE or DRMSE $> \varepsilon$. The original, calculated early-eluted, later-eluted peaks and the error curve are shown as solid (a), dotted (b) and (c) and dashed (d) lines, respectively.

The noise-added overlapped peak was then smoothed and differentiated numerically utilizing the Savitzky–Golay seven-point quadratic least-squares method [28,29]. The smoothed peak and the differential peak wera used as raw data for computation of starting points, maxima and end points of component peaks utilizing the Weimann algorithm [34]. The number of component peaks was then obtained by counting these sets. In order to extract later eluted component peak parameters, the range of the time pocket had to be established. This was done by choosing the maximum and its 20% height point in the tail part of an overlapped peak as initial starting and final time points, respectively. The initial starting point was then shifted 5 points stepwise toward the valley for each iteration until the minimum PRMSE was obtained. The later eluted peak parameters were then extracted in this optimized time pocket. The early-eluted peak parameters were obtained by subtracting these values from the overall peak and optimization process. The measure of the goodness of fit of the calculated peak to the original peak was tested utilizing the method of root mean square error of normal (NRMSE) and derivative peaks (DRMSE). If both calculations met an execution criterion, both NRMSE and DRMSE less than a value ε, our initial guessing routine was completed for peak deconvolution. The graphical representation of these procedures is illustrated in Fig. 1, steps 1–3, together with error curve, step 3. If the criteria were not met, the deconvolution was processed further utilizing a non-linear least-squares routine.

In all simulation procedures, statistical estimations such as mean values, confidence limit, reproducibility and relative percentage error of each parameter were calculated from twenty runs.

EXPERIMENTAL

Reagents

Nitrogen (99.95%) was used as the carrier gas after passing it through a molecular sieve. Ethylene (Matheson) and its deuterated isotope (Merck Sharp and Dohme of Canada) were used without further purification.

Column

A 30 m × 2 mm I.D. PTFE column packed with 228.6 mg of dicarbonylrhodium(I) 3-trifluoroacetyl-(1*R*)-camphorate (Johnson Matthey) in 9.0 g of squalane (Merck) coated on 52.9 g of Chromosorb P AW (30–60 mesh) was used to separate ethylene isotopes.

Apparatus

A Hewlett-Packard HP 5880A and a laboratory-made gas chromatograph equipped with flame ionization detectors were used. Samples were injected by use of a 1.0-ml internal loop gas sampling valve (Valco) and the pressure was monitored by use of a pressure transducer (Datametrics). The signal was

taken as an averaged point every 6 s (equivalent to 180 points average) for the HP 5880A and every 3 s (equivalent to 30 points average) for the laboratory-made gas chromatograph.

RESULTS AND DISCUSSION

Simulation studies

Computer simulation studies were carried out to demonstrate the applicability of the present technique to real chromatograms. The resolution of asymmetric chromatograms is governed by the number of component peaks, noise, peak shape, peak size and degree of overlap. The number of component peaks in this study was limited to two for simplicity and to avoid any confounding effects, as mutli-component systems with more than three components are simply extensions of two-component systems (see also the end of this section). For the noise effect, a 1.0% noise level (corresponding to a maximum signal-to-noise ratio = 100), a possible worst case in a commercial chromatogram, was chosen for the studies as the noise level is indirectly proportional to the degree of recovery of peak parameters [9,26]. The peak shape was measured by observing the τ/σ value for a single-peak chromatogram. For an overlapped chromatogram, the peak shapes were studied in two distinct cases separately, *i.e.*, with constant τ and with variable τ. With constant τ, there could be two different cases of peak shapes. If the σ values of two components were the same, the peak shapes of both components were represented in terms of τ/σ and, if not ($\sigma_1 \neq \sigma_2$), by τ and σ_1/σ_2. With variable τ, the peak shape was represented mainly by τ_1/τ_2 as the effect of τ predominated over the σ values. The peak size effect was expressed by the peak-area ratio, A_1/A_2, of two components. For the measure of overlap we introduced a variance-independent reduced resolution (RR) as its description by conventional resolution, as pointed out by previous workers [35,36], is inadequate for an asymmetric peak. The RR was defined by a given resolution (a function of retention times and peak shapes) divided by the critical resolution (a function of peak shapes only), the value at the complete disappearance point of the valley between two component peaks. In order to obtain RR, the critical resolution had to be calculated. This could be done by bringing two component peaks (with τ/σ and A_1/A_2 known) from infinite separation to the disappearance point of the valley. The collection of all possible values then formed a contour map on the τ/σ and A_1/A_2 surface, as shown in Fig. 2. Simulated chromatograms are displayed in Fig. 3 as functions of τ/σ, A_1/A_2 and RR, obtained from the map.

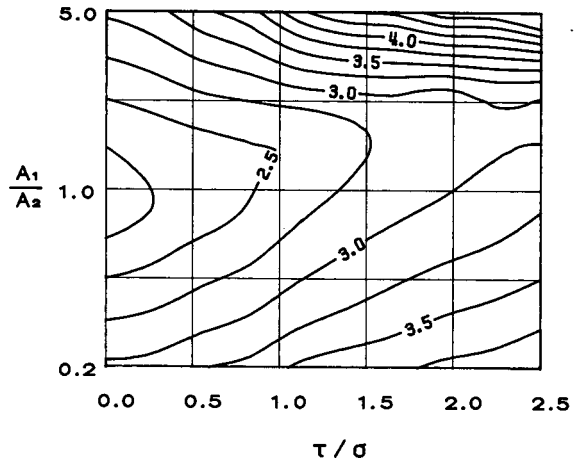

Fig. 2. Contour map of critical separation on the τ/σ and A_1/A_2 surface. Critical resolution = critical separation/total peak variance.

Case 1. Constant τ. The applicability of the technique was tested for various conditions and the results are listed in Tables I–III for constant ($\sigma_1 = \sigma_2$) and Table IV for different peak broadening parameters ($\sigma_1 \neq \sigma_2$). In Table I for a comparative study between initial guesses and non-linear regressions at $A_1 = A_2$ and Table II for intitial guessing routines as functions of RR, τ/σ and A_1/A_2, the relative percentage errors of extracted peak parameters from initial guesses showed decreasing tendencies from $RR = 0.6$, the complete merging point of two peaks, to $RR = 1.4$, from where conventional geometrical methods [1–4] could be applied with reasonable accuracies. In these regions the relative percentage errors were found to be $<2\%$ in most instances for RR from >1.0 to 1.4 applying an initial guessing routine alone, while the errors were increased drastically for $0.6 \leqslant RR \leqslant 1.0$ where the accuracies could only be improved up to $<2.2\%$ by applying a non-linear least-squares routine. The study was stopped at $RR = 0.6$, the complete merging point of two peaks, as its lower limit, as it is impractical below this point (see Fig. 3). Through-

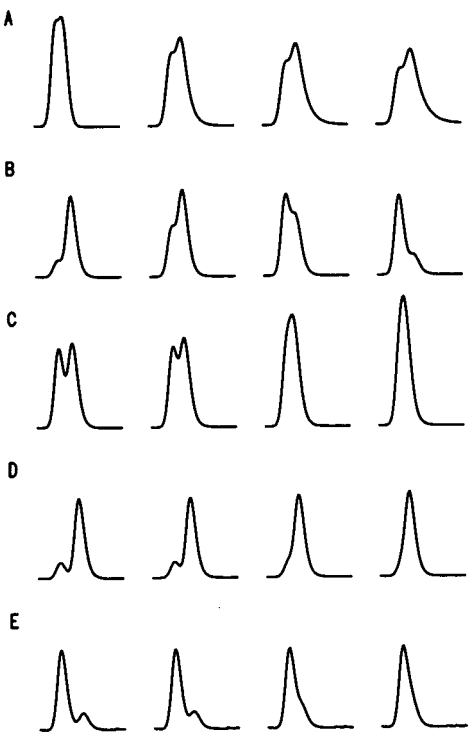

Fig. 3. Simulated chromatograms as a function of reduced resolution (RR), peak-area ratio (A_1/A_2) and asymmetry (τ/σ). (A) Chromatograms for τ/σ = 0.5, 1.5, 2.0 and 2.5 at fixed RR = 1.0 and A_1/A_2 = 1.0. (B) Chromatograms for A_1/A_2 = 0.2/1, 0.6/1, 1/0.6 and 1/0.2 at fixed RR = 1.0 and τ/σ = 1.0. (C) Chromatograms for RR = 1.4, 1.2, 0.8 and 0.6 at fixed A_1/A_2 = 1.0 and τ/σ = 1.0. (D) Same conditions as (C), except A_1/A_2 = 0.2/1. (E) Same conditions as (C), except A_1/A_2 = 1/0.2.

out the studies it was also found that RR was a major factor for the accuracies of peak recovery processes because of its prominent effect compared with those of A_1/A_2 and τ/σ. The present technique showed a general tendency for underestimation for early-eluted peaks and overestimation for later-eluted peaks. These effects indicated a positive contribution from the tail part of an early-eluted peak to the later-eluted peak parameters and, in turn, a negative contribution to the early-eluted peak, obtained by subtracting the later-eluted peak from the convoluted peak. Hence the greater the later-eluted peak area was, the better was the recovery of peak parameters because it suffered relatively less perturbation from the early-eluted peak. The recovery was also more effective in the case of larger τ/σ values for given RR and A_1/A_2. This may be attributed to the fact that the overlapped peak with relatively larger τ/σ value has a larger retention time difference (Δt_G) and hence the obtained peak parameters from the resulting Gaussian component show better precision. In Table III, the relative percentage errors and reproducibility of the extracted peak parameters by non-linear regression at constant peak shape ($\sigma_1 = \sigma_2$) are found to be <2% in most instances and the worst values are 5.94 and 4.29%, respectively. In Table IV, for the parameters with different peak broadenings ($\sigma_1 \neq \sigma_2$), the errors show very minor differences from the case of constant τ/σ even for large variations of σ_1/σ_2 as long as τ remains constant. From the foregoing discussion, it may be concluded that the tailing parameter τ plays a major role in the extraction of peak parameters.

Case 2. Variable τ. Comparative studies were performed using a full EMG with variable τ and a simplified EMG with constant τ, and the results are listed in Table V. The relative percentage errors of t_G and A obtained by eqn. 3 were <2% for all calculations, whereas with eqn. 5 they increased by an average of 2.5% for every 10% difference in τ values ($\Delta\tau = |\tau_1 - \tau_2|$). The average computing times for these procedures were also compared and were 9 s for initial guessing 2 min for non-linear regression at constant τ and 20 min for non-linear regression at variable τ with an IBM-XT personal computer. Therefore, one may conclude that the simplified EMG calculation is more practical than the full EMG calculation for constant τ and still useful even for variable τ at the expense of reproducibility up to 5% when the difference in two τ values is less than 10%.

Although the detailed consideration of the technique was limited to a two-component system, the technique was also tested on a four-component system to see the possibility of extending it to multi-component systems. Deconvolution was performed using the last peak as a starting component and the remainder was thereby obtained by subtracting the calculated peak from the overall peak. The same procedure was repeated using the remainder until the whole peak was deconvoluted and the resolved peaks are displayed in Fig. 4. The relative percentage errors and reproducibilities were found to be <2.1 and <1.1%, respectively.

TABLE I

RELATIVE PERCENTAGE ERRORS OF EXTRACTED PEAK PARAMETERS WITH THE INITIAL GUESSING AND WITH THE NON-LINEAR LEAST-SQUARES ROUTINES AT VARIOUS *RR*

Data were obtained at fixed $\tau/\sigma = 1.0$, $A_1/A_2 = 1.0$ and with added normal random noise of signal-to-noise ratio = 100 with respect to the maximum peak height.

RR	Peak[a]	Initial guessing				Non-linear least-squares			
		τ	σ	t_G	A	τ	σ	t_G	A
0.6	L	−5.52	1.75	−0.45	24.62	−2.10	2.15	0.07	0.92
	E	−62.48	−3.98	0.75	−32.45	–	−1.75	0.05	−1.04
0.8	L	−1.58	1.05	−0.16	9.25	−1.84	1.96	0.05	0.51
	E	−22.73	−2.43	0.20	−8.45	–	1.12	0.04	−0.84
1.0	L	−0.87	1.63	−0.08	3.27	−1.54	1.33	0.02	0.13
	E	−6.78	0.52	0.07	−3.49	–	1.15	0.01	−0.19
1.2	L	−0.52	0.65	−0.02	0.94				
	E	−2.45	0.46	0.05	−1.14				
1.4	L	−0.33	0.20	0.01	0.17				
	E	−1.05	0.10	0.14	−0.22				

[a] E and L denote the early- and the later-eluted peaks, respectively.

TABLE II

RELATIVE PERCENTAGE ERRORS OF EXTRACTED PEAK PARAMETERS WITH THE INITIAL GUESSING ROUTINE AT VARIOUS *RR*, τ/σ AND A_1/A_2

Data were taken from noise-added peaks. The noise was normal random noise of signal-to-noise ratio = 100 with respect to the maximum peak height.

RR	τ/σ	A_1/A_2	Later-eluted component				Early-eluted component			
			τ	σ	t_G	A	τ	σ	t_G	A
1.0	0.5	1/1	−7.35	2.63	0.27	6.57	−6.51	2.13	0.50	−4.25
	1.5	1/1	−0.36	1.95	−0.06	3.39	−1.33	−1.37	0.20	−3.96
	2.5	1/1	0.20	−0.56	−0.49	2.53	−0.06	−0.57	0.04	−2.33
1.2	0.5	1/1	−4.52	0.54	0.06	0.74	−3.09	0.36	−0.01	−0.96
	1.5	1/1	−0.31	0.45	−0.01	0.61	−1.82	0.35	0.03	−0.48
	2.5	1/1	0.62	−0.21	−0.01	0.45	0.14	−0.42	0.11	−0.18
1.0	1.0	0.2/1	−2.45	1.52	0.07	0.07	−8.45	1.62	0.04	−0.84
	1.0	0.6/1	−1.55	1.87	0.10	0.89	−3.23	2.03	0.15	−1.27
	1.0	1/0.6	−1.75	1.58	0.20	1.63	−2.75	1.38	0.15	−1.78
	1.0	1/0.2	−4.61	3.62	−0.33	5.09	−10.51	1.66	0.22	−2.23
1.2	1.0	0.2/1	−0.34	0.48	−0.00	0.05	−1.99	0.11	0.01	−0.23
	1.0	0.6/1	−0.13	0.11	−0.00	0.11	−1.31	0.13	0.02	−0.14
	1.0	1/0.6	−0.70	0.62	−0.01	1.02	−3.68	0.24	0.05	−1.08
	1.0	1/0.2	−1.35	1.46	−0.03	2.32	−6.53	0.91	0.08	−2.48

TABLE III

RELATIVE PERCENTAGE ERRORS AND REPRODUCIBILITIES OF EXTRACTED PEAK PARAMETERS WITH THE NON-LINEAR SQUARE ROUTINE AT VARIOUS RR, τ/σ AND A_1/A_2

Data were taken from noise-added peaks. The noise was normal random noise of signal-to-noise ratio = 100 with respect to the maximum peak height.

RR	τ/σ	A_1/A_2	Peak[a]	Relative error (%)				Reproducibility (%)			
				τ	σ	t_G	A	τ	σ	t_G	A
0.6	0.5	1/1	L	−5.94	1.82	0.21	1.09	4.21	0.92	0.24	1.42
			E	–	1.21	0.10	−0.95	–	1.32	0.13	1.59
0.6	1.5	1/1	L	−2.21	1.14	0.10	0.75	2.14	1.22	0.15	1.21
			E	–	0.48	0.14	−0.54	–	0.63	0.21	1.35
0.6	2.5	1/1	L	−3.29	1.54	−0.12	0.75	2.62	1.37	0.04	0.97
			E	–	−0.82	−0.17	−0.95	–	0.14	0.05	1.02
0.8	0.5	1/1	L	−2.07	0.52	0.08	0.63	1.49	0.31	0.00	0.16
			E	–	0.44	0.07	−0.72	–	0.46	0.00	0.10
0.8	1.5	1/1	L	−0.92	0.37	0.02	0.62	0.87	0.21	0.01	0.49
			E	–	0.51	0.02	−0.69	–	0.39	0.01	0.05
0.8	2.5	1/1	L	−1.44	0.21	−0.00	0.36	1.38	0.40	0.01	0.26
			E	–	0.21	−0.04	−0.55	–	0.15	0.01	0.31
0.6	1.0	0.2/1	L	−1.44	−2.63	1.82	−4.20	0.74	1.24	0.04	1.69
			E	–	1.16	0.42	2.33	–	0.10	0.25	1.51
0.6	1.0	0.6/1	L	−1.30	1.23	0.03	0.04	0.08	0.09	0.10	0.16
			E	–	1.14	0.02	−0.18	–	0.08	0.00	0.31
0.6	1.0	1/0.6	L	−1.54	1.38	0.04	0.05	0.23	0.25	0.01	0.37
			E	–	1.29	0.02	−0.18	–	0.80	0.00	0.19
0.6	1.0	1/0.2	L	−1.88	1.69	0.14	0.74	3.92	3.63	0.04	4.29
			E	–	2.18	0.04	−1.46	–	0.18	0.01	2.01
0.8	1.0	0.2/1	L	−0.17	−1.20	0.02	0.09	0.25	0.05	0.00	0.05
			E	–	1.27	0.14	−0.19	–	0.17	0.05	0.47
0.8	1.0	0.6/1	L	−1.27	1.18	0.04	−0.00	0.12	0.08	0.00	0.06
			E	–	1.15	0.04	−0.00	–	0.09	0.00	0.11
0.8	1.0	1/0.6	L	−1.52	1.31	0.04	0.11	0.31	0.22	0.00	0.23
			E	–	1.17	0.04	−0.10	–	0.08	0.00	0.15
0.8	1.0	1/0.2	L	−1.88	1.33	0.03	0.63	2.92	2.16	0.18	3.12
			E	–	1.19	0.42	−1.48	–	0.19	0.00	1.94

[a] E and L denote the early- and the later-eluted peaks, respectively.

Experimental verification

An experimental study was carried out to test the validity of the present algorithm using a PC-based data acquisition system. An isotopic mixture of [$^2H_2$]ethylene and [$^2H_3$]ethylene was chosen as a prototype of deconvolution problems among three typical cases such as isotopic mixture, enantiomer and isomer separations, utilizing the complexation gas chromatographic (GC) technique [37]. The reference values of peak parameters for individual components were obtained by injecting each sample into the GC system separately and utilizing our previous technique [26]. Premixed samples of known compositions of each component were then injected to test the algorithm. The GC conditions, such as carrier gas flow-rate and column temperature, were

TABLE IV

RELATIVE PERCENTAGE ERROR CHANGES OF t_G AND A AT CONSTANT τ/σ AND AT VARIOUS σ_1/σ_2

Data were obtained from noise-added peaks using the non-linear least-squares routine. The noise was normal random noise of signal-to-noise ratio = 100 with respect to the maximum peak height.

σ_1/σ_2	Later-eluted component		Early-eluted component	
	t_G	A	t_G	A
0.2/1	0.07	0.14	0.03	0.09
0.6/1	0.05	0.07	0.01	0.04
1/0.6	0.04	0.02	0.06	0.07
1/0.2	0.03	0.08	0.03	0.12

controlled to generate two different RR regions, *i.e.*, one with $RR > 1$ required the initial guessing routine only, and the other with $RR \leqslant 1$ required the non-linear regression. Averaged chromatograms from ten runs with the mixture samples under two different conditions and those of the two individual components are displayed in Fig. 5A for $RR > 1$ and Fig. 5B for $RR \leqslant 1$, as dotted lines together with the calculated values (open circles). The verified results of the present algorithm are presented in Table VI, with relative errors $<1.52\%$ under both conditions and standard deviations $<2.14\%$. The present technique demonstrates reasonable agreement between the computed peak profiles from the overlapped peaks of mixtures and the measured peak profiles obtained from individual injections.

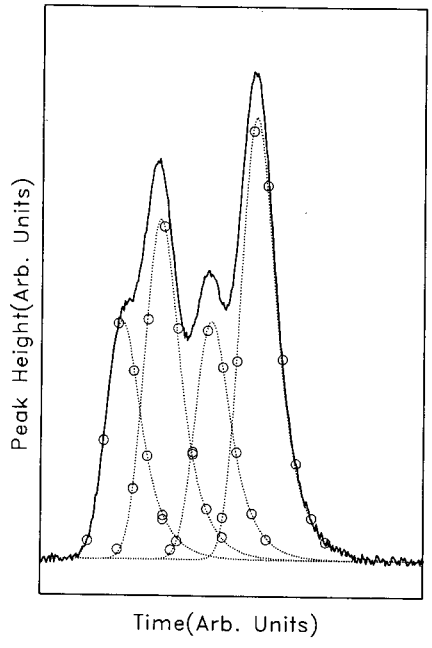

Fig. 4. Typical deconvolution from an overlapped four-component system. The overlapped chromatogram was synthesized from four sets of known peak parameters. The solid line, dotted lines and open circles are the overlapped peak, component peaks and deconvoluted component peaks utilizing this technique, respectively.

We also investigated the linearity of the peak area

TABLE V

RELATIVE PERCENTAGE ERRORS OF t_G AND A USING THE SIMPLIFIED EMG AND THE FULL EMG FUNCTIONS FOR VARIOUS τ_1/τ_2

Data were obtained from noise-added peaks using the non-linear least-squares routine. The noise was normal random noise of signal-to-noise ratio = 100 with respect to the maximum peak height.

τ_1/τ_2	Simplified EMG				Full EMG			
	Later-eluted component		Early-eluted component		Later-eluted component		Early-eluted component	
	t_G	A	t_G	A	t_G	A	t_G	A
0.8/1	−0.30	5.08	0.29	−5.13	0.05	0.84	0.04	−0.91
0.9/1	0.00	2.61	0.16	−2.65	0.07	0.72	0.02	−0.73
1/1	0.04	0.06	0.04	−0.10	0.03	0.12	0.05	−0.19
1/0.9	0.08	−2.59	−0.07	2.48	0.06	0.59	0.03	−0.72
1/0.8	0.12	−5.23	−0.16	5.10	0.04	1.21	0.07	−1.32

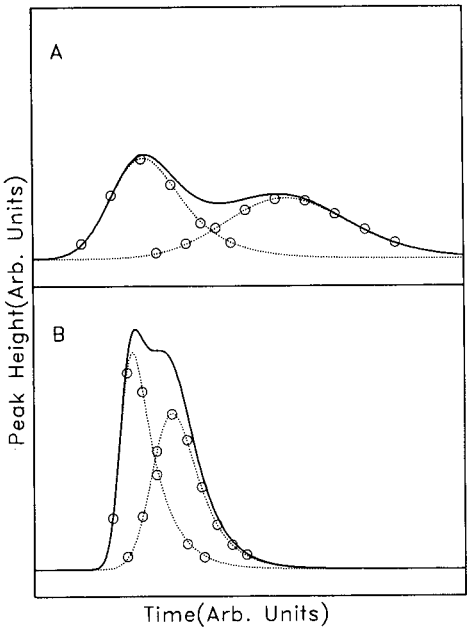

Fig. 5. Comparison between the observed and the deconvoluted chromatograms calculated from overlapped peaks for two distinct cases, *i.e.*, (A) for $RR > 1$ and (B) for $RR \leq 1$. (A) For $RR > 1$: the dotted lines are obtained by injecting two individual samples separately and the solid line by injecting the mixture of two components with GC conditions of carrier gas flow-rate 17 ml/min, oven temperature 20°C and samples [$^2H_2$]ethylene and [$^2H_3$]ethylene. The open circles represent the resolved peak points from the chromatogram of the mixture by the present algorithm. (B) For $RR \leq 1$: the lines and the open circles are same in (A) except for the GC conditions: carrier gas flow-rate 25 ml/min, oven temperature 60°C and samples [$^2H_2$]ethylene and [$^2H_3$]ethylene.

TABLE VII

RECOVERED PEAK AREAS USING THE PROPOSED TECHNIQUE

Sample used (Torr)		Recovered peak area[a]	
[$^2H_2$]	[$^2H_3$]	[$^2H_2$]	[$^2H_3$]
0.201	0.401	1.00	2.03
0.398	0.197	1.94	1.01
0.604	0.605	2.96	3.09

[a] The chromatographic peak areas recovered by the proposed method are represented as reduced peak areas with respect to [$^2H_2$]ethylene.

to test the applicability of this method in quantitative analysis, and the results are presented in Table VII. The observed area of the later-eluted peak of an equimolar mixture of two components was always greater than that of the early-eluted peak, and these results were also consistent with those of our simulation studies. The correction factors of the computed values against the initially known amounts of samples were found to be 0.982 for [$^2H_2$]ethylene and 1.006 for [$^2H_3$]ethylene. These findings also indicate that the present technique is suitable for the quantitative analysis of overlapped components.

TABLE VI

RELATIVE PERCENTAGE ERRORS AND STANDARD DEVIATIONS OF EXTRACTED PEAK PARAMETERS FROM EXPERIMENTAL CHROMATOGRAMS

Conditions[a]	Peak[b]	Relative error (%)[c]				Standard deviation (%)			
		τ	σ	t_G	A	τ	σ	t_G	A
A	L	−0.27	0.47	−0.01	0.38	1.32	1.07	0.03	0.51
	E	−1.13	0.20	0.03	−0.43	2.14	1.45	0.07	0.74
B	L	−0.10	0.13	−0.00	0.01	1.84	1.42	0.07	0.98
	E	−0.07	−0.04	0.00	−0.00	—	1.64	0.25	1.24

[a] Conditions A: the acquired conditions are $RR = 1.27$, $\tau_1/\tau_2 = 0.97$, $\sigma_1/\sigma_2 = 0.36$ and $A_1/A_2 = 1.00$. Peak parameterization requires the initial guessing routine only (see also Fig. 5A). Conditions B: the acquired conditions are $RR = 0.94$, $\tau_1/\tau_2 = 0.96$, $\sigma_1/\sigma_2 = 0.40$ and $A_1/A_2 = 1.00$. Peak parameterization requires the non-linear least-squares method using simplified EMG (see also Fig. 5B).

[b] E and L denote the early-eluted ([$^2H_2$]ethylene) and the later-eluted component ([$^2H_3$]ethylene), respectively.

[c] Relative percentage error of peak parameters, P, is defined by

$$P = \frac{(P_{sep} - P_{mix})}{P_{sep}} \cdot 100$$

where P_{sep} and P_{mix} are the peak parameters of a single peak obtained by the method of ref. 26 and those of the convoluted peak, respectively.

ACKNOWLEDGEMENTS

This work was done with financial assistance from the Korea Standards Research Institute and the Korea Science and Engineering Foundation, which is gratefully acknowledged.

REFERENCES

1 J. D. Hettinger, J. R. Hubbard, J. M. Gill and L. A. Miller, *J. Chromatogr. Sci.*, 9 (1971) 710.
2 H. A. Hancock, Jr., L. A. Dahm and J. F. Muldoon, *J. Chromatogr. Sci.*, 8 (1970) 57.
3 A. W. Westerberg, *Anal. Chem.*, 41 (1969) 1770.
4 A. N. Papas and T. P. Tougas, *Anal. Chem.*, 62 (1990) 234.
5 R. F. Lacey, *Anal. Chem.*, 58 (1986) 1404.
6 A. H. Andreson, T. C. Gibb and A. B. Littlewood, *J. Chromatogr. Sci.*, 8 (1970) 640.
7 R. A. Vaidya and R. D. Hester, *J. Chromatogr.*, 287 (1984) 231.
8 M. Rosenbaum, V. Hancil and R. Komers, *J. Chromatogr.*, 191 (1980) 157.
9 K.-H. Jung and Y. H. Shin, *Bull. Korean Chem. Soc.*, 7 (1986) 403.
10 C. F. Lam, A. Forst and H. Bank, *Appl. Spectrosc.*, 33 (1979) 273.
11 R. A. Caruana, R. B. Searle, T. Heller and S. I. Shupack, *Anal. Chem.*, 58 (1986) 1162; R. A. Caruana, R. B. Searle and S. I. Shupack, *Anal. Chem.*, 60 (1988) 1896.
12 A. S. Said, *Theory and Mathematics of Chromatography*, Hüthig, Heidelberg, Basle, New York, 1981, p. 69.
13 K. Yamaoka and T. Nakagawa, *Anal. Chem.*, 47 (1975) 2050.
14 A. Jaulmes and C. Vidal-Madjar, *Anal. Chem.*, 63 (1991) 1165.
15 V. Maynard and E. Grushka, *Anal. Chem.*, 44 (1972) 1427.
16 A. B. Littlewood, *Gas Chromatography*, Academic Press, New York, 2nd ed., 1970, p. 169.
17 I. G. McWilliam and H. C. Bolton, *Anal. Chem.*, 41 (1969) 1755.
18 I. G. McWilliam and H. C. Bolton, *Anal. Chem.*, 41 (1969) 1762.
19 I. G. McWilliam and H. C. Bolton, *Anal. Chem.*, 43 (1971) 883.
20 T. S. Buys and K. de Clark, *Anal. Chem.*, 44 (1972) 1273.
21 E. Grushka, M. N. Myers and J. C. Giddings, *Anal. Chem.*, 42 (1970) 21.
22 O. Grubner, *Anal. Chem.*, 43 (1971) 1934.
23 R. E. Pauls and L. B. Rogers, *Anal. Chem.*, 49 (1977) 625.
24 J. P. Foley, *Anal. Chem.*, 59 (1987) 1984.
25 J. P. Foley and J. G. Dorsey, *J. Chromatogr. Sci.*, 22 (1984) 40.
26 K.-H. Jung, S. J. Yun and S. H. Kang, *Anal. Chem.*, 56 (1984) 457.
27 R. Kolvoda, *Operation Amplifiers in Chemical Instrumentation*, Wiley, New York, 1975, p. 49.
28 P. A. Gorry, *Anal. Chem.*, 62 (1990) 570.
29 A. Savitzky and M. J. E. Golay, *Anal. Chem.*, 36 (1964) 1672.
30 D. W. Maquardt, *J. Soc. Ind. Appl. Math.*, 11 (1963) 431.
31 W. H. Press, B. P. Flannery, S. A. Teukolsky and W. T. Vetterling, *Numerical Recipes*, Cambridge University Press, Cambridge, 1986, p. 523.
32 S. J. Yun, *Ph. D. Thesis*, Korea Advanced Institute of Science and Technology, Seoul, 1987.
33 W. H. Press, B. P. Flannery, S. A. Teukolsky and W. T. Vetterling, *Numerical Recipes*, Cambridge University Press, Cambridge, 1986, p. 202.
34 B. Weimann, *Chromatographia*, 7 (1974) 472.
35 J. J. Kirkland, W. W. Yau, H. J. Stoklosa and C. H. Diks, Jr., *J. Chromatogr. Sci.*, 15 (1977) 303.
36 J. P. Foley, *J. Chromatogr.*, 384 (1987) 301.
37 V. Schurig, *Chromatographia*, 13 (1980) 263.

Journal of Chromatography, 591 (1992) 31–45
Elsevier Science Publishers B.V., Amsterdam

CHROM. 23 792

Optimization of the experimental conditions and the column design parameters in overloaded elution chromatography

Attila Felinger☆ and Georges Guiochon*

**Department of Chemistry, University of Tennessee, Knoxville, TN 37996-1501, and Division of Analytical Chemistry, Oak Ridge National Laboratory, Oak Ridge, TN 37831-6120 (USA)*

(First received July 16th, 1991; revised manuscript received October 7th, 1991)

ABSTRACT

A theoretical study of the optimization of the separation of a binary mixture in overloaded elution chromatography was performed. The elution band profiles were calculated using the semi-ideal model of chromatography and assuming competitive Langmuir isotherms. In a first step, the experimental (operating) conditions (*i.e.*, the reduced velocity of the mobile phase and the loading factor) were optimized using a simplex algorithm. In a second step, the column design parameters (*i.e.*, the column length and the average particle diameter) and the operating conditions were optimized for the maximum production rate of either the more or the less retained component. The optimum value of the capacity factor of the first component, was also determined. Binary mixtures having relative retentions between 1.1 and 1.8 and relative concentrations of 1:3 and 3:1 were studied. The maximum production rates were obtained for very low values of the capacity factor of the first component, of the order of 0.3–0.5, depending slightly on the relative retention.

INTRODUCTION

There is currently considerable interest in the preparative applications of liquid chromatography, especially in the pharmaceutical and the fine chemicals industries. However, there are great uncertainties regarding the procedures to be followed for optimizing the column design and operating conditions for a new separation. Although it has been shown that an overlapping band separation can provide a 5–10-fold increase in production rate, some persist in aiming for a touching band separation. Even the definition of the goal of an optimization procedure remains controversial. For an industrial-scale separation, the optimum conditions should correspond to the lowest cost possible. For laboratory separations, time spent in preparing the products needed tends to dominate the costs and the maximum production rate becomes more desirable. However, finding rapidly sub-optimum conditions may permit considerable savings in time, and hence in cost. In an academic environment, it is difficult to price properly the various components of the cost of a separation. Hence, the optimization of the experimental conditions for the maximum possible production rate, with some constraints of product purity, recovery yield and inlet pressure, becomes the simplest goal. We adopted it in this work.

The achievement of a high production rate in preparative liquid chromatography means that the column has to be operated with a high feed load, and hence under non-linear conditions. The individual elution bands are asymmetric and overlap to some extent. Therefore, the composition and the size of the feed sample injected have a strong influence on the chromatograms obtained. Although the theory

☆ On leave from the Department of Analytical Chemistry, University of Veszprém, H-8201 Veszprém, Hungary.

0021-9673/92/$05.00

of non-linear chromatography has developed considerably in recent years [1,2], the system of mass balance equations for a binary mixture has no closed-form solution for the semi-ideal model, the best suited to account for the behavior of modern high-performance liquid chromatographic (HPLC) columns [1]. The optimum conditions must be determined using the numerical solutions of this model. There are two approaches to this problem, one theoretical and the other numerical.

Golshan-Shirazi and Guiochon [3–6] used the analytical solution of the ideal model of chromatography which can be derived for a binary mixture [7]. From this solution, they calculated analytical expressions for the optimum experimental conditions (optimum sample size, column length and particle size, cutting times) for the recovery yield and the production rate [3]. The ideal model assumes infinite column efficiency. Actual columns have a finite efficiency, a function of the mobile phase velocity. By using an approximate solution of the semi-ideal model of chromatography, expressions were also derived for the optimum conditions taking into account the finite column efficiency [4]. These results were later elaborated and applied to the study of several practical problems of optimization [8,9].

The other approach is purely computational. It involves combining the numerical solution of the system of mass balance equations with a maximum search method. Because it is entirely based on numerical solutions, it makes it very difficult to give general rules for the optimum experimental conditions in non-linear chromatography. The non-linear simplex method, a simple but, in most instances, efficient algorithm was used by Ghodbane and Guiochon [10] and by Katti *et al.* [11]. The simulations showed that the maximum production rate is achieved at a much higher value of the mobile phase reduced velocity than its efficiency optimum value, and the necessary resolution between components is usually lower than unity. The optimum values of the experimental parameters are very different, depending on whether one wishes to purify the more or the less retained component. If the relative amount of the second-eluting component is large enough, self-displacement may occur, which increases the production of the first component [12,13].

In previous work, the simultaneous optimization of more than two parameters was not performed. Accordingly, these studies were focused on the optimization of the operating conditions using a given column. Much was learned regarding the influence of the mobile phase velocity, the sample size, the column length and the relative retention. The influence of other parameters, especially the retention factor of one of the components of the mixture, was neglected. This paper reports a more general approach, using a simplex procedure permitting the simultaneous optimization of the column length, particle size, mobile phase flow velocity and feed amount.

THEORY

The individual elution profiles of the components of binary mixtures were calculated using an equilibrium-diffusive model of chromatography [2]. The calculations of these profiles are carried out by numerical integration of the system of mass balance equations of chromatography for the two components, using a finite difference method [2,14]. Constant equilibrium between the mobile and stationary phases is assumed, as in the ideal (equilibrium) model, and the competitive Langmuir isotherm model is used. The smoothing effect of the axial dispersion and the mass transfer resistance on the band profiles is accounted for by adjusting properly the numerical dispersion [14,15]. Then, given a purity requirement for both components, a simple integration routine permits the determination of the cutting times for the two fractions, the amounts produced, the recovery yields and the production rate [11].

Column characteristics

For all the calculations of optimum conditions, we assumed the characteristics of the chromatographic system to be as follows: the column porosity was 0.80, the viscosity of the mobile phase was 1 cP, and the diffusion coefficient of each compound in the mobile phase was $D_m = 1 \cdot 10^{-5}$ cm^2/s, the column inside diameter was $d = 4.6$ mm, the maximum inlet pressure allowed was assumed to be 125 atm, which was chosen as a compromise between the current performance of laboratory and industrial equipment used in preparative chromatography, and the sample was injected as a rectangular plug.

The column efficiency was calculated using the Knox equation [16]:

$$h = 2/v + v^{1/3} + v/10 \quad (1)$$

where $h = H/d_p$ is the reduced plate height, H is the actual height equivalent to a theoretical plate, $v = ud_p/D_m$ is the reduced mobile phase velocity and u is the actual mobile phase velocity.

In the first part of the work, we optimized the operating parameters of a given column for the chosen separation. The column dimensions were chosen arbitrarily as follows: column length $L = 25$ cm and average particle diameter $d_p = 20$ μm. The experimental conditions (the loading factor and the reduced velocity of the mobile phase) were optimized. In the second part, the column design parameters (the column length and the average particle diameter) were also optimized.

Equilibrium isotherms

We assumed that the isotherms of the two compounds are given by the competitive Langmuir isotherm model [17]:

$$q_i = a_iC_i/(1 + b_1C_1 + b_2C_2) \quad i = 1, 2 \quad (2)$$

where q_i and C_i are the concentrations of the component i at equilibrium in the stationary and the mobile phase, respectively. All concentrations are in mg/ml. a_i and b_i are numerical coefficients. The choice of the Langmuir model is a simplification. This model is valid only if the column saturation capacities for the two components, *i.e.*, the ratios of their coefficients a_i/b_i, are the same [18], otherwise major deviations from this model may be observed. When the column saturation capacities of the components of a binary mixture are different, the Levan–Vermeulen model [18] is much more satisfactory [19]. In keeping with the theoretical rigor of the model, we selected values of the isotherm coefficient giving the same value of the column saturation capacity for the two components.

The numerical values chosen for the isotherm coefficients were $a_1 = k'_1/0.25$, $a_2 = \alpha k'_1/0.25$, $b_1 = k'_1/325$ ml/mg and $b_2 = \alpha k'_1/325$ ml/mg. With this choice of coefficients, $q_1 = q_2 = 1300$ mg/ml. k'_1 is the retention factor, or column capacity factor, of the first component at infinite dilution and α is their separation factor.

Definitions

The production rate was defined as the amount of the purified component produced per unit cross-sectional area of the column per unit time (mg/cm^2 · s). The cycle time, *i.e.*, the time between two consecutive injections, was defined as $\Delta t_c = t_{c,2} - t_{c,1}$, where $t_{c,1}$ is the time when the concentration of the first component reaches $1 \cdot 10^{-6}$ mg/ml and $t_{c,2}$ is the time when the concentration of the second component drops below $1 \cdot 10^{-6}$ mg/ml. Although arbitrary, especially as far as the concentration thresholds are chosen, this definition has some merit over the alternative, $\Delta t = t_{R,2o} - t_o = k'_2t_o$, where $t_{R2,o}$ is the limiting retention time of the second component at infinite dilution and t_o is the column hold-up time [3–6,8,9].

Calculation procedures

The modified simplex algorithm described by Dose [20] was used. The calculations of the optimum values of the parameters assumed a desired purity of both components of 99%. Two constraints were applied, a maximum inlet pressure, which determines the maximum allowed reduced velocity, and a minimum required recovery yield. The standard deviations of the coordinates of the simplex vertices were used as convergence criteria. The convergence was reached when the standard deviation for all parameters to be optimized dropped below 0.1%.

The optimum experimental conditions of the separation were calculated for both the less and the more retained components. As we see, they are often very different. Two mixture compositions (relative concentrations 1:3 and 3:1) were chosen and four values of the separation factor (α = 1.1, 1.2, 1.5 and 1.8) were studied.

RESULTS AND DISCUSSION

In Fig. 1 we compare typical results obtained in the calculation of an optimum loading factor. As can be seen, if the cycle time is defined as the corrected retention time of the second component [4], the production rate of the second component (dotted line) rises very fast at first, then increases slowly, but indefinitely with increasing loading factor. The production rate has no well defined maximum, and this result is not practical for the purpose of optimi-

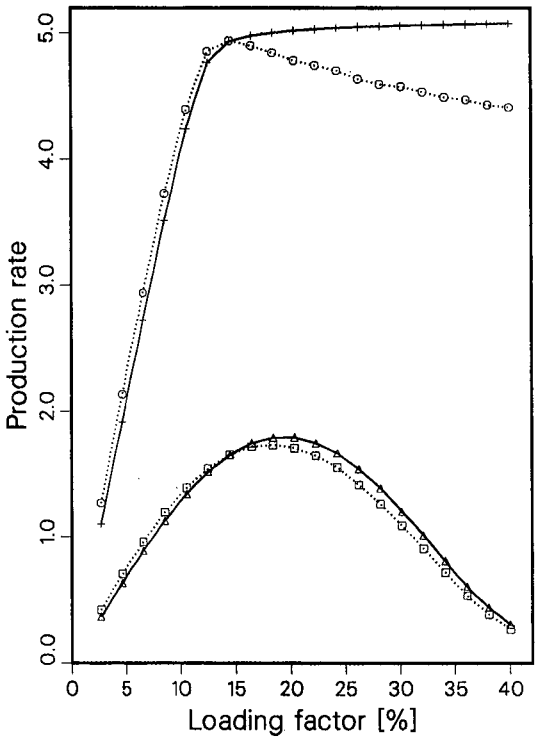

Fig. 1. Effect of the definition of the cycle time on the production rate of the two components of a binary mixture. Solid lines: production rate of (△) the first and (+) the second component if the cycle time is $\Delta t_c = t_{R2,0} - t_0$. Dotted lines: production rate of (□) the first and (○) the second component if the cycle time is $\Delta t_c = t_{c,2} - t_{c,1}$. In both instances, the mixture composition is 1:3, $\alpha = 1.5$, $k'_1 = 6$, $v = 300$. The reduced velocity of the mobile phase and the loading factor have been optimized.

zation by numerical calculations. More importantly, it leads to misleading conclusions for the practical applications of the results. There would be no point in injecting large sample amounts if most of the throughput has to be cut off and recycled or, still worse, wasted.

On the contrary, with the definition of the cycle time used in this work, the higher the loading factor the longer is the cycle time. Hence the production rate of the second component (Fig. 1, dotted line) decreases after reaching a maximum. Below this maximum, the two curves are almost identical. For the first component, both the location of the optimum and the maximum production rate differ slightly, but the two plots of the loading factor *versus* the production rate are essentially identical.

Optimization of experimental conditions for a given column

In this first part of the work a two-parameter optimization was performed to determine the operating conditions giving the maximum production rate for 99% purity. The loading factor and the reduced velocity of the mobile phase were optimized simultaneously, the other parameters remaining unchanged.

Influence of retention factor. The optimization procedure for L_f and v was repeated for several values of k'_1 between 0.5 and 6. The values of the retention factor giving the maximum production rate were determined for the two components for several values of the retention factor and of the mixture composition. The numerical results, including the optimum values of the parameters and the maximum production rate, are listed in Table I.

The maximum production rate is plotted *versus* the retention factor, k'_1, in Figs. 2 and 3 for mixtures with relative concentrations of 1:3 and 3:1 and a relative retention $\alpha = 1.2$. The production rate increases very rapidly at first with increasing retention factor. An optimum is reached for k'_1 in the range 1.5–1.9, depending on the relative concentration and on whether the production rate of the first or of the second component is being maximized. The optimum capacity factor is slightly smaller if the component at the higher concentration is being purified.

This result is in agreement with previous results derived on a purely theoretical basis [5,6]. Optimum values of the order of unity for the retention factor had been expected.

Influence of recovery yield constraint. The maximum production rate was determined without yield constraint and with 60% and 90% yield constraints. The recovery yield is poor at the optimum value of the retention factor; it is only 27–48% for a separation factor $\alpha = 1.2$. When setting a 60% constraint on the recovery yield, the loss of production rate is only *ca.* 3–17%, whereas the yield actually doubles. The decrease in production rate is much more significant (38–62%) when a constraint of 90% is set on the recovery yield. To increase the recovery yield as required, both the reduced velocity and the loading factor must be lowered significantly. As a consequence, the optimum value of the retention factor, k'_1, is shifted towards higher values

TABLE I

OPTIMUM VALUES OF THE EXPERIMENTAL OPERATING CONDITIONS FOR A GIVEN COLUMN

L = 25 cm; d_p = 20 μm

α	C_1/C_2	Component No.	k'_1	Production rate (mg/cm^2 · s)	Recovery yield (%)	v	L_f (%)
1.2	3:1	1	1.5	2.371	37.0	124	6.84
1.2	3:1	1	1.6	1.970	60.0	102	4.14
1.2	3:1	1	2.3	0.909	90.0	62	2.21
1.2	3:1	2	1.7	0.278	27.5	89	4.08
1.2	3:1	2	2.0	0.241	60.0	69	2.17
1.2	3:1	2	2.7	0.137	90.0	45	1.35
1.2	1:3	1	1.8	0.413	48.7	55	6.11
1.2	1:3	1	1.9	0.401	60.0	52	4.79
1.2	1:3	1	2.4	0.252	90.0	39	2.90
1.2	1:3	2	1.5	1.725	26.3	171	5.53
1.2	1:3	2	1.7	1.547	60.0	121	2.79
1.2	1:3	2	1.9	1.064	90.0	64	2.15
1.5	3:1	1	0.9	18.354	59.0	400	12.48
1.5	3:1	1	0.9	18.338	60.0	368	12.45
1.5	3:1	1	1.3	12.233	90.0	179	10.53
1.5	3:1	2	1.2	3.534	49.5	294	12.76
1.5	3:1	2	1.3	3.392	60.0	235	12.40
1.5	3:1	2	1.4	2.329	90.0	163	6.60
1.5	1:3	1	1.2	3.513	62.7	195	13.76
1.5	1:3	1	1.7	2.608	90.0	152	11.28
1.5	1:3	2	1.0	15.536	53.8	400	13.65
1.5	1:3	2	1.0	14.991	60.0	400	10.55
1.5	1:3	2	1.3	11.034	90.0	247	8.56
1.8	3:1	1	0.7	42.596	61.7	400	36.56
1.8	3:1	2	1.0	8.736	62.4	400	27.75
1.8	1:3	1	1.0	8.295	66.2	400	20.34
1.8	1:3	2	0.7	30.132	61.6	400	23.73

(up to 2.65 if we want to recover the more retained component at 99% purity from a 3:1 mixture, with a 90% recovery yield at α = 1.2).

The production rate of the first component is always higher than that of the second if account is taken of the difference in relative concentration. This was found to be true not only for the 1:3 mixture but in all instances when the concentration of the more retained component is higher than that of the less retained component. This can be explained by the effect of self-displacement [13], which is significant only if the loading factor of the second component is higher than that of the less retained component. The optimum loading factor for maximum production rate is always higher for the purification of the first component. On the other hand, the optimum reduced velocity is higher if one optimizes the purification of the component of higher relative concentration, whether it is the more or the less retained component.

Influence of relative retention or separation factor. The same calculations were repeated for binary mixtures at a relative retention α = 1.5. The dependence of the maximum production rate on the retention factor in this instance is shown in Fig. 4 (3:1 mixture) and 5 (1:3 mixture). We observe that the optimum value of the retention factor is markedly shifted towards smaller values (0.9–1.2, instead

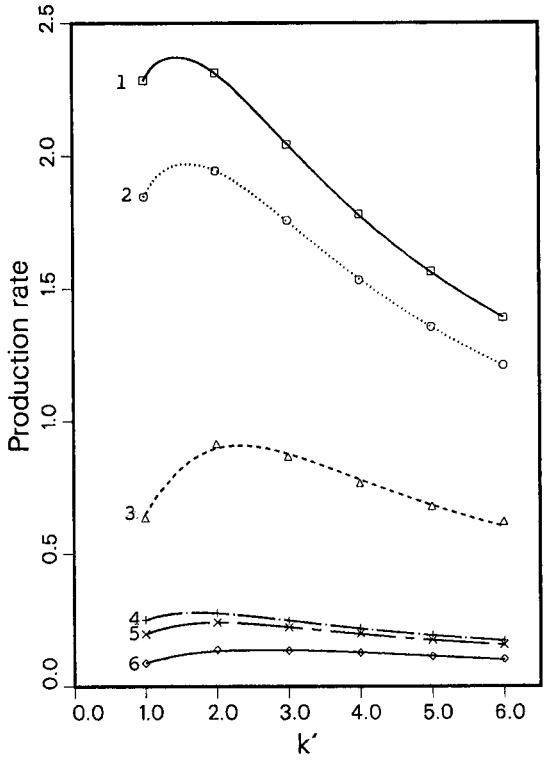

Fig. 2. Plots of the maximum production rates of either component *versus* the retention factor of the less retained component and influence of a yield constraint. Feed composition, 3:1; separation factor, $\alpha = 1.2$. 1, First component without yield constraint; 2, first component, 60% recovery yield; 3, first component, 90% recovery yield; 4, second component without yield constraint; 5, second component, 60% recovery yield; 6, second component, 90% recovery yield.

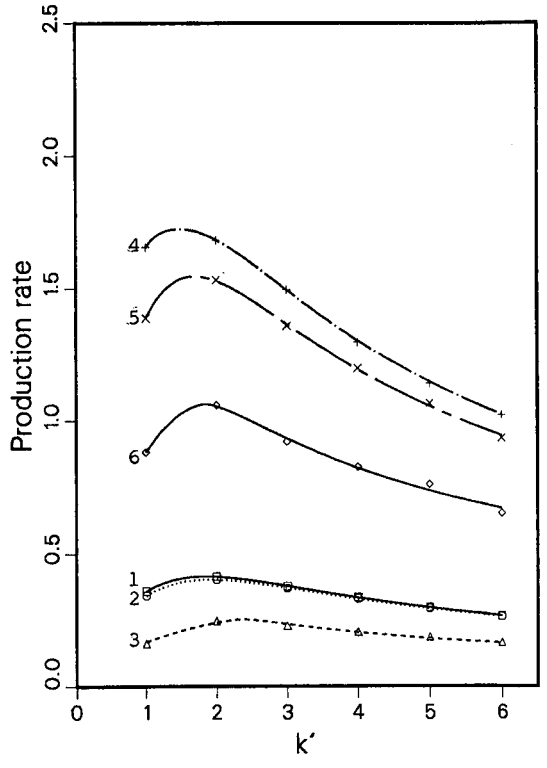

Fig. 3. Same as Fig. 2, except feed composition 1:3.

of 1.5–1.9) and that the recovery yield is much better at the optimum retention factor than for $\alpha = 1.2$. The yield exceeds 60% at the maximum production rate of the first component from a 1:3 mixture. When the retention factor is higher than 2, the recovery yield under the optimum conditions is always better than 60%. The larger separation factor allows the use of a 3–4 times higher reduced velocity and of a 2–4 times higher loading factor. The combination of these changes results in an 8–12 times higher production rate than with $\alpha = 1.2$. This increase is intermediate between a dependence on $(1 - \alpha)^2$ and on $(1 - \alpha)^3$, as was predicted by theory [3–7]. In some instances, the optimum reduced velocity is below the maximum ($\nu = 400$) allowed by the maximum inlet pressure constraint ($p = 125$ bar).

Calculations were also performed with a very high relative retention, $\alpha = 1.8$. In this instance, the optimum capacity factor is shifted towards still lower values, 0.7–1.0 (Fig. 6). The recovery yield under optimum experimental conditions always exceeds 60%. However, the gain in production rate is only about 2.3-fold, compared with the production rate obtained for $\alpha = 1.5$. This gain is not as significant as when the separation factor was raised from 1.2 to 1.5. It corresponds barely to a dependence on $(1 - \alpha)^2$. One of the reasons for this is the pressure constraint. The optimum reduced velocity increases with increasing retention factor. When the retention factor increases from 1.2 to 1.5, the optimum reduced velocity increases to near the upper limit corresponding to the pressure constraint of 125 atm ($\nu = 400$). When the separation factor is increased to 1.8, the reduced velocity cannot be raised. The loading factor only can be increased, by about 20–

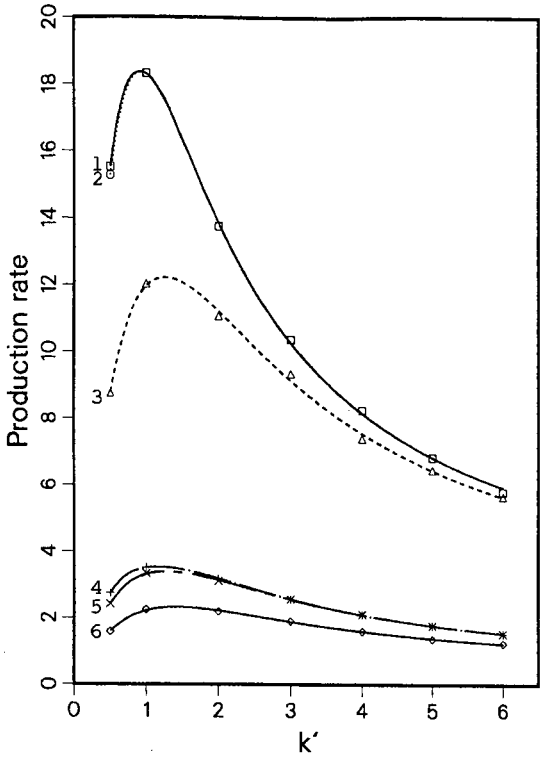

Fig. 4. Same as Fig. 2, except $\alpha = 1.5$.

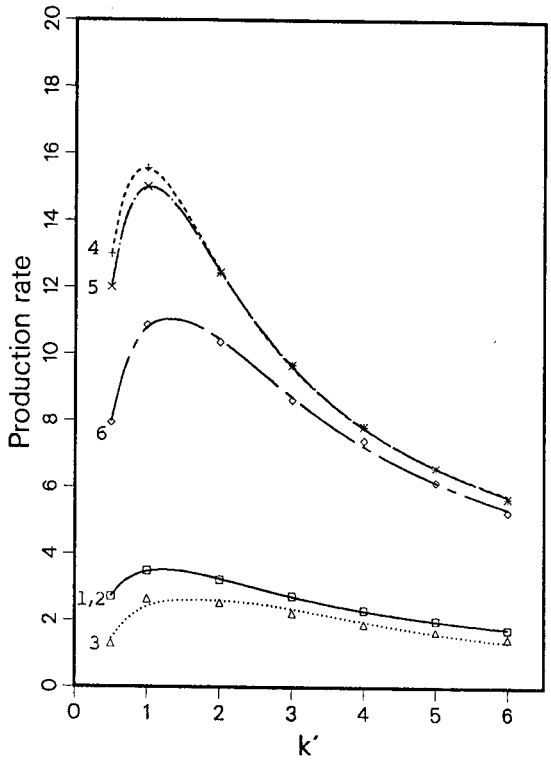

Fig. 5. Same as Fig. 4, except feed composition 1:3.

36%, to raise the production rate, as the cycle time cannot decrease.

The use of a higher inlet pressure would permit significant improvements in the production rate of components that are easy to separate, as we do not need a high efficiency and we are using a given column, of constant length.

Simultaneous optimization of column design parameters and operating conditions

In the second part of the work, the column characteristics (column length and average particle diameter) and the operating conditions (reduced velocity of the mobile phase and column loading factor) were optimized simultaneously. The same values were used for the relative composition of the mixture (1:3 and 3:1) and for the separation factor ($\alpha = 1.1$, 1.2, 1.5 and 1.8). The optimum conditions were determined without any yield constraint, however.

Optimum value of the ratio d_p^2/L[a]. A detailed investigation of the solution of the ideal model of chromatography [7] shows that, for infinitely efficient columns, there is no separate optimum value of either the column length or the particle diameter, but that there is an optimum for the ratio d_p^2/L [3]. The reason for this phenomenon is that short columns packed with small particles have a short cycle time but accept small sample sizes, whereas longer columns packed with coarser particles may accommodate larger amounts of feed but have a longer cycle time. It was shown that, with certain assumptions, this result can be reasonably extended to col-

[a] The values of d_p^2/L should be given in length units. As d_p is conveniently expressed in μm and L in cm, the natural unit (or rather the most convenient) is 1 $\mu m^2/cm$ = 1 Å. This is the unit used for the ratio d_p^2/L throughout this paper. Such a small unit should not impress; d_p^2/L has no physical reality, it is merely a convenient parameter.

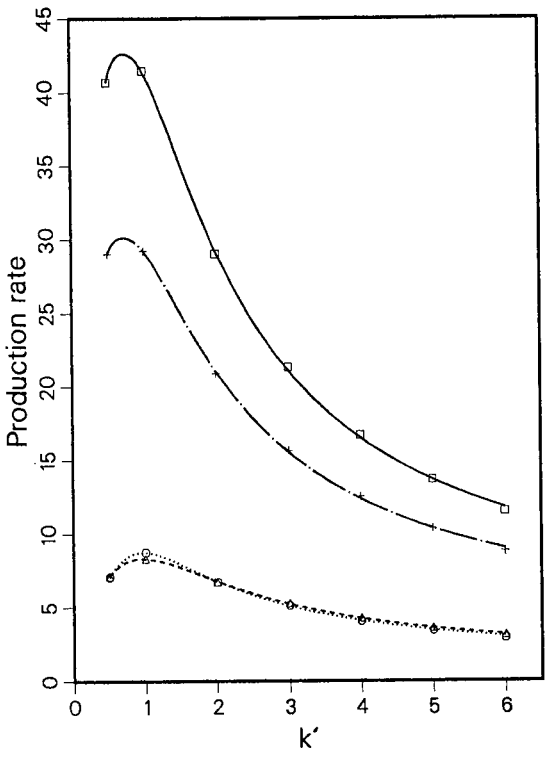

Fig. 6. Plot of the maximum production rate of the two components of a mixture *versus* the retention factor of the first component. (□) First and (○) second components of a 3:1 mixture; (△) first and (+) second components of a 1:3 mixture. Relative retention, $\alpha = 1.8$.

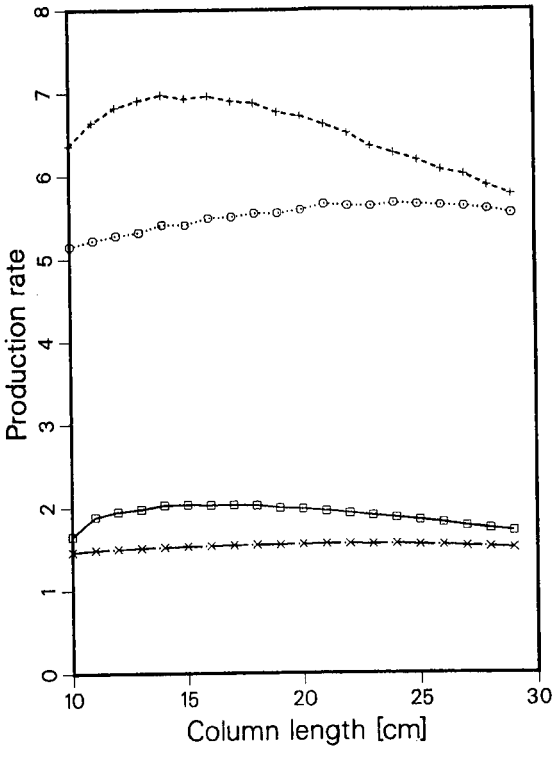

Fig. 7. Plot of the maximum production rate *versus* the column length. The particle diameter is optimized for the maximum production rate for each column length. (+) First and (×) second components in a 3:1 mixture; (□) first and (○) second components in a 1:3 mixture. $\alpha = 1.5$.

umns of finite efficiency (semi-ideal model) [4]. To investigate the range of validity of this rule, numerical optimization was carried out to investigate the degree and range of validity of this conclusion by calculating the exact optimum conditions for various combinations of these two parameters.

Calculations were performed for 3:1 and 1:3 binary mixtures with $\alpha = 1.5$ and $k'_1 = 6$. The optimum particle size was searched for with values of the column length set successively between 10 and 30 cm. In Fig. 7, we see that the maximum production rate varies only very slightly. It is almost constant for the production of the second component from 3:1 mixture and has a very weak optimum around $L = 15$ cm for the production of the first component. In Figs. 8 and 9, we show contour plots of the production rate as a function of the column length (ordinate) and the particle size (abscissa) for the first (Fig. 8) and the second (Fig. 9) component of a 3:1 mixture.

By comparing these two figures and Fig. 10, which shows the lines along which d_p^2/L is constant in an L *versus* d_p graph, we observe that the contour plots of the production rate of the second component (Fig. 9) and the lines along which d_p^2/L is constant (Fig. 10) are parallel. Hence the production rate of the second component is nearly constant along these curves. Only a very slight maximum is found at $L = 21.2$ cm and $d_p = 17.4$ μm ($d_p^2/L = 14.3$). For the first component, the contours of constant production rate and constant d_p^2/L are not exactly parallel. They intersect each other, but with a very shallow angle. There are separate optimum values of the column length and the particle size. However, at a constant value of d_p^2/L, the column length optimum is very flat, at $L = 15$ cm and $d_p = 16.2$ μm ($d_p^2/L = 17.5$).

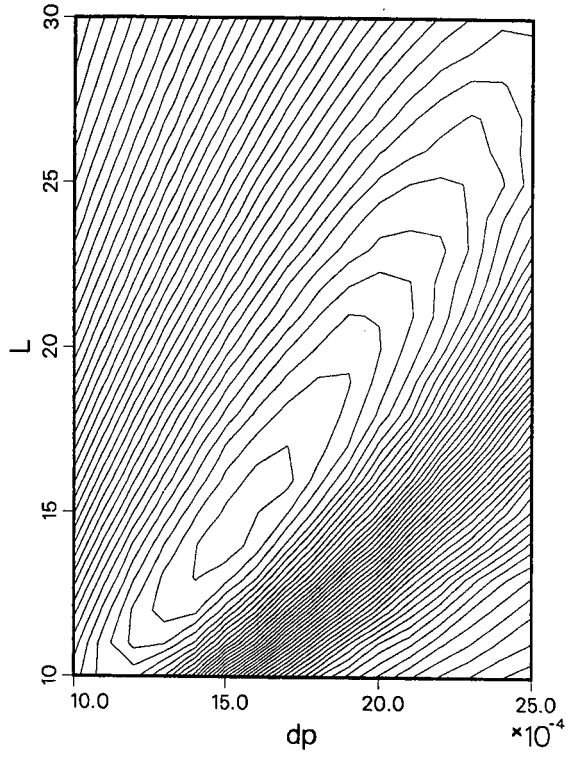

Fig. 8. Contour plots of the production rate of the first component as a function of the column length (L) and the average particle diameter (d_p). Mixture composition, 3:1; $\alpha = 1.5$; $k'_1 = 6$.

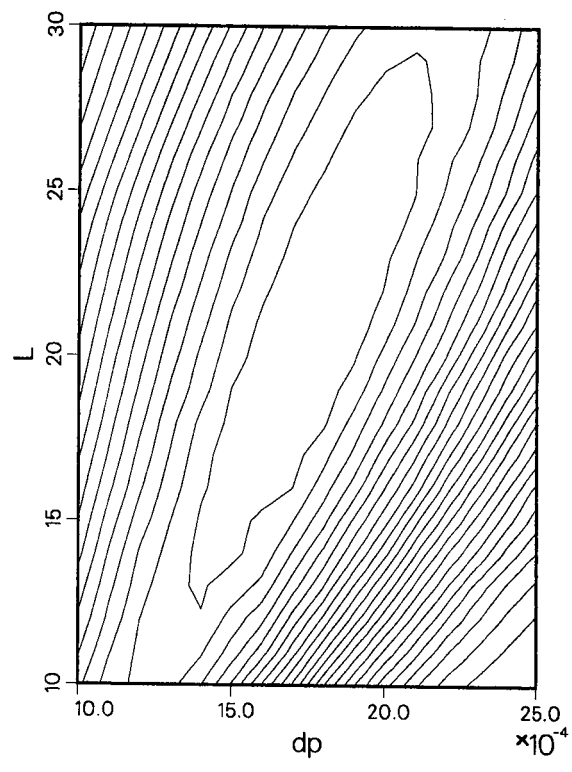

Fig. 9. Same as Fig. 8, but for the second component.

As the expressions derived for the optimum parameters using the approximate soluton of the semi-ideal model [4] are correct only for high values of the reduced velocity, it can be expected that for smaller values of the separation factor and the retention factor, where the optimum reduced velocity is also smaller, the maximum is better defined. In consequence, when one tries to optimize the column design parameters, both the column length and the particle diameter should be optimized separately.

Optimization of retention factor. Compared with the value obtained for a given column, the optimum retention factor is much smaller when the column design parameters are also optimized (see Figs. 11–14 and Table II). The optimum value of k'_1 was found to be between 0.3 and 0.5 in all the cases investigated. Only a very slight dependence on the separation factor can be observed. The optimum value of the retention factor is found in the range $k'_1 = 0.4$–0.5 for $\alpha = 1.1$ (Fig. 11) and in the range $k'_1 = 0.3$–0.4 for $\alpha = 1.8$ (Fig. 14).

Figs. 15 and 16 show chromatograms corresponding to the maximum possible production rate for values of the retention factor around the optimum value. The production rates of the less and the more retained component were optimized in Figs. 15 and 16, respectively, for a binary mixture having a relative concentration of 1:3; the separation factor is $\alpha = 1.5$. These chromatograms show that the band width increases rapidly with increasing retention factor, as the optimum column efficiency decreases as the retention factor increases. Consequently, the concentration of the purified components collected decreases with increasing retention factor.

For a separation factor $\alpha = 1.2$, the maximum production rate under the optimum conditions (including the optimum retention factor) is 3.5–6 times higher than it was for the 25-cm column packed

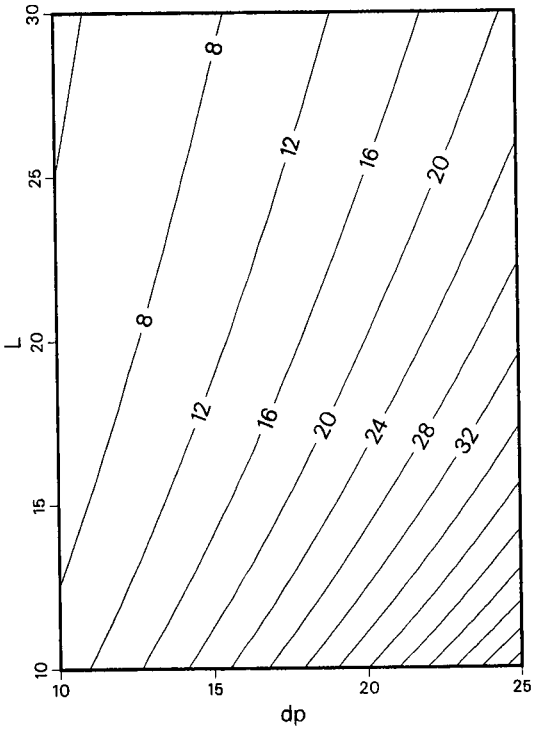

Fig. 10. Contour plots of constant d_p^2/L (μm^2/cm) as a function of L and d_p.

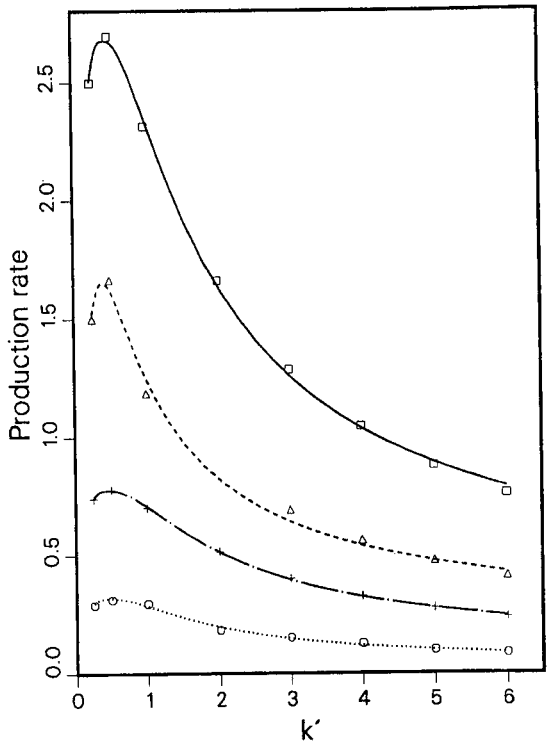

Fig. 11. Plots of the maximum production rates of either component *versus* the retention factor of the less retained component. (□) First and (○) second components of a 3:1 mixture; (△) first and (+) second components of a 1:3 mixture. Separation factor, α = 1.1. The mobile phase reduced velocity, the loading factor, the column length and the particle diameter have been optimized.

with 20-μm particles operated under its optimum conditions. The production rate gain is only 1.5–2.3 times at α = 1.5 and 1.3–1.6 times for α = 1.8 (compare Tables I and II).

Dependence of maximum production rate on retention factor. It is not always possible to optimize the retention factor to such low values as required for k'_1. Other considerations may require the separation to be performed at high values of k'_1. The gain in production rate that we can achieve by optimizing the column characteristics at a constant value of the retention factor is smaller when we want a high retention factor. For a constant value of the retention factor of 6, this gain is 50–150% for a α = 1.2, 1–20% for α = 1.5 and 0–5% for α = 1.8. This means that the 25-cm column packed with 20-μm particles considered in the first part of this work is almost optimum for the separation of a mixture of relative retention α = 1.8 and a retention factor k'_1 = 6. We note that the value of the ratio d_p^2/L is 16 for the above column, whereas the optimum ratio for such a mixture (k'_1 = 6, α = 1.8) was found to be between 14 and 22, depending on the composition of the mixture.

The dependence of the optimum value of d_p^2/L on the first component retention factor in a 1:3 mixture is illustrated in Fig. 17 for the four values of the separation factor considered. The plots are almost linear, and the slope of the lines increases with increasing separation factor. The optimum value of the ratio also depends on the sample composition and on whether we want to purify the less or the more retained component of the mixture, but to a much smaller extent. The optimum ratio is usually smaller when we need to optimize the separation for the less concentrated component of the mixture than for the more concentrated component.

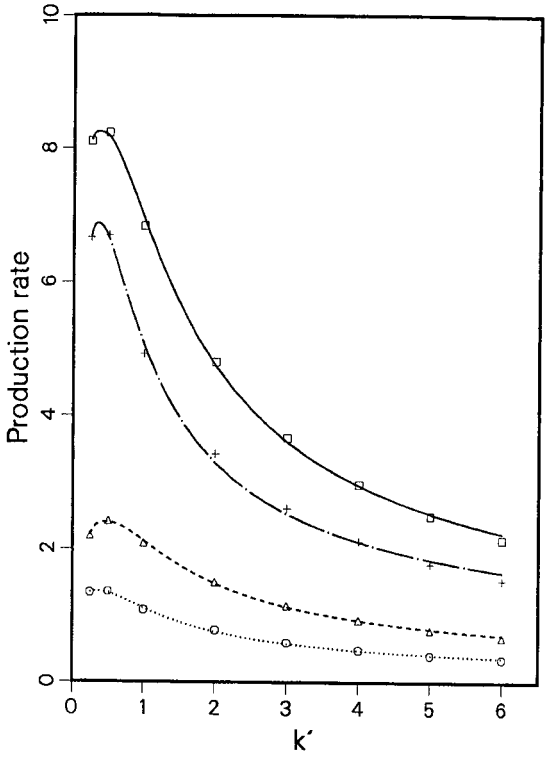

Fig. 12. Same as Fig. 11, except $\alpha = 1.2$.

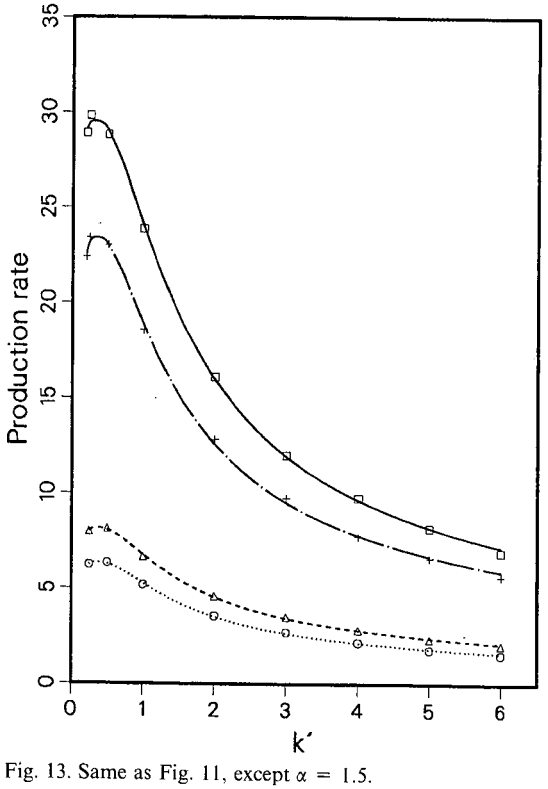

Fig. 13. Same as Fig. 11, except $\alpha = 1.5$.

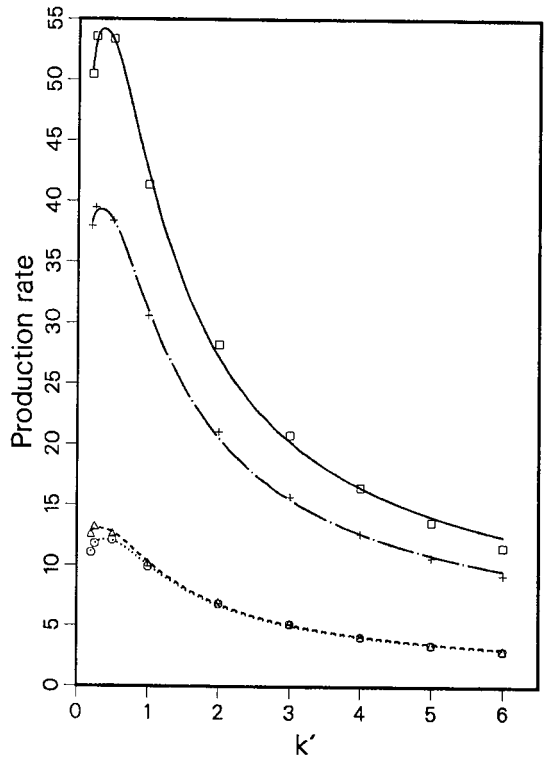

Fig. 14. Same as Fig. 11, except $\alpha = 1.8$.

Optimum column design. As we have shown earlier, there are an optimum column length and an optimum particle size (Table II), although significant variations around these optimum values do not cause a large decrease in production rate provided that d_p^2/L is kept constant. We see in Table II that the separation factor has a strong influence on the optimum column length. This length also depends on whether we need to purify the less or the more retained component. For the purification of the more retained component, the optimum column is much longer than that for the purification of the less retained component.

We see in Table II that the separation factor has a strong influence on the optimum column efficiency. This results from the influence of the separation factor on both the optimum column length and the optimum flow velocity, but also from the low value of the optimum retention factor. This latter relationship is illustrated in Fig. 18. If the column is operated at $k'_1 = 0.25$, we need a column that is nearly ten times more efficient than the optimum

TABLE II

OPTIMUM VALUES OF THE PARAMETERS OF OPERATING CONDITIONS AND COLUMN DESIGN

α	C_1/C_2	Component No.	k'_1	Production rate (mg/cm^2 · s)	Yield (%)	v	L_f (%)	L (cm)	d_p (μm)	d_p^2/L (μm^2/cm)	N
1.1	3:1	1	0.5	2.675	42.3	28	3.72	93.4	12.9	1.78	12 453
1.1	3:1	2	0.5	0.318	67.6	27	0.67	189.3	14.8	1.17	18 700
1.1	1:3	1	0.5	0.775	57.6	17	2.88	120.0	12.0	1.19	22 755
1.1	1:3	2	0.4	1.653	49.5	32	0.86	227.0	18.1	1.44	19 791
1.2	3:1	1	0.4	8.248	53.4	36	7.84	50.5	11.5	2.62	6310
1.2	3:1	2	0.4	1.362	58.4	39	3.42	114.8	15.6	2.13	9998
1.2	1:3	1	0.5	2.399	64.5	25	6.75	51.5	10.7	2.24	8710
1.2	1:3	2	0.4	6.881	54.4	69	4.36	142.0	20.4	2.93	6310
1.5	3:1	1	0.3	29.506	59.4	60	21.67	17.4	9.6	5.32	1820
1.5	3:1	2	0.4	6.345	72.5	66	12.40	29.5	12.1	4.93	2291
1.5	1:3	1	0.4	8.133	74.6	40	17.27	19.9	8.8	3.92	3020
1.5	1:3	2	0.3	23.404	81.4	70	11.45	26.4	11.3	4.86	2082
1.8	3:1	1	0.4	54.154	70.3	88	34.34	11.9	9.6	7.75	933
1.8	3:1	2	0.4	12.112	77.7	85	21.92	15.6	10.2	6.73	1175
1.8	1:3	1	0.3	13.033	74.6	60	25.00	13.9	8.8	5.57	1589
1.8	1:3	2	0.3	39.312	80.3	76	19.61	17.4	10.8	6.72	1202

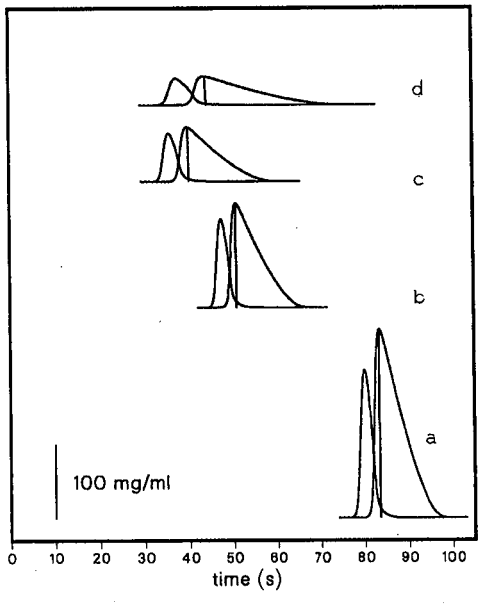

Fig. 15. Optimum chromatograms corresponding to the maximum production rate of the less retained component in a mixture of relative concentration 1:3; the separation factor is α = 1.5. Retention factor, k'_1: (a) = 0.25; (b) = 0.5; (c) = 1.0; (d) = 2.0.

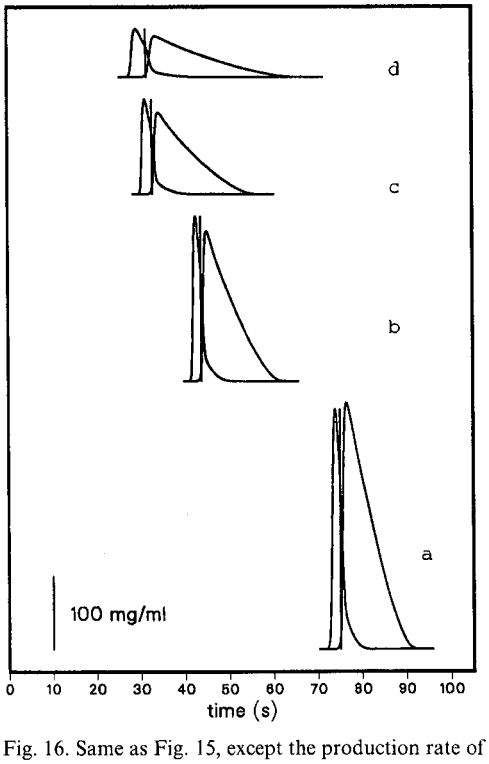

Fig. 16. Same as Fig. 15, except the production rate of the more retained component is optimized.

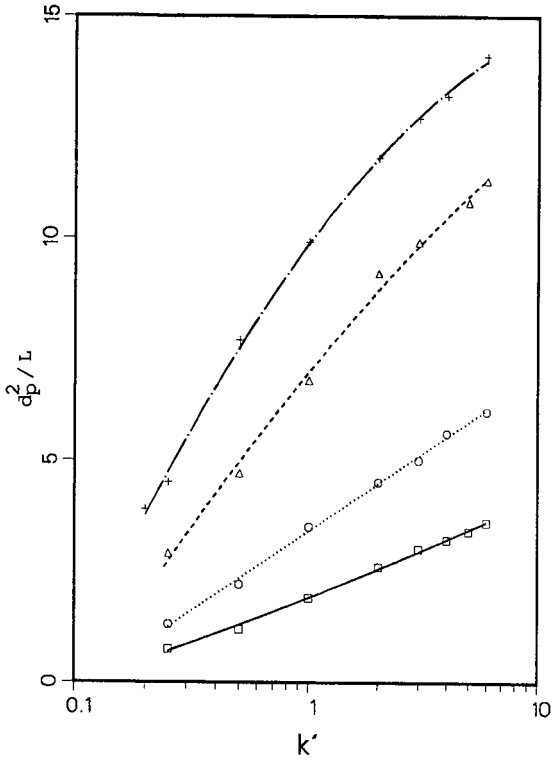

Fig. 17. Plot of the optimum value of the ratio d_p^2/L *versus* the retention factor of the less retained component of a 1:3 mixture. Separation factors: □ = 1.1; ○ = 1.2; △ = 1.5; + = 1.8.

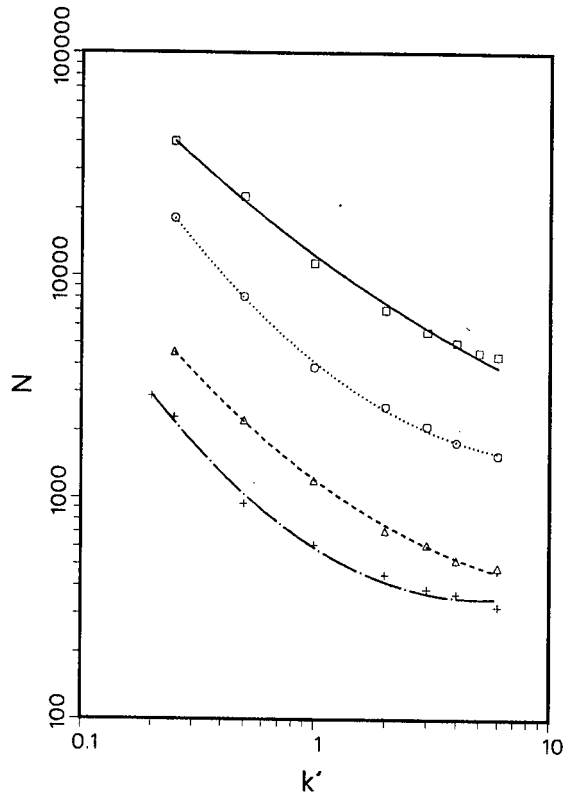

Fig. 18. Plot of the column efficiency required to perform the separation under the same experimental conditions as in Fig. 17.

column needed when the same separation is carried out at $k'_1 = 6$. For the separation of a mixture with $\alpha = 1.1$ a column having more than 20 000 theoretical plates is needed, whereas a column with 1000 theoretical plates is sufficient at $\alpha = 1.8$. Generally, a more efficient column is needed for the preparation of the more retained component and for the purification of the component which has the smaller relative concentration.

Mobile phase velocity. We found that the optimum reduced velocity of the mobile phase is usually small at the optimum retention factor, although it is markedly higher than the reduced velocity corresponding to the maximum column efficiency. It is rarely limited by the maximum inlet pressure (never in Table II, and only for the easiest problems in Table I). For example, the reduced velocity is small (15–30) at the optimum capacity factor for $\alpha = 1.1$ (*i.e.*, $k'_1 = 0.5$), whereas the optimum column length is large (100–200 cm) and the optimum particle size moderate (12–15 μm). Whereas the optimum column length depends only slightly on the composition of the mixture, it depends much more on whether we want to prepare the more or the less retained component. The column should be operated at a lower mobile phase reduced velocity if we want to prepare the component with the smaller relative concentration.

In contrast, if the column is operated at a non-optimum value of the retention factor, the optimum reduced velocity may be high (compare Tables I and II). The optimum reduced velocity increases almost linearly with increasing log k'_1, as illustrated in Fig. 19 for the less retained component in a 1:3 mixture. This result explains the apparent disagreement between previous results. General theoretical considerations on the optimization problem lead to the prediction of a moderate value of the mobile phase

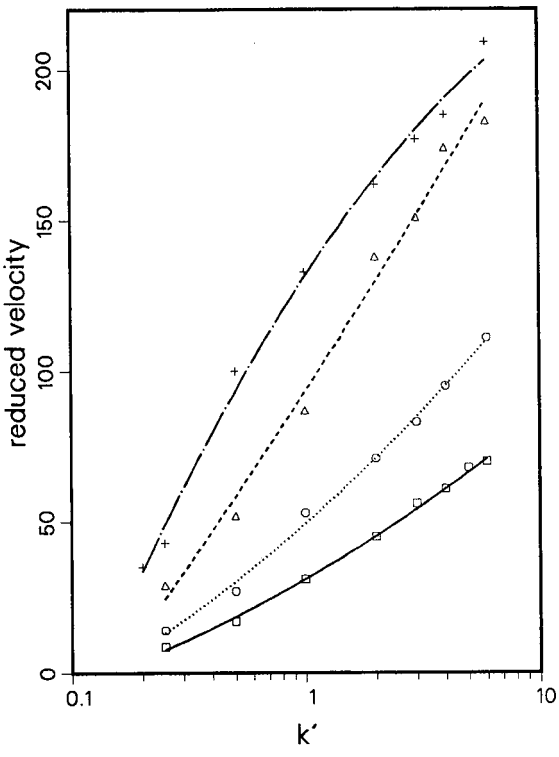

Fig. 19. Plot of the optimum reduced velocity of the mobile phase *versus* the retention factor of the first component. Same experimental conditions as in Fig. 17.

reduced velocity [4]. On the other hand, numerical optimization of the experimental conditions for a given column and chromatographic system resulted in large values of the optimum reduced velocity [11]. However, in these numerical calculations, we have assumed constant values of α and k'_1, and the selected value of k'_1 was large compared with the optimum values recommended in this work.

Optimum sample size. Based on the ideal model of liquid chromatography, an equation was derived for the optimum loading factor of the sample when the purification of the more retained component is optimized [3]. In Table III, we compare the optimum loading factors predicted by the ideal model for different values of the separation factor and of the feed composition with the results of the numerical optimization obtained in this work.

To check whether or not the difference is due only to the error caused by the simplex algorithm, we computed the standard deviation of the optimum

TABLE III

OPTIMUM LOADING FACTORS BASED ON THE IDEAL MODEL AND ON THE SEMI-IDEAL MODEL

The purification of the more retained component is optimized.

α	3:1 mixture		1:3 mixture	
	I^a	S^a	I^a	S^a
1.1	0.89	0.67	1.12	0.86
1.2	3.17	3.42	3.87	4.36
1.5	13.57	12.40	14.30	11.45
1.8	19.14	21.92	18.11	19.61

[a] I = optimum loading factor predicted by the ideal model of chromatography; S = optimum loading factor calculated by the semi-ideal model.

parameters by repeating the simplex optimization 25 times, starting the simplex algorithm with a very different initial vertex. The relative standard deviations of the optimum values obtained for the column length, the average particle diameter and the loading factor are all between 4 and 5%. The relative standard deviation of the mobile phase reduced velocity is twice as high (8.5%), whereas that of the maximum production rate is very small (less than 1%).

The difference between the two sets of data in Table III is approximately within the $\pm 2\sigma$ confidence interval, although in five cases out of eight it is slightly higher.

CONCLUSIONS

One of the most important results of this work is the confirmation of an optimum value of the retention factor of the first component of a pair of components to be separated in preparative chromatography. Of equal importance is the fact that this optimum retention factor is very low, always below unity when all the parameters are optimized for a given separation (Table II), rarely above 1.5 when the operating conditions of a given column are optimized (Table I). The optimum retention factor decreases slightly with increasing separation factor when all parameters are optimized simultaneously. It decreases more rapidly when the operating parameters of a given column are optimized. Although typical of most columns currently used in preparative applications, the column considered here (L = 25

cm, d_p = 20 μm) is close to the optimum design only for the relatively simple separation of a binary mixture with a high separation factor, α = 1.8, and at a high value of the retention factor, between 5 and 6.

In contrast, if all the parameters of the separation are optimized together, the optimum retention factor is very small, of the order of 0.3–0.5, depends only slightly on the separation factor and is almost independent of the composition of the mixture and of whether the more or the less retained component is prepared. The optimum is sharp, and small changes in the retention factor around the optimum may lead to significant losses of the production rate.

It could appear unacceptable to a chromatographer to operate a preparative column under conditions where the retention factor is a fraction of a unit. It is recognized that optimum analytical results are obtained when the retention factor is between 3 and 6. This difference between the two results is a further illustration of the dangers encountered in applying carelessly the principles of analytical chromatography to preparative chromatography. In addition to permitting the achievement of the maximum production rate possible, the choice of a low retention factor has the further advantage of giving a relatively low optimum mobile phase velocity.

Another important result is the strong dependence of the column design parameters on the retention factor of the first component of the sample if a non-optimum value of this retention factor has to be chosen. Also, there is a strong dependence of the column design parameters on whether we prefer to optimize the separation for the production of the more or the less retained component of the mixture. For the production of the more retained component we need a longer column.

ACKNOWLEDGEMENTS

We thank A. M. Katti (Mallinckrodt, St. Louis, MO, USA) and S. Golshan-Shirazi (University of Tennessee, Knoxville, TN, USA), for fruitful discussions. This work was supported in part by grant CHE-8901382 from the National Science Foundation and by the cooperative agreement between the University of Tennessee and the Oak Ridge National Laboratory. We acknowledge support of our computational effort by the University of Tennessee Computing Center.

REFERENCES

1 A. M. Katti and G. Guiochon, *Adv. Chromatogr.*, 31 (1991) 1.
2 S. Golshan-Shirazi and G. Guiochon, *J. Chromatogr.*, 506 (1990) 495.
3 S. Golshan-Shirazi and G. Guiochon, *Anal. Chem.*, 61 (1989) 1276.
4 S. Golshan-Shirazi and G. Guiochon, *Anal. Chem.*, 61 (1989) 1368.
5 S. Goshan-Shirazi and G. Guiochon, *Am. Biotechnol.*, 8, No. 2 (1990) 24.
6 S. Golshan-Shirazi and G. Guiochon, *Am. Biotechnol.*, 8, No. 8 (1990) 26.
7 S. Golshan-Shirazi and G. Guiochon, *J. Phys. Chem.*, 93 (1989) 4143.
8 S. Golshan-Shirazi and G. Guiochon, *J. Chromatogr.*, 517 (1990) 229.
9 S. Golshan-Shirazi and G. Guiochon, *J. Chromatogr.*, 536 (1991) 57.
10 S. Ghodbane and G. Guiochon, *Chromatographia*, 26 (1988) 53.
11 A. M. Katti, E. V. Dose and G. Guiochon, *J. Chromatogr.*, 540 (1991) 1.
12 S. Ghodbane and G. Guiochon, *J. Chromatogr.*, 444 (1988) 275.
13 J. Newburger and G. Guiochon, *J. Chromatogr.*, 523 (1990) 63.
14 G. Guiochon, S. Golshan-Shirazi and A. Jaulmes, *Anal. Chem.*, 60 (1988) 1856.
15 M. Czok and G. Guiochon, *Anal. Chem.*, 62 (1990) 189.
16 J. H. Knox, *J. Chromatogr. Sci.*, 15 (1977) 352.
17 G. M. Schwab, *Ergebnisse der Exacten Naturwissenschaften*, Vol. 7, Springer, Berlin, 1928, p. 276.
18 M. D. Levan and T. Vermeulen, *J. Phys. Chem.*, 85 (1981) 3247.
19 S. Golshan-Shirazi, J.-X. Huang and G. Guiochon, *Anal. Chem.*, 63 (1991) 1147.
20 E. V. Dose, *Anal. Chem.*, 59 (1987) 2420.

Journal of Chromatography, 591 (1992) 47–54
Elsevier Science Publishers B.V., Amsterdam

CHROM. 23 787

Peak capacity of columns for size-exclusion chromatography*

Lars Hagel

Department of Analytical Chemical R&D, Pharmacia LKB Biotechnology, S-751 82 Uppsala (Sweden)

(First received July 30th, 1991; revised manuscript received October 4th, 1991)

ABSTRACT

The practical peak capacity of columns for size-exclusion chromatography (SEC) is related to the pore fraction (V_p/V_t), plate number (N) and resolution (R_s) and may be estimated from $n_{SEC} \approx 1 + V_p/V_t)\ N^{1/2}/(4R_s)$. This equation yields a value of 80–90% of the maximum peak capacity, in contrast to earlier proposed equations which yield a large overestimate of the peak capacity. The practical peak capacities of columns packed with microparticulate materials is *ca.* 13 for completely resolved peaks, which is roughly equal to the peak capacity of columns traditionally used for SEC, the reason being the small pore volume of rigid materials and the short column lengths used. However, the maximum peak capacity is obtained with a considerably shorter separation time.

INTRODUCTION

In size-exclusion chromatography (SEC) (also known as gel filtration for aqueous system and gel permeation chromatography for non-aqueous systems), solutes are, ideally, eluted strictly according to decreasing size. This is due to the increasing proportion of the pore volume that becomes sterically available to successively smaller molecules with an increased retention time as a result. The maximum effective separation volume is thus restricted by the total pore volume of the packing material used. This limits the theoretical peak capacity of columns for SEC to a fraction of that for adsorptive chromatographic techniques for which solutes may be selectively retained and eluted after several column volumes of effluent [1]. As the peak-to-peak distance in SEC is limited, minimizing the peak widths becomes an important factor for achieving high peak capacities. Peak widths can be kept small through the use of columns of high efficiency and the following simple equation has been proposed for the calculation of the peak capacity (n) from the column plate number (N) (see, *e.g.*, refs. 2–4):

$$n \approx 1 + 0.2N^{1/2} \quad (1)$$

This relationship implies that peak capacities of 23–33 should be common for columns packed with microparticulate materials with $N = 12\ 500$–$25\ 000$. However, such peak capacities have so far not been realized in practice. This is due to the fact that eqn. 1 is an oversimplification and, further, it does not accurately account for variations in the pore volume. Chang *et al.* [5] illustrated the effect of pore volume on resolution in SEC and concluded that 2.6 times as many plates were required for Glycophase G/CPG for obtaining a resolution factor comparable to that for Sephadex G-200, owing to the small pore volume of the former material.

The complete equation for peak capacity (the maximum number of peaks separated on a given column) in gel filtration as described by Giddings [1] is

$$n = 1 + \ln(V_t/V_0)N^{1/2}/m \quad (2)$$

where V_t is the total liquid volume, V_0 is the void

* Parts of this work were presented at the *Tenth International Symposium on HPLC of Proteins, Peptides and Polynucleotides, October 29–31, 1990, Wiesbaden, Germany.*

0021-9673/92/$05.00

volume of the column and m is the spacing between peaks in terms of the standard deviation of solutes within a peak. The equation was derived under the assumption that the plate number is constant over the separation range. However, this assumption seems not to be valid as variations of N have been found to be considerable whereas variations in peak widths are small for various solutes [6–9]. From a study of the broadening effect in the SEC of polyethylene by Tung *et al.* [6], it may be calculated that the peak widths varied by 2.6 times and the plate numbers by 28.7 times over the separation range. Hagel and Andersson [7] presented data on proteins from which variations in peak widths of 2 times and in plate counts of 13 times may be inferred. Basedow and co-workers [8,9] found that the variation in peak widths of narrow dextran fractions was almost negligible when the solutes were chromatographed at low flow-rates.

Horváth and Lipsky [10] derived an equation for peak capacity in gradient elution, where all peaks have the same peak width. The equation was generalized by Grushka [11] to

$$n = 1 + N^{1/2}/4[(V_p/V_i) - 1] \quad (3)$$

where N is the plate number of the first peak and V_p is the pore volume of the material. This equation should also be applicable to the calculation of peak capacities of columns for SEC provided that the plate number of the first peak, *i.e.*, the void peak, is readily attainable. Unfortunately, in practice, this is seldom the case.

In a recent study of the separation characteristics of gel filtration by simulations it was found that the equations suggested (*i.e.*, eqns. 1 and 2) were not in accordance with the expected peak capacities [12]. Further, published chromatograms indicates peak capacities of *ca.* 7–8 also for columns packed with microparticulate materials [3,13–17], which shows that the simple dependence of merely plate number as expressed by eqn. 1, is erroneous. Thus, for estimations of the inherent performance of different media–column combinations, it is necessary to find a more accurate equation for expressing the peak capacity in SEC.

THEORETICAL

The zone broadening of solutes in SEC can be calculated from the well known Van Deemter equation as adapted to gel filtration by Giddings and Mallik [18], and Knox and Scott [19]:

$$H = 2\lambda d_p + 2[0.6D_m + \gamma_s D_m(1/R - 1)]/u + R(1 - R)d_p^2 u/30\gamma_s D_m \quad (4)$$

assuming that coupling effects between column dispersion and axial diffusion can be neglected (this is normally the case in SEC, which is carried out at reduced velocities exceeding 1) [20]. The plate height, H, is dependent on a geometric factor λ, the particle size d_p, the diffusion coefficient of the solute D_m, the obstruction factor to diffusion in the porous material γ_s, the relative zone velocity R and the interstitial velocity of the mobile phase u. A characteristic of the Van Deemter equation is the minimum plate height, which for SEC of macromolecules is given by [12]

$$H_{min} = d_p(2\lambda + 2\{2/30[0.6R(1 - R)/\gamma_s + (1 - R)]^2\}^{1/2}) \approx \text{constant} \cdot d_p \quad (5)$$

The proportionality constant, called the minimum reduced plate height, h_{min}, is dependent on, among other factors, how well the column is packed. Minimum reduced plate heights around 2 are regarded as excellent and values around 4 acceptable for high-performance columns [21,22].

The plate number and the peak width can be calculated from the plate height by

$$N = L/H \quad (6)$$

and

$$\sigma = V_R/N^{1/2} = V_R(H/L)^{1/2} \quad (7)$$

where L is the column length, V_R the retention volume of the solute and σ the peak width expressed in standard deviation, assuming a Gaussian distribution of solutes within a peak.

The maximum number of resolved peaks may be estimated from simulations of chromatograms using eqns. 4 and 7 as illustrated in Fig. 1. Identical separation patterns for different columns were obtained by selecting parameters in accordance with published data for commercial columns, as stated in the caption. For traditional media, a long column is necessary for providing high peak capacity. Note that the peak widths are roughly constant over the separation range at these flow velocities (as found

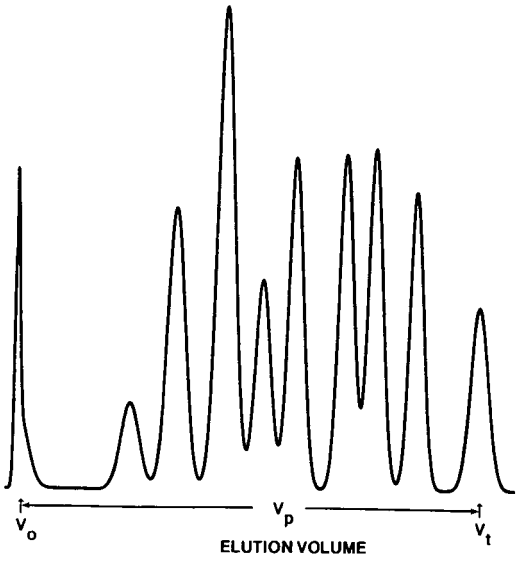

Fig. 1. Theoretical peak capacities of SEC columns as obtained by computer simulations. Peak widths are calculated from eqn. 7 for the solutes used under Experimental (see caption to Fig. 6). Conditions were selected according to published data [7,23,24], except for the column length of the 100-μm material, and identical separation patterns were obtained by minor adjustments of the pore fraction of the various materials:

Particle size (μm)	5	10	30	100
Bead pore fraction (%)	52	75	92	96
Nominal velocity (cm/h)	54	27	9	3
Column length (cm)	25	30	60	214

The resolutions between adjacent peaks are, from left to right, 2.93, 1.29, 1.45, 1.17, 1.10, 1.75, 1.02, 1.49 and 2.04. Peaks are, in ideal SEC, only eluted in the pore volume region, V_p, between the void volume, V_0, and the total liquid volume, V_t.

experimentally by Basedow *et al.* [8]). The separation systems seem to be able to resolve approximately eleven peaks with baseline separation. As illustrated in Figs. 2 and 3, the variations in peak width are considerably smaller than variations in plate number over the separation range normally encountered in SEC. It is also seen that the peak widths are virtually constant over a large portion of the separation range at the flow velocities commonly recommended for protein separations, *i.e.*, 27 cm/h for a 50-kilodalton protein chromatographed on a 10-μm material [23].

These results, together with experimental observations, encourage the use of eqn. 3 for the calculation of column peak capacity in SEC. However, determination of the plate number for the void peak is difficult. Instead, an equation that is related to the

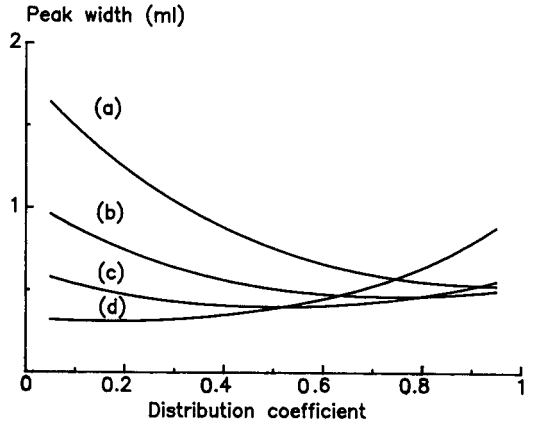

Fig. 2. Variations in peak widths over the separation range of SEC at various eluent velocities. Peak widths in ml calculated from eqn. 7 for solutes with molecular weights from 100 to 10 000 000 chromatographed on a 30 × 1 cm I.D. column packed with a 10-μm material. Nominal velocity: (a) 90; (b) 30; (c) 10; (d) 2 cm/h.

maximum plate number should be very useful for purposes of comparison between different materials packed in different columns. This may be obtained by a slight modification of the discussion made by Grushka [11] (see Fig. 1). The volume between the void peak, V_0, and the totally permeating peak, V_t, is equal to the pore volume, V_p, of the chromatographic material. This space may be filled with V_p/W peaks of width W. The width of a peak can be

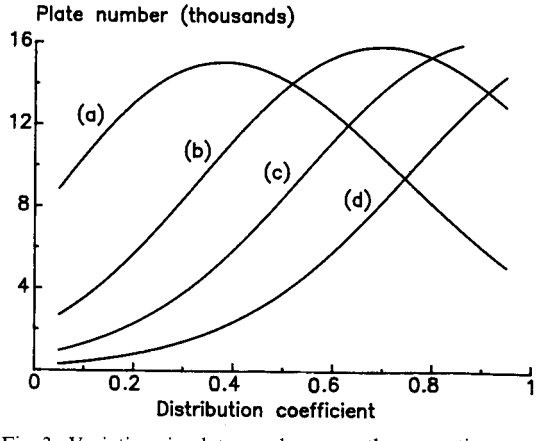

Fig. 3. Variations in plate numbers over the separation range of SEC at various eluent velocities. Plate numbers calculated from eqn. 6 with conditions given in the caption to Fig. 2. Nominal velocity: (a) 2; (b) 10; (c) 30; (d) 90 cm/h.

expressed in multiples of the standard deviation, σ, assuming a Gaussian distribution of solutes within the peak. The multiple factor is related to the resolution, R_s, of adjacent peaks. A spacing of the centre of two peaks (of equal widths) of 6σ, *i.e.*, $W = 6\sigma$, will yield $R_s = 1.5$, whereas $W = 4\sigma$ will yield $R_s = 1.0$. The influence of the resolution may be incorporated into the equation for peak capacity by expressing the width as $W = 4\sigma R_s$.

The width of the peaks will vary with both eluent velocity and retention volume (Fig. 2). At very low velocities, excessive broadening of fast-diffusing solutes will take place owing to the dominating influence of axial diffusion, and at very high velocities non-equilibrium effects will cause broadening of slow-diffusing species. A guideline for high-resolution gel filtration of proteins is to use a flow velocity yielding a reduced plate height of four for the solute of interest [23]. Assuming that this solute is eluted in the middle of the separation range (*i.e.*, a situation between curves b and c in Fig. 2), the peak width may, with the aid of eqn. 7, be calculated from

$$\sigma = (V_0 + K_D V_p)(4h)^{1/2}\sigma_{t,min}/[V_t(2h)^{1/2}] = (1.0 \pm 0.1)\sigma_{t,min} \quad (8)$$

where the distribution coefficient, K_D, is set to 0.5, the permeability, V_p/V_0, is between 0.8 and 2.2 and $\sigma_{t,min}$ is the minimum peak width of totally permeating solutes in standard deviations. Thus, at the eluent velocities commonly recommended for protein separations, the peak widths are approximately constant (Fig. 2) and roughly equal to the minimum peak width of a totally permeating peak (eqn. 8). From these assumptions and with the use of eqn. 7, and realizing that owing to column dispersion (and the definitions of V_0 and V_t), half a peak will appear before V_0 and half a peak will appear after V_t, the total number of peaks that, in practice, can be separated by SEC may be estimated from

$$n_{SEC} = V_p/[4(V_R/N^{1/2})R_s] + 0.5 + 0.5 = 1 + (V_p/V_t)(N_{max})^{1/2}/(4R_s) \quad (9)$$

where the plate count is calculated for the totally permeating peak (hence V_R becomes V_t). The practical peak capacity as calculated from eqn. 9 will be fairly close to the maximum theoretical peak capacity of the column (see below).

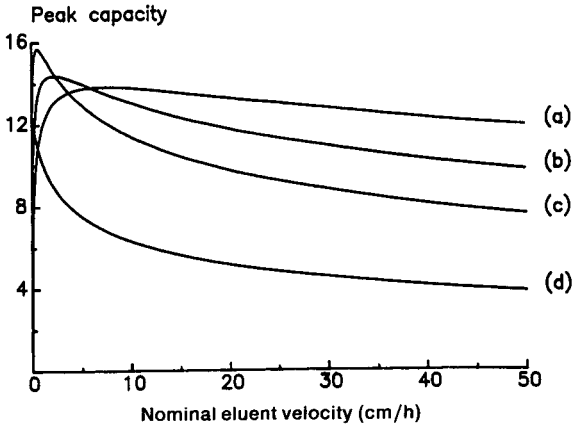

Fig. 4. Theoretical peak capacities of SEC columns. Number of peaks resolved by $R_s = 1.5$ obtained by successive calculations of peak widths with aid of eqn. 4, starting with the void peak. Separation range same as in Fig. 2. Column parameters:

	d_p (μm)	V_p/V_0	h_{min}	L (cm)
(a)	4	0.78	2.5	25
(b)	10	1.30	2.0	30
(c)	30	2.20	2.0	60
(d)	100	2.25	2.0	100

The plate number may be expressed in terms of the minimum reduced plate height from eqns. 5 and 6, which yields

$$n_{SEC} = 1 + (V_p/V_t)[L/(h_{min}d_p)]^{1/2}/(4R_s) \quad (10)$$

Hence the practical peak capacity is roughly inversely proportional to the resolution and to the square root of the particle size and proportional to the pore fraction and to the square root of the column length. It is also evident that optimum peak capacity is only obtained with columnss that are well packed. The influence of some of these parameters is illustrated in Fig. 4, showing the peak capacities of optimally packed columns at various eluent velocities. The peak capacity at each velocity was obtained by successive calculations of peak widths [14], starting from the void peak, with the aid of eqns. 4 and 7. The total peak capacity will decrease at very low eluent velocities owing to the excessive broadening of low-molecular-weight solute peaks and at very high velocities owing to broadening of high-molecular-weight solute peaks. The latter effect is reduced by using small-particle-size materials, possessing small diffusion distances. The maximum peak capacity is obtained, in most instances, at an unrealistically low

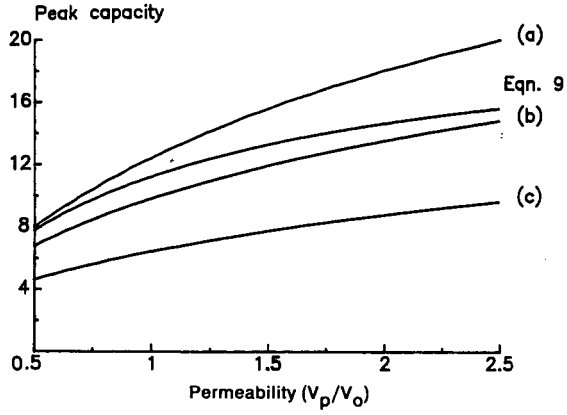

Fig. 5. Comparison of theoretical peak capacities and that calculated from eqn. 9 at various permeabilities, V_p/V_o, of the chromatographic material. Maximum peak capacity derived as for Fig. 4b with the following nominal eluent velocities: (a) 2; (b) 27; (c) 150 cm/h.

eluent velocity. In the calculation of the practical peak capacity, the eluent velocity exceeds the optimum velocity (as often is the case in experimental SEC) and therefore the peak capacity calculated with the aid of eqn. 9 will be 15–20% lower than the true peak capacity of the column (Fig. 5a). However, as illustrated in Fig. 5, the peak capacity as calculated from eqn. 9 will be close to the true peak capacity obtained at recommended eluent velocities (Fig. 5b), which was the assumption in eqn. 9.

The eluent velocity yielding the minimum plate height, and thus minimum zone broadening of a particular solute, is given by [23]

$$u_{opt} = (D_m/d_p)\gamma_s(60\{2/[3\gamma_s R(1-R)] + 1/R^2\})^{1/2} \quad (11)$$

and is thus inversely proportional to the particle size of the chromatographic material employed. It can be shown that the flow velocity will be proportional to D_m/d_p also when $H = 2H_{min}$. This means that the inherent peak capacity of small-particle-size media is obtained at a higher eluent velocity and consequently with a shorter time of analysis (Fig. 4). By combining eqns. 10 and 11, it is seen that the practical peak capacity is held constant by keeping the column length proportional to the particle size and the flow velocity inversely proportional to the particle size, which results in an analysis time proportional to $[d_p/(V_p/V_t)]^2$. However, this is only true for media of similar pore fractions, as the pore fraction will influence R and thus u_{opt}. Low pore fractions will result in relatively longer separation times, as is evident from the data in the caption to Fig. 1. The analysis time on the 5-μm material is twice as long as expected on the basis of differences in particle sizes of the materials.

EXPERIMENTAL

For an experimental study of the peak capacity as a function of the particle size, it is necessary to use a set of materials possessing very similar selectivity properties. For this purpose, we selected a family of gels based on 6% agarose of various particle sizes. The peak capacities of Superose 6 ($d \approx 13$ μm), Superose 6 Prep Grade ($d \approx 33$ μm) and Sepharose CL 6B ($d_p \approx 95$ μm), packed into columns of various lengths (Table I), were examined by size exclusion of a protein mixture using phosphate buffer as mobile phase (Fig. 6). The instrumentation used was a Model P-500 high-precision pump, a Model V-7 injector, equipped with a 200- or 500-μl loop, a Model UV-M UV detector with a 10-μl flow cell and 280-nm filter and a Model REC-2 recorder (Pharmacia LKB Biotechnology, Uppsala, Sweden).

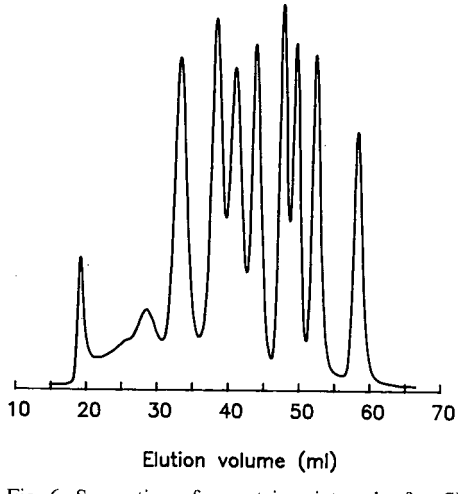

Fig. 6. Separation of a protein mixture by fast SEC. Column: 31.6 × 1.6 cm I.D. packed with Superose 6. Sample: 200 μl of a mixture of thyroglobulin (2 mg), ferritin (0.6 mg), IgG (1 mg), bovine serum albumin (1.6 mg), carbonic anhydrase (0.6 mg), cytochrome *c* (0.4 mg), aprotinin (1.4 mg) and glycyltyrosine (0.2 mg). Eluent: 0.05 M phosphate in 0.15 *M* NaCl (pH 7.0). Flow-rate: 50 ml/h.

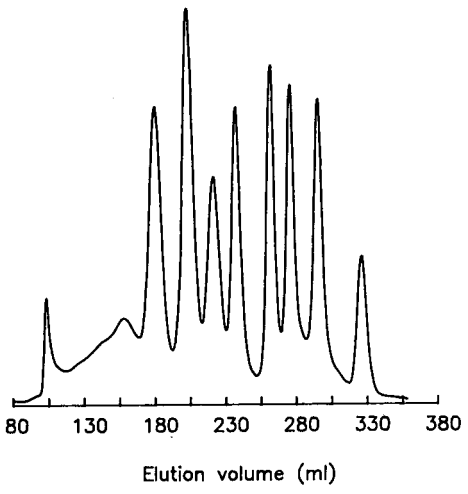

Fig. 7. Separation of a protein mixture by standard SEC. Column: 64.0 × 2.6 cm I.D. packed with Superose 6 Prep Grade. Solutes and eluent as in Fig. 6. Sample volume: 200 μl. Flow-rate: 43 ml/h.

Simulations were performed on a Hewlett-Packard Series 9000/200 computer.

RESULTS AND DISCUSSION

The chromatograms illustrated in Figs. 6–8 confirm that the predicted peak capacities of the different columns, as calculated from eqn. 9 (see Table I, are in good accordance with those found experimentally and that similar separation patterns and peak capacities are obtained under optimum conditions for traditional, standard and fast SEC. Further, the chromatograms are very similar to the separation patterns expected from the simulations shown in Fig. 1, although a lower resolution between peaks is obtained experimentally. The peak widths are fairly constant over the entire separation range. It is evident from the chromatograms that the selectivities of the materials differ slightly, especially at the extremes of the separation range. The separation in the high-molecular-weight region is overestimated by the computer simulation, which is due to the problem of assigning a correct obstruction factor for solutes eluted at $K_D < 0.2$ [23]. The separation on Superose 6 Prep Grade is better than that on Superose 6, which can be attributed to the too high eluent velocity used with the latter column (*i.e.*, 20 cm/h should give a more realistic picture of the separation ability of this material [23]). For Sepharose CL 6B, a change in the experimental conditions to L = 156 cm and u_{nom} = 2.5 cm/h can be expected to yield a similar separation to that with Superose 6 Prep Grade.

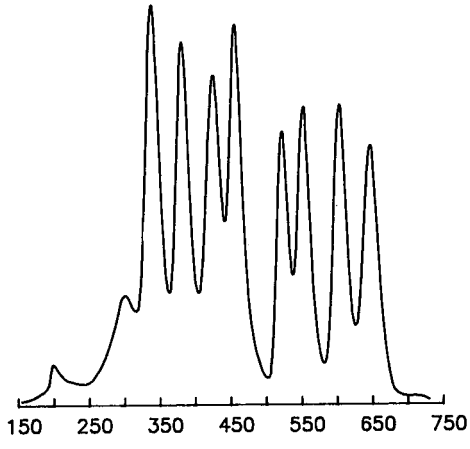

Fig. 8. Separation of a protein mixture by traditional SEC. Column: 137.9 × 2.5 cm I.D. packed with Sepharose CL 6B. Solutes and eluent as in Fig. 6. Sample volume: 500 μl. Flow-rate: 9.6 ml/h.

TABLE I

EXPERIMENTAL PARAMETERS

Parameter	Superose 6	Superose 6 Prep Grade	Sepharose CL 6B
$d_{p,50,v}$ (μm)	13.6	29.2	95.0
V_0 (ml)[a]	19.7	105.7	204.8
V_t (ml)[b]	58.8	328.2	652.8
V_p/V_t	0.664	0.678	0.686
L (cm)	31.6	64.0	137.9
N_{max}[c]	10 000	12 500	5140
u_{nom} (cm/h)	24.9	8.1	1.96
$L/\{u_{nom}[d_p/(V_p/V_t)]^2\}$	$3.0 \cdot 10^5$	$4.2 \cdot 10^5$	$3.7 \cdot 10^5$
$n_{1.5}$ from eqn. 9	12.0	13.6	9.2
$n_{1.5}$ experimental[d]	11.6	13.6	8.7

[a] Calculated from the peak apex of the void peak.
[b] Calculated from the peak apex of glycyltyrosine.
[c] Determined from the peak width at half-height of acetone.
[d] Calculated from the mean peak widths of bovine serum albumin and carbonic anhydrase in Figs. 6–8 and the distance between the void volume and the total volume.

TABLE II

THEORETICAL PEAK CAPACITIES OF SOME COMMERCIAL COLUMNS FOR AQUEOUS SEC

Column	L (cm)	d_p (μm)	V_p/V_t	N	$n_{1.0}$	$n_{1.5}$
Prepacked columns[a]						
Zorbax GF-250	25.0	4	0.44	25 000[b]	18	13
Superose 12	30.0	10	0.65	12 000	18	13
TSK 3000 SW	30.5	10	0.57	9220	15	10
Synchropak GPC 300	24.5	10	0.59	4200	11	7
Waters I-125	25.0	10	0.48	4950	10	7
Synchropak GPC 100	25.0	10	0.55	2080	6	4
LiChrosorb Diol	30.0	10	0.39	1760	5	4
Laboratory-packed columns[a]						
Superose 6 Prep Grade	30.0	33	0.69	3640	11	8
Superose 6 Prep Grade	60.0	33	0.69	7200	16	11
Sephacryl S 300 HR	60.0	54	0.62	6900	14	10
Sepharose CL 6B	100.0	110	0.70	4170	12	9

[a] Data for the columns collected from refs. 23 and 24.
[b] Calculated assuming $h_{min} = 2.5$.

The peak capcities of some different commercially availble columns for high-performance SEC and those of traditional media packed in laboratory columns, as calculated from eqn. 9, are given in Table II. It is seen tht the inherent high peak capacity of small-particle-size media is in some instances ruined by an extremely low pore volume of the material or sacrificed for a decrease in column length as compared with traditional media. As noted elsewhere [25], the plate numbers determined for some of the columns are surprisingly low, which might yield an unfair picture of the expected peak capacity of these silica-based materials. Assuming that the columns are well packed, *e.g.*, $h_{min} = 2.5$, the peak capacity for completely resolved peaks, *i.e.*, $R_s = 1.5$, varies between 8 and 13 owing to the different pore volumes of the different materials. This shows that the peak capacity of columns for fast SEC are of the same order as laboratory-packed columns of traditional media, provided that the columns are operated close to the optimum velocity. This is also illustrated by Fig. 4, showing the peak capacities of optimally packed columns at various flow velocities. However, the peak capacities of microparticulate materials are substantially less sensitive to high flow velocities, owing to the small diffusion distances of these materials. Hence the optimum performance is not dramatically [higher] but [faster] with microparticulate materials with the column lengths normally used. This is also evident from Fig. 1, where the difference between the materials is not peak capacity but separation time, *i.e.*, the number of peaks separated per unit time. Grushka [26] discussed the influence of particle size, column length and eluent velocity on the "rate of peak capacity production".

The detrimental impact of large matrix volumes on the peak capacities of microparticulate materials was noted by Engelhardt and Ahr [14]. They found that the theoretical peak capacities of 10- and 3-μm silica materials packed in 25-cm columns were 15 and 27, respectively. Corresponding data from eqn. 9 using their data for pore fractions, plate height and resolution factor, *e.g.* $R_s = 1.0$, are 13 and 23, respectively, which is in fair agreement considering that eqn. 9 will yield a slight underestimate of the maximum peak capacity, as outlined above.

The example given is valid for macromolecules. However, the discussion is equally applicable to small solutes, the maximum peak capacity will appear at higher flow velocities (proportional to the diffusivity) and as the slope of the C term of the Van Deemter plot will be smaller than for solutes of large D_m, the operational range of high peak capacities

will be large. This is also the case for smaller-particle-size materials. It may be noted that in general it seems to be more difficult to obtain optimally packed beds of smaller particles, which also partially explains the modest peak capacities displayed by some novel media. The small zone broadening of microparticulate media will, of course, be very important when low sample dilution is critical, *e.g.*, in micropreparative work or high-sensitivity analysis.

As the optimum eluent velocity is directly related to the diffusivity of the solute, a continuous increase in velocity as the solutes are being eluted should not only provide more optimum resolution but also a decrease in separation time, sometimes by a factor of two [23]. In the ideal case, it may be expected that a flow gradient may be constructed such as to allow each solute to elute with $H = H_{min}$. However, this situation can never be realized as the low eluent velocity necessary to yield small peak widths of early eluting substances will have to be constant for 30–40% of the run, and this will have a detrimental effect on the peak width of fast-diffusing solutes.

A resolution of 1 is assumed in the calculations of peak capacity by eqns. 1 and 2. However, as can be seen from Fig. 1, $R_s = 1$ will result in overlapping peaks (*e.g.*, peaks 7 and 8 from the left), whereas $R_s = 1.5$ yields almost completely resolved peaks (*e.g.*, peaks 8 and 9 from the left). It may therefore be recommended that the peak capacity be calculated from $R_s = 1.5$.

CONCLUSIONS

The practical peak capacities of columns for SEC can be calculated from

$$n = 1 + (V_p/V_t)[L/(h_{min}d_p)]^{1/2}/(4R_s)$$

Owing to the reduction in the relative pore volume and column length with decreasing particle size, the practical peak capacity of columns for SEC is around 10–15. This value will be lower for non-optimally packed columns.

The maximum peak capacity is obtained at a flow velocity inversely proportional to the particle size and, thus, the gain achieved with using microparticulate media is in separation speed and low sample dilution, not peak capacity.

ACKNOWLEDGEMENT

The author is grateful to Mr. Torvald Andersson for the preparation of the columns used in the experimental work.

REFERENCES

1 J. C. Giddings, *Anal. Chem.*, 39 (1967) 1027.
2 D. D. Bly, K. A. Boni, M. R. J. Cantow, J. Cazes, D. J. Harmon, J. N. Little and E. D. Weir, *Polym. Lett.*, 9 (1971) 401.
3 T. Takeuchi, T. Saito and D. Ishii, *J. Chromatogr.*, 351 (1986) 295.
4 J. V. Dawkins, in C. Booth and C. Price (Editors), *Comprehensive Polymer Science, Vol. 1, Polymer Characterisation*, Pergamon Press, Oxford, 1989, p. 256.
5 S. H. Chang, K. M. Gooding and F. E. Regnier, *J. Chromatogr.*, 125 (1976) 103.
6 L. H. Tung, J. C. Moore and G. W. Knight, *J. Appl. Polym. Sci.*, 10 (1966) 1261.
7 L. Hagel and T. Andersson, *J. Chromatogr.*, 285 (1984) 295.
8 A. M. Basedow, K. H. Ebert, H. Ederer and H. Hunger, *Macromol. Chem.*, 177 (1976) 1501.
9 A. M. Basedow, K. H. Ebert, H. J. Ederer and E. Fosshag, *J. Chromatogr.*, 192 (1980) 259.
10 C. G. Horváth and S. R. Lipsky, *Anal. Chem.*, 39 (1967) 1893.
11 E. Grushka, *Anal. Chem.*, 42 (1970) 1142.
12 L. Hagel and J.-C. Janson, in E. Heftmann (Editor), *Chromatography*, Elsevier, Amsterdam, 5th ed., 1991, Part A, Ch. 6, p. A267.
13 R. V. Vivilecchia, B. G. Lightbody, N. Z. Thimot and H. M. Quinn, *J. Chromatogr. Sci.*, 15 (1977) 424.
14 H. Engelhardt and G. Ahr, *J. Chromatogr.*, 282 (1983) 385.
15 Y. Kato, Y. Yamasaki, H. Moriyama, K. Tokunaga and T. Hashimoto, *J. Chromatogr.*, 404 (1987) 333.
16 *Zorbax Bio Series GF-250, Technical Report*, DuPont, Wilmington, DE.
17 *PLgel GPC Columns*, Polymer Laboratories, Church Stretton, 1981.
18 J. C. Giddings and K. L. Mallik, *Anal. Chem.*, 38 (1966) 997.
19 J. H. Knox and P. H. Scott, *J. Chromatogr.*, 282 (1983) 297.
20 J. C. Giddings, in E. Heftmann (Editor), *Chromatography*, Van Nostrand Reinhold, New York, 3rd ed., 1975, p. 39.
21 W. Heitz and W. Kern, *Angew. Makromol. Chem.*, 1 (1967) 150.
22 P. A. Bristow and J. H. Knox, *Chromatographia*, 10 (1977) 279.
23 L. Hagel, in J.-C. Janson and L. Rydén (Editors), *Protein Purification, Methods for High Resolution Protein Separation and Analysis*, VCH, Deerfield Beach, FL, 1989, Ch. 6.
24 E. Pfannkoch, K. C. Lu, F. E. Regnier and H. G. Barth, *J. Chromatogr. Sci.*, 18 (1980) 430.
25 K. K. Unger and J. N. Kinkel, in P. L. Dubin (Editor), *Aqueous Size-Exclusion Chromatography*, Elsevier, Amsterdam, 1988, p. 229.
26 E. Grushka, *J. Chromatogr.*, 316 (1984) 81.

Journal of Chromatography, 591 (1992) 55–63
Elsevier Science Publishers B.V., Amsterdam

CHROM. 23 806

Retention processes on α_1-acid glycoprotein-bonded stationary phase

E. Arvidsson* and S. O. Jansson

Analytical Chemistry, Astra Hässle AB, S-431 83 Mölndal (Sweden)

G. Schill

Department of Analytical Pharmaceutical Chemistry, Uppsala University Biomedical Centre, P.O. Box 574, S-751 23 Uppsala (Sweden)

(First received July 2nd, 1991; revised manuscript received October 16th, 1991)

ABSTRACT

Stereoselective separations of charged enantiomers on CHIRAL-AGP can be controlled by varying the pH and adding charged and uncharged additives to the mobile phase. The interaction with the selector, α_1-acid glycoprotein, was studied by monitoring the effects of the variables on retention and by indirect detection, in part using a simple multivariate design. The stereoselectivity is due to simultaneous retention processes involving ion-exchange and ion-pairing mechanisms. The predominant mode of interaction for different solutes was elucidated from variables that promote or counteract either of the processes. Considerable improvements in the stereoselectivity were achieved with chiral or achiral anionic and cationic additives that act in a synergistic or competitive mode.

INTRODUCTION

The dramatic development of chromatographic separation methods for enantiomeric compounds during the last decade has been achieved by different techniques. In many of them, such as with silica-bonded α_1-acid glycoprotein (Chiral-AGP), the character of the chiral binding process is incompletely known and the choice of conditions for stereoselective separation is more or less empirical. It is apparent from the separation of enantiomeric solutes of different structures that Chiral-AGP has binding sites of different character. By varying the properties of the mobile phase, a basis for the optimization of stereoselective separations and an insight into the binding mechanisms are obtained [1].

Chiral-AGP can be applied to the separation of both charged and uncharged enantiomers. The selector, α_1-acid glycoprotein (AGP), is an acidic protein with negatively charged groups in the aspartic acid residues and in the terminal serine group, whereas positively charged groups are present in the arginine, lysine and histidine residues. Uncharged, hydrogen-bonding chiral sites appear in the peptide chain and in the carbohydrate units that constitute 45% of the molecular weight [2]. Advanced studies of the chiral recognition properties by, *e.g.*, binding experiments with partly modified AGP have not been reported.

It has been found that the retention and stereoselectivity on Chiral-AGP can be varied over a wide range by changing the pH of the aqueous mobile phase and the content of charged and uncharged organic components [1]. The effects of these changes are highly dependent on the structure of the solute and bear no simple relationship to general properties such as charge or hydrophobicity. The complex nature of the binding process was illustrated in a previous paper by the effects of charged additives on retention and indirect detection [3]. The relationships were partly analysed by a two-level experimen-

0021-9673/92/$05.00

tal design with three variables using β-values to describe the effects of the variables, which is a systematic way to collect information. Enantiomers were affected differently, which indicates binding to several sites. The reversal of the retention order of the enantiomers of pseudoephedrine on addition of the counter ion octanoate [4] has the same basis.

The aim of this study was to develop models for the binding process to the chiral AGP-selector which can be used in the optimization of the stereoselective separation of charged enantiomers. The interaction between the solute and selector was studied by monitoring the effects of 2-propanol, pH and cationic and anionic additives on retention, selectivity and indirect detection. Solutes having an asymmetric centre in an aliphatic chain were included in the study.

EXPERIMENTAL

Apparatus

The chromatographic system consisted of a Model 2150 liquid chromatographic pump (LKB, Bromma, Sweden), a Rheodyne (Cotati, CA, USA) Model 7010 injector with a 20-μl loop and a Kratos (Ramsey, NJ, USA) Spectroflow 783 variable-wavelength detector. The temperature of the analytical column, injector and connecting tubes was controlled by immersing the system in a thermostated bath (RMS, Lauda-Königshofen, Germany). The chromatograms were recorded on a Perkin-Elmer (Norwalk, CT, USA) Model 56 instrument or a Spectra-Physics (San José, CA, USA) SP 4270 integrator.

Chromatographic conditions and chemicals

The separation column was Chiral-AGP (100 × 4.0 mm I.D.; 5 μm) from ChromTech (Norsborg, Sweden). The flow-rate was 0.4 ml/min and the system was thermostated at 22°C. If not stated otherwise, the mobile phases were phosphate buffers (ionic strength $I = 0.05\ M$) to which modifiers were added. The wavelength of detection was the UV absorption maximum or, when studying indirect detection, 220 nm. Atropine sulphate, homatropine bromide and sodium octanoate were purchased from Merck (Darmstadt, Germany). Metoprolol succinate was synthesized at Astra Hässle (Mölndal, Sweden). 1-(2-Hydroxyphenyl)-2-(*tert.*-butylamino)-ethanol (2HPE), 1-(4-hydroxyphenyl)-2-(*tert.*-butylamino)ethanol (4HPE) and ipratropine were kindly supplied by Astra Draco (Lund, Sweden). 4-Phenylbutyric acid, (*R*)- and (*S*)-3-phenylbutyric acid and racemic 2-phenylbutyric acid were purchased from Fluka (Buchs, Switzerland) and (*S*)- and (*R*)-2-phenylbutyric acid from Sigma (St. Louis, MO, USA).

Factorial design

Factorial design allows in a systematic way conclusions to be drawn about retention mechanisms from β-coefficients. The effects of pH, octanoate and 2-propanol on the retention were studied. A full-factorial design was made with 2^3 experiments, giving possibilities of calculating both the individual and combined effects of the three variables on retention and stereoselectivity. Calculations of effects expressed as β-values at different compositions of the mobile phases were made as described previously [3]. The magnitude of the effects of the variables depends on both the range studied and the magnitude of the response, which limits the use of the β-coefficients to a quantitative comparison of a certain variable on different solutes. The three variables were studied at two levels: pH in the mobile phase, 6.0 (−1) and 7.5 (+1); concentration of 2-propanol, 0% (−1) and 3% (+1); and concentration of octanoate, 0 mM (−1) and 4 mM (+1).

Indirect detection

A solute without an inherent detector response can be detected and quantified by an indirect detection technique. In a reversed-phase system the principle is as follows [5]: a detectable compound with moderate retention is included in the aqueous mobile phase. When a solution deviating in composition from the mobile phase is injected, the established equilibria are disturbed. Each retained component will form a zone which travels through the column with constant composition. When eluted, the zones appear as peaks as the concentration of the detectable compound deviates from that in the bulk of the mobile phase. The peaks can be positive or negative and they are given both by injected solutes and by mobile phase components (system peaks). The nature of the retention processes appears from the directions and relative retention of the solute and system peaks as shown previously [5]. Studies of system peaks, peak direction and solute peak size

combined with retention and selectivity data can give valuable information about retention principles.

RESULTS AND DISCUSSION

Binding processes

Two major retention principles have to be considered, *viz.*, binding to charged and uncharged sites. If the binding site is charged, the solid phase can act as an ion exchanger. The capacity factor of a solute HA^+ retained on a cation-exchanging site can be expressed as

$$k'_{HA,ie} = \frac{qC_R K_{HA}}{[H^+] + K_Q[Q^+]} \quad (1)$$

where q is the phase volume ratio [6], H^+ and Q^+ are mobile phase ions, K_{HA} and K_Q are equilibrium constants expressing the exchange of H^+ for HA^+ and Q^+, respectively, and C_R is the total binding capacity for cations.

AGP has an isoelectric point of 2.7 and its cation-exchanging capacity, C_R, increases with increasing pH. The retention of cations is dependent not only on $[H^+]$ but also on the concentration of other mobile phase cations, represented in eqn. 1 by Q^+. The effect of Q^+ is highly dependent on its affinity for the charged site.

The retention of an anionic solute is in an analogous way dependent on the OH^- concentration and the concentration and type of other mobile phase anions. The total binding capacity for anions decreases with increasing pH.

Eqn. 1 shows that an ion with a charge opposite to that of the solute has no direct influence on the retention. However, the presence of anion-exchanging sites might give rise to special retention effects. If a divalent anion, *e.g.*, HPO_4^{2-}, is bound to a monovalent site it will give rise to a negative charge that might retain cations.

An uncharged site can bind a charged solute as an ion pair with a counter ion. Assuming Langmuir adsorption, the retention of a cation, HA^+, can be expressed as

$$k'_{HA,ip} = \frac{qK_0 K_{HAX}[X^-]}{1 + K_{QX}[Q^+][X^-]} \quad (2)$$

where X^- and Q^+ are ions added to the mobile phase [7], K_0 is the total binding capacity and K_{HAX} and K_{QX} are the ion-pair distribution constants [6].

Eqn. 2 shows that additives of the same and opposite charge as the solute affect the retention. For any charged solute, both ion-exchange and ion-pairing processes are possible. An additive of the same charge as the solute has the same kind of effect on both processes whereas a counter ion to the solute directly affects only the ion-pair binding process. It should also be remembered that weak protolytes can be distributed to the solid phase in uncharged form, carboxylic acids usually at pH below 6 and aliphatic amines at pH above 8.

pH and mobile phase additives can affect both unspecific and stereoselective retention processes or sites, using a simple approach. A stereoselective site can bind two enantiomeric solutes with different strength. When applied to eqns. 1 and 2 this means that the equilibrium constants of the solutes are different whereas the remainder of the interaction pattern remains the same. If a single stereoselective site is responsible for the retention, the separation factor, $\alpha = k'_2/k'_1$, will be independent of the concentration of a mobile phase variable. If α changes with a mobile phase variable, more than one site must be involved in the retention process. The effect of the variable on k' and α can give information of the character of the binding sites. If the variable has a dominant influence on a stereoselective site, k' of the two enantiomers and α change in the same direction. If a reversal of the retention order is obtained [4], at least two stereoselective sites with different retention order are involved.

Retention studies

A rational way of approaching the complex influence of mobile phase components using a factorial design [8] was briefly demonstrated in a previous study [3]. Application of the method to analytes of different structures and charge can be based on conclusions on the properties of the binding sites in the chiral selector.

The effects of the three variables, pH, content of 2-propanol and the hydrophobic anion of octanoic acid, are expressed as β-coefficients and presented in Table I. The β-coefficients illustrate changes in retention and selectivity. The solutes are five cationic compounds. Atropine and homatropine have an ester and an alcohol group in the vicinity of the

TABLE I

CALCULATED EFFECTS OF pH, 2-PROPANOL AND OCTANOATE FOR FIVE SOLUTES

Solute	Parameter	β_{pH}	β_{pr}[a]	β_{oc}[a]
Atropine	k'_1	6.4	−5.8	−0.6
	k'_2	8.9	−8.3	1.8
	α	0.06	−0.10	0.20
Homatropine	k'_1	5.0	−3.5	−0.1[b]
	k'_2	7.1	−5.4	−1.2
	α	0.04	−0.11	−0.15
Metoprolol	k'_1	3.5	−3.1	−1.2
	k'_2	4.7	−4.5	−2.1
	α	0.06	−0.12	−0.08
4HPE	k'_1	1.4	−1.0	0.1[b]
	k'_2	1.9	−1.5	0.8
	α	0.13	−0.14	0.13
2HPE	k'_1	6.7	−6.8	−3.6
	k'_2	21	−22	−11.6
	α	0.39	−0.42	−0.19

[a] pr = 2-Propanol; oc = octanoate.
[b] Non-significant effect.

chiral centre, 4HPE and 2HPE have a 4-hydroxyphenyl or a 2-hydroxyphenyl group at the chiral carbon whereas metoprolol is an alkanolamine with a hydroxyl group at the chiral centre.

The experimental variation was determined using higher order interactions [9] and effects lower than this interaction effect are indicated in Table I as non-significant. Comparative calculations using a computer program, RS-Discover (BBN Software Products, Cambridge, MA, USA), confirmed our manual calculations. It should also be emphasized that the model did not completely describe the response, possibly owing to a lack of quadratic terms in the model. However, the aim was to use β-coefficients as a simple tool to visualize the dominant effects of mobile phase components.

Effects of pH

β_{pH}-values for k', $\beta_{pH}(k')$, of all the cationic enantiomers are positive, which shows that the dominant effect of increasing pH is an increase in k'. This indicates retention on a cation-exchanging site in accordance with eqn. 1. The β_{pH}-values for α, $\beta_{pH}(\alpha)$, are positive for all the cationic solutes, which indicates that the cation-exchange sites have stereoselective binding properties.

The cation-exchanging properties of the protein dominate in the pH range used and the anion-exchange capacity must be limited. However, the influence of anion-exchange groups is indicated by the significant retention of dihydrogenphosphate [10]. The effects of pH on a chiral anion, 2-phenylbutyrate, are discussed below in connection with the studies of influences of hydrophobic, cationic components in the mobile phase.

Effects of 2-propanol

$\beta_{pr}(k')$ is negative for all the enantiomers, indicating that the dominant effect of addition of 2-propanol is a decrease in the retention. This may be due to increased solvation of the enantiomers in the mobile phase, *i.e.*, a process that affects chiral and non-chiral binding to the same extent and is without effect on the stereoselectivity. 2-Propanol can also block the binding at uncharged sites on the solid phase and as $\beta_{pr}(\alpha)$ is negative for all the solutes it seems that blocking of a stereoselective uncharged site is one of the effects of 2-propanol.

Effect of octanoate

The $\beta_{oc}(k')$-values are fairly small in most instances. Positive effects are obtained for k'_2 of atropine and 4HPE whereas negative effects are found for k'_2 of homatropine and for k'_1 and k'_2 for metoprolol and 2HPE. This indicates that octanoate affects different sites or retention processes for the two enantiomers of atropine, homatropine and 4HPE whereas the same kind of site dominates the retention of both enantiomers of metoprolol and 2HPE.

$\beta_{oc}(\alpha)$ is positive for atropine and 4HPE and negative for the other solutes. If both $\beta_{oc}(k')$ and $\beta_{oc}(\alpha)$ are taken into account, it is obvious that octanoate influences stereoselective processes for all the cations.

The positive effects of octanoate on k'_2 are obviously due to an ion-pair binding process in accordance with eqn. 2. Octanoate can compete for the binding to uncharged sites as an ion pair with mobile phase cations or, at least at pH 6.0, in uncharged form.

The combined effects were generally smaller than the individual effects and hence more uncertain. However, the combined effects support the conclusions above.

Influence of anionic buffers

Not only hydrophobic anions such as octanoate but also the highly hydrophilic anions in the buffer can affect retention and stereoselectivity, as shown in Table II. This effect may be due to ion-pair binding to the uncharged site. However, it is also possible that the difference between phosphate and acetate is due to influences from anion-exchange sites as they can give rise to negative charges on the solid phase on binding of HPO_4^{2-} whereas the binding of acetate gives a neutral product. The difference between the buffers is maintained in the presence of a hydrophobic additive, which shows that all the anions participate in the retention process.

The buffer anions can give rise to major effects: homatropine has a high separation factor when the mobile phase contains (*S*)-2-phenylbutyric acid in phosphate buffer but the stereoselectivity is lost when the buffering is made with acetate. The retention decreases on increase in the buffer concentration. It might be due to competing effects in an ion-pair binding process but the increase in $[Na^+]$ has the same kind of effect on the cation-exchange site.

The system peaks achieved by use of the principle of indirect detection technique can give information of the retention process. The presence of a system peak shows the existence of an interaction between the solute and mobile phase components. The direction of the system peaks shows the type of interaction, *e.g.*, competitive or synergistic, and the number of system peaks indicates the number of mobile phase additives retained on the solid phase and interacting with the solute. Fig. 1 shows a separation of the enantiomers of homatropine using a mobile phase containing the detectable (*S*)-2-phenylbutyrate in phosphate buffer. The two negative system peaks show that the interaction is synergistic, *i.e.*, ion-pair retention, and that two mobile phase ions, the detectable (*S*)-2-phenylbutyrate and the buffer anion, are involved in the retention process.

The participation of all the anions in the retention process is further demonstrated by the retention of one of the system peaks being altered when phosphate is exchanged for acetate as buffering component. With racemic 2-phenylbutyrate as additive three system peaks appear as (*S*)- and (*R*)-2-phenylbutyrate have different retentions.

Retention effects of cationic additives

Mobile phase cations can affect retention both by interaction at a cation-exchanging site and as a counter ion in ion-pair interactions at an uncharged site. Two studies each with two variables, pH + tetrabutylammonium (TBA) and pH + dimethyloctylamine (DMOA), respectively, are presented in Table III.

For the anionic 2-phenylbutyrate the increase in pH gives a decrease in k' and an increase in the stereoselectivity. The considerable decrease in the retention with pH shows that the process involves

TABLE II

INFLUENCE OF BUFFERING ANIONS AND IONIC STRENGTH ON RETENTION AND STEREOSELECTIVITY FOR ATROPINE AND HOMATROPINE

Mobile phase: 0.5 m*M* additive and 1% 2-propanol in buffer of pH 6.0.

Buffer	Ionic strength	Additive[a]	Atropine		Homatropine	
			k'_1	α	k'_1	α
Acetate	0.05	–	2.1	1.2	1.9	1.4
Phosphate	0.05	–	2.8[b]	–	2.7	1.3
Acetate	0.05	(*S*)-2-phBA	2.7	3.9	4.3	1.0
Phosphate	0.05	(*S*)-2-phBA	3.2	3.0	3.0	1.4
Phosphate	0.05	2-phBA (racemic)	3.2	3.2	3.2	1.5
Phosphate	0.10	2-phBA (racemic)	2.6	3.4	2.4	1.6

[a] phBA = Phenylbutyric acid.
[b] Only (−)-atropine injected.

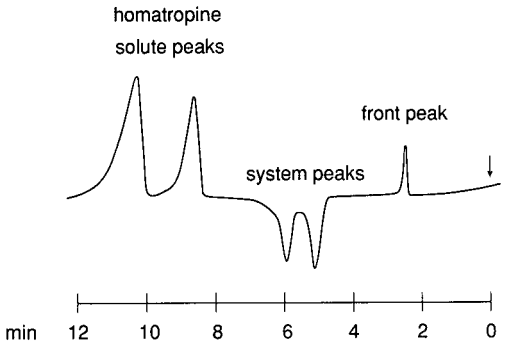

Fig. 1. Resolution of homatropine enantiomers. Mobile phase: 0.5 m*M* (*S*)-2-phenylbutyric acid + 1% 2-propanol in phosphate buffer (pH 6.0). Detection wavelength: 220 nm.

anion exchange or/and binding of 2-phenylbutyrate as an acid. The fact that k' and α change in opposite directions implies that pH influences the binding to a site with low or no stereoselectivity. It was further found that addition of 2-propanol gave an increase in α in addition to a decrease in k'. As 2-propanol mainly decreases the binding to uncharged sites, this means that it is the binding of 2-phenylbutyrate as acid that has no or low stereoselectivity.

The effects of TBA and DMOA on 2-phenylbutyrate are different. TBA gives a decrease in k' with a minor change in α. DMOA increases k' of the second-eluted enantiomer, which indicates ion-pair binding to an uncharged site. The k' value of the first-eluted enantiomer is almost unaffected and there is an increase in the stereoselectivity, which is particularly strong at pH 7.5. The substantially different effects of DMOA on the two enantiomers of 2-phenylbutyrate imply different retention processes. One of them is obviously an ion-pairing process. The different influences of DMOA and TBA might imply that ion pairs of quaternary ammonium ions are too polar for an interaction with the uncharged chiral sites (*cf.*, Table V).

The retention increases with increasing pH for the two cations, homatropine and 2HPE (Table III). The simultaneous increase in α shows that the cationic solutes are retained by a stereoselective cation-exchanging site, which is in agreement with the results presented in Table I.

The aprotic TBA and the basic DMOA have slightly different effects on the cationic enantiomers but k' decreases in accordance with the relationships for retention by ion-exchange (eqn. 1) or ion-pair binding (eqn. 2). There is no significant change in the stereoselectivity for homatropine but a decrease in α for 2HPE.

Influence of enantiomeric and isomeric ionic additives

The effect of the counter ions is dependent on their configuration, as shown in Table IV. This implies binding to an uncharged site with chiral character.

It is of special interest that atropine and its quaternized derivatives interact differently with chiral counter ions, as shown in Table V. (*S*)-2-Phenylbutyrate does not give rise to stereoselective separation of methylatropine and isopropylatropine,

TABLE III

EFFECT OF CATIONIC MOBILE PHASE ADDITIVES ON RETENTION AND STEREOSELECTIVITY

Mobile phase: 3 m*M* additive and 1% 2-propanol in phosphate buffer.

Solute	Parameter	Variable					
		pH 6.0			pH 7.5		
		–	TBA	DMOA	–	TBA	DMOA
2-Phenylbutyrate	k'_1	1.28	0.62	1.34	0.15	0.12	0.15
	α	1.52	1.59	1.97	1.97	1.84	5.70
2HPE	k'_1	2.42	1.13	1.56	11.6	3.24	5.70
	α	1.80	1.62	1.79	2.58	1.87	2.28
Homatropine	k'_1	3.14	1.52	2.04	16.2	4.66	8.30
	α	1.24	1.24	1.27	1.41	1.40	1.48

TABLE IV

EFFECT OF COUNTER ION ON RETENTION AND STEREOSELECTIVITY

Mobile phase: 0.5 m*M* additive and 1% 2-propanol in phosphate buffer of pH 6.0.

Additive[a]	Atropine		Homatropine	
	k'_1	α	k'_1	α
–	2.24	1.00	1.97	1.34
(*S*)-2-phBA	2.71	3.34	2.46	1.58
(*R*)-2-phBA	1.81	1.57	1.94	1.08
(*S*)-3-phBA	3.27	1.38	3.24	1.05
(*R*)-3-phBA	3.17	1.15	2.98	1.16
4-phBA	2.24	1.16	2.28	1.17

[a] phBA = Phenylbutyric acid.

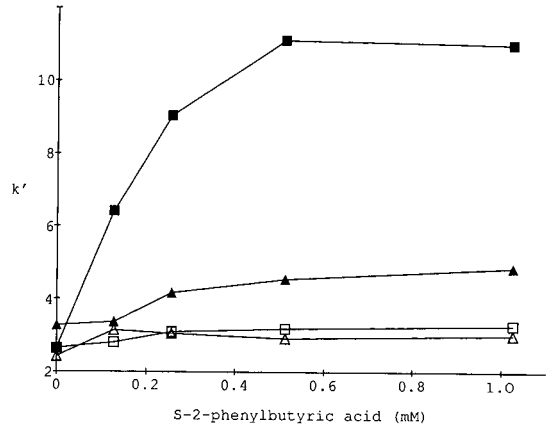

Fig. 2. Influence of (*S*)-2-phenylbutyric acid on capacity factors. Mobile phase: (*S*)-2-phenylbutyric acid + 1% 2-propanol in phosphate buffer (pH 6.0). Detection wavelength: 220 nm. □ = Atropine; △ = homatropine. Open symbols = k'_1; filled symbols = k'_2.

only a competitive interaction. As shown above, ion-pair binding is necessary for the chiral separation of atropine and it might be that ion pairs of quaternary ammonium ions are too polar for an interaction with the uncharged chiral site. Homatropine, which has its main stereoselective interaction with the cation-exchanging site, is easily separated in quaternized form.

Even counter ions with small structural differences can give different effects, as shown in two examples giving the retention as a function of the counter ion concentration. (*S*)-2-Phenylbutyrate (Fig. 2) gives with increasing concentration a retention increase for the second-eluted enantiomers that is typical of an ion-pair binding process, whereas the first-eluted enantiomers are almost unaffected. This indicates different retention processes for the two enantiomers, in accordance with the results obtained with octanoate as counter ion. The assumption of a synergistic process is supported by the chromatogram in Fig. 1. The system peaks are negative, which is one of the characteristics of an ion-pair distribution.

4-Phenylbutyrate gives a different pattern: the retention decreases for all the enantiomers, as is illustrated in Fig. 3. This might be due to competition at the uncharged site by an ion pair between the additive and a mobile phase cation. The chromatogram in Fig. 4 supports this view. The positive system peak before the solute peak is typical of a competitive interaction between solutes and an additive.

Chiral cations as additives can give large improvements in the stereoselectivity for cationic solutes. The effect of (−)-atropine is demonstrated in Table VI. The retention of all the cationic solutes decreases but the enantiomers are affected to a different extent as they are probably retained by different retention processes. This gives rise to a considerable improvement in the chiral separation of ipratropine, a quaternized atropine, whereas the

TABLE V

RETENTION AND STEREOSELECTIVITY OF ATROPINE, HOMATROPINE AND QUATERNIZED DERIVATIVES WITH AND WITHOUT (*S*)-2-PHENYLBUTYRATE AS MOBILE PHASE ADDITIVE

Mobile phase: 0.5 m*M* additive and 1% 2-propanol in phosphate buffer of pH 6.0. Performed on a Chiral-AGP column with a different batch number to that used in Table IV.

Solute	Additive			
	–		(*S*)-2-Phenylbutyrate	
	k'_1	α	k'_1	α
Atopine	2.5	1.0	2.7	3.2
Methylatropine	2.9	1.0	1.8	1.0
Ipratropine	4.6	1.0	3.1	1.0
Homatropine	2.7	1.3	2.5	1.6
Methylhomatropine	2.8	1.7	–	–

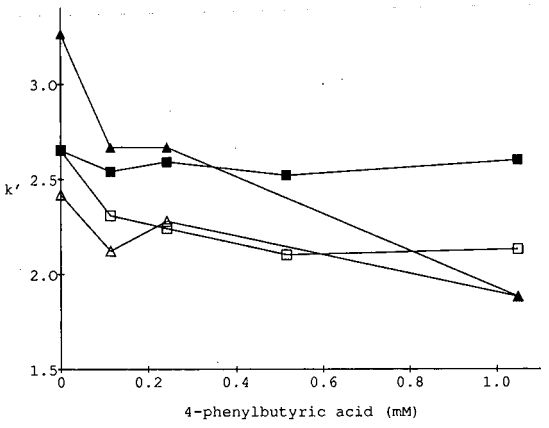

Fig. 3. Influence of 4-phenylbutyric acid on capacity factors. Mobile phase: 4-phenylbutyric acid + 1% 2-propanol in phosphate buffer (pH 6.0). Detection wavelength: 220 nm. Symbols as in Fig. 2.

effect on homatropine is the opposite, *i.e.*, a decrease in α. The retention of the (+)-atropine is also decreased when the (−)-antipode is present in the mobile phase.

The character of the site for the interaction of (−)-atropine cannot be elucidated from the results in Table VI, but some indications are given by studies with the enantiomers of uncharged methyl mandelate as mobile phase additive. These enantiomers, which have the same groups at the chiral carbon as homatropine, are easily separated on the AGP phase with $\alpha = 1.5$. As mobile phase additives they give rise to a decrease in the retention of

TABLE VI

EFFECT OF RETENTION AND STEREOSELECTIVITY USING (−)-ATROPINE AS MOBILE PHASE ADDITIVE

Mobile phase: additive and 1% 2-propanol in phosphate buffer of pH 6.0.

Solute	Additive			
	−		(−)-Atropine (0.55 m*M*)	
	k'_1	α	k'_1	α
Ipratropine	4.6	1.0	2.4	1.5
Homatropine	2.7	1.3	2.0	1.3
Atropine (racemic)	2.8	1.0	1.6[a]	1.3

[a] System peak.

homatropine, atropine and their quaternized derivatives, but no chiral separation for atropine and its derivative is achieved and only a decrease in α for the other solutes. It seems that an additive with a competitive effect must interact at a charged chiral site to give rise to improvements in the stereoselectivity for this group of compounds.

Indirect detection of enantiomers

A detectable mobile phase additive can give rise to indirect detection effects that provide information about the retention processes. Fig. 5 shows the effects on cations in a system with the counter ion, (*S*)-2-phenylbutyrate, as detectable component. The

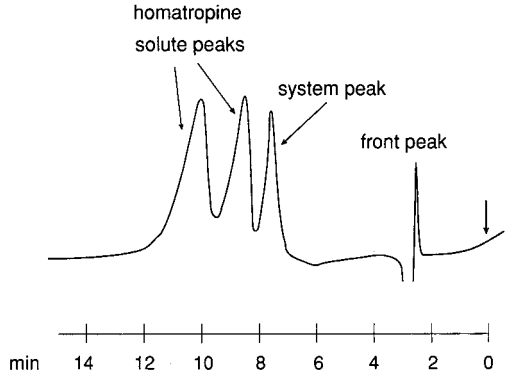

Fig. 4. Resolution of homatropine enantiomers. Mobile phase: 0.5 m*M* 4-phenylbutyric acid + 1% 2-propanol in phosphate buffer (pH 6.0). Detection wavelength: 220 nm.

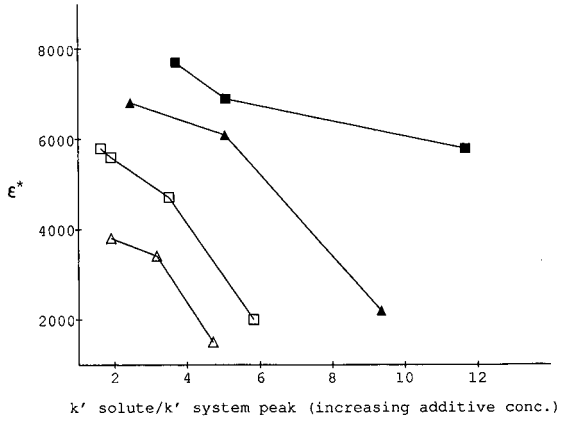

Fig. 5. Effects of (*S*)-2-phenylbutyrate on the apparent molar absorptivity for atropine and homatropine. Symbols, mobile phase and detection wavelength as in Fig. 2.

apparent molar absorptivity, ε^*, is calculated from the peak area and the amount of solute injected [11]. It is given as a function of the increase in relative retention, $k'_{\text{enantiomer}}/k'_{\text{main system peak}}$ occurring with an increase in the counter ion concentration.

Fig. 5 shows that ε^* decreases with increasing counter ion concentration, which is in accordance with the theory of ion-pairing systems with an adsorbing stationary phase [5]. However, on the AGP-phase the last-eluted enantiomer has a significantly higher ε^* than the first-eluted enantiomer. This is an important deviation from the effects appearing in a system with an adsorbing stationary phase, where the component eluted closer to the system peak is more influenced by interaction effects and has a higher ε^*. The results in Fig. 5 give further support to the view that the enantiomers of a solute are bound by different processes, *e.g.*, to sites with different fractional loadings of an anionic additive.

CONCLUSIONS

The stereoselectivity on silica-bonded AGP is due to ion-exchanging and ion-pairing processes and the effect is highly dependent on the structure of the solute. Small structural differences can alter the dominant chiral interaction, as shown by the solute pairs atropine–homatropine and 2HPE–4HPE. The retention and stereoselectivity are affected by different kinds of ions from hydrophilic buffers to hydrophobic cations and anions. Counter ions to the solute can improve the stereoselectivity by both increasing and decreasing the retention. Enantiomers of charged chiral additives can give stereoselectivity for new classes of compounds, *e.g.*, quaternized atropine derivatives, but their effect is also highly dependent on the configuration.

REFERENCES

1 J. Hermansson and G. Schill, in M. Zief and L. J. Crane (Editors), *Chromatographic Chiral Separation*, Marcel Dekker, New York, 1987, p. 245.
2 K. Schmid, in F. W. Putnam (Editor), *The Plasma Proteins*, Academic Press, New York, 1975, p. 184.
3 E. Arvidsson, S.-O. Jansson and G. Schill, *J. Chromatogr.*, 506 (1990) 579.
4 G. Schill, I. Wainer and S. Barkan, *J. Chromatogr.*, 365 (1986) 73.
5 J. Crommen, G. Schill, D. Westerlund and L. Hackzell, *Chromatographia*, 24 (1987) 252.
6 E. Arvidsson, J. Crommen, G. Schill and D. Westerlund, *Chromatographia*, 24 (1987) 460.
7 A. Sokolowski and K.-G. Wahlund, *J. Chromatogr.*, 189 (1980) 299.
8 D. L. Massart, B. G. M. Vandeginste, S. N. Deming, Y. Mechotte and L. Kaufman, *Chemometrics: a Textbook* (*Data Handling in Science and Technology*, Vol. 2), Elsevier, Amsterdam, 1988, p. 271.
9 G. E. P. Box, W. G. Hunter and J. S. Hunter, *Statistics for Experimenters —An Introduction to Design, Data Analysis and Model Building*, Wiley, New York, 1978, p. 327.
10 K. Balmér, B.-A. Persson and G. Schill, *J. Chromatogr.*, 477 (1989) 107.
11 L. Hackzell and G. Schill, *Chromatographia*, 15 (1982) 437.

Journal of Chromatography, 591 (1992) 65–73
Elsevier Science Publishers B.V., Amsterdam

CHROM. 23 796

Direct liquid chromatographic separation of enantiomers on immobilized protein stationary phases

IX. Influence of the cross-linking reagent on the retentive and enantioselective properties of chiral sorbents based on bovine serum albumin

Shalini Andersson*

Department of Chemistry, University of Linköping, S-581 83 Linköping (Sweden)

Richard A. Thompson and Stig G. Allenmark

Laboratory of Microbiological Chemistry, University of Gothenburg, Guldhedsgatan 10A, S-413 46 Gothenburg (Sweden)

(First received May 22nd, 1991; revised manuscript received October 8th, 1991)

ABSTRACT

Three modifications of silica-bound, cross-linked bovine serum albumin (BSA) were evaluated as chiral sorbents for use in the liquid chromatographic separation of enantiomers. Glutaraldehyde, formaldehyde and di-(N-succinimidyl) carbonate were used as bifunctional reagents for the immobilization of BSA. The sorbents all contain the same loading of BSA (14.4 ± 0.1%, w/w) and differ only with respect to the cross-linker used for immobilization. Despite their apparent similarity, the sorbents show very different chromatographic properties, not only with respect to retention of analyte enantiomers (k' and α), but also with respect to column efficiency (affecting R_s values). The data obtained indicate that the chemical structure of the cross-linking reagent affects to a large extent the accessibility of important chiral binding sites. Although the data obtained are difficult to interpret in any detail, certain generalizations concerning the different behaviour of the sorbents can be made.

INTRODUCTION

Chiral stationary phases (CSPs) based on bovine serum albumin (BSA) have been used for the reversed-phase separation of a variety of enantiomers [1–3]. A number of different techniques have been described for the immobilization of BSA to silica, *e.g.*, adsorption, covalent binding and entrapment by cross-linking of the protein [4–9]. The retention behaviour and the enantioselectivity of chiral compounds were found to be highly influenced by the choice of the immobilization technique; indeed, in some instances a total loss of chiral recognition was observed [5,9]. For the past few years we have been working with glutaraldehyde-cross-linked BSA sorbents which have shown high stability towards organic solvents. However, the increase in hydrophobicity of these sorbents due to incorporation of the cross-linking reagent was generally found to give undesirably longer retention times [6,8].

One of our aims has been to decrease the degree of achiral hydrophobic interaction generated by the cross-linking reagent, since theoretically this would lead to decreased capacity factors (k') and larger

0021-9673/92/$05.00

separation factors, provided that the chiral binding sites of BSA are unaffected. For this purpose, three different cross-linking reagents were used under otherwise equivalent conditions for the entrapment of BSA in 3-aminopropylsilica. The prepared sorbents were evaluated with respect to their retentive and enantioselective properties for a number of racemic compounds.

EXPERIMENTAL

Chemicals

The benzodiazepinones (**Ia–d**) were obtained from the Department of Drug Control, Biomedical Centre, Uppsala University. Albendazole S-oxide (SO.ABZ) and its structural analogues (**IIa–d**) were kindly supplied by Professor P. Delatour (Charbonnieres, France). Racemic tryptophan (**III**) and methaqualone {2-methyl-3-(*o*-tolyl)-4[3*H*]-quinazolinone} (**VI**) were obtained from Sigma (St. Louis, MO, USA). (±)-Benzoin and di-(N-succinimidyl) carbonate (DSC) were purchased from Fluka (Buchs, Switzerland). Both formaldehyde (FA) and glutaraldehyde (GLA) solutions (Merck, Darmstadt, Germany) were diluted with water to give 5% solutions before use. Bovine serum albumin (BSA) was obtained from Sigma. The spherical 3-aminopropylsilica (100 Å, 7 μm), was a gift from EKA Nobel (Surte, Sweden).

Structures of compounds **III–VII** are given in Fig. 1.

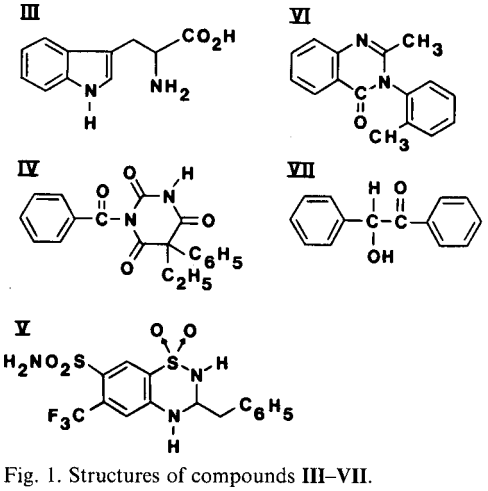

Fig. 1. Structures of compounds **III–VII**.

Preparation of BSA–silica sorbents

Three different BSA-based stationary phases (CSPs I–III) were prepared under equivalent experimental conditions. CSP I was glutaraldehyde-cross-linked BSA entrapped in 3-aminopropylsilica (BSA–GLA sorbent); BSA/g silica, 143 mg (nitrogen analysis) and 147 mg (suphur analysis). CSP II was formaldehyde-cross-linked BSA entrapped in 3-aminopropylsilica (BSA–FA sorbent); BSA/g silica, 144 mg (nitrogen analysis) and 146 mg (sulphur analysis). CSP III was BSA cross-linked into 3-aminopropylsilica using N-succinimidyl carbonate (BSA–DSC sorbent); BSA/g silica, 143 mg (nitrogen analysis) and 146 mg (sulphur analysis).

CSPs I and II were obtained using the procedure described previously [8,9]. BSA–DSC sorbent was prepared as follows: BSA (1 g) dissolved in 0.1 *M* phosphate buffer (pH 7.0, 1% of (2-propanol) and 3-aminopropylsilica (2 g) were ultrasonicated for 3 min. Thereafter, the slurry was agitated overnight at room temperature for 24 h, 1 g of DSC suspended in buffer was added and the slurry agitated overnight at 35°C, isolated and washed thoroughly with 0.1 *M* phosphate buffer (pH 7) containing 40% of 2-propanol. The sorbents were then resuspended and packed into 125 × 4 mm I.D. columns as described previously [8].

Liquid chromatography

Chromatography at ambient temperature was performed using an LKB Model 2150 pump, a Rheodyne Model 7125 injection valve with a 20-μl loop and an LKB Model 2151 variable-wavelength UV detector. The mobile phase was a phosphate buffer containing 0–7% of 2-propanol. All chromatography was carried out under isocratic conditions. Retention times and peak areas were obtained using a Waters Model 740 electronic integrator interfaced with the detector.

Sorbent analysis

The amount of BSA incorporated into the silica was determined from elemental analysis data (NS) for the dried materials. The 3-aminopropylsilica used contained 1.84% (w/w) of nitrogen.

RESULTS AND DISCUSSION

The amount of BSA per gram of silica is approxi-

mately the same (14.4 ± 0.1%, w/w) in all the three BSA sorbents studied. This indicates that the steps in the preparation of the packing material prior to the addition of the cross-linking reagent determine to a large extent the amount of protein loaded into the silica. Hence the choice of the cross-linking reagent for the immobilization of BSA is of minor importance.

As the loading of BSA is the same, one can assume that the difference in retention and availibility of chiral binding sites for solutes chromatographed on the CSPs can be mainly attributed to the chemical structure of the cross-linker and to changes in protein conformation as a result of cross-linking. One would also expect the degree of achiral hydrophobic interaction generated by the cross-linking reagent to increase in the order DSC < FA < GLA.

Column performance

The column performance was evaluated using *p*-nitroaniline as the analyte. Asymmetry factors (*asf*) and plate heights (*h*) were calculated and plotted as shown in Fig. 2a and b. These results indicate that the BSA–DSC column has a lower column efficiency than the other two types of columns. Further, the BSA–FA sorbent shows the highest column load threshold. Similar results were found for racemic oxazepam (see Fig. 5), which will be discussed later.

The type of organic modifier added to the mobile phase was generally found to affect both the plate height and asymmetry factors. Hence the use of aprotic solvents such as acetonitrile results in better column efficiency and peak shape.

Influence of the cross-linking reagent on the retention and enantioseparation of different compounds on BSA sorbents

*Benzodiazepinones (**Ia–d**).* The benzodiazepinones (**Ia–d**) were generally found to be less retained on BSA–DSC columns, which was in accordance with expectation as this material was assumed to be the least hydrophobic. Further, the use of DSC as a cross-linker also leads to the highest separation factors (α) for three of the diazepinones studied (Table I). It is interesting that substitution of the amide hydrogen in lorazepam (**Ib**) with a methyl group results in a total loss of chiral recognition on the BSA–DSC and BSA–GLA sorbents, indicating participation of the amide hydrogen atom in the binding to BSA and that this is crucial for the enantiodiscrimination on these sorbents. This is not so, however, for the BSA–FA sorbent, on which lormetazepam (**Ic**) is well resolved, even if there is a decrease in the α value compared with lorazepam. One may therefore conclude that the enantioselective properties of the BSA–FA column differ substantially from those of the other two

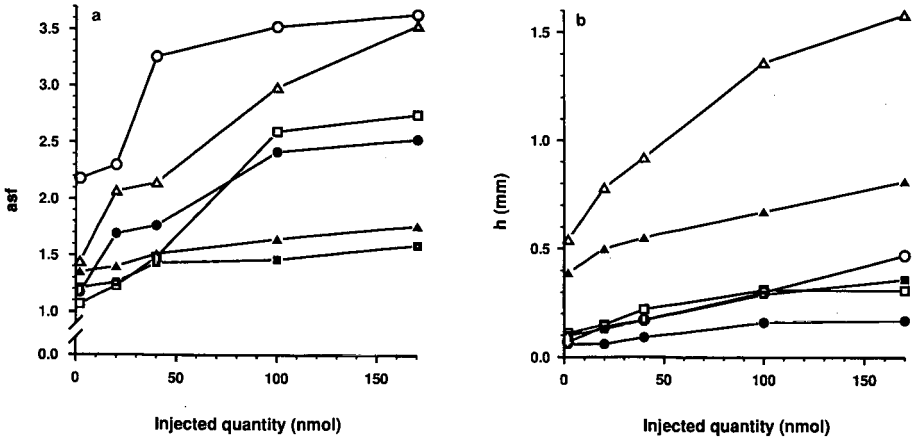

Fig. 2. Dependence of (a) peak symmetry and (b) plate height on column load and eluent composition on three different types of BSA-based columns. Mobile phase, 50 m*M* phosphate buffer (pH 7.2) containing 5% of organic modifier; flow-rate, 1.0 ml/min; UV detection, 254 nm; solute, *p*-nitroaniline. Organic modifier 2-propanol: △ = BSA–DSC; ○ = BSA–FA; □ BSA–GLA column. Organic modifier acetonitrile: ▲ = BSA–DSC; ● = BSA–FA; ■ = BSA–GLA column.

TABLE I

INFLUENCE OF CROSS-LINKING REAGENT ON RETENTION AND RESOLUTION OF BENZODIAZEPINONES ON BSA SORBENTS

Mobile phase, 50 m*M* phosphate buffer (pH 7.1) containing 7% of 2-propanol; flow-rate, 1.0 ml/min; column, 125 × 4 mm I.D.; amount injected, 4 nmol; UV detection at 230 nm. Solute structure:

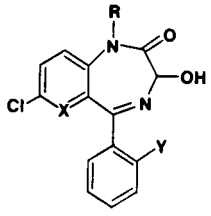

No.	Compound	BSA–DSC			BSA–FA			BSA–GLA		
		k'_1	α	R_s	k'_1	α	R_s	k'_1	α	R_s
Ia	Oxazepam (R = H, X = CH, Y = H)	4.38	5.78	5.69	5.87	5.16	9.10	5.70	3.53	7.16
Ib	Lorazepam (R = H, X = CH, Y = Cl)	6.86	2.33	2.46	9.80	1.69	2.52	8.47	2.11	3.66
Ic	Lormetazepam (R = CH_3, X = CH, Y = Cl)	5.86	1.0	–	5.66	1.44	1.75	6.63	1.0	–
Id	Lopirazepam (R = H, X = N, Y = Cl)	1.36	3.33	2.53	1.75	2.54	3.71	2.07	2.30	3.72

types of columns. It is therefore reasonable to assume that accessibility to the various chiral binding sites is dependent on the type of cross-linking reagent used in the immobilization procedure.

Further, the low efficiency of BSA–DSC columns results in lower resolution (R_s) values. Lopirazepam (**Id**), for example, is least resolved on the BSA–DSC column even though it is best separated on this column (Fig. 3).

*Albendazole sulphoxide and structural analogues (**IIa–d**).* The parent compound albendazole sulphoxide (**IIa**) and the free amine (**IIb**) were retained on all three types of columns but were resolved only on the BSA–FA column and then only partially. Fig. 4 shows the enantioseparation of *rac*-albendazole sulphoxide. Substitution of the propyl group for a phenyl group (**IIc** and **d**) has a marked effect on the enantioseparation of these compounds, the largest α values being obtained on a BSA–DSC column (Table II). However, the low column efficiency of the BSA–DSC column leads to low R_s values for these compounds. The BSA–FA column shows a drastic increase in retention for **IIc** and **IId**, indicat-

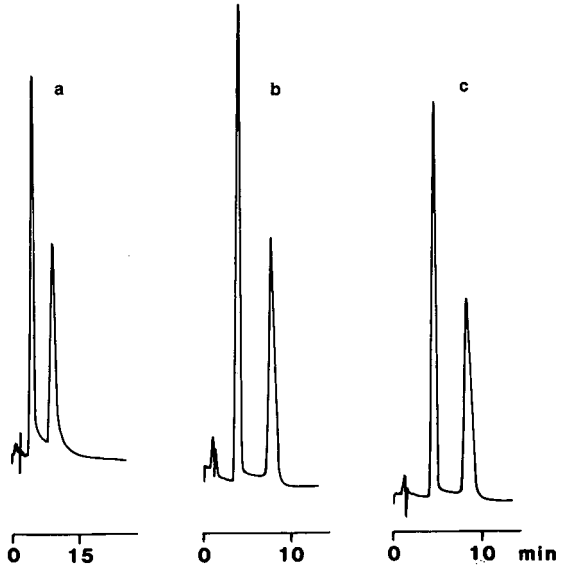

Fig. 3. Optical resolution of *rac*-lopirazepam (**Id**) on (a) BSA–DSC, (b) BSA–FA and (c) BSA–GLA columns. Mobile phase, 50 m*M* phosphate buffer (pH 7.1) containing 7% of 2-propanol; flow-rate, 1.0 ml/min; UV detection, 230 nm; amount injected, 4 nmol.

Fig. 4. Separation of enantiomers of *rac*-albendazole sulphoxide (**IIa**) on BSA–FA column. Mobile phase, 50 m*M* phosphate buffer (pH 7.7) containing 2% of methanol; flow-rate, 1.0 ml/min; detection UV 254 nm; amount injected, 4 nmol.

ing and the hydrophobic interaction between the solute and the CSP is strengthened; however, the enantioseparation is not significantly affected. One can therefore assume that the aromatic ring at the asymmetric centre is a prerequisite for chiral discrimination on the BSA–GLA and BSA–DSC sorbents but not on the BSA–FA sorbent. The free amines (**IIb** and **d**) were generally retained more strongly, indicating that hydrogen bonding is also involved in the retention process.

Miscellaneous compounds. As shown in Table III, under basic mobile phase conditions (pH 7.7), the BSA–DSC sorbent gives very large α values for compounds displaying acidic character, *i.e.*, D,L-tryptophan (**III**), benzonal (**IV**) and bendroflumethiazide (**V**). This indicates that the charged groups in the solutes can interact more easily with the protein when DSC is the cross-linking reagent, leading to an increase in enantiodiscrimination. Tryptophan, which is amphoteric, is best separated on the BSA–GLA column, however.

Earlier studies of methaqualone (**VI**) and benzoin (**VII**) have shown that the dominant interaction between the solute and BSA-based CSPs is hydrophobic in character [10]. The BSA–FA sorbent was found to interact more strongly with these compounds, which is reflected in both the k' and α values. The α values of **VI** and **VII** decrease in the series FA > DSC > GLA used as cross-linking reagents.

TABLE II

CHROMATOGRAPHIC DATA OBTAINED ON DIFFERENT BSA COLUMNS FOR ALBENDAZOLE SULPHOXIDE AND STRUCTURAL ANALOGUES

Mobile phase, 50 m*M* phosphate buffer (pH 7.7) containing 2% of 2-propanol; flow-rate, 1.0 ml/min; column, 125 × 4 mm I.D.; amount injected, 4 nmol; UV detection at 254 nm. Solute structure:

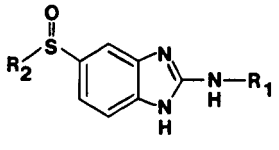

No.	Compound	BSA–DSC			BSA–FA			BSA–GLA		
		k'_1	α	R_s	k'_1	α	R_s	k'_1	α	R_s
IIa	$R_1 = COOCH_3$ $R_2 = C_3H_7$	0.86	1.0	–	1.03	1.69	0.72	0.96	1.0	–
IIb	$R_1 = H$ $R_2 = C_3H_7$	1.33	1.0	–	1.28	1.42	1.08	1.46	1.0	–
IIc	$R_1 = COOCH_3$ $R_2 = C_6H_5$	5.06	1.85	1.11	23.1	1.20	0.87	6.42	1.57	1.44
IId	$R_1 = H$ $R_2 = C_6H_5$	6.59	1.70	1.46	19.3	1.40	2.02	7.47	1.55	2.52

TABLE III

OPTICAL RESOLUTION DATA FOR VARIOUS COMPOUNDS ON DIFFERENT BSA SORBENTS

Mobile phase, 50 m*M* phosphate buffer (pH 7.7) containing 2-propanol; flow-rate, 1.0 ml/min; column, 125 × 4 mm I.D.; amount injected, 4 nmol.

Compound	2-Propanol (%)	BSA–DSC			BSA–FA			BSA–GLA		
		k'_1	α	R_s	k'_1	α	R_s	k'_1	α	R_s
III	2	1.34	6.71	4.34	0.50	2.02	1.96	0.90	9.24	5.27
IV	5	25.8	1.47	1.85	28.3	1.40	1.73	32.5	1.12	0.56
V	5	8.19	1.79	1.63	10.1	1.16	1.07	9.04	1.47	2.04
VI	2	3.93	1.29	0.67	4.08	1.50	1.68	3.42	1.20	0.74
VII	5	3.85	2.60	2.62	5.05	3.09	3.56	3.93	2.23	3.70

TABLE IV

INFLUENCE OF ORGANIC MOBILE PHASE ADDITIVES ON RETENTION AND COLUMN EFFICIENCY

Mobile phase, 50 m*M* phosphate buffer (pH 7.7) containing 2% of organic modifier; flow-rate, 1.0 ml/min; column, 125 × 4 mm I.D., amount injected, 4 nmol.

CSP	Solute	Organic modifier	k'_1	α	R_s	h_1 (mm)	h_2 (mm)
BSA—DSC	Methaqualone	Methanol	5.83	1.18	0.40	1.02	0.88
		Acetonitrile	4.58	1.24	0.49	0.87	1.08
		2-Propanol	3.93	1.29	0.67	0.63	0.61
	SO.ABZ.NH_2 (**IIb**)	Methanol	8.15	1.47	1.15	0.62	0.51
		Acetonitrile	6.92	1.50	1.17	0.53	0.70
		2-Propanol	6.59	1.70	1.46	0.52	0.64
	D,L-Tryptophan	Methanol	1.21	14.0	5.03	0.24	0.42
		Acetonitrile	0.69	11.2	4.21	0.32	0.29
		2-Propanol	1.34	6.71	4.34	0.24	0.57
BSA–FA	Methaqualone	Methanol	7.41	1.31	1.09	0.40	0.30
		Acetonotrile	5.17	1.39	1.39	0.29	0.24
		2-Propanol	4.08	1.50	1.68	0.30	0.23
	SO.ABZ.NH_2 (**IIb**)	Methanol	28.7	1.62	2.71	0.15	0.16
		Acetonitrile	18.0	1.54	2.56	0.14	0.14
		2-Propanol	19.3	1.40	2.02	0.16	0.14
	D,L-Tryptophan	Methanol	0.56	2.54	2.08	0.23	0.98
		Acetonitrile	0.48	2.10	2.03	0.13	0.24
		2-Propanol	0.50	2.02	1.96	0.13	0.60
BSA–GLA	Methaqualone	Methanol	5.48	1.19	0.88	0.19	0.40
		Acetonitrile	4.66	1.18	1.09	0.11	0.15
		2-Propanol	3.42	1.20	0.74	0.26	0.35
	SO-ABZ.NH_2 (**IIb**)	Methanol	9.46	1.44	2.19	0.13	0.21
		Acetonitrile	7.01	1.46	2.63	0.09	0.16
		2-Propanol	7.47	1.55	2.52	0.13	0.18
	D,L-Tryptophan	Methanol	1.30	11.1	5.73	0.17	1.19
		Acetonitrile	0.76	6.93	5.75	0.12	0.33
		2-Propanol	0.90	9.24	5.27	0.18	0.66

Effect of organic modifiers in the mobile phase on retention and resolution on BSA-based CSPs

The use of glutaraldehyde as a cross-linking reagent for the immobilization of BSA results in a more "hydrophobic" sorbent compared with BSA–DSC and BSA–FA sorbents. To gain further insight into the behaviour of the CSPs, a study of the hydrophobic interaction between structurally different solutes and BSA sorbents was conducted by using different organic mobile phase additives.

The chirality of metaqualone (**VI**) is generated by restricted internal rotation in the molecule. As already mentioned, the dominant interaction between this compound and BSA is hydrophobic, which can be seen in that the lowest k' values are obtained for the most hydrophobic mobile phase additive, 2-propanol. With the BSA–FA column, 2-propanol as mobile phase additive also leads to the highest enantioseparation and resolution of methaqualone, mainly owing to the faster elution of the first enantiomer (Table IV). A similar behaviour is seen on the BSA–DSC column.

This is not the case on the BSA–GLA column, where the α values remain basically the same irrespective of the hydrophobicity of the mobile phase additive. However, there is a marked increase in resolution when acetonitrile is used as the retention modifier, mainly owing to a large increase in column efficiency. It is interesting that although the enantioseparation of methaqualone on the BSA–DSC column is greater than or equal to that on the BSA–GLA sorbent, the low column efficiency of the former leads to unexpectedly low R_s values on the BSA–DSC column.

As mentioned previously, both the free amino group and the aromatic phenyl group at the chiral centre participate in the retentive process of the basic compound **IId**, a structural analogue of albendazole sulphoxide. Retention on the BSA–DSC sorbent decreases with increasing eluting power of the organic modifier in the mobile phase, especially for the first-eluted enantiomer. Consequently, α increases with increasing hydrophobicity of the mobile phase modifier (Table IV). The more hydrophobic sorbents, BSA–FA and BSA–GLA, show an interesting retention behaviour, namely that both enantiomers of **IId** are less retained when acetonitrile is used instead of 2-propanol as the mobile pase modifier. However, the effect on enantioselectivity is different on the two sorbents. On the BSA–GLA column, α increases with increasing hydrophobicity of the mobile phase additive whereas α decreases on the BSA–FA column. The latter is mainly due to faster elution of the last-eluted enantiomer.

We have reported previously the enantioseparation of D,L-tryptophan on BSA sorbents [11]. The interaction between tryptophan and the protein is highly pH dependent and separation is afforded at basic pH (>7.5). The large α value attained (Table IV) reflects the presence of a specific indole binding site on BSA, which has a very high affinity for the D-enantiomer [12]. In contrast to the two earlier compounds (**IIb** and **VI**), the DSC-cross-linked BSA sorbent displays the largest enantioselectivity towards tryptophan ($\alpha \geqslant 6.7$). All three columns show a similar retention behaviour, *i.e.*, D,L-tryptophan is least retained on BSA sorbents when acetonitrile is the organic modifier in the mobile phase. However, the enantioseparation of tryptophan is affected differently on these sorbents; on BSA–DSC and BSA–FA columns, α decreases with increasing hydrophobicity of the mobile phase additive whereas on the BSA–GLA column α decreases on using acetonitrile as a mobile phase modifier (Table IV). Further, there is a drastic decrease in the enantioseparation of tryptophan on the BSA–FA column ($\alpha \approx 2$) compared with the other two types of sorbents. One can therefore assume that the availibility of the indole binding site is restricted when formaldehyde is used as a cross-linking reagent.

Influence of column load on peak symmetry and column efficiency

The binding capacity of protein columns is relatively low owing to the small part of the molecule actually involved in the chiral recognition process [13]. At small amounts of solute injected (<10 nmol) there is no significance difference in the extent of deterionation of the peak symmetry of the enantiomers of oxazepam and plate height on the three different columns (Fig. 5a and b). However, as the column load increases, the peaks show increasing tailing and at injected solute quantities $\geqslant 40$ nmol a tendency towards fronting and thereby an overall lower peak asymmetry factor is found for all the three types of BSA columns. The last-eluted peak on the BSA–GLA column, however, shows

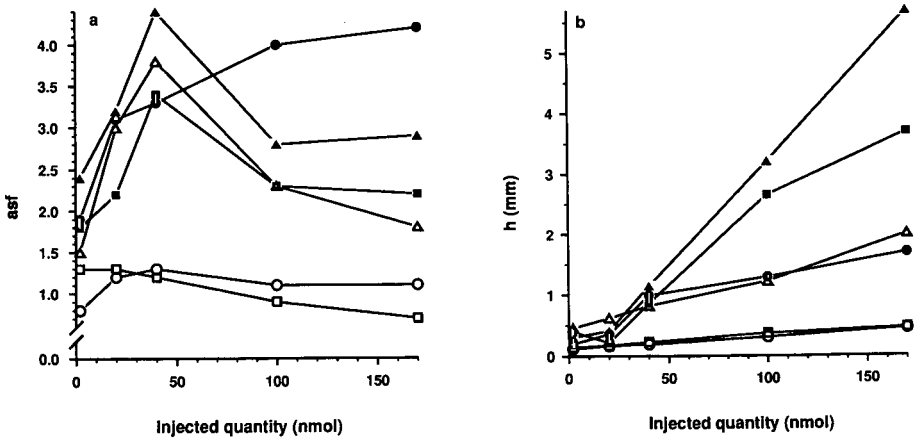

Fig. 5. Influence of column load on (a) peak symmetry and (b) plate height of *rac*-oxazepam. Column: △,▲ = BSA–DSC; ○,● = BSA–FA; □,■ = BSA–GLA. Open symbols represent the first-eluted enantiomer. Mobile phase, 50 m*M* phosphate buffer (pH 7.1) containing of 7% of 2-propanol; flow-rate, 1.0 ml/min; UV detection, 230 nm.

increasing tailing with increasing amounts of injected solute. These results are in general agreement with the binding model suggested by Guiochon and co-workers [13,14], *i.e.*, there are two types of binding sites on BSA, one of which is chiral selective and the other a non-selective binding site having a roughly ten times larger capacity. Hence, as the column load increases, the stereoselective site is saturated and the non-selective binding sites begin to contribute in the retention process. This phenomenon could also explain the peak fronting observed as the column load increases.

CONCLUSIONS

The hydrophobicity of the cross-linking reagent used for immobilization of BSA is reflected by the retentive properties of the BSA-based sorbents. The least hydrophobic sorbent, BSA–DSC, was generally found to show the lowest k' values and high enantioselectivity, particularly for acidic compounds. However, the low column efficiency displayed by this type of sorbent results in broader peaks and consequently low R_s values. Further, the enantioselective properties of BSA sorbents are greatly affected by the choice of the cross-linking reagent used during the immobilization procedure. The BSA–FA sorbent displays substantially different enantioselectivity to the BSA–DSC and BSA–GLA columns. One can assume that during the immobilization procedure the protein attains different conformations with different cross-linking reagents and as a result availibility of some of the chiral binding sites is affected.

The type of organic modifier in the mobile phase was found to influence not only retention and enantioselectivity but also column efficiency and peak shape. Generally, an aprotic solvent such as acetonitrile was found to give better peak symmetry and higher column efficiency. Further, of the three cross-linked sorbents, the BSA–FA column had the highest capacity.

ACKNOWLEDGEMENT

This work was supported by the Swedish Natural Science Research Council (K-KU 2508-300).

REFERENCES

1 C. Lagercrantz, T. Larsson and I. Denfors, *Comp. Biochem. Physiol.*, 690 (1981) 375.
2 S. Allenmark, *Chromatographic Enantioseparation: Methods and Applications*, Ellis Horwood/Wiley, Chichester, New York, 2nd ed., 1991, pp. 130–132.
3 I. W. Wainer, *J. Pharm. Biomed. Anal.*, 7 (1989) 1033.
4 S. Allenmark, B. Bomgren and H. Borén, *J. Chromatogr.*, 264 (1983) 63.

5 P. Erlandsson, L. Hansson and R. Isaksson, *J. Chromatogr.*, 370 (1986) 475.
6 M. Aubel and L. B. Rogers, *J. Chromatogr.*, 392 (1987) 415.
7 J. Vindevogel, J. Van Dijck and M. Verzele, *J. Chromatogr.*, 447 (1988) 297.
8 R. A. Thompson, S. Andersson and S. Allenmark, *J. Chromatogr.*, 465 (1989) 263.
9 S. Andersson, S. Allenmark, P. Erlandsson and S. Nilsson, *J. Chromatogr.*, 498 (1990) 81.
10 S. Allenmark and S. Andersson, *Chirality*, 1 (1989) 154.
11 S. Allenmark, B. Bomgren and H. Borén, *J. Chromatogr.*, 316 (1984) 617.
12 K. K. Stewart and R. F. Doherty, *Proc. Natl. Acad. Sci. U.S.A.*, 70 (1973) 2850.
13 S. Jacobson, S. Golshan-Shirazi and G. Guiochon, *J. Am. Chem. Soc.*, 112 (1990) 6492.
14 S. Jacobson, S. Golshan-Shirazi and G. Guiochon, *J. Chromatogr.*, 522 (1990) 23.

Journal of Chromatography, 591 (1992) 75–88
Elsevier Science Publishers B.V., Amsterdam

CHROM. 23 767

Physico-chemical properties of electron-acceptor stationary phases in liquid chromatography

Kenneth J. Welch☆ and Norman E. Hoffman*

Chemistry Department, Marquette University, Milwaukee, WI 53233 (USA)

(First received July 30th, 1991; revised manuscript received September 24th, 1991)

ABSTRACT

Some new electron-acceptor (EA) stationary bonded phases (BPs) for liquid chromatography were synthesized and compared with existing EA BPs. The following EA BPs were compared: dinitrophenylmercaptopropylsilica (DNPMP); dinitrodibenzoylmercaptopropylsilica (DNBMP); dinitroanilinopropylsilica (DNAP); dinitrobenzamidopropylsilica (DNBAP); tetranitrofluoreniminopropylsilica (TNFP); tetranitrodibenzosuberiminopropylsilica (TNDBSP); trinitrophenylmercaptopropylsilica (TNPMP); pentafluorophenylsilica (PFPh); aminopropylsilica (NH_2) and Nucleosil 5-NO_2 (5-NO_2). Entropy–enthalpy compensation data indicated that the mechanism of retention (first six BPs) was the same for planar and non-planar aromatic solutes, but it was less informative than the vector-analysis techniques of linear correlation coefficient and Euclidian distance calculations. The latter provided a quantitative comparison of the BPs. All EA BPs had close similarity except for TNFP. NH_2 and 5-NO_2 were similar to the EA BPs. PFPh was not similar to the other EA BPs. The EA BPs were also examined for their ability to group aromatic solutes of similar ring size regardless of alkyl substitution. A new performance parameter, R_r (group resolution), was proposed and applied to these data. Using the calculated values for R_r, the group-resolution effectiveness of the various BP followed the sequence DNAP ≫ DNPMP, TNPMP, 5-NO_2 > TNDBSP, DNBMP, DNBAP > NH_2 > TNFP ≫ PFPh. Retention of aromatic solutes as a function of planarity was also investigated. DNPMP was found to be slightly better than DNAP at separating bridged biphenyls.

INTRODUCTION

Bonding electron-acceptor (EA) groups to silica produces a stationary bonded phase (BP) for effective class separation of polycyclic aromatic hydrocarbons (PAHs) by high-performance liquid chromatography (HPLC). A variety of EA phases have been developed; however, the most common EA phases consist of nitroaromatic molecules bonded to silica via a suitable linking group [1]. Examples of these EA phases include nitrated fluoreniminopropyl [2–5], 2,4-dinitroanilinopropyl [5–12], 2,4-dinitroanilinooctyl [11], picramidopropyl [10–15], picramidooctyl [11], 3,5-dinitrobenzenesulphamidopropyl [10] and 3,5-dinitrobenzamidopropyl [10,16] silicas. The EA phases based on bonded dinitrophenyl or picryl groups have been preferred over the nitrofluorenyl EA phases because they exhibit less peak asymmetry and less selectivity within PAH class types [2,5].

The length of the alkyl group attaching the EA group to the silica surface has had little effect on the grouping of PAH classes [11]. When non-polar solvents are used, the solvophobic electron-acceptor groups remain adsorbed on the silica surface regardless of the size of the linking group.

With EA groups bonded to aminopropylsilica, an acidic hydrogen is available for silanophilic interactions with the surface or for secondary polar interaction with the analyte. The significance of this has not been investigated; however, there are a few EA phases that have been made using linking groups not based on aminopropylsilica: picryl propyl ether-silica [17], dinitrophenylmercaptopropylsilica [18],

☆ Present address: Scientific Support and Government Affairs Division, S. C. Johnson and Son, Inc., Racine, WI 53403-5011, USA.

0021-9673/92/$05.00

dinitrobenzoylmercaptopropylsilica [18] and picrylmercaptopropylsilica [18].

A model for the retention of aromatics on EA phases may be extrapolated from the observations of electron donor–acceptor (or charge-transfer) complexes in solutions [19], in solids [20] and liquid–solid adsorption chromatography (LSC) [21–24]. The retention process consists of displacing sufficient mobile phase molecules to allow the formation of a localized electron donor–acceptor (EDA) complex between a π-electron donor (π-base) solute molecule and a bonded π-electron acceptor (π-acid) group in approximately parallel planes at a short distance (*ca.* 3 Å) [19,20]. An EDA model for chromatography was inferred from the observed correlation between ln k' values (k' = capacity factor) and the first ionization energies for electron-donor molecules. This model was in agreement with the charge-transfer UV spectrum of a solution of anthracene and 2,4-dinitrophenylanilinoethane [9]. Later, a charge-transfer spectrum was observed in the photoacoustic spectrum of anthracene adsorbed on picramidopropylsilica [25]. EDA complex formation is reversible and rapid with a heat of formation of less than 6 kcal/mol [4,8]. The net free-energy change is the sum of the energies of interaction for each group in the donor molecule (*e.g.*, the π electrons [18], aromatic carbons [12] or aromatic rings [11]) with the EA phase less the energy expended to displace the mobile phase molecules. The strength of complex formation is influenced by steric effects. For example, alkylbiphenyls (twelve π-electrons) elute with the same retention time as alkylnaphthalenes (ten π-electrons) instead of with alkylfluorenes (*i.e.*, bridged biphenyls with twelve π-electrons) [18]. Since the acceptor surface may be regarded as planar, the greatest interaction is anticipated with planar donor molecules [21,26,27].

Typically, electron-acceptor phases have been examined with linear free-energy techniques [4,9,10,12,18] or with retention indices [11,28]. The latter technique is well suited for establishing the group-selective aptitude of a particular stationary phase. Two methods used for comparing the retention behaviors of reversed-phase BPs are the extrathermodynamic approaches of enthalpy–entropy compensation [29–38] and homoenergetic–heteroenergetic plots. Neither enthalpy–entropy compensation, derived from techniques used to study solute–solvent interactions [39,40], nor homoenergetic–heteroenergetic plots, used to investigate empirically solute interactions in reversed-phase HPLC [40], have been systematically applied to EA phases.

In this work, we acquired or prepared a variety of EA phases and evaluated them with planar and non-planar solutes. The aim was to compare the various EA phases and observe if certain EA phases had advantages in "grouping", "selecting" or "recognizing" various types of aromatic solutes. The adsorption characteristics of six stationary phases were compared using the techniques of enthalpy–entropy compensation. All stationary phases were compared using vector-analysis techniques and the phases were ranked according to their ability to group alkyl PAHs and recognize planar *versus* non-planar solutes.

EXPERIMENTAL

2,4-Dinitrochlorobenzene, 3,5-dinitrobenzoyl chloride, picryl chloride, pyridine, dibenzosuberone and triethylamine were obtained from Aldrich (Milwaukee, WI, USA). Tetrahydrofuran (THF, "Non-Spectro", Burdick & Jackson Labs., Muskegon, MI, USA) and toluene (Sargent-Welch Scientific, Skokie, IL, USA) were dried over sodium sulphate and sodium metal, respectively, and filtered prior to use. Silica gel (8-μm RoSil, 400 m^2/g) (Alltech, Deerfield, IL, USA) was dried *in vacuo* at 150°C for 3 h. Aminopropylsilica (5-μm RSil, 550 m^2/g) (Alltech) (NH_2 in Fig. 1), Nucleosil 5 NO_2 (Alltech) (5-NO_2 in Fig. 1) and Supelcosil LC-18 octadecyldimethylsilylsilica (Supelco, Bellefonte, PA, USA) (C_{18} in Fig. 1) were used as received.

Mercaptopropylsilica was made, as described previously [17,18], by adding 3.7 g of 3-mercaptopropyltrimethoxysilane (Petrarch Systems, Bristol, PA, USA) to 2.5 g of silica gel and 200 ml of toluene in a reflux apparatus. A mild reflux was maintained for 24 h. The silica was recovered by filtration, washed with toluene, acetone, water and acetone and dried at 60°C *in vacuo*.

Dinitrophenylmercaptopropylsilica (DNPMP in Fig. 1) was prepared by combining 2.5 g of freshly prepared mercaptopropylsilica, 3.0 g of 2,4-dinitrochlorobenzene, 1.2 ml of pyridine and 150 ml of THF in a reflux apparatus [18]. The mixture was allowed to react for 24 h and treated as for

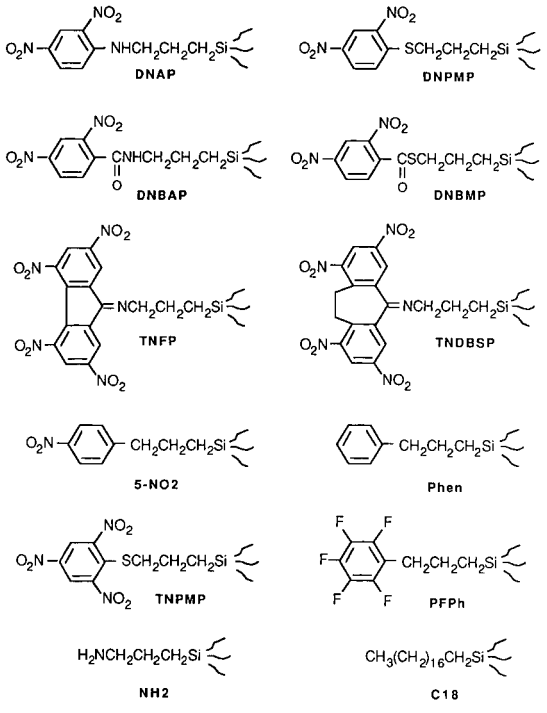

Fig. 1. Various bonded stationary phases used to study the physico-chemical properties of electron-acceptor groups.

mercaptopropylsilica above. Based on elemental analysis (Galbraith Labs., Knoxville, TN, USA), the surface coverage was calculated as 1.12 μmol/m^2.

Dinitrobenzoylmercaptopropylsilica (DNBMP in Fig. 1) and trinitrophenylmercaptopropylsilica (TNPMP in Fig. 1) were prepared by adding 5.2 g of 3,5-dinitrobenzoyl chloride and 3.7 g of picryl chloride to freshly prepared mercaptopropylsilica and completing the steps as for DNPMP above. Based on elemental analyses, the surface coverages were 1.34 and 1.74 μmol/m^2, respectively.

Dinitroanilinopropylsilica (DNAP in Fig. 1) was prepared by combining 3.0 g of 2,4-dinitrochlorobenzene, 2.5 g of 8-μm aminopropylsilica, 1.2 ml of pyridine and 150 ml of THF in a reflux apparatus. After 48 h of refluxing, the mixture was treated as for DNPMP above. Based on elemental analysis, the surface coverage was 1.13 μmol/m^2.

3,5-Dinitrobenzamidopropylsilica (DNBAP in Fig. 1) was prepared [16] by combining 3.5 g of 3,5-dinitrobenzoyl chloride, 2.5 g of 8-μm aminopropylsilica, 2 ml of triethylamine and 150 ml of THF in a septum-sealed reaction flask. The system was stirred and maintained at 60°C. After 24 h, the mixture was treated as for DNPMP above. Based on elemental analysis, the surface coverage was 1.95 μmol/m^2.

2,4,5,7-Tetranitrofluoreniminopropylsilica (TNFP in Fig. 1) was prepared similarly to a procedure described previously [2]. A 2.5-g amount of 8-μm aminopropylsilica was dried by collecting water for 5 h (as the benzene–water azeotrope) with a Dean–Stark moisture trap, 6 g of 2,4,5,7-tetranitro-9-fluorenone were added to the boiling flask and azeotroping was continued for 18 h. The dark-brown silica was collected by filtration and washed with hexane and THF. Based on elemental analysis, the surface coverage was 0.73 μmol/m^2.

The aromatic nitration of dibenzosuberone was performed using the procedure for the nitration of fluorenone [41]. Fuming nitric acid and sulphuric acid (*ca.* 1:1) were slowly added to a refluxing mixture of sulphuric acid (190 ml), fuming nitric acid (325 ml) and 21 g of dibenzosuberone. After 18 h the material was precipitated by pouring the contents into 5 l of cold water. The precipitate was collected by filtration and washed (three times) with hot hexane. Crude product (11 g) was dissolved in a hot solution of 6% acetic anhydride in glacial acetic acid. On cooling, 5.5 g of yellow precipitate with m.p. 197°C recrystallized: ^{1}H NMR ([$^2H_6$]acetone), δ = 8.95 (2H, s), 8.93 (2H, s), 3.72 (4H, s). The nuclear Overhauser effect was observed for ^{13}C nuclei at δ = 128.8 and 123.6. Tetranitrodibenzosuberone was confirmed as the precipitate by direct-probe mass spectrometry (*m/z* 388) and the spot-test for *m*-dinitroaromatics was positive [42]. Based on these data, a structure of 1,3,7,9-tetranitrodibenzosuberone was assigned to this product. 1,3,7,9-Tetranitrodibenzosuberiminopropylsilica (TNDBS in Fig. 1) was made through the same sequence as TNFP. Based on elemental analysis, the surface coverage was 1.48 μmol/m^2.

Pentafluorophenylsilica (PFPh in Fig. 1) and phenylsilica (Phen in Fig. 1) were prepared by adding 3.97 g of pentafluorophenyldimethylchlorosilane and phenyldimethylchlorosilane (Petrarch Systems) to reflux apparatus containing 2.5 g of silica gel, 1.2 ml of pyridine and 150 ml of THF. The mixtures were allowed to react for 24 h and treated as for mercaptopropylsilica above.

The bonded phases were slurry packed with a Micromeritics (Norcross, GA, USA) Model 705 stirred slurry packer at 6000 p.s.i. into 50 × 4.6 mm I.D. stainless-steel columns (Alltech). Each column was installed in an HPLC apparatus consisting of a Waters (Milford, MA, USA) Model 6000A pump with the high-sensitivity pulse damper installed and retrofitted with Model 510 heads, a Rheodyne Model 7125 injector with a 6-μl sample loop, a 2.8-l Equatherm water bath (Curtin Matheson Scientific, Houston, TX, USA), a Vari-Chrom UV-10 variable-wavelength detector (Varian, Sunnyvale, CA, USA), a 300-p.s.i. back-pressure regulator (Alltech) and an SP-4270 printer/plotter (Spectra-Physics, San Jose, CA, USA). Solvent flowing from the pump to the injector passed through a 2-ml stainless-steel loop, immersed in a constant-temperature bath, prior to entering the injector. The columns were evaluated by injecting solutions of various PAHs (*ca.* 200 mg/l) with isooctane (1.0 ml/min) as a mobile phase and monitoring the eluate at 254 nm. Column void volumes were established as the retention time of carbon tetrachloride.

Data analysis was performed with the aid of a VAX 8650 or 6430 computer (Digital Equipment, West Concord, MA, USA) operating the RS1 software package (Bolt Beranek and Newman, Cambridge, MA, USA).

RESULTS AND DISCUSSION

HPLC packings containing a variety of covalently bonded electron-acceptor groups were prepared. 2,4-Dinitroanilinopropylsilica (DNAP) and 3,5-dinitrobenzamidopropylsilica (DNBAP), among the most frequently used EA phases, provided the potential for secondary adsorption owing to the presence of polar hydrogens or a carbonyl group. 2,4-Dinitrophenylmercaptopropylsilica (DNPMP) and 3,5-dinitrobenzoylmercaptopropylsilica (DNBMP) avoided the possibility for secondary adsorption by a polar hydrogen. 2,4,5,7-Tetranitrofluoreniminopropylsilica (TNFP) and 1,3,7,9-tetranitrodibenzosuberiminopropylsilica (TNDBS) provided the possibility of secondary adsorption from an adjacent electron-acceptor ring with planar or non-planar orientation. The capacity factors of various planar and non-planar PAHs were determined over a range of temperatures on each stationary phase using carbon tetrachloride to mark the column volume. Evidence for the "charge-transfer" mechanism in chromatography has generally been regarded as an observed increase in the retention time of aromatic solutes on phases containing electron-withdrawing bonded groups relative to the underivatized stationary phase [13]. This phenomenon has been reported previously for DNAP [8,9], DNPMP [18], DNBAP [10,16], DNBMP [18] and TNFP [2], and was observed for all of the EA phases.

As the EDA complex is reversible, the capacity factor (k') would be proportional to the equilibrium constant (eqn. 1) for the complex and the Van 't Hoff equation (eqn. 3) would apply:

$$k' = K\phi \tag{1}$$

$$\ln k' = \ln K + \ln \phi = -\Delta G^0/RT + \ln \phi \tag{2}$$

$$\ln k' = -\Delta H^0/RT + \Delta S^0/R + \ln \phi \tag{3}$$

where ΔH^0 and ΔS^0 are the standard-state enthalpy and entropy for transfer of the solute molecule from the mobile phase to the stationary phase, R is the gas constant, T is the absolute temperature and ϕ is the phase ratio of the column [29]. A plot of $\ln k'$ *vs.* $1/T$ would yield a straight line (*i.e.*, constant enthalpy) if there is no change in the mechanism or structure of the complex. As Melander *et al.* [29] have demonstrated, when enthalpy–entropy compensation is observed for a family of solutes or stationary phases, the following equation applies:

$$\ln k'(T) = (-\Delta H^0/R)(1/T - 1/\beta) - \Delta G^0_\beta/R_\beta + \ln \phi \tag{4}$$

where $\ln k'(T)$ is the capacity factor for a solute at a particular temperature T, ΔH^0 is the enthalpy of adsorption of the solute and ΔG^0_β is the Gibbs free energy for the adsorption at the compensation temperature β. It is possible to obtain β from a plot of $\ln k'$ *vs.* ΔH^0 for a family of solutes on a stationary phase. If values of β for different chromatographic systems agree (such as within a 95% confidence interval), the retention mechanisms are considered to be the same (or isokinetic).

Linear Van 't Hoff plots have a rigorous thermodynamic basis in the absence of heat-capacity effects. If the mechanism of a process is invariant (*i.e.*, constant enthalpy) over the chosen temperature range, a Van 't Hoff plot yields a straight line. The

Van 't Hoff plots for various EA phases were plotted, and linear regressions (ln k' *vs.* $1/T$) for the solutes on each EA phase were calculated. With this information, the enthalpies of adsorption were calculated using eqn. 3. These data are summarized in Table I. Applying eqn. 4, the ln k' values at 45°C for each analyte were plotted against their calculated enthalpies of adsorption on each stationary phase

TABLE I

STATISTICS FROM THE VAN 'T HOFF PLOTS OF VARIOUS ELECTRON-ACCEPTOR STATIONARY PHASES

The columns contain the slope, intercept (Int.), their standard deviations (S.D.) and the coefficient of determination (r^2) calculated for each analyte. The enthalpy and its standard deviation were calculated from the slope data. The mean ln k' is the logarithm of the capacity factor at the mean temperature of 45°C.

Compound	Column	Slope	S.D. (slope)	Int.	S.D. (Int.)	r^2	ΔH (kcal mol^{-1})	S.D. (ΔH)	Mean ln k'
Benzene	DNAP	826.4	143.4	−3.4	0.4	0.917	1.64	0.28	−0.841
Naphthalene		915.5	107.0	−2.5	0.3	0.961	1.82	0.21	0.399
Anthracene		2060.3	605.1	−4.7	2.1	0.794	4.09	1.20	1.590
Phenanthrene		1779.8	505.5	−3.9	1.7	0.805	3.54	1.00	1.565
Pyrene		1915.6	72.9	−3.7	0.2	0.996	3.81	0.14	2.333
Fluoranthene		1846.9	49.4	−3.4	0.1	0.998	3.67	0.10	2.435
Chrysene		2533.0	65.7	−4.6	0.2	0.998	5.03	0.13	3.408
Fluorene		1245.9	54.8	−2.8	0.1	0.994	2.48	0.11	1.186
Dihydrophenanthrene		977.1	59.2	−2.2	0.1	0.989	1.94	0.12	0.928
Dibenzosuberane		921.8	79.1	−2.0	0.2	0.978	1.83	0.16	0.904
Biphenyl		1355.2	469.7	−3.8	1.4	0.735	2.69	0.93	0.546
Benzene	DNBAP	614.2	356.7	−3.6	1.1	0.497	1.22	0.71	−1.705
Naphthalene		1482.0	208.9	−4.5	0.7	0.944	2.94	0.42	0.148
Anthracene		2185.2	248.4	−5.2	0.9	0.963	4.34	0.49	1.654
Phenanthrene		1946.1	191.3	−4.4	0.7	0.972	3.87	0.38	1.675
Pyrene		2121.8	168.5	−4.3	0.6	0.981	4.22	0.33	2.323
Fluoranthene		2127.4	153.7	−4.4	0.6	0.985	4.23	0.31	2.296
Chrysene		2818.2	316.2	−5.8	1.1	0.964	5.60	0.63	2.998
Fluorene		1869.6	215.3	−5.0	0.8	0.962	3.71	0.43	0.821
Dihydrophenanthrene		1730.2	203.5	−5.1	2.9	0.960	3.44	0.40	0.343
Dibenzosuberane		1641.8	167.8	−4.8	0.6	0.970	3.26	0.33	0.327
Biphenyl		1486.8	224.8	−4.7	0.7	0.936	2.95	0.45	−0.071
Benzene	DNPMP	265.6	84.4	−2.0	0.2	0.767	0.53	0.17	−1.221
Naphthalene		915.5	107.0	−2.5	0.3	0.961	1.82	0.21	0.399
Anthracene		1657.2	81.0	−3.4	0.2	0.993	3.29	0.16	1.882
Phenanthrene		1712.3	72.8	−3.6	0.2	0.995	3.40	0.14	1.824
Pyrene		1915.6	72.9	−3.7	0.2	0.996	3.81	0.14	2.333
Fluoranthene		1846.9	49.4	−3.4	0.1	0.998	3.67	0.10	2.435
Chrysene		2533.0	65.7	−4.6	0.2	0.998	5.03	0.13	3.408
Fluorene		1245.9	54.8	−2.8	0.1	0.994	2.48	0.11	1.186
Dihydrophenanthrene		977.1	59.2	−2.2	0.1	0.989	1.94	0.12	0.928
Dibenzosuberane		921.8	79.1	−2.0	0.2	0.978	1.83	0.16	0.904
Biphenyl		915.7	157.0	−3.0	0.5	0.919	1.82	0.31	−0.094
Benzene	DNBMP	92.4	317.4	−2.4	1.0	0.027	0.18	0.63	−2.004
Naphthalene		773.7	163.7	−3.1	0.5	0.882	1.54	0.33	−0.592
Anthracene		1499.9	95.8	−4.1	0.3	0.988	2.98	0.19	0.646
Phenanthrene		1538.5	96.7	−4.2	0.3	0.988	3.06	0.19	0.697
Pyrene		1707.6	70.6	−4.3	0.2	0.995	3.39	0.14	1.084
Fluoranthene		1751.5	75.4	−4.4	0.2	0.994	3.48	0.15	1.140
Chrysene		2045.7	64.5	−4.7	0.2	0.997	4.06	0.13	1.752
Fluorene		1062.3	87.7	−3.3	0.2	0.980	2.11	0.17	0.082

(Continued on p. 80)

TABLE I *(continued)*

Compound	Column	Slope	S.D. (slope)	Int.	S.D. (Int.)	r^2	ΔH (kcal mol^{-1})	S.D. (ΔH)	Mean ln k'
Dihydrophenanthrene		936.2	117.5	−3.1	0.3	0.955	1.86	0.23	−0.066
Dibenzosuberane		1014.3	132.2	−3.3	0.4	0.952	2.02	0.26	−0.022
Biphenyl		881.7	133.4	−3.3	0.4	0.936	1.75	0.27	−0.449
Benzene	TNFP	677.4	51.8	−3.2	0.1	0.983	1.35	0.10	−1.053
Naphthalene		1180.6	162.1	−3.5	0.5	0.946	2.35	0.32	0.280
Anthracene		2271.3	254.5	−5.1	0.7	0.964	4.51	0.51	2.137
Phenanthrene		1325.7	136.8	−2.4	0.4	0.969	2.63	0.27	1.710
Pyrene		2044.7	139.1	−4.3	0.4	0.986	4.06	0.28	2.083
Fluoranthene		2186.9	128.2	−4.6	0.4	0.990	4.35	0.25	2.294
Chrysene		2583.9	181.2	−4.4	0.6	0.985	5.13	0.36	3.650
Fluorene		2217.1	120.4	−5.8	0.3	0.991	4.41	0.24	1.227
Dihydrophenanthrene		1990.6	274.0	−5.5	0.8	0.946	3.96	0.54	0.750
Dibenzosuberane		1731.6	462.4	−4.7	1.5	0.824	3.44	0.92	0.722
Biphenyl		1151.9	284.3	−3.3	0.9	0.846	2.29	0.56	0.302
Benzene	TNDBSP	434.0	105.9	−3.6	0.3	0.848	0.86	0.21	−2.186
Naphthalene		1208.2	113.7	−4.1	0.3	0.974	2.40	0.23	−0.248
Anthracene		2158.9	29.0	−5.3	0.0	0.999	4.29	0.06	1.523
Phenanthrene		2040.1	155.9	−5.1	0.4	0.983	4.05	0.31	1.343
Pyrene		2163.2	72.0	−4.9	0.1	0.997	4.30	0.14	1.960
Fluoranthene		2318.8	66.5	−5.2	0.2	0.998	4.61	0.13	2.104
Chrysene		3048.8	11.9	−6.4	0.1	1.000	6.06	0.02	3.143
Fluorene		1688.8	96.4	−4.7	0.2	0.990	3.36	0.19	0.604
Dihydrophenanthrene		1516.9	91.9	−4.8	0.2	0.989	3.01	0.18	0.024
Dibenzosuberane		1349.0	121.5	−4.2	0.3	0.976	2.68	0.24	0.024
Biphenyl		1249.4	75.4	−4.3	0.2	0.989	2.48	0.15	−0.418

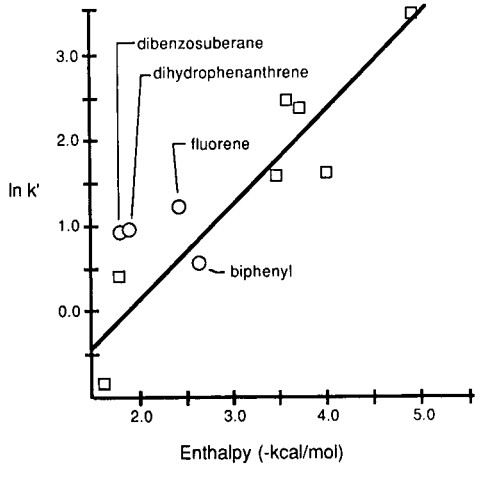

Fig. 2. Entropy–enthalpy compensation plot for (□) planar and (○) non-planar aromatic solutes on dinitroanilinopropylsilica (DNAP).

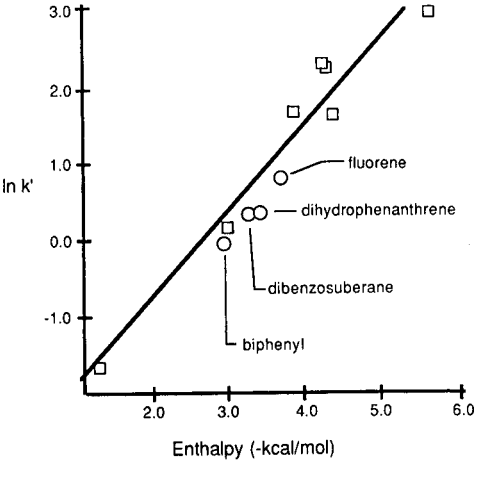

Fig. 3. Entropy–enthalpy compensation plot for (□) planar and (○) non-planar aromatic solutes on dinitrobenzamidopropylsilica (DNBAP).

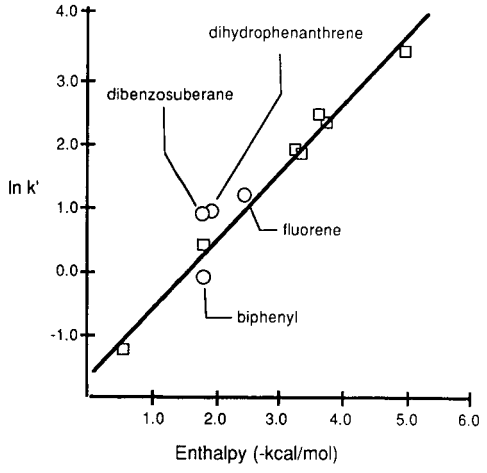

Fig. 4. Entropy–enthalpy compensation plot for (□) planar and (○) non-planar aromatic solutes on dinitrophenylmercaptopropylsilica (DNPMP).

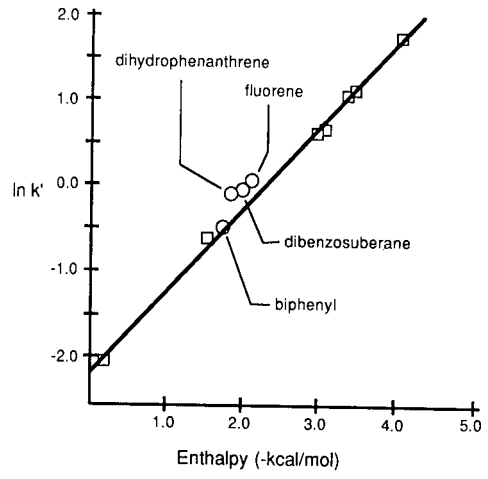

Fig. 5. Entropy–enthalpy compensation plot for (□) planar and (○) non-planar aromatic solutes on dinitrobenzoylmercaptopropylsilica (DNBMP).

(Figs. 2–7). The uncertainties in the enthalpy values were calculated from the uncertainties in the slopes of the Van 't Hoff plots. Compensation of an enthalpy change, produced from an outside stress (such as temperature), by an entropy change is a common occurrence in systems involving small molecules. Common mechanisms are characterized by having $\delta\Delta H$ proportional to $\delta\Delta S$, where δ denotes a change in the thermodynamic parameter caused by a difference in solute, mobile phase or stationary phase. For the various EA stationary phases (Figs. 2–7), the linear locus of data points for the planar compounds indicates consistent enthalpy–entropy compensation, and that the mechanism of adsorption under these conditions was the same for benzene through chrysene. DNAP (Fig. 2), DNBAP (Fig. 3) and TNFP (Fig. 6) had a greater scatter in this linear distribution, as observed from the plots of ln k' *vs.* enthalpy and the standard deviations for the slopes calculated during the linear regression

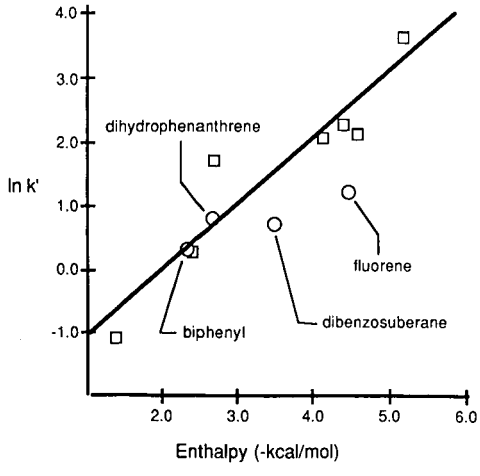

Fig. 6. Entropy–enthalpy compensation plot for (□) planar and (○) non-planar aromatic solutes on tetranitrofluoreniminopropylsilica (TNFP).

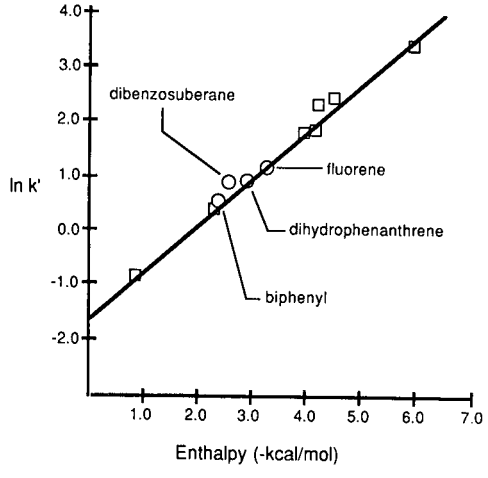

Fig. 7. Entropy–enthalpy compensation plot for (□) planar and (○) non-planar aromatic solutes on tetranitrodibenzosuberiminopropylsilica (TNDBSP).

(Table II). These observations, although reproducible, cannot be explained in terms of the thermodynamic parameters that were evaluated.

The non-planar aromatics (fluorene is grouped with the non-planar compounds for this discussion), had approximately (*i.e.*, within 95% confidence level) the same mechanism for adsorption of the planar solutes. The TNDBS stationary phase was prepared in an attempt to optimize the retention of non-planar aromatics (in particular its dibenzosuberane counterpart). Apparently the sublimity of this stationary phase was ignored by the non-planar solutes in favor of random multi-site orientations which resulted in adsorption behavior similar to those of the other phases. This may be additional indirect evidence for the Monte Carlo model of EDA adsorption [12,43].

If the compensation temperatures (β) are identical for species in different chemical processes, they are believed to share a common physico-chemical property. In this case, similar compensation temperatures for the adsorption of planar aromatic hydrocarbons on different electron-acceptor phases would suggest a common adsorption mechanism among the various phases. Using the recommendations of Krug *et al.* [44,45], compensation temperatures were calculated (Table II) and compared. The compensation temperature of TNDBSP differed from those of DNBAP and DNPMP (>95% confidence level). This suggests that the mechanism of retaining planar solutes may be different on TNDBSP than on either DNBAP and DNPMP. This observation would have been more encouraging had a difference in

TABLE II

ENTROPY–ENTHALPY COMPENSATION IN ELECTRON-ACCEPTOR STATIONARY PHASES

The slope and standard deviation were obtained from the linear regression for the planar solutes. The compensation temperature and the 95% confidence level were calculated from the slope data. The harmonic mean temperature was 318 ± 20 K (95% C.L.).

Stationary phase	Slope of entropy–enthalpy compensation plot (planar)	n	Compensation temperature (95% C.L.)
DNAP	1.07 ± 0.18	7	985 ± 426
DNBAP	1.14 ± 0.12	7	1142 ± 309
DNPMP	1.04 ± 0.05	7	931 ± 115
DNBMP	0.95 ± 0.02	7	798 ± 43
TNFP	1.04 ± 0.17	7	930 ± 391
TNDBSP	0.84 ± 0.04	7	679 ± 83

TABLE III

LN k' VALUES FOR AROMATIC SOLUTES ON VARIOUS STATIONARY PHASES

No. of π-electrons	Compound	ln k'				
		DNAP	DNPMP	TNPMP	5-NO_2	TNDBSP
6	Benzene	−1.825	−1.147	−1.221	−1.551	−2.361
	Toluene	−1.825	−1.099	−1.166	−1.551	−2.179
	o-Xylene	−1.729	−1.147	−1.338	−1.625	−1.891
	Mesitylene	−1.930	−1.371	−1.472	−1.992	−2.179
	Tetralin	−1.562	−1.199	−1.066	−1.551	−1.668
10	Naphthalene	−0.138	0.251	0.180	−0.452	−0.142
	1-Methylnaphthalene	−0.120	0.346	0.284	−0.428	0.000
	1-Ethylnaphthalene	−0.235	0.214	0.152	−0.452	−0.164
	1,5-Dimethylnaphthalene	−0.050	0.492	0.378	−0.361	0.055
14	Anthracene	1.349	2.095	1.697	0.773	1.847
	Phenanthrene	1.354	2.077	1.676	0.794	1.624
	2-Methylanthracene	1.406	2.280	1.767	0.752	2.107
	9,10-Dimethylanthracene	1.587	2.508	1.994	0.834	2.438
	3,6-Dimethylphenanthrene	1.529	2.472	1.927	0.879	2.228
	2-Methylphenanthrene	1.441	2.298	1.767	0.834	1.823
	2-Ethylanthracene	1.302	2.079	1.593	0.693	1.859

mechanism for planar and non-planar solutes been observed for TNDBSP. The compensation temperature treatment may be detecting that TNDBSP has the bulkiest electron-acceptor surface among the EA phases. Similar compensation temperatures were observed for the remaining EA phases (>95% confidence level), indicating a common adsorption mechanism. The compensation temperatures observed for the EA phases (679–1142 K) were slightly higher than those reported for reversed-phase stationary phases (360–897 K) [29,30].

Another extrathermodynamic approach to studying reversed-phase stationary phases is the vector-analysis approach called homoenergetic–heteroenergetic plots [46]. As shown in eqn. 2, the retention of an analyte on a column depends on the phase ratio and the Gibbs free energy for the adsorption process. Consider the retention of an analyte on two different stationary phases at the same temperature:

$$\ln k'_A = -\Delta G^0_A/RT + \ln \phi_A \quad (5)$$

$$\ln k'_B = -\Delta G^0_B/RT + \ln \phi_B \quad (6)$$

If the Gibbs energies for two stationary phases are proportional so that

$$\Delta G^0_A = \rho \Delta G^0_B$$

then eqns. 5 and 6 can be combined to yield

$$-RT(\ln k'_A - \ln \phi_A) = -RT\rho(\ln k'_B - \ln \phi_B) \quad (7)$$

Eqn. 7, with some rearrangement, becomes

$$\ln k'_A = \rho \ln k'_B + \ln \phi_A - \rho \ln \phi_B \quad (8)$$

Capacity factors ($\ln k'$) for a set of analytes (i) on a stationary phase (A) *versus* the $\ln k'$ values for the same analytes on a different stationary phase (B) are vectors that can be used to examine the similarity of A and B. Melander *et al.* [46] stated that when ρ_i/ρ_{i+1} is 1 (*i.e.*, a linear correlation coefficient $\geqslant 0.95$), the phases are homoenergetic (homo = same), and if ρ_i/ρ_{i+1} is not equal to 1 (*i.e.*, a linear correlation coefficient $\leqslant 0.95$), the phases are homeoenergetic (homeo = similar).

The linear correlation coefficient (r) is not unique to homoenergetic–heteroenergetic plots, and is one of the ways to examine similarity between sets of data:

$$r = \delta_{ab}/(\delta_a \delta_b) = \frac{\sum (a_i - \bar{a})(b_i - \bar{b})}{[\sum (a_i - \bar{a})^2 \sum (b_i - \bar{b})^2]^{1/2}} \quad (9)$$

The linear correlation coefficient has the geometric significance of representing the cosine of the angle (Θ) formed between the vectors $[\boldsymbol{a}_i]$ and $[\boldsymbol{b}_i]$.

DNBMP	DNBAP	NH_2	TNFP	C_{18}	PFPh	Phen
−1.626	−1.386	−1.640	−3.045	−3.219	−1.578	−1.386
−1.546	−1.317	−1.314	−2.351	−2.813	−1.745	−1.204
−1.914	−1.253	−1.902	−2.351	−3.219	−1.578	−1.609
−2.031	−1.192	−1.902	−3.045	−3.219	−2.064	−1.897
−1.546	−0.934	−1.497	−1.946	−2.813	−2.197	−1.099
−0.447	0.417	−0.467	−0.742	−2.120	−1.371	−0.916
−0.350	0.609	−0.567	−0.693	−2.120	−1.099	−0.693
−0.397	0.441	−0.567	−0.847	−2.303	−1.008	−0.660
−0.219	0.850	−0.491	−0.480	−2.303	−1.008	−0.539
0.977	1.996	0.440	1.211	−1.514	0.031	0.049
0.945	2.020	0.505	0.795	−1.514	0.076	0.095
0.983	2.136	0.523	1.266	−1.427	0.091	0.182
1.060	2.630	0.540	1.580	−1.514	0.120	0.312
1.109	2.564	0.557	1.580	−1.715	0.188	0.348
0.906	2.234	0.566	1.344	−1.609	0.091	0.236
0.725	2.066	0.440	1.319	−1.609	−0.136	0.125

TABLE IV

LOGARITHM OF CAPACITY FACTORS (LN k') *VERSUS* THE COSINE OF DIHEDRAL ANGLE (DH) FOR BIPHENYL SPECIES ON VARIOUS ELECTRON-ACCEPTOR STATIONARY PHASES

Compound	Cos(DH)	TNFP	TNDBSP	DNBAP	DNPMP	DNAP
Biphenyl	0.775	0.627	−0.150	0.368	0.508	0.604
9,10-Dihydrophenanthrene	0.956	1.251	0.299	0.799	1.092	1.092
Fluorene	1.000	1.679	0.912	1.358	1.405	1.405
Slope [ln k' *vs.* cos(DH)]		4.318	4.070	3.814	3.768	3.309
S.D.		1.012	1.847	1.666	0.624	0.711
y-Intercept		−2.745	−3.351	−2.630	−2.429	−1.978
r^2		0.948	0.829	0.840	0.973	0.956

Another way to compare analytical data that is conveniently in the form of vectors is by calculating the Euclidian distance (D_{ab}):

$$D_{ab} = [\sum(a_i - b_i)^2]^{1/2} = [\boldsymbol{a}_i - \boldsymbol{b}_i][\boldsymbol{a}_i - \boldsymbol{b}_i]^T \quad (10)$$

Massart and Kaufman [47] state that comparison of Euclidian distance calculations is useful in detecting differences in polarity and specificity in liquid stationary phases whereas comparison of linear correlation coefficients detects only specificity, albeit better than Euclidian distance.

Twelve stationary phases were examined using sixteen aromatic hydrocarbons with and without alkyl substituents. These data were collected at a temperature of 25°C using a constant-temperature bath. The linear correlation coefficient and Euclidian distance were calculated for each vector pair (*i.e.*, column of data) in Table III according to eqns. 9 and 10, respectively. The results for the 66 combinations are presented in Table V. To aid in interpreting these data, the combinations were arranged according to some clusters that became apparent through inspection. The group assignments were made as follows: A, $r \geqslant 0.992$ and $D_{ab} \leqslant 3.1$; B, $0.992 > r \geqslant 0.975$ and $3.1 < D_{ab} \leqslant 5.0$; and C, $r < 0.975$ and $D_{ab} > 5.0$. These groups were assigned the more descriptive labels of "close similarity" (A), "some similarity" (B) and "no similarity" (C). As one might expect, the C_{18} phase had little in common with the EA phases, and, under these conditions, C_{18} also differed from the Phen and PFPh phases. It was interesting that NH_2 and TNFP did not have close similarity (*i.e.*, group A) to many of the other EA phases. It was also interesting that the combination with the greatest difference in compensation temperatures (DNBAP–TNDBSP) had a higher group assignment (Group A) than combinations with a smaller difference in compensation temperatures (*e.g.*, DNBMP–TNDBSP in Group B). This is not necessarily in conflict with the entropy–enthalpy compensation data; however, it does suggest that a vector analysis using correlation coefficient and Euclidian distance calculations may be more informative when comparing the subtleties of stationary phases. PFPh, if it behaved as an EA phase at all under these conditions, was not similar to the other EA phases.

The model for EDA chromatography, as described in the Introduction, involves parallel planes between donor and acceptor molecules. As noted previously [18], the lack of planarity in biphenyl (twelve π-electrons) causes it to have a retention time similar to naphthalene (ten π-electrons). To investigate this phenomenon further, the logarithms of the capacity factors (ln k') for biphenyl, 9,10-dihydrophenanthrene and fluorene on several stationary phases were plotted against the cosines of the dihedral angle (cos φ) for the analytes (Table IV). The multi-ring acceptor phases, TNFP and TNDBSP, appeared to have better selection of planar *vs.* non-planar species based on the slope of ln k' *vs.* cos φ. The standard deviations of the slopes and coefficients of determination (r^2) for TNDBSP and DNBAP were large relative to the other EA phases. This may suggest secondary equilibria. Alumina was included with these data because it has been accepted as a useful stationary phase in resolving planar and non-planar analytes. One can see

TNPMP	5-NO_2	DNBMP	Alumina	C_{18}	NH_2	PFPh	Phen
0.389	0.258	−0.058	−0.400	−1.966	0.000	−0.405	−0.244
0.779	0.611	0.264	−0.270	−1.715	0.284	−0.083	0.125
1.071	0.804	0.436	0.131	−1.514	0.339	−0.016	0.080
2.777	2.288	2.074	1.884	1.829	1.525	1.746	0.353
0.722	0.392	0.343	1.356	0.468	0.053	0.044	0.054
−1.781	−1.525	−1.674	−1.894	−3.396	−1.180	−1.758	−0.243
0.937	0.972	0.973	0.659	0.928	0.999	0.999	0.977

that alumina is only mildly effective in that role.

Each stationary phase was also evaluated for its ability to group alkyl-substituted PAHs in narrow bands. In previous studies [11,28] of the grouping behavior of stationary phases, retention indices were used. A model compound is chosen as representing a particular group and all other compounds in the group under study are evaluated in terms of how closely to the model compound they elute. It is not obvious that the collective distance of a series of solutes from a model compound is a better measurement than simply noting the overall width of the

TABLE V

LINEAR CORRELATION COEFFICIENT (r) AND EUCLIDIAN DISTANCE (D_{ab}) CALCULATED FROM THE PAIR OF VECTORS [LN k' a_1, LN k' a_2, ..., LN k' a_n] AND [LN k' b_1, LN k' b_2, ..., LN k' b_n], WHERE LN k' ϕ_i IS THE LOGARITHM OF THE CAPACITY FACTOR OF THE iTH COMPONENT ON STATIONARY PHASE ϕ

The group assignments were made as follows: A, $r \geqslant 0.992$ and $D_{ab} \leqslant 3.1$; B, $0.992 > r \geqslant 0.975$ and $3.1 < D_{ab} \leqslant 5.0$; and C, $r < 0.975$ and $D_{ab} > 5.0$.

Combination	r	D_{ab}	Group	Combination	r	D_{ab}	Group	Combination	r	D_{ab}	Group
TNPMP–DNAP	0.998	1.694	A	TNPMP–TNFP	0.991	3.788	B	C_{18}–DNBMP	0.981	8.198	C
TNPMP–DNBMP	0.998	2.708	A	NH_2–DNAP	0.990	2.611	B	C_{18}–DNAP	0.979	9.381	C
5-NO_2–TNPMP	0.997	3.073	A	DNBAP–DNBMP	0.990	4.098	B	C_{18}–TNPMP	0.978	10.88	C
5-NO_2–DNBMP	0.997	0.589	A	DNBAP–TNFP	0.990	4.715	B	C_{18}–5-NO_2	0.978	7.853	C
TNPMP–DNPMP	0.997	1.327	A	5-NO_2–TNDBSP	0.990	3.480	B	Phen–DNPMP	0.976	5.894	C
5-NO_2–DNAP	0.996	1.817	A	DNBMP–TNDBSP	0.989	3.013	B	C_{18}–TNFP	0.974	8.300	C
DNBAP–TNDBSP	0.996	2.414	A	5-NO_2–DNBAP	0.989	4.489	B	Phen–DNAP	0.974	3.576	C
DNAP–TNDBSP	0.996	1.739	A	DNPMP–TNFP	0.988	4.550	B	C_{18}–TNDBSP	0.973	10.60	C
DNAP–DNBAP	0.996	2.913	A	5-NO_2–TNFP	0.988	2.672	B	Phen–DNBAP	0.972	6.052	C
NH_2–DNBMP	0.995	1.299	A	DNBMP–TNFP	0.986	2.389	B	Phen–TNDBSP	0.971	5.187	C
TNPMP–DNBAP	0.995	1.489	A	Phen–DNBMP	0.984	2.272	B	PFPh–TNPMP	0.971	5.495	C
DNAP–DNPMP	0.995	2.747	A	NH_2–TNFP	0.983	3.108	B	PFPh–DNBMP	0.969	2.927	C
TNPMP–TNDBSP	0.995	2.093	A	NH_2–TNDBSP	0.982	4.241	B	C_{18}–DNBAP	0.968	12.23	C
DNAP–DNBMP	0.995	1.386	A	Phen–NH_2	0.982	1.135	B	PFPh–DNAP	0.967	4.176	C
TNDBSP–TNFP	0.994	2.570	A	Phen–TNPMP	0.981	4.634	B	C_{18}–DNPMP	0.967	12.06	C
NH_2–5-NO_2	0.993	0.880	A	Phen–5-NO_2	0.981	1.814	B	PFPh–TNDBSP	0.962	5.659	C
DNPMP–TNDBSP	0.993	2.303	A	Phen–TNFP	0.980	3.938	B	Phen–C_{18}	0.961	6.644	C
DNPMP–DNBAP	0.992	0.745	A	PFPh–5-NO_2	0.975	2.492	B	PFPh–DNBAP	0.959	6.895	C
5-NO_2–DNPMP	0.994	4.301	B	C_{18}–NH_2	0.987	7.168	C	PFPh–NH_2	0.957	1.943	C
NH_2–TNPMP	0.993	3.815	B	NH_2–DNPMP	0.987	5.067	C	PFPh–TNFP	0.953	4.006	C
DNPMP–DNBMP	0.992	3.919	B	NH_2–DNBAP	0.983	5.236	C	Phen–PFPh	0.952	1.561	C
DNAP–TNFP	0.991	2.271	B	PFPh–DNPMP	0.982	6.669	C	PFPh–C_{18}	0.923	5.636	C

TABLE VI

GROUPING OF LN k' VALUES AND COMPARATIVE STATISTICS FOR AROMATIC SOLUTES ON VARIOUS STATIONARY PHASES

No. of π-electrons	Parameter	DNAP	DNPMP	TNPMP	5-NO_2	TNDBSP
6	Mean ln k'	−1.774	−1.193	−1.253	−1.654	−2.055
	Variance	0.019	0.011	0.025	0.037	0.075
	Range	0.368	0.272	0.405	0.442	0.693
	Skewness	0.880	−1.637	−0.432	−2.090	0.614
	Kurtosis	1.013	2.952	−0.541	4.408	−0.831
10	Mean ln k'	−0.136	0.325	0.248	−0.423	−0.063
	Variance	0.006	0.015	0.011	0.002	0.011
	Range	0.186	0.278	0.226	0.091	0.219
	Skewness	−0.512	0.976	0.605	1.635	0.188
	Kurtosis	1.371	−0.063	−2.045	2.513	−4.528
14	Mean ln k'	1.424	2.258	1.774	0.794	1.989
	Variance	0.011	0.034	0.020	0.004	0.078
	Range	0.284	0.431	0.401	0.186	0.814
	Skewness	0.618	0.351	0.555	−0.375	0.501
	Kurtosis	−0.823	−1.765	−0.654	−0.094	−0.607
	Γ $(10\pi - 6\pi)$	1.638	1.518	1.501	1.230	1.993
	Γ $(14\pi - 10\pi)$	1.560	1.933	1.526	1.218	2.052
	$\Gamma \times \Gamma$	2.555	2.934	2.291	1.498	4.089
	Sum of variance	0.036	0.060	0.055	0.043	0.165
	$G(\Gamma)$	71.968	48.817	41.392	35.228	24.764

elution range of the group. As the logarithm of capacity factor is proportional to a retention index for a particular group, the same grouping information can be obtained with the former. The selection of which compounds belong to which group is important in comparing the performances of EA phases. The mechanism of EDA chromatography operates primarily on the basis of the number of π-electrons in the donor molecule and secondarily on the planarity of the donor molecule. Therefore, the groups were categorized according to π-electron numbers of six, ten and fourteen. The biphenyls and bridged biphenyls (9,10-dihydrophenanthrene and fluorene) were not included in this evaluation.

In addition to grouping alkyl PAHs in narrow bands, it is important to insure that the bands are well separated from one another. This is important when one is considering switching fractions of HPLC effluent to other techniques such as multidimensional HPLC or gas chromatography. A study of grouping behavior was designed to consider practically the stationary phases in terms of grouping and separation. This was accomplished by calculating a single value from the ln k' values of aromatic solutes on each stationary phase.

Within each group on a stationary phase, comparative statistics (mean, variance, range, skewness and kurtosis) were calculated. The grouping aptitude of the EA phases could readily be compared. The mean ln k' for each was used to calculate a value called Γ, the difference in mean ln k' for adjacent groups. The similarity of Γ (group separation number) to α (separation number) can be seen:

$$\alpha = k'_2/k'_1$$
$$\Gamma = \ln k'_2 - \ln k'_1 \qquad (11)$$

The best separation would occur when individual Γ values were each at a maximum or when the product of the Γ values was a maximum. Similarly, the best grouping would occur when the combined variance for all groups was at a minimum. These

DNBMP	DNBAP	NH_2	TNFP	C_{18}	PFPh	Phen
−1.733	−1.217	−1.651	−2.548	−3.057	−1.833	−1.439
0.051	0.030	0.066	0.233	0.049	0.081	0.103
0.486	0.452	0.588	1.099	0.405	0.619	0.799
−0.670	1.318	0.251	−0.047	0.609	−0.495	−0.609
−2.374	2.025	−1.841	−2.117	−3.333	−2.460	−0.799
−0.353	0.579	−0.523	−0.690	−2.211	−1.121	−0.702
0.010	0.040	0.003	0.024	0.011	0.029	0.025
0.228	0.433	0.100	0.368	0.182	0.363	0.377
1.067	1.082	0.184	0.972	0.000	−1.657	−0.922
1.206	−0.036	−4.946	1.606	−6.000	2.608	1.788
0.958	2.235	0.510	1.299	−1.558	0.066	0.193
0.015	0.068	0.003	0.071	0.009	0.010	0.013
0.384	0.634	0.126	0.786	0.288	0.323	0.300
−1.018	0.896	−0.634	−1.051	−0.480	−1.424	0.226
1.811	−1.085	−1.343	1.834	0.183	3.121	−1.446
1.379	1.796	1.128	1.857	0.845	0.711	0.737
1.311	1.656	1.033	1.990	0.654	1.187	0.895
1.809	2.973	1.165	3.695	0.553	0.844	0.659
0.076	0.138	0.071	0.328	0.069	0.121	0.141
23.929	21.596	16.352	11.275	7.987	7.007	4.693

opposing performance measures were combined in a single equation to make comparison easier:

$$R_\Gamma = \frac{[\Gamma(10\pi - 6\pi) \times \Gamma(14\pi - 10\pi)]}{[s^2(6\pi) + s^2(10\pi) + s^2(14\pi)]} \qquad (12)$$

The results of these calculations are shown in Table VI. The significance of this new performance parameter (R_Γ or "group resolution") is that it is a single value that combines the effectiveness of a stationary phase to place related solutes into narrow bands and the effectiveness of the stationary phase to maintain separation among the groups. Using the calculated values for R_Γ, the group-resolution effectiveness of the various phases followed the sequence DNAP ≫ DNPMP, TNPMP, 5-NO_2 > TNDBSP, DNBMP, DNBAP > NH_2 > TNFP. PFPh was ranked with C_{18} and Phen.

In summary, the entropy–enthalpy compensation technique was not very helpful in providing comparisons among the various electron-acceptor phases. The vector-analysis techniques of linear correlation coefficient calculation and Euclidian distance calculation provided two quantitative measures for comparing stationary phases that were much more useful. As the most effective application of electron-acceptor phases is group separation, the parameter R_Γ (group resolution) should be helpful in evaluating these electron-acceptor phases and those to come. It has been shown that electron-acceptor phases are also effective at separating bridged-biphenyl compounds based on dihedral angle. With this added understanding, new applications of these curious stationary phases may emerge.

By applying the comparison techniques described here, it was found that DNAP was better at grouping aromatic solutes than DNPMP (R_Γ 72 and 49, respectively). Conversely, DNPMP was found to be slightly better than DNAP at separating species based on dihedral angle (slope in Table V 3.8 and 3.3, respectively).

ACKNOWLEDGEMENT

We thank S. C. Johnson and Son, Inc. (Racine, WI, USA) for financial support and the loan of equipment.

REFERENCES

1 W. Holstein and H. Hemetsberger, *Chromatographia*, 15 (1982) 251.
2 C. H. Lochmüller and C. W. Amoss, *J. Chromatogr.*, 108 (1975) 85.
3 C. H. Lochmüller, R. R. Ryall and C. W. Amoss, *J. Chromatogr.*, 178 (1979) 298.
4 H. Hemetsberger, H. Klar and H. Ricken, *Chromatographia*, 13 (1980) 277.
5 W. E. Hammers, A. G. M. Theeuwes, W. K. Brederode and C. L. Delingny, *J. Chromatogr.*, 234 (1982) 321.
6 P. L. Grizzle and J. S. Thomson, *Anal. Chem.*, 54 (1982) 1071.
7 E. P. Lankmayr and K. Müller, *J. Chromatogr.*, 155 (1978) 139.
8 L. Nondek and J. Málek, *J. Chromatogr.*, 155 (1978) 187.
9 L. Nondek, M. Minárik and J. Málek, *J. Chromatogr.*, 178 (1979) 427.
10 L. Nondek and R. Ponec, *J. Chromatogr.*, 294 (1984) 175.
11 J. S. Thomson and J. W. Reynolds, *Anal. Chem.*, 56 (1984) 2434.
12 L. Nondek and M. Minárik, *J. Chromatogr.*, 324 (1985) 261.
13 S. A. Matlin, J. S. Tinker, A. Tito-Lloret, W. J. Lough, L. Chan and D. Bryan, *Proc. Anal. Div. Chem. Soc.*, 16 (1979) 354.
14 S. A. Matlin, W. J. Lough and D. G. Bryan, *J. High Resolut. Chromatogr. Chromatogr. Commun.*, 3 (1980) 33.
15 G. Eppert and T. Schinke, *J. Chromatogr.*, 260 (1983) 305.
16 G. Félix and C. Bertrand, *J. High Resolut. Chromatogr. Chromatogr. Commun.*, 7 (1984) 160.
17 G. Félix and C. Bertrand, *J. High Resolut. Chromatogr. Chromatogr. Commun.*, 7 (1984) 714.
18 K. J. Welch and N. E. Hoffman, *J. High Resolut. Chromatogr. Chromatogr. Commun.*, 9 (1986) 417.
19 R. S. Mulliken and W. B. Person, *Molecular Complexes*, Wiley-Interscience, New York, 1969, p. 448.
20 S. C. Wallwork, *J. Chem. Soc.*, (1961) 494.
21 L. R. Snyder, *Principles of Adsorption Chromatography*, Marcel Dekker, New York, 1968.
22 L. R. Snyder, in Cs. Horváth (Editor), *High Performance Liquid Chromatography*, Vol. 3, Academic Press, New York, 1963, p. 157.
23 L. R. Snyder, *LC Mag.*, 1 (1983) 478.
24 R. P. W. Scott, *J. Chromatogr.*, 122 (1976) 35.
25 L. Nondek, P. Dienstbier and R. Rericha, *J. High Resolut. Chromatogr. Chromatogr. Commun.*, 11 (1988) 217.
26 L. R. Snyder, *J. Phys. Chem.*, 67 (1963) 240.
27 L. R. Snyder, *J. Chromatogr.*, 25 (1966) 274.
28 M. Popl, V. Dolonsky and J. Mostecky, *J. Chromatogr.*, 91 (1974) 649.
29 W. Melander, D. E. Campbell and Cs. Horváth, *J. Chromatogr.*, 158 (1978) 215.
30 K. Jinno and N. Ozaki, *J. Liq. Chromatogr.*, 7 (1984) 877.
31 R. J. Laub and S. J. Madden, *J. Liq. Chromatogr.*, 8 (1985) 187.
32 K. Jinno, T. Ohshima and Y. Hirata, *J. High Resolut. Chromatogr. Chromatogr. Commun.*, 5 (1982) 621.
33 C. M. Riley, E. Tomlinson and T. L. Hakenscheid, *J. Chromatogr.*, 218 (1981) 427.
34 H. Colin, J. C. Díez-Masa, G. Guiochon, T. Czajkowska and I. Miedziak, *J. Chromatogr.*, 167 (1978) 41.
35 K. Jinno and Y. Hirata, *J. High Resolut. Chromatogr. Chromatogr. Commun.*, 5 (1982) 621.
36 C. A. Chang, C.-F. Tu and C.-S. Huang, *J. Chromatogr. Sci.*, 22 (1984) 321.
37 M. Kuchar, E. Draus, V. Rejholec and V. Miller, *J. Chromatogr.*, 449 (1988) 391.
38 H. Issaq and M. Jaroniec, *J. Liq. Chromatogr.*, 12 (1989) 2067.
39 K. J. Laidler, *Trans. Faraday Soc.*, 55 (1959) 1725.
40 R. Lumry and S. Rajender, *Biopolymers*, 9 (1970) 1125.
41 H. E. Baumgarten, *Org. Synth.*, 5 (1973) 1029.
42 S. A. Nabi, S. Haque and P. M. Qureshi, *Talanta*, 30 (1983) 989.
43 J. Sedlácek and L. Nondek, *J. High Resolut. Chromatogr. Chromatogr. Commun.*, 8 (1985) 364.
44 R. R. Krug, W. G. Hunter and R. A. Grieger, *J. Phys. Chem.*, 80 (1976) 2335.
45 R. R. Krug, W. G. Hunter and R. A. Grieger, *J. Phys. Chem.*, 80 (1976) 2341.
46 W. Melander, J. Stoveken and Cs. Horváth, *J. Chromatogr.*, 199 (1980) 35.
47 D. L. Massart and L. Kaufman, *The Interpretation of Analytical Chemical Data by the Use of Cluster Analysis*, Wiley, New York, 1983, p. 15.

Journal of Chromatography, 591 (1992) 89–97
Elsevier Science Publishers B.V., Amsterdam

CHROM. 23 764

Chromatography on Poly-RP and its cyano and diol derivatives using both polar and non-polar solvent systems

Jacek J. Jagodzinski, Gary T. Marshall, Barton J. Poulsen, Giselle Raza and Wesley A. Rolls*

Interaction Chemicals Inc., 1615 Plymouth St., Mountain View, CA 94043 (USA)

(First received April 17th, 1991; revised manuscript received September 24th, 1991)

ABSTRACT

A 4-μm polystyrene–divinylbenzene resin, Poly-RP CO, was synthesized for high-performance liquid chromatography. The surface of this resin was functionalized with cyano and diol groups that are capable of enhancing the selectivity and capacity of the base resin. Chromatography was performed with traditional polar solvent systems, such as acetonitrile–water, and also with non-polar solvent systems, such as dichloromethane–hexane; the latter solvent system can give separations that are otherwise difficult to achieve with acetonitrile–water. Good separations of simple isomer mixtures were achieved on these resins.

INTRODUCTION

Over the last decade, the use of polymeric resins in reversed-phase liquid chromatography has grown dramatically. In 1980, virtually all commercial reversed-phase columns were alkyl-bonded silicas [1], whereas now the list of commercial polymeric columns for reversed-phase high-performance liquid chromatography (HPLC) includes PRP-1 [2], PLRP-S [3] and ACT-1 [4], all of which are polystyrene–divinylbenzene-based resins, as well as Asahipak ODP-50 [5], a vinyl alcohol polymer gel with bonded octadecyl groups, and Hypercarb [6], a porous graphitic carbon stationary phase. One of the driving forces behind the development of these polymeric columns is the inherent pH instability of silica-based columns, especially above pH 7, which places severe limitations on their practical use [7]. Numerous attempts have been made to improve the pH stability of silica-based columns, including the use of bulky silane reagents [8] and the coating of polymers on the surface of silica [9], but these materials still do not have the pH stability associated with the polystyrene–divinylbenzene matrix (stability from pH 0 to 14). Although there have been many recent reports on the HPLC properties of more pH-stable inorganic supports, such as alumina [10], zirconia [11] and titania [12], these supports are not yet available in the same wide range of particle sizes and pore sizes as silica gel and polymer resins. Currently, commercial silica-based columns are still far superior to polymer-based columns in terms of column efficiency and mechanical rigidity.

One advantage of polystyrene-based resins in the ease with which the phenyl rings can be functionalized with a variety of different organic moieties, so that a wide range of sorbents with different properties and applications can be derived from a single base material. Polystyrene beads have been modified with a number of useful functional groups, including amino [13], nitro [14] and hydroxyl [15] groups. Although interesting HPLC separations on these resins have been reported, all of the chromatography was performed with methanol–water and/or

0021-9673/92/$05.00

acetonitrile–water mobile phases, which are the standard polar solvent systems used for reversed-phase chromatography.

This paper demonstrates that good separations can be achieved on polystyrene-based resins by using non-polar solvent systems, such as dichloromethane–hexane and tetrahydrofuran–hexane. A 4-μm macroporous polystyrene resin, Poly-RP CO, was used for the chromatography, together with two hydrophilic derivatives, Poly-RP CYANO and Poly-RP DIOL. It is demonstrated that the use of non-polar solvent systems allows separations that are difficult to achieve with acetonitrile–water, and that the addition of the cyano and diol functional groups to the base resin vastly improves the resolution of simple mixtures of isomers in non-polar solvent systems.

EXPERIMENTAL

Equipment

All polymer resins were packed into 15 × 0.46 cm I.D. stainless-steel columns for 20 min at 4000 p.s.i. using a Shandon HPLC packing apparatus (Keystone Scientific, State College, PA, USA). Valco end-fittings with 2-μm pressed-in frits were used to end-cap the columns (Valco Instruments, Houston, TX, USA). The chromatographic system consisted of two Hitachi (Danbury, CT, USA) Model 655A-12 pumps, a Hitachi L-5000 LC gradient controller, a Hitachi D-2000 ChromatoIntegrator, a Kratos (Ramsey, NJ, USA) Spectroflow 773 absorbance detector and a Rheodyne (Cotati, CA, USA) Model 7125 sample injector equipped with a 20-μl sample loop. Infrared spectra were recorded on a Perkin-Elmer (Norwalk, CT, USA) 1600 Series Fourier transform (FT) IR spectrometer equipped with a diffuse-reflectance sample accessory.

Materials and methods

All chromatographic solvents were purchased from EM Science (Cherry Hill, NJ, USA) and were of OmniSolve grade. Test solutes for HPLC were obtained from Aldrich (Milwaukee, WI, USA). Solute solutions were made up by dissolving 0.1–0.5 g of the compound in either hexane, acetonitrile, dichloromethane or the mobile phase and then diluting these stock solutions by a factor of 1:100 with the mobile phase or with pure hexane. Triton N-101 was purchased from Polysciences (Warrington, PA, USA). Capacity factors (k') and efficiencies (plates per meter; N/m) were determined according to the method described by Snyder and Kirkland [16]. All of the chromatographic runs were performed at ambient temperature.

The base polymer, Poly-RP CO, is a 4-μm, 300-Å, macroporous polystyrene–divinylbenzene resin available from Interaction Chemicals (Mountain View, CA, USA). Poly-RP CYANO and Poly-RP DIOL resins were obtained by chemical derivatization of the Poly-RP CO base resin. The success of the synthetic procedures and the presence of the functional groups was confirmed by FT-IR spectrometry; the Poly-RP CYANO resin showed a strong absorption at 2250 cm^{-1}, which is uniquely characteristic of the cyano moiety [17], while the Poly-RP DIOL resin displayed intense broad bands centered at 3400 and 1100 cm^{-1}, which confirms the presence of hydroxyl groups [17]. Elemental analysis (Galbraith Labs., Knoxville, TN, USA) was performed on the Poly-RP CYANO and Poly-RP DIOL resins, and gave levels of functionalization of 0.9 mmol/g for the cyano group and 1.1 mmol/g for the diol group.

RESULTS AND DISCUSSION

Comparison of the polarity of Poly-RP CO and its derivatives

Fig. 1 shows a standard test chromatogram of a Poly-RP CO column packed in acetonitrile–water (70:30) and then tested with the same mobile phase containing 0.01 M dibasic potassium phosphate buffer. The description of the solute mixture and the corresponding efficiencies, asymmetries and capacity factors are given in Table I, with the retention time of potassium nitrite being used as the t_0 value. The peak efficiencies are good relative to other polymer-based columns, with several peaks having efficiencies above 50 000 N/m, but are still much lower than those of commercial silica-based columns. This difference in efficiency between polymer- and silica-based columns has been reviewed by other workers [18,19] and is believed to be caused mainly by the microporous gel structure of polymer resins.

The unfunctionalized Poly-RP CO is by nature extremely hydrophobic. In contrast, the Poly-RP CYANO and the Poly-RP DIOL were easily dis-

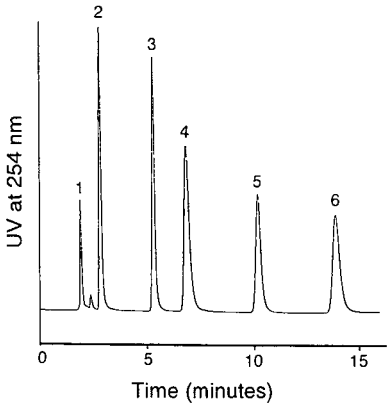

Fig. 1. Separation of a standard test mixture on a Poly-RP CO column. Mobile phase, acetonitrile–water (70:30) with 0.01 *M* dibasic potassium phosphate buffer; flow-rate, 0.75 ml/min. Peaks: 1 = potassium nitrite; 2 = physostigmine; 3 = acetophenone; 4 = diethyl phthalate; 5 = butyrophenone; 6 = valerophenone.

persed in water (*i.e.*, hydrophilic) and, in fact, we were able to pack both of these polymers at 4000 p.s.i. into 15 × 0.46 cm I.D. columns using water as both the slurry solvent and packing solvent. In order to compare all three resins closely, some Poly-RP CO was packed into a 15 × 0.46 cm I.D. column at 4000 p.s.i. using a 1% solution of Triton N-101 in water as the packing and slurry solvent. Triton N-101 is a non-ionic surfactant that enabled the hydrophobic Poly-RP CO to be dispersed and packed in aqueous media.

After packing, all three columns were equilibrated in water and then the mobile phase was changed to acetonitrile–water (70:30) by subjecting each column to a 30-min gradient at 0.75 ml/min. Each column was then tested and the *N*/m values for valerophenone were found to be 42 000, 25 000 and 32 000 for Poly-RP CO, Poly-RP CYANO and Poly-RP DIOL, respectively, as indicated in Table II. A second gradient from 100% acetonitrile to 100% water and then to acetonitrile–water (70:30) was performed on each column. While the hydrophilic Poly-RP CYANO and Poly-RP DIOL columns showed no decrease in efficiency after the gradient, the *N*/m value for valerophenone on the Poly-RP CO decreased from 42 000 to 27 000, probably because the hydrophobic Poly-RP CO partly collapsed when subjected to 100% water. In general, we have found that Poly-RP CO performs best in the range from acetonitrile–water (30:70) to 100% acetonitrile, whereas the Poly-RP CYANO and Poly-RP DIOL columns can operate anywhere from 100% water to 100% acetonitrile.

TABLE I

CHARACTERISTICS OF A POLY-RP CO COLUMN USING A STANDARD TEST MIXTURE

The peak asymmetry factor, A_s, was calculated at 10% of the peak height, as described in ref. 16, p. 222. Conditions: mobile phase, acetonitrile–water (70:30) with 0.01 *M* dibasic potassium phosphate buffer; flow-rate, 0.75 ml/min; back-pressure, 1400 p.s.i.

Component	Retention time (min)	k'	A_s	Efficiency (*N*/m)
Potassium nitrite[a]	1.93	0.00	2.7	16 000
Physostigmine	2.84	0.47	1.4	27 000
Acetophenone	5.34	1.77	1.3	56 000
Diethyl phthalate	6.89	2.57	1.6	33 000
Butyrophenone	10.21	4.29	1.4	57 000
Valerophenone	13.93	6.21	1.4	55 000

[a] The potassium nitrite peak is obscured by some oxidation products of physostigmine.

Conversion of the columns to non-polar solvent systems from polar solvent systems

To change from acetonitrile to hexane, a much more non-polar solvent, it was necessary to use an intermediate solvent because hexane and acetonitrile are not totally miscible. Acetone was chosen because it wets polystryrene resins very well, it is

TABLE II

WATER COMPATIBILITY OF POLY-RP CO AND ITS DERIVATIVES

Gradient 1 = 100% water to acetonitrile–water (70:30) at 0.75 ml/min over a 30-min period. Gradient 2 = 100% acetonitrile to 100% water to acetonitrile–water (70:30) at 0.75 ml/min over a 1-h period. Conditions: flow-rate, 0.75 ml/min; back-pressure, *ca.* 2000 p.s.i. for all three columns. k' = Capacity factor of valerophenone. Efficiency = *N*/m value of valerophenone.

Column	k'	Efficiency after gradient 1 (*N*/m)	Efficiency after gradient 2 (*N*/m)
Poly-RP CO	6.2	42 000	27 000
Poly-RP CYANO	4.7	25 000	25 000
Poly-RP DIOL	4.5	32 000	32 000

TABLE III

INTERCHANGE OF SOLVENTS ON A POLY-RP CYANO COLUMN

Conditions: 1-h linear gradients from 100% of the original solvent to 100% of the final solvent at 0.5 ml/min with UV detection at 350 nm; the time required for a baseline is the total time measured from the start of the gradient.

Original solvent	Final solvent	Time required for baseline (min)
Acetonitrile	Acetone	70
Acetone	Hexane	102
Hexane	Acetone	70
Acetone	Acetonitrile	88

miscible with both acetonitrile and hexane and it has a low viscosity, thereby leading to low column back-pressures. All columns were subjected to 1-h linear gradients from 100% acetonitrile to 100% acetone at 0.5 ml/min, followed by 1-h linear gradients from 100% acetone to 100% hexane; this is similar to a procedure used by other workers for changing mobile phases on a cyanopropylsilica column [20]. A reverse gradient, from hexane to acetone to acetonitrile, was run on the Poly-RP CYANO column and the efficiency was re-evaluated in acetonitrile–water (70:30) using valerophenone as the test solute. The efficiency was found to be 25 000 N/m, which is the same efficiency that this resin displayed before the gradient runs. These data show that the derivatized resins can be used in mobile phases of virtually any polarity. Table III summarizes the times required to achieve the baseline with these gradients on the Poly-RP CYANO column.

pH stability of Poly-RP CO, Poly-RP CYANO and Poly-RP DIOL

In order to demonstrate the pH stability of Poly-RP CO and its derivatives, the columns were tested under both strongly basic conditions [acetonitrile–water (70:30) containing 1% of triethylamine] and strongly acidic conditions [acetonitrile–water (70:30) containing 1% of phosphoric acid]; the results are reported in Table IV. Each column was equilibrated in the appropriate mobile phase and then the capacity factor (k'), efficiency (N/m) and peak asymmetry factor (A_s) were measured using valerophenone as a test solute. After pumping 1000 ml of mobile phase through each column, these parameters were remeasured and are reported in parentheses in Table IV next to the original values. The results show that all three resins suffered little or no deterioration in capacity factor, efficiency or peak asymmetry under conditions of strong base or strong acid.

Choice of non-polar mobile phase solvents

Most of the early HPLC work was carried out on polar silica gels using relatively non-polar mobile phases. Later, non-polar bonded-phase silica columns using polar mobile phases became more popular. The former type of chromatography is known as "normal-phase" and the latter as "reversed-phase" [21]. There have been many recent

TABLE IV

pH STABILITY OF POLY-RP CO AND ITS DERIVATIVES

Basic conditions: 0.75 ml/min of acetonitrile–water (70:30) containing 1% of triethylamine. Acidic conditions: 0.75 ml/min of acetonitrile–water (70:30) containing 1% of phosphoric acid. The initial values of k', N/m and A_s for the valerophenone test solute are listed, followed in parentheses by the values obtained after pumping 1000 ml of mobile phase through each column.

Conditions	Parameter	Poly-RP CO	Poly-RP CYANO	Poly-RP DIOL
Basic	k'	6.5 (6.6)	5.3 (5.2)	4.6 (4.5)
	N/m	45 000 (45 000)	35 000 (35 000)	25 000 (26 000)
	A_s	1.3 (1.2)	1.2 (1.2)	1.0 (0.9)
Acidic	k'	7.0 (7.1)	5.7 (5.6)	4.8 (4.9)
	N/m	45 000 (45 000)	34 000 (34 000)	26 000 (26 000)
	A_s	1.3 (1.3)	1.2 (1.1)	0.9 (1.0)

reports of separations on bonded-phase silicas using non-polar solvents because of the unique separation selectivities that these mobile phases can offer. Some examples include the separations of fat-soluble vitamins [22], polyhydroxysteroids [23], flavonoids [24] and metal–diethyldithiocarbamate chelates [25].

In most of these reports, hexane was chosen as the base or "weak" solvent and various percentage of "strong" solvent modifiers, such as dichloromethane, tetrahydrofuran, ethyl acetate or isopropanol, were added to adjust the retention times of the solutes to reasonable levels. For our purposes, isopropanol was rejected because its high viscosity leads to very high column back-pressures with small polymer particles. Ethyl acetate was rejected because it is not transparent in the UV range of interest for typical HPLC applications. Because initial testing showed that higher column efficiencies were obtained with the dichloromethane–hexane system than with the tetrahydrofuran–hexane system, all of the "normal-phase" chromatography reported in this paper was done in the former solvent system. An increase in the percentage of dichloromethane gave shorter retention times for all the solutes studied on both the base resin and its functionalized derivatives. These results are analogous to those found for solvent strength studies performed on silica columns and their polar bonded-phase derivatives. For example, the mobile phase strength on an aminosilica column was found to increase as the percentage of tetrahydrofuran in hexane was raised [26]. A decrease in retention time with an increase in the amount of polar modifier in a non-polar solvent is generally observed in normal-phase chromatography [27].

Separation of aniline derivatives

Fig. 2 shows the separation of N,N-diethylaniline (2.93 min), N,N-dimethylaniline (3.38 min) and aniline (5.75 min) on a Poly-RP CO column in a mobile phase consisting of dichloromethane–hexane (10:90) containing 0.1% of triethylamine. As has been noted in previous work on bonded-phase silica columns [28], the peak elution order is the opposite of that observed in reversed-phase chromatography with the most non-polar compound, N,N-diethylaniline, eluting first and the most polar compound, aniline, eluting last.

The effects of the cyano and diol functional

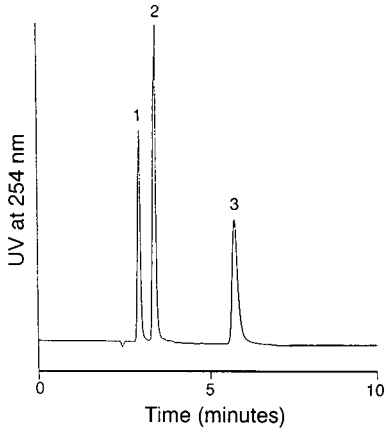

Fig. 2. Separation of anilines on a Poly-RP CO column using a non-polar mobile phase. Mobile phase, dichloromethane–hexane (10:90) containing 0.1% of triethylamine; flow-rate, 0.75 ml/min. Peaks: 1 = N,N-diethylaniline; 2 = N,N-dimethylaniline; 3 = aniline.

groups can be seen in the separation of the isomers of dimethylaniline (Fig. 3); the corresponding numerical data for these separations and the others reported in this work are presented in Table V. A

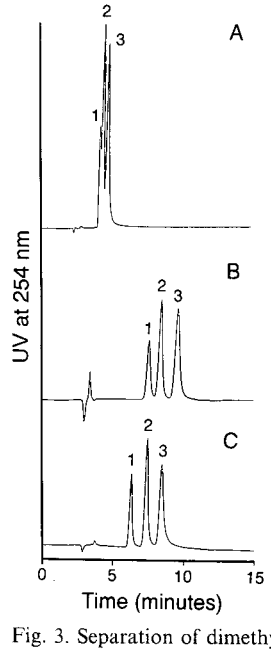

Fig. 3. Separation of dimethylanilines on (A) Poly-RP CO, (B) Poly-RP CYANO and (C) Poly-RP DIOL columns. Mobile phase, dichloromethane–hexane (10:90) containing 0.1% of triethylamine; flow-rate, 0.75 ml/min. Peaks: 1 = 2,6-dimethylaniline; 2 = 2,4-dimethylaniline; 3 = 3,5-dimethylaniline.

TABLE V

CAPACITY FACTORS (k') FOR VARIOUS SOLUTES ON POLY-RP CO AND ITS DERIVATIVES USING BOTH POLAR (P) AND NON-POLAR (NP) MOBILE PHASES

All experiments were done at a flow-rate of 0.75 ml/min.

Solute	k'					
	Poly-RP CO		Poly-RP CYANO		Poly-RP DIOL	
	NP	P	NP	P	NP	P
2,6-Dimethylaniline[a]	1.15	3.26	3.12	2.99	2.00	2.52
2,4-Dimethylaniline[a]	1.24	2.76	3.58	2.64	2.52	2.20
3,5-Dimethylaniline[a]	1.41	2.75	4.22	2.64	3.03	2.23
o-Xylene[a]	0.52		0.72		0.39	
m-Xylene[a]	0.49		0.64		0.35	
p-Xylene[a]	0.47		0.65		0.34	
2,6-Dimethylpyridine[b]	0.65	2.81	2.08	2.67	2.26	2.47
2,5-Dimethylpyridine[b]	0.69	3.34	2.79	3.27	3.23	3.08
2,4-Dimethylpyridine[b]	0.73	3.05	3.15	3.03	3.72	2.91
2,6-Dimethylphenol[c]	0.33	3.58	1.30	3.86	0.76	2.99
2,4-Dimethylphenol[c]	0.50	2.78	3.32	3.70	2.23	2.61
2,3-Dimethylphenol[c]	0.54	2.79	3.73	3.69	2.57	2.61
3,5-Dimethylphenol[c]	0.56	2.26	5.02	3.13	3.30	2.16
1-Naphthol[d]	0.97	8.43	9.60	16.30	7.24	10.97
2-Naphthol[d]	0.98	6.41	11.15	12.24	8.06	8.45

[a] NP = dichloromethane–hexane (10:90) with 0.1% triethylamine; P = acetonitrile–water (60:40) with 0.1% triethylamine.
[b] NP = dichloromethane–hexane (10:90) with 0.1% triethylamine; P = acetonitrile–water (30:70) with 0.1% triethylamine.
[c] NP = dichloromethane–hexane (50:50); P = acetonitrile–water (55:45).
[d] NP = dichloromethane–hexane (50:50); P = acetonitrile–water (45:55).

mixture of 2,6-, 2,4- and 3,5-dimethylaniline was injected on to each of the three columns under identical conditions of dichloromethane–hexane (10:90) containing 0.1% of triethylamine at a flow-rate of 0.75 ml/min. Under these conditions, the unfunctionalized Poly-RP CO showed a low capacity ($k' = 1.1$–1.4) and poor resolution of the isomer mixture, while the functionalized resins, Poly-RP CYANO and Poly-RP DIOL, showed much higher capacities ($k' = 2.0$–4.2) and better resolution of the isomer mixture. A possible explanation for this increase in retention and resolution is that the unfunctionalized Poly-RP CO is capable of interacting with solute molecules primarily through only dispersion and π–π forces, whereas the functionalized resins can interact with solute molecules through a much broader range of forces, including dispersion, π–π, dipole–dipole, acid–base and hydrogen-bonding interactions. For example, because of their polar cyano and hydroxyl functional groups, the Poly-RP CYANO and Poly-RP DIOL resins could undergo strong dipole–dipole and hydrogen-bonding interactions with the nitrogen-containing aniline solutes; such strong interactions would not be possible between the unfunctionalized Poly-RP CO and the aniline solutes. Also, the sample retention is expected to increase as the polarity of the stationary phase is increased because the driving force for retention in normal-phase chromatography is the attraction of polar solute molecules by a polar stationary phase.

To illustrate our point further, we injected some aromatic isomers without any polar functional substituents, namely a mixture of *o*-, *m*- and *p*-xylene, onto all three columns under the same experimental conditions as used for the aniline isomers; the corresponding numerical data are given in Table V. These three isomers could not be separated on any of

the columns (they virtually co-eluted) and, in fact, they had very similar capacity factors on both the functionalized and unfunctionalized resins, with the Poly-RP DIOL actually giving lower capacity factors than the Poly-RP CO resin. The xylene isomers would only be able to interact with the three resins through dispersion and π–π forces and not through strong dipole–dipole and hydrogen-bonding interactions, and so one would expect the separations to be very similar on all three resins in this instance.

The order of elution of these dimethylaniline isomers (2,6- followed by 2,4- and 3,5-) is similar to that observed by Truedsson and Smith [29] using a cyanosilica column with normal-phase solvents. They postulated that the 2,6-isomer would elute first, partly because its amino nitrogen is the most sterically shielded from interaction with the nitrile group of the resin.

Comparison of the separation of pyridine derivatives in non-polar vs. polar solvent systems

A mixture of 2,6-, 2,5- and 2,4-dimethylpyridine was injected on to each of the three columns under the same conditions as used for the aniline derivatives; the results are reported in Fig. 4A and Table V. Once again, the unfunctionalized Poly-RP CO showed a much lower capacity (k' = 0.65–0.73) than the functionalized resins (k' = 2.08–3.72). The best separation of this mixture of isomers was obtained on the Poly-RP DIOL column (see Fig. 4A), which gave a broader range of capacity factors (k' = 2.26–3.72) than the Poly-RP CYANO column (k' = 2.08–3.15).

In order to demonstrate the usefulness of non-polar solvent systems with polymeric columns, the same separation was attempted on all three columns using a mobile phase of acetonitrile–water (30:70) containing 0.1% of triethylamine, which gave capacity factors similar to those obtained with dichloromethane–hexane (10:90). These results are reported in Fig. 4B and Table V. The data show that the Poly-RP DIOL column is capable of good resolution of all three isomers in dichloromethane–hexane, whereas the use of acetonitrile–water resulted in very poor resolution for the 2,5- and 2,4-dimethylpyridines. Research on bonded-phase silica columns has also shown that isomer selectivity is generally superior in normal-phase systems than reversed-phase systems, as was shown for the separation of retinol isomers on silica columns in both types of mobile phases [30].

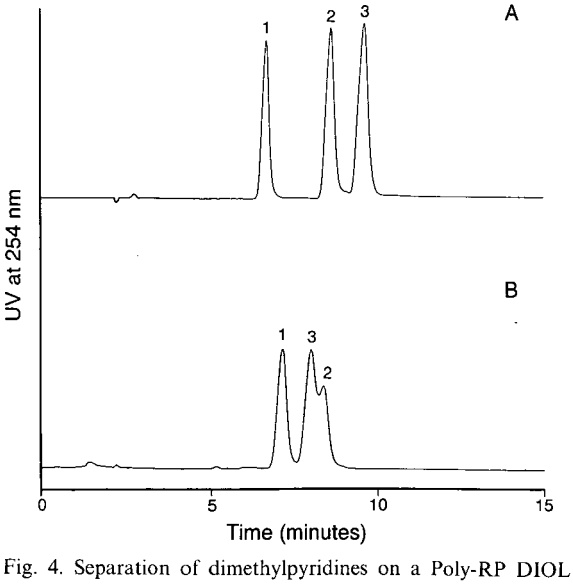

Fig. 4. Separation of dimethylpyridines on a Poly-RP DIOL column using both (A) non-polar and (B) polar mobile phases. Mobile phase, (A) dichloromethane–hexane (10:90) containing 0.1% of triethylamine and (B) acetonitrile–water (30:70) containing 0.1% of triethylamine; flow-rate, 0.75 ml/min. Peaks: 1 = 2,6-dimethylpyridine; 2 = 2,5-dimethylpyridine; 3 = 2,4-dimethylpyridine.

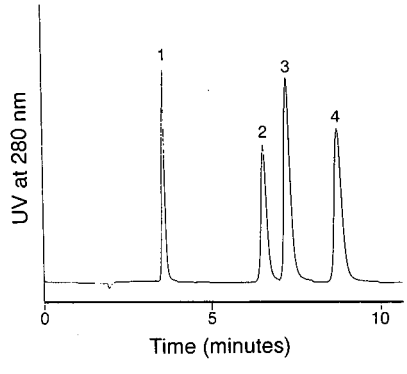

Fig. 5. Separation of dimethylphenols on a Poly-RP DIOL column using a non-polar mobile phase. Mobile phase, dichloromethane–hexane (50:50); flow-rate, 0.75 ml/min. Peaks: 1 = 2,6-dimethylphenol; 2 = 2,4-dimethylphenol; 3 = 2,3-dimethylphenol; 4 = 3,5-dimethylphenol.

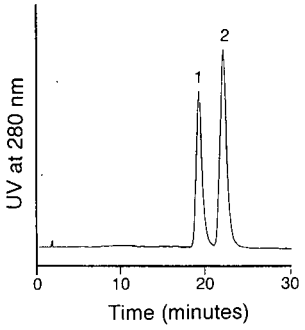

Fig. 6. Separation of naphthols on a Poly-RP CYANO column using the same conditions as in Fig. 5. Peaks: 1 = 1-naphthol; 2 = 2-naphthol.

Separation of phenolic compounds in non-polar solvent systems

The elution of the isomers of dimethylphenol and naphthol (hydroxynaphthalene) on the functionalized columns required a very strong solvent system, dichloromethane–hexane (50:50) (Figs. 5 and 6 and Table V). Fig. 5 shows the separation of four isomers of dimethylphenol on the Poly-RP DIOL column. Fig. 6 shows that baseline resolution of 1- and 2-naphthol can be achieved with the Poly-RP CYANO column. It is also interesting to note the large difference in capacity factors for these compounds on the unfunctionalized and on the functionalized resins (see Table V). This is probably caused by strong hydrogen-bonding interactions between the acidic phenolic hydrogens of the solutes and the polar functional groups on the cyano and diol resins, because we have found that the corresponding solutes without the phenolic groups, namely xylene and naphthalene, can easily be eluted from the cyano and diol resins with dichloromethane–hexane (10:90).

Most of the isomers in this study have been tested using both acetonitrile–water and dichloromethane–hexane (Table V). Generally, acetonitrile–water gave very similar separations and capacity factors on all three columns; the differences between the functionalized and unfunctionalized columns were much more exaggerated in dichloromethane–hexane. Unlike normal-phase chromatography, where the driving force for retention is the attraction of polar solutes to a polar stationary phase, the driving force for retention in reversed-phase chromatography is the rejection of less polar solutes by the highly polar mobile phase. When the polar Poly-RP CYANO and Poly-RP DIOL resins are used with the polar mobile phases employed in reversed-phase chromatography, the difference in polarity between the mobile phase and stationary phase relative to that of a polystyrene–divinylbenzene packing is much lower and the driving force for retention is much less, which explains the similarity in capacity factors among all three stationary phases in reversed-phase solvents. Similar results have been observed on bonded-phase silica columns in reversed-phase systems [31].

CONCLUSIONS

This work demonstrates that good separations can be achieved on polymeric separation media using non-polar solvent systems. The use of these non-polar solvents allows for separations that might be difficult to achieve using the traditional polar solvent systems that are based on mixtures of various organic solvents with water. By avoiding the use of viscous, aqueous-based mobile phases, low operating pressures can be achieved even with 4-μm polymeric particles. The functionalization of the polymer surface with diol and cyano moieties increases the capacity and resolving power of these columns in non-polar solvents.

ACKNOWLEDGEMENTS

The support of Mr. D. Hometchko and Mr. N. Kitagawa, and the management of Interaction Chemicals and E.M. Science, is gratefully acknowledged, as are the efforts of the production and applications divisions of Interaction Chemicals.

REFERENCES

1 R. E. Majors, *J. Chromatogr. Sci.*, 18 (1980) 488.
2 D. P. Lee and J. H. Kindsvater, *Anal. Chem.*, 52 (1980) 2425.
3 L. D. Bowers and S. Pedigo, *J. Chromatogr.*, 371 (1986) 243.
4 D. MacBlane, N. Kitagawa and J. R. Benson, *Am. Lab.*, 19 (1987) 134.
5 T. Ohtani, Y. Tamura, M. Kasai, T. Uchida, Y. Yanagihara and K. Noguchi, *J. Chromatogr.*, 515 (1990) 175.
6 B. J. Bassler and R. A. Hartwick, *J. Chromatogr. Sci.*, 27 (1989) 162.
7 J. R. Benson and D. J. Woo, *J. Chromatogr. Sci.*, 22 (1984) 386.

8 J. J. Kirkland, J. L. Glajch and R. D. Farlee, *Anal. Chem.*, 61 (1989) 2.
9 H. Engelhardt, H. Low, W. Eberhardt and M. Maub, *Chromatographia*, 27 (1989) 535.
10 T. Cserhati, *Chromatographia*, 29 (1990) 593.
11 T. P. Weber, P. W. Carr and E. F. Funkenbusch, *J. Chromatogr.*, 519 (1990) 31.
12 M. Kawahara, H. Nakamura and T. Nakajima, *J. Chromatogr.*, 515 (1990) 149.
13 K. T. Howang, K. Iwamoto, N. Takai and M. Seno, *J. Liq. Chromatogr.*, 8 (1985) 2387.
14 C. Grosse-Rhode, H. G. Kicinski and A. Kettrup, *Chromatographia*, 26 (1988) 209.
15 Y.-B. Yang and M. Verzele, *J. Chromatogr.*, 387 (1987) 197.
16 L. R. Snyder and J. J. Kirkland, *Introduction to Modern Liquid Chromatography*, Wiley, New York, 1979, pp. 24 and 31.
17 R. M. Silverstein, G. C. Bassler and T. C. Morrill, *Spectrometric Identification of Organic Compounds*, Wiley, New York, 1981, pp. 112 and 129.
18 F. Nevejans and M. Verzele, *J. Chromatogr.*, 406 (1987) 325.
19 N. Tanaka and M. Araki, *Adv. Chromatogr.*, 30 (1989) 81.
20 M. De Smet, G. Hoogewijs, M. Puttemans and D. L. Massart, *Anal. Chem.*, 56 (1984) 2662.
21 R. E. Majors, in C. Horváth (Editor), *High-Performance Liquid Chromatography: Advances and Perspectives*, Academic Press, New York, 1980, p. 76.
22 S. Hara, T. Ando and Y. Nakayama, *J. Liq. Chromatogr.*, 12 (1989) 729.
23 N. Kaouadji and R. Lafont, *J. Chromatogr.*, 505 (1990) 408.
24 M. C. Pietrogrande, C. Bighi, G. Blo, Y. D. Kahie, P. Reschiglian and F. Dondi, *Chromatographia*, 27 (1989) 625.
25 P. L. Zhu, D. J. Wang, J. Q. Jin and S. L. Cao, *Chromatographia*, 25 (1988) 419.
26 L. R. Snyder, *LC Mag.*, 1 (1983) 478.
27 L. R. Snyder and J. J. Kirkland, *Introduction to Modern Liquid Chromatography*, Wiley, New York, 1979, p. 284.
28 L. R. Snyder and J. J. Kirkland, *Introduction to Modern Liquid Chromatography*, Wiley, New York, 1979, p. 282.
29 L.-A. Truedsson and B. E. F. Smith, *J. Chromatogr.*, 214 (1981) 291.
30 B. Stancher and F. Zonta, *J. Chromatogr.*, 234 (1982) 244.
31 P. E. Antle, A. P. Goldberg and L. R. Snyder, *J. Chromatogr.*, 321 (1985) 1.

Journal of Chromatography, 591 (1992) 99–106
Elsevier Science Publishers B.V., Amsterdam

CHROM. 23 786

Oriented immobilization of peptide ligands on solid supports

Giorgio Fassina

Protein Engineering Unit, Tecnogen ScpA, Via Ampere 56, I-20131 Milan (Italy)

(First received March 26th, 1991; revised manuscript received October 2nd, 1991)

ABSTRACT

A synthetic procedure was developed for the direct immobilization on preactivated affinity supports of peptidic ligands requiring free α-amino groups to recognize their targets properly. The peptidic ligand is assembled by solid-phase peptide synthesis on an octa-branched heptalysine core through a polyglycine spacer, similarly to the method developed for the production of multiple antigenic peptides. After deblocking from the resin, peptide is dialysed, lyophylized and used directly for coupling to preactivated supports. Following immobilization, only a limited number of peptide chains are covalently linked to the solid phase, leaving the remainder facing the mobile phase and sufficiently spaced to interact properly. This procedure was applied successfully to the design, synthesis and oriented immobilization of a multimeric tripeptide ligand (Met–Tyr–Phe) for affinity purification of bovine neurophysin.

INTRODUCTION

Retention of the molecular recognition properties of immobilized ligands requires their orientation on the solid phase [1,2]. A vast number of peptidic ligands used for polypeptide purification need complete accessibility of the α-amino groups, often involved in stabilizing interactions in the forming complex [3]. In these instances, to achieve full retention of recognition properties, is necessary to immobilize the peptidic ligand through its C-terminal carboxyl group, following an often laborious route which requires reversible protection of all the ligand amino groups, activation of the ligand C-terminal carboxyl group with usually the formation of an active ester, coupling to an amino group-derivatized solid support and removal of the α-amino protecting groups. If the peptide ligand bears other carboxyl groups in the side-chains, the activation cannot be directed towards a specific group and the peptide will be randomly immobilized through all the activatable carboxyl groups. A procedure has been developed to overcome these problems, based on the direct synthesis of the peptide ligand in a multimeric form starting from a polydentate lysinic core, similarly to the syntesis of multiple antigenic peptides for antisera production [4]. This procedure has been applied to the design, synthesis and immobilization of a tripeptide Met–Tyr–Phe, able to associate bovine neurophysins non-covalently [3,5]. Neurophysins are a class of small (10 000 dalton) neuroendocrine proteins which form multimolecular non-covalent complexes with the neurohypophysial peptide hormones oxitocin and vasopressin, and also di- and tripeptide analogues of the α-amino terminal sequence of the hormones [6]. Peptides containing only the first three residues of the hormones contribute almost two thirds of the binding free energy of the natural hormones, and binding interactions at the side-chain in position 1 appear to be hydrophobic and an aromatic side-chain in position 2 is necessary for binding [7]. Removal of the free α-amino group in position 1 by substitution with H or by derivatization diminishes binding to neurophysins by a factor of at least 100. The requirement of availability of the peptidyl α-amino group precluded the non-directed coupling of peptides, hormones and analogues to solid supports for affinity column preparation [8].

0021-9673/92/$05.00

EXPERIMENTAL

Materials

9-Fluorenylmethoxycarbonyl (Fmoc)-derivatized amino acids and 4-hydroxymethylphenoxyacetic (HMP) resin for solid-phase peptide synthesis were purchased from Novabiochem (Laufelfingen, Switzerland). High-performance liquid chromatographic (HPLC)-grade, dichloromethane (DCM), N-methylpyrrolidone (NMP), methanol, water and acetonitrile were purchased from Merck (Darmstadt, Germany) and trifluoroacetic acid (TFA) from Pierce (Rockford, IL, USA). Reagents used as scavengers during deblocking of peptides from resins, such as phenol, thioanisole and ethanedithiol, were obtained from Aldrich (Milan, Italy). Eupergit C 30N, an acrylic support for affinity chromatography preactivated with epoxy groups, was obtained from Rohm (Weiterstadt, Germany). Glass affinity columns used for packing peptide derivatized support were purchased from Omni (Cambridge, UK). Freeze-dried bovine posterior pituitary glands were obtained from Peel-Freeze (Roger, AR, USA).

Solid-phase synthesis

Octameric MYFGGGGG ligand (8[MYF-G_5] (MYF = Met–Tyr–Phe) was synthesized by solid-phase peptide synthesis following the Fmoc methodology [9] on a fully automated Model 431 A Applied Biosystems synthesis, software version 1:1.

The solvent systems for dissolving derivatized amino acids were NMP–DCM mixtures and peptide chains were assembled from subsequent coupling of dicyclohexylcarbodiimide (DCC)–hydroxybenzotriazole-activated amino acids on HMP resin. The attachment of the first amino acid, glycine, to the resin was accomplished automatically using 4-dimethylaminopyridine as catalyst. On the Gly–HMP resin, three subsequent coupling cycles of Fmoc-Lys(Fmoc) were performed, and then the MYFGGGGG chain was assembled. After completion of the synthesis cycles, the peptide resin was dried overnight under vacuum. Peptide was cleaved from the resin (200 mg) using 10 ml of TFA–phenol–thioanisole–ethanedithiol (95:2:2:1) and incubating at room temperature for 1.5 h. The mixture was then filtered and vacuum-concentrated to 1 ml and peptidic material was precipitated by adding 10 ml of cold diethyl ether. The collected precipitate was dissolved in 20 ml of 0.1 *M* acetate acid, extensively dialysed against 0.1 *M* acetic acid and lyophilized. The peptide 8[G_5], structurally identical with 8[MYF-G_5] except for the first three MYF N-terminal residues, was synthesized and purified similarly as a control.

Affinity column preparation

Immobilization of 8[MYF-G_5] on Eupergit C 30N was carried out by incubating 10 mg of peptide dissolved 10 ml of 0.1 *M* $NaHCO_3$–0.5 *M* NaCl (pH 8.5) with 1.0 g of support with agitation for 24 h. The extent of peptide incorporation was followed by reversed-phase (RP) HPLC, indicating that 95% of the starting peptide was support bound. Subsequently, the resin was repeatedly washed with 0.1 *M* Tris (pH 8.5) and slurry packed on an 80 × 6.6 mm I.D. glass column. In a similar way were prepared control columns, incubating 1.0 g of Eupergit C 30N with 10 ml of 0.5 *M* Tris (pH 8.5) or 10 mg of MYF-NH_2 or 10 mg of 8[G_5].

Determination of binding constants

Dissociation constants for the interaction between immobilized 8[MYF-G_5] and soluble neurophysin (NP) were determined by competitive elution experiments [10,11]. The extent of retardation of the NP elution volume on the (8[MYF-G_5])Eupergit column was measured in the presence of increasing amounts of MYF-NH_2 dissolved in the elution buffer. Data were plotted according to the equation

$$\frac{1}{V - V_0} = \frac{K_{M/P}}{M_T} + \frac{[L]K_{P/L}}{M_T K_{M/P}} \quad (1)$$

where V is the elution volume of NP, V_0 the column void volume, $K_{M/P}$ the dissociation constant for the interaction between immobilized 8[MYF-G_5] and soluble NP, [L] the concentration of MYF-NH_2 in the buffer, $K_{P/L}$ the dissociation constant for the interaction between soluble NP and soluble MYF-NH_2 and M_T the total amount of immobilized 8[MYF-G_5].

Amino acid analysis

The amino acid composition of synthetic peptides, peptide fragments obtained by neurophysin proteolytic digestion and the peptide loading of de-

rivatized supports were evaluated by RP-HPLC analysis of Fmoc-derivatized acid hydrolysates [12].

Purification of NP II from bovine pituitary glands

Crude neurophysin mixtures were obtained from freeze-dried bovine pituitaries by acid extraction, sodium chloride precipitation and gel filtration on Sephadex G-25 in 1 *M* formic acid [13]. Isolation of bovine neurophysin II isoforms from mixtures of neurophysin I and other non-NP-related peptides was achieved by ion-exchange chromatography on a DEAE-Trisacryl column (70 × 2.4 cm I.D.) using a linear gradient from 0.1 *M* (1 l) to 0.5 *M* (1 l) ammonium acetate (pH 6.0). The identity of the purified neurophysin II was confirmed by amino acid analysis and tryptic mapping of performic acid-oxidized material, under the conditions described previously [14]. In detail, samples of neurophysin II (100 μg) were treated with 100 μl of performic acid, incubated for 3 h at 4°C and then diluted with water and lyophilized. Trypsin digestion was performed by incubating the performic acid-oxidized protein with 2% L-1-tosylamide-2-phenylethyl-chloromethyl ketone (TPCK) trypsin for 2 h at 37°C in 0.1 *M* NH_4HCO_3 (pH 8.6). At the end the mixture was lyophilized and subjected to RP-HPLC analysis. Fragments corresponding to neurophysin II residues 1–8, 9–18, 21–43, 44–66 and 67–93, purified by RP-HPLC, were identified by amino acid analysis.

High-performance electrophoresis

Determination of the molecular weight of 8[MYF-G_5] was carried out by high-performance electrophoresis on an ABI Model 230A instrument using a 50 × 2.5 mm I.D. 12% polyacrylamide gel tube. Gels, prepared according to the manufacturer's instructions in the native and denaturing form, were run at 1.5 mA, and the effluent was monitored by measuring the UV absorbance at 225 nm. Under these conditions, the multimeric peptide eluted after 135 min, bromophenol blue (700 dalton) after 50 min, neurophysin (10 000 dalton) after 120 min and α-lactalbumin (14 200 dalton) after 130 min.

Thermolysin treatment of 8[MYF-G_5] and (8[MYF-G_5])Eupergit

Samples of 8[MYF-G_5] (100 μg) and (8[MYF-G_5])Eupergit (50 mg) were treated with 0.1 μg of thermolysin (TLN) in 1 ml of 0.1 *M* Tris (pH 7.0). The mixtures were incubated for 3 h at room temperature under agitation. Subsequently, aliquots of 100 μl were analysed by RP-HPLC and compared with the digestion products of MYF-NH_2 (50 μg) obtained by similar treatment.

RESULTS

Design, synthesis and characterisation of 8[MYF-G_5]

The tripeptide vasopressin analogue Met–Tyr–Phe was synthesized starting from an octadentate branching heptalysine core, obtained after three subsequent couplings of Fmoc–Lys(Fmoc) on a Gly–HMP resin. A pentaglycine spacer was introduced before the MYF sequence to provide augmented accessibility of the tripeptide for NP interaction. The structure of the resulting product, denoted 8[MYF-G_5], is shown in Fig. 1. After cleavage from the resin, peptide was purified by dialysis against 0.1 *M* acetic acid and lyophilized. The purified material gave a satisfactory amino acid analysis (M 6.9, Y 6.5, F 7.4, G 41.3, K 7.2). RP-HPLC analysis of dialysed material provided a non-homogeneous profile (Fig. 2, top), probably indicative of some deletions occurred during synthesis, caused by the steric hindrance created by the chains growing in close proximity from the polylysinic core. The non-homogeneity of the elution profile could also be enhanced by non-homogeneous types of interac-

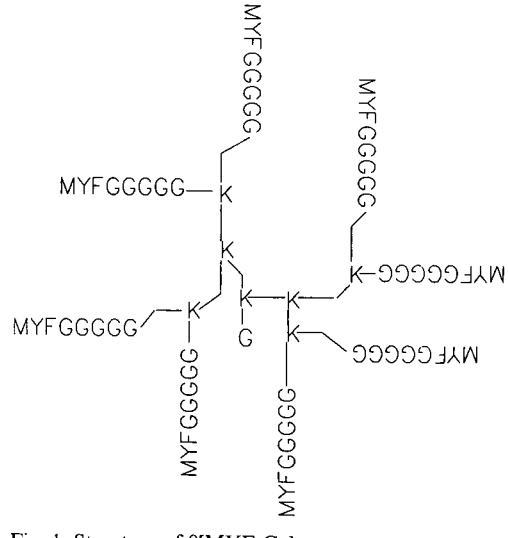

Fig. 1. Structure of 8[MYF-G_5].

tions of the branched peptide with the stationary phase of the reversed-phase column (C_4, 300 Å pore size). Determination of the molecular weight of 8[MYF-G_5] on a calibrated gel filtration column (Fig. 2, bottom) provided a value higher than the expected theoretical value (8000 dalton). The same behaviour was observed in gel electrophoresis under denaturing and non-denaturing conditions. This effect could be explained by a larger molecular volume filled by the 8[MYF-G_5] molecule compared with that occupied by a folded protein of the same molecular weight. Incorporation of the tripeptide at the head of the pentaglycine octamer was also confirmed comparing the digestion products of 8[MYF-G_5] and MYF-NH_2 treated with TLN (Fig. 3). Under the same proteolysis conditions, the dipeptide MY-COOH is obtained in both instances, indicating that the tripeptide MYF is correctly assembled in 8[MYF-G_5] after the polyglycine spacer.

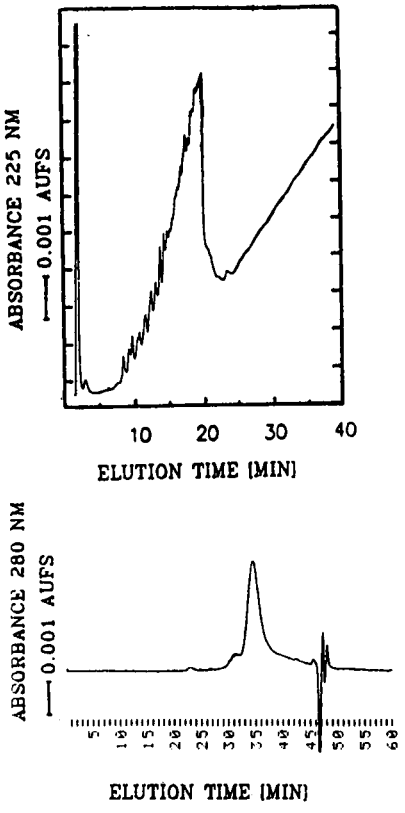

Fig. 2. Chromatographic characterization of 8[MYF-G_5]. Top: RP-HPLC profile of dialysed 8[MYF-G_5]. The sample (50 μg) was eluted on a Brownlee Labs. C_4 RP-HPLC column (50 × 3 mm I.D.) equilibrated at a flow-rate of 0.5 ml/min with acetonitrile–water–(5:95:0.1), with a linear gradient of acetonitrile from 5% to 60% in 30 min. The effluent was monitored at 225 nm (0.1 a.u.f.s.). Bottom: gel filtration profile of dialysed 8[MYF-G_5]. The sample (100 μg) was eluted on a TSK-SW 2000 gel filtration column (300 × 4.6 mm I.D.) equilibrated at a flow-rate of 0.5 ml/min with 0.1 *M* acetic acid. The effluent was monitored at 280 nm (0.01 a.u.f.s.).

Recognition properties of immobilized 8[MYF-G_5]

The binding characteristics of immobilized 8[MYF-G_5] were first evaluated by zonal and competitive elutions of ion-exchange chromatographically purified NP on the (8[MYF-G_5]) Eupergit high-performance liquid affinity chromatography (HPLAC) column. A small amount of NP (100 μg) was applied to the column equilibrated at a flow-rate of 1 ml/min with 0.1 *M* ammonium acetate (pH 5.7), monitoring the effluent at 280 nm, and after 25

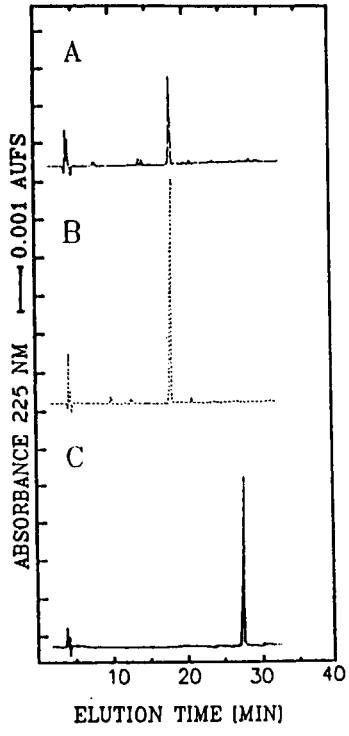

Fig. 3. Thermolysin proteolytic degradation of 8[MYF-G_5]. RP-HPLC profile of (C) MYF-NH_2, (B) TLN-treated MYF-NH_2 and (A) TLN-treated 8[MYF-G_5] obtained on a Zorbax C_{18} column (250 × 4.6 mm I.D.) using a linear gradient from 5 to 50% acetonitrile in 30 min. Eupergit-immobilized 8[MYF-G_5] after TLN treatment provided the same peptide fragment as in chromatogram A.

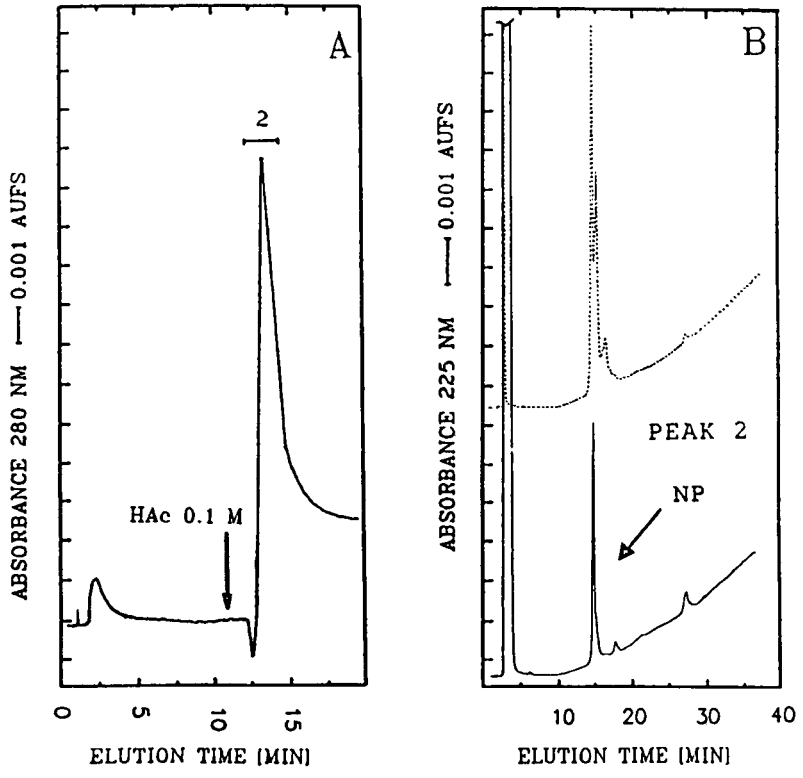

Fig. 4. Binding of partially purified NP to (8[MYF-G_5])Eupergit. (A) HPLAC profile of 100 μg of NP obtained after ion-exchange chromatography on the (8[MYF-G_5])Eupergit column. The column was equilibrated at a flow-rate of 1.0 ml/min with 0.2 *M* ammonium acetate (pH 5.7). At the position indicated by the arrow, the eluent was changed to 0.1 *M* acetic acid. Eluted material, denoted peak 2, was collected for RP-HPLC analysis. (B) RP-HPLC analysis of 50 μg of NP after the ion-exchange chromatographic step (top) and HPLAC-purified peak 2 (bottom).

min the eluent was changed to 0.1 *M* acetic acid (Fig. 4A). Bound material, denoted peak 2, was collected and analysed by RP-HPLC (Fig. 4B, bottom) and compared with the starting material (Fig. 4B, top). The affinity column retained NP almost quantitatively (90%) and allowed the removal of closely eluting RP-HPLC contaminants. Under the identical elution conditions and column geometry, a (Tris)Eupergit column failed to retain any NP sample applied (Fig. 5A). Similarly, columns of the same overall dimensions prepared by immobilizing MYF-NH_2, or 8[G_5], similar in structure to 8[MYF-G_5] but missing the N-terminal tripeptide MYF, did not retain NP under the conditions tested (Fig. 5B and C). Further, treatment of Eupergit-immobilized 8[MYF-G_5] with thermolysin released the MY-NH_2 dipeptide in solution, as reported in Fig. 3, providing clear evidence that not all the chains are covalently bound to the support. Overall, these results indicate (a) that the interaction between NP and 8[MYF-G_5] occurs through the N-terminal tripeptide moiety MYF, and not with the polyglycine core, (b) that the interaction with the tripeptide occurs only if the α-amino group is not covalently linked to the support, and consequently (c) that not all of the eight peptide chains in 8[MYF-G_5] are covalently linked to the solid support, and some of them face the mobile phase and can interact properly with NP.

Further evidence of interaction specificity was shown by the competitive effect of MYF-NH_2 dissolved in the elution buffer. According to eqn. 1, in this situation the elution volume of NP should be reduced proportionally to the amount of MYF-NH_2 in the buffer (Fig. 6). The same amount of NP (50 μg) was applied to the column equilibrated with

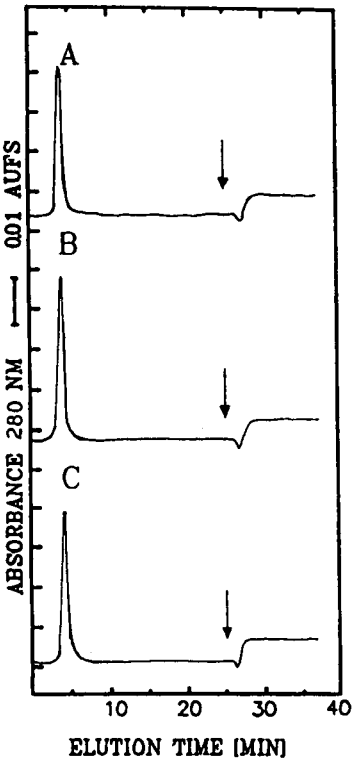

Fig. 5. Elution profile of ion-exchange purified NP on control columns. HPLAC profiles of 100 μg of NP on (A) [MYF-NH_2]Eupergit, (B) [Tris]Eupergit and (C) (8[MYF-G_5])Eupergit. Columns were equilibrated at a flow-rate of 1.0 ml/min with 0.2 *M* ammonium acetate (pH 5.7). At the positions indicated by the arrows, the eluent was changed to 0.1 *M* acetic acid.

0.1 *M* ammonium acetate (pH 5.7) and increasing amounts of MYF-NH_2, and data plotted according to eqn. 1 allowed the determination of dissociation constants for immobilized 8[MYF-G_5]–soluble NP ($K_{M/P} = 3.1 \cdot 10^{-4}$ *M*) and soluble NP–soluble MYF-NH_2 ($K_{P/L} = 6.1 \cdot 10^{-4}$ *M*) interactions. The amount of immobilized MYF-G_5 ($M_T = 30$ μmol) used for calculations of dissociation constants was determined by quantitative amino acid analysis of the derivatized support, assuming 8[MYF-G_5] to be octavalent, and does not take into account the unknown number of chains covalently linked to the solid support and thus not available for the interaction. The correct dissociation constant values can range from *ca.* $2.7 \cdot 10^{-4}$ *M*, for only one chain linked to the solid phase ($M_T = 26$ μmol), to $0.4 \cdot 10^{-4}$ *M*, for seven chains linked to the solid phase ($M_T = 4$ μmol). The close agreement of the dissociation constant values determined by competitive elution experiments with the value obtained fully in solution by other methods ($K_{DISS} = 1.3 \cdot 10^{-4}$ *M*) [2], and by analytical affinity chromatography on Met–Tyr–Phe–Affi-Gel 102 [13] ($K_{DISS} = 1.2 \cdot 10^{-4}$ *M*) suggest that immobilized 8[MYF-G_5] retains similar binding characteristics to the tripeptide MYF-NH_2 in solution.

Further, the multi-branched ligand recognizes NP probably as a monomer, because NP, able to self-associate in solution, in its dimeric form binds the hormone analogue MYF-NH_2 with a one order

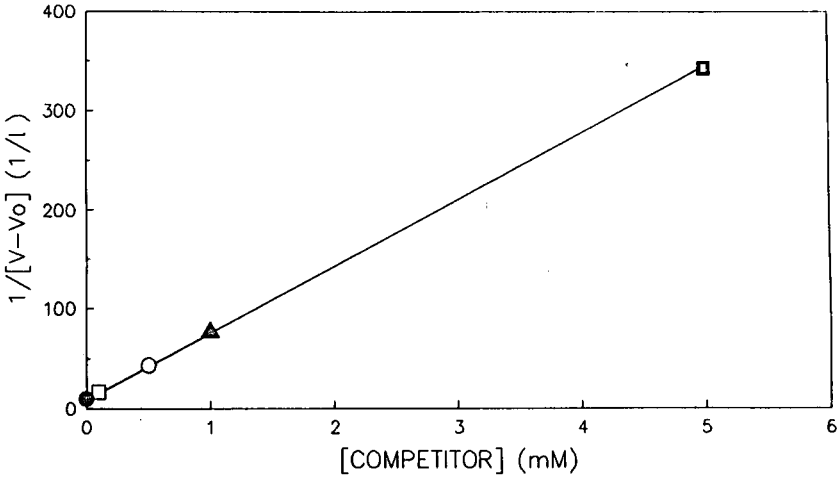

Fig. 6. Competitive elution of NP on the (8[MYF-G_5])Eupergit column. The column was equilibrated with 0.2 *M* ammonium acetate (pH 5.7) containing different amounts of MYF-NH_2 and 50 μg of NP were applied, monitoring the effluent at 280 nm. The dependence of NP retardation on MYF-NH_2 concentration in the elution buffer is plotted according to eqn. 1.

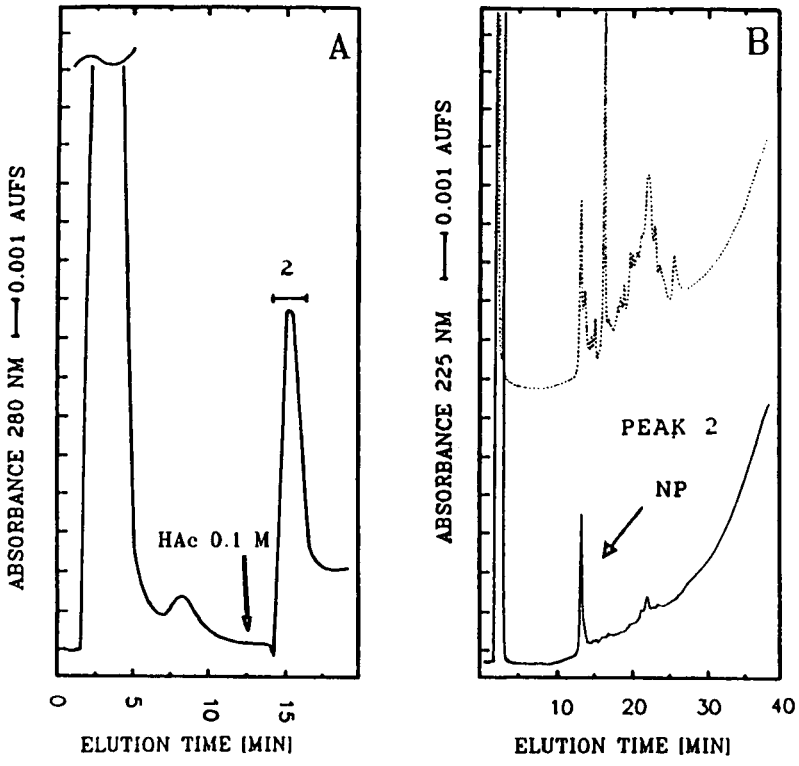

Fig. 7. HPLAC purification of NP from crude extracts. (A) HPLAC profile of crude extract applied to the (8[MYF-G_5])Eupergit column, equilibrated with 0.2 *M* ammonium acetate (pH 5.7). At the position indicated by the arrow, the eluent was changed to 0.1 *M* acetic acid. Eluted material, denoted peak 2, was collected for RP-HPLC analysis. (B) RP-HPLC analysis of crude extract (top) and HPLAC-purified peak 2 (bottom).

of magnitude higher affinity than monomeric NP [15].

Purification of NP from crude extract

To examine the selectivity of immobilized 8[MYF-G_5]–NP recognition, a crude protein mixture (1 mg/ml total proteins) was prepared combining together different *Escherichia coli* extracts, spiked with a small amount of NP (50 μg/ml), and applied to the 8[MYF-G_5]Eupergit column. After elution of unbound material, the eluent was changed to 0.1 *M* acetic acid (Fig. 7A), and bound material, denoted peak 2, was collected for RP-HPLC analysis (Fig. 7B, bottom) and compared with the crude starting material (Fig. 7B, top). The overall recovery was close to 90%, and most contaminants were efficiently removed. The same column has been used for more than 30 runs without any apparent decrease in capacity.

DISCUSSION

The non-directed coupling of neurohypophysial peptide hormones to solid supports has precluded their interaction with neurophysin, as this process depends on the availability of the peptidyl α-amino groups. This problem has been overcome by the coupling of a reversible acetone-blocked lysine vasopressin to cyanogen bromide-activated agarose and subsequent deprotection [16], and by DCC-mediated incorporation of α-nitrophenylsulphenyl–Met–Tyr–Phe–COOH to aminohexylagarose and subsequent deprotection [17]. Either procedure required complex synthetic steps. In the latter instance, moreover, the introduction of the aminohexyl spacer produced aspecific interactions with neurophysin at low ionic strength. Direct immobilization of branched peptidic ligands on preactivated solid supports may represent an actractive alterna-

tive to C-terminal covalent linkage for oriented coupling. In the immobilized form, multi-branched peptidic ligands are properly oriented for interactions with target molecules requiring ligand-free α-amino groups, and at the same time are sufficiently spaced from the solid support through the entire length of the chains involved in the covalent linkage with the preactivated solid phase. Further, in the case of poorly soluble ligands, the branched polylysinic core can be designed with the incorporation of charged residues, such as Arg or Glu, to improve the solubility of the final product.

Current automated instrumentation for solid-phase peptide synthesis allows an easy and convenient preparation of multimeric ligands in very short time. Preactivated solid supports for ligand immobilization and subsequent column preparation are also widely available.

In the case system analysed here, immobilized 8[MYF-G_5] retained binding properties for neurophysin similarly to carboxyl-terminal immobilized monomeric MYF-COOH. Recognition was selective, as evidenced by the ability of immobilized 8[MYF-G_5] to purifying NP from a crude mixture, and specific, as demonstrated by the competing effect of MYF-NH_2 in the buffer. The absolute values of the dissociation constants determined using competitive elutions on the 8[MYF-G_5] column cannot be very accurate because the exact number of MYF-GY_5 chains covalently linked cannot be precisely calculated, and hence the amount of M_T that is functionally active. In any event, the relative magnitude of $K_{M/P}$ and $K_{P/L}$ is correct, because the same M_T value is used in both calculations. The close similarity of the dissociation constants obtained for the interaction between immobilized 8[MYF-G_5] and soluble NP and between soluble NP and soluble MYF-NH_2 indicates that the presence of the pentaglycine spacer in 8[MYF-G_5] does not noticeably affect the recognition.

The method developed can be easily adapted to other ligands requiring C-terminal immobilization for proper functioning. Spacer length, incorporation of solubilizing residues and a reduced or augmented number of chains linked to the central core can be selected according to the characteristics of the ligand under consideration.

ACKNOWLEDGEMENTS

The author is grateful to Simona Germani for excellent technical assistance and to Professor Giovanni Cassani for his support and critical discussions.

REFERENCES

1 E. Chiancone and M. Gattoni, *Methods Enzymol.*, 135 (1987) 484.
2 T. M. Phillips, N. S. More, W. D. Queen, T. V. Holohan, N. C. Kramer and A. M. Thompson, *J. Chromatogr.*, 317 (1984) 173.
3 E. Breslow, J. Weis and C. J. Menendez-Botet, *Biochemistry*, 13 (1973) 4644.
4 J. P. Tam, *Proc. Natl. Acad. Sci. U.S.A.*, 85 (1988) 5409.
5 P. Nicolas, M. Camier, P. Dessen and P. Cohen, *J. Biol. Chem.*, 251 (1976) 3965.
6 E. Breslow, *Ann. N.Y. Acad. Sci.*, 248 (1975) 423.
7 V. Sardana, J. D. Carlson, E. Breslow and D. Peyton, *Biochemistry*, 26 (1987) 995.
8 J. P. Frenoy, J. Menard, P. Pesquies and P. Corval, *Eur. J. Biochem.*, 26 (1974) 995.
9 E. Atherton and R. C. Sheppard, *Solid Phase Peptide Synthesis: a Practical Approach*, IRL Press, Oxford, 1989.
10 I. M. Chaiken, *Analytical Affinity Chromatography*, CRC Press, Boca Raton, FL, 1987.
11 G. Fassina and I. M. Chaiken, *Adv. Chromatogr.*, 27 (1987) 247.
12 S. Einarsson, B. Josefsson and S. Lagerkvist, *J. Chromatogr.*, 282 (1983) 609.
13 T. Kanmera and I. M. Chaiken, *J. Biol. Chem.*, 260 (1985) 8474.
14 I. M. Chaiken and C. J. Hough, *Anal. Biochem.*, 107 (1980) 11.
15 P. Nicolas, P. Dessen, M. Camier and P. Cohen, *FEBS Lett.*, 86 (1978) 188.
16 I. C. A. F. Robinson, D. H. Edgar and J. M. Walker, *Neurosciences*, 1 (1976) 35.
17 I. M. Chaiken, *Anal. Biochem.*, 97 (1979) 302.

Journal of Chromatography, 591 (1992) 107–113
Elsevier Science Publishers B.V., Amsterdam

CHROM. 23 798

Surface-modified membranes as a matrix for protein purification

P. Langlotz and K. H. Kroner*

GBF-Gesellschaft für Biotechnologische Forschung mbH, Mascheroder Weg 1, 3300 Braunschweig (Germany)

(First received April 8th, 1991; revised manuscript received October 11th, 1991)

ABSTRACT

Recently introduced membrane-based chromatographic supports for protein separation are available either with a coupled ligand, *e.g.*, protein A, protein G or ion-exchange groups, or as activated matrices for coupling a desired ligand. The coupling conditions for protein A and immunoglobulin G to an epoxy-activated membrane were determined. The performance of the prepared affinity membranes was investigated using pure rabbit immunoglobulin G and protein A as a model system. For practical application monoclonal antibodies from cell culture supernatant were purified with a prepared protein A membrane and for comparison with a sulphonic acid ion exchange membrane.

INTRODUCTION

Affinity chromatography using particulate materials is a highly developed method for the purification of biomolecules [1]. It is commonly used in the final steps of purification procedures. However, there are some drawbacks for large-scale application even for the commonly used soft gels. The compressibility of the gels and pore diffusion limit the flow-rates. To overcome these disadvantages the particle diameter has been reduced and more rigid materials, *e.g.*, synthetic polymers or silica-based particles, have been introduced [2], but such supports require high-pressure equipment and silica-based particles are not stable at pH >8.

Alternatively, the use of membranes as chromatographic matrices has been proposed. In recent years microporous membranes, generally used for separation of cells and whole-broth clarification, were successfully modified for coupling ligands covalently. These new supports are rigid, pore diffusion is negligible (mass transfer is governed mainly by forced convection) and high-pressure equipment is not necessary [3].

Affinity membranes promise some advantages over common particulate materials, and several applications have already been published: fibronectin was purified using gelatin hollow fibres [3]; a *p*-benzamidine membrane was used for removal of thrombin and kallikrein from blood [4]; Hou and Zaniewski [5] isolated urokinase by means of metal chelate affinity membranes; Cibacron Blue membranes were useful for isolating microbial enzymes [6,7]; and protein A cartridges were tested for binding immunoglobulin G (IgG) from serum [8]. In combination with common particulate chromatographic materials, ion-exchange membrane-based cartridges gave good results in purifying recombinant interleukin [9], recombinant tissue plasminogen activator [10], β-1,4-xylanase [11] and antibodies [12].

The scope of this work was to study the coupling conditions for an epoxy-activated membrane and to determine the amount of protein coupled covalently. Further, the protein-binding capacity and stability of the prepared affinity membranes were investigated by using pure rabbit IgG and protein A. For practical application monoclonal antibodies from cell culture supernatant were purified. Alternatively, a monoclonal antibody reacting poorly with pro-

0021-9673/92/$05.00

tein A was isolated with a sulphonic acid ion-exchange membrane.

EXPERIMENTAL

Materials

Protein A (from a *Staphylococcus aureus* mutant secreting protein A), rabbit IgG and soybean trypsin inhibitor were purchased from Sigma and bovine serum albumin from Serva.

Cell culture supernatant from murine hybridomas containing a monoclonal antibody (mouse IgG_{2a} or mouse IgG_1) were kind gifts from Dr. U. Marx (Department of Medical Immunology, Medical School, Humboldt University, Berlin, Germany) and Dr. Wagner (Zellkulturtechnik GBF, Braunschweig, Germany), respectively. The cells were grown in a serum-free medium supplemented with BSA, transferrin, insulin and some minor additives as described previously [13].

The studies were performed with an epoxy-activated polymeric composite membrane (Sartobind Epoxy, pore size 0.2 μm) and a sulphonic acid ion-exchange membrane (Sartobind S, pore size 0.45 μm), which were kind gifts from Sartorius (Göttingen, Germany).

All solutions applied to the membranes were prefiltered using a 0.2-μm sterile filter. In order to achieve a uniform flow distribution, single membrane sheets were placed in an ultrafiltration cell (Amicon type 8050, 13.4 cm^2 membrane area, and Amicon type 8400, 42 cm^2 membrane area), without stirring and pressure equipment. Constant flow-rates were maintained by means of a peristaltic pump on the filtrate line (Pharmacia P-1).

Protein was determined according to the method of Lowry *et al.* [14] with BSA as standard, if not indicated otherwise. All investigations were carried out at room temperature.

Coupling of proteins to Sartobind Epoxy

Proteins were dissolved in appropriate coupling buffer (0.5 *M* phosphate, pH 5, 7 and 8, or 0.5 *M* carbonate, pH 9), resulting in concentrations of 0.9–1 mg/ml. The protein solutions were circulated through the membranes for 2–26 h at a flow-rate of 1 ml/min using a peristaltic pump (Pharmacia P-1).

Membranes to be used for chromatography were coupled for 16 h and treated with 2% ethyl glycinate in 0.1 *M* borate buffer (pH 8.3) for 2–3 h to block remaining reactive groups. Subsequently the membranes were washed three times with coupling buffer followed by 0.1 *M* citric acid (pH 2.5).

Membranes to be assayed for covalently coupled protein were washed with coupling buffer, 0.1 *M* citric acid (pH 2.5), 10% sodium dodecyl sulphate (SDS), 6 *M* urea and water.

Determination of protein bound covalently to Sartobind Epoxy

Method I. The amount of protein coupled covalenty was determined by amino acid analysis (similarly to the previous method for gel materials [15]). Membranes were hydrolysed in 6 *M* HCl–0.1% phenol in evacuated tubes for 24 h at 110°C. The HCl was evaporated and the remaining residue dissolved in 0.1 *M* sodium citrate buffer (pH 2.2), centrifuged and aliquots of the supernatant were applied to a Biotronic LC 5001 amino acid analyser. The separation was effected on a BTC 2710 cation-exchange resin column (210 × 3.2 mm I.D.) with step gradients, including pH, temperature and salt concentration changes. After reaction with ninhydrin, detection was applied at 440 and 570 nm. Calibration was performed using a Pierce amino acid standard containing 1 nmol of each amino acid. Membranes without protein were treated in the same way as a control.

Method II. Membranes were hydrolysed in 6 *M* HCl for 24 h at 37°C. After neutralization with 6 *M* NaOH, the solution was centrifuged and the supernatant analysed according to the method of Lowry *et al.* [14]. Calibration graphs were obtained by hydrolysing known amounts of the appropriate protein in the presence of the starting membrane under the same conditions (similarly to the previous method for gel materials [16]).

Determination of protein-binding capacity of protein A and IgG membranes

The adsorption characteristics of the prepared affinity membranes were investigated by passing solutions of different concentrations of protein A or rabbit IgG in 50 m*M* phosphate (pH 7.5) through the corresponding membrane. Protein solutions were applied until the concentration in the outlet was nearly the same as that in the starting solution.

Unbound protein was washed out with 50 m*M*

phosphate (pH 7.5) and desorption was effected with 0.1 *M* citric acid (pH 2.5). The area of the protein A membrane was 13.4 cm^2 and that of the IgG membrane 42 cm^2.

Affinity chromatography

Cell culture supernatant containing mouse IgG_{2a} antibody was concentrated by ultrafiltration and applied to a protein A membrane (13.4 cm^2) previously equilibrated with 0.1 *M* phosphate (pH 8.3) at a flow-rate of 1 ml/min. Washing was performed with 0.1 *M* phosphate–2 *M* NaCl and elution with 0.1 *M* citric acid (pH 3.5). The antibody concentration was determined by enzyme-linked immunosorbent assay (ELISA).

Ion-exchange chromatography

Cell culture supernatant containing mouse IgG_1 monoclonal antibody (conductivity 12 mS, pH 7.8, protein content 1 mg/ml, mainly BSA, antibody concentration 120 μg/ml) was diluted with 20 m*M* citrate (pH 5.5) and the pH adjusted, resulting in a conductivity of 4.5 mS (pH 5.5) a protein content of 0.25 mg/ml and an antibody concentration of 30 μg/ml.

The prefiltered supernatant was applied to a sulphonic acid ion-exchange membrane (42 cm^2), previously equilibrated with 20 m*M* citrate (pH 5.5). Washing was performed with equilibration buffer and elution with equilibration buffer supplemented with 140 m*M* and 1 *M* NaCl, respectively. The flow-rate throughout the whole process was 5 ml/min.

Electrophoresis

SDS–polyacrylamide gel electrophoretic (SDS-PAGE) analysis was done using Pharmacia Phast Gels (8–25% polyacrylamide–SDS) and the silver staining method according to Butcher and Tomkins [17].

RESULTS AND DISCUSSION

Preparation and characterization

Coupling of proteins to Sartobind Epoxy. We chose the direct determination of covalently coupled protein by hydrolysis of the membranes, as this method has proved to work well for gel materials [15,16]. The indirect method often used for measuring the difference of protein concentration before and after coupling needs a large amount of material for analysis to give reasonable values and reduced errors.

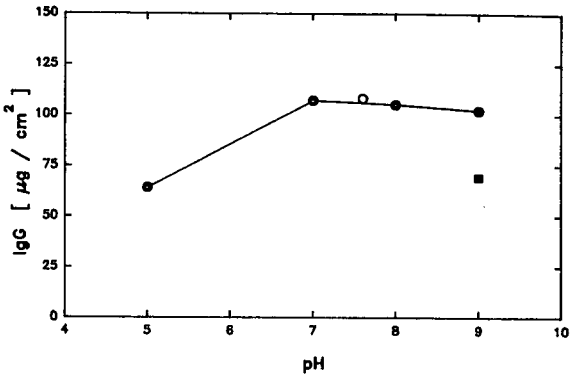

Fig. 1. Coupling of rabbit IgG to epoxy-activated membrane. Coupling buffer: 0.5 *M* phosphate (pH 5–8) or 0.5 *M* carbonate (pH 9); values obtained by amino acid analysis. Coupling time: ■ = 5 h; ● = 16.5 h; ○ = 26 h.

Fig. 1 shows the results for coupling rabbit IgG at different pH values. At pH 7–9 the amount of coupled protein was 107 μg/cm^2 (= 0.67 nmol, IgG MW = 160 000 dalton), whereas only 60% of the maximum value was obtained at pH 5. This value is in good agreement with the value stated by the producer obtained by radioactive assay (100 μg/cm^2). Using the volume conversion factor for the membrane, 45 cm^2 ≙ 1 ml ≙ 265 mg, 4.8 mg protein was bound per ml membrane or 18.1 mg protein per g membrane.

Coupling was performed overnight for 16.5 h. A prolonged incubation time in the optimum pH range did not result in a higher coupling yield, whereas a shorter time (5 h) reduced the amount of IgG coupled covalently to 64%.

Protein A was coupled at pH 8 for various incubation times (Fig. 2). The maximum capacity was reached after 16 h, corresponding to 35 μg/cm^2 or 0.83 nmol/cm^2, but in contrast to IgG shorter incubation times decreased the total amount only to 85%, which might be due to the lower molecular weigth of protein A (42 000 dalton), leading to better access to the activated groups. For comparison, with an even smaller protein, soybean trypsin inhibitor (MW = 23 000 dalton), the value obtained for coupling after 16 h at pH 8 was 20 μg/cm^2 or 0.87 nmol/cm^2.

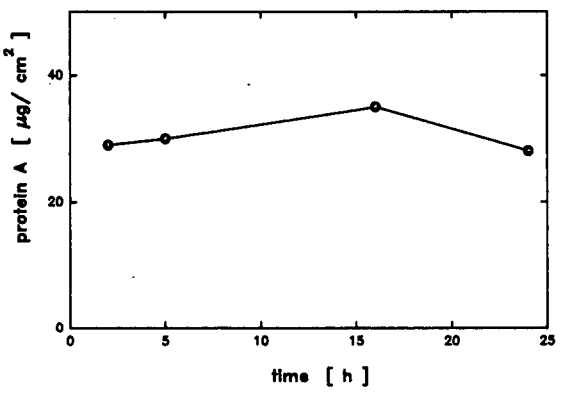

Fig. 2. Protein A bound covalently to epoxy-activated membrane. Protein A in 0.5 *M* phosphate (pH 8) was circulated for 2–24 h. Subsequently, the membranes were washed, hydrolysed and assayed by method II.

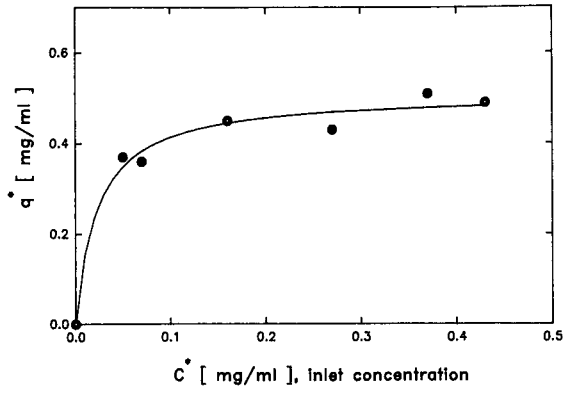

Fig. 3. Adsorption isotherm of protein A membrane. Pure rabbit IgG in 50 m*M* phosphate (pH 7.5) was applied until the outlet concentration was identical with the inlet concentration. After washing with 50 m*M* phosphate (pH 7.5), bound IgG was eluted with 0.1 *M* citric acid (pH 2.5). Flow-rate, 3 ml/min.

Protein-binding capacity of protein A and IgG membranes. Figs. 3 and 4 show the adsorption isotherms for the protein A membrane and IgG membrane, respectively. The shapes of the isotherms indicate Langmuir-type adsorption, which can be described by the equation

$$dq/dt = k_1C(q_m - q) - k_2q \qquad (1)$$

where C is the concentration of adsorbate in solution, q the solid-phase concentration of adsorbed molecules and q_m the maximum capacity of the adsorbent. At equilibrium, eqn. 1 leads to

$$q^* = \frac{q_mC^*}{K_d + C^*} \qquad (2)$$

where $K_d = k_2/k_1$ is the dissociation constant of the system. The following values were obtained: K_d = 0.047 mg/ml ($2.9 \cdot 10^{-7}$ *M*) and q_m = 4.74 mg/ml for the system protein A membrane–rabbit IgG, and K_d = 0.023 mg/ml ($5.5 \cdot 10^{-7}$ *M*) and q_m = 0.51 mg/ml for the system IgG membrane–protein A.

A binding ratio of more than one bound IgG molecule for each protein A molecule (1.3 nmol IgG/nmol protein A) was found for the protein A membrane by using the maximum amount of IgG bound obtained from the isotherm and the amount of protein A coupled covalently to the membrane determined as described. For the system IgG membrane–protein A the binding ratio was calculated to be 2.5 nmol IgG/nmol protein A. These values are in agreement with findings for particulate materials [18] and are reasonable as one protein A molecule was found to bind two molecules of IgG [19].

The lower binding ratio obtained in the system protein A membrane–IgG might be due to multipoint attachment of protein A. Shorter coupling times may be useful in preventing this phenomenon. Another point to be considered is the steric hindrance of the large IgG molecule.

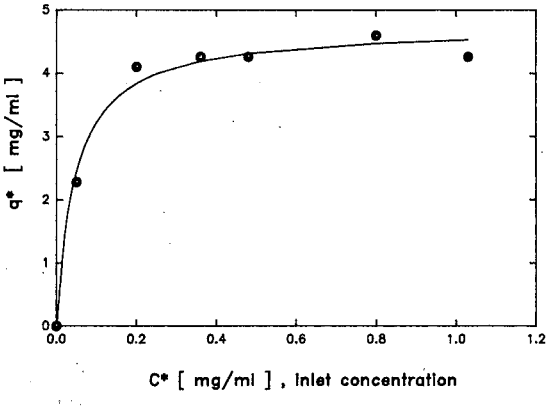

Fig. 4. Adsorption isotherm of IgG membrane. Pure protein A in 50 m*M* (pH 7.5) was applied until the outlet concentration was identical with the inlet concentration. Washing was done using 50 m*M* phosphate (pH 7.5) and elution with 0.1 *M* citric acid (pH 2.5). Flow-rate, 2 ml/min.

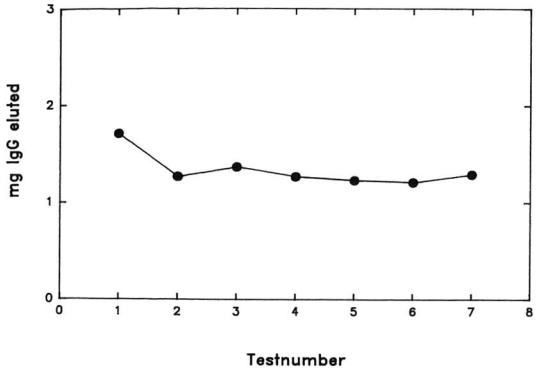

Fig. 5. Repeated use of protein A membrane. Saturating concentrations of IgG in 50 m*M* phosphate (pH 7.5) were applied. After washing with 50 m*M* phosphate (pH 7.5) and elution with 0.1 *M* citric acid (pH 2.5) the membrane was re-equilibrated and used again.

Stability of protein A membrane. For practical applications, the stability of the prepared affinity membranes is very important. The results of repeated use of the protein A membrane are shown in Fig. 5. After the first run a decrease of *ca.* 20% in IgG capacity was observed, and this value remained stable in subsequent runs. This result is similar to those of other workers for protein A columns, and is probably due to non-covalently bound protein being washed out after the first run rather than to ligand leakage [20]. The protein A membrane used for chromatography was washed under mild conditions compared with the membranes needed for amino acid analysis and some non-covalently bound protein A may have been retained on the matrix. From the difference in IgG adsorption in the first and the following runs and the binding ratio of 1.3 nmol IgG/nmol protein A, about 10 μg/cm^2 non-covalently bound protein A were retained on the matrix material after coupling and washing.

The membrane was re-used about 30 times, including runs with pure rabbit IgG and crude cell culture supernatant. During this period a decrease in capacity of 30% was observed. Cleaning with 6 *M* urea was done occasionally, but cleaning procedures for matrices containing proteins, which cannot be cleaned with NaOH and used with high protein concentrations and crude solutions, still have to be optimized.

Resolution. When considering the chromatographic feature of the membranes, the resolution of such matrices is of concern. Generally, high resolution could be expected. Plate heights can be predicted from the theoretical relation of 2–5 d_p, where d_p is the nominal pore size of the membrane, resulting in values of 0.4–2 μm for the present membranes. From the experiments performed (*e.g.*, see Fig. 6), values of about 3–7 μm can be calculated for flow-rates of 1–3 ml/min (bed height 200 μm), which are larger than expected but in agreement with earlier findings [21]. The main reason for this discrepancy is probably the unfavourable ratio of the dead volume of the filter device to the membrane bed volume, rather than axial dispersion in the membrane, which may lead to some back-mixing effects and result in peak broadening. This is supported by other workers [22]. Nevertheless, a resolution as high as for very small particulate high-performance liquid chromatographic materials (1–5 μm) can be assumed for the membrane matrices [21].

Applications

Affinity chromatography. Fig. 6 shows the purification of a monoclonal antibody (mouse IgG_2) from cell culture supernatant. The cell-free supernatant was concentrated by ultrafiltration using an Amicon PM 30 membrane. A 5-ml volume of the supernatant, containing 13.2 mg/ml of protein (mainly BSA) and 300 μg/ml of antibody, was applied to a protein A membrane (13.4 cm^2) previously equilibrated with 0.1 *M* phosphate (pH 8.3). Washing was done with 20 ml of equilibration buffer suplemented with 2 *M* NaCl and desorption was carried out using 0.1 *M* citric acid (pH 3.5). During the whole process the flow-rate was maintained constant at 1 ml/min. The first peak represents the unbound fraction and the second the eluted antibody. The recovery of the applied amount of antibody was 93% (Table I). As judged by SDS-PAGE the antibody was pure (Fig. 7), showing two bands corresponding to the heavy and light chains of IgG.

Ion-exchange chromatography. Ion-exchange chromatography is an alternative to affinity chromatography when the antibody reaction with protein A is weak; also ion-exchange matrices might be preferred when isolating antibodies for pharmaceutical use, in order to prevent contamination with

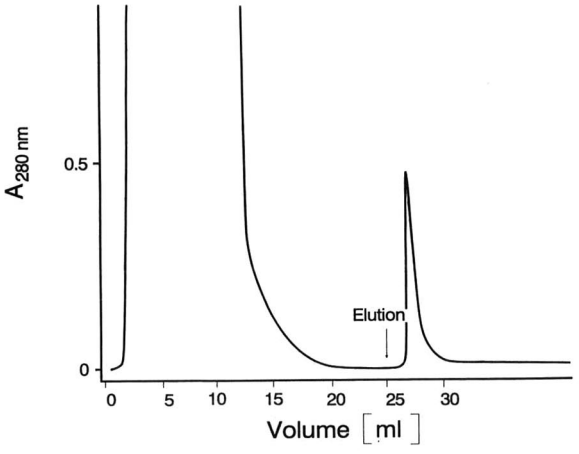

Fig. 6. Purification of monoclonal antibody from cell culture supernatant. Concentrated serum-free supernatant containing 300 μg/ml of monoclonal antibody and 13.2 mg/ml of protein was applied at a flow-rate of 1 ml/min to a protein A membrane (13.4 cm^2). Washing was performed using 0.1 *M* phosphate (pH 8.3)–2 *M* NaCl and elution with 0.1 *M* citric acid (pH 3.5). The arrow indicates the start of elution.

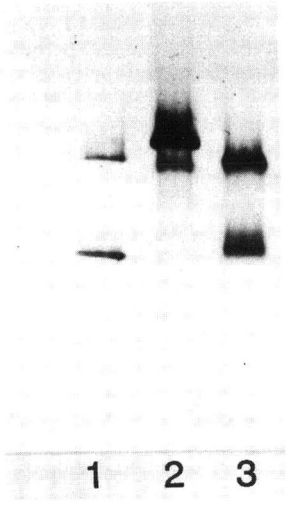

Fig. 7. SDS polyacrylamide gradient gel (8–25%) electrophoresis with silver staining. Lanes: 1 = protein A-membrane purified monoclonal antibody; 2 = crude cell culture supernatant; 3 = pure rabbit IgG.

protein A [23]. We therefore compared the results from affinity membranes with those from the purification of a mouse IgG_1 antibody by means of sulphonic acid ion-exchange membrane. From the manufacturer's information the ion-exchange membrane used has a capacity for proteins of 10–100 mg/ml (1 ml ≙ 50 cm^2), depending on the type of protein, protein concentration and buffer system.

Fig. 8 illustrates the antibody purification with an ion-exchange membrane. By dilution with the chromatographic buffer the conductivity and pH of the cell culture supernatant were decreased appropriately and applied at a flow-rate of 5 ml/min to a

TABLE I

PURIFICATION OF MONOCLONAL ANTIBODY FROM CELL CULTURE SUPERNATANT BY PROTEIN A MEMBRANE (VALUES OBTAINED BY ELISA)

Step	Antibody (μg/ml)	Volume (ml)	Total amount of antibody (mg)
Supernatant	300	5.0	1.5
Breakthrough (unbound proteins)	0.18	6.8	<0.01
Wash[a]	0	7.2	0
Elution	500	2.8	1.40

[a] Only the first fractions were assayed.

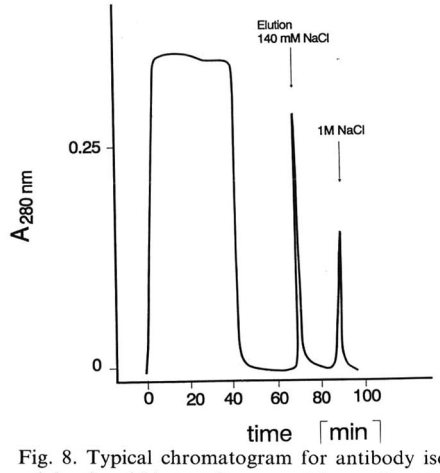

Fig. 8. Typical chromatogram for antibody isolation with the sulphonic acid ion-exchange membrane. Serum-free cell culture supernatant containing 30 μg/ml of antibody and 0.25 mg/ml of protein was applied at a flow-rate of 5 ml/min to a sulphonic acid ion-exchange membrane (42 cm^2). Elution of the antibody was performed using 50 m*M* citrate (pH 5.5)—140 m*M* NaCl. Additional cleaning was effected with 1 *M* NaCl.

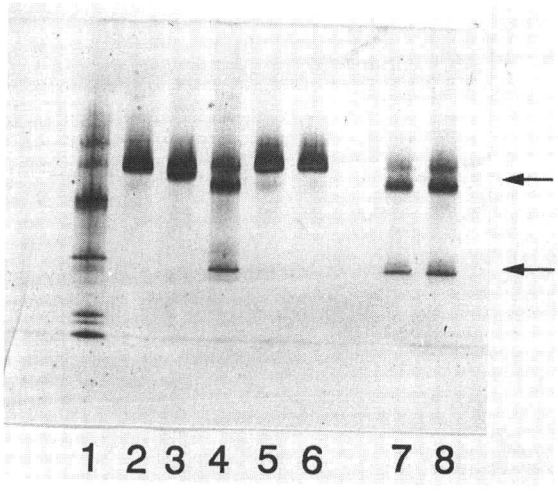

Fig. 9. SDS polyacrylamide gradient gel (8–25%) electrophoresis with silver staining; isolation of monoclonal antibodies with sulphonic acid ion-exchange membrane (fractions from two runs). Lanes: 1 = Pharmacia molecular weight markers (78 000, 66 250, 45 000, 30 000, 17 200, 12 300 dalton); 2 = cell culture supernatant; 3 = breakthrough; 4 = monoclonal antibody eluted with 140 m*M* NaCl; 5 = cell culture supernatant; 6 = breakthrough; 7 and 8 = monoclonal antibody eluted with 140 m*M* NaCl. Arrows indicate the light and heavy chains.

sulphonic acid ion-exchange membrane (42 cm^2). Elution (second peak in Fig. 8) with 140 *M* NaCl resulted in 1.63 mg of antibody in 7.7 ml; no more antibody was eluted with 1 *M* NaCl. The antibody obtained was slightly contaminated with BSA as judged by SDS-PAGE (Fig. 9) and required an additional purification step by gel filtration.

CONCLUSION

Affinity and ion-exchange membranes are useful matrices for purifying monoclonal antibodies. They are simple to handle, as bed packing procedures are not necessary, and scale-up can be performed easily. Cross-flow filtration experiments are under investigation and seem to be even more promising than dead-end filtration, because crude homogenates and cell culture supernatants can be applied without prior clarification.

ACKNOWLEDGEMENTS

The expert technical assistance of Mrs. Sandra Fritzsche is greatly appreciated. We thank Dr. Wagner (Zellkulturtechnik, GBF, Braunschweig) and Dr. Uwe Marx (Department of Medical Immunology, Medical School, Humboldt University, Berlin) for providing cell culture supernatant and the ELISA technique. This work was supported by a grant from BMFT.

REFERENCES

1 Y. D. Clonis, *Bio/Technology*, 5 (1987) 1290.
2 S. Ohlson, L. Hansson, M. Glad, K. Mosbach and P.-O. Larsson, *Tibtech*, 7 (1989) 179.
3 S. Brandt, R. A. Goffe, S. B. Kessler, J. L. O'Conner and S. E. Zale, *Bio/Technology*, 6 (1988) 779.
4 S. H. Huang, S. Roy, K. C. Hou and G. T. Tsao, *Biotechnol. Prog.*, 4 (1988) 159.
5 K. C. Hou and R. Zaniewski, *J. Chromatogr.*, 525 (1990) 297.
6 S. Krause, K. H. Kroner and W.-D. Deckwer, *Biotechnol. Tech.*, 5 (1991) 199.
7 B. Champluvier, G. Briefs and M.-R. Kula, in C. Christiansen, L. Munck and J. Villadsen (Eds.), *5th ECB, Copenhagen, July 1990*, Munksgaard, Copenhagen, 1990, Vol. I, p. 525–528.
8 R. M. Mandaro, S. Roy and K. C. Hou, *Bio/Technology*, 5 (1987) 928.
9 Y. Kikumoto, Y.-M. Hong, T. Nishida, S. Nakai, Y. Masui and Y. Hirai, *Biochem. Biophys. Res. Commun.*, 147 (1987) 315.
10 A. Upshall, A. A. Kumar, M. C. Bailey, M. D. Parker, M. A. Favreau, K. P. Lewison, M. L. Joseph, J. M. Maragnora and G. L. McKnight, *Bio/Technology*, 5 (1987) 1301.
11 L. U. L. Tan, E. K. C. Yu, G. W. Louis-Seize and J. N. Saddler, *Biotechnol. Bioeng*, 30 (1987) 96.
12 A. Jungbauer, F. Unterluggauer, K. Uhl, A. Buchacher, F. Steindl, D. Pettauer and E. Wenisch, *Biotechnol. Bioeng*, 32 (1988) 326.
13 V. Jäger, J. Lehmann and P. Friedel, *Cytotechnology*, 1 (1988) 319.
14 O. H. Lowry, N. J. Rosebrough, A. L. Farr and R. J. Fandall, *J. Biol. Chem.*, 193 (1951) 265.
15 M.-R. Kula, *Dechema Monogr.*, 84 (1979) 182.
16 H. A. Chase and S. L. Fowell, *J. Biotechnol.*, 4 (1986) 1.
17 L. A. Butcher and J. K. Tomkins, *Anal. Biochem.*, 148 (1986) 384.
18 D. C. Herak and E. W. Merill, *Biotechnol. Prog.*, 6 (1990) 33.
19 J. Sjöquist, B. Meloun and H. Hjelm, *Eur. J. Biochem.*, 29 (1972) 572.
20 M. T. Dertzbaugh, M. C. Flickinger and W. B. Lebherz, III, *J. Immunol. Methods*, 83 (1985) 169.
21 S. Krause and K. H. Kroner, in N. Li (Ed.), *Proceedings of International Congress on Membranes and Membrane Processes, Chicago, August 1990*, North American Membrane Society, Chicago, 1990, Vol. I, p. 166.
22 B. Champluvier and M. R. Kula, *J. Chromatogr.*, 539 (1991) 315.
23 S. A. Duffy, B. J. Moellering, G. M. Prior, K. R. Doyle and C. P. Prior, *BioPharm*, 2, No. 6 (1989) 34.

Journal of Chromatography, 591 (1992) 115–120
Elsevier Science Publishers B.V., Amsterdam

CHROM. 23 795

Diffusion of proteins in Sepharose Cl-B gels

Mohsen Moussaoui, Mohammed Benlyas and Philippe Wahl*

Centre de Biophysique Moléculaire, CNRS, 1A Avenue de la Recherche Scientifique, 45071 Orléans Cedex 2 (France)

(First received June 28th, 1991; revised manuscript received October 8th, 1991)

ABSTRACT

The reduced diffusion coefficient, D/D_0, of fluorescein-labelled globular proteins in the agarose gels Sepharose Cl-2B, 4B and 6B were measured by the FRAP method. Comparison of the partition coefficients of the native and the labelled proteins in the gel showed that the fluorescein residues did not introduce new interactions between the solute and the gel matrix. D/D_0 decreased as a function of the Stokes radius. The variation of D/D_0 as a function of the partition coefficient of the proteins in the gel did not agree with a previously published prediction. This is in contrast with the diffusion of globular proteins in ACA34 gel, in which the sieving matrix is made of cross-linked polyacrylamide.

INTRODUCTION

The diffusion coefficient of a solute in gel beads is one of the factors that determine the efficiency of the separation of macromolecules by gel chromatography [1]. Only a few measurements of the diffusion of macromolecules in gels have been published until now [2–4]. In previous work, we determined the reduced coefficient, D/D_0, of the diffusion of fluorescein-labelled dextran fractions in Sephadex gel beads [5] and of fluorescein-labelled proteins in the ACA34 gel [6]. The technique used was the fluorescence recovery after photobleaching (FRAP) [5]. It was found that D/D_0 of the proteins in the gel AC34 decreased exponentially as the Stokes radius of the molecules increased. Further, D/D_0 varied as a function of the partition coefficient of the proteins in the gel, as predicted by the theory of Ogston *et al.* [7]. In this work, the same method was used for measuring the diffusion of fluorescein-labelled globular proteins in three Sepharose Cl-B gels.

The sieving properties of ACA34 gel are those of its polyacrylamide component, which means that the gel behaves as a microporous gel. On the other hand, the Sepharose Cl-B gels are essentially composed of agarose. The structure of agarose gels has been described as reticulated [8].

EXPERIMENTAL

The origin of the protein samples and of the fluorescein isothiocyanate isomer I (FITC) was as described previously [6]. Sepharose Cl-6B (Lot KI 38317), Cl-4B (Lot MB 01610) and Cl-2B (Lot 5204) were purchased from Pharmacia (Upsala, Sweden).

The technique of protein labelling with FITC has already been described, and the values of the labelling ratios of these samples were given [6]. Dextran blue was purchased from Pharmacia and DNA of phage lambda was purchased from Sigma.

The chromatography of proteins was performed on columns (90 × 1.35 cm) filled with the gels studied. Each column was equilibrated with buffer A [10 m*M* sodium phosphate–0.15 *M* sodium chloride–1 m*M* sodium azide (pH 8).

The partition coefficient was determined by the equation of Laurent and Killander [9]:

$$K_{AV} = \frac{V_e - V_0}{V_t - V_0} \quad (1)$$

where V_e is the elution volume, V_t the volume of the gel bed in the column and V_0 the void volume. V_0 was determined by the chromatography of DNA of

0021-9673/92/$05.00

phage lambda. With Sepharose C1-6B dextran blue was also used.

Microfluorimetric measurements of the partition coefficient

The gel beads were immersed in a solution of a fluorescent protein, contained in a small optical cuvette which was placed on the microscope stage of the FRAP apparatus, as described [5]. The fluorimetric partition coefficient was defined by the following expression [5]:

$$K_f = F_B/F_f \quad (2)$$

where F_B and F_f are the fluorescences measured with the microscope–photometer assembly centred on a bead and on the free solvent respectively. K_f is equal to K_{AV} when the quantum efficiency of the macromolecule fluorescence is the same in the bead and in the free solvent. The diameter of the gel beads was in the range 100–150 μm. As mentioned previously, there was a stray fluorescence which came from the contribution of the fluorescent track of the laser beam in the solvent surrounding the bead [5,6]. The measured intensity, F'_B, was related to the corrected intensity by

$$F'_B = F_B + \alpha F_f$$

where α is a constant. If one puts

$$K'_f = F'_B/F_f$$

then

$$K_f = K'_f - \alpha (1 - K'_f) \quad (3)$$

We determined α by measuring the apparent fluorimetric partition coefficient of a high-molecular-weight fluorescein dextran excluded from the gel. The value of α was 0.04.

Measurement of the reduced diffusion coefficient

The relative diffusion coefficient of labelled proteins in a gel bead was determined by FRAP, as already described [5,6]. FRAP curves were recorded with the microscope alternately centred on a gel bead and on the surrounding solvent. These curves were analysed with the following function [10]:

$$F(t) = \frac{F_0 + F_\infty\, t/t_{\frac{1}{2}}}{1 + t/t_{\frac{1}{2}}} \quad (4)$$

where F_0 and F_∞ are the fluorescence intensities emitted immediately after the bleaching pulse and at a infite time after bleaching, respectively, and $t_{\frac{1}{2}}$ is the half-time of the fluorescence recovery.

The bleaching fraction was defined as

$$B = (F_i - F_0)/F_i \quad (5)$$

and the fraction of freely diffusing molecules (or recovery fraction), by

$$L = (F_\infty - F_0)/(F_i - F_0) \quad (6)$$

where F_i is the prebleaching fluorescence intensity. The reduced diffusion coefficient was obtained by applying the following relationship [5,6]:

$$\frac{D}{D_0} = \frac{(t_{\frac{1}{2}})_f}{(t_{\frac{1}{2}})_b} \cdot \frac{\beta_b}{\beta_f} \quad (7)$$

where D and D_0 are the diffusion coefficients of the solute in the gel and in the free solvent, respectively, $(t_{\frac{1}{2}})_f$ and $(t_{\frac{1}{2}})_b$ are the half-times of the fluorescence recovery and β_f and β_b are factors (depending on B) [10] measured in the free solvent and in the bead, respectively. Eqn. 4 is a very good approximation of the theoretical function of Axelrod *et al.* [11] provided that $B < 0.7$, which always applied in our experiments. Eqn. 7 then gives accurately the ratio D/D_0. The values of β were given as function of B by Yguerabide *et al.* [10].

We have shown that the influence of the stray fluorescence on the FRAP curves determined with the microscope centred on the bead depended on the value of K_{AV} [6]. In this work, this stray fluorescence was negligible as K_{AV} was $\geqslant 0.3$ in all instances [6].

RESULTS

Chromatography of proteins on a gel column

Six native proteins, namely ribonuclease A, α-chymotrysinogen A, ovalbumin, bovine serum albumin, aldolase and thyroglobulin, were chromatographed on columns of Sepharose C1-2B, 4B and 6B. These proteins were labelled with fluorescein isothiocyanate and purified as described previously [6]. The labelled proteins were also chromatographed on the Sepharose C1-6B column. Table I shows that the partition coefficients of a labelled and of the corresponding native protein were identical within the experimental accuracy.

TABLE I

PARTITION COEFFICIENTS OF NATIVE AND LABELLED PROTEINS IN SEPHAROSE CL-6B GEL

Protein	K_{AV}	
	Native	Labelled
Ribonuclease	0.80	0.87
Chymotrypsinogen A	0.71	0.76
Ovalbumin	0.58	0.57
Aldolase	0.49	0.50
Thyroglobulin	0.29	0.31

In addition, we measured the microfluorimetric partition coefficient K_f of the labelled proteins on the three Sepharose gels, and found that it was equal to the K_{AV} of the parent native protein (Figs. 1–3). These results showed that the fluorescein residues did not induce any interaction between the labelled proteins and the gel matrix.

Determination of the reduced diffusion coefficient of proteins in a bead of Sepharose gel

This was performed by FRAP as described under Experimental. The bleaching fraction was about 0.5. After its fitting, eqn. 4 satisfactorily reproduced the experimental curves. In every instance we found that the fraction of fluorescence recovery L was equal to 1. This showed that there was no slow exchange between a free species and a species bound to the gel matrix. The reduced diffusion coefficient D/D_0 was determined as described above.

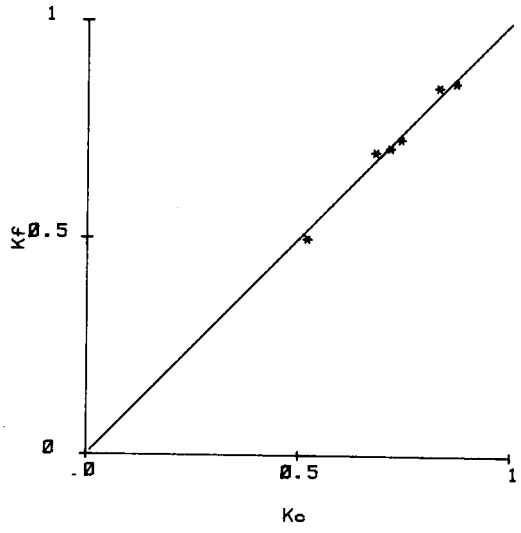

Fig. 2. Variation of the K_f as a function of the K_{AV} of native proteins in Sepharose Cl-4B gel.

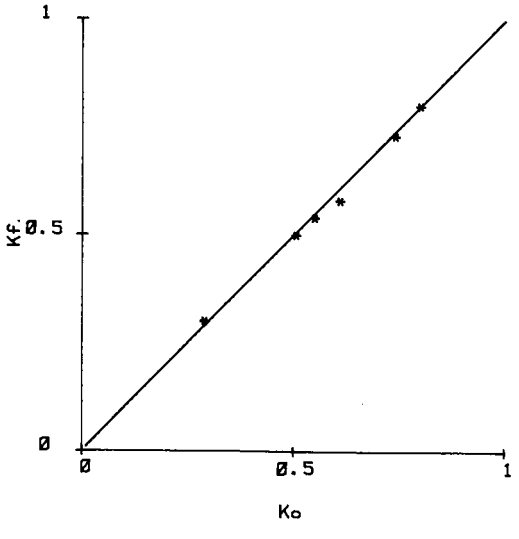

Fig. 1. Variation of the microfluorimetric partition coefficient K_f of labelled proteins as a function of the chromatographic partition coefficient K_{AV} of the native proteins in Sepharose Cl-6B gel.

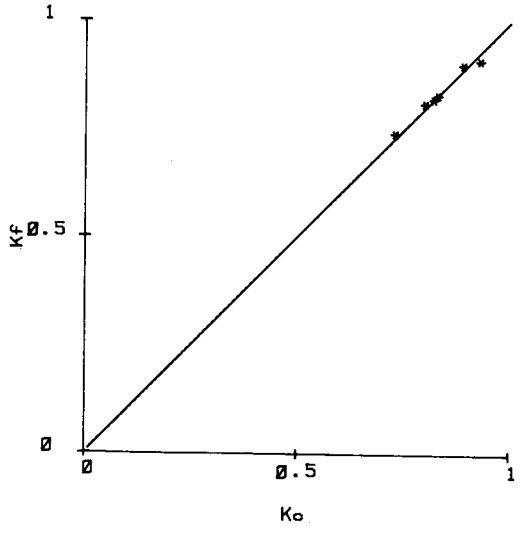

Fig. 3. Variation of the K_f as a function of the K_{AV} of native proteins in Sepharose Cl-2B gel.

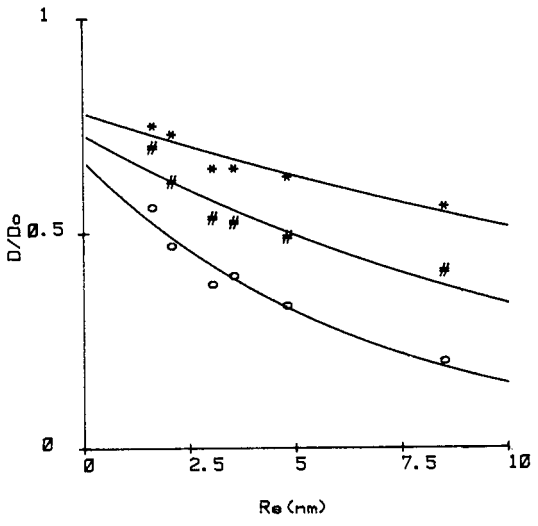

Fig. 4. Variation of the reduced diffusion coefficient of the fluorescein-labelled proteins as a function of their Stokes radius in (○) Sepharose C1-6B, (#) C1-4B and (*) C1-2B. The continuous curves represent the fitted eqn. 9.

The variation of D/D_0 is plotted as a function of the Stokes radius of the protein in Fig. 4 and as a function of K_{AV} in Fig. 5.

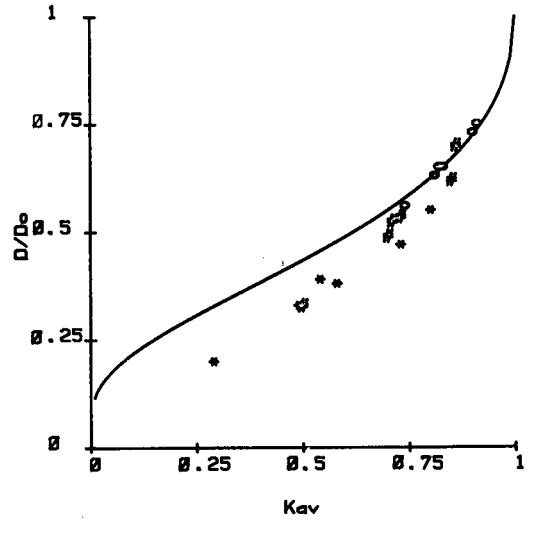

Fig. 5. Variation of the reduced diffusion coefficient of the proteins as a function of their partition coefficient in (○) Sepharose C1-2B, (#) C1-4B and (*) C1-6B. The continuous curve represents eqn. 12.

DISCUSSION

The partition coefficient measurements showed that the fluorescein residues do not induce interactions between the labelled proteins and the matrix of the Sepharose C1-B gels. Therefore, the diffusion coefficient of the labelled proteins determined by FRAP is equal to the diffusion coefficient of the parent native proteins.

For solute molecules which do not bind to the gel matrix, there are two possible causes of their diffusion retardation by the gel: the hydrodynamic effect and the obstruction effect [4]. The present theories of diffusion in gels assume that the solute molecules are spherical. These theories rest on simplified models of the gel matrix and lead to expressions of D/D_0 as functions of the molecular radius.

We first tried to apply the equation of Faxen derived from a hydrodynamic theory [12]. It did not represent our data satisfactorily.

The gel model of Ogston [13] consists of a random network of straight fibres. The partition coefficient of spherical molecules between the gel and the free solution is given by the following equation [9]:

$$K_{AV} = \exp\left[-\pi l\,(R_f + R_s)^2\right] \tag{8}$$

where R_f is the radius of the cross-section, l the linear concentration of the fibres and R_s is the Stokes radius of the solute molecule. The same matrix model was used in Ogston *et al.*'s theory of diffusion in gels [7]. In addition, the retardation was ascribed to the obstruction effect. The equation proposed by Ogston *et al.* can be written as:

$$D/D_0 = A \exp\left(-BR_s\right) \tag{9}$$

where

$$A = \exp\left[-(\pi l)^{\frac{1}{2}} R_f\right] \tag{10}$$

$$B = (\pi l)^{\frac{1}{2}}$$

We fitted the parameters A and B of eqn. 9 to our experimental data by the non-linear least-squares method. The parameter values are given in Table II and the corresponding calculated curves are shown in Fig. 4.

From A and B, R_f and l could be calculated by eqn. 10. Finally, the average radius of the cavities of the gels could be calculated according to the following equation [13,14]:

$$R_c = 0.5\, l^{-\frac{1}{2}} - R_f \tag{11}$$

TABLE II

DIFFUSION OF GLOBULAR PROTEINS IN SEPHAROSE Cl-B GELS

Parameter values of eqns. 9, 10 and 11 fitted to the experimental variation of D/D_0 as a function of R_s.

Sepharose gel	A	B (nm^{-1})	$l \times 10^4$ (nm^{-2})	R_f (nm)	R_c (nm)
Cl-2B	0.78 ± 0.03	0.042 ± 0.008	5.6	5.9	31
Cl-4B	0.73 ± 0.03	0.078 ± 0.016	19.3	4.0	16
Cl-6B	0.67 ± 0.05	0.15 ± 0.02	72.6	2.7	8

These parameters are also given in Table II.

The theory of Cukier [15] is based on hydrodynamic interactions. The results can also be expressed by eqn. 9 in which $A = 1$. This last prediction is obviously not verified by our data (see Table II). The theory of Altenberg and Tirrel [16] takes both the hydrodynamic and the obstruction effects into account. In this theory, the gel model is constituted of fixed spheres randomly distributed in a viscous fluid.

By fitting the theoretical equation of these authors to our experimental data, we found that the hydrodynamic terms were negligible. The function of Altenberg and Tirrel did not fit our data as well as eqn. 9.

Taken together, these analyses suggest that the obstruction effect may play an important role in the diffusion retardation of proteins in Sepharose Cl-B gels.

A relationship between the reduced diffusion coefficient and the partition coefficient can be obtained from eqn. 8–10 [7]:

$$D/D_0 = \exp\left[-(\ln K_{AV})^{\frac{1}{2}}\right] \quad (12)$$

The curve representing the theoretical function 12 is shown in Fig. 5. It can be seen that the points representing the experimental data corresponding to large values of K_{AV} ($K_{AV} > 0.8$) are on the theoretical curve. For smaller values of K_{AV}, the experimental points are below the theoretical curve. The difference between the experimentral and theoretical points increases when K_{AV} decreases. For a given K_{AV}, the diffusion is more retarded than is predicted by the theory.

In contrast, we found in previous work that eqn. 12 represented the diffusion measurements of proteins in ACA34 gel fairly well [6]. The sieving properties of the ACA34 gel are ascribed to its polyacrylamide component. The fibres of polyacrylamide gels are composed of single or a small number of polymer molecules [14]. These fibres are cross-linked by covalent bonds. On the other hand, the fibres of Sepharose consist of aggregates of a large number of agarose molecules linked by hydrogen bonds [17–19]. The structure has been described as reticulated [8].

Ogston's model of gels seems more appropriate to describe the sieving properties of microporous gels such as polyacrylamide gels and cross-linked dextran gels than reticulated gels such as agarose [8,9,14,20]. This may explain why eqn. 12 describes the results of experiments with ACA34 gel better than those with sepharose Cl-B gels.

The diffusion of dextran fractions with a Stokes radius between 33 and 100 nm have been studied in gels containing 0.3–4% of agarose using the quasi-elastic laser light-scattering method (QELS) [2]. For gels containing 2% and 4% of agarose (equal to the nominal concentrations of Sepharose Cl-2B and Cl-4B, respectively), the variation of D/D_0 as a function of the partition coefficient is qualitatively similar to the experimental data in Fig. 5, that is the experimental points are on the curve representing eqn. 12 for high partition coefficients and below this curve for small partition coefficients. With the FRAP method we also obtained similar results by measuring the diffusion of fluorescein-labelled dextran in Sepharose Cl-B (results not shown).

It should be noted, however, that the diffusion coefficient of a solute in gels may depend of the probe distance associated with the method of measurement [21]. In QELS, the probe distance is a few tenths of a micrometre whereas in our FRAP measurements it is of the order of 20 μm. Further exper-

iments may reveal systematic differences between the diffusion coefficients determined by these techniques and help to reach a better understanding of the diffusion mechanism in gels. In any case, FRAP measurement of proteins in chromatographic gels appears to be a useful and simple technique.

REFERENCES

1 J. C. Giddings, *Dynamics of Chromatography*, Marcel Dekker, New York, 1965.
2 P. Y. Key and D. B. Sellen, *J. Polym. Sci. Polym. Phys. Ed.*, 20 (1982) 659.
3 I. Noshio, J. C. Reina and R. Bansil, *Phys. Rev. Lett.*, 59 (1987) 684.
4 A. H. Muhr and J. M. U. Blanshard, *Polymer*, 23 (1982) 1012.
5 E. Poitevin and P. Wahl, *Biophys. Chem.*, 31 (1988) 247.
6 M. Moussaoui, M. Benlyas and P. Wahl, *J. Chromatogr.*, 338 (1991) 71.
7 A. Ogston, B. N. Preston and J. D. Wells, *Proc. Roy. Soc. London, Ser. A*, 333 (1973) 297.
8 R. West, *Biopolymers*, 26 (1987) 343.
9 T. C. Laurent and J. Killander, *J. Chromatogr.*, 14 (1964) 317.
10 J. Yguerabide, J. A. Schmit and F. E. Yguerabide, *Biophys. J.*, 40 (1982) 69.
11 D. Axelrod, D. E. Koppel, J. Schlessinger, F. Elson and W. W. Webb, *Biophys. J.*, 16 (1976) 1055.
12 F. J. Renkin, *Gen. Phys.*, 38 (1954) 225.
13 A. G. Ogston, *Trans. Faraday Soc.*, 54 (1958) 1754.
14 J. S. Fawcett and C. J. O. R. Morris, *Sep. Sci.*, 1 (1966) 9.
15 R. F. Cukier, *Macromolecules*, 17 (1984) 252.
16 A. R. Altenberg and M. Tirrel, *J. Chem. Phys.*, 80 (1984) 2208.
17 S. Arnott, A. Fulmer, W. E. Scott, I. C. M. Dea, R. Moorhouse and D. A. Rees, *J. Mol. Biol.*, 90 (1974) 269.
18 A. Amsterdam, Z. Er-El and S. Shaltiel, *Arch. Biochem. Biophys.*, 171 (1975) 673.
19 T. K. Attwood, B. J. Nelmes and D. B. Sellen, *Biopolymers*, 27 (1988) 201.
20 M. Le Maire, A. Chazi, J. Moller and L. P. Aggerbeck, *Biochem. J.*, 243 (1987) 399.
21 J. Newman and K. Schick, *Biopolymers*, 28 (1989) 1969.

Journal of Chromatography, 591 (1992) 121–128
Elsevier Science Publishers B.V., Amsterdam

CHROM. 23 789

Analysis of pH-dependent protein interactions with gel filtration medium

Nikolai P. Golovchenko*, Irina A. Kataeva and Vasily K. Akimenko

Department of Anaerobic Processes, Institute of Biochemistry and Physiology of Microorganisms, Pushchino, Moscow Region, 142292 (USSR)

(First received February 12th, 1991; revised manuscript received October 4th, 1991)

ABSTRACT

A prepacked Superose 12 HR 10/30 column was used to study the effects of elution ionic strength and pH on the chromatographic behaviour of a strong hydrophobic *Clostridium thermocellum* endoglucanase (1) and two weak hydrophobic proteins, *Clostridium thermocellum* endoglucanase C and egg white lysozyme. Ion-exclusion or ion-exchange interactions between weakly hydrophobic proteins and the gel matrix were observed at low ionic strength, depending on whether the pH of the elution buffer was higher or lower than the p*I* values of the proteins. These interactions were due to the presence of negatively charged groups on the surface of Superose and could be eliminated at any pH by adding electrolyte at a concentration determined by its chemical identity. The optimum results were observed with sodium sulphate at a concentration of 100 m*M*. The chromatographic behaviour of strong hydrophobic endoglucanase (1) on a Superose column as a function of pH was much more complex because of two interplaying effects, electrostatic and hydrophobic. Ideal size-exclusion chromatography could be achieved only in a narrow range of the conditions: first, the mobile phase must contain a weak salting-out electrolyte such as NaCl, and second, the mobile phase pH must be high enough that hydrophobic interactions between the solute and support are balanced by their electrostatic repulsion. At pH > p*I*, the retardation of endoglucanase (1) gradually increased with decreasing pH as a result of lowering of repulsive electrostatic interactions whether or not the buffer ionic strength was high. At pH < p*I* a drastic increase in the capacity factor k' was observed owing to the additivity of hydrophobic and ion-exchange effects. Overall, the chromatographic behaviour of endoglucanase (1) on a Superose column could be adequately described in terms of the theory of potential barrier chromatography. The explanation presented could obviously be valid for the behaviour of any protein on any gel matrix, as its mechanism was described using lumped physical notions such as hydrophobic and electrostatic interactions, charges and potentials. Virtually all currently known gel filtration media are more or less hydrophobic and are weak cation exchangers.

INTRODUCTION

Non-ideal behaviour of proteins and other high- and low-molecular-weight substances in size-exclusion chromatography (the so-called non-ideal SEC or nSEC) is a well known phenomenon [1–21]. The major reason for such deviation from "pure" SEC is electrostatic interactions between charged solutes and charged support surfaces determined by the presence of ionogenic groups in all of the commercially available SEC packings and hydrophobic interactions. The influence of the mobile phase ionic strength on these interactions is well understood. The electrostatic interactions are considered to be suppressed at high ionic strength and, conversely, the hydrophobic interactions are minor at low ionic strength. The influence of the mobile phase pH at low ionic strength on the retention mechanism has also been well studied [4,8,15,16,19,21]. Depending on the relative values of pH and isoelectric point of a protein, there is either an earlier elution compared with ideal SEC (the so-called "ion-exclusion effect"), or later elution ("ion-exchange effect"), which are due to amphoteric properties of protein molecules. As the residual charges of SEC packings are negative, the ion-exclusion effect occurs at mobile phase pH values above the isoelectric point when protein and matrix are similarly charged, and ion-exchange effect at pH values below p*I*, when protein and matrix are oppositely charged. The only

0021-9673/92/$05.00

exception would be when the pH is too low for the support to be ionized.

The influence of pH in nSEC at high ionic strengths, *i.e.*, under conditions when the hydrophobic interactions are maximized, is far from being understood. All the workers concerned with this question observed increased interactions between the solute and support at low mobile phase pH and a high ionic strength [2,9,13,14], but it was only Holmes *et al.* [14], who suggested the possible cause of this effect, namely the exposure at acidic pH of the key sites of the solute molecules responsible for hydrophobic interactions. As this suggestion is speculative and the purification of proteins at high salt concentrations using unsubstituted gel matrices (termed "salting-out", "hydrophobic salting-out" or "solvophobic" chromatography) has became a widely used technique [6,22–26], the aim of this work was to reinvestigate in more detail the mechanism of the protein–gel matrix interactions under these conditions.

EXPERIMENTAL

Equipment

Chromatographic experiments were performed on a prepacked Superose 12 HR 10/30 column which was part of a complete fast protein liquid chromatographic system (Pharmacia, Uppsala, Sweden).

Materials and reagents

Strongly hydrophobic endoglucanase (1) [EG (1)] of *Clostridium thermocellum* was isolated as described in ref. 27 and non-hydrophobic endoglucanase C (EG C) of the same organism as in ref. 11. Three-times recrystallized egg white lysozyme was purchased from Reakhim (USSR). Elution buffers were prepared using analytical-reagent grade reagents and Milli-Q quality deionized water. Buffers were degassed and passed through a 0.22-μm filter before use. Samples were clarified by centrifugation at 20 000 *g* before application.

The following buffers were used: ethanolamine–HCl (pH 10.0), Tris–HCl (pH 8.5), imidazol–HCl (pH 7.0), histidine–HCl (pH 6.0), sodium succinate (pH 5.5 and 4.0), sodium acetate (pH 5.0 and 4.5) and β-alanine (pH 3.5) at concentrations of 25 m*M*.

Chromatographic procedure

The column was equilibrated with two volumes of elution buffer. A 25-μl loop and MV-7 injector were used to apply the samples. Isocratic elution at a flow-rate of 1 ml/min was used throughout. The protein concentration in the effluent was followed at 280 nm using a UV-1 monitor. The magnitude of protein retardation was expressed by the capacity factor k':

$$k' = (V_R - V^0)/V^0 \quad (1)$$

where V_R is the retention volume and V^0 is the elution volume of an unretained solute. The latter value was calculated from the calibration graph for the Superose column as a function of protein molecular weights, which are 41 000–42 000 dalton for EG (1) [27], 39 000 dalton for EG C [28] and 14 000 dalton for lysozyme [13]. The calibration graph was obtained under the optimum conditions (pH 5.5, $I = 0.38$) under which the interactions between the Superose column and proteins are minimal [8]. Weakly hydrophobic protein standards were used: ferritin (440 000 dalton), aldolase (158 000 dalton), bovine serum albumin (67 000 dalton), ovalbumin (43 000 dalton) and cytochrome *c* (12 300 dalton).

RESULTS AND DISCUSSION

Endoglucanase (1)

Experiments on the non-ideal chromatographic behaviour of proteins and other compounds in gel filtration media have usually been performed at fixed pH values and varying ionic strengths of elution buffers [2,4,8,9,13–16,19,21]. In our opinion, this could hardly provide useful information to explain adequately the pH dependence of solute–support interactions. In this work the elution position of proteins was investigated *vs.* pH at different (but fixed in a given set of experiments) ionic strengths.

The results of experiments with strongly hydrophobic endoglucanase (1) are presented in Fig. 1, where curve 1 shows the dependence of k' on pH at low ionic strength (buffers without any additives), curve 2 shows the dependence of k' on pH at higher ionic strength (buffers with 100 m*M* NaCl added) and curve 3 that at still higher ionic strength (buffers with 100 m*M* sodium sulphate added).

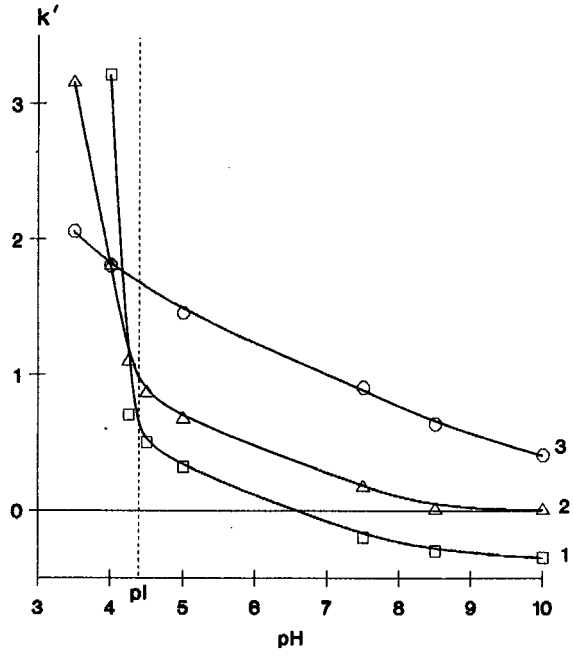

Fig. 1. Effect of pH on capacity factor k' of endoglucanase (1) in buffers of different ionic strength. Curves: 1 = buffers at a concentration of 25 mM with no additional electrolyte; 2 = the same buffers supplemented with 0.1 M NaCl; 3 = the same buffers supplemented with 0.1 M Na_2SO_4.

The results can be properly described and analysed separately for pH regions above and below the isoelectric point of EG (1), which is 4.4 [27]. In Fig. 1 these regions are demarcated by a broken line.

In the pH region above pI, curve 2 is located above curve 1, and curve 3 above curve 2. In earlier work [11] the retarded elution of EG (1) on addition of a salt to the elution buffer was attributed to the hydrophobic interaction of enzyme with the matrix; therefore, the later elution of the enzyme in the presence of NaCl and even more later in the presence of Na_2SO_4 may be associated with stronger salting-out conditions.

The chromatographic process was found to be strongly dependent not only on ionic strength but also on pH. The ideal SEC with $k' = 0$ could be achieved in the presence of NaCl and a mobile phase pH > 8.5 (Fig. 1, curve 2). Under stronger salting-out conditions occurring in the presence of Na_2SO_4 the hydrophobic interactions are superior at any pH tested (Fig. 1, curve 3). Under weaker salting-out conditions occurring without added electrolyte to the buffers the hydrophobic interactions are in excess at pH < 6.5 and the electrostatic repulsion of EG (1) (the "ion-exclusion effect") is in excess at pH > 6.5 (Fig. 1, curve 1).

The true cause of the monotonic increase in the interactions with decreasing pH at all three ionic strengths tested is not easily understood. Intuitively, it is clearly associated with hydrophobic interactions because this effect is absent in the case of non-hydrophobic EG (1) (see Fig. 6). The simplest explanation of this result could be the increased protein hydrophobicity or exposure of hydrophobic sites on the protein surface with decrease in pH, as suggested by other workers for tRNA [14]. Although possible in principle, the suggestion needs to be proved.

However, the pH dependence of interactions can be explained without this speculative supposition. Indeed, Superose contains some carboxylic and sulphate groups that are negatively charged within the working pH range [5,8]. Similarly charged is endoglucanase (1) at pH > pI, its net negative charge being the larger the higher is the pH. In this situation, Hesselink's theory of polyelectrolyte adsorption on charged surfaces [29] and the thermodynamic theory of protein adsorption of Norde and Lyklema [30] predict an increase in sorption with decrease in pH as a result of an increase in the electric contribution to the free energy of sorption. Certainly, neither theory is fully adequate for the experimental results of our work, as they were developed not for the chromatographic process *per se* but just for the adsorption on solid charged surfaces.

A more adequate and comprehensible analysis of the results can be made in terms of the theory of potential barrier chromatography proposed by Rukenstein and Lesins [31]. Below we give some postulates of this theory.

The total potential Φ of the adsorbate–adsorbent interaction is obtained by summing the individual contributions:

$$\Phi = \Phi_{DL} + \Phi_{vdW} + \Phi_B \quad (2)$$

where Φ_{DL} is the electrical double-layer interaction potential, Φ_{vdW} is the London–Van der Waals potential essentially determining the strength of hydrophobic interactions in an aqueous medium and Φ_B is the potential of repulsive short-range Born

interaction. Complex expressions for all three individual potentials and a discussion of their origin, nature and importance have been published [31]. The double-layer interaction arises from the charged surfaces of the adsorbate and the adsorbent. Therefore, its magnitude is readily modified by a pH change of the mobile phase as the degree of ionization of the surface groups is a function of pH. Further, the changes in the ionic strength of the mobile phase also greatly affect the double-layer potential owing to the screening of the surface charges and the binding of the counter ions to the charged surfaces. It should be noted that the chemical identity of the ions will determine the extent to which they bind to the charged surface and consequently reduce the double-layer interaction.

The attractive Van der Waals interaction between the adsorbate and adsorbent originates from the orientation, induction and dispersion interactions and can be altered by the addition of organic solvents to the mobile phase or salts at high concentrations.

The repulsive short-range interaction originates from steric and Born repulsion (the major contribution) and hydration forces and becomes important when the adsorbate approaches the adsorbent within very short distances. Like the Van der Waals potential, the Born potential is not significantly altered by pH or small changes in the ionic strength of the mobile phase.

The general idealized profiles of three individual (curves A, B and C) and total interaction potential (curve D) are illustrated in Fig. 2, taken from ref. 31. Curve A represents the repulsive double-layer interaction, *i.e.*, with a negatively charged matrix such as Superose it holds for pH > p*I* of the protein, where the latter is similarly charged. At short distances between the solute and the support an adsorption energy well (primary minimum) occurs on the total potential profile whereas at intermediate distances a potential barrier to adsorption appears. The solute can move over the potential barrier (if it is not too high) into the primary minimum and subsequently can escape from the adsorption energy well (if it is not too deep) to the bulk solution. The lower the barrier the more readily adsorption occurs, and the deeper the energy well the slower is the process of desorption.

In chromatographic theory, the elution behaviour of a solute is described as repeated adsorption–desorption cycles. The greater the characteristic time for adsorption during the cycle, the slower the solute moves along the column, *i.e.*, the larger is its retention volume, and *vice versa*.

Let us now examine the experimental results in Fig. 1 (region of pH > p*I*) and the potential profiles in Figs. 2–5. First, the analysis provides a simple explanation of increased k' on addition of the salt to the mobile phase. Indeed, the salt decreases the double-layer repulsion by screening the surface charges of the protein and the matrix. Curve A in Fig. 2 shifts to the left whereas the positions of curves B and C do not change significantly, as the Van der Waals potential and, especially, the Born potential are insensitive to small changes in ionic strength of the mobile phase, as mentioned above. As a result, the potential barrier on the total potential profile D will decrease and the potential well will become deeper (Fig. 3). In other words, EG

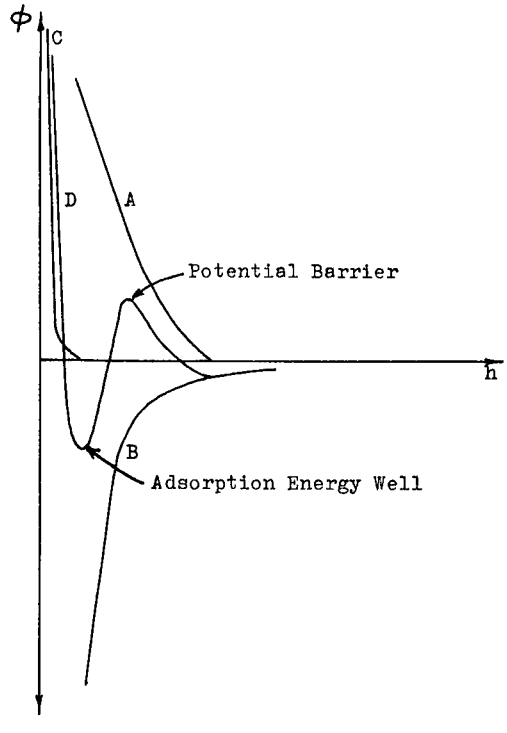

Fig. 2. Schematic profiles of the (A) double-layer, (B) Van der Waals, (C) Born and (D) total interaction potential for negatively charged protein and matrix at low ionic strength [31]. h = Distance between the protein molecule and the matrix.

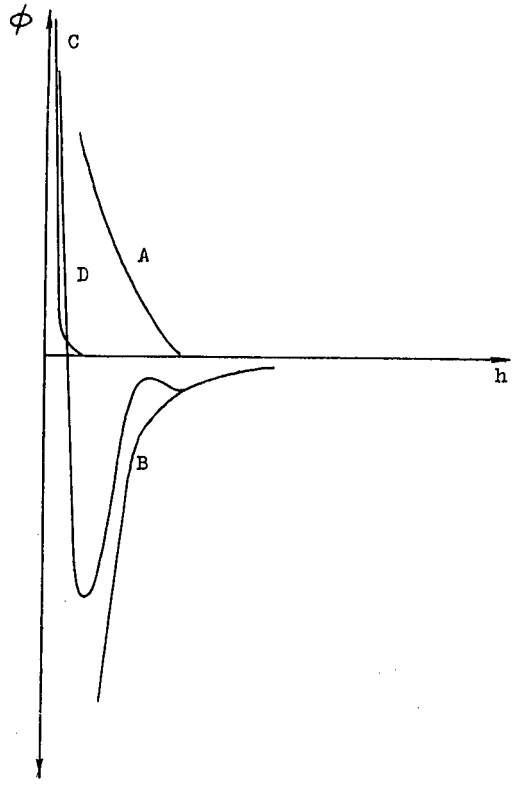

Fig. 3. Schematic representation of the effect of increased ionic strength or decreased pH (but still above the p*I* of the protein) on the individual contributions and the total interaction potential. Curves as in Fig. 2.

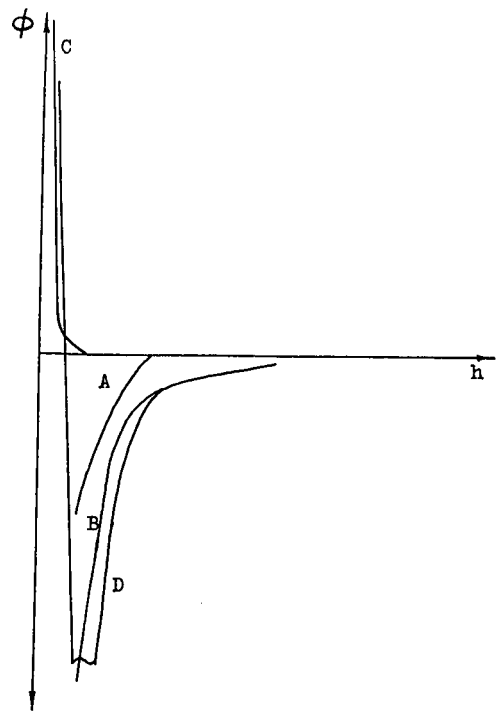

Fig. 4. Schematic potential profiles at pH slightly lower than p*I* of protein and low ionic strength of the mobile phase. Curves as in Fig. 2.

(1) will be more readily adsorbed and more slowly desorbed, which results in an increase in k'. A larger k' in the presence of Na_2SO_4 as compared with an equimolar concentration of NaCl can be explained by the higher ionic strength and stronger salting-out capacity of the former salt (and, consequently, by some enhancement of hydrophobic interactions) and its stronger efficiency in screening of protein and matrix charges.

In much the same manner the potential barrier decreases and the adsorption energy well becomes deeper during the lowering of the pH, which results in an increase in k' (Fig. 1, pH > p*I*). In this instance the double-layer potential is diminished, mainly owing to the decrease in the net negative charge of EG (1), as the degree of ionization of carboxyl groups of Superose is less sensitive to pH in this region, which is far from pK′ values of this group.

Hence the monotonic pH dependence of the sorption of EG (1) on Superose is conditioned by the fact that the potential barrier for sorption is dependent on pH. Therefore, this effect can be observed only when both electrostatic and pronounced hydrophobic interactions take place between the solute and support.

Let us consider now the region of pH < p*I* when the net charge of EG (1) is opposite to that of Superose. The double-layer potential profile (curve A) in this instance tends to go downwards (electrostatic attraction). As a result, the total potential (Fig. 4, curve D) has no barrier for sorption and the potential well becomes deeper. The adsorption–desorption equilibrium sharply changes towards adsorption, which explains the drastic increase in k' at pH < p*I* (the left-hand side of Fig. 1). Interestingly, in this region of pH the relative positions of curves 1, 2 and 3 were inverted as compared with the region of pH > p*I*. This is due to the screening effect of the salt with a consequent attenuation of the

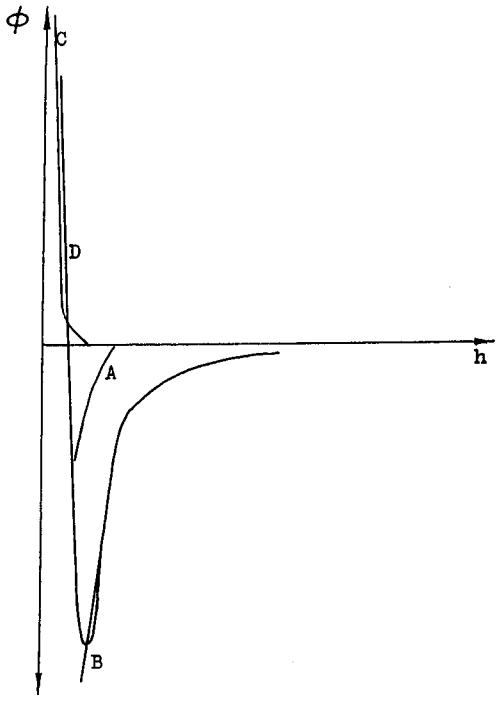

Fig. 5. Schematic representation of the effect of increased ionic strength on the interaction potentials at pH < p*I* of the protein. Curves as in Fig. 2.

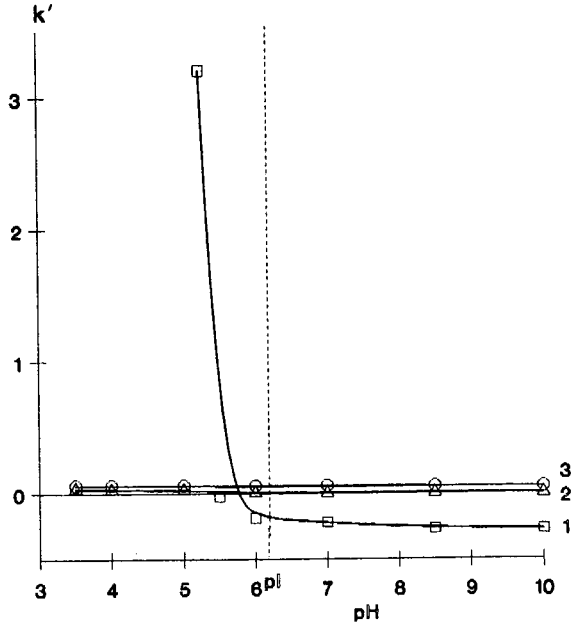

Fig. 6. Effect of pH on the capacity factor k' of endoglucanase C in buffers of different ionic strength. Curves: 1 = buffers at a concentration of 25 m*M* with no additional electrolyte; 2 = the same buffers supplemented with 0.1 *M* Na_2SO_4; 3 = the same buffers supplemented with 0.5 *M* Na_2SO_4.

double-layer potential and the decrease in the depth of the potential well (Fig. 5, curve D). The fact that on the left-hand side of Fig. 1 curve 3 proves to be below curve 2 is further evidence for the larger efficiency of Na_2SO_4 in reducing the ionic interactions as compared with NaCl. This conclusion is also supported by the experiments with lysozyme (see below).

Endoglucanase C

The results of chromatographic experiments with non-hydrophobic protein, EG C, are given in Fig. 6. In contrast to the corresponding experiments with EG (1), curve 2 represents the k' values in the presence of 100 m*M* Na_2SO_4 and curve 3 in the presence of 500 m*M* Na_2SO_4, *i.e.*, under more salting-out conditions. In spite of this, we found no noticeable hydrophobic interaction of EG C with Superose in the pH range studied. Non-size exclusion of protein from the gel at pH > p*I* and the strong retardation at pH < p*I*, observed at low ionic strength (Fig. 6, curve 1), are apparently due to electrostatic interactions of EG C with the negatively charged matrix because they are eliminated at high ionic strengths (Fig. 6, curves 2 and 3).

Lysozyme

This protein was assayed as the reason for the observed retardation of this and some other proteins on gel-filtration matrices at low pH and high ionic strength [2,9,13] remained unclear. Indeed, our previous results [11] showed that the relative hydrophobicity of lysozyme is closer to that of weakly hydrophobic EG C but not of strongly hydrophobic EG (1). Therefore, the mechanism of the pH-dependent retardation described above for EG (1) is inapplicable for lysozyme.

The results of chromatographic experiments with this protein are shown in Fig. 7. Owing to the very basic properties of the lysozyme (p*I* 11.0), at low ionic strength (buffers with no additional electrolyte) this protein is completely adsorbed on Superose by the ion-exchange mechanism within the pH range investigated, so Fig. 7 lacks a corresponding curve.

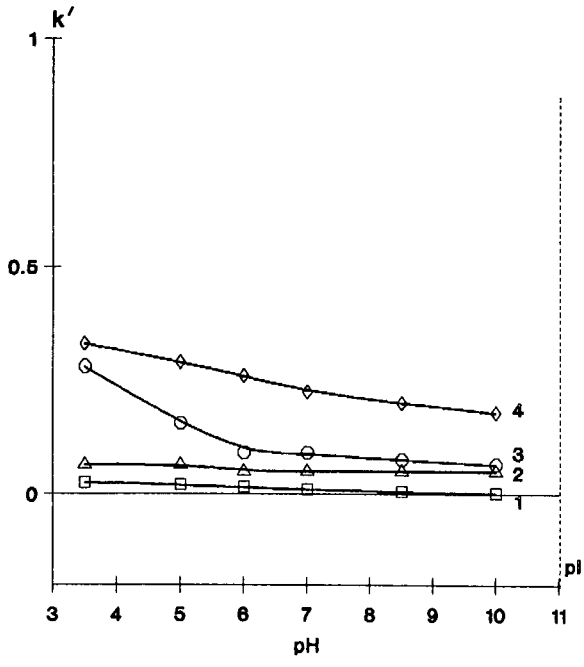

Fig. 7. Effect of pH on the capacity factor k' of lysozyme in buffers of different ionic strength. Curves: 1 = buffers supplemented with 0.1 M Na_2SO_4; 2 = buffers supplemented with 0.5 M Na_2SO_4; 3 = buffers supplemented with 0.5 M NaCl; 4 = buffers supplemented with 0.1 M NaCl.

Four other curves show the pH dependence of k' at increased ionic strengths: in the presence of 100 mM sodium sulphate (curve 1), 500 mM sodium sulphate (curve 2), 500 mM NaCl (curve 3) and 100 mM NaCl (curve 4). In the presence of 100 mM sodium sulphate the chromatographic process approaches the ideal gel filtration, as indicated by $k' = 0$. Sodium sulphate at a concentration of 500 mM evidently stimulates some hydrophobic interaction of lysozyme with the matrix (curve 2). The fact that in the presence of 500 mM NaCl (curve 3), 100 mM NaCl (curve 4) and 500 mM Na_2SO_4 (curve 2) the interaction is inversely dependent on the salting-out strength indicates that in the presence of NaCl some lysozyme adsorption is due not to hydrophobic interactions but to incomplete elimination of the ion-exchange interaction.

As the latter becomes stronger at acidic pH owing to the increased positive charge of lysozyme, it is not surprising that at both NaCl concentrations the retardation of this protein on Superose is enhanced with decrease in pH, as is seen in Fig. 7. Na_2SO_4 effectively eliminates ion-exchange interactions and no pH dependence in the presence of this salt is observed (Fig. 7, curves 1 and 2).

CONCLUSIONS

The aim of this work was mainly to elucidate the cause of the gradual increase of retardation of proteins and some other solutes on gel filtration matrices with decrease in pH, even at high ionic strengths when electrostatic interactions are assumed to be absent or at least negligible.

It should be emphasized that the existing hypothesis on the exposure of hydrophobic sites on the surface of macromolecules at low pH requires justification, whereas the above phenomenon can be well explained from the fact that all known gel filtration matrices are not only weakly hydrophobic but also contain some ionogenic groups that are negatively charged at the working pH.

As a result, at low ionic strengths and pH > pI when proteins are negatively charged, the ion-exclusion effect is observed and at pH < pI the ion-exchange effect. With weakly hydrophobic proteins, such as EG C or lysozyme, these interactions can be easily avoided by adding a salt to the eluent. It should be noted that NaCl, the electrolyte usually used in gel filtration for this purpose, sometimes does not eliminate them totally (*e.g.*, in the case of lysozyme) even at a concentration of 500 mM. Apparently, this is the cause of the increased distribution coefficient (k_D) of lysozyme and other proteins at low pH and high ionic strength observed by some workers [2,9,13]. Nevertheless, 0.1 M sodium sulphate totally suppresses these interactions at any pH tested, which is consistent with the high elution strength of this salt as compared with NaCl [32].

A more complicated situation occurs with strongly hydrophobic proteins such as EG (1). In this instance an ideal SEC can be obtained only under restricted conditions. First, the mobile phase must contain an electrolyte whose concentration and salting-out strength are not high in order to attenuate the electrostatic interactions but not to promote significantly the hydrophobic interactions. Second, the mobile phase pH must be high enough to balance the attractive hydrophobic interactions with the repulsive electrostatic interactions.

As for the true cause of the monotonic increase in the retardation of hydrophobic proteins on gel filtration matrices with decrease in pH, it is most readily explained in terms of the theory of potential barrier chromatography [31] as a result of a gradual decrease in the potential barrier for the sorption of charged solutes on a charged support.

REFERENCES

1 D. E. Schmidt, R. W. Giese, D. Conron and B. L. Karger, *Anal. Chem.*, 52 (1980) 177–182.
2 P. Strop, F. Mikes and Z. Chytilova, *J. Chromatogr.*, 156 (1978) 239–254.
3 H. G. Barth, *J. Chromatogr. Sci.*, 18 (1980) 409–429.
4 E. Pfannkoch, K. C. Lu, F. E. Regnier and H. G. Barth, *J. Chromatogr. Sci.*, 18 (1980) 430–441.
5 T. Andersson, M. Carlsson, L. Hagel and P.-A. Pernemalm, *J. Chromatogr.*, 326 (1985) 33–44.
6 H. Imai, G. Tamai and S. Sakura, *J. Chromatogr.*, 371 (1986) 29–35.
7 A. Zaton, R. R. de Alegria and J. M. de Gandarias, *J. Liq. Chromatogr.*, 10 (1987) 3073–3083.
8 P. L. Dubin and J. M. Principi, *J. Chromatogr.*, 479 (1989) 159–164.
9 B.-L. Johansson and J. Gustavsson, *J. Chromatogr.*, 457 (1988) 205–213.
10 P. L. Dubin and J. M. Principi, *Anal. Chem.*, 61 (1989) 780–781.
11 N. P. Golovchenko, I. A. Kataeva and V. K. Akimenko, *Enzyme Microb. Technol.*, in press.
12 M. Belew, J. Porath, J. Fohlman and J.-C. Janson, *J. Chromatogr.*, 147 (1978) 205–212.
13 I. Drevin, L. Larsson, I. Eriksson and B.-L. Johansson, *J. Chromatogr.*, 514 (1990) 137–146.
14 W. M. Holmes, R. E. Hurd, B. R. Reid, R. A. Rimerman and G. W. Hatfield, *Proc. Natl. Acad. Sci. U.S.A.*, 72 (1975) 1068–1071.
15 F. E. Regnier, *Methods Enzymol.*, 91, Part 1 (1983) 137–190.
16 W. Kopaciewicz and F. E. Regnier, *Anal. Biochem.*, 126 (1982) 8–16.
17 T. Arakawa, *Arch. Biochem. Biophys.*, 248 (1986) 101–105.
18 M. G. Cacace, M. Santin and A. Sada, *J. Chromatogr.*, 510 (1990) 41–46.
19 H. D. Crone, *J. Chromatogr.*, 92 (1974) 127–135.
20 N. V. B. Marsden, *Naturwissenschaften*, 64 (1977) 148–149.
21 S. Mori and M. Kato, *J. Liq. Chromatogr.*, 10 (1987) 3113–3126.
22 N. Sakihama, H. Ohmori, N. Sugimoto, Y. Yamasaki, R. Oshino and M. Shin, *J. Biochem.*, 93 (1983) 129–134.
23 M. Mevarech, W. Leicht and M. M. Werber, *Biochemistry*, 15 (1976) 2383–2387.
24 W. Leicht and S. Pundak, *Anal. Biochem.*, 114 (1981) 186–192.
25 J. Lascu, J. Abrudan, L. Muresan, E. Presecan, A. Vonica and J. Proinov, *J. Chromatogr.*, 357 (1986) 436–439.
26 D. F. Tikhomirov, N. N. Nutsubidze, V. M. Lakhtin and A. A. Klyosov, *Biokhimiya*, 52 (1987) 1097–1106.
27 N. P. Golovchenko, I. A. Kataeva, M. G. Buchtijarova, R. I. Aminov, T. V. Tsoi, V. K. Akimenko and A. M. Boronin, *Biokhimiya*, 56 (1991) 49–54.
28 D. Petre, J. Millet, R. Longin, P. Beguin, H. Girard and J.-P. Aubert, *Biochimie*, 68 (1986) 687–695.
29 F. Th. Hesselink, *J. Colloid Interface Sci.*, 60 (1977) 448–466.
30 W. Norde and J. Lyklema, *J. Colloid Interface Sci.*, 71 (1979) 350–366.
31 E. Ruckenstein and V. Lesins, *Biotechnol. Bioeng.*, 28 (1986) 432–451.
32 *FPLC Ion Exchange and Chromatofocusing*, Pharmacia LKB Biotechnology, Uppsala, 1985, p. 135.

Journal of Chromatography, 591 (1992) 129–137
Elsevier Science Publishers B.V., Amsterdam

CHROMSYMP. 2451

Limits and effects of precolumn addition of thioglycerol in liquid chromatographic–fast atom bombardment mass spectrometric systems☆

Alain Carrier, Jean-Pierre Gagné and Michel J. Bertrand*

Regional Center for Mass Spectrometry, Department of Chemistry, University of Montreal, P.O. Box 6128, Montreal H3C 3J7 (Canada)

(First received July 17th, 1991; revised manuscript received September 12th, 1991)

ABSTRACT

A series of experiments were conducted in order to determine the effect of the precolumn addition of a viscous matrix such as thioglycerol on the chromatographic performance of liquid chromatographic–fast atom bombardment mass spectrometric (LC–FAB-MS) systems. In those experiments, the concentration of thioglycerol in a mobile phase consisting of acetonitrile–water–trifluoroacetic acid was varied and important chromatographic parameters such as retention times, capacity factors, number of theoretical plates, peak widths, resolution and impedance of separation were monitored for analytes such as met-enkephalin, leu-enkephalin and *p*-hydroxybenzoic acid. The results obtained indicate that for concentrations of thioglycerol in the mobile phase below 3% most chromatographic indicators are only slightly affected. However, for concentrations of the viscous matrix above that value the capacity factors are significantly decreased, indicating that thioglycerol is behaving as an efficient organic moderator, and peak broadening becomes important, having a detrimental effect on the performance of the system. Van Deemter plots obtained for the analytes at concentrations of thioglycerol in the mobile phase of 0–15% reveal that the major effect of thioglycerol is to reduce the mass transfer efficiency in the chromatographic system at high linear velocities and concentrations of thioglycerol above 3%. Comparison of the effects of viscous matrices such as thioglycerol and glycerol on the chromatographic performance of LC–FAB-MS systems indicates that the chromatographic efficiency is almost independent of the matrix concentration when the systems are operated near their optimum linear velocities and that high matrix contents and high linear velocities can be used with little decrease in efficiency if the systems are operated at higher temperatures.

INTRODUCTION

The technique of fast atom bombardment mass spectrometry (FAB-MS) is now confirmed as a powerful tool in the mass spectral analysis of polar, thermally labile or involatile compounds. In its application [1], the analyte was dissolved in a viscous matrix such as glycerol, which was subsequently introduced into the ion source of the mass spectrometer and bombarded with a beam of high-energy (5–8 keV), fast-moving neutral species (FAB). High-energy Cs^+ ions can also be used as in liquid secondary ion mass spectrometry (LSIMS) and yield similar results, although some differences exist because the ion beam is generally more focused than the neutral beam and usually has a higher density of particles. The liquid matrix used in these desorption–ionization techniques provides a means by which the molecules on the surface can be replenished by molecular diffusion in the liquid, thus allowing for the presence of fresh material at the surface and partial elimination of secondary products issuing from the radiation damage caused to the solution. The role of the liquid matrix, however, is not simply to dissolve the analyte but it is also involved

☆ Presented at the *8th (Montreux) Symposium on Liquid Chromatography–Mass Spectrometry (LC–MS, SFC–MS, CE–MS, IC–MS), Ithaca, NY, July 17–19, 1991.*

0021-9673/92/$05.00

intimately in the ionization process. The mass spectra obtained in FAB-LSIMS are affected by the nature of the matrix [2,3] and strong matrix–analyte interactions exist in the solution [2,4–7].

FAB-MS has in recent years extended the scope of its application primarily as a result of the introduction of dynamic FAB or continuous-flow FAB (CF-FAB) [8,9]. The latter technique allows the continuous introduction of aqueous solutions into the mass spectrometer by delivering the mobile phase through a fused-silica capillary located in the hollow shaft of the FAB probe [10,11]. The advent of CF-FAB has not only increased the power of the technique but it has also allowed its interfacing with liquid chromatography (LC–FAB-MS) [12–25]. Severals approaches have been used in order to couple LC to CF-FAB systems. The most commonly used interface involves the direct coupling of conventional [12,13], microbore [14] or packed capillary columns [15–19, 24–26] with CF-FAB. The columns are connected with the FAB probe tip through a transfer fused-silica capillary (50–75 μm I.D.) and split-flow devices are used to reduce the flow through the interface below typically 10 μl/min when appropriate. In all of these LC–FAB-MS systems, it is necessary to add a viscous matrix to the mobile phase in order to optimize the ionization efficiency. Matrix concentrations ranging from 0 to 25% have been reported [8,12–16,21,22,27,28] and the optimum concentration required for proper ionization is usually a compromise between absolute sensitivity and signal-to-noise ratio. The addition of the viscous matrix can be done before the chromatographic separation (precolumn) [14,16,18,19,24,25] or after the separation (postcolumn) [12,16,17].

Although postcolumn addition has been suggested, in most instances precolumn addition is easier to achieve and offers advantages in conventional systems. It should be noted, however, that the precolumn addition of the matrix will significantly alter the polarity and viscosity of the mobile phase and therefore will affect the chromatographic process.

Although many studies have focused on the optimization of FAB probes and CF-FAB systems [8,9,26,27], few have dealt with the optimization of LC–FAB-MS systems [16,17,27–32]. Occasionally, some of the effects of precolumn addition on the chromatographic performance have been mentioned [8,16,17], but until recently not many systematic studies were focused on the optimization of the chromatographic systems [16,33,34]. Previous work in this laboratory [33,34] has shown that the precolumn addition of a viscous matrix such as glycerol over a wide range of concentrations affects most chromatographic indicators (R_s, k', E, t_R, $w_{1/2}$, N). The extent of the changes observed depends on the actual glycerol content in the mobile phase. The overall performance of the chromatographic system was seen to decrease when the concentration of glycerol in the mobile phase exceeded 3%, whereas minor decreases in performance were observed when the glycerol content was maintained below 3% for a wide range of flow rates. Further work conducted on the optimization of LC–FAB-MS systems using analytes from several chemical classes has revealed that the main source of chromatographic band broadening in these systems was related to the increase in the viscosity of the mobile phase and changes in the diffusivity of the analytes with glycerol content [33].

In seeking to broaden the scope of our previous studies and to evaluate the general boundaries within which precolumn addition of a matrix can be used, we undertook this work, which included the characterization of the effect of precolumn addition of various amounts of thioglycerol to a mobile phase consisting of acetonitrile–water–trifluoroacetic acid and the study of the kinetic optimization of the chromatographic process in the presence of such a matrix. The objectives of the study were (i) to quantify the effects of the addition of thioglycerol to the mobile phase over the concentration range 0–15% on most chromatographic indicators, (ii) to identify the source of broadening in LC–FAB-MS systems by kinetic studies and determine the optimum operational conditions to be used in these systems, (iii) to compare the effects of the addition of different matrices in order to establish general guidelines for precolumn addition and (iv) to determine the effect of an increase in the temperature of analysis on the performance of the chromatographic system. The results obtained indicate that general guidelines can be formulated, as was indicated by our earlier findings, and that the deleterious effects of precolumn addition can be compensated under selected conditions.

EXPERIMENTAL

Instrumentation

The LC system consisted of a Perkin-Elmer Model 410 pump connected to a Rheodyne Model 7125 injector with a 6-μl sample loop. Detection (280 nm) was effected with a Perkin-Elmer LC-90 variable-wavelength detector. The chromatographic column used [Spherisorb ODS-2, d_p = 5 μm, 125 mm × 4.6 mm I.D. (CSC, Montreal, Canada)] was maintained at constant temperature by a water jacket regulated by a Haake (Berlin-Steglitz, Germany) circulator. Viscosity measurements were performed with a ball viscosimeter (Haake).

Chemicals

The peptides met-enkephalin and leu-enkephalin were obtained from Sigma (St. Louis, MO, USA) and *p*-hydroxybenzoic acid and Glass-distilled thioglycerol (THIO) (>95%) were purchased from Aldrich (Milwaukee, WI, USA). The solvents used in the preparation of the mobile phases were distilled and deionized water (Milli-Q system; Millipore, Bedford, MA, USA), HPLC-grade acetonitrile (ACN) and trifluoroacetic acid (TFA), obtained from Aldrich. All compounds were used as received.

Preparation of mobile phase

The mobile phases were prepared by mixing appropriate volumes of distilled, deionized water and organic modifiers. The mobile phase contained fixed proportions of trifluoroacetic acid (0.05%) and acetonitrile (30%) and the amount of water added was adjusted to component the volume of thioglycerol added to the solution (ACN–water–THIO/TFA = 30:70 − *x*:*x*:0.05). Sufficient amounts of each mixture were prepared in order to ensure that all experiments would be conducted with the same mobile phase. In all instances, the solvents used were filtered (0.45 μm) and degassed prior to use.

Chromatographic measurements

All chromatographic experiments were conducted at 25 or 38.5°C after the chromatographic system had equilibrated for at least 90 min. Precise values for the volumetric flow rate were measured for each experiment. The retention of sodium nitrate was taken as the dead volume indicator and the average linear velocity of the mobile phase was calculated using the length of the chromatographic column. The number of theoretical plates (N) was calculated from the peak width at half-height. The Van Deemter plots were generated by measuring the theoretical plate heigth (H) with linear velocities in the range 0.1–7 mm/s, corresponding to flow-rates of 0.05–3 ml/min in our chromatographic system. Other measurements were made at a constant linear velocity.

RESULTS AND DISCUSSION

It is common practice in LC to add an organic modifier to the mobile phase in order to alter the chromatographic process and the retention characteristics of the analytes. The modifier is usually of low viscosity in order to obtain high chromatographic efficiency and minimize pressure build-up in the system. In LC–FAB-MS systems, however, the matrix added to the mobile phase is used to optimize ionization and is fairly viscous, leading to the use of rather unusual mobile phases in terms of chromatography. Recently, the use of thioglycerol as a matrix in LC–FAB-MS and FAB-MS has been

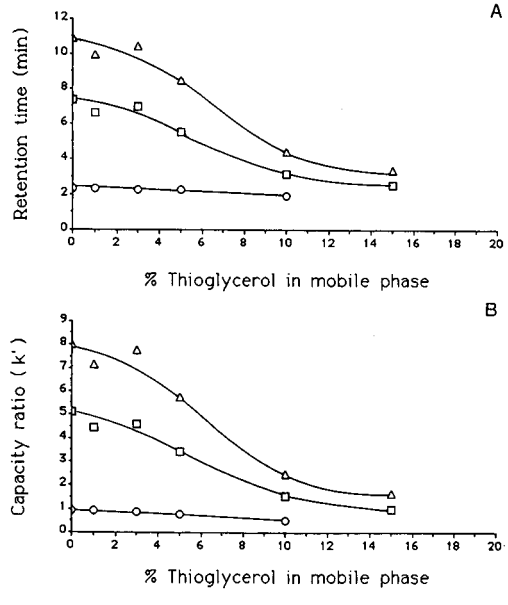

Fig. 1. Effect of concentration of thioglycerol in the mobile phase on (A) retention times and (B) capacity factors (k'), □ = Met-enkephalin; △ = leu-enkephalin; ○ = *p*-hydroxybenzoic acid.

reported to offer advantages over glycerol in the analysis of oligosaccharides, peptides and eicosanoic compounds [15,18,35,36], but its effects on the overall chromatographic performance were not described. The effect of an increasing concentration of this particular matrix in the mobile phase on the chromatographic properties of the analytes can be seen in Fig. 1*a* and *b*, which show the effect of the variation of the thioglycerol content in the mobile phase (0–15%) on the retention times and capacity factors of two peptides, met- and leu-enkephalin, and of a less retained analyte, *p*-hydroxybenzoic acid. As can be observed, higher contents of thioglycerol reduce the capacity factor of met- and leu-enkephalin by *ca.* 80%. This indicates that small increases in thioglycerol in the mobile phase alter the distribution of these compounds significantly. The reduction observed for *p*-hydroxybenzoic acid is *ca.* 40%, which is consistent with the much lower capacity factor of this compound, which is only sligtly retained. Hence, thioglycerol acts as an efficient organic moderator, behaving as other viscous matrices that have been studied [32]. Thioglycerol behaves as a less polar moderator than glycerol, causing greater changes in retention characteristics than glycerol for small changes in concentrations in the mobile phase. As for systems containing glycerol, however, essentially no change is observed when the added concentration of the matrix in the mobile phase is below 3%.

The chromatographic performance of the system was also monitored as the thioglycerol content in the mobile phase was increased. This was done by evaluating the relative variation in the normalized theoretical plate number (N/N_0) with and without thioglycerol present in the mobile phase. As shown in Fig. 2, the efficiency of the chromatographic system as measured by N/N_0 is only slightly affected when the thioglycerol content is below 3%, but above this value a reduction of up to 25% can be observed for the compounds studied. The reduction in efficiency observed for *p*-hydroxybenzoic acid is greater, possibly indicating dead volume effects for this less retained compound. The broadening induced by the addition of thioglycerol to the mobile phase can be evaluated by examining the variation of the normalized peak width ($w_{1/2}/t_R$) with thioglycerol content. The behavior of this chromatographic indicator with increasing thioglycerol content in the mobile phase is shown in Fig. 3, which indicates that peak broadening increases with increasing thioglycerol concentration for all the compounds studied, being greater for *p*-hydroxybenzoic acid, which correlates well with the findings that the decrease in efficiency is greater for the less retained compounds, indicating that instrumental dead volume diffusion is important.

The overall effect of the addition of thioglycerol to the mobile phase can be reflected by examining the behavior of two important chromatographic parameters, the resolution and the impedance of separation [37]. The influence of thioglycerol on the resolution is shown in Fig. 4 for the pair met- and leu-enkephalin. The resolution decreases almost linearly with increase in the thioglycerol content in the mobile phase, demonstrating the deleterious effects of the decrease in efficiency and increase in peak broadening on the separation power of the

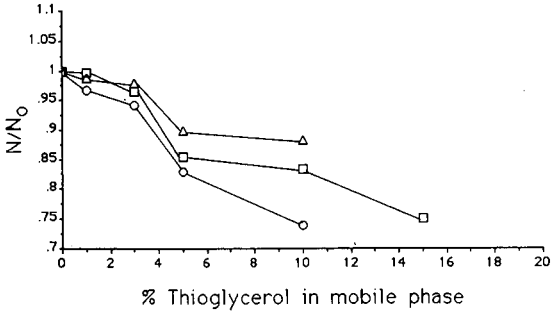

Fig. 2. Effect of concentration of thioglycerol in the mobile phase on the normalized number of theoretical plates, N/N_0. □ = Met-enkephalin; △ = leu-enkephalin; ○ = *p*-hydroxybenzoic acid.

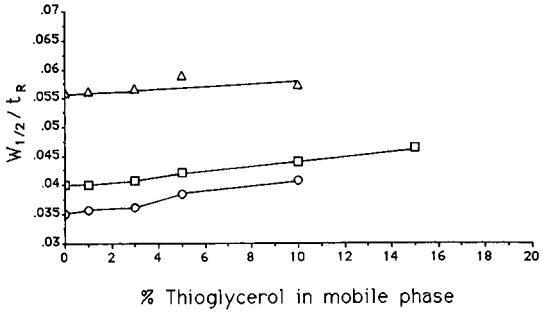

Fig. 3. Effect of concentration of thioglycerol in the mobile phase on the normalized peak width, $w_{1/2}/t_R$. □ = Met-enkephalin; △ = leu-enkephalin; ○ = *p*-hydroxybenzoic acid.

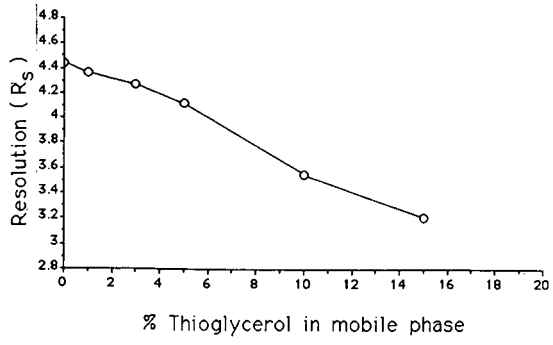

Fig. 4. Effect of concentration of thioglycerol in the mobile phase on the resolution, R_s, for met- and leu-enkephalin.

system. The decrease in performance of the chromatographic system can be measured using the separation impedance (E), which is related to the efficiency and to the physical properties of the system. The variation of the separation impedance (E) normalized to that in the absence of thioglycerol (E_0) can be observed in Fig. 5, which gives the normalized impedance (E/E_0) as a function of thioglycerol content in the mobile phase. The results clearly indicate that this parameter is more than doubled as the concentration varies from 0 to 15%. The sharp increase observed in E/E_0 for thioglycerol contents above 10% is indicative that the chromatographic system is perturbed under these conditions, which results in a dramatic decrease in performance. For thioglycerol contents below 3%, however, the impedance is stable, suggesting that the performance is retained.

In order to access the factors responsible for the decrease in chromatographic performance and obtain qualitative information on the system, Van

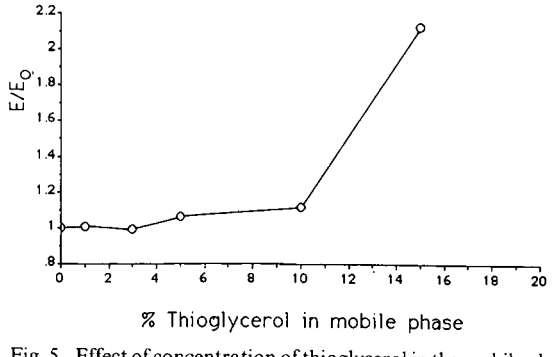

Fig. 5. Effect of concentration of thioglycerol in the mobile phase on the normalized separation impedance, E/E_0.

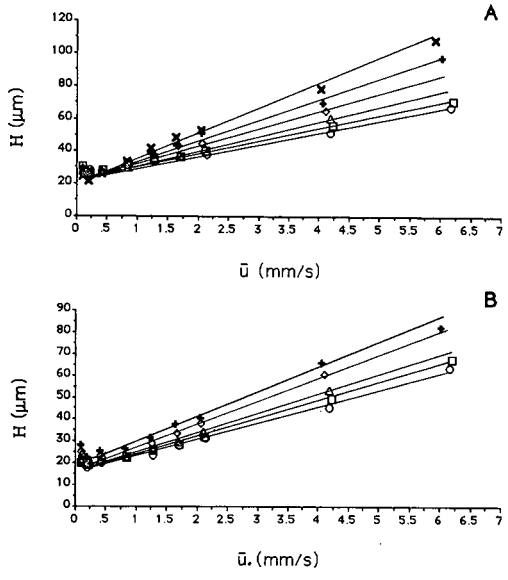

Fig. 6. Van Deemter plots for met-enkephalin at various thioglycerol concentrations in the mobile phase: ○ = 0%; □ = 1%; △ = 3%; ◇ = 5%; + = 10%; × = 15%. (A) Met-enkephalin; (B) *p*-hydroxybenzoic acid.

Deemter plots were generated with the thioglycerol content in the mobile phase varying in the range 0–15% and for linear velocities between 0.2 and 7 mm/s. The plots that were obtained under these experimental conditions using met-enkephalin and *p*-hydrobenzoic acid are shown in Fig. 6a and b, respectively. The data indicate that as the thioglycerol content is increased from 0 to 15% the slopes of the Van Deemter plots increase steadily and significantly. This means that the presence of thioglycerol affects the mass transfer kinetics in the system. It can also be observed that for both compounds the plots converge at lower linear velocities (0.2–0.6 mm/s), indicating that the system can be operated near optimum performance and that only small differences in chromatographic performance occur under these conditions as the concentration of thioglycerol in the mobile phase changes. This important effect, which has also been observed when glycerol was used as a viscous matrix [33], implies that it is possible to use precolumn addition or high concentrations of the viscous matrix and retain the chromatographic performance, provided that the system is operated near its optimum kinetic conditions.

The systematic reduction of the capacity factor, the normalized number of theoretical plates and the resolution occurring for all the different compounds studied clearly demonstrates that the presence of thioglycerol in the mobile phase produces significant changes in the kinetics of the chromatographic process. This is well supported by experimental evidence of the increase in broadening as demonstrated by the variation of the normalized peak width and the increase in the slope of the Van Deemter plots. The processes that occur within the chromatographic column can be represented by the three kinetic effects which are expressed as terms in the Van Deemter equation relating the height equivalent to a theoretical plate (H) to the average linear velocity of the mobile phase ($\bar{u}$) [38–40]. For the system under investigation, the Van Deemter equation has the form [40]

$$H = 2\lambda d_p + \frac{2\gamma D_m}{\bar{u}} + \left[\frac{f_1(k')d_p^2}{D_m} + \frac{f_2(k')d_f^2}{D_s}\right]\bar{u} \qquad (1)$$

where λ and γ are constants, d_p *and* d_f are the particle size and film thickness, respectively, D_m and D_s are the diffusion coefficients in the mobile phase and the stationary phase, respectively, and $f_1(k')$ and $f_2(k')$ are functions of the capacity factor. As the film thickness is considered to be small [39,41], eqn. 1 can be approximated by

$$H = 2\lambda d_p + \frac{2\gamma D_m}{\bar{u}} + \frac{(1 + 6k' + 11k'^2)d_p^2\bar{u}}{24(1 + k')^2} \qquad (2)$$

which represents an expanded form of the more general Van Deemter equation

$$H = A + \frac{B}{\bar{u}} + C\bar{u} \qquad (3)$$

where A, B and C represent the contributions from eddy diffusion, longitudinal diffusion and mass transfer, respectively. As shown in Fig. 6, the term which is mostly affected by the presence of thioglycerol in the mobile phase is the mass transfer term (C), which involves $f_1(k')$, and the diffusion coefficient in the mobile phase, D_m.

It is possible from available data on *p*-hydroxybenzoic acid to evaluate D_m at different thioglycerol concentrations using the Wilke–Chang equation [42]. Knowledge of the $f_1(k')$ function and the estimated values for D_m should allow a qualitative

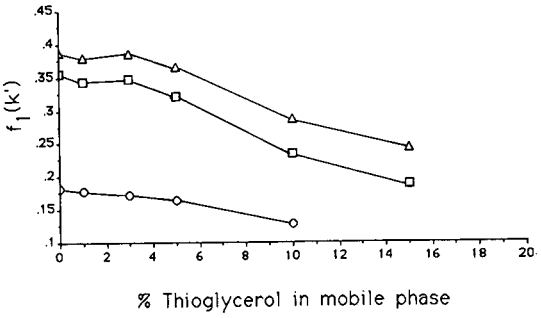

Fig. 7. Effect of concentration of thioglycerol in the mobile phase on $f_1(k')$. □ = Met-enkephalin; △ = leu-enkephalin; ○ = *p*-hydrobenzoic acid.

discussion of the relative contributions of both $f_1(k')$ and D_m to the mass transfer term in the Van Deemter equation. The variation in $f_1(k')$ with thioglycerol content is shown in Fig. 7 for met-enkephalin, leu-enkephalin and *p*-hydroxybenzoic acid. It can be observed that $f_1(k')$ decreases significantly for all compounds studied as the concentration of thioglycerol in the mobile phase is increased. This decrease in $f_1(k')$ should induce a decrease in the mass transfer term, but this is not observed experimentally (Fig. 6). This apparent discrepancy can easily be explained if it is assumed that D_m decreases with increase in thioglycerol content, therefore producing an opposite effect on the mass transfer term. This hypothesis can be verified by examination of Fig. 8, where the variations of $1/D_m$ and $f_1(k')/D_m$ with the thioglycerol content are shown. It is clearly seen that $1/D_m$ decreases as the thioglycerol content is increased and that the opposite variations of D_m and $f_1(k')$ result in a small increase in the mass

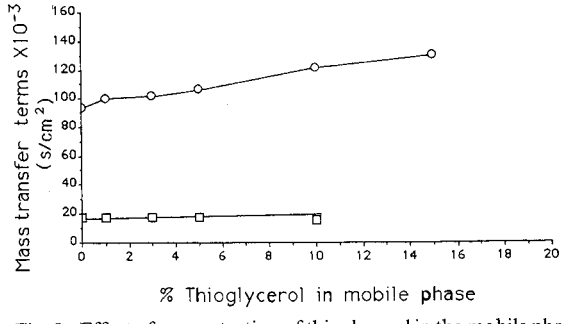

Fig. 8. Effect of concentration of thioglycerol in the mobile phase on the variation of (○) $1/D_m$ and (□) $f_1(k')/D_m$ for *p*-hydroxybenzoic acid.

transfer term with increase in the thioglycerol content. Therefore, the net effect of the presence of thioglycerol in the mobile phase is to reduce the efficiency of mass transfer in the system at higher thioglycerol contents or at higher linear velocities. However, the situation around the optimum linear velocity is different, because under these conditions the theoretical plate height becomes independent of the diffusion coefficient, as can be shown using the Van Deemter equation.

The conclusion that the theoretical plate height becomes independent of the diffusion coefficient D_m around the optimum linear velocity seems to be confirmed by the experimental data shown in Fig. 6, where only slight variations in H are observed near the optimum linear velocity. As the measured values of H represent the resultant contribution to broadening produced by the column and extra-column dead volume, the weak variation observed under optimum conditions can be attributed to the extra-column dead volume. This is confirmed by the data shown in Fig. 9, where the increase in broadening as measured by the variance of an unretained compound ($NaNO_3$) is seen to increase at higher thioglycerol concentrations. This effect will cause a vertical translation of the Van Deemter plots for high contents of thioglycerol, as can be observed by close examination of Fig. 6B. The finding that the chromatographic performance becomes independent of the thioglycerol content under optimized conditions implies that working at the optimum linear velocity will significantly increase the time of analysis. Higher linear velocities can be used to reduce the time of analysis with only a slight

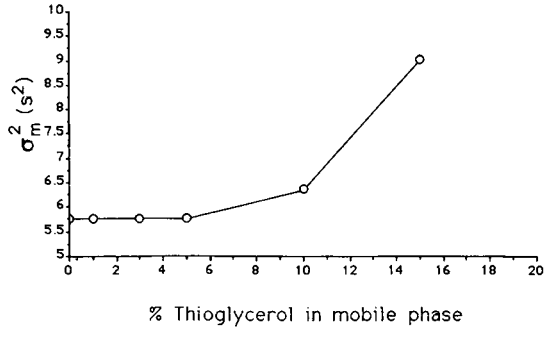

Fig. 9. Effect of concentration of thioglycerol in the mobile phase on the variance associated with the elution of an unretained compound.

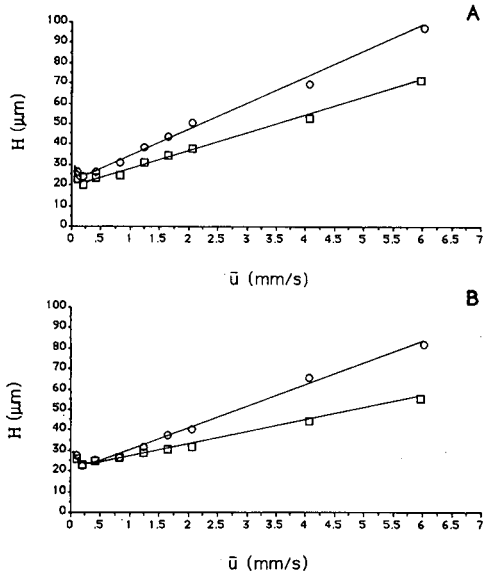

Fig. 10. Temperature dependence of Van Deemter plots for (A) met-enkephalin and (B) *p*-hydroxybenzoic acid at 10% thioglycerol in the mobile phase. ○ = 25°C; □ = 38.5°C.

deterioration in the chromatographic performance, but the results in this study indicate that this is possible only at thioglycerol concentrations below 3%. This is due to the fact that most chromatographic indicators are not significantly affected for thioglycerol contents up to that value. However, if the thioglycerol content is above 3%, the use of higher linear velocities will result in a severe deterioration of the chromatographic performance. The dependence of $f_1(k')$ on temperature and of D_m on both viscosity and temperature suggests that this parameter could possibly be used to nullify the adverse effect of high concentrations of thioglycerol in the mobile phase. In order to increase the chromatographic performance at elevated thioglycerol contents or high linear velocity, Van Deemter plots were generated at 38.5°C to verify the effect of temperature on the mass transfer term. The results are shown in Fig. 10, which compares the theoretical plate height (H) at 25 and 38.5°C for (A) met-enkephalin and (B) *p*-hydroxybenzoic acid in a mobile phase containing 10% of thioglycerol. As expected, the plot at 38.5°C indicates that the increase in temperature has the desired effect and allows the performance to be restored. The theoretical plate height measured at 38.5°C is similar to that

at 25°C with no thioglycerol present in the mobile phase. Hence higher linear velocities can be used with minor decreases in performance at high thioglycerol contents provided that the experiments are conducted at higher temperatures.

In order to obtain general guidelines for the precolumn addition of viscous matrices in LC–FAB-MS systems, it can be useful to compare the results obtained in the investigation of the effects of these matrices. Using the results of this study for thioglycerol and those from our previous work with glycerol [32,33], it becomes possible to compare the effects of both matrices on the chromatographic performance of LC–FAB-MS systems using precolumn addition and to identify similarities and differences in their behavior. For chromatographic indicators such as retention times, capacity factors, number of theoretical plates and resolution, the effect of the addition of a viscous matrix to the mobile phase is to reduce these parameters significantly at high contents of the matrix. Thioglycerol produces a more significant change in the capacity factors than glycerol for concentrations above 3%. For other chromatographic indicators such as normalized peak widths and impedance of separation, these parameters show an increase at higher contents of the matrix in the mobile phase, indicating that the viscous matrix increases broadening in the system and reduces the overall performance. For example, the presence of 15% of thioglycerol in the mobile phase doubles the separation impedance whereas 30% of glycerol is required to produce a similar effect. In terms of increasing the viscosity of the mobile phase, thioglycerol and glycerol are seen to have equivalent effects, as shown by the viscosity measurements given in Table I.

TABLE I

VARIATION OF THE VISCOSITY OF THE MOBILE PHASE WITH VISCOUS MATRIX CONTENT

Data taken from ref. 33.

Matrix content (%)	Viscosity (cP)	
	ACN–water–THIO–TFA (30:70 – *x*:*x*:0.05)	ACN–water–GLY–TFA (30:70 – *x*:*x*:0.1)
0	0.93	0.95
1	0.99	0.96
3	1.02	1.01
5	1.07	1.05
10	1.24	1.26
15	1.36	

The Van Deemter plots obtained for peptides, acidic compounds and phenols using three different mobile phases and two different matrices show typical characteristics that are believed to represent common trends: (i) all the systems studied seem to retain their chromatographic performance near optimum linear velocities (0.1–0.6 mm/s) with almost no dependence on the matrix concentration in the mobile phase in the range of concentrations studied (0–30%); (ii) the effect of the increase in the concentration of the viscous matrix systematically results in a decrease in the mass transfer efficiency in the chromatographic system for linear velocities greater than 1 mm/s; and (iii) an increase in the temperature of analysis significantly improves the efficiency of the system at high matrix contents and high linear velocities. These three characteristics imply that under the appropriate experimental conditions, it is possible to use a wide range of concentrations of the viscous matrix in the mobile phase while retaining the chromatographic efficiency, contrary to the general belief that high concentrations of the matrix will necessarily result in inadequate chromatographic performance. However, the increase in matrix content can induce broadening effects outside the chromatographic column, and effects mostly apparent in the interface (droplet) have been partly documented [17,33].

CONCLUSIONS

As previously observed for glycerol, the precolumn addition of thioglycerol as a viscous matrix in LC–FAB-MS systems results in alterations to the chromatographic process. This is confirmed by the observation that an increase in the thioglycerol content induces a decrease in the capacity factor, an increase in broadening, a decrease in resolution and a decrease in the chromatographic performance. At concentrations of thioglycerol in the mobile phase below 3%, these changes are minor. The effects of the presence of thioglycerol in the mobile phase on chromatographic performance are minimized, however, if the system is operated near its optimum conditions for average linear velocities. Under those

conditions, high concentrations of the viscous matrix can be used and the efficiency of the chromatographic system is retained. At high thioglycerol contents and high linear velocities, the detrimental effect of the added matrix is apparent but it can be reduced substantially by increasing the temperature of the system, which allows the analysis to be conducted in a reasonable time and at almost any concentrations of matrix in the mobile phase with essentially no decrease in chromatographic performance.

ACKNOWLEDGEMENTS

The authors acknowledge the financial contributions of the Natural Science and Engineering Research Council of Canada (NSERC), Hydro-Québec and Fonds FCAR, Government of Québec, which permitted this study.

REFERENCES

1 M. Barber, R. Bordoli, R. D. Sedgwick and N. J. Tyler, *J. Chem. Soc., Chem. Commun.*, (1981) 325.
2 J. L. Gower, *Biomed. Mass Spectrom.*, 12 (1985) 191.
3 W. D. Lehman, M. Kessler and W. A. Konig, *Biomed. Mass Spectrom.*, 11 (1984) 217.
4 G. M. Allmaier, *Rapid Commun. Mass Spectrom.*, 2 (1988) 74.
5 B. L. Bentz and P. J. Gale, *Int. J. Mass Spectrom. Ion Processes*, 878 (1987) 115.
6 J. Meili and J. Siebl, *Org. Mass Spectrom.*, 19 (1984) 581.
7 J. Visentini, J. Gauthier and M. J. Bertrand, *Rapid Commun. Mass Spectrom.*, 3 (1989) 390.
8 Y. Ito, T. Takeuchi, D. Ishii and M. Goto, *J. Chromatogr.*, 346 (1985) 161.
9 R. M. Caprioli, T. Fan and J. S. Cottrell, *Anal. Chem.*, 58 (1986) 2949.
10 M. J. Bertrand, V. Benham, R. St.-Louis and M. J. Evans, *Can. J. Chem.*, 67 (1989) 910.
11 M. J. Bertrand and V. Benham, in T. Theophanides (Editor), *Spectroscopy of Inorganic Bioactivators, Theory and Applications (NATO ASI Series)*, Kluwer, Dordrecht, 1989, pp. 349–377.
12 D. E. Games, S. Pleasance, E. D. Ramsay and M. A. McDowall, *Biomed. Environ. Mass Spectrom.*, 15 (1988) 179.
13 D. W. Hutchinson, A. R. Woolfitt and A. E. Ashcroft, *Org. Mass Spectrom.*, 22 (1987) 304.
14 A. E. Ashcroft, *Org. Mass Spectrom.*, 22 (1987) 734.
15 P. Boulenguer, Y. Leroy, J. M. Alonso, J. Montreuil, G. Ricard, C. Colbert, D. Duquet, C. Dewaele and B. Fournet, *Anal. Biochem.*, 168 (1988) 164.
16 S. Pleasance, P. Thibault, M. A. Moseley, L. J. Deterding, K. B. Tomer and J. W. Jorgenson, *J. Am. Soc. Mass Spectrom.*, 1 (1990) 321.
17 M. A. Moseley, L. J. Deterding, J. S. M. de Wit, K. B. Tomer, R. T. Kennedy, N. Bragg and J. W. Jorgenson, *Anal. Chem.*, 61 (1989) 1577.
18 D. B. Kassel, B. D. Musselman and J. A. Smith, *Anal. Chem.*, 63 (1991) 1091.
19 W. J. Henzel, J. H. Bourell and J. T. Stults, *Anal. Biochem.*, 187 (1990) 228.
20 L. J. Deterding, M. A. Mosely, K. B. Tomer and J. W. Jorgenson, *Anal. Chem.*, 61 (1989) 2504.
21 P. Dobberstein, E. Korte, G. Memerhoff and R. Pesch, *Int. Mass Spectrom. Ion Phys.*, 46 (1985) 185.
22 J. G. Stroh, J. C. Cook, R. M. Milberg, L. Brayton, T. Kihara, Z. Huang, K. L. Rinehart, Jr., and I. A. S. Lewis, *Anal. Chem.*, 57 (1985) 985.
23 P. S. Kokonen, W. M. A. Niessen, U. R. Tjaden and J. Van Der Greef, *Rapid Commun. Mass Spectrom.*, 5 (1991) 19.
24 A. Capiello, P. Palma, I. A. Papayannopoulos and K. Biemann, *Chromatographia*, 30 (1990) 477.
25 A. C. Barefoot, R. W. Reiser and S. A. Cousins, *J. Chromatogr.*, 474 (1989) 39.
26 S. A. Martin, C. E. Costello and K. Biemann, *Anal. Chem.*, 54 (1982) 2362.
27 T. Takeuchi, S. Watanabe, N. Kondo, D. Ishii and M. Goto, *J. Chromatogr.*, 435 (1988) 482.
28 K. Tomer and C. E. Parker, *J. Chromatogr.*, 492 (1989) 189.
29 P. Kokkonen, E. Schröder, W. M. A. Niessen, U. R. Tjaden and J. Van Der Greef, *J. Chromatogr.*, 54 (1990) 35.
30 R. M. Caprioli, in R. M. Caprioli (Editor), *Continuous Flow Fast Atom Bombarment Mass Spectrometry*, Wiley, Chichester, 1990, p. 1.
31 R. M. Caprioli, B. B. Dague and K. Wilson, *J. Chromatogr. Sci.*, 26 (1988) 640.
32 J. P. Gagné, A. Carrier and M. J. Bertrand, *J. Chromatogr.*, 554 (1991) 61.
33 J. P. Gagné, A. Carrier and M. J. Bertrand, *J. Chromatogr.*, 554 (1991) 47.
34 J. P. Gagné, A. Carrier and M. J. Bertrand, in *Proceedings of the 39th ASMS Annual Conference on Mass Spectrometry and Allied Topics, Nashville, TN, May 24–28, 1991*, ASMS, East Lansing, MI, p. 372.
35 U. Justesen and G. Bojesen, *J. Chromatogr.*, 562 (1991) 59.
36 L. Shampine, D. B. Kassel and R. J. Andereg, in *Proceedings of the 39th ASMS Annual Conference on Mass Spectrometry and Allied Topics, Nashville, TN, May 24–28, 1991*, ASMS, East Lansing, MI, p. 777.
37 P. A. Bristow and J. H. Knox, *Chromatographia*, 10 (1977) 279.
38 J. J. van Deemter, F. J. Zuiderweg and A. Klinkenberg, *Chem. Eng. Sci.*, 5 (1956) 271.
39 J. A. Jonsson, in J. A. Jonsson (Editor), *Chromatographic Theory and Basic Principle*, Marcel Dekker, New York, 1987, p. 27.
40 E. D. Katz, K. L. Ogan and R. P. W. Scott, *J. Chromatogr.*, 270 (1983) 51.
41 C. Gluckman, A. Hirose, V. L. McGiffin and M. Novotny, *Chromatographia*, 17 (1983) 303.
42 C. R. Wilke and P. Chang, *AIChE J.*, 1 (1955) 264.

Journal of Chromatography, 591 (1992) 139–148
Elsevier Science Publishers B.V., Amsterdam

CHROM. 23 794

Interfacing gradient elution ion-exchange chromatography and low-angle laser light-scattering photometry for analysis of proteins

Rohin M. Mhatre and Ira S. Krull*

Department of Chemistry and Barnett Institute (341MU), Northeastern University, 360 Huntington Avenue, Boston, MA 02115 (USA)

(First received July 10th, 1991; revised manuscript received October 8th, 1991)

ABSTRACT

Molecular weights (MWs) of different proteins were determined by interfacing gradient elution ion-exchange chromatography and low-angle laser light-scattering photometry (IEC–LALLS). A high-performance strong cation-exchange column was used to elute proteins using fast (5 min) and conventional (15–30 min) gradients. The eluted proteins were characterized on-line by determining their MWs using LALLS. The specific refractive index (RI) increment (dn/dc) and the RI of the solvent used over the gradient range were determined off-line and used to calculate the absolute weight-average MWs. Four proteins, ribonuclease A, α-chymotrypsinogen A, trypsinogen and β-lactoglobulin A (β-LACT) were studied. Accurate MWs were obtained for all the proteins using fast and conventional gradients, except for β-LACT, which aggregated as a function of the gradient employed. The degree of aggregation of β-LACT increased as the rapidity of the gradient was increased over a fixed gradient range. This study indicated that it is possible to separate and characterize proteins rapidly using IEC–LALLS.

INTRODUCTION

The separation of biopolymers, especially proteins, has gained significant advantage in the past decade or so [1–6]. The development of high-performance liquid chromatography (HPLC) for biopolymers has been due to the development of supports specially designed for biopolymer separation, and understanding the chromatographic behavior of different biopolymers. In spite of the advances in column chemistry, no great importance has been given to characterizing or identifying proteins separated by HPLC. Most of the detection approaches, such as UV, fluorescence and refractive index, provide insufficient information for characterizing biopolymers. Mass spectrometry is the only detection technique that has been able to provide qualitative information in terms of molecular weight (MW), but it is not currently practical for the routine MW determination of high-MW biopolymers.

We have been interested in interfacing low-angle laser light-scattering photometry (LALLS) for on-line detection for HPLC to characterize proteins by determining their absolute MW [7–11]. LALLS had been used for this purpose in the past few years, but only under isocratic conditions, and mainly for size-exclusion chromatography (SEC) [12–16]. Over the past few years, we have succesfully interfaced gradient reversed-phase (RP) and hydrophobic interaction chromatography (HIC) with LALLS. This encouraged us to look at interfacing gradient elution ion-exchange chromatography (IEC).

High-performance IEC has not been used as extensively as RP chromatography or SEC for the separation of proteins. However, as the mass recovery is very high and the biological activity of the protein is maintained in IEC, it has become an important tool for the biotechnology industry. Many research groups have, over the past few years, developed various high-efficiency IEC columns and

0021-9673/92/$05.00

have also concentrated on understanding the retention mechanisms in IEC [17–21]. Fast IEC separations of proteins have been accomplished using non-porous packings [22,23]. Recently, Lloyd and Warner [24] demonstrated the use of wide-pore polymer matrix columns, which have been able to separate proteins very rapidly with high resolution. The columns have also been shown to have a higher loading capacity and rigidity than non-porous columns. The introduction of rigid polymer-based columns has allowed the use of high flow-rates and steep gradients for rapid separations of proteins.

In this paper, we demonstrate the coupling of a wide-pore, polymer-based, strong cation-exchange column for on-line LALLS–UV detection. Our previous attempts at interfacing RP-chromatography and LALLS had indicated that aggregates of proteins were formed on-column as a function of the rapidity of the gradient employed for elution. We have tried to investigate whether similar aggregates would be formed under rapid IEC elution conditions. Detailed discussions of the equations and theory of LALLS can be found elsewhere [8,25–28].

EXPERIMENTAL

Apparatus

The HPLC–LALLS–UV system was obtained from LDC Analytical (Riviera Beach, FL, USA), and consisted of a Model CM4000 ternary gradient pump, a Model SM4000 variable-wavelength UV detector and a Model KMX-6 LALLS detector. The injector was a Rheodyne (Cotati, CA, USA) Model 7125 syringe-loading type, fitted with a 20-μl loop. The ion-exchange column was a 10-μm HP-SCX strong cation-exchange column (100 × 7.8 mm I.D.) (Interaction Chemicals, CA, USA).

Three different instrumental set-ups used in this work were an IEC–HPLC system with LALLS–UV detection, an SEC system with LALLS–UV detection and a flow-injection analysis (FIA) system connected to a LALLS detctor.

System I, used for the gradient IEC–HPLC, consisted of a CM4000 gradient system, KMX-6 LALLS detector and an SM4000 UV detector, in series. The detector signals were collected on a Soltec (Sun Valley, CA, USA) Model 1242 strip-chart recorder and an IBM compatible computer using PCLALLS data collection and processing software from LDC Analytical.

System II, used for SEC studies, consisted of an LDC ConstaMetric III metering pump and an injector fitted with a 100-μl injection loop, a TSKgel G4000 SW column (30 cm × 8 mm I.D.) (Phenomenex, Ranchos Palos Verdes, CA, U.S.A.) and an LDC SpectroMonitor-D variable wavelength UV–VIS detector. The remaining experimental set-up was similar to system I.

System III, used for FIA, consisted of a 2-ml injection loop and 1/8-in. narrow-bore tubing of 12 in. length connected between the injector and the LALLS instrument. The LALLS output was collected on a Soltec recorder.

Refractive index (RI) increment (dn/dc) measurements were made in an off-line mode using a KMX-16 633-nm laser-based differential refractometer. RIs of the mobile phases were measured using a Bausch and Lomb (Rochester, NY, USA) Model 3L Abbé refractometer with a 632.8-nm narrow bandpass filter (Melles Griot, Rochester, NY, USA).

Mobile phases

Three mobile phases were used. The first was 5 m*M* Bis-Tris, (pH 5.8) (A) and 5 m*M* Bis-Tris + 0.5 *M* NaCl (pH 5.8) (B). This mobile phase was used to elute α-chymotrypsinogen A (CHY), trypsinogen (TRP) and ribonuclease A (RNase). The second was 10 m*M* sodium phosphate (monobasic) (pH 4.0) (A) and 10 m*M* sodium phosphate (monobasic) + 0.5 *M* NaCl (pH 4.0) (B), and was used to elute β-lactoglobulin (β-LACT). The third was a modified protein buffer (MPB) and was prepared as described [9]. All mobile phases were filtered through a 0.2-μm filter (Millipore, Bedford, MA, USA) and degased before use. The column was equilibrated with mobile phase A (protein dependent) overnight at a flow-rate of 0.2 ml/min.

Chemicals and supplies

HPLC-grade water was purchased from EM Science (Gibbstown, NJ, USA) and Bis-Tris, dibasic sodium phosphate and sodium chloride from Aldrich (Milwaukee, WI, USA). All protein standards were purchased from Sigma (St. Louis, MO, USA). Proteins were used as received.

Procedures

IEC–LALLS–UV studies. Fresh mobiles phases were prepared for each study. Protein standards in

the concentration range 8–10 mg/ml were prepared in 5 m*M* Bis-Tris, except β-LACT, which was prepared in 10 m*M* monobasic sodium phosphate, and refrigerated for about 1 h prior to use. Samples were kept refrigerated between each injection. The mobile phase flow-rate used throughout was 1 ml/min. The UV detector was set at 280 nm and 0.2 a.u.f.s. To study the effect of gradient times (over a fixed gradient range) on MWs of proteins, three gradients of 5, 10, and 15 min were run. Gradient ranges for the elution of individual proteins were as follows: TRP was eluted using a gradient from 5 to 75% B, α-CHY was eluted using a gradient from 15 to 100% B, RNase was eluted using a gradient from 0 to 100% B and a gradient from 0 to 80% B was used for β-LACT.

FIA–LALLS. FIA–LALLS studies were done using protein concentrations in the range 0.25–5.0 mg/ml. Proteins were dissolved in mobile phase A, which was also the mobile phase used for elution. The plots generated from the FIA–LALLS studies were used to calculate the second virial coefficient (A_2), which was eventually used to calculate the MW by IEC–LALLS.

SEC–LALLS–UV studies. System II described under *Apparatus* was used for this study. Protein concentrations ranging from 5 to 10 mg/ml prepared in buffer A were injected. Buffer A was also the mobile phase. Proteins were eluted at a flow-rate of 0.7 ml/min. LALLS and UV peak areas were integrated for calculating the MW of individual proteins [8,25–28].

Calculation of refractive index (RI), specific refractive index increment (dn/dc) and percentage recovery. RI of the mobile phase was measured over the entire gradient range (0–100% B) using an Abbé refractometer. The RI was measured to determine changes in RI over the gradient range used for elution of proteins. For gradient elution to be coupled successfully with LALLS, the two solvents (A and B) have to be "isorefractive"; solvents are considered to be isorefractive if the difference in their RI is $\leqslant 0.025$ units [27]. The differences in the RI of the two buffers was found to be 0.0045, which is much below the limit for isorefractivity. To measure the RI, different concentrations of B and A were prepared with that of B increasing by 10% over the 0–100% B range. The solutions were prepared in volumes of 10 ml. RI measurements were made by following standard operating procedures outlined in the operator's manual.

The d*n*/d*c* measurements were made using a KMX-16 differential laser-based (633-nm) refractometer. The refractometer was connected to a water-bath to maintain a cell temperature of 25°C. Protein solutions were prepared in buffer A and the concentrations ranged from 1 to 5 mg/ml. In previous studies we had determined d*n*/d*c* values at the point of elution of the protein [7,9]. In this particular study, as the *RI*s of the solvents were very close, d*n*/d*c* measurements were determined in buffer A. This assumption was based on calculation of d*n*/d*c* values at the point for β-LACT, which was about 30% B. The d*n*/d*c* values calculated by dissolving the protein in 30% B matched very well those using 100% A. Also, as most of the proteins analyzed seemed to elute at about or below 30–35% B buffer composition, it was safe to assume that the d*n*/d*c* values calculated in buffer A were accurate. Protein solutions were prepared and refrigerated for about 1 h prior to use. The solutions were then placed in the refractometer cell and 6–8 readings were determined for each solution; d*n*/d*c* values were calculated for 4–5 different concentrations of the protein.

The molar absorptivity of β-LACT was calculated on-line by FIA, using a B concentration at the point of elution in IEC, and was used to determine the percentage recovery as described in detail previously [10].

RESULTS AND DISCUSSION

The purpose of this study was primarily to determine the compatibility of interfacing gradient IEC with LALLS. To the best of our knowledge, there are no published reports on interfacing gradient IEC with on-line LALLS detection for determining the MWs of proteins. In our previous attempts, we were successful at interfacing gradient RP chromatography with LALLS for determining MWs on-line [9]. However, we noticed that all the proteins studied seemed to aggregate as a function of the gradient time over a fixed gradient range. At gradient times below 15 min, higher MWs were obtained, indicating the formation of aggregates. When longer gradient times were used (>15 min), the MWs obtained matched literatures values.

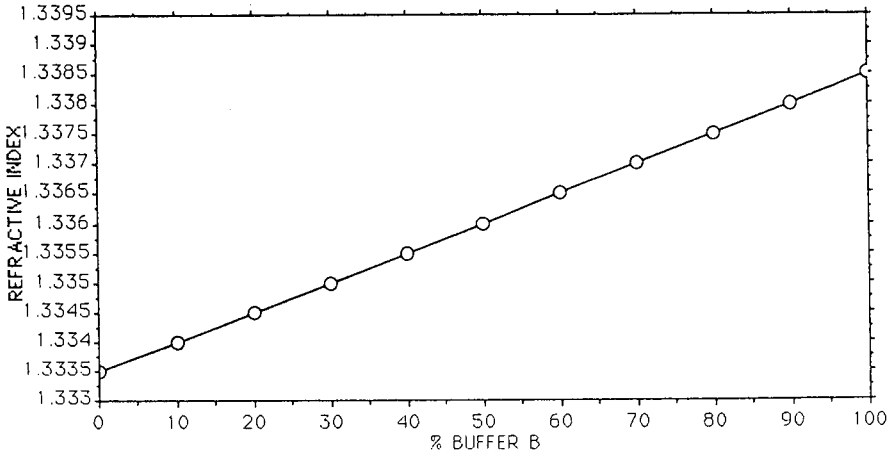

Fig. 1. Plot of refractive index *versus* percentage of buffer B. Mobile phase: (A) 5 m*M* Bis-Tris; (B) A + 0.5 *M* sodium chloride (pH 5.8).

Those results had indicated that RP separations using conventional means of detection may have led to the formation of higher MW species of proteins. However, this could not be determined as the precise nature of the eluting species was not known.

Based on the above results, we tried to study the effects of changes in gradient times in ion-exchange chromatography on the MWs of some commercially available proteins. In most of these studies, the gradient times used were 5, 10 and 15 min over a fixed gradient range. We report several studies done to determine the MWs of proteins, including (1) n and dn/dc calculations; (2) IEC–LALLS–UV for four commercially available proteins with MWs obtained at different gradient times; (3) SEC–LALLS–UV studies using MPB and phosphate buffer to calculate the MW of β-LACT; and (4) FIA–LALLS–UV studies to calculate A_2.

n and dn/dc determinations

Fig. 1 shows a plot of the change in RI over the gradient range 0–100% B (5 m*M* Bis-Tris + 0.5 *M* NaCl). The change in RI was minimal (0.0045), which satisfied the condition of isorefractivity. The change in RI for the buffer system used to separate β-LACT was also well below the isorefractivity limit of 0.025. These results indicated that gradient IEC could be interfaced with LALLS without any further corrections for RI changes.

Table I is a list of the calculated dn/dc values for the different proteins. As seen, all the dn/dc values fell between 0.16 and 0.17. These values were typical of what we have determined for various proteins in related studies [7–11].

IEC–LALLS–UV analysis of proteins

The purpose of this study was to determine if the rapidity of the gradient caused any alterations in the biopolymer, such as the formation of aggregates, as observed with RP gradients. RNase aggregated as a function of the rapidity of the gradient (percentage change in B per minute) when eluted using RP-HPLC–LALLS [9]. Mixtures of aggregates were obtained for RNase when a 10-min RP gradient was used, and the degree of aggregation

TABLE I

dn/dc VALUES OF DIFFERENT PROTEINS

Relative standard deviations (%) (n = 3) are given in parentheses.

Protein	dn/dc[a]
Trypsinogen	0.171 (1.75)
α-Chymotrypsinogen A	0.168 (0.8)
Ribonuclease A	0.162 (0.6)
β-Lactoglobulin A	0.166 (100% A) (1.3)
	0.164 (30% B–70% A) (0.7)

[a] dn/dc measurements were made in buffer A (5 m*M* Bis-Tris) for all proteins except β-LACT, where buffer A was 10 m*M* sodium phosphate (monobasic) and B was A + 0.5 *M* NaCl.

TABLE II

MOLECULAR WEIGHT DATA FOR PROTEINS OBTAINED BY IEC–LALLS

Mobile phase: A = 5 m*M* Bis-Tris, B = A + 0.5 *M* NaCl (pH 5.8). Column: HP-SCX, 10 μm, 100 × 7.8 mm I.D. Detection: UV at 280 nm, 0.2 a.u.f.s. LALLS: 0.2 mm field stop, 6–7° annuli, G_o = 400–425 mV [2–4]. Relative standard deviations (%) (n = 3) are given in parentheses.

Gradient time (min)	CHY	TRP	RNase
5	25 500 (4.7)	25 100 (4.2)	15 200 (1.3)
10	26 150 (2.7)	25 200 (6.0)	14 900 (3.5)
15	25 300 (6.3)	24 900 (4.0)	14 400 (1.9)
Theoretical MW	26 000	24 000	13 800

increased with a 5-min RP gradient. The first IEC results that were obtained for gradient times of 5–15 min are shown in Table II. As seen from the results, the MW for CHY, TRP and RNase agreed well with literature values of monomer MWs. This suggested that some proteins could be eluted under fast gradient conditions without aggregate formation. These results seemed very encouraging, and indicated that fast IEC separations were compatible with LALLS. Figs. 2, 3 and 4 illustrate the LALLS and UV results for TRP, CHY and RNAse, respectively. At least three injections were made to determine the relative standard deviations (R.S.D.) of the MWs. In general, there was excellent reproducibility and precision (low R.S.D.).

β-LACT was studied next. Previous reports indicated that β-LACT aggregated very easily, as a function of pH [29–32]. Based on the above, we studied β-LACT to investigate the effect of fast gra-

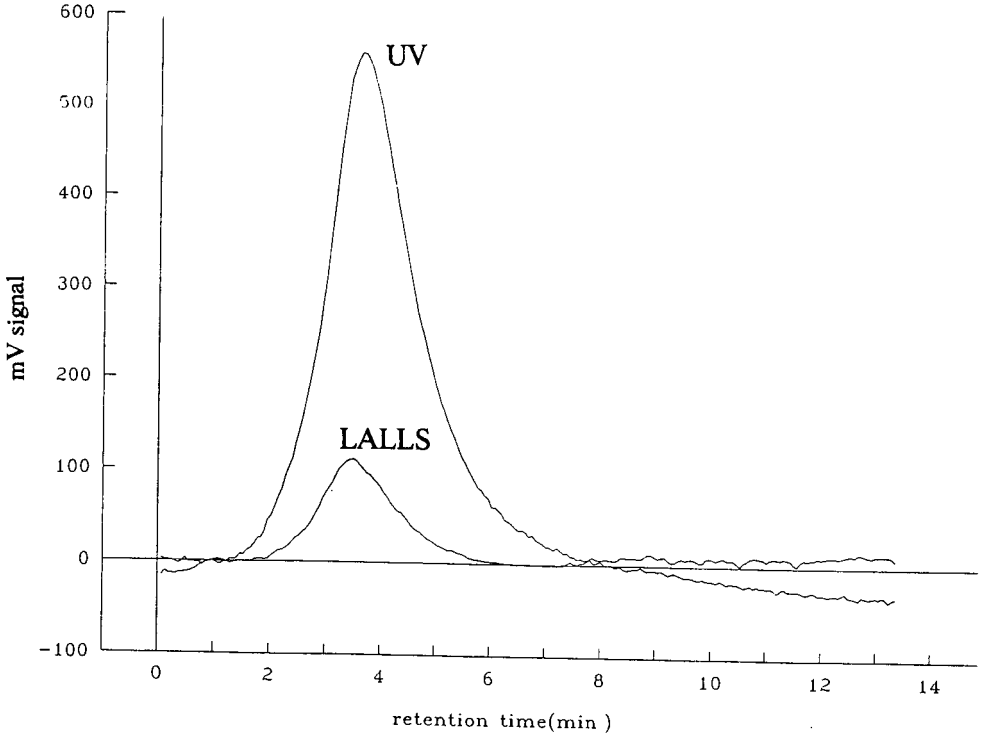

Fig. 2. LALLS–UV signals of trypsinogen 10-min gradient. Column, HP-SCX; mobile phase, (A) 5 m*M* Bis-Tris, (B) A + 0.5 *M* sodium chloride (pH 5.8), 15–75% B in 10 min at 1 ml/min; UV-detection, 280 nm, 0.2 a.u.f.s.; LALLS, 0.2 mm field stop, 6–7° annuli, G_o = 400 mV; concentration 10 mg/ml through a 20-μl loop.

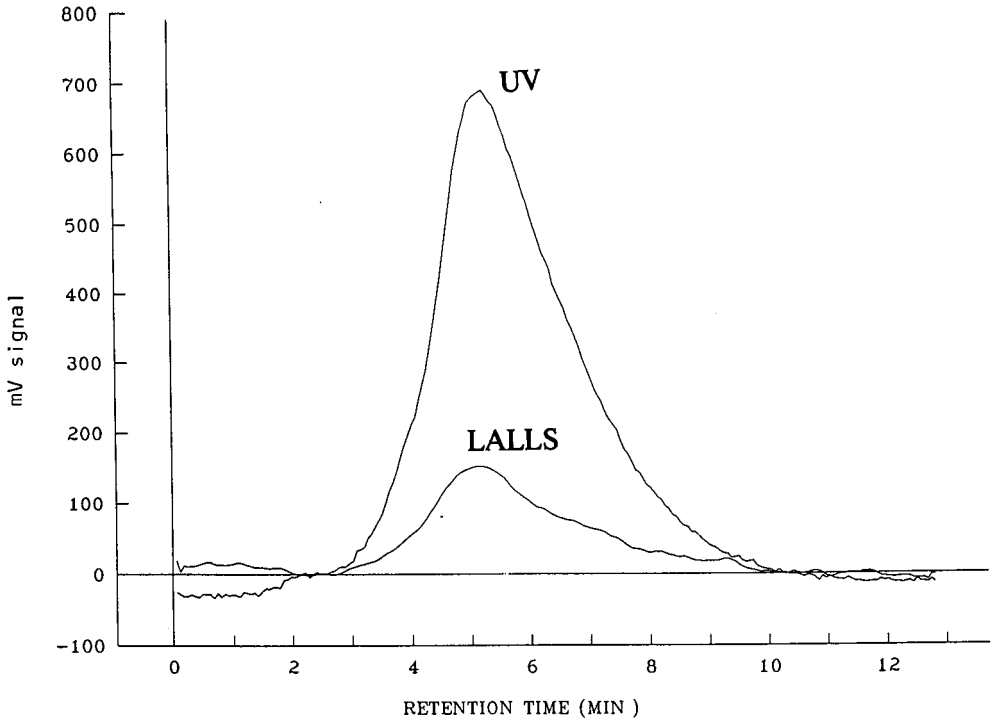

Fig. 3. LALLS–UV signals of α-chymotrypsinogen 5-min gradient. Conditions as in Fig. 2 except gradient 15–100% B in 5 min.

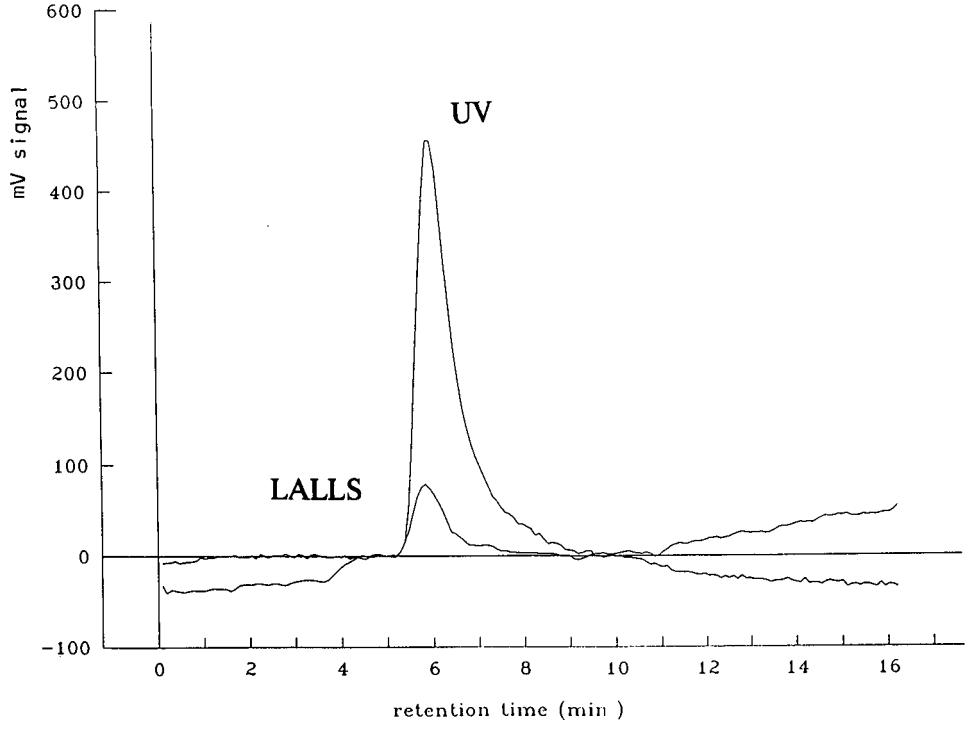

Fig. 4. LALLS–UV signals of ribonuclease A 15-min gradient. Conditions as in Fig. 2 except gradient 0–100% B in 15 min.

TABLE III

MW OF β-LACTOGLOBULIN A

Mobile phase: A = 10 m*M* NAH_2PO_4; B = A + 0.5 *M* NaCl. Gradient 0–80% B. Relative standard deviations in % (n = 3) are given in parentheses.

Gradient time (min)	MW
5	71 000 (5.1)
15	63 300 (2)
30	46 000 (2.1)
Theoretical MW	18 700

dients (5 min) on MW. Table III shows the MW of β-LACT obtained for the 30-, 15- and 5-min gradients. The MW increased from that obtained in the 30-min gradient (46 000 dalton) to the 15-min (63 000 dalton) and the 5-min gradients (71 000 dalton). This was the first protein studied that exhibited such behaviour. β-LACT was always present as a dimer or higher aggregate under the elution conditions. What remained to be determined was whether the protein was present as a dimer when supplied, aggregated in the injection solution, or aggregated on-column. The above results suggested that β-LACT was probably aggregating on-column, from a dimeric to higher aggregate states. Figs. 5 and 6 illustrate the LALLS and UV signals of β-LACT at 30 and 5 min, respectively. As seen, the LALLS and UV peaks were fairly symmetrical. In the RP studies, peaks for the 5-min gradients were unsymmetrical as mixed aggregates were formed and were partially resolved [9]. The symmetry of the LALLS peak indicated that mixed aggregates were probably not formed for the 5-min gradient. The MW from the 30-min gradient was slightly higher than that for a dimer, indicating that a dimer and some other aggregate form were present. The 5-min gradient indicated the formation of a tetramer. The MW from the 15-min gradient again indicated the formation of mixed aggregates which were not being separated owing to the low resolution of IEC.

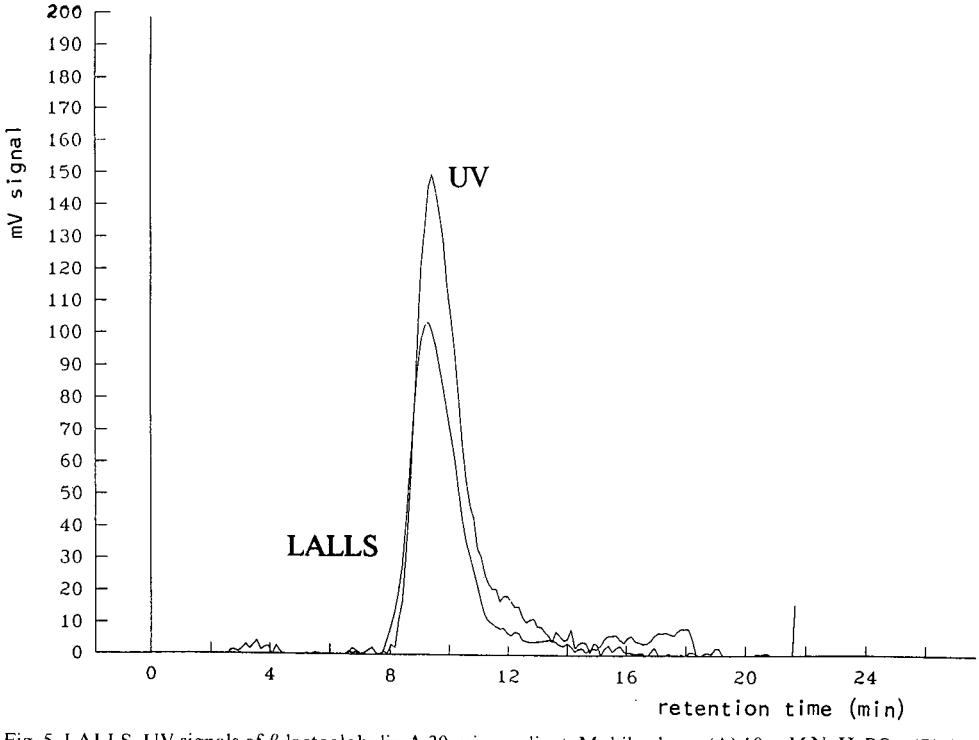

Fig. 5. LALLS–UV signals of β-lactoglobulin A 30-min gradient. Mobile phase, (A) 10 m*M* NaH_2PO_4, (B) A + 0.5 *M* sodium chloride (pH 4.0), 0–80% B in 30 min; other conditions as in Fig. 2.

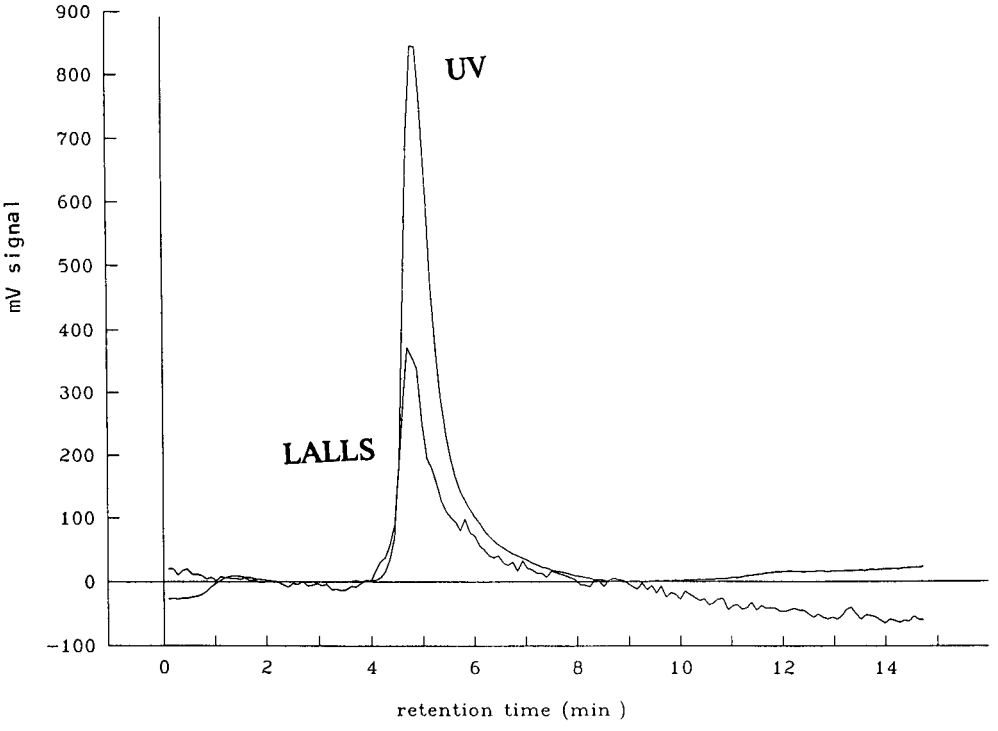

Fig. 6. LALLS–UV signals of β-lactoglobulin A 5-min gradient. Conditions as in Fig. 5 except gradient 0–80% B in 5 min.

The recoveries of β-LACT were above 95% for all the gradient times. This suggested that there was little loss of sample on-column. Also, the decrease in MW from the 5- to 30-min gradient time was due to a lower degree of aggregation with the latter gradient, and not to lower recovery of sample. Recoveries for the other proteins were assumed to be 100%. As the MWs for these proteins matched literature values, our assumptions were indeed correct. In a separate study, the recoveries for some other proteins eluted from a column similar to that used in this work were above 95% [33]. The increase in MW of β-LACT could not be an artifact of the system as none of the other proteins aggregated under any gradient conditions.

TABLE IV

SEC-LALLS OF β-LACTOGLOBULIN A

Column: TSK-GEL G4000SW. Flow-rate: 0.7 ml/min. Injection volume: 100 μl. Relative standard deviations (%) (n = 3) are given in parentheses.

Mobile phase	Concentration injected (mg/ml)	MW
MPB	4.2	19 200 (4.4)
10 mM Na_2HPO_4	10.68	37 900 (2.6)

TABLE V

MOLECULAR WEIGHTS DETERMINED BY FIA–LALLS

FIA conditions: 5 mM Bis-Tris at 0.2 ml/min; 2-ml injection loop, except for β-LACT, where 10 mM NaH_2PO_4 was used for elution. LALLS: 0.2 mm field stop, 6–7° annuli, G_o = 200 mV. Relative standard deviations (%) (n = 3) are given in parentheses.

Protein	MW	Literature value[a]
Trypsinogen	25 600 (3.5)	24 000
α-Chymotrypsinogen A	26 968 (1.6)	26 000
Ribonuclease A	15 000 (1.2)	13 800
β-Lactoglobulin A	37 700 (2.6)	18 700

[a] Taken from Sigma Chemical Co. catalog (1991).

SEC–LALLS–UV of β-LACT

SEC–LALLS studies were performed to determine whether β-LACT was present as an aggregate as received from the supplier and aggregated further on-column, or if it aggregated in the injection solution prior to injection. To determine the state of β-LACT in the sample, it was dissolved in a non-aggregating buffer, MPB. MPB has been reported not to aggregate proteins [7–11]. Table IV shows that the MW obtained using SEC–LALLS and MPB matched that of the monomer (19 200 dalton).

β-LACT was then dissolved in buffer A, the injection solvent, and eluted using the same solvent. The MW was 37 900 dalton (97% recovery). This was close to the MW obtained using the 30-min gradient. As *ca.* 10 mg/ml of β-LACT were used per injection, these results suggested that the protein was present as a dimer prior to injection and aggregated further on-column as a function of the gradient. Fig. 7 shows the LALLS–UV signals for a 10 mg/ml concentration of β-LACT.

FIA–LALLS

Table V shows the MWs of RNase, CHY, TRP and β-LACT obtained by FIA–LALLS. The MWs matched well with literature values, except for β-LACT (MW 37 700 dalton), which formed a dimer.

CONCLUSIONS

This study has helped us to understand further the significance of LALLS as a qualitative detection technique for biopolymer analysis. UV peaks that seem to be single/monomeric species may in fact be aggregates or mixtures of aggregates, as with β-LACT. It is possible to interface gradient elution IEC and LALLS for the rapid separation and characterization of biopolymers on-line. Of the four proteins studied, it was possible to interface very steep gradients (5-min 0–80% B) and deduce accurate MW information. β-LACT was the only protein studied that aggregated as a function of the gradient. We have also been able to interface suc-

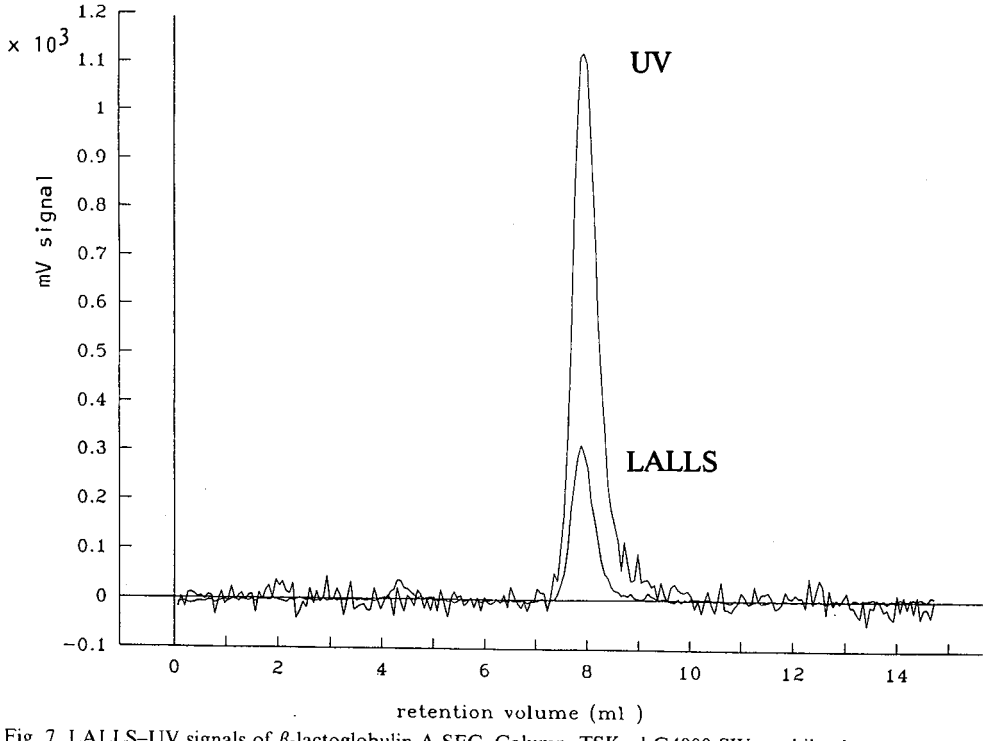

Fig. 7. LALLS–UV signals of β-lactoglobulin A SEC. Column, TSKgel G4000 SW; mobile phase, 10 m*M* NaH_2PO_4 at 0.7 ml/min; concentration, 10 mg/ml; LALLS conditions as in Fig. 2.

cessfully fast-gradient HIC with LALLS and the results will be published in the near future.

ACKNOWLEDGEMENTS

Gratitude is expressed to Laboratory Data Control (LDC) Analytical, Division of Thermo Instruments, (Riviera Beach, FL, USA), for their instrumentation donations, funding and technical support. This work would not have been possible without the continuing support of certain individuals within LDC, especially H. Kenny, B. Freeman, W. Mahn, M. Munk and B. Howe. We also acknowledge Interaction Chemicals, Division of E. Merck (D. Hometchko), for their donation of the ion-exchange column used. Additional funding for this work was provided, in part, by Merck Sharp & Dohme Research Laboratories (H. Perpall and M. Brooks), Pfizer (G. Forcier and K. Bratin) and the NIH-Biomedical Research Support Grant to NU, NO. RR07143 (DHHS) (S. Fine). Various individuals within Northeastern University have shown considerable interest in the work described, especially B. Karger, D. Magiera and A. Quazi. We appreciate their interest and continued encouragement. This is contribution No. 486 from the Barnett Institue at Northeastern University.

REFERENCES

1 M. T. W. Hearn, F. E. Regnier and C. T. Wehr (Editors), *High Performance Liquid Chromatography of Proteins and Peptides*, Academic Press, New York, 1983.
2 Cs. Horváth (Editor), *High Performance Liquid Chromatography: Advances and Perpectives*, Vols. 1–5, Academic Press, New York, 1981–1988.
3 O. Mikeš, *High Performance Liquid Chromatography of Biopolymers and Biooligomers, Part A: Principles, Materials and Techniques*, Elsevier, Amsterdam, 1988.
4 O. Mikeš, *High Performance Liquid Chromatography of Biopolymers and Biooligomers, Part B: Separation of Individual Compound Classes*, Elsevier, Amsterdam, 1988.
5 K. M. Gooding and F. E. Regnier (Editors), *HPLC of Biological Macromolecules*, Marcel Dekker, New York, 1990.
6 S. Yamamoto and R. Matsuno, *Ion-Exchange Chromatography of Proteins*, Vol. 43, Marcel Dekker, New York, 1988.
7 I. S. Krull, H. H. Stuting and S. C. Krzysko, *J. Chromatogr.*, 492 (1988) 29.
8 H. H. Stuting, I. S. Krull, R. Mhatre, S. C. Krzysko and H. G. Barth, *LC · GC*, 7 (1989) 402.
9 R. Mhatre, I. S. Krull and H. H. Stuting, *J. Chromatogr.*, 502 (1990) 21.
10 H. H. Stuting and I. S. Krull, *Anal. Chem.*, 62 (1990) 2107.
11 H. H. Stuting and I. S. Krull, *J. Chromatogr.*, 539 (1991) 91.
12 K. Kelichi, N. Taj and T. Toshio, *Biochim. Biophys. Acta*, 70 (1982) 19.
13 J. G. Bindels, N. B. Dewar and M. J. Hoerdes, *J. Chromatogr.*, 252 (1982) 523.
14 W. Flapper, P. J. M. Van der Oetelaar, C. P. M. Breed, J. Steenberg and H. J. Hoenders, *Clin. Chem.*, 32 (1986) 363.
15 S. Maezawa and T. Takagi, *J. Chromatogr.*, 280 (1983) 124.
16 T. Nakao, O. Fujitani and M. Nakao, *J. Biochem.*, 94 (1983) 689.
17 R. A. Barford, B. J. Sliwinski, H. L. Rothobart, *J. Chromatogr.*, 185 (1979) 393.
18 K. M. Gooding and M. N. Schmuck, *J. Chromatogr.*, 296 (1984) 321.
19 G. Vanecek and F. E. Regnier, *Anal. Biochem.*, 109 (1980) 345.
20 K. M. Gooding and M. N. Schmuck, *J. Chromatogr.*, 327 (1985) 139.
21 Z. E. Rassi and Cs. Horváth, *J. Chromatogr.*, 359 (1986) 255.
22 J. K. Duncan, A. J. C. Chen and C. J. Siebert, *J. Chromatogr.*, 397 (1987) 3.
23 Y. Kato, T. Kitamura, A. Mitsui and T. Hashimoto, *J. Chromatogr.*, 398 (1989) 327.
24 L. L. Lloyd and F. P. Warner, paper presented at the *40th Pittsburgh Conference of Analytical Chemistry and Applied Spectroscopy, Atlanta, GA, March 1989.*
25 M. Kerker, *The Scattering of Light and Other Electromagnetic Radiation*, Academic Press, New York, 1969.
26 P. Kratochvil, *Classical Light Scattering From Polymer Solutions*, Elsevier, Amsterdam, 1987.
27 H. Eisenberg, *Biological Macromolecules and Polyelectrolytes in Solutions*, Clarendon Press, Oxford, 1976.
28 J. Stepamen, P. Anzenbacher and B. Sedlacek (Editors), *Laser Light Scattering Spectroscopy of Biological Objects*, Elsevier, Amsterdam, 1987.
29 N. Grinberg, R. Blanco, D. M. Yarmush and B. L. Karger, *Anal. Chem.*, 61 (1989) 514.
30 R.Blanco, A. Arai, N. Grinberg, D. M. Yarmush and B. L. Karger, *J. Chromatogr.*, 482 (1989) 1.
31 S. N. Timasheff and R. Townend, *J. Am. Chem. Soc.*, 83 (1961) 464.
32 T. F. Kumosinki and S. N. Timasheff, J. Am. Chem. Soc., 88 (1960) 5635.
33 N. F. Nelson and N. Kitagawa, *J. Liq. Chromatogr.*, 20 (1990) 4037.

Journal of Chromatography, 591 (1992) 149–157
Elsevier Science Publishers B.V., Amsterdam

CHROM. 23 791

Comparison of ethoxylated alcohols and polyethylene glycols by high-performance liquid chromatography and supercritical fluid chromatography using evaporative light-scattering detection☆

S. Brossard, M. Lafosse* and M. Dreux

Laboratoire de Chimie Bioorganique et Analytique (LCBA), URA 499, Université d'Orléans, B.P. 6759, 45067 Orléans Cedex 2 (France)

(First received August 23rd, 1991; revised manuscript received October 4th, 1991)

ABSTRACT

Ethoxylated alcohols are surfactants whose oligomer distributions are conventionally determined by high-performance liquid chromatography. However, this method cannot resolve individual oligomers with a high degree of ethoxylation. Further, normal- and reversed-phase liquid chromatography cannot give the fingerprints for both the ethoxylated alcohols and polyethylene glycols, the synthetic residues without surfactant properties. Supercritical fluid chromatography coupled with evaporative light-scattering detection was developed for the analysis of these mixtures which do not contain chromophores.

INTRODUCTION

Commercial surfactant compounds [C_nH_{2n+1}-$(OCH_2CH_2)_xOH$] are complex mixtures because of the various numbers of ethylene oxide units declared by the manufacturer. They are synthesized by condensation of ethylene oxide units on a long chain alcohol ($C_nH_{2n+1}OH$) and, as a result, the oligomer index (x) varies over a considerable range [x = 2–40 ethylene oxide (EO) units for BC–X (see Experimental part)]. Further, when the starting alcohol is an isomeric mixture, the chromatographic fingerprint becomes more complex. Moreover, these surfactant mixtures can contain polyethylene glycols (PEGs), synthetic residues without surfactant properties. McClure [1] proposed a method using chemical derivatization to eliminate terminal hydroxyl groups from the surfactant mixtures. However, these groups undergo derivatization, thus altering the chromatographic properties. Zeman [2] used a back-flushing technique in order to elute PEGs. These compounds are strongly adsorbed on polar stationary phases. In addition to the difficulty of obtaining a good separation of individual ethylene oxides, detection is problematic. For non-UV-absorbing compounds, hydroxyl groups derivatized with 3,5-dinitrobenzoyl chloride allow, for example, UV detection [3,4], but, this involves a supplementary step in the analysis. With alkylphenol ethoxylated oligomers, Bear [5] and Ahel and Geiger [6] pointed out that the UV response depends on the number of ethylene oxide units, and this behaviour makes quantitative analysis difficult. Moreover, the differential refractometer is not adapted to the study of these mixtures because only an isocratic analysis is possible, which causes the peaks occuring near the end of the chromatogram to be deformed and too weak. Gradient elution is possible with flame ionization detection (FID) [1,7,8], but for very small amounts it is not sensitive enough for a proper analysis. For these reasons, the evaporative

☆ Poster presented at the *Congrès de Chromatographies en Phases Liquide et Supercritique, Paris, January 22–24, 1991.*

0021-9673/92/$05.00

light-scattering detection (ELSD) appeared to be the best choice for this type of study [9,10] because the instrumentation is universally available and the method is sensitive (20 ng) and compatible with gradient elution.

Supercritical fluid chromatography (SFC) with capillary columns has been used as a complementary technique in the analysis of PEGs because of its capacity for new selectivities, hence circumventing the limitations of high-performance liquid chromatography (HPLC). However, surfactants having high molecular weights were not resolved. Moreover, simultaneous analysis of the two families (ethoxylated alcohols and PEGs) was not mentioned, and the analysis times were long [11–13]. Giorgetti *et al.* [14] applied packed columns to analyses of surfactants containing chromophores. In SFC on packed columns it appeared necessary to add polar modifiers to the supercritical fluid to elute these compounds. This allows the neutralization of residual silanol groups on bonded silica. This is the reason why FID cannot be used for the non-UV-absorbing compounds. Thus ELSD seems to be a quasi-universal detection method for SFC on packed columns [15]. Hagen *et al.* [16] recently used ELSD with polymeric particles as stationary phase to resolve PEG 1000, but there was no mention of surfactant analyses.

The aim of this work was to show the superiority of SFC over HPLC and to illustrate the coupling of SFC and ELSD to resolve PEGs and surfactants. Thus we used HPLC and SFC to resolve the ethylene oxide oligomer distributions inside of each of these two families.

EXPERIMENTAL

Apparatus

In HPLC, a Bruker Model LC-31 ternary pump (Merck, Darmstadt, Germany) was coupled with a Sedex 45 evaporative light-scattering detector (Sedere, Vitry-sur-Seine, France).

The SFC apparatus was as follows. Carbon dioxide was pumped with a Waters (Milford, MA, USA) Model M 501 pump. An ethanol cooling bath was used to cool the pump head in order to increase the pump-down efficiency. A polar modifier was added using a Jasco (Tokyo, Japan) Model 2510 pump. The two solvents were mixed at a controlled temperature (Jasco 860-CO oven) in a dynamic mixing chamber (Knauer, Berlin, Germany). An injection valve was placed in the Jasco oven. A Sedex Model 45 evaporative light-scattering detector with the interface adjusted to SFC was used.

Chromatographic columns

Various stationary phases and columns were used: 5-μm LiChrospher Diol, 125 mm × 4 mm I.D. (Merck); 5-μm Hypersil C_{18}, 150 mm × 4.6 mm I.D. (Shandon, Runcorn, UK); 5-μm Nucleosil C_{18}, 150 mm × 4.6 mm I.D. (Macherey-Nagel, Düren, Germany); 5-μm PLRPS, 150 mm × 4.6 mm I.D. (Polymer Labs., Shropshire, UK); 5-μm Zorbax Sil, 150 mm × 4.6 mm I.D. (DuPont, Wilmington, DE, USA); 5-μm Zorbax Diol, 250 mm × 9.4 mm I.D. (DuPont); and 5-μm Ultrasphere Si, 250 mm × 4.6 mm I.D. (Beckman, Berkeley, CA, USA).

Chemicals and reagents

Carbon dioxide was of B 50 grade (Air Liquide, Paris, France), methanol of HPLC grade (Prolabo) and all other polar modifiers of analytical-reagent grade.

Brij 76, BC-10, BC-20, BC-30 and BC-40 [$C_{16}H_{33}(OCH_2CH_2)_xOH$] are complex industrial mixtures purchased from Nikko Chemicals (Tokyo, Japan). $C_{12}H_{25}(OCH_2CH_2)_9OH$ are industrial mixtures (Diversey, Ozoir la Ferrière, France). Ethylene glycol monohexadecyl ($C_{16}OE_1$), diethylene glycol monohexadecyl ($C_{16}OE_2$), tetraethylene glycol monohexadecyl ($C_{16}OE_4$), hexaethylene glycol monohexadecyl ($C_{16}OE_6$), hexaethylene glycol monodecyl ($C_{10}OE_6$), hexaethylene glycol monododecyl ($C_{12}OE_6$), hexaethylene glycol monotetradecyl ($C_{14}OE_6$) and hexaethylene glycol monooctadecyl ethers ($C_{18}OE_6$) and androsterone were purchased from Fluka (Buchs, Switzerland).

PEG 300, 400 and 1540 waxes were used as stationary phases in gas chromatography.

RESULTS AND DISCUSSION

High-performance liquid chromatography

Normal-phase HPLC is the technique mainly used for surfactant analyses because it furnishes rich fingerprints. Bonded silicas with groups such as diol and amino were used instead of bare silicas

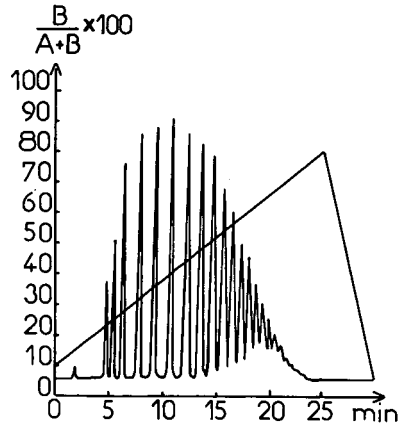

Fig. 1. Brij 76, $C_{18}H_{37}(OCH_2CH_2)_{10}OH$. Chromatographic conditions: column, LiChrospher 100 Diol (125 mm × 4 mm I.D.); mobile phase, linear gradient from 90% to 20% A in 25 min, A = hexane, B = chloroform–2-propanol (98:2); flow-rate, 1 ml min^{-1}; detection, ELSD.

because the activity of the latter depends on the amount of water in the mobile phase, making column equilibration time very long. *n*-Hexane–2-propanol–water mixtures are often used as mobile phases [3,4] because chloroform and dichloromethane cause a baseline drift in UV detection with gradient elution and a decrease in sensitivity. On the other hand, the use of *n*-hexane–dichloromethane–methanol mixtures with ELSD affords different polarities. Dichloromethane can be replaced with chloroform because of its larger donor character, and 2-propanol is easier to use than methanol for regulating retention times. Fig. 1 shows a very good separation of a surfactant mixtures having an octadecyl chain and an average of ten EO (according to the manufacturer). These oligomers without chromophores are detected by ELSD and the gradient elution does not cause baseline drift. In normal-phase elution, mixtures are separated according to the number of EO units (x). The retention of lower molecular weight oligomers increases with increasing number of repeat EO units (Table I). However, normal-phase HPLC has the following four major drawbacks: (1) for high-molecular-weight surfactants, the resolution of oligomers decreases with increase in the number of EO units (Fig. 1); (2) when there are over twenty EO units, these surfactant mixtures are completely adsorbed on a chromatographic support; these mixtures can be desorbed

TABLE I

RETENTION TIMES OF PURE ETHOXYLATED ALCOHOLS HAVING THE SAME ALKYL CHAIN LENGTH

Chromatographic conditions: column, LiChrospher 100 Diol (125 mm × 4 mm I.D.); mobile phase, linear gradient from 90% to 20% A in 25 min, A = hexane, B = chloroform–2-propanol (98:2); flow-rate, 1 ml min^{-1}; detection, ELSD.

Compound	Retention time (min)
$C_{16}H_{33}OE_1$	2.99
$C_{16}H_{33}OE_2$	4.51
$C_{16}H_{33}OE_4$	7.38
$C_{16}H_{33}OE_6$	10.65

with a considerable increase in the alcohol content in the mobile phase (methanol, ethanol, 2-propanol, etc.), but all species are eluted as a single peak without any resolution under such elution conditions; (3) the same chromatographic system is not able to resolve PEGs and ethoxylated alcohol mixtures; and (4) Table II shows that normal-phase chromatography cannot resolve alkyl chain homologues with common degrees of ethoxylation.

Consequently, studies [4] have been carried out in reversed-phase chromatography to obtain the simplest chromatographic fingerprint but showing different alkyl chain lenghts present in these polyethoxylated alcohol mixtures. Such systems allowed, first, the elution of PEGs, then surfactants according to their alkyl chain length in methanol–water without gradient elution (Fig. 2). The retention times of the second and third chromatographic peaks corresponded to those of the $C_{16}OE_6$ and

TABLE II

RETENTION TIMES OF PURE ETHOXYLATED ALCOHOLS HAVING THE SAME NUMBER OF EO UNITS

Chromatographic conditions as in Table I.

Compound	Retention time (min)
$C_{10}H_{21}OE_6$	10.99
$C_{12}H_{25}OE_6$	10.93
$C_{14}H_{29}OE_6$	10.71
$C_{16}H_{33}OE_6$	10.65
$C_{18}H_{37}OE_6$	10.47

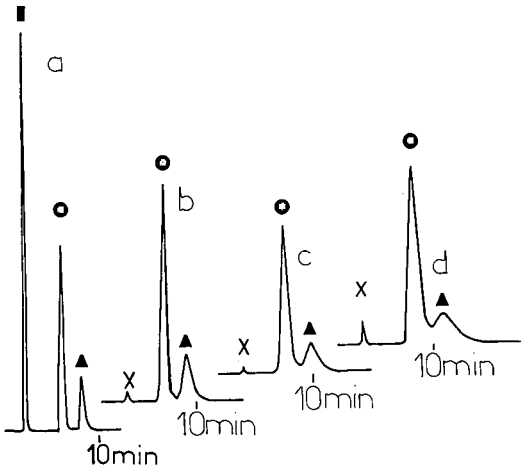

Fig. 2. (a) □ = PEG 300; ○,▲ = BC-7; ○ = BC7–C_{16}; ▲ = BC7–C_{18}. (b) × = Unknown; ○,▲ = BC-20; ○ = BC20–C_{16}; ▲ = BC20–C_{18}. (c) × = Unknown; ○,▲ = BC-30; ○ = BC30–C_{16}; ▲ = BC30–C_{18}. (d) × = Unknown ○,▲ = BC-40; ○ = BC40–C_{16}; ▲ = BC40–C_{18}. Chromatographic conditions: column, Nucleosil C_{18} (150 mm × 4.6 mm I.D.); mobile phase, methanol–water (19:1); flow-rate, 1 ml min^{-1}; pressure, 104 atm; detection, ELSD.

$C_{18}OE_6$ standards, respectively, indicating that the starting alcohol is a mixture. The reversed-phase system allows an easy separation according to the number of methylene units (Fig. 3). Moreover, several studies [17] showed, contrary to the normal-phase system, good resolutions of PEGs with the reversed-phase system but poor surfactant fingerprints (Fig. 4). The results were similar with many apolar adsorbents using alkyl, TMS, C_8 or C_{18}

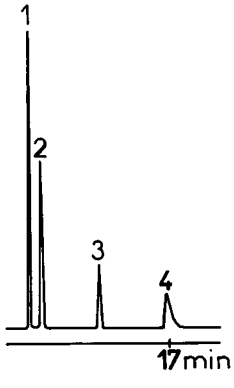

Fig. 3. 1 = PEG 300; 2 = $C_{10}OE_6$; 3 = $C_{14}OE_6$; 4 = $C_{18}OE_6$. Chromatographic conditions: column, Hypersil C_{18} (150 mm × 4.6 mm I.D.); mobile phase, methanol–water (9:1); flow-rate, 1 ml min^{-1}; pressure, 49 atm; detection, ELSD.

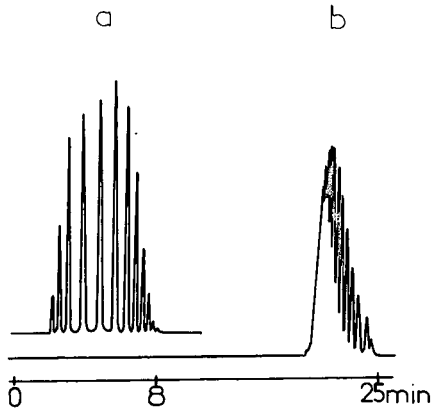

Fig. 4. Chromatograms of (a) PEG 400 and (b) $C_{12}H_{25}(OCH_2CH_2)_9OH$. Chromatographic conditions: column, PLRP-S (150 mm × 4.6 mm I.D.), mobile phase, linear gradient from 10% to 90% A in 30 min, A = acetonitrile, B = water; flow-rate, 1 ml min^{-1}; detection, ELSD.

types of bonded silicas or polymeric particles. The advantage of combined HPLC–ELSD, as shown in Fig. 2, is the possibility of performing a fast determination of each component. Indeed, Ahel and Giger [6] and Bear [5] pointed out the dependence between the polyethoxylated alkylphenol UV response and the number of EO units, whereas the PEGs cannot be detected. ELSD is universal in that all of these ethoxylated products have similar response factors, as shown in Fig. 5. When methanol–water mixtures are used as the eluent and solvent, linear calibration graphs, log (peak area) = f[log (concentration)] are parallel for PEGs and surfactants and also for androsterone, which is a different component used as a reference. The quantitative analysis of one family of mixtures can be achieved with a precision of less than 20% [18].

If the eluent and solvent are a dichloromethane–methanol mixture, a similar response for the same oligomer series can be observed, except for androsterone and PEG 300 (Fig. 6). Androsterone is a solid whereas PEG 300 is a liquid and the other families are waxy. When nebulization occurs, the particle size of drops may be affected by mobile phase characteristics such as density, viscosity, surface tension and velocity, thus explaining the differences in response curves observed. After evaporation of the organic solvent (dichloromethane–methanol) and just before detection, the microparticles probably return to an aspect close to their physical state,

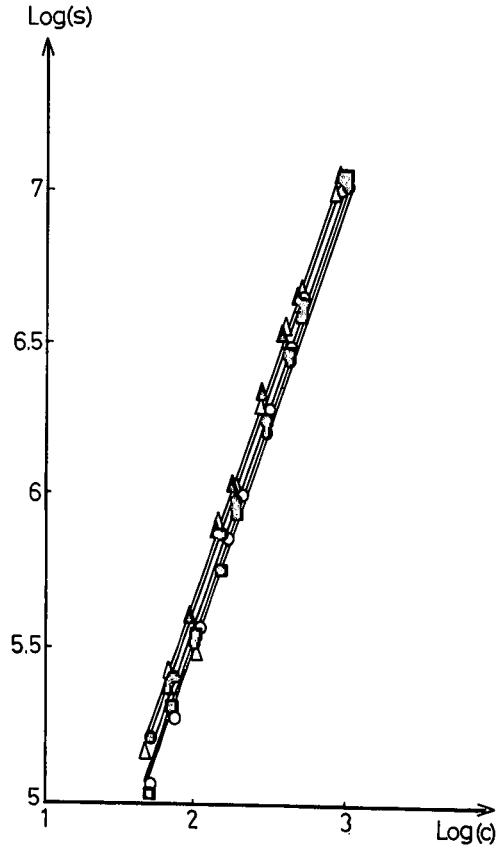

Fig. 5. Linear calibration graph log (peak area) *vs.* log (concentration). ● = BC-7; ▲ = BC-40; ■ = PEG 300; ○ = PEG 1540; △ = androsterone. Chromatographic conditions: column, LiChrospher 100 Diol (125 mm × 4 mm I.D.); mobile phase, methanol–water (4:1); flow rate, 1 ml min^{-1}; detection, ELSD.

which is not the case in an aqueous solution. Because liquid microparticles scatter less light than oily or solid particles, the androsterone response is greater than that of PEG 300.

In HPLC, we can conclude that in the normal-phase mode it is possible to obtain low-molecular-weight oligomer distributions, whereas surfactants with more than 10–15 EO units could not be resolved and PEG mixtures could not be eluted. In the reversed-phase mode, it was possible to evaluate PEGs and surfactants quantitatively, even those with high molecular weights. PEG mixtures were better resolved than in the normal-phase mode, although the surfactant fingerprints were poor (Table III). To obtain richer chromatograms, we therefore decided to investigate SFC with packed columns coupled with ELSD.

Supercritical fluid chromatography

Above 31°C and 73 bar, carbon dioxide has become a popular supercritical fluid because of its particular combining qualities with analytes and stationary phases. Other studies of PEGs [16] and non-ionic surfactants [19] have been done using apolar or slightly polar capillary columns with carbon dioxide as the mobile phase. These showed that surfactants and PEGs with low molecular weight can be resolved. However, the selectivity of the surfactant mixtures decreases with an increasing number of EO units, whereas PEG mixtures are totally adsorbed on the chromatographic support. In order to elute polar compounds, it is necessary to add

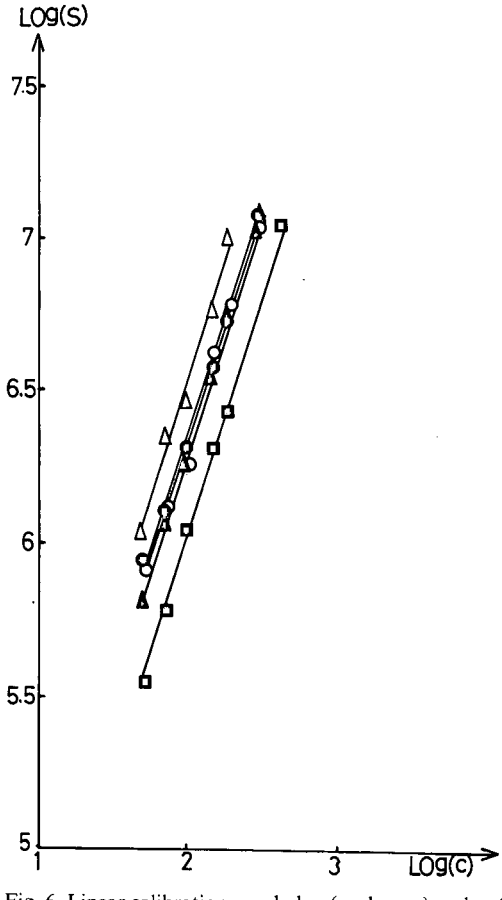

Fig. 6. Linear calibration graph, log (peak area) *vs.* log (concentration). ● = BC-7; ▲ = BC-40; ■ = PEG 300; ○ = PEG 1540; △ = androsterone. Chromatographic conditions: column, LiChrospher 100 Diol (125 mm × 4 mm I.D.); mobile phase, dichloromethane–methanol (9:1); flow-rate, 1 ml min^{-1}; detection, ELSD.

TABLE III

SUMMARY OF ANALYSES OF ETHOXYLATED ALCOHOLS AND PEGs BY HPLC

Mode	Compound	n	x	Separation	Little or no separation	No separation
Normal phase	$C_nH_{2n+1}(OCH_2CH_2)_xOH$	Constant	Variable	×		
	$C_nH_{2n+1}(OCH_2CH_2)_xOH$	Variable	Constant		×	
	$H(OCH_2CH_2)_xOH$		Variable			×
Reversed-phase	$C_nH_{2n+1}(OCH_2CH_2)_xOH$	Constant	Variable		×	
	$C_nH_{2n+1}(OCH_2CH_2)_xOH$	Variable	Constant	×		
	$H(OCH_2CH_2)_xOH$		Variable	×		

modifiers to the carbon dioxide, which is incompatible with the flame ionization detector.

Columns packed with octadecyl-bonded silicas were also investigated by Giorgetti *et al.* [14], and these studies showed excellent non-ionic surfactant separations, but no separations of highly ethoxylated surfactants and PEGs were obtained. To reduce the residual silanol groups on this type of apolar adsorbent, Hagen *et al.* [16] used columns of polymeric particles with carbon dioxide–methanol as the mobile phase. They observed excellent separations of PEG 1540 with baseline resolution, although no work was carried out on surfactant mixtures.

Following these results, we decided to carry out investigations by adopting the chromatographic system used in normal-phase HPLC in SFC. Carbon dioxide–methanol was used as the mobile phase instead of *n*-hexane–chloroform–2-propanol and bare or diol-bonded silicas were used as stationary phases. Modifiers were chosen according to their suitability for obtaining the best elution and resolution for both families of PEGs and surfactants. ELSD with SFC was shown to be compatible [12,14,15] using different modifiers as in the following examples.

On bare silicas under isocratic conditions with carbon dioxide–methanol, a very rich chromatographic fingerprint may be obtained for the surfactants (Fig. 7). However, the retention decreases if there is an increase in water content, causing split peaks in the chromatographic signal. The causes of this phenomenon are that two surfactant families have different alkyl chain lengths and that the starting alcohol was not pure. Under the same conditions, PEGs were well eluted when a small amount of water was added to the carbon dioxide–methanol eluent and also the chromatographic signal symmetry increased (Fig. 8). On the other hand, surfactants and PEGs with a high degree of ethoxylation could not be eluted. However, if a small amount of triethylamine is added to the polar modifier, high-molecular-weight polymers such as PEG 1540 (34 EO) may be eluted under isocratic conditions, but the resolution decreases with increasing amounts of triethylamine (Fig. 9). It is interesting to note the peak symmetry, never observed before in HPLC under these isocratic conditions, although the column equilibration times are very long. Moreover, amino adsorption on bare silica seems to be more or less irreversible, thus modifying the stationary phase surface. This polar modifier containing nitrogen is the only one which allows the elution of such high-molecular-weight PEGs. In comparison, diethylamine and pyridine clearly require longer analysis times. In an elution gradient with triethylamine, not only high-molecular-weight surfactants may be eluted but also two different alkyl chain lengths can be confirmed (Fig. 10). The baseline drift observed even without the chromatographic columns was not due to a non-homogeneous eluent mixture, because with on-line UV detection no baseline drift was observed. Nevertheless, increasing the additional gas at the SFC–ELSD interface level makes this phenomenon disappear. This prevents the effluents from the column recondensing at the opening of the nebulizer block, leaving the fused-silica capillary restrictor.

To find a simpler method of analysis, diol-bonded silicas with a supercritical fluid were used again. Using LiChrospher 100 Diol with isocratic elution, a carbon dioxide–methanol mixture offers a differ-

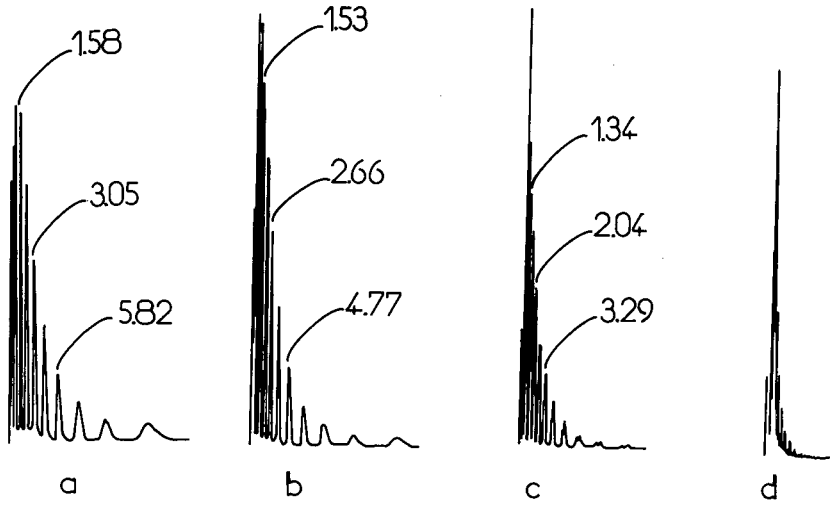

Fig. 7. BC-10: $C_{16}H_{33}(OCH_2CH_2)_{10}OH$. Chromatographic conditions: column, Zorbax Sil (150 mm × 4.6 mm I.D.); flow-rate, 4.2 ml min^{-1}; detection, ELSD. Retention times in minutes. (a) CO_2–CH_3OH (80:20, w/w), pressure 264 atm; (b) CO_2–CH_3OH–H_2O (80:19.5:0.5, w/w/w), pressure 268 atm; (c) CO_2–CH_3OH–H_2O (80:18.76:1.24, w/w/w), pressure 277 atm; (d) CO_2–CH_3OH–H_2O (80:17.56:2.44, w/w/w), pressure 277 atm.

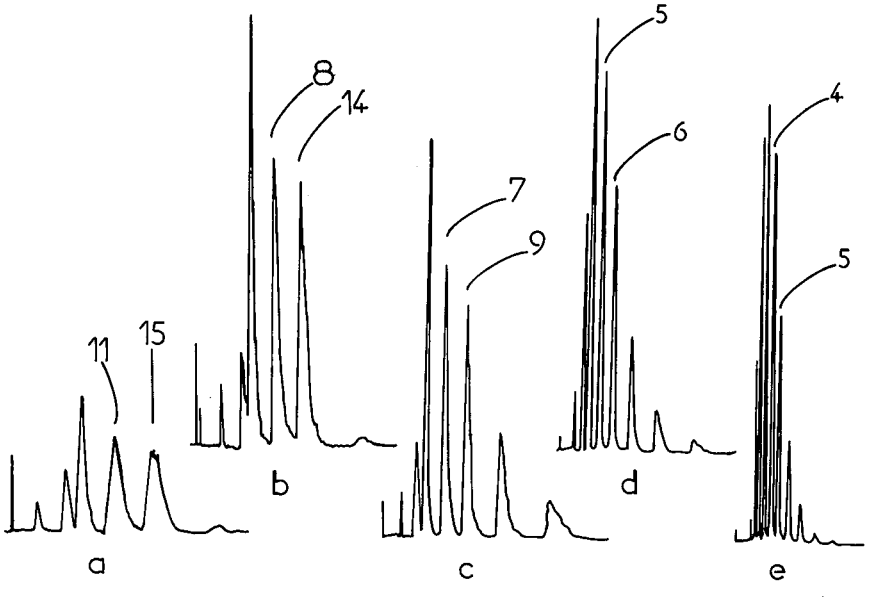

Fig. 8. PEG 400. Chromatographic conditions: column, Zorbax Sil (150 mm × 4.6 mm I.D.); flow-rate, 4.2 ml min^{-1}; detection, ELSD. Retention times in minutes. (a) CO_2–CH_3OH (80:20, w/w) pressure 264 atm. (b) CO_2–CH_3OH–H_2O (80:19.75:0.25, w/w/w), pressure 264 atm; (c) CO_2–CH_3OH–H_2O (80:19.5:0.5, w/w/w), pressure 268 atm; (d) CO_2–CH_3OH–H_2O (80:18.76:1.24, w/w/w), pressure 277 atm; (e) CO_2–CH_3OH–H_2O (80:17.56:2.44, w/w/w), pressure 274 atm.

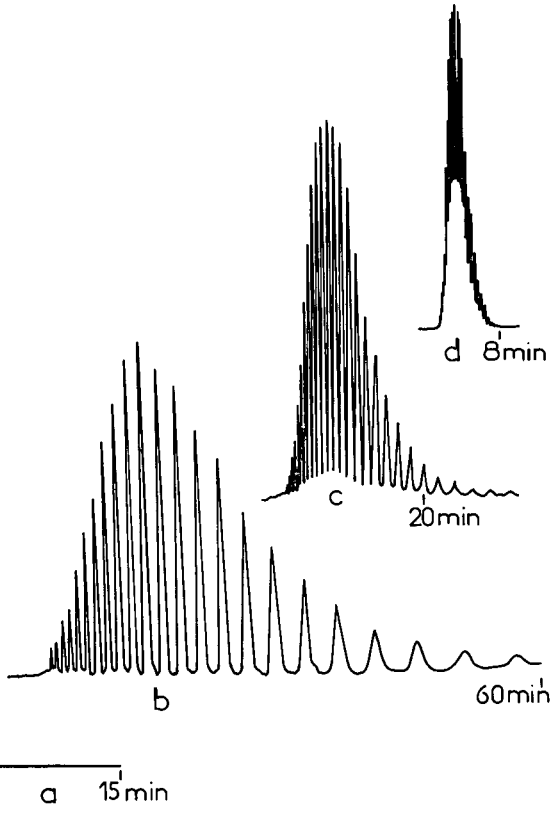

Fig. 9. PEG 1540. Chromatographic conditions: column, Ultrasphere Si (250 mm × 4.6 mm I.D.); flow-rate, 4.2 ml min^{-1}; detection, ELSD. (a) CO_2–CH_3OH–H_2O (80:18.77:1.23, w/w/w), pressure 272 atm; (b) CO_2–CH_3OH–H_2O–$(C_2H_5)_3N$ (80:18.68:1.23:0.09, w/w), pressure 272 atm; (c) CO_2–CH_3OH–H_2O–$(C_2H_5)_3N$ (80:18.60:1.22:0.18, w/w), pressure 288 atm; (d) CO_2–CH_3OH–H_2O–$(C_2H_5)_3N$ (80:18.43:1.21:0.36, w/w), pressure 280 atm.

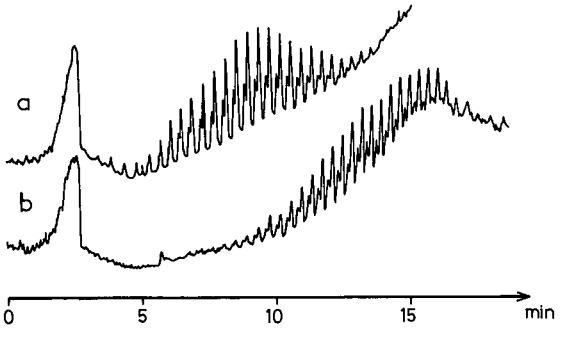

Fig. .10. (a) BC-20, $C_{16}H_{33}(OCH_2CH_2)_{20}OH$; (b) BC-30, $C_{16}H_{33}(OCH_2CH_2)_{30}OH$. Chromatographic conditions: column, Zorbax Sil (150 mm × 4.6 mm I.D.); linear gradient from CO_2–CH_3OH–H_2O–$(C_2H_5)_3N$ (94:5.55:0.4:0.05, w/w) to CO_2–CH_3OH–H_2O–$(C_2H_5)_3N$ (77.2:21.2:1.4:0.2, w/w) in 15 min; flow-rate, 3.46 ml min^{-1}; detection, ELSD.

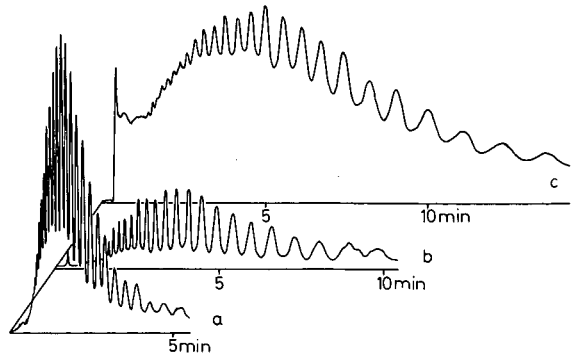

Fig. 11. (a) BC-20, $C_{16}H_{33}(OCH_2CH_2)_{20}OH$; (b) BC-30, $C_{16}H_{33}(OCH_2CH_2)_{30}OH$; (c) BC-40, $C_{16}H_{33}(OCH_2CH_2)_{40}OH$. Chromatographic conditions: column LiChrospher 100 Diol (125 mm × 4 mm I.D.). (a) CO_2–CH_3OH (87:13, w/w), flow-rate 3.88 ml min^{-1}; (b) CO_2–CH_3OH (93:7, w/w), flow-rate 3.88 ml min^{-1}; (c) CO_2–CH_3OH (87:13, w/w), flow-rate 3.88 ml min^{-1}. Detection, ELSD.

ent fingerprint of BC-20, -30 and -40 without peak splitting (Fig. 11). To increase the resolution of this type of separation, a 10-μm Zorbax Diol column (250 mm × 9.4 mm I.D.) was used because of its larger stationary phase volume. In this instance, with a small amount of water, the BC-10 fingerprint was even richer but the peak splitting already observed in Fig. 10 continued. This chromatographic system allows the simple elution of the corresponding PEG 300 and Fig. 12 shows that the two fingerprints are overlapped. It must be noted that triethy-

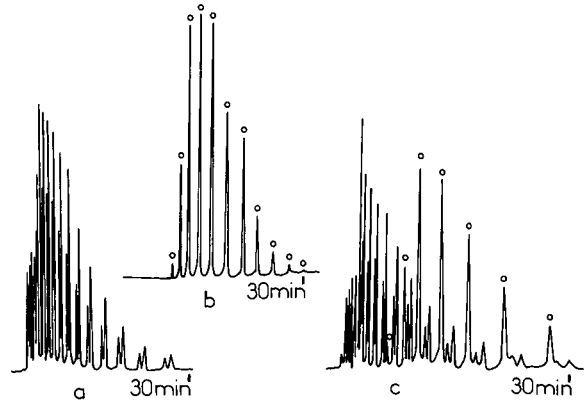

Fig. 12. (a) BC-10, $C_{16}H_{33}(OCH_2CH_2)_{10}OH$; (b) PEG 400; (c) BC-10 + PEG 400. Chromatographic conditions: column, Zorbax Diol (250 mm × 9.4 mm I.D.); mobile phase, CO_2–CH_3OH–H_2O (80:18.76:1.24, w/w/w); flow-rate, 4.2 ml min^{-1}; pressure, 243 atm; detection, ELSD.

lamine is not indispensable with this last bonded adsorbent.

CONCLUSIONS

In SFC, contrary to HPLC, it is possible to obtain richer polyethoxylated alcohol fingerprints and to elute high-molecular-weight polyethoxylated alcohols and PEGs. Both the surfactant and PEG mixtures can be clearly resolved, but the two distributions continue to be overlapped. This problem is currently being studied. Otherwise, SFC with ELSD appears to be well adapted for the analysis of these solutes.

ACKNOWLEDGEMENT

This thesis work (S. Brossard) was supported by a grant provided by Laboratoires Parfums Christian Dior, Saint-Jean-de-Braye, France.

REFERENCES

1 J. D. McClure, *J. Am. Oil Chem. Soc.*, 59 (1982) 364.
2 I. Zeman, *J. Chromatogr.*, 363 (1986) 223.
3 P. L. Desbene, V. Even, B. Desmazieres, J. J. Basselier and L. Minssieux, *Analusis*, 16 (1988) 44.
4 A. Nozawa and T. Ohnuma, *J. Chromatogr.*, 187 (1980) 261.
5 G. R. Bear, *J. Chromatogr.*, 459 (1988) 91.
6 M. Ahel and W. Giger, *Anal. Chem.*, 57 (1985) 2584.
7 R. J. Maxwell, E. H. Nungesser, W. N. Marmer and T. A. Foglia, *LC · GC Int.*, 1 (1987) 56.
8 E. H. McKerrel, presented at the *18th International Symposium on Chromatography, Amsterdam, September 23–28, 1990.*
9 M. Lafosse, M. Dreux, L. Morin-Allory and J. M. Colin, *J. High Resolut. Chromatogr. Chromatogr. Commun.*, 8 (1985) 39.
10 M. Lafosse, M. Dreux and L. Morin-Allory, *J. Chromatogr.*, 404 (1987) 95.
11 M. L. Lee, B. Xu, E. C. Huang, N. M. Djordjevic, H. C. K. Chang and K. E. Markides, *J. Microcol. Sep.*, 1 (1989) 1.
12 J. D. Pinkston, in K. Markides and M. Lee (Editors), *Symposium/Workshop on Supercritical Fluid Chromatography, Snow Bird, UT, June 13–15, 1989,* Brigham Young University Press, Snow Bird, UT, 1989, p. 279.
13 Y. Hirata, in K. Markides and M. Lee (Editors), *Symposium/Workshop on Supercritical Fluid Chromatography, Snow Bird, UT, June 13–15, 1989,* Brigham Young University Press, Snow Bird, UT, 1989, p. 302.
14 A. Giorgetti, N. Pericles, H. M. Widmer, K. Anton and P. Datwyler, *J. Chromatogr. Sci.*, 27 (1989) 318.
15 P. Carraud, D. Thiebaut, M. Caude, R. Rosset, M. Lafosse and M. Dreux, *J. Chromatogr. Sci.*, 25 (1987) 395.
16 H. M. Hagen, K. E. Landmark and T. Greibrokk, *J. Microcol. Sep.*, 3 (1991) 27.
17 M. Lafosse, unpublished results.
18 M. Lafosse, C. Elfakir, L. Morin-Allory and M. Dreux, *Anal. Chem.*, submitted for publication.
19 F. Hofler, in K. Markides and M. Lee (Editors), *Symposium/Workshop on Supercritical Fluid Chromatography, Snow Bird, UT, June 13–15, 1989,* Brigham Young University Press, Snow Bird, UT, 1989, p. 291.

Journal of Chromatography, 591 (1992) 159–164
Elsevier Science Publishers B.V., Amsterdam

CHROM. 23 770

3-Bromomethyl-7-methoxy-1,4-benzoxazin-2-one as a highly sensitive fluorescence derivatization reagent for carboxylic acids in high-performance liquid chromatography

Akio Nakanishi*, Hideo Naganuma, Junichi Kondo, Keiko Watanabe, Kimie Hirano, Takao Kawasaki and Yukinori Kawahara

Product Development Laboratories, Sankyo Co. Ltd., 2–58 Hiromachi 1-chome, Shinagawa-ku, Tokyo 140 (Japan)

(First received July 19th, 1991; revised manuscript received September 20th, 1991)

ABSTRACT

A fluorescence labelling reagent, 3-bromomethyl-7-methoxy-1,4-benzoxazin-2-one (BrMB), was synthesized from 2-amino-5-methoxyphenol and ethyl pyruvate by the Wislecenus reaction followed by bromination. Picomole to nanomole amounts of saturated aliphatic fatty acids were converted into the corresponding fluorogenic esters in the presence of anhydrous potassium carbonate and a crown ether as catalysts. BrMB derivatives of fatty acids were separated on a reversed-phase column and were sensitively detected fluorimetrically at 440 nm with excitation at 345 nm. Quantitative studies revealed that *n*-caproic acid was esterified completely under mild conditions and with sufficient reproducibility. The detection limit of the BrMB derivative of *n*-caproic acid was just below 2 fmol.

INTRODUCTION

Fatty acids are difficult to determine at low concentrations because of their weak UV absorption. High-performance liquid chromatography (HPLC) with fluorescence detection is useful for the determination of trace compounds. Therefore, many fluorogenic reagents have been developed for the determination of carboxylic acids by HPLC, *e.g.*, 4-bromomethyl-7-methoxycoumarin (BrMMC) [1,2], 1-bromoactylpyrene (BAP) [3], 4-bromomethyl-6,7-methylenedioxycoumarin (BrMDC) [4], 4-bromomethyl-6,7-dimethoxycoumarin (BrDMC) [5], 4-bromomethyl-6,7-dimethoxy-1-methyl-2-(1*H*)-quinoxalinone (BrMQ) [6], 9-anthryldiazomethane (ADAM) [7] and others [8–13]. Of these reagents, BrMMC has been widely applied in HPLC assays, but it is poorly soluble in reaction media such as acetonitrile and ethyl acetate used to obtain acyl derivatives, and further the fluorescence intensity of MMC derivatives of carboxylic acids was affected by the solvent composition.

This paper describes the preparation of 3-bromomethyl-7-methoxy-1,4-benzoxazin-2-one (BrMB), which possesses a new 1,4-benzoxazin-2-one moiety, a highly fluorescent compound, and the applicability of the reagent to the determination of femtomole levels of carboxylic acids by HLC with fluorescence detection.

EXPERIMENTAL

Materials

All chemicals for synthesis were of guaranteed-reagent grade and all organic solvents for chromatographic purposes were of special grade for HPLC, obtained from Wako (Osaka, Japan). Water was purified with a Milli-Q water purification unit (Millipore, Bedford, MA, USA). Linear C_3–C_{20} saturated fatty acids and 18-crown-6 were pur-

0021-9673/92/$05.00

chased from Sigma (St. Louis, MO, USA) and phenyltrimethylammonium tribromide from Aldrich (Milwaukee, WI, USA).

Instruments

A Hitachi (Tokyo, Japan) Model 650-40 spectrofluorimeter photometer was used for the measurement of fluorescence spectra. The HPLC system consisted of a Model LC-5A solvent-delivery pump (Shimadzu, Kyoto, Japan) equipped with a Rheodyne (Cotati, CA, USA) Model 7125 sample injector and a Shimadzu Model RF-550 fluorescence HPLC monitor, which was linked to a Shimadzu Model C-R6A chromatographic integrator.

Synthesis of reagents

The following methods were used for analysis of the products of the syntheses. Proton nuclear magnetic resonance (^{1}H NMR) spectra were measured using a Model JNM-GX270 spectrometer (JEOL, Tokyo, Japan) at 270 MHz and chemical shift values were expressed in ppm downfield from tetramethylsilane as a internal standard. A Perkin-Elmer (Norwalk, CT, USA) Model 1750 infrared spectrometer was used for infrared spectra determinations. Mass spectra were measured with a Model DX-300 mass spectrometer (JEOL) in the electron impact mode.

3-Methyl-7-methoxy-1,4-benzoxazin-2-one (**1**). This synthesis was performed using the Wislecenus reaction [14]. To an aqueous solution (60 ml) of 5-methoxy-2-nitrophenol (0.03 mol) was added sodium hydrosulphite (36 g) and the mixture was refluxed for 30 min under an inert gas. 2-Amino-5-methoxyphenol was separated as amber-coloured prisms after cooling on ice. Ethyl pyruvate (0.03 mol) was added to a solution of 2-amino-5-methoxyphenol (0.03 mol) in ethanol (45 ml) and acetic acid (11 ml). The mixture was kept in the dark with stirring overnight at ambient temperature. The orange-yellow crystals formed were separated by filtration and recrystallized from ethanol, 2.38 g, yield 41.6%, m.p. 126°C. Elemental analysis: calculated for $C_{10}H_9NO_3$, C 62.82, H 4.75, N 7.33; found, C 62.91, H 4.85, N 7.30%. NMR (C^2HCl_3), ppm: 2.52 (3H, s, CH_3); 3.87 (3H, s, OCH_3); 6.75 (1H, d, J=2.6 Hz); 6.90 (H, dd, J=2.6 and 8.8 Hz); 7.60 (1H, d, J=8.8 Hz). Mass spectrum: m/z 192 (M^+), 106 (base peak). IR (KBr): 3040–2956, 1730, 1616, 1566, 1442, 1356, 1256, 1164, 1096, 1024 cm^{-1}.

3-Bromomethyl-7-methoxy-1,4-benzoxazin-2-one (**2**). To an ice-cold solution of **1** (1.09 g) in tetrahydrofuran (20 ml) was added phenyltrimethyl ammonium tribromide (0.01 mol) and the mixture was stirred gently overnight in a refrigerator. The crude mixture was diluted with 50 ml of diethyl ether and washed with 25 ml of 0.1 *M* $NaHSO_3$, followed by 25 ml of 0.1 *M* $NaHCO_3$ and distilled water. The organic layer was dried over anhydrous Na_2SO_4 and evaporated *in vacuo*. The residue was purified by silica gel (50 g) column chromatography and eluted with *n*-hexane–dichloromethane (1:1). The dried material was recrystallized from *n*-hexane–dichloromethane (1:1). BrMB was obtained as faint yellow prisms, 1.66 g, yield 62.0%, m.p. 146°C. NMR (C^2HCl_3), ppm: 3.90 (3H, s, OCH_3); 4.54 (2H, s, CH_2); 6.78 (1H, d, J=2.6 Hz); 6.94 (1H, dd, J=2.6 and 8.8 Hz); 7.67 (1H, d, J=8.8 Hz). Elemental analysis: calculated for $C_{10}H_8NO_3Br$, C 44.47, H 2.99, N 5.19, Br 29.59; found, C 44.42, H 2.99, N 5.18, Br 29.41%. Mass spectrum: m/z 271 (M^+), 190 (base peak). IR (KBr): 3072–2948, 1730, 1620, 1544, 1364, 1272, 1214, 1198, 1124, 1022 cm^{-1}.

*Preparation of n-caproic acid derivative (**3**) as fluorescence reference.* The authentic BrMB derivative of *n*-caproic acid was synthesized on a semi-micro preparative scale in order to evaluate its reactivity. To a solution of *n*-caproic acid (1.2 mmol) in 5 ml of acetonitrile were added BrMB (0.6 mmol) and triethylamine (1.2 mmol). The resulting solution was allowed to stand at 40°C for 1 h, then evaporated to dryness *in vacuo*. The residue was purified on a silica gel column with a mixture of *n*-hexane and dichloromethane (1:1) as eluent. The main fraction was evaporated to dryness *in vacuo* and the residue was purified by repeated recrystallization from diethyl ether to give faint yellow needles (**3**), yield 42.0%, m.p. 48°C. NMR (C^2HCl_3), ppm: 0.92 (3H, t, J=6.3 Hz, CH_3); 1.2–1.9 [6H, m, $(CH_2)_3$]; 2.47 (2H, t, J=7.5 Hz, $OCOCH_2$); 3.89 (3H, s, OCH_3); 5.26 (2H, s, CH_2OCO); 6.78 (1H, d, J=2.6 Hz); 6.92 (1H, dd, J=2.6 and 8.8 Hz); 7.65 (1H, d, J=8.8 Hz). Elemental analysis: calculated for $C_{16}H_{19}NO_5$, C 62.94, H 6.27, N 4.59; found, C 62.99, H 6.23, N 4.55%. Mass spectrum: m/z 305 (M^+), 207 (base peak). IR (KBr): 2932, 1726, 1620, 1566, 1420, 1340, 1284, 1172, 1158, 1026 cm^{-1}.

Analytical derivatization of carboxylic acids

In a 4-ml amber-coloured screw-capped vial were placed 1 ml of acetonitrile solution of carboxylic acids, 0.05 ml of 40 m*M* BrMB in acetonitrile, 0.05 ml of 40 m*M* 18-crown-6 in acetonitrile and 10 mg of potassium carbonate. After being mixed, the reaction solution was allowed to stand at 40°C for 10 min. A 10-μl aliquot of the reaction mixture was injected into the HPLC system. The BrMB derivatives of carboxylic acids were separated by HPLC and quantified by fluorescence detection.

Chromatographic conditions

Optimum separation of BrMB derivatives of C_6–C_{13} straight-chain fatty acids could be achieved by using a reversed-phase ODS YMC Pack A-312 column (150 × 6 mm I.D.; particle size 5 μm) (YMC, Kyoto, Japan) and acetonitrile–water (80:20) as mobile phase. The mobile phase was degassed by brief sonication before use and then pumped isocratically at 1.5 ml/min at ambient temperature. The excitation and emission wavelengths were adjusted to 345 and 440 nm, respectively.

RESULTS AND DISCUSSION

Synthesis of 7-methoxy-1,4-benzoxazin-2-one as a fluorescent probe

Many fluorescent labelling reagents are known for the sensitive chromatographic determination of carboxylic acids [1–13]. ADAM [7] and BrMMC [1,2] have been used extensively for trace determinations of prostanoids in biological specimens. However, the former reagent is unstable and the fluorescence intensity of the latter derivatives is affected by solvents. Various 1,4-benzoxazin-2-ones have been reported [14–17], which were synthesized by condensation of α-keto esters with *o*-aminophenols, but no mention was made of their fluorescence properties except for 6,7-methylenedioxy [18], 6,7-dimethoxy [18] and 7-amino derivatives [19]. Our attention became directed toward substituted 1,4-benzoxazin-2-ones, especially with electron-donating substituents, such as amino, alkylamino, hydroxy and alkyloxy groups, in the 7-position as new fluorescent probes for the sensitive determination of trace drugs by HPLC. Of these compounds, we synthesized 7-methoxy-1,4-benzoxazin-2-one with a reactive functional group at the 3-position, because the 7-methoxy derivative of 3-methyl-1,4-benzoxazin-2-one has the strongest fluorescence intensity, as shown in Table I. The order of the relative fluorescence intensities is essentially the same as the order of the Hammett substituent constants, except for the amino derivatives.

The synthetic route is shown in Fig. 1. 2-Amino-5-methoxyphenol was previously obtained [20] by catalytic hydrogenation (PtO_2–H_2) of 5-methoxy-2-nitro-phenol in hydrochloric acid–ethanol. In this work, 2-amino-5-methoxyphenol was obtained by reduction using sodium hydrosulphite. The aminophenol reacted with ethyl pyruvate under mild conditions and gave the condensed-ring 3-methyl-7-methoxy-1,4-benzoxazin-2-one. This

TABLE I

FLUORESCENCE SPECTRAL PROPERTIES OF 3-METHYL-1,4-BENZOXAZIN-2-ONE ANALOGUES

Substituent		I_F[a]	Fluorescence[b]	
6-position	7-position		λ_{ex} (max.) (nm)	λ_{em} (max.) (nm)
H	H	4.5	355	430
H	CH_3	13	336	428
H	OH	450	400	472
H	OCH_3	520	342	436
–OCH_2O–		480	370	480
H	NH_2	42	380	510
H	$N(CH_3)_2$	120	410	535

[a] I_F = relative fluorescence intensity [4-methyl-7-methoxycoumarin (MMC) = 100].
[b] Fluorescence spectra were measured in ethanol solution.

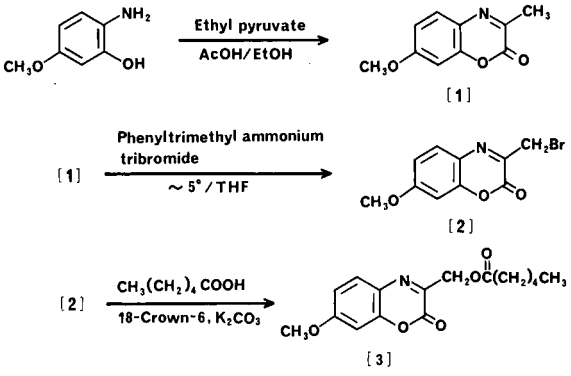

Fig. 1. Synthesis scheme for the fluorescent derivatization reagent BrMB (**2**), and derivatization of *n*-caproic acid with BrMB. AcOH = Acetic acid; EtOH = ethanol; THF = tetrahydrofuran.

TABLE II

FLUORESCENCE SPECTRAL PROPERTIES OF BrMB ESTER OF *n*-CAPROIC ACID IN VARIOUS SOLVENTS

Solvent	I_F[a]	Fluorescence	
		λ_{ex} (max.) (nm)	λ_{em} (max.) (nm)
n-Hexane	4.7	338	426
Benzene	11	346	429
Dichloromethane	29	374	427
Acetone	25	343	427
Ethyl acetate	15	337	423
Acetonitrile	38	341	429
Ethanol	51	342	436
Methanol	69	340	440
Water	100	346	451

[a] I_F = relative fluorescence intensity (water = 100).

compound was easily converted into the bromomethyl derivative (BrMB) by bromination of the methyl group at the 3-position on treatment with phenyltrimethylammonium tribromide.

The reagent, BrMB, proved to be stable at room temperature for at least 6 months with protection from humidity and light, and the acetonitrile solution was also stable for at least 1 week when stored in a refrigerator.

Fluorescence properties of BrMB derivatives

The excitation and emission spectra of the fluorescent ester **3** in methanol–water (80:20) were measured. The solution is similar to the mobile phase used for the chromatographic separation of BrMB derivatives of fatty acids. Under this condition, the excitation and emission maxima were obtained at 345 and 440 nm, respectively.

The fluorescence intensity of BrMB derivatives was affected by the polarity and pH of the solvent. The effects of the solvent on the fluorescence were therefore examined before the analytical technique was developed.

Table II lists the excitation and emission maxima and the relative fluorescence intensities of the purified BrMB ester of *n*-caproic acid in various media. Strong fluorescence was observed in methanol and acetonitrile.

The effects of water concentration and pH on the fluorescence intensity of **3** were investigated. The fluorescence intensity was almost maximum and constant at water concentrations of 20–40% in aqueous methanol and 20–60% in aqueous acetonitrile. The most intense fluorescence was constant between pH 3 and 6.

These results suggest that aqueous acetonitrile is suitable as a mobile phase in the reversed-phase HPLC of BrMB derivatives of fatty acids.

Derivatization of carboxylic acids with BrMB

The derivatization reaction of carboxylic acids with BrMB afforded the ester in the presence of a phase-transfer catalyst in acetonitrile. The fluorescence intensity–time profile of the reaction of *n*-caproic acid with BrMB was tested in the presence of 18-crown-6 and potassium carbonate in acetonitrile at 25 and 40°C. Under these derivatization conditions, the rate of formation of the fluorescent ester was rapid, the reaction being completed within 10 min at 40°C, and a slow decrease in the fluorescence intensity was observed. However, when the reaction mixture was stored in an amber-coloured glass vial at 4°C, the fluorescent derivatives were stable for at least 1 day. This property of BrMB is better than that of BrMMC and BrMDC, where complete esterification of *n*-caproic acid took at least 30 min at the same temperature [4].

Separation of BrMB derivatives of fatty acids

Fig. 2 shows a typical chromatogram of a reaction mixture of fatty acids with BrMB obtained by reversed-phase HPLC using aqueous acetonitrile as

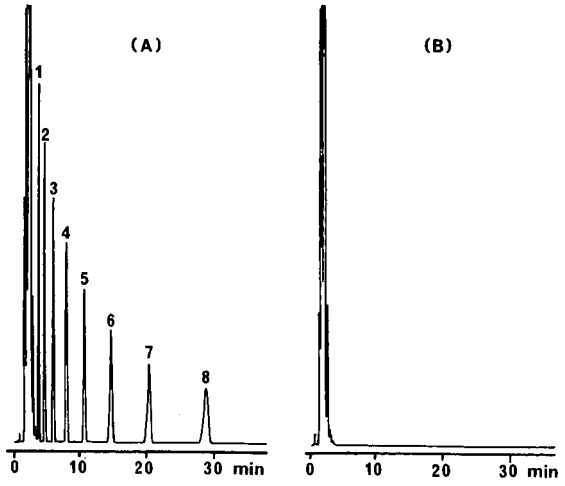

Fig. 2. Chromatographic separation of BrMB derivatives of fatty acids. (A) Reaction mixture of C_6–C_{13} fatty acids. Peaks: 1 = hexanoic acid (C_6), 2 = heptanoic acid (C_7), 3 = octanoic acid (C_8), 4 = nonanoic acid (C_9), 5 = decanoic acid (C_{10}), 6 = undecanoic acid (C_{11}), 7 = dodecanoic acid (C_{12}), 8 = tridecanoic acid (C_{13}). (B) Blank of reaction mixture without fatty acid. HPLC conditions are given in the text. Amount injected: 5 pmol each.

the eluent. A good separation can be achieved with the YMC-Pack A-312 column and acetonitrile–water (80:20) as the mobile phase. The eight fatty acids derivatives were resolved within 30 min.

The capacity factors (k') increased with increasing number of methylene groups in the carboxylic acid; the plot of log k' *versus* carbon number gave approximately a straight line, as illustrated in Fig. 3.

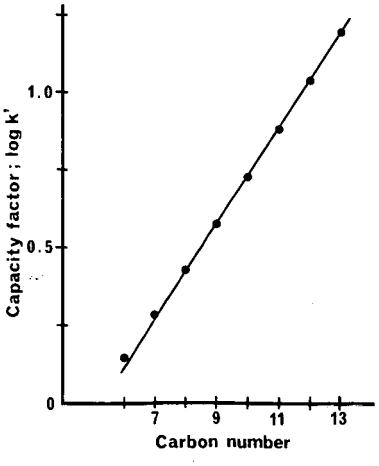

Fig. 3. Relationship between carbon chain number of fatty acids and capacity factor (log k') of BrMB derivatives in reversed-phase HPLC.

TABLE III

REPRODUCIBILITY OF THE PROPOSED METHOD

Fatty acid	Relative standard deviation (%)[a]		
	1.8 pmol	9.0 pmol	45 pmol
C_6	1.86	2.43	0.75
C_7	2.30	2.22	0.79
C_8	2.25	3.15	1.08
C_9	2.11	2.07	0.97
C_{10}	2.00	1.88	0.93
C_{11}	1.60	1.92	0.86
C_{12}	2.56	2.07	0.95
C_{13}	2.76	1.40	0.65

[a] $n = 5$.

Linearity of response, precision and detection limit

Calibration graphs of peak areas *versus* concentrations of fatty acids labelled with BrMB were plotted. A good linear detector response (linear regression coefficient = 0.999) was observed for all the fatty acids in the range 0.7– 45 pmol injected on-column (number of fatty acid concentrations tested = 7, $n = 3$ at each concentration). The detection limits of the fatty acids are in the range 2–10 fmol at a signal-to-noise ratio of 3.

Multiple derivatization ($n = 5$) of fatty acids followed by HPLC gave peak areas with relative standard deviations of 0.65–3.15% in the range 1.8–45 pmol of fatty acids analysed, as shown in Table III.

It is expected that this method will be suitable for the derivatization and separation of carboxylic acids with satisfactory reliability and its high sensitivity may provide much more precise information on biologically important various organic acids. This methods is now being applied to trace determinations of some non-steroidal anti-inflammatory drugs in biological specimens for pharmacokinetic studies.

REFERENCES

1 W. Dunges, *Anal. Chem.*, 49 (1977) 442.
2 J. F. Lawrence, *J. Chromatogr. Sci.*, 17 (1979) 147.
3 S. Kamada, M. Maeda and A. Tsuji, *J. Chromatogr.*, 272 (1983) 29.

4 H. Naganuma and Y. Kawahara, *J. Chromatogr.*, 478 (1989) 149.
5 P. Farinotti, Ph. Siard, J. Bouson, S. Kirkiacharian, B. Valeur and G. Mahuzier, *J. Chromatogr.*, 269 (1983) 81.
6 M. Yamaguchi, S. Hara, R. Matsunaga, M. Nakamura and Y. Ohkura, *J. Chromatogr.*, 346 (1985) 227.
7 N. Nimura and T. Kinoshita, *Anal. Lett.*, 13 (1981) 191.
8 N. Nimura, T. Kinoshita, T. Yoshida, A. Uetake and C. Nakai, *Anal. Chem.*, 60 (1988) 2067.
9 M. Yamaguchi, O. Takehiro, S. Hara, M. Nakamura and Y. Ohkura, *Chem. Pharm. Bull.*, 36 (1988) 2263.
10 J. B. F. Lloyd, *J. Chromatogr.*, 189 (1980) 59.
11 W. D. Watkins and M. B. Peterson, *Anal. Biochem.*, 124 (1982) 30.
12 H. Tsuchiya, T. Hayashi and M. Sato, *J. Chromatogr.*, 309 (1984) 43.
13 Y. M. Lee, H. Nakamura and T. Nakajima, *Anal. Sci.*, 5 (1989) 681.
14 W. Wislecenus and W. Beekh, *Justus Liebigs Ann. Chem.*, 295 (1897) 339.
15 E. Biekert, D. Hoffman and F. J. Meyer, *Chem. Ber.*, 94 (1961) 1664.
16 R. B. Moffett, *J. Med. Chem.*, 9 (1966) 475.
17 A. McKillop, A. Henderson, P. S. Ray, C. Avendano and E. G. Molinero, *Tetrahedron Lett.*, 23 (1982) 3357.
18 D. G. Orphanos and A. Taurins, *Can. J. Chem.*, 44 (1966) 1795.
19 M. T. Le Bris, *J. Heterocycl. Chem.*, 22 (1985) 1275.
20 E. E. Smissman, J. B. Lapiduo and S. D. Beck, *J. Org. Chem.*, 22 (1957) 220.

Journal of Chromatography, 591 (1992) 165–173
Elsevier Science Publishers B.V., Amsterdam

CHROM. 23 788

Determination of organic acids, amino acids and saccharides by high-performance liquid chromatography and a postcolumn enzyme reactor with amperometric detection

R. Mögele, B. Pabel and R. Galensa*

Institute of Food Chemistry, University of Braunschweig, Schleinitzstrasse 20, W-3300 Braunschweig (Germany)

(First received April 18th, 1991; revised manuscript received October 2nd, 1991)

ABSTRACT

A technique for the determination of organic acids, amino acids and sugars is described. The compounds of interest are separated by high-performance liquid chromatography (HPLC) and converted on-line by immobilized enzymes. The enzymes employed are covalently bound to a synthetic carrier. Hydrogen peroxide, which is produced in the reaction with oxidases, makes possible the application of an electrochemical detector. This arrangement combines the separation efficiency of HPLC, the substrate specificity of enzymes and the high sensitivity of electrochemical detection. The enzymes act according to known reaction mechanisms, but coupling with HPLC leads to a promising extension in the field of biosensors. The simple pretreatment of the samples (often a dilution step is sufficient) allows a rapid analysis of foodstuffs and biological or clinical extracts. The examples presented demonstrate the very high sensitivity of the method with detection limits in the nano- to picomolar range and a wide field of application.

INTRODUCTION

The demand for rapid but specific and exact methods in analytical chemistry, *e.g.*, in the food industry and the biochemical and environmental fields, has increased substantially recently. High-performance liquid chromatography (HPLC) has been widely applied and the disadvantage of insufficient sensitivity has been overcome by the development of sensitive detectors, *e.g.*, the electrochemical detector. By pre- and postcolumn derivatization it is possible to detect electrochemically inactive substances. One form of selective postcolumn reaction is conversion with immobilized enzyme reactors (IMER) [1–4], based on known enzyme reactions [5–7]. IMERs are commonly used in flow-injection analysis (FIA) [8–11]. Because there is no separation in FIA, the coupling of HPLC with biosensors is advantageous. In the method proposed here, the compounds of interest are separated by HPLC and converted in the IMER and the reaction product is detected amperometrically [12]. For example, this approach has already been employed for the determination of the neurotransmitters choline and acetylcholine [13–16].

The presented one-step determination of organic acids, amino acids and sugars represents a development of the combination of HPLC separation, enzymatic conversion and electrochemical detection. Examples of some successful applications are given.

EXPERIMENTAL

Apparatus

For the separation of acids, two HPLC pumps, an LC-XPD from Pye Unicam (Kassel, Germany) and an Economy 2/E from Techlab (Erkerode, Germany), a Model 3512 degasser from ERC (Alteglofsheim, Germany), Model EP 30 electrochemical de-

0021-9673/92/$05.00

tector from Biometra (Göttingen, Germany) equipped with a platinum cell (working potential 0.6 V *versus* Ag/AgCl, range 50 nA) and a Model 7125 injection valve (Rheodyne, Berkeley, CA, USA) equipped with a 10-μl sample loop. The results were recorded with a Shimadzu (Duisburg, Germany) C-R6A instrument. The following columns were used: Superspher 100, 125 × 4.5 mm I.D., packed with 5-μm ODS (Merck, Darmstadt, Germany); Polyspher OA HY, 300 × 6.5 mm I.D. filled with cation-exchange resin (Merck); and Inertsil ODS 2, 250 × 4.6 mm I.D., packed with 5-μm ODS (VDS Optilab, Berlin, Germany).

The HPLC separation of sugars was carried out with two Beckman (Munich, Germany) pumps, an ERC 3512 degasser, a Biometra EP 30 electrochemical detector and a Model 7125 injection valve (Rheodyne) equipped with a 10-μl sample loop. The results were recorded with a Model 3390 A integrator from Hewlett-Packard (Bad Homburg, Germany). The following columns were used: Supelcosil LC 18, 250 × 4.6 mm I.D., filled with 5-μm ODS (Supelco, Bad Homburg, Germany); LiChrospher, 125 × 4 mm I.D., packed with ODS (Merck); and a mixing column, 60 × 4 mm I.D. filled with glass beads, diameter 40 μm.

Reagents

D,L-Amino acids, ascorbic acid, $Co(NO_3)_2 \cdot 6H_2O$, L-lactic acid, $MgSO_4 \cdot 7H_2O$, $Na_2HPO_4 \cdot 2H_2O$, $NaH_2PO_4 \cdot H_2O$, nicotinamide adenine dinucleotide free acid, oxalic acid, phosphoric acid and sugars (fructose, galactose, glucose, lactose, maltose, maltotriose and saccharose) were obtained from Merck, citric acid, succinic acid and tris(hydroxymethyl)aminomethane (Tris) from Serva (Heidelberg, Germany) and lithium-D,L-lactate, lithium-D-lactate and maltooligosaccharides from corn syrup were purchased from Sigma (Deisenhofen, Germany). All reagents were of analytical-reagent grade. Water obtained with a NANOpure-A system (Sybron/Barnstead, Boston, MA, USA) was used to prepare all stations.

Enzymes

The following were obtained from Sigma: L-amino acid oxidase (EC 1.4.3.2) type V from *Crotalus adamanteus* venom, lyophilized, A-3016, 8.5 U [U = amount (units) of enzyme used for immobilization]; D-amino acid oxidase (EC 1.4.3.3) type II from porcine kidney, suspension in $(NH_4)_2SO_4$ solution, A-1789, 73 U; amyloglucosidase (EC 3.2.1.3) from *Aspergillus niger*, suspension in 3.2 *M* $(NH_4)_2SO_4$ solution, pH 6.0, A-3514, 940 U; ascorbate oxidase (EC 1.10.3.3) from *Cucurbita* species, lyophilized, A-0157, 250 U; galactose oxidase (EC 1.1.3.9) from *Dactylium dendroides*, lyophilized, G-3385, 150 U; β-galactosidase (EC 3.2.1.23) from *Escherichia coli*, lyophilized, G-6008, 1000 U; glucose oxidase (EC 1.1.3.4) from *Aspergillus niger* lyophilized, G-6125, 2000 U; invertase (EC 3.2.1.26) from baker's yeast, solid, I-4504, 6000 U; L-lactate oxidase from *Pediococcus* species, lyophilized, L-0638, 25 U; oxalate oxidase (EC 1.2.3.4) from barley seedlings, lyophilized, O-4127, 5 U; mutarotase (EC 5.1.3.3) from porcine kidney, lyophilized, M-9776, 5000 U. L-Lactate dehydrogenase (EC 1.1.1.27) from porcine muscle, solution in glycerin, 127221, 160 U, and D-lactate dehydrogenase (EC 1.1.1.28) from *Lactobacillus leichmannii*, suspension in $(NH_4)_2SO_4$ solution, 106914, 160 U, were commercially available from Boehringer (Mannheim, Germany). Glucose isomerase (EC 5.3.1.5), crystalline 9 U, was a gift from Kalie Chemie (Hannover, Germany).

Immobilization

The enzymes were covalently bound to a polymeric carrier by the Biometra method (Galensa *et al.* [12]). Eupergit C, which is based on poly(methylmethacrylamide), from Röhm Pharma (Weiterstadt, Germany) was used as a polymeric matrix. Bearing oxirane groups, it is capable of binding proteins via their amino, thio and hydroxy groups. The immobilized enzymes are filled in steel cartridges (40 × 2.5 mm I.D.), maximum pressure 150 bar.

Sample preparation

Samples and standards were dissolved in and diluted with water or phosphate buffer (0.1 *M*), sonicated and filtered (0.45-μm membrane filters) if necessary.

RESULTS AND DISCUSSION

Different instrumental arrangements were used for the determination of the particular acids, amino acids and sugars. Fig. 1 shows the simplest way if

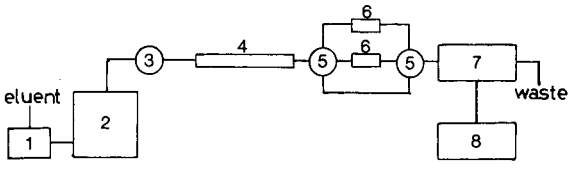

Fig. 1. Schematic diagram of the experimental arrangement without a second eluent. 1 = Degasser; 2 = pump; 3 = injection valve; 4 = HPLC column; 5 = switching valve; 6 = enzyme reactor; 7 = electrochemical detector; 8 = integrator.

the same eluent is needed for the separation and for the enzyme reaction. By the use of switching valves, it is possible to select different enzyme reactors. Interfering electroactive components in the samples can be detected with a reference device, without enzyme. Attention must be paid to the compatibility of the conditions for HPLC separation and enzyme reaction. Enzymes exhibit an optimum pH range for activity, which depends not only on pH but also on ionic strength and type of buffer. The optimum pH can be shifted by the immobilization, *e.g.*, by binding on a multi-charged support [17]. Activity profiles have to be recorded by evaluating the effect of pH on the peak current. If the HPLC separation requires water or an eluent with an unsuitable pH value, the optimum pH is adjusted by feeding a second eluent after the column (see Fig. 2).

To enhance the separation efficiency organic modifiers are sometimes added to the HPLC eluent. Although the covalently immobilized enzymes exhibit an increased stability towards organic solvents compared with the native enzymes [17], the use of such eluents is limited. Among the factors governing the catalytic activity of the IMERs, attention must be paid to the dependence on the presence of a coenzyme or special activators, *e.g.*, inorganic ions [18]. In addition to the investigation of the enzyme parameters, the optimum potential on the working electrode in the flow cell has to be determined. Signal-to-noise ratios and peak current as a function of applied potentials give plots characteristic of the individual electroactive substances. In most instances we used oxidases. The generated hydrogen peroxide was measured at a potential of 0.6 V (*versus* Ag/AgCl/KCl) on a platinum electrode:

$$H_2O_2 \longrightarrow O_2 + 2\,H^+ + 2e^- \qquad (1)$$

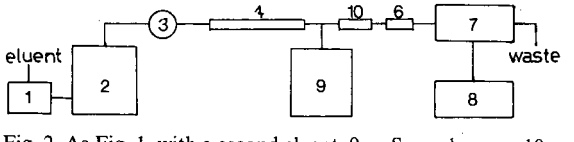

Fig. 2. As Fig. 1, with a second eluent. 9 = Second pump, 10 = mixing column.

Determination of acids

Oxalic acid. Because of the toxicity of free oxalic acid and its salts, determinations in vegetable foodstuffs such as spinach, mangold and rhubarb and in clinical samples are of great interest. Among the various methods for determining oxalic acid [19], the use of enzymes provides a high degree of specificity and sensitivity.

Oxalic acid is converted to H_2O_2 and CO_2 with oxalic acid oxidase (OAD):

$$\text{oxalic acid} + O_2 \xrightarrow{\text{OAD}} CO_2 + H_2O_2 \qquad (2)$$

In contrast to the published FIA method with immobilized OAD and the detection of the liberated hydrogen peroxide by a colour reaction [20,21], no additional reagent is necessary in our method with electrochemical detection. The separation (and also protection of the IMER) takes place by HPLC.

With respect to the optimum pH of the immobilized OAD, a 0.1 *M* citrate or succinate buffer solution (pH 5.0) is used as eluent [21,22]. A linear calibration graph is obtained in the 1–10 ppm range using a 10-μl sample loop (0.1–1 n*M* per injected volume), with a detection limit of 0.63 ppm.

Lactic acid. Lactic acid is important in food technology. It is employed for mild acidification and conservation of sour milk products, sour vegetables, etc. Its determination can serve for fermentation control. The content of lactic acid is also a quality factor indicating the beginning of food degradation. Further, the examination of the lactate blood concentration is an important clinical parameter, *e.g.*, for the diagnosis of lactic acidosis or shock states. Lactic acid can be determined with lactic acid oxidase (LOD), which catalyses the following reaction:

$$\text{lactic acid} + O_2 \xrightarrow{\text{LOD}} \text{pyruvate} + H_2O_2 \qquad (3)$$

Several studies with immobilized LOD have been published, *e.g.*, combined with a Clark oxygen elec-

trode [23], fluorimetric detection [24], differential-pulse polarography [25] or FIA with amperometric detection [26]. In this work, lactic acid is also determined with immobilized LOD, but in combination with HPLC separation and an electrochemical detector. The immobilized LOD has a pH optimum of 7.0–7.5. The eluent is 0.1 *M* phosphate buffer solution (pH 7.3). Under these conditions, the calibration graph is linear from 0.6 to 63 ppm using a 10-μl injection volume (0.07–7 n*M* per injection). The limit of detection is 0.18 ppm. Chromatograms of food samples are presented in Fig. 3.

Lactic acid is an optically active substance that occurs naturally in the dextrorotatory L-(+)-form. The determination of D-(−)-lactic acid as a product of microbial metabolism is of interest, *e.g.*, in the analysis of foodstuffs such as tomato products [27]. LOD only converts the L-enantiomer of lactic acid. For the determination of both forms, we use L- and D-lactic acid dehydrogenase (LDH). L-LDH has also been employed in a FIA system [28]. In our method, nicotinamide adenine dinucleotide (NAD), which is necessary as a coenzyme for the reaction, is added to the eluent (0.1 *M* phosphate buffer, pH 7.3) at a concentration of 1 m*M*.

$$\text{lactic acid} + \text{NAD}^+ \xrightarrow{\text{LDH}} \text{pyruvate} + \text{NADH} + \text{H}^+ \qquad (4)$$

NADH is detected electrochemically at a potential of 0.7 V (in contrast to the usually applied potential of 0.6 V). Separation of the enantiomers is not possible with the tested columns. The determination is achieved by reactor switching as shown in Fig. 1.

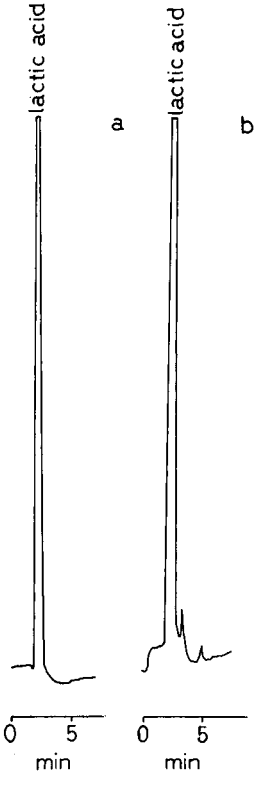

Fig. 3. Chromatography of food samples, diluted in buffer, on a Superspher 100 RP-18e column (125 × 4.5 mm I.D.) with an L-lactate oxidase reactor. Chromatographic conditions: experimental arrangement as in Fig. 1; mobile phase, 0.1 *M* phosphate buffer (pH 7.4); flow-rate, 0.5 ml/min; working potential, 0.6 V; range, 50 nA. (a) Yoghurt, 380 mg/l, L-lactic acid 1.2%; (b) concentrated tomatoes, 1.836 g/l, L-lactic acid 0.5%.

Ascorbic acid. Ascorbic acid can be detected by electrochemical oxidation on a platinum electrode at a potential of 0.6 V. Because of the similar retention times on RP-18 columns, the determination of organic acids in real samples is disturbed and ascorbic acid must be eliminated. By the use of ascorbate oxidase (AOD), it is converted into dehydroascorbic acid, which is not electrochemically active. AOD has a pH optimum at pH 5.0–5.5, so the in-line elimination with the immobilized enzyme is only possible during the determination of oxalic acid. AOD and OAD are co-immobilized or two reactors are coupled in series and a buffer solution of pH 5.5 is used as eluent [21]. To determine other analytes, the pH must be changed after the reaction with ascorbic acid oxidase, *e.g.*, for lactic acid from pH 5 to 7.3.

Attempts to shift the pH optimum of AOD by immobilization on another carrier substance are in progress. Alternatively to the destruction, ascorbic acid can be separated chromatographically from oxalic or lactic acid with a suitable chromatographic system. Fig. 4 shows the separation of ascorbic acid, lactic acid and uric acid in blood serum with the IMER system.

Amino acids. L-Amino acids are essential for the biosynthesis of proteins. The optical antipodes, D-amino acids, can be found, *e.g.*, in fermented foods such as dairy products, lactic acid-fermented vegetables and alcoholic beverages [29,30]. The identification of D-amino acids can be evidence of the addi-

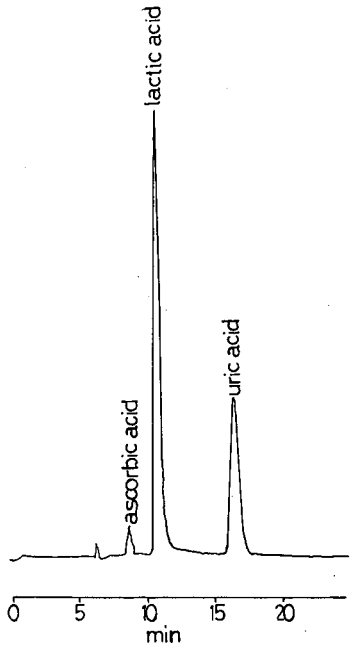

Fig. 4. Separation of ascorbic acid (0.1 μmol/l added), L-lactic acid and uric acid in blood serum, diluted 1:40, on a Polyspher OA HY column (300 × 6.5 mm I.D.) with an L-lactate oxidase reactor. Chromatographic conditions: experimental arrangement as in Fig. 2; mobile phase 1, 0.005 *M* H_3PO_4; mobile phase 2, 0.2 *M* phosphate buffer (pH 7.4); flow-rate, 0.4 ml/min each; working potential, 0.6 V; range, 50 nA.

tion of synthetic, racemic amino acids as adulterants in fruit juices [31]. A method with immobilized L-amino acid oxidase (L-AAOD) as an amperometric enzyme electrode has been proposed [32]. L-AAOD catalyses the oxidative deamination of a number of L-amino acids:

$$\text{amino acid} + H_2O + O_2 \xrightarrow{\text{L-AAOD}} \text{2-oxo acid} + NH_3 + H_2O_2 \qquad (5)$$

The performance of a sensor with L-AAOD has been investigated with the FIA technique. Determination of particular amino acids in one single run is not possible in this way. Other sensors are based on selective oxidases for L-glutamate, L-lysine and L-tyrosine [33]. Recently, a combined FIA–HPLC method was presented, which used immobilized L-AAOD and D-AAOD with amperometric detection [34]. In other studies, racemic resolution of amino acid esters into L-amino acids and D-amino acid esters was achieved using enzyme reactors with immobilized α-chymotrypsin [35] or trypsin [36] as HPLC columns [37]. An HPLC system with immobilized L-AAOD as a postcolumn reactor in combination with chemiluminescence detection has been described [38].

In our work, we also use the optical specificity of immobilized L-AAOD and D-AAOD, but with amperometric detection of the generated hydrogen peroxide. With 0.1 *M* phosphate buffer (pH 7.3), several amino acids, corresponding to the specificity of the oxidase [5,39], were determined after separation on a reversed-phase column (see Fig. 5). The simultaneous determination of both enantiomers with a parallel configuration of two IMERs and a multi-channel flow-through cell should be possible,

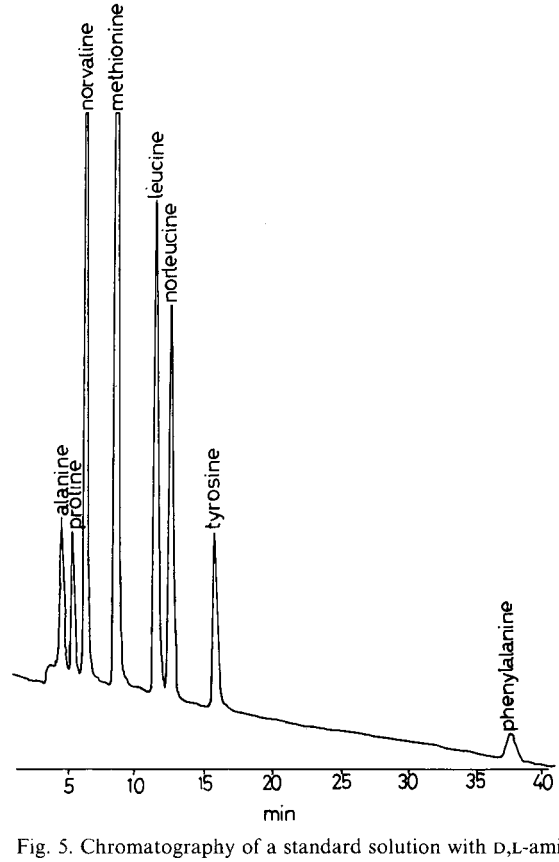

Fig. 5. Chromatography of a standard solution with D,L-amino acids (0.05 m*M*) on an Inertsil ODS-2 column (250 × 4.6 mm I.D.) with a D-amino acid oxidase reactor. Chromatographic conditions: experimental arrangement as in Fig. 1; mobile phase, 0.1 *M* phosphate buffer (pH 7.4); flow-rate, 0.45 ml/min; working potential, 0.6 V; range, 50 nA.

as has been described with a FIA system for sugars, lactate, sulphite and ethanol [40]. Another possibility has been presented for malate and ethanol with a system consisting of two solution lines and a single electrode [41]. A train of two peaks appears in the FIA-trace. To reduce problems in recovery and reproducibility caused by the splitting of the solution line, we prefer alternation of the two amino acid oxidases by means of a switching valve.

Determination of sugars

Another current study is the determination of sugars. Only for glucose and galactose are oxidases available, which produce hydrogen peroxide directly. Galactose oxidase is not very specific, and lactose and raffinose are also suitable substrates.

Other sugars, such as sucrose, maltose and fructose, do not react. Enzymatic hydrolysis of these di- and oligosaccharides and conversion of monosaccharides is necessary before the application of the oxidases [42–44].

Another very sensitive way to determine sugars is high-performance anion-exchange chromatography with pulsed amperometric detection (PAD) [45–50]. However PAD is a universal method, whereas in the method presented the sugars of interest are selectively determined by substrate-specific enzymes.

Glucose. The determination of glucose is accomplished by glucose oxidase (GOD) [7,12]:

$$\beta\text{-D-glucose} + O_2 + H_2O \xrightarrow{GOD} \text{D-gluconic acid} + H_2O_2 \qquad (6)$$

Because GOD is specific only for β-D-glucose, a higher sensitivity can be obtained if GOD is combined with a mutarotase (MUT). MUT catalyses the conversion of α-D-glucose into β-D-glucose [42].

GOD is stable over a wide pH range with maximum activity at pH 5.6. The detection limit in our system is 0.02 ppm (1 p*M* glucose using a 10-μl injection volume).

Sucrose. Sucrose can be hydrolysed in the presence of invertase (IV) to glucose and fructose [42]:

$$\text{sucrose} + H_2O \xrightarrow{IV} \alpha\text{-D-glucose} + \beta\text{-D-fructose} \qquad (7)$$

$$\alpha\text{-D-glucose} \xrightarrow{MUT} \beta\text{-D-glucose} \qquad (8)$$

Direct conversion of the formed α-D-glucose by

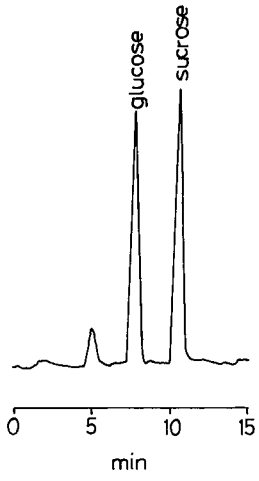

Fig. 6. Separation of glucose and sucrose in a pear juice, diluted 1:40 000, on a Supelcosil LC 18 column (250 × 4.6 mm I.D.) with an invertase, mutarotase and glucose oxidase reactor. Chromatographic conditions: experimental arrangement as in Fig. 2; mobile phase 1, water, flow-rate 0.4 ml/min; mobile phase 2, 0.2 *M* phosphate buffer (pH 6.4), flow-rate 0.3 ml/min; working potential, 0.6 V; range, 50 nA.

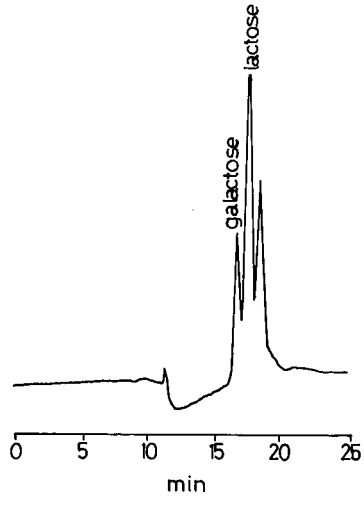

Fig. 7. Separation of galactose and lactose in a soft cheese (130 mg in 100 ml) on a Supelcosil LC 18 column (250 × 4.6 mm I.D.) with a galactose oxidase reactor. Chromatographic conditions: experimental arrangement as in Fig. 2; mobile phase 1, water, flow-rate 0.2 ml/min; mobile phase 2, 0.2 *M* phosphate buffer (pH 6.4), flow-rate 0.25 ml/min; working potential, 0.6 V; range, 50 nA.

GOD to gluconic acid and H_2O_2 (see eqn. 6) is not possible, because GOD is specific for β-D-glucose. For the determination of trace amounts of glucose mutarotase must be used. The detection limit with MUT is 0.1 ppm and without 10 ppm (pH 6.4), corresponding to 3 and 300 p*M* sucrose, respectively, with an injection volume of 10 μl.

Fig. 6 shows the simultaneous determination of glucose and sucrose in a pear juice.

Galactose. The enzymatic conversion is directly possible, because a corresponding oxidase is available [7]. Galactose oxidase (GALOD) reaches maximum activity at pH 5.8 and catalyses the reaction:

$$\text{D-galactose} + O_2 \xrightarrow{\text{GALOD}} \text{D-galactohexodialdose} + H_2O_2 \quad (9)$$

The detection limit is 0.15 ppm (8 p*M* with a 10-μl injection volume).

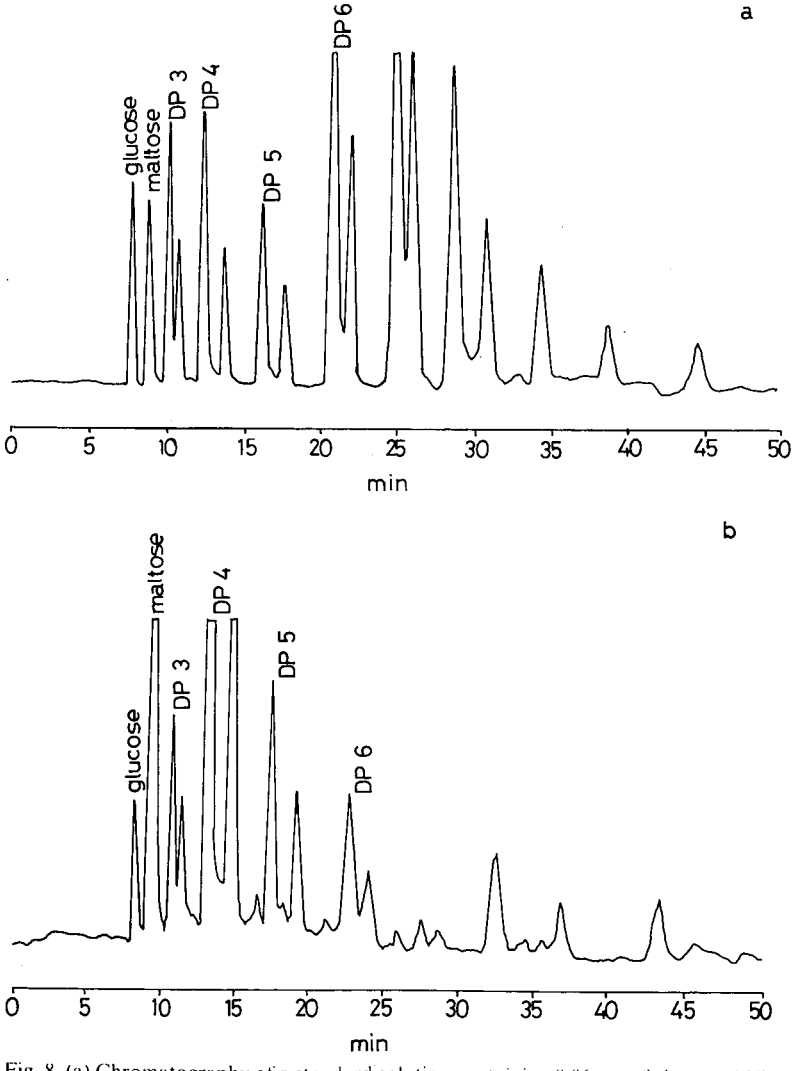

Fig. 8. (a) Chromatography of a standard solution containing 0.06 mg of glucose, 0.08 mg of maltose, 0.14 mg of maltotriose and 3.18 mg of maltooligosaccharides from corn syrup per 100 ml on a Supelcosil LC 18 column (250 × 4.6 mm I.D.) with an amyloglucosidase and glucose oxidase reactor. (b) Separation of glucose, maltose and maltooligosaccharides in a Pils beer, diluted 1:1200, on a Supelcosil LC 18 column (250 × 4.6 mm I.D.) with an amyloglucosidase and glucose oxidase reactor. Chromatographic conditions: experimental arrangement as in Fig. 2; mobile phase 1, water, flow-rate 0.4 ml/min; mobile phase 2, 0.2 *M* phosphate buffer (pH 6.4), flow-rate 0.3 ml/min; working potential, 0.6 V; range, 50 nA.

Lactose. Lactose (β-D-galactose-1→4-D-glucose) can be detected by two different methods.

Hydrolysis of lactose is effected by β-galactosidase, giving galactose and glucose [42]. In a second reaction, glucose can be converted in the presence of GOD (see eqn. 6). The detection limit at pH 7.0 is 0.05 ppm (1.5 p*M* for a 10-μl injection volume).

Likewise, it is possible to determine the galactose with GALOD (see eqn. 9). For the determination using GALOD, because the oxidation with GALOD does not occur at the C-1 position as with GOD, but in the C-6 position [51], enzymatic hydrolysis of lactose to galactose and glucose is not necessary. The detection limit is 5 ppm (150 p*M* for a 10-μl injection).

The separation of galactose and lactose in a soft cheese is shown in Fig. 7.

Maltose. The enzymatic hydrolysis of maltose to glucose can be catalysed by either α-glucosidase or amyloglucosidase (AG). AG hydrolyses α-1,4-glucan linkages in polysaccharides and is therefore not specific for maltose [42]. Nevertheless, AG was most preferred because the sensitivity with AG is much greater and maltooligosaccharides can also be determined (see Fig. 8).

The detection limit is 0.03 ppm (1 p*M* for a 10-μl injection), pH 6.4.

Fructose. Fructose can be converted into glucose with glucose isomerase (GI) [42,43]:

$$\text{fructose} \overset{\text{GI}}{\rightleftharpoons} \text{glucose} \qquad (10)$$

For all of the previous enzymatic sugar reactions, a 0.1 *M* phosphate buffer was taken, whereas the conditions with GI are 5 m*M* Tris buffer (pH 7.5) containing 0.5 m*M* Mg^{2+} and 0.125 m*M* Co^{2+}. To increase the enzyme activity, the GI reactor is heated at 45°C.

Magnesium ions are essential for the glucose isomerase reaction and cobalt ions increase the lifetime of the enzyme, especially when the reactor works at a higher temperature [18]. The magnesium and cobalt ions do not affect the following GOD reactor. Behind the GI reactor, a 0.2 *M* phosphate buffer (pH 6.4) is added by a second pump to the Tris buffer stream (same flow) to change the pH value.

The detection limit is 5 ppm fructose (0.28 n*M* for a 10-μl injection).

CONCLUSION

The method presented offers wide range of applications in the analysis of complex samples. The reagents used are non-toxic and commercially available. The high sensitivity, the specificity of the enzymes and the simple sample pretreatment make the method rapid and inexpensive. The lifetime and stability of the biosensors (often over 1 year) are higher than for FIA techniques. The HPLC separation with reversed-phase or cation-exchange columns allows the simultaneous determination of several substances in various extracts. Additionally, the column protects the enzyme reactor. Currently we are able to determine lactic acid, oxalic acid, ascorbic acid, amino acids and sugars with detection limits in the n*M* to p*M* range. The relative standard deviation in all the cases examined is between 2 and 5%. From the results it can be deduced that the stability of the electrochemical detector is a decisive factor for reproducibility. We are working on further improvements regarding the validity of quantitative results.

ACKNOWLEDGEMENT

The authors thank Biometra (Biomedizinische Analytik, Göttingen, Germany) for support and cooperation.

REFERENCES

1 K. Shimada and T. Oe, *J. Chromatogr.*, 492 (1989) 345.
2 K. Matsumoto, H. Matsubara, M. Hamada, H. Ukeda and Y. Osajima, *J. Biotechnol.*, 14 (1990) 115.
3 G. A. Marko-Varga, *Anal. Chem.*, 61 (1989) 831.
4 G. G. Guilbault and J. H. Luang, *Chimia*, 42 (1988) 267.
5 H. U. Bergmeyer, J. Bergmeyer and M. Grassl (Editors), *Methods of Enzymatic Analysis*, Vol. II, Verlag Chemie, Weinheim, 3rd ed., 1983.
6 H. L. Schmidt and R. Kittsteiner-Eberle, *Naturwissenschaften*, 73 (1986) 314.
7 F. Scheller and F. Schubert, *Biosensoren*, Birkhäuser, Basel, Boston, Berlin, 1989.
8 G. Wagner and R. Schmid, *Food Biotechnol.*, 4 (1990) 215.
9 B. G. Osborne and J. F. Tyson, *Int. J. Food Sci. Technol.*, 23 (1988) 241.
10 L. Lemieux, R. Puchades and R. E. Simard, *Lebensm. Wiss. Technol.*, 22 (1989) 254.
11 B. A. A. Dremel, B. P. H. Schaffar and R. D. Schmid, *Anal. Chim. Acta*, 225 (1989) 293.
12 R. Galensa, G. Müller, A. Schirmer, H. Hippe and H. Stadler, *Lebensmittelchem. Gerichtl. Chem.*, 42 (1988) 94.

13 H. Stadler and T. Nesselhut, *Neurochem. Int.*, 9 (1986) 127.
14 G. Damsma, D. Lammerts van Bueren, B. H. C. Westerink and A. S. Horn, *Chromatographia*, 24 (1987) 827.
15 J. L. Meek and C. Eva, *J. Chromatogr.*, 317 (1984) 343.
16 T. Yao and M. Sato, *Anal. Chim. Acta*, 172 (1985) 371.
17 W. Hartmeier, *Immobilisierte Biokatalysatoren*, Springer, Berlin, Heidelberg, New York, Tokyo, 1986.
18 W. Gerhartz, *Enzymes in Industry*, VCH, Weinheim, 1990.
19 J. A. Hodgkinson, *Oxalic Acid in Biology and Medicine*, Academic Press, New York, 1977.
20 R. Bais, N. Potezny, J. B. Edwards, A. M. Rofe and R. A. Conyers, *Anal. Chem.*, 52 (1980) 508.
21 S. v. Laffert, B. Pabel, G. Müller and R. Galensa, in R. D. Schmid and F. Scheller (Editors), lecture presented at the *GBF Biosensor Workshop* (*GBF Monographs*, No. 13, 293), VCH, Weinheim, 1989.
22 H. Hippe, H. Stadler and R. Galensa, *BioTec*, 3 (1990) 22.
23 F. Mizutani, K. Sasaki and Y. Shimura, *Anal. Chem.*, 55 (1983) 35.
24 K. Zaitsu, M. Nakayana and Y. Ohkura, *Anal. Chem.*, 201 (1987) 351.
25 K. Hasebe, S. Hikima and H. Yoshida, *Fresenius' J. Anal. Chem.*, 339 (1991) 261.
26 M. Mascini, D. Moscone, G. Palleschi and R. Pilloton, *Anal. Chim. Acta*, 213 (1988) 101.
27 S. Hanewinkel-Meshkini and W. Hackmann, *Dtsch. Lebensm.-Rundsch.*, 85 (1989) 351.
28 T. Yao, Y. Kobayashi and S. Musha, *Anal. Chim. Acta*, 138 (1982) 81.
29 H. Brückner and M. Hausch, *J. High Resolut. Chromatogr.*, 12 (1989) 680.
30 H. Brückner and M. Hausch, *Chromatographia*, 28 (1989) 487.
31 H. J. Hofsommer, I. Klein, J. Grüning and H. R. Höpker, *Flüssiges Obst*, 56 (1989) 646.
32 G. G. Guilbault and G. J. Lubrano, *Anal. Chim. Acta*, 69 (1974) 183.
33 D. Pfeiffer, L. Risinger, U. Wollenberger, G. Johansson and F. W. Scheller, lecture presented at the *GBF Biosensor Workshop, Braunschweig*, (*GBF Monographs*, No. 13, 27), VCH, Weinheim, 1989.
34 T. Yao, lecture presented at the *GBF Biosensor Workshop, Braunschweig, 1990*, in press.
35 I. W. Wainer, P. Jadaud, G. R. Schonbaum, S. V. Kakodkae and M. P. Henry, *Chromatographia*, 25 (1988) 903.
36 S. Thelohan, Ph. Jadaud and I. W. Wainer, *Chromatographia*, 28 (1989) 551.
37 J. Kalbe, H. Höcker and H. Berndt, *Chromatographia*, 28 (1989) 193.
38 H. Jansen, U. A. Th. Brinkman and R. W. Frei, *J. Chromatogr.*, 440 (1988) 217.
39 M. Dixon and K. Kleppe, *Biochim. Biophys. Acta*, 96 (1965) 357.
40 K. Matsumoto, lecture presented at the *GBF Biosensor Workshop, Braunschweig, 1990*, in press.
41 H. Ukeda, Y. Nakada, K. Matsumoto and Y. Osajima, lecture presented at the *GBF Biosensor Workshop, Braunschweig, 1990*, in press.
42 C. A. Swindlehurst and T. A. Nieman, *Anal. Chim. Acta*, 205 (1988) 195.
43 L. Olsson and C. F. Mandenius, *Anal. Chim. Acta*, 224 (1989) 31.
44 K. Matsumoto, H. Kamikado, H. Matsubara and Y. Osajima, *Anal. Chem.*, 60 (1988) 147.
45 D. R. White, Jr., and W. W. Widmer, *J. Agric. Food Chem.*, 38 (1990) 1918.
46 *Technical Note 20, LPN 03421-01, 4/89*, Dionex Idstein, 1989.
47 W. R. LaCourse, D. A. Mead, Jr., and D. C. Johnson, *Anal. Chem.*, 62 (1990) 220.
48 R. M. Pollmann, *J. Assoc. Off. Anal. Chem.*, 72 (1989) 425.
49 D. A. Martens and W. T. Frankenberger, Jr., *Chromatographia*, 29 (1990) 7.
50 A. T. Hotchkiss, Jr., and K. B. Hicks, *Anal. Biochem.*, 184 (1990) 200.
51 D. Amaral, L. Bernstein, D. Morse and B. L. Horecker, *J. Biol. Chem.*, 238 (1963) 2281.

Journal of Chromatography, 591 (1992) 175–180
Elsevier Science Publishers B.V., Amsterdam

CHROM. 23 776

Improvement of extraction procedure for biogenic amines in foods and their high-performance liquid chromatographic determination

Sabrina Moret and Renzo Bortolomeazzi

Istituto di Tecnologie Alimentari, Università degli Studi di Udine, Via Marangoni 97, 33100 Udine (Italy)

Giovanni Lercker*

Dipartimento di Scienze e Tecnologie Alimentari e Microbiologiche, Sezione di Industrie e Tecnologie Alimentari, Università di Firenze, Via Donizetti 6, 50144 Florence (Italy)

(First received August 1st, 1991; revised manuscript received September 27th, 1991)

ABSTRACT

A high-performance liquid chromatography method is described for the simultaneous determination of the biogenic amines tryptamine, 2-phenylethylamine, putrescine, cadaverine, histamine, tyramine, spermidine and spermine in cheese. The optimization of the procedure for the extraction of amines from the matrix is described. The separation of dansyl derivatives of the amines was achieved by reversed-phase liquid chromatography with gradient elution, followed by UV detection at 254 nm. The mobile phase was acetonitrile–0.01 *M* phosphate buffer (pH 7)–water. Under these conditions, rapid elution of the amines in less than 13 min was obtained. Validation of the method included calibration experiments, addition of standard amines for the determination of amine recoveries and repeatability tests.

INTRODUCTION

The formation of biogenic amines, primarily as a consequence of microbial decarboxylation of specific amino acids, is a problem related to proteolytic processes, taking place during the production of fermented food such as cheese, fish products, sausages, wine and beer [1,2]. Biogenic amines are vasoactive products; the consumption of large amounts of these substances may cause problems to some consumers such as headache, nausea, hypo- or hypertension, cardiac palpitation and, in severe cases, intracerebral haemorrhage and death [3–5]. Cheese represents an ideal environment for amine production, but it is a complex matrix for amine determination.

All the analytical methods employed for amines involve two steps: extraction and determination. The extraction of different amines from the matrix represents a very critical step, often resulting in very low analytical recoveries. This problem arises from their different chemical structures. In this case it is necessary to find a compromise in order to obtain a satisfactory recovery for each analyte amine. Many different solvents have been used for the extraction of amines from cheese, such as perchloric acid [6,7], trichloroacetic acid [8], hydrochloric acid [9–11], methanol and other organic solvents [6,12].

The determination of biogenic amines has been carried out with different chromatographic methods: thin-layer chromatography [13–15], gas chromatography [16–18] and high-performance liquid chromatography (HPLC) [19–26], mostly with the last method owing to its high resolution and sensitivity.

In this work we developed an extraction proce-

0021-9673/92/$05.00

dure and a rapid HPLC method for the simultaneous determination of eight biogenic amines in cheese: histamine, tyramine, tryptamine, 2-phenylethylamine, putrescine, cadaverine, spermidine and spermine.

EXPERIMENTAL

Reagents and samples

Tryptamine (Try), 2-phenylethylamine (2-Phe), putrescine (Put), cadaverine (Cad), histamine (His), tyramine (Tyr), spermidine (Spd), spermine (Spm), 1,7-diaminoheptane (1,7-Dh) and dansyl chloride (>99%) were obtained from Fluka (Buchs, Switzerland). Amines, except for 1,7-diaminoheptane, were purchased as hydrochloride salts, and the results were corrected on the basis of their purity and referred to the free base. Orthophosphoric acid (85%) and anhydrous sodium carbonate were obtained from Merck (Darmstadt, Germany). HPLC-grade solvents (Carlo Erba, Milan, Italy) and water purified with a Milli-Q system (Millipore, Bedford, MA, USA) were used throughout.

Parmigiano Reggiano cheese samples were obtained from commercial sources.

Standard solutions

A stock standard solution was prepared by adding an accurately weighed amount of each amine (*ca.* 100 mg) to a 100 ml volumetric flask and diluting to volume with water. Five working standard solutions at different concentrations were prepared from the stock solution, adding a fixed and known amount of internal standard before dilution. Fresh dilute standard solutions must be prepared weekly because some amines are subject to decomposition.

TABLE I

HPLC ELUTION PROGRAMME FOR AMINE ANALYSIS

A = acetonitrile; B = phosphate buffer (pH 7); C = water. Flow-rate, 0.8 ml/min.

Time (min)	A (%)	B (%)	C (%)
0.0	65	35	0
1.0	65	35	0
5.0	80	20	0
5.1	80	0	20
6.0	90	0	10

High-performance liquid chromatography

HPLC determinations were performed with a Varian (Palo Alto, CA, USA) Model 9010 liquid chromatograph and a Rheodyne Model 7161 manual injector with a 10-μl loop. The detector was a Varian Model 9050 UV–VIS spectrophotometer set at 254 nm. An IBM Personal System/2 Model 30 286 computer and an Epson LX-400 printer were used for data aquisition and registration.

The column was a reversed-phase Spherisorb 3S TG (15 cm × 4.6 mm I.D.; particle size 3 μm), with a Spherisorb 5 ODS-2 guard column (Phase Separations, Queensferry, UK). The three solvent reservoirs contained the following eluents: (A) acetonitrile, (B) 0.01 M dipotassium hydrogenphosphate buffer solution, adjusted to pH 7 with orthophosphoric acid (85%), and (C) water. The elution programme consisted of the gradient system shown in Table I, with a flow-rate of 0.8 ml/min. Before use, the eluents were filtered through a 0.22-μm Durapore filter (Millipore) and degassed under vacuum. The eluted dansylamines were detected by monitoring the UV absorbance at 254 nm.

Amine extraction

A modification of the procedure developed by Voigt *et al.* [11] and Lovenburg and Engelman [10] was used for the extraction of all the investigated amines. A 10-g amount of ground cheese, accurately weighed into a centrifuge tube, was homogenized with 20 ml of 0.1 *M* hydrochloric acid containing a known amount of 1,7-diaminoheptane (internal standard) in a Politron homogenizer (Kinematica, Lucerne, Switzerland) at speed 5 for 1 min. The cheese slurry obtained with this step was centrifuged at about 14 000 *g* for 20 min at 4°C with a Cryofuge 20-3 centrifuge, rotor No. 8780 (Heraeus, Karlsruhe Germany). The aqueous layer was collected and the residue was re-extracted with the same procedure.

The two aqueous extracts were combined and, when necessary, filtered through a paper filter. A portion (10 ml) of this extract was saturated with solid sodium carbonate [27] (pH > 12), then an equal volume of *n*-butanol–chloroform 1:1 (v/v) was added and the mixture was blended with a horizontal orbital motion blender for 30 min. After decanting, the upper organic phase was removed, 1 ml of it was introduced into a screw-capped test-tube and two drops of 1 *M* hydrochloric acid were added.

The solution was then evaporated to dryness at ambient temperature with a Uniequip System (Uniequip, Martinsried, Munich, Germany), consisting of a centrifuge (Univapo 100 H) and a refrigerated aspirator (Uniject II). The residue was finally dissolved in 1 ml of 0.1 *M* hydrochloric acid prior to the derivatization step.

Derivative preparation

Other minor modifications to the analytical procedure [19] were introduced for the derivative preparation. A 0.5-ml volume of saturated $NaHCO_3$ solution and 1 ml of dansyl chloride reagent (5 mg/ml) were added in the same test-tube to the sample obtained from previous steps. The test-tube was sealed and the mixture was thoroughly mixed with a Vortex mixer (Tecno Vetro, Monza, Italy) for 20–30 s. The reaction mixture was then left for 1 h at 40°C, with occasional shaking. Finally, instead of extracting the mixture with several portions of diethyl ether and evaporating the combined ether extracts to dryness [19], the mixture was directly evaporated at 40°C with the Uniequip system and the residue was dissolved in 1 ml of acetonitrile for HPLC analysis.

It is assumed that the amine conversion to dansyl derivatives is complete (100%); unfortunately, at present analytical techniques for independently validating this assumption are not available.

RESULTS AND DISCUSSION

Chromatographic conditions

Different solvent mixtures and gradient programmes were tried in order to reduce the analysis time while maintaining a good resolution of all the amine peaks. The achievement of a good resolution of all the eluted peaks was made difficult by the presence of interfering peaks, probably related to the excess of dansyl chloride.

Initially, good results were obtained using as the mobile phase a mixture of acetonitrile and water with a solvent gradient. It was observed that, after a few injections, visible deterioration of the column efficiency occurred, manifested by the appearance of peak broadening and shoulders on the peaks. The replacement of water with 0.01 *M* phosphate buffer solution (pH 7) re-established the optimum column efficiency.

The solvent gradient procedure employed is reported in Table I. In order to avoid precipitation of phosphate buffer salt in the chromatographic system, occurring at acetonitrile concentrations higher than 80%, the HPLC elution computer program provides an exchange between the two reservoirs of phosphate buffer and water. It was observed that it was possible to use a solvent gradient of acetonitrile and water by washing the column every 10–20 injections with phosphate buffer for about 10 min to regenerate the column efficiency. Under these conditions all the amines were eluted in less than 13 min.

Optimization of extraction procedure

According to Voigt *et al.*'s method [11], cheese is extracted with a 0.1 *M* HCl, centrifuged and the aqueous extract is saturated with NaCl, adjusted to pH 10 with Na_2CO_3 and finally extracted with *n*-butanol. Using this procedure, some amines, in particular Put, Cad, Spd and Spm, were not extracted in detectable amounts. In order to obtain a satisfactory extraction recovery for each investigated compound, two extractions of a cheese sample with 0.1 *M* HCl were performed and the pH of the extract was increased above 12 with solid sodium carbonate.

When *n*-butanol–chloroform mixture (1:1, v/v) was used in place of *n*-butanol to accelerate subsequent solvent evaporation, no significant difference in amine recoveries was observed. Before evaporating to dryness, two drops of 0.1 *M* HCl were added to the organic extract in order to obtain amines in their ionic form (hydrochloride) to reduce their volatility. The addition of hydrochloric acid considerably improved the recovery of 2-Phe, but it reduced the recovery of Spd and Spm.

The whole procedure involves multiple steps, and for this reason the use of an internal standard (I.S.) is desirable. 1,7-Dh was chosen as the I.S. for several reasons: it has a retention time not corresponding to the other eluted components, it does not occur naturally in cheese samples and it gives good extraction recoveries.

Fig. 1 compares two different procedures: chromatogram A is for a cheese sample spiked with a known amount of each amine and extracted following the method of Voigt *et al.* [11], and chromatogram B was obtained for the same sample using the extraction method presented here. The improve-

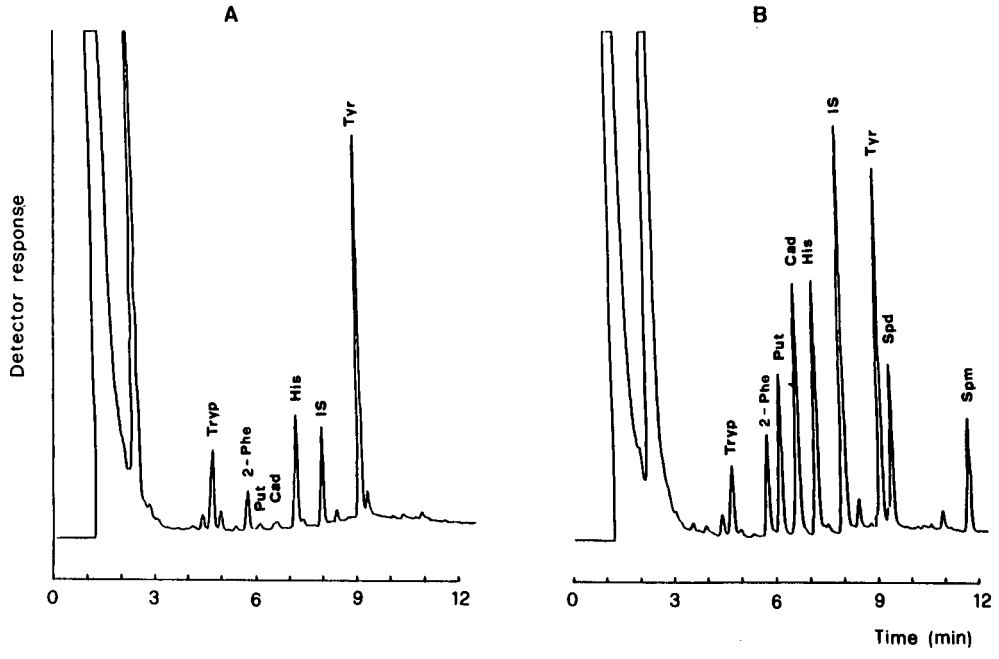

Fig. 1. Chromatograms of two aliquots of the same fortified cheese (see Table V) extracted following different procedures: (A) procedure of Voigt *et al.* [11]; (B) proposed procedure. For chromatographic conditions, see Experimental.

ment in amine recoveries with the present procedure is clear.

Linearity

In order to verify the linearity of the UV detector response at 254 nm for the working concentration of each amine, a portion of each of the five working standard solutions was derivatized and injected into the HPLC system. Calibration graphs were constructed by plotting the amine to I.S. peak-area ratios against the amine to I.S. weight ratios. Linear least-squares regression was used to calculate the slope, intercept and correlation coefficient (r^2). Data on linearity and detection limits are given in Table

TABLE II

DETECTION LIMIT AND LINEARITY

Detection limit is expressed as the amount of amine required to procedure a signal three times the background noise. Linearity data were obtained from a five-level calibration.

Amine	Detection limit (ng)	Range of linearity (ng)	Slope	Intercept	Correlation coefficient (r^2)
Tryp	0.08	6.6–829	0.4430	0.0045	0.9999
2-Phe	0.06	6.1–736	0.5073	0.0039	0.9998
Put	0.02	3.7–463	1.3995	0.0131	0.9998
Cad	0.03	4.0–503	1.1755	0.0105	0.9998
His	0.04	8.0–1003	0.9639	0.0236	0.9997
Tyr	0.02	9.0–1130	0.8682	0.0501	0.9995
Spd	0.03	4.0–503	0.9843	0.0168	0.9990
Spm	0.05	4.1–512	0.8205	0.0069	0.9989

TABLE III

INSTRUMENTAL REPEATABILITY

Results are means of ten replicates of the same sample. $\bar{x}$ = Mean; S.D. = standard deviation; R.S.D. = relative standard deviation.

Amine	$\bar{x}^a$	S.D.	R.S.D. (%)
Tryp	2.110	0.004	0.2
2-Phe	1.949	0.008	0.4
Put	0.703	0.003	0.4
Cad	0.743	0.002	0.3
His	0.986	0.005	0.5
Tyr	1.003	0.003	0.3
Spd	0.845	0.011	1.3
Spm	1.084	0.011	1.0

[a] x = [(I.S. area/standard amine area) × (standard amine concentration/I.S. concentration)].

TABLE IV

ANALYTICAL REPEATABILITY

Results are means for ten cheese samples which underwent the whole analytical procedure. For abbreviations, see Table III.

Amine	$\bar{x}^a$	S.D.	R.S.D. (%)
Tryp	2.631	0.099	3.8
2-Phe	3.516	0.076	2.2
Put	0.388	0.036	9.3
Cad	0.933	0.060	6.4
His	5.719	0.188	3.3
Tyr	21.890	0.578	2.6
Spd	0.415	0.042	10.1
Spm	0.403	0.043	10.7

[a] x = [(amine area/I.S. area)/cheese weight] × 100.

II; a linear relationship with $r^2 > 0.999$ was always obtained. The concentration ranges are representative of amine concentrations detected in cheese samples.

Repeatability

A standard solution was derivatized and the mixture was injected ten times to evaluate the repeatability of the chromatographic system. Means ($\bar{x}$), standard deviations (S.D.) and relative standard deviations (R.S.D.) of the response factors are reported in Table III.

The repeatability of the whole method was examined on a Parmigiano Reggiano cheese sample with a low amine content. Ten aliquots of the same sample were extracted with 20 ml of 0.1 *M* HCl, containing a known amount of each amine, and analysed using the proposed procedure. Results are given in Table IV.

Recovery

The recovery of the method was determined by a standard addition technique. A sample of cheese was spiked with a known amount of amine standard

TABLE V

RECOVERY

Results are means for three cheese samples which underwent the whole analytical procedure.

Amine	Amount determined in sample (mg per 100 g)	Amount of standard added (mg per 100 g)	Amount found in sample (mg per 100 g)	Recovery (%)
Tryp	ND[a]	1.66	1.17	70.5
2-Phe	0.08	1.53	1.51	93.8
Put	0.03	0.93	0.50	52.1
Cad	0.01	1.01	0.78	76.5
His	0.45	2.01	2.46	100.1
Tyr	4.20	2.26	5.35	82.8
Spd	0.01	1.01	0.64	62.7
Spm	0.04	1.02	0.43	40.6
IS	ND	3.93	3.82	97.2

[a] ND = Not detectable.

solution in triplicate. The extraction recovery was determined by carrying out the proposed procedure. To calculate the percentage recovery, concentrations determined before and after standard addition were compared. Results calculated as means of three values, and expressed as milligrams of amine per 100 g of cheese sample, are summarized in Table V together with the percentage recoveries.

We observed that the acid extracts of cheese samples were not stable. Indeed, the recoveries of some amines, particularly Put, Cad, Spd and Spm, decreased considerably after only 3 days of storage in a freezer (−18°C).

CONCLUSIONS

The proposed method appears to be suitable for the rapid detection of a relatively large number of amines in cheese samples. Both a linear response of the detector with increasing analyte concentration and good repeatability of the results were obtained. The recoveries were good for all amines except for Put, Spd and Spm. However, a compromise between optimization of amine recovery and number of biogenic amines detected had to be made, owing to the differences in the partition coefficients of amines in the extraction medium. We expect this method also to be suitable for the detection of biogenic amines in other food matrices.

ACKNOWLEDGEMENTS

This work was carried out within the framework of the Ministero dell' Agricolture e delle Foreste (MAF)-application oriented project "Moderne Strategie Lattiero-Casearie" (No. 3). To support of MAF (Italy) is gratefully acknowledged.

REFERENCES

1 E. Marley and E. Blackwell, *Adv. Pharmacol. Chemother.*, 8 (1970) 85.
2 J. A. Maga, *CRC Crit. Rev. Food Sci. Nutr.*, 10 (1978) 373.
3 W. Lovenberg, *J. Agric. Food Chem.*, 22 (1974) 23.
4 D. M. Kuhn and W. Lovenberg, in J. N. Hathcock (Editor), *Nutritional Toxicology*, Vol. I, Academic Press, New York, 1982, Ch. 13, p. 473.
5 P. Antila, *Kieler Milchwirtsch. Forschungsber.*, 35 (1983) 373.
6 U. Pechanek, G. Blaicher, W. Pfannhauser and H. Woidich, *Z. Lebensm.-Unters.-Forsch.*, 171 (1980) 420.
7 P. E. Koehler and R. R. Eitenmiller, *J. Food Sci.*, 43 (1978) 1245.
8 E. Karmas and J. L. Mietz, *Lebensm. Wiss. Technol.*, 11 (1978) 333.
9 D. Horowitz, D. Lovenberg, K. Engelman and A. Sjoerdsma, *J. Am. Med. Assoc.*, 188 (1964) 1108.
10 W. Lovenburg and K. Engelman, in D. Glick (Editor), *Methods of Biochemical Analysis*, Suppl. Vol., Interscience, New York, 1971, p. 1.
11 M. N. Voigt, R. R. Eitenmiller, P. E. Koehler and M. K. Hamdy, *J. Milk Food Technol.*, 37 (1974) 377.
12 J. W. Redmont and A. Tseng, *J. Chromatogr.*, 170 (1979) 479.
13 P. Spettoli, *Ind. Agrar.*, 9 (1971) 1.
14 B. Wortberg and G. Zieprath, *Lebensmittelchem. Gerichtl. Chem.*, 35 (1981) 89.
15 K. D. Henry Chin and P. E. Koehler, *J. Food Sci.*, 48 (1983) 1826.
16 P. Capella and E. C. Horning, *Anal. Chem.*, 38 (1966) 316.
17 W. F. Staruszkiewicz and J. F. Boun, *J. Assoc. Off. Anal. Chem.*, 64 (1981) 584.
18 S. Yamamoto, H. Itano, H. Kataoka and M. Makita, *J. Agric. Food Chem.*, 30 (1982) 435.
19 J. L. Mietz and E. Karmas, *J. Food Sci.*, 421 (1977) 155.
20 C. Buteau, C. L. Duitschaever and G. C. Ashton, *J. Chromatogr.*, 284 (1984) 201.
21 P. Antila, V. Antila, J. Matttila and H. Hakkarainen, *Milchwissenschaft*, 39 (1984) 81.
22 G. Tiecco, G. Tantillo, E. Francioso and G. De Natale, *Ind. Aliment.*, 1 (1984) 1.
23 H. M. L. J. Joosten and C. Olieman, *J. Chromatogr.*, 356 (1986) 311.
24 M. A. J. S. Van Boekel and A. P. Arentsen-Stasse, *J. Chromatogr.*, 389 (1987) 267.
25 G. Chiavari, G. C. Galletti and P. Vitali, *Chromatographia*, 27 (1989) 216.
26 S. Suzuki, K. Kobayashi, J. Noda, T. Suzuki and K. Takama, *J. Chromatogr.*, 508 (1990) 225.
27 S. T. Edwards and W. E. Sandine, *J. Dairy Sci.*, 64 (1981) 2431.

Journal of Chromatography, 591 (1992) 181–186
Elsevier Science Publishers B.V., Amsterdam

CHROM. 23 769

Amino acid analysis by high-performance liquid chromatography after derivatization with diethyl ethoxymethylenemalonate

Manuel Alaiz, José L. Navarro, Julio Girón and Eduardo Vioque*

Instituto de la Grasa y sus Derivados (CSIC), Apartado 1078, E-41012 Seville (Spain)

(First received July 12th, 1991; revised manuscript received September 20th, 1991)

ABSTRACT

Amino acids were determined by precolumn derivatization with diethyl ethoxymethylenemalonate and reversed-phase high-performance liquid chromatography (HPLC) with spectrophotometric detection at 280 nm. The reaction time was 50 min and the derivatives were stable at room temperature. Chromatographic resolution of a mixture of the derivatives of seventeen amino acids, including proline and cystine, was achieved within 35 min using a binary gradient system. The detection limit was 3 pmol. Amino acid analyses of acid hydrolysates of two proteins gave results equivalent to those obtained by conventional ion-exchange-based amino acid analysis. The simplicity of the procedure allows its use on any multi-purpose HPLC system.

INTRODUCTION

In an effort to increase instrument productivity and sensitivity with respect to amino acid analyses, several alternatives to traditional ion-exchange chromatography and postcolumn derivatization with ninhydrin have been explored [1]. For the most part, the alternative approaches rely on precolumn derivatization with hydrophobic reagents, which in turn allows rapid and efficient resolution of the derivatives by reversed-phase high-performance liquid chromatography (HPLC). Moreover, the nature of these compounds is such that the absorbance or fluorescence signals of the compounds often extend the sensitivity to the picomole or femtomole range.

The most common reagents used for amino acid derivatization in this context are *o*-phthalaldehyde [2–6], 5-dimethylaminonaphthalene-1-sulphonyl chloride [7–10], 4-dimethylaminoazobenzene-4′-sulphonyl chloride [11,12], phenyl isothiocyanate [13–15], 9-fluorenylmethyl chloroformate [16,17], 1-fluoro-2,4-dinitrobenzene [18], 1-fluoro-2,4-dinitrophenyl-5-L-alaninamide [19] and 4-N,N-dimethylaminoazobenze-4′-isothiocyanate [20]. Each of these reagents provides the general advantages associated with precolumn derivatization.

A new reagent which gives amino acid derivatives detectable in the ultraviolet region is diethyl ethoxymethylenemalonate [21]. The derivatives are easily obtained and are very stable. In this paper, we report the HPLC determination of the derivatives of all the commonly occurring L-amino acids in proteins (except those which are destroyed by acid hydrolysis). The run, using a binary elution programme, is complete in 35 min.

EXPERIMENTAL

Reagents and samples

Diethyl ethoxymethylenemalonate was obtained from Fluka (Buchs, Switzerland). Sodium acetate, sodium hydroxide, boric acid and hydrochloric acid were purchased from Panreac (Barcelona, Spain). Acetonitrile of HPLC grade was from Romil Chemicals (Loughborough, UK). Sodium azide was obtained from Merck (Darmstadt, Germany) and L-amino acids from Serva (Heidelberg, Germany). Insulin and lysozyme were purchased from

0021-9673/92/$05.00

Boehringer (Mannheim, Germany). Deionized, distilled water was used for the preparation of buffers. The buffers used for the HPLC analysis were filtered through a 0.22-μm filter (Millipore, Bedford, MA, USA). All the HPLC solvents were degassed with helium.

Instruments

The HPLC system (Waters) consisted of a Model 600E multi-solvent delivery system, a Wisp Model 712 automatic injector, a Model 484 UV–VIS detector and an APC IV NEC personal computer. Data adquisition and processing were effected with Maxima 820 3.3 version software (Waters). Separations were attained using a 300 × 3.9 mm I.D. reversed-phase column (Nova-Pack C_{18}, 4 μm; Waters). The column was maintained at 18°C by a temperature controller (Julabo F 10).

Hydrolysis

Mixtures of amino acids, or a protein, with D,L-α-aminobutyric acid as internal standard were dissolved in 6.0 *M* hydrochloric acid. The solutions were gassed with nitrogen and sealed in hydrolysis tubes under nitrogen, then incubated in an oven at 110°C for 24 h.

Derivatization

Formation of N-[2,2-bis(ethoxycarbonyl)vinyl] derivatives of mixtures of amino acids, or protein hydrolysates, was achieved as follows: to a dried sample of standard amino acid mixture, or a protein hydrolysate (2–200 μg), in 1 *M* sodium borate buffer (pH 9.0) (1 ml) containing 0.02% of sodium azide was added 0.8 μl of diethyl ethoxymethylenemalonate. The reaction was carried out at 50°C for 50 min with vigorous shaking. The resulting mixture was cooled to room temperature and 15 μl were injected into the chromatograph.

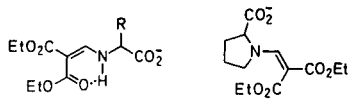

a b

Fig. 1. Derivatives obtained in the reaction of diethyl ethoxymethylenemalonate with amino acids. (a) R = characteristic lateral chain of each amino acid, except proline; (b) derivative of proline. Et = Ethyl.

Chromatography

Resolution of the amino acid derivatives was routinely accomplished using a binary gradient system. The solvents used were (A) 25 m*M* sodium acetate containing 0.02% of sodium azide (pH 6.0) and (B) acetonitrile. Solvent was delivered to the column at a flow-rate of 0.9 ml/min as follows: Time 0.0–3.0 min, linear gradient from A–B (91:9) to A–B (86:14); 3.0–13.0 min, elution with A–B (86:14);

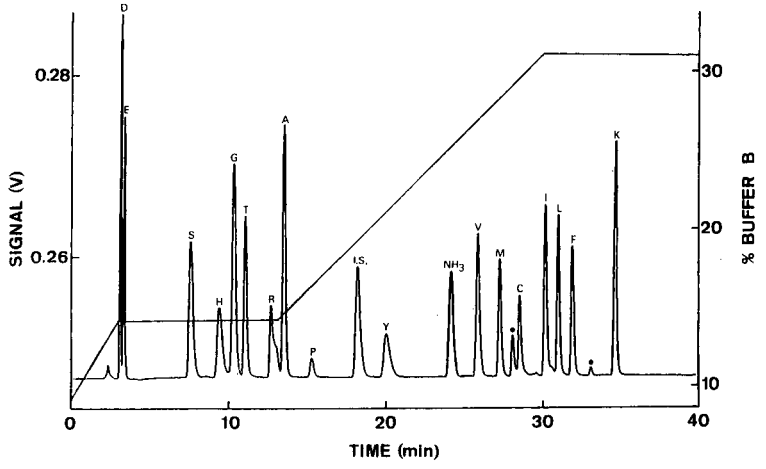

Fig. 2. Elution pattern of a standard amino acid mixture chromatographed as described in the text. The amount of each standard N-[2,2-bis(ethoxycarbonyl)vinyl]amino acid present in the mixture ranged from 50 to 200 pmol, except proline (300 pmol). Peaks are labelled with single-letter notations for amino acids. I.S. = D,L-α-aminobutyric acid (internal standard); ❶ = unidentified peaks.

13.0–30.0 min, linear gradient from A–B (86:14) to A–B (69:31); 30.0–35.0 min, elution with A–B (69:31).

RESULTS AND DISCUSSION

Fig. 1 shows the structures of the derivatives obtained in the reaction of L-amino acids with diethyl ethoxymethylenemalonate.

Reversed-phase HPLC resolution of the N-[2,2-bis(ethoxycarbonyl)vinyl] derivatives of seventeen commonly occurring L-amino acids is shown in Fig. 2. The 2,2-bis(ethoxycarbonyl)vinyl group provided not only the neccesary interactions with the apolar stationary phase but also a high absorptivity for easy spectrophotometric detection at 280 nm [21]. Another characteristic of this derivatization that should be noted is the absence of the reagent peak in the chromatogram because the diethyl ethoxymethylenemalonate has an absorption maximum at 240 nm. The derivatization blank did not give any peak. The limit of detection was 3 pmol with a signal-to-noise ratio of 5. The identity of each peak was established either by adding a threefold molar excess of the amino acid in question, or by omitting the amino acid from the standard mixture. Lysine and cystine were separated as disubstituted derivatives. Analysis of individual amino acids standards allowed the identification of the unknown peak with a retention time of 28.10 min produced in cystine hydrolysis. Direct derivatization of cystine standard without hydrolysis did not afford this peak. Although the separation between aspartic and glutamic acids seems to be too close, the retention times of the peaks show good repeatability and allow reliable integration of the areas.

The derivatization of free amino acids with diethyl ethoxymethylenemalonate is easy and quantitative, and the N-[2,2-bis(ethoxycarbonyl)vinyl] derivatives are stable for several weeks at room temperature [21]. Response factors for all derivatives were calculated from calibration runs employing 10–2000 pmol of amino acid, using D,L-α-aminobutyric acid as an internal standard. The response was found to be linear in all instances (correlation coefficient $\geqslant 0.996$). Fig. 3 shows a typical calibration graph for the range 10–1000 pmol for glycine. The derivatives of aspartic acid, glycine, isoleucine and

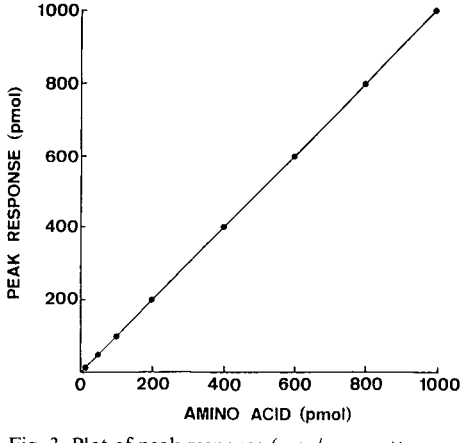

Fig. 3. Plot of peak response (area/area$_{I.S.}$ × amount of I.S.) of N-[2,2-bis(ethoxycarbonyl)vinyl] derivative for glycine. Each point represents the mean of five different analyses.

TABLE I

RETENTION TIMES AND RESPONSE FACTORS FOR N-[2,2-BIS(ETHOXYCARBONYL)VINYL] DERIVATIVES OF AMINO ACIDS

Amino acid	Retention time (min)[a]	Response factor
Aspartic acid	3.10	1.00
Glutamic acid	3.31	1.04
Serine	7.48	0.96
Histidine	9.35	0.92
Glycine	10.25	1.00
Threonine	11.02	1.02
Arginine	12.66	0.98
Alanine	13.45	1.03
Proline	15.25	0.04[b]
D,L-α-Amino butyric acid	18.15	1.00[c]
Tyrosine	20.05	0.91
Ammonia	24.21	–
Valine	25.84	1.04
Methionine	27.22	0.92
Cystine	28.52	1.08
Isoleucine	30.19	1.00
Leucine	31.02	1.00
Phenylalanine	31.95	0.95
Lysine	34.73	1.86

[a] Values represent averages determined from twenty standard chromatograms with a standard deviation of 0.1 min for each compound.

[b] The lowest response factor of the compounds evaluated; this is due to its different structure (Fig. 1).

[c] 1 pmol of D,L-α-aminobutyric acid (internal standard) represents 1380 μV s.

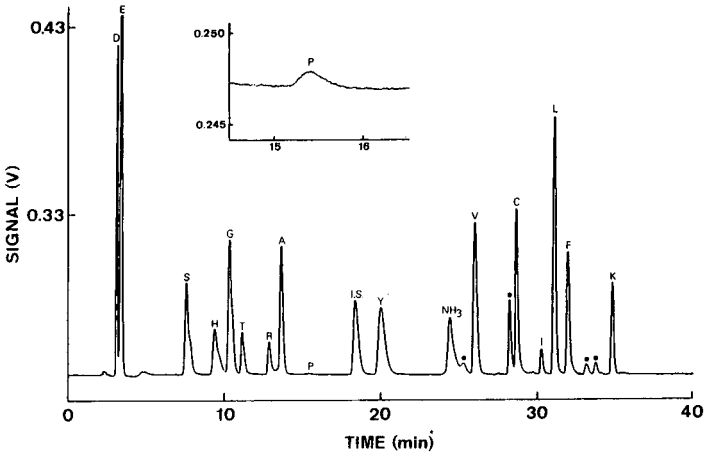

Fig. 4. Elution pattern of N-[2,2-bis(ethoxycarbonyl)vinyl] derivatives in an insulin hydrolysate. The sample contained 9488 pmol of amino acids and 617 pmol of internal standard. Peaks are designated as in Fig. 2.

leucine essentially follow the same line. The slope, 1.00, represents the response factor.

Table I summarizes the retention times and response factors for the N-[2,2-bis(ethoxycarbonyl) vinyl] derivatives evaluated.

After the verification of the method using several mixtures of amino acid standards with different compositions, its applicability to the determination of amino acids in a protein hydrolysate was assessed by the determination of the amino acid compositions of insulin and lysozyme (Figs. 4 and 5). The results agreed with those obtained with a conventional amino acid analyser based on ion-exchange chromatography and were equivalent to the reported values (Table II).

Several widely used methods for amino acid analysis have lower detection limits [13–17] and some of them shorter derivatization [2–10, 13–18] or analysis times [2–17] than the method presented here. However, many of them have disadvantages such as the use of unstable derivatives [2–10, 13–15], the presence of reagent or reagent-derived peaks in the

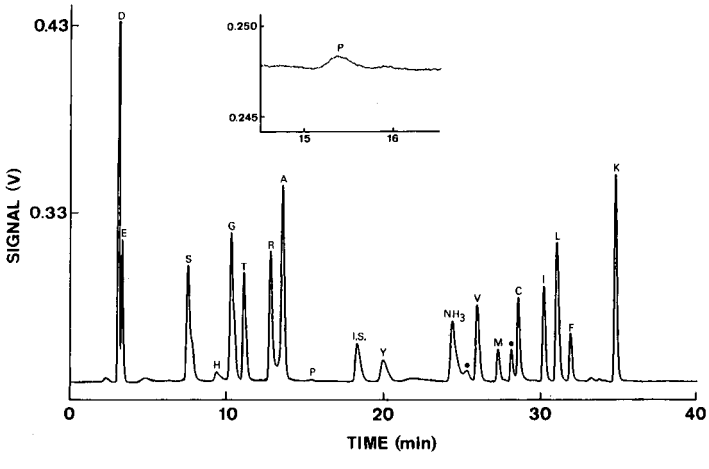

Fig. 5. Elution pattern of N-[2,2-bis(ethoxycarbonyl)vinyl] derivatives in a lysozyme hydrolysate. The sample contained 9188 pmol of amino acids and 308 pmol of internal standard. Peaks are designated as in Fig. 2.

TABLE II

AMINO ACID COMPOSITIONS OF PROTEINS DETERMINED BY THE DESCRIBED HPLC METHOD AND BY CONVENTIONAL ION-EXCHANGE CHROMATOGRAPHY (IEC)

Amino acid	Insulin[a,b]			Lysozyme[a,c]		
	Present	HPLC	IEC[d]	Present	HPLC	IEC[e]
Aspartic acid	3	3.0	2.9	21	20.0	22.2
Glutamic acid	7	6.8	6.8	5	5.1	5.2
Serine	3	3.1	2.8	10	9.9	8.1
Histidine	2	2.1	1.8	1	1.1	0.8
Glycine	4	4.0	4.0	12	11.6	12.5
Threonine	1	1.0	2.8	7	6.9	6.2
Arginine	1	0.9	1.1	11	9.9	11.6
Alanine	3	3.1	1.1	12	12.4	12.0
Proline	1	1.0	1.0	2	1.9	2.4
Tyrosine	4	4.0	3.7	3	3.2	3.5
Valine	5	4.3	3.0	6	5.6	5.3
Methionine	0	0.0	0.0	2	2.4	1.8
Cystine (half)	6	6.4	4.9	8	8.1	6.6
Isoleucine	1	0.6	1.2	6	5.7	5.0
Leucine	6	6.1	5.9	8	9.8	8.3
Phenylalanine	3	3.2	2.8	3	3.0	2.8
Lysine	1	1.0	1.0	6	6.1	5.3

[a] For hydrolysis and derivatization, see Experimental.
[b] Residues per 51 total residues.
[c] Residues per 123 total residues.
[d] Ion-exchange on a Durrum 500 column provided by J. Johansen, Carlsberg Bio Tech, Carlsberg, Sweden.
[e] See ref. 22.

chromatograms [7–20] or extra steps (*e.g.*, extraction, concentration and evaporation) in sample processing after the derivatization reaction [7–20].

The present derivatization reaction is clean (no side-reaction products have been observed) and the shift in the absorbance maximum from 240 to 280 nm on derivatization provides a novel means for eliminating the interference from excess of reagent. These aspects, in addition to the stability and the good chromatographic behaviour of the N-[2,2-bis (ethoxycarbonyl)vinyl] derivatives in reversed-phase HPLC, make possible an easy and reproducible derivatization, injection and elution process.

In conclusion, the derivatization of amino acids with diethyl ethoxymethylenemalonate and their subsequent reversed-phase HPLC is recommended as an alternative to the dedicated amino acid analyser when subpicomole sensitivity is not required.

ACKNOWLEDGEMENTS

This study was supported in part by the Comisión Interministerial de Ciencia y Tecnología (Project ALI 88-0169) and the Junta de Andalucía (Project 2075). We thank Drs. F. J. Hidalgo, R. Zamora and F. Millán for helpful discussions.

REFERENCES

1 R. W. Zumbalt and C. W. Gehrke, in J. P. Cherry and R. A. Barford (Editors), *Amino Acids Analysis: a Survey of Current Techniques*, American Oil Chemists' Society, Champaign, IL, 1988, p. 13.
2 P. Lindroth and K. Mopper, *Anal. Chem.*, 51 (1979) 1667.
3 B. N. Jones and J. P. Gilligan, *J. Chromatogr.*, 266 (1983) 471.
4 B. N. Jones, S. Pabbo and S. Stein, *J. Liq. Chromatogr.*, 4 (1981) 565.
5 J. P. H. Burback, A. Prins, J. L. M. Leboville, J. Verhoef and A. Witter, *J. Chromatogr.*, 237 (1982) 339.
6 H. W. Jarrett, K. D. Cooksy, B. Ellis and J. M. Anderson, *Anal. Biochem.*, 153 (1986) 189.

7 E. Bayer, E. Grom, B. Kaltenegger and R. Uhman, *Anal. Chem.*, 48 (1976) 1106.
8 N. Kaneda, M. Sato and K. Yagi, *Anal. Biochem.*, 127 (1982) 49.
9 C. De Jong, G. J. Hughes, E. Van Wieringen and K. J. Wilson, *J. Chromatogr.*, 241 (1982) 345.
10 Y. Tapuhi, D. E. Schmidt, W. Lindner and B. L. Karger, *Anal. Biochem.*, 115 (1981) 123.
11 J.-Y. Chang, R. Knecht and G. Broun, *Biochem. J.*, 199 (1981) 547.
12 V. Stocchi, G. Piccoli, M. Magnani, F. Palma, B. Biagiarelli and L. Cucchiarini, *Anal. Biochem.*, 178 (1989) 107.
13 R. I. Heinrikson and S. C. Meredith, *Anal. Biochem.*, 136 (1984) 65.
14 S. A. Cohen and D. J. Strydom, *Anal. Biochem.*, 174 (1988) 1.
15 R. F. Ebert, *Anal. Biochem.*, 154 (1986) 431.
16 S. Einarsson, B. Josefsson and S. Lagerkvist, *J. Chromatogr.*, 282 (1983) 609.
17 R. Cunico, A. G. Mayer, C. T. Wehr and T. L. Sheehan, *Biochromatography*, 1 (1986) 6.
18 R. C. Morton and G. E. Gerber, *Anal. Biochem.*, 170 (1988) 220.
19 S. Kochhar and P. Christen, *Anal. Biochem.*, 178 (1989) 17.
20 J.-Y. Chang, P. Martin, R. Bernasconi and D. G. Braun, *FEBS Lett.*, 132 (1981) 117.
21 M. Alaiz, J. Girón, F. J. Hidalgo, M. P. Maza, F. Millán, R. Zamora and E. Vioque, *Synthesis*, (1989) 544.
22 S.-H. Chiou and K.-T. Wang, *J. Chromatogr.*, 491 (1989) 424.

Journal of Chromatography, 591 (1992) 187–193
Elsevier Science Publishers B.V., Amsterdam

CHROM. 23 808

Rapid isolation of human complement component C9 to verify the specificity of a haemolytic C9 microassay☆

Hester J. Bootsma, Carmen W. van den Berg and Hans van Dijk*

Eijkman–Winkler Laboratory of Medical Microbiology, Section of Experimental Microbiology, University Hospital G04.614, P.O. Box 85 500, NL-3508 GA Utrecht (Netherlands)

(First received May 13th, 1991; revised manuscript received October 4th, 1991)

ABSTRACT

A sensitive, haemolytic microassay of human complement component C9 was developed. The assay is based on the principle of reactive (C5b6-initiated) haemolysis and uses commercially available C9-depleted serum as reagent for C9. The specificity of the assay was verified by rapid, activity-guided isolation of the haemolytic component from human serum using high-performance liquid chromatography (HPLC) on a system for fast protein liquid chromatography. This isolation yielded a single component with characteristics of C9. The results suggest that rapid, activity-guided isolation as a new application of HPLC can be a useful tool to demonstrate the specificity of a functional assay.

INTRODUCTION

C9 is the last complement (C) component participating in the generation of membrane attack complexes (MAC). It is a single-chain glycoprotein with a relative molecular mass (M_r) of 66 000–71 000 [1,2]. During activation, the component is oligomerized by C5b-8 complexes formed as a consequence of classical and/or alternative C pathway activation. Despite the presumed role of C9 in completing MAC, C9-deficient subjects show substantial classical complement pathway activity in *in vitro* assays using antibody-coated sheep erythrocytes as target cells [3]. This implies that lysis of sheep erythrocytes via the classical C pathway as used by others [1,4] is not the optimum system to determine C9 activity [5]. We therefore searched for other principles that could be applied for the functional assay of C9. C5b6-mediated (reactive) lysis [6] of chicken erythrocytes was tested for suitability. C5b6, prepared by incubating human serum with inulin [7], was combined with low concentrations of commercially available C9-depleted serum as reagent for C9 (R9). The mixture appeared to be a very useful and sensitive tool for determining functional C9 in human serum.

To test the specificity of the method developed, the haemolytic component(s) was (were) isolated from human serum on the basis of activity in the assay. To this end, a rapid separation procedure was developed based on stepwise polyethylene glycol (PEG) precipitation followed by high-performance liquid chromatography (HPLC) on hydroxyapatite (HA), anion-exchange and gel permeation chromatographic columns using an instrument for fast protein liquid chromatography. The identity of the isolated component was confirmed by polyacrylamide gel electrophoresis.

EXPERIMENTAL

Buffers

Veronal-buffered (25 m*M*) saline (750 m*M*) of pH 7.35 ± 0.05 (VSB-5x) [8,9] served as a five-times concentrated stock solution for the preparation of VSB^0, VSB^0-gel (containing 0.1% gelatine and heated at 56°C for 15 min) and EDTA-VB (containing 10 m*M* EDTA).

☆ Presented at the *Fourth FPLC Symposium, Maarssen, Netherlands, March 26th, 1991.*

0021-9673/92/$05.00

Cells

Chicken blood, diluted 50% in Alsever's old solution (114 m*M* citrate–27 m*M* glucose–72 m*M* NaCl, pH 6.1) was obtained from BioTrading (Wilnis, Netherlands) and was used as a source of erythrocytes (ChE). The ChE were stored at 4°C for at least 2 weeks before use. The cells were washed three times with saline (4000 *g*, room temperature, 8 min) before use.

Sera

Human AB serum from a rhesus-positive individual (HS) was obtained from the central blood bank in Utrecht and used as source of either C5 and C6 or C9.

C9-depleted normal HS (R9) was obtained from Cytotech (San Diego, CA, USA) and used as source of C7 and C8.

Functional assay of human C9

Preparation of human C5b6 [7]. Inulin (obtained from BDH, Poole, UK) was washed once with VSB^0 (2500 *g*, room temperature, 10 min). HS (1 ml per 5 mg of inulin) was added to the pellet and the mixture was incubated at 37°C for 30 min. Subsequently, the suspension was chilled on ice, spun (2500 *g*, 4°C, 10 min) and the pellet was washed once with ice-cold VSB^0-gel. After this wash, the pellet was reconstituted in VSB^0 and incubated at 37°C for 30 min. The inulin was removed by centrifugation (4000 *g*, room temperature, 10 min) and the supernatant (containing C5b6) was used directly or after storage in small aliquots at −70°C.

Preparation of ChEC5b6 cells (EC5b6). EC5b6 were prepared by incubating 3×10^8 of ChE per ml of EDTA-VB (4% suspension) with the same volume of C5b6 at 37°C for 45 min. EC5b6 were kept at 4°C until use.

Functional assay of human C9. A variant of the microassay as described by Klerx *et al.* [10] for classical and alternative pathway activation was used. The test was performed in U-welled microtitre plates. Unless stated otherwise, R9 was diluted 1:100 in EDTA-VB before use. A 50-μl volume of R9 was mixed with 50 μl of EC5b6 and a similar volume of C9-containing sample. After incubation at 37°C for 60 min, the remaining cells and ghosts were spun down (2000 *g*, room temperature, 10 min), and 50 μl of the supernates were transferred to flat-bottomed microtitre plates containing 200 μl of water per well. Lysis was read at 405 nm in a Titertek Multiskan PLUS apparatus (Flow Labs., McLean, VA, USA). A mixture of 50 μl of EC5b6 and 100 μl of water served as 100% lysis control.

C9-containing samples were routinely tested in one concentration. For quantification purposes, duplicate dilution series of C9-containing samples were used. C9 activity was expressed in units corresponding to the amount of serum giving rise to 50% haemolysis.

Isolation procedure

The procedure developed to isolate C9 was essentially an HPLC adaptation of existing methods published by Biesecker and Müller-Eberhard [1] and DiScipio and Hugli [2]. The procedure was executed on a system for fast protein liquid chromatography equipped with an LCC-500 controller (Pharmacia, Uppsala, Sweden). To improve the separation characteristics of the procedure, chromatography on hydroxyapatite was performed before anion-exchange chromatography. All purification steps were carried out between 2 and 4°C.

– *Buffers.* All separation buffers contained 1m*M* phenylmethyl sulphonylfluoride (PMSF) (Sigma, St. Louis, MO, USA) taken from a stock solution of 100 m*M* PMSF in isopropanol. The starting buffer for Mono Q and hydroxyapatite chromatography consisted of 5 m*M* veronal and 100 m*M* NaCl (pH 7.0). Phosphate buffers were prepared with Na_2HPO_4 and KH_2PO_4. Before use, all buffers were filtered through 0.22-μm filters (Millipore, Bedford, MA, USA) and degassed.

– *Polyethylene glycol precipitation.* HS was mixed with a double volume of 12% (w/v) PEG 4000 (BDH) in EDTA-VB and centrifuged at 4000 *g* and 4°C for 1 h. The precipitate was discarded and the PEG concentration in the supernatant was increased to, unless mentioned otherwise, 16% (w/v). The mixture was centrifuged again at 4000 *g* and 4°C for 1 h. The serum PEG precipitate (8–16%) was reconstituted in starting buffer and filtered through an Acrodisc 0.2-μm filter (Gelman, Ann Arbor, MI, USA).

– *Hydroxyapatite chromatography.* Hydroxyapatite (HA) was obtained from Calbiochem (La Jolla, CA, USA). It was poured into a Pharmacia HR 10/10 column and was equilibrated with starting

buffer. After application of 8–16% PEG precipitate of HS, the column was washed with 15 ml of starting buffer. The column was then equilibrated with 15 ml of 80 m*M* phosphate buffer (pH 7.7). C9 was eluted at a flow-rate of 0.5 ml/min (fraction size 2 ml) with 40 ml of 300 m*M* phosphate buffer (pH 7.7), forming a linear phosphate gradient. Fractions containing functional activity were pooled.

– *Dialysis.* The pooled fractions were dialysed against 1 l of starting buffer for 4 h.

– *Mono Q anion-exchange chromatography.* The pooled HA material was loaded on a Mono Q column (Type HR 5/5) (Pharmacia) and eluted with a linear NaCl concentration gradient from 100 to 500 m*M* in 5 m*M* veronal. The flow-rate was 1.0 ml/min and the fraction size 1 ml. Before testing, fractions were diluted 1:3 in EDTA-VB. Fractions containing C9 activity were pooled.

– *Superose 12 gel permeation chromatography.* Further purification was performed on a 24 ml Superose 12 column (Type HR 10/30) (Pharmacia) using EDTA-VB as eluent. The flow-rate was 0.3 ml/min and the fraction size 1 ml.

Sodium dodecyl sulphate–polyacrylamide gel electrophoresis (SDS-PAGE)

The purity of fractions was checked by SDS-PAGE (12.5% gel) according to Laemmli [11]. The gels were developed by a silver staining method [12].

Protein determination

Protein concentrations were determined by the Bradford method [13] using BSA (Sigma) as reference.

Statistics

Vertical bars in the figures represent the arithmetic mean ± the standard error of the mean (S.E.M.). Differences from *P* values of <0.05 were considered to be statistically significant.

RESULTS

A functional assay of human C9 was developed. The assay is based on the lysis of chicken erythrocytes in EDTA by limiting amounts of C9 and excess of both C5b6 and commercially available C9-depleted human serum (R9) as source of C7 and C8. The optimum conditions for the C9 assay were studied by varying the concentrations of both R9 and human serum (HS; source of C9). As shown in Fig. 1, the dose–response curve for R9 showed a biphasic course with an optimum at 0.5 μl; higher concentrations of R9 were inhibitory, probably owing to the presence in serum of a terminal route inhibitor. In further experiments, 0.5 μl of R9 (50 μl, diluted 1:100) per well was used. At this concentration of R9, the optimum amount of HS was determined. Fig. 2A and B show that lysis in the C9 assay again followed a biphasic course, in this instance with an optimum at 160 nl. At low doses (5–160 nl per well) lysis appeared to be linearly dependent on the amount of HS. In some individual sera the optimum was at 50 nl.

To demonstrate the specificity of the assay, C9 was isolated from HS by HPLC on the basis of its haemolytic activity. The following separation techniques were used successively: fractionated PEG precipitation, HA chromatography, Mono Q anion-exchange chromatography and Superose 12 gel permeation chromatography. On stepwise PEG precipitation, no haemolytic activity was recovered in precipitates prepared with percentages of PEG below 8 (not shown), whereas most of the activity was precipitated between 8 and 16% PEG (Fig. 3). Above 16% PEG a slight decrease in activity was observed, probably due to the coprecipitation of a terminal route inhibitor and/or to residual PEG in the precipitate (inhibitory at final test concentra-

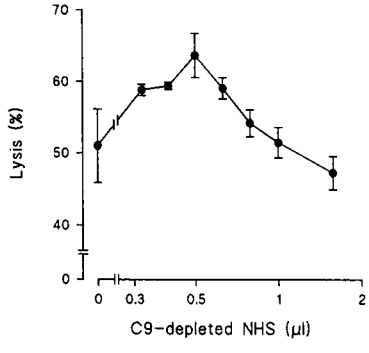

Fig. 1. Dose–effect curve for C9-depleted serum in the presence of a constant amount (50 nl) of human serum in the C9 assay. Circles and vertical bars represent the mean ± S.E.M. ($n=2$–4). The difference between the values obtained with 0 and 0.5 μl of C9-depleted NHS is statistically significant ($p<0.05$). The same holds for the decreased haemolysis above 0.8 μl of C9 reagent ($P<0.025$).

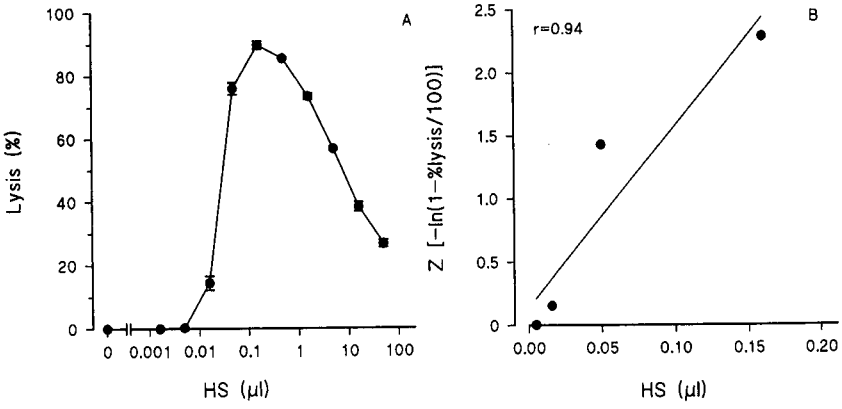

Fig. 2. Dose–effect curve for human serum when tested in the C9 assay in the presence of 0.5 µl of C9-depleted serum (left-hand panel; $n = 2$). The right-hand panel shows the kinetics after transformation to "active sites per cell" [$-\ln(1 - \%\text{lysis}/100)$] according to Borsos and Rapp [14]. The values for 0.016, 0.05 and 0.16 µl of HS are significantly enhanced in comparison with 0, 0.0016 and 0.005 µl ($P < 0.001$). The decrease in activity at serum doses above 0.16 µl is also significant ($P < 0.025$).

tions of >1%; not shown). On the HA column, haemolytic activity was eluted at phosphate concentrations between 130 and 300 m*M* (Fig. 4). On Mono Q separation, haemolytic activity was recovered in fractions containing 190–320 m*M* NaCl (Fig. 5). The final chromatographic step on Superose 12 (24-ml column) showed that the haemolytic component was present in the 13th and 14th 1-ml fractions, and in lower concentration in the 15th fraction (Fig. 6). The three active Superose 12 fractions were qualitatively analysed by SDS-PAGE. Fraction 14 showed a single band (Fig. 7), corresponding to an M_r of 74 000. Summarized separation characteristics are given in Table I.

Finally, the distribution of C9 levels in a normal population was studied. To this end, serum samples from 38 healthy students were tested in triplicate. The titres showed a slightly unequal distribution pattern with some deviants at higher levels. Minimum, median, mean and maximum values were 3248, 11 446, 13 741 and 35 313 units/ml, respectively (Fig. 8). The detection limit was 20 units/ml.

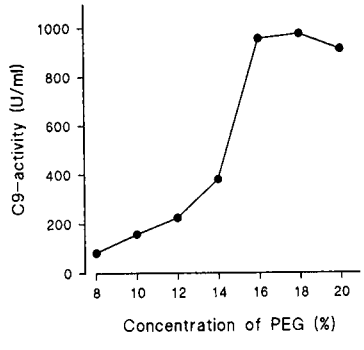

Fig. 3. PEG-precipitation characteristics of functional C9 in human serum. An 8% PEG supernatant of HS was incubated and spun (4000 *g*, 4°C, 1 h) with the indicated percentage of PEG. The precipitates were reconstituted in EDTA-containing buffer and tested for functional activity in the C9 assay.

DISCUSSION

A novel, haemolytic microassay for determining C9 activity in human serum and serum fractions was developed. The assay is based on the lysis of chicken erythrocytes by C9 and an excess of C5b6 and C9-depleted serum (R9) in EDTA. The C9-assay is specific, as it follows first-order kinetics (Fig. 2B) [14], and purification of the functional molecule from human serum yields a single protein with an apparent M_r of 74 000. This is in the range of known M_rs of human C9 [1,2]. The method is also sensitive, as test samples can be applied in high dilution. As the mean C9 level in the population is about 60 µg/ml [15] and the mean level in a random sample of the population was determined to be 13 741 units/ml, the detection limit of the assay (20 units/ml; 0.1%) is about 90 ng/ml. This limit is of

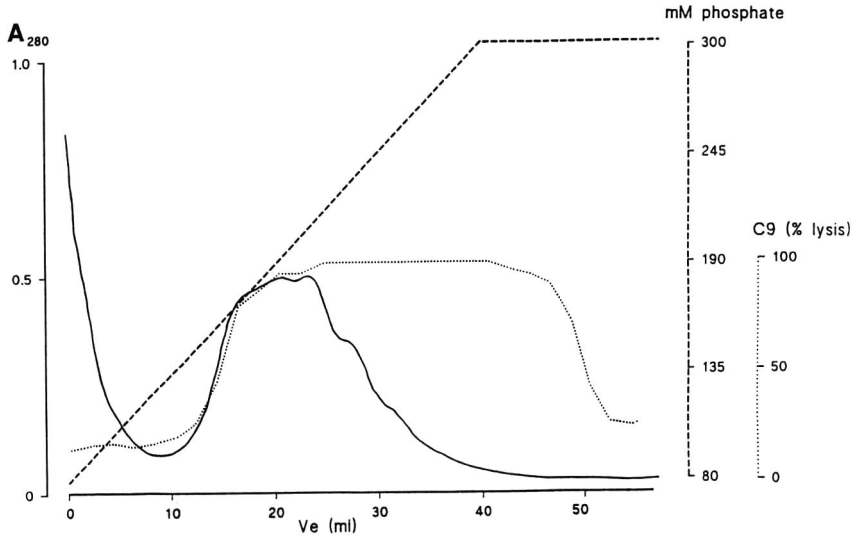

Fig. 4. Elution profile of the 8–16% PEG precipitate on hydroxyapatite chromatography. Fractions were tested for haemolytic activity in the C9 assay.

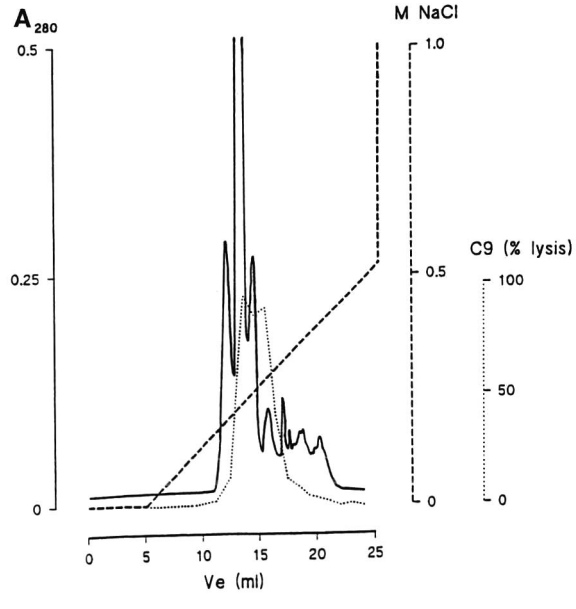

Fig. 5. Elution profile of pooled hydroxyapatite fractions on Mono Q. Fractions were diluted 1:3 in EDTA-VB and tested for haemolytic activity in the C9 assay.

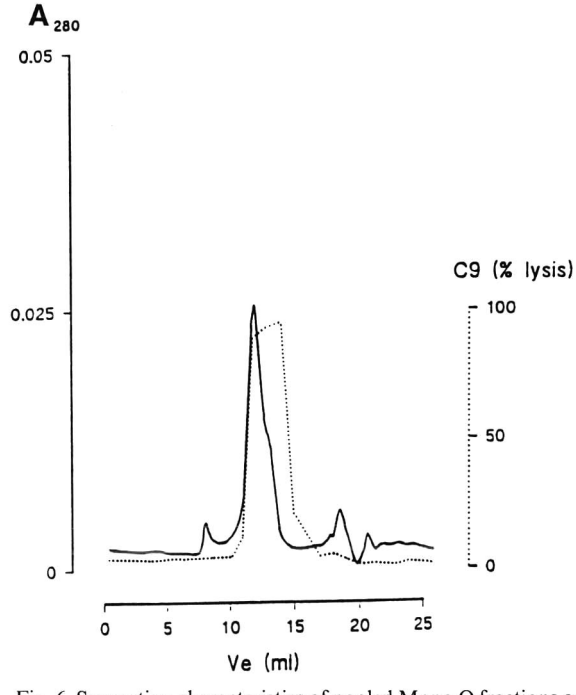

Fig. 6. Separation characteristics of pooled Mono Q fractions on Superose 12. Fractions were tested for haemolytic activity in the C9 assay.

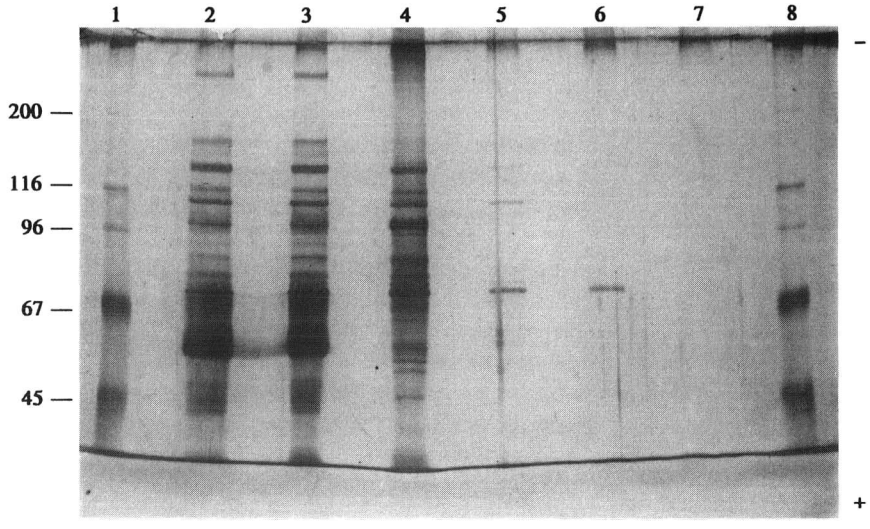

Fig. 7. SDS-PAGE under reducing conditions of C9-containing fractions at different steps of the isolation procedure. Lanes: 1 and 8 = M_r markers (M_r indicated $\times 10^{-3}$); 2 and 3 = pooled hydroxyapatite fractions before and after dialysis; 4 = pooled Mono Q fraction; 5–7 = Superose 12 fraction 13–15.

the same order of magnitude as that of other haemolytic C9 assays used to determine C9 deficiency in patients with meningococcal meningitis [16]. The detection limit of immunochemical assays varies between 100-times higher [16] and 180-times lower [17] than that of the present assay. Finally, the proposed test is easily accessible and inexpensive, because isolated C components are not required, all reagents are commercially available and the most expensive reagent, C9-depleted serum, is needed in only a 0.5-μl amount per well.

TABLE I

YIELDS OF FUNCTIONAL C9 AT THE DIFFERENT STAGES OF THE ISOLATION PROCEDURE

Fraction	Specific activity (U/mg)[a]	Yield (%)	Purification factor
Human serum	866	100	1
8–16% PEG	1479	33	1.7
Hydroxyapatite	41 275	15	48
Mono Q	125 632	10	145
Superose 12	333 492	5	385

[a] Functional C9 was measured by the lysis of chicken erythrocytes (7.5×10^6 per well) in the presence of an excess of inulin-generated human C5b6 and 1:300 diluted C9-depleted human serum.

Other functional C9 assays are based on classical C pathway activation and use either isolated C components [1], C8-depleted serum and isolated C8 [5] or 5 μl of C9-depleted human serum per test-tube [4]. Classical pathway activation, however, has the disadvantage that sera from C9-deficient subjects show considerable C8-dependent background activity (3,5], which does not occur in our assay. Other workers [17] use immunochemical C9 assays that detect antigenic, but not necessarily functional, C9.

The reason for the very low background values in our assay may be the use of chicken erythrocytes as target cells. Chicken, unlike sheep, erythrocytes belong to the very few target cells that are sensitive to

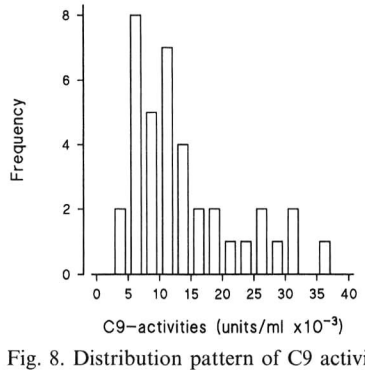

Fig. 8. Distribution pattern of C9 activities as determined in a group of 38 healthy students (20–27 years of age).

human C5b6-initiated or "reactive" lysis [7,18]. The resistance of sheep erythrocytes to reactive lysis by human complement therefore points to a functional cross-reactivity of human and sheep erythrocytes at the level of one of the late complement inhibitors (LCI; C8-binding protein and/or CD59 [19,20]). Recently, we succeeded in showing immunogenic cross-reactivity between human and sheep erythrocytes at that level [21]. This means that sheep erythrocytes could boost an LCI-neutralizing antibody response in mice induced by immunization with human erythrocytes and *vice versa*. In those experiments the anti-LCI antibodies were measured by a functional assay based on the lysis of human erythrocytes by cobra venom factor-activated, homologous complement. Because of the cross-reactivity between human and sheep LCI, the contribution of C9 to lysis of sheep erythrocytes may be relatively low, resulting in a co-determination of C8 in functional C9 assays using these erythrocytes as target cells [1,4,5]. The absence of cross-reactive LCI on chicken erythrocytes may therefore be the explanation for the high sensitivity of these cells to haemolysis by human C9 and their relative resistance to human C8.

The main purpose of isolating C9 from human serum was to show the specificity of the C9 assay. Therefore, a rapid HPLC adaptation of existing methods [1,2] was used. Using this isolation procedure, one fraction was obtained with functional activity and containing a single protein as judged by SDS-PAGE. In this sense, the fast protein isolation procedure for human C9 developed was very successful. For preparative purposes, however, the procedure might not be entirely optimal and could need some adaptation.

The M_r of the functionally active C9 as described in this paper (74 000) is slightly higher than those found by other workers (71 000) [1,22] or 68 000 [2,23]. By gel permeation chromatographic analysis of human C9, however, a higher M_r (80 000) [23], 79 000 [24] or 78 000 [25] is found.

The unequal distribution pattern of C9 levels in the population as observed with our haemolytic assay and especially the higher deviants may be attributed to the ability of C9 to behave as an acute phase reactant [26–28].

In conclusion, our results suggest that rapid, activity-guided isolation of a component by, *e.g.*, HPLC may in general be a fruitful approach to the determination of the specificity of a functional assay for the component involved.

REFERENCES

1 G. Biesecker and H. J. Müller-Eberhard, *J. Immunol.*, 124 (1980) 1291.
2 R. G. DiScipio and T. E. Hugli, *J. Biol. Chem.*, 260 (1985) 14802.
3 T. F. Lint, H. J. Zeitz and H. Gewurz, *J. Immunol.*, 125 (1981) 2252.
4 S. S. Asghar, H. Siem and H. J. van der Helm, *Clin. Chim. Acta*, 165 (1987) 387.
5 A. F. Esser and J. M. Sodetz, *Methods Enzymol.*, 162 (1988) 551.
6 R. A. Thompson and D. S. Rowe, *Immunology*, 14 (1968) 745.
7 M. D. P. Boyle, A. P. Gee, M. Okada and T. Borsos, *J. Immunol.*, 125 (1980) 2818.
8 H. van Dijk, P. M. Rademaker and J. M. N. Willers, *J. Immunol. Methods*, 39 (1980) 257.
9 H. van Dijk, P. M. Rademaker, J. P. A. M. Klerx and J. M. N. Willers, *J. Immunol. Methods*, 85 (1985) 233.
10 J. P. A. M. Klerx, C. J. Beukelman, H. van Dijk and J. M. N. Willers, *J. Immunol. Methods*, 63 (1983) 215.
11 U. K. Laemmli, *Nature (London)*, 277 (1970) 680.
12 J. H. Morrisey, *Anal. Biochem.*, 117 (1981) 307.
13 M. M. Bradford, *Anal. Biochem.*, 72 (1976) 248.
14 T. Borsos and H. J. Rapp, *J. Immunol.*, 91 (1963) 851.
15 K. Rother and G. O. Till, *The Complement System*, Springer, Berlin, 1988, p. 1.
16 M. Nagata, T. Hara, T. Aoki, Y. Mizuno, H. Akeda, S. Inaba, K. Tsumoto and K. Ueda, *J. Pediatr.*, 114 (1989) 260.
17 Y. Takata, T. Moriyama, Y. Fukumori, A. Yoden, M. Shima and S. Inai, *J. Immunol. Methods*, 117 (1989) 107.
18 P. J. Baker, T. F. Lint, B. C. McLeod, C. L. Behrends and H. Gewurz, *J. Immunol.*, 114 (1975) 554.
19 S. Schönemark, E. W. Rauterberg, M. L. Shin, S. Löke, D. Roelcke and G. M. Hänsch, *J. Immunol.*, 136 (1986) 1772.
20 A. Davies, D. L. Simmons, G. Hale, R. A. Harrison, H. Tighe, P. J. Lachmann and H. Waldmann, *J. Exp. Med.*, 170 (1989) 637.
21 H. J. Bootsma and H. van Dijk, in preparation.
22 J. Tschopp, S. Engel and E. R. Podack, *J. Biol. Chem.*, 259 (1984) 1922.
23 G. M. Hänsch, G. Rummel and F. Gänzler, *Complement*, 1 (1984) 116.
24 U. Hadding and H. J. Müller-Eberhard, *Immunology*, 16 (1969) 719.
25 E. W. Rauterberg, Ch. Schieck and G. M. Hänsch, *Immunobiology*, 155 (1979) 365.
26 M. Takahashi, S. Kawachi-Takahashi and K. Yamamoto, *Int. Arch. Allergy Appl. Immunol.*, 47 (1974) 887.
27 M. Adinolfi and T. Lehner, *Genet. Complement*, 5 (1988) 123.
28 P. Späth, Berne, Switzerland, personal communication.

Journal of Chromatography, 591 (1992) 195–206
Elsevier Science Publishers B.V., Amsterdam

CHROMSYMP. 2425

Determination of aminoglycoside antibiotics by reversed-phase ion-pair high-performance liquid chromatography coupled with pulsed amperometry and ion spray mass spectrometry☆

Lee G. McLaughlin and Jack D. Henion*

Drug Testing and Toxicology, NYS College of Veterinary Medicine, Cornell University, 925 Warren Drive, Ithaca, NY 14850 (USA)

(First received July 17th, 1991; revised manuscript received August 25th, 1991)

ABSTRACT

This work constitutes a preliminary investigation of a high-performance liquid chromatographic (HPLC)–mass spectrometric (MS) method for confirming aminoglycoside residues in bovine tissues. A reversed-phase ion-pair HPLC method for the separation of four aminoglycosides was developed using volatile ion-pairing agents and optimized for detection with an ion spray HPLC–MS interface. The method is also compatible with a commercial pulsed amperometric detector that was used for HPLC method development and that may be useful for the screening and quantification phases of a regulatory method. Several column phases, eluent compositions, and pairing ions were evaluated for optimum HPLC–MS sensitivity. Detection limits are in the low nanogram range with the pulsed amperometric detector and with HPLC–MS in the selected ion monitoring mode. Results with bovine kidney, fortified to 20 ppm and extracted by matrix solid-phase dispersion, obtained using both detectors are presented.

INTRODUCTION

There is a great need for improved analytical methods for confirmation of aminoglycoside (AG) antibiotic residues in the edible tissues of livestock. Certain members of this class are used widely for veterinary purposes and because of their nephro- and ototoxicity, and the potential for acquired bacterial resistance, their residues in food products are of concern to the US Food and Drug Administration (FDA). For confirmation, especially in a regulatory setting, mass spectrometry has been cited as an ideal choice [1]. However, the hydrophilicity, basicity and thermal lability of these analytes preclude their direct determination by gas chromatography (GC)–mass spectrometry (MS). Therefore, high-performance liquid chromatographic (HPLC)–MS (HPLC–MS) and HPLC–MS–MS methods may have the greatest potential for accomplishing direct multi-residue identifications in complex biological matrices.

Direct determination of AGs by HPLC has been reported using refractive index [2] and ultraviolet (UV) detection [3], which lack sensitivity and selectivity. Other reports include detection by pulsed amperometry [4], including its novel combination with high-performance anion-exchange chromatography [5], and d.c. amperometry [6]. Shaikh and Allen [7] have reviewed physico-chemical methods used for AG determination in animal tissues. Traditionally, microbiological assays have been used [8], but there are an increasing number of reports of reversed-phase ion-pair HPLC methods using fluorescence detection of derivatized analytes. Such methods have been used to detect neomycin in bovine and porcine tissues [8,9] and bovine milk

☆ Presented at the *8th (Montreux) Symposium on Liquid Chromatography–Mass Spectrometry (LC–MS, SFC–MS, CE–MS, IC–MS), Ithaca, NY, July 17–19, 1991.*

0021-9673/92/$05.00

[10,11], gentamicin in bovine milk [12] and muscle tissue [13] and rabbit renal cortex [14] and streptomycin in chicken meat [15]. There are no reports of the direct spectrometric determination of AGs in animal tissue of which we are aware.

There are only a few literature reports on the on-line HPLC–MS detection of AGs. Tobramycin, kanamycin and neamine have been detected using the moving belt interface and ammonia chemical ionization [16]. Atmospheric pressure chemical ionization (APCI) mass spectra have been shown for the kanamycin components [17] with detection limits between 1 and 50 ng reported for the gentamicin C and kanamycin components by flow-injection analysis in the selected ion monitoring (SIM) mode [18]. Dihydrostreptomycin was detected by continuous-flow fast atom bombardment MS using capillary HPLC at a flow-rate of 50 nl/min [19]. Most recently, the gentamicin C components have been determined using thermospray HPLC–MS [20].

The unique features of the ion spray interface for HPLC–MS [21] make it worth investigating for the determination of these compounds. That is, for analytes that exist as ions in solution, ion desorption from the liquid to the gas phase occurs under the influence of an electric field without the need for heat or other severe conditions. Other HPLC–MS techniques such as thermospray and heated pneumatic nebulization for APCI rely on heat for either solvent or analyte vaporization, or both. There are, however, limitations to the mobile phase composition for good performance of the ion spray interface. Although the characterization of these effects is on-going, it is generally believed that use of mobile phases with low ionic strength, significant concentrations of organic modifiers such as methanol or acetonitrile and avoidance of non-volatile additives will achieve the best performance [21,22]. Therefore, it is necessary in some instances to compromise between ideal chromatographic conditions and conditions that support the ionization, desolvation and desorption processes of the ion spray HPLC–MS interface.

The AGs are difficult to retain in the reversed-phase mode even with purely aqueous eluents [2]. Therefore, most chromatographic methods are based on some form of ion chromatography, typically ion-exchange or ion-pair modes. Most of the reported ion chromatographic eluents are not well suited for use with the ion spray interface owing to the presence of non-volatile electrolytes that suppress analyte desorption and increase the background ion current in the mass spectrometer. For instance, ion-pair methods commonly employ sodium alkyl sulfonate pairing ions together with high concentrations of sodium salt buffers to improve the chromatographic peak shape [14].

Inchauspé and Samain [2] have reported the use of volatile perfluorinated carboxylic acids as ion-pairing agents to facilitate the retention of AGs in the reversed-phase mode for their preparative isolation by HPLC [2]. They later found this approach to be useful for the characterization of AGs in culture broths by off-line field desorption MS and predicted the applicability of these volatile surfactants to evolving HPLC–MS techniques [23]. Indeed, mobile phases containing trifluoroacetic acid (TFA) have been used successfully for the thermospray HPLC–MS determination of gentamicin C [20] and with ion spray HPLC–MS for the determination of peptides in the positive-ion mode [24]. TFA was not found to be effective for retaining the AGs, with the exception of the gentamicins, for which it has a unique selectivity [25]. However, Inchauspé and co-workers have successfully used the three- and four-carbon homologues, pentafluoropropionic acid (PFPA) and heptafluorobutyric acid (HFBA), to separate mixtures of AGs [2,23,25,26].

It should be noted that, in some instances, post-column suppressors can be used on-line to remove ionic species that interfere with detection [27]. However, this adds complexity in addition to post-column dead volume and the attendant band broadening to the system. More work is needed to discover if suppressor technology can improve HPLC–MS determinations of these compounds. In this work, we explored reversed-phase ion-pair HPLC with volatile pairing ions as a means of determining AGs by ion spray HPLC–MS in the positive-ion mode without post-column suppression or make-up flows.

The feasibility of ion spray HPLC–MS for AG determinations is demonstrated here in the full-scan and SIM modes. Ultimately, confirmation will be accomplished by HPLC–MS–MS in the selected reaction monitoring (SRM) mode. With post-column addition of strong base, the method is also compatible with pulsed amperometric detection (PAD),

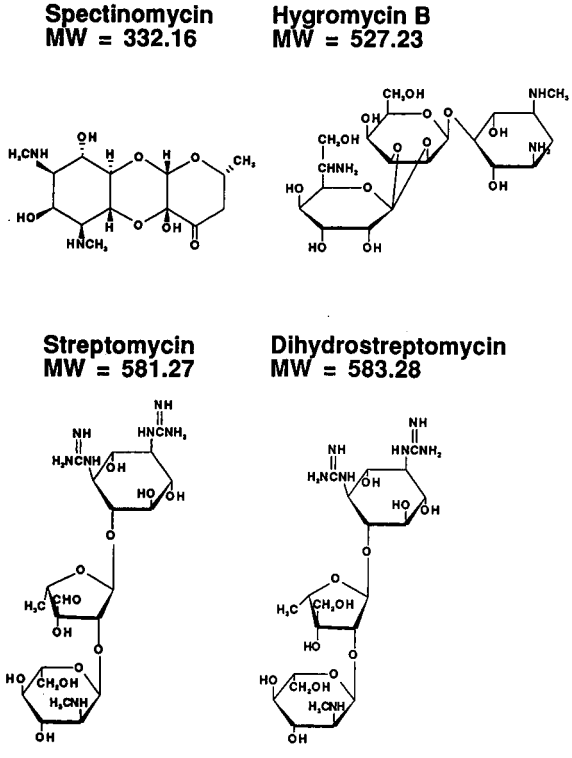

Fig. 1. Structures of the aminocyclitol and aminoglycoside antibiotics and their monoisotopic molecular weights (MW).

which could possibly be used for the screening and quantification phases of a regulatory method. Data are presented for four antibiotics of immediate interest to the US FDA (Fig. 1). Streptomycin and dihydrostreptomycin are aminoglycosides whereas spectinomycin and hygromycin B are classified as aminocyclitols [28]. They are all approved for some veterinary uses, although tolerance levels do not exist for all specific uses [29]. Current levels of regulatory interest in bovine kidney are 0.02 ppm for hygromycin B, 0.1 ppm for spectinomycin and 0.5 ppm for streptomycin and dihydrostreptomycin [30].

EXPERIMENTAL

Chemicals

Water was distilled in-house and purified with a Barnstead (Boston, MA, USA) Nanopure system. Methanol, hexane and ethyl acetate were of HPLC grade from Fisher Scientific (Rochester, NY, USA) and acetonitrile (ACN) was of Fisher Optima grade. Sodium hydroxide solution was of Fisher Certified 50% (w/w) and ammonia solution was of Fisher ACS reagent grade. Sulfuric acid, doubly-distilled from Vycor, was purchased from GFS Chemicals (Columbus, OH, USA). Spectinomycin dihydrochloride, hygromycin B, streptomycin sesquisulfate, dihydrostreptomycin sesquisulfate, pentafluoropropionic acid (PFPA) and heptafluorobutyric acid (HFBA) were products of Sigma (St. Louis, MO, USA). The aminoglycoside standards were stored in a desiccator at 4°C and were not dried or purified further before use. Aqueous stock solutions with a free base concentration of 4 μmol/ml were found to be stable for at least 5 months at 4°C. All solutions were stored in polypropylene or polyethylene containers to avoid adsorption on glassware [31]. The amounts and concentrations specified in this paper refer to the free base form of the analytes.

Sample extraction procedure

The matrix solid-phase dispersion (MSPD) method of Barker *et al.* [32] as modified by Schenck [9] was used to extract analytes added to control bovine kidney. Control kidney was obtained at a local supermarket and homogenized in 300-g batches for 45 s at low speed in a Waring blender (VWR Scientific, Rochester, NY, USA). Tissue homogenate (0.5 g) was placed in an agate mortar and spiked with 5 μl of a 2 μg/μl aqueous stock solution of the four analytes and allowed to equilibrate for 5 min. Bondesil cyanopropyl 40-μm bulk packing material (Analytichem International, Harbor City, CA, USA) (2 g) was added to the tissue and blended manually with a pestle for 2 min. The resulting mixture was transferred through a funnel into an empty 8-ml solid-phase extraction reservoir (Analytichem International) with 20-μm frits placed at the top and bottom and compressed to a bed volume of *ca.* 4 ml. The mortar was then rinsed with 3 ml of hexane, which was poured on to the top of the column and washed with water and methanol before the next dispersion was performed. Using a Supelco (Bellefonte, PA, USA) vacuum manifold, the 3-ml hexane wash was eluted at 6.77 kPa (2 in.Hg), as were successive 5-ml aliquots of ethyl acetate, methanol and methanol–water (50:50). The analytes were eluted with 1 ml of water followed by 8 ml of

0.05 *M* sulfuric acid at 3.39 kPa (1 in.Hg). For PAD the eluate was neutralized with NaOH (50%, w/w) and 15 μl of the 9-ml eluate were injected. Sample pH was measured with a Fisher Scientific Model 815MP pH meter. For HPLC–MS an aliquot of the 9-ml eluate was concentrated by a factor of four in a SpeedVac SVC 100 (Savant Instruments, Farmingdale, NY, USA) and neutralized with ammonia solution and 10 μl were injected on to the column.

Chromatography

Separations were developed using a Dionex (Sunnyvale, CA, USA) gradient pump module equipped with a Model 4500i pulsed amperometric detector. The gradient pump module was used at a flow rate of 1 ml/min while eluents were sparged and pressurized with a Dionex eluent degas module using ultra-high-purity helium. The system included a pneumatically actuated injector with a 25-μl sample loop.

The HPLC columns used for this work were as follows: 3-μm Spherisorb ODS-2 (100 mm × 4.6 mm I.D.), packed by Keystone Scientific (Bellefonte, PA, USA), 5-μm Inertsil ODS-2 (100 mm × 4.6 mm I.D.), purchased from Keystone Scientific, and 10-μm PRP-1 (220 mm × 4.6 mm I.D.), from Hamilton (Reno, NV, USA). For HPLC–MS work, a Waters (Milford, MA, USA) Model 510 pump delivered eluent at a flow-rate of 200 μl/min to a 5-μm Spherisorb ODS-2 column, (100 mm × 2 mm I.D.), also packed by Keystone Scientific. The injector was a Rheodyne (Cotati, CA, USA) Model 7125 with a 20-μl sample loop. Spherisorb ODS-2 (3 μm) guard columns (10 mm × 4.0 mm I.D. or 10 mm × 2 mm I.D.) were used with each of the Spherisorb ODS-2 analytical columns (Keystone Scientific).

The various mobile phases tested ranged from 8 to 16% ACN and 5 to 40 m*M* PFPA or HFBA. They were prepared by diluting the acid with ACN to 50 ml in a volumetric flask and mixing this with 575 ml of water. Water and ACN were filtered through 0.2-μm nylon filter disks before use (Rainin Instrument, Woburn, MA, USA). The pH of an 8% ACN–20 m*M* PFPA eluent was measured to be 1.9. The HPLC column void volume was determined by injection of methanol. Columns were flushed overnight with ACN–water (40:60) at a flow-rate of 0.1 ml/min.

Pulsed amperometry

The pulsed amperometric detector was a Dionex Series 4500i with a solvent-compatible cell (3.5-μl volume) and a gold working electrode. The applied potential for oxidation (E_1) was 0.1 V with a pulse duration of 480 ms and a current sampling period of 200 ms. Potentials used for cleaning the working electrode (E_2 and E_3) were 0.6 and −0.8 V with pulse durations of 120 and 300 ms, respectively. The response time was set at 1 s. A Dionex post-column pneumatic controller maintained at 207 kPa (30 p.s.i.) supplied 0.3 *M* NaOH at a flow-rate of 0.8 ml/min to the HPLC column effluent, making the total flow-rate to the PAD cell 1.8 ml/min. A 122-cm reaction coil (Dionex) was used for mixing of the two streams. Full-scale output was set on the PAD to a value of 100 or 300 nA and chromatograms were recorded with a Hewlett-Packard (Avondale, PA, USA) Model 3390A integrator. The 0.3 *M* NaOH solution was prepared by sparging water with helium for 15 min and then adding the NaOH solution and swirling gently to effect mixing. The reference electrode was soaked in water for *ca.* 30 min before use and was stored in certified potassium hydrogenphthalate buffer solution (pH 4) when not in use (Fisher Scientific).

Mass spectrometry

The HPLC column effluent (200 μl/min) was connected to the ion spray HPLC–MS interface [21] via a splitting device consisting of a 1/16-in. polyether ether ketone (PEEK) tee purchased from Upchurch Scientific (Oak Harbor, WA, USA) with a 9-cm length of 0.005 in. I.D. PEEK tubing attached. The splitting ratio was estimated to be 1:5 such that 40 μl/min of effluent reached the interface. The interface was maintained at 3.4 kV and the nebulizing nitrogen pressure at 414 kPa (60 p.s.i.). The mass spectrometer was a TAGA 6000E triple quadrupole instrument, upgraded to an API III, equipped with an atmospheric pressure ion source which was used in the positive-ion mode (Sciex, Thornhill, Canada). The optimum sprayer position was determined by infusing a 100 ng/μl solution of dihydrostreptomycin dissolved in mobile phase (*i.e.*, 8% ACN in 10 or 20 m*M* PFPA) at 40 μl/min. A declustering potential of 30 V was used unless indicated otherwise. The scan rate under HPLC–MS conditions was 3 s per scan with data collected in 0.5-u steps

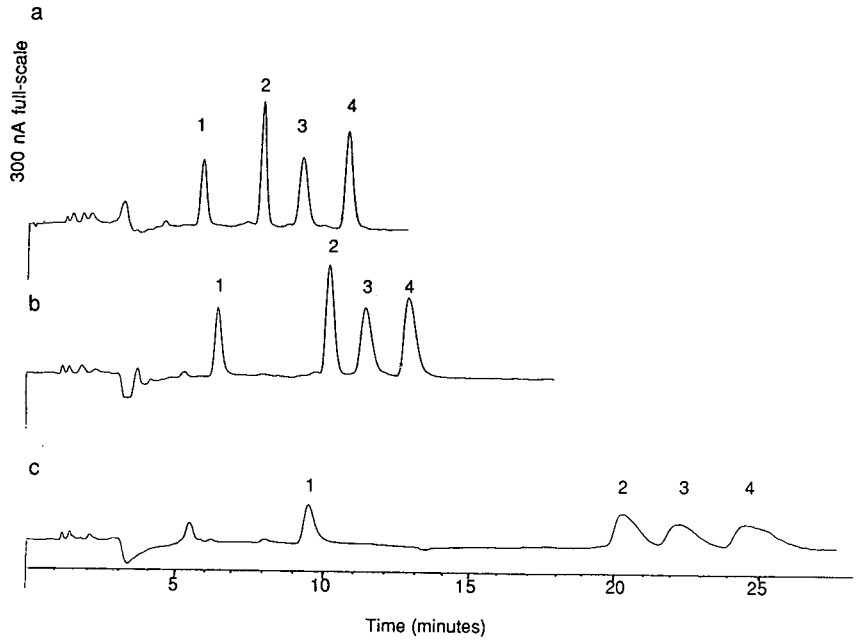

Fig. 2. HPLC–PAD elution profiles of a synthetic mixture of the four analytes using the Spherisorb ODS-2 column with various concentrations of PFPA in 8% ACN–water: (a) 20 m*M*; (b) 10 m*M*; (c) 5 m*M*. Peaks: 1 = spectinomycin (80 ng); 2 = hygromycin B (110 ng); 3 = streptomycin (145 ng); 4 = dihydrostreptomycin (145 ng).

for full-scan acquisition. Dwell periods of 750 ms were used in the SIM mode. Flow-injection analysis (FIA) was used to assess ion spray sensitivity as a function of pairing-ion concentration. For this experiment, a Brownlee micropump (Applied Biosystems, Foster City, CA, USA) delivered eluent at 40 μl/min directly to the interface with no splitting. Analytes were dissolved in the mobile phase being evaluated. The injector was a Rheodyne Model 7520 with a 1-μl internal sample loop. Data were acquired in the SIM mode with dwell periods of 75 ms. The data system was the standard Macintosh system provided by the manufacturer (Sciex).

RESULTS AND DISCUSSION

Effect of pairing-ion concentration on reversed-phase HPLC separation

For ion spray HPLC–MS it is desirable to minimize the concentration of pairing ion while using as much organic modifier as possible (see below). Also, a certain amount of chromatographic resolution

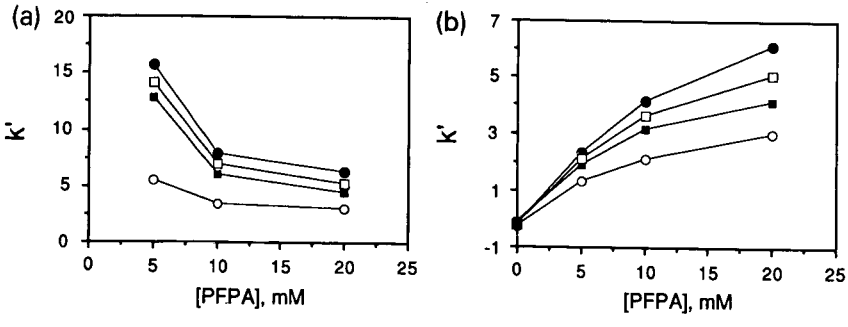

Fig. 3. Dependence of *k'* on the concentration of PFPA in 8% ACN–water for (a) Spherisorb ODS-2 column and (b) Inertsil ODS-2 ultra-end-capped column. With the Spherisorb column and no PFPA none of the analytes was observed to elute within 40 min. Data were obtained using PAD. ○ = Spectinomycin; ■ = hygromycin B; □ = streptomycin; ● = dihydrostreptomycin.

between component peaks is required in order to scan the peaks during discrete time windows with the mass spectrometer. This is necessary for monitoring ions from many analytes in one chromatographic profile in the SIM or SRM mode of operation. Of the eluents and columns tested with PAD, the highest efficiency and resolution were achieved using 8% ACN in 20 m*M* PFPA on the Spherisorb ODS-2 column. The elution profile for a synthetic mixture of the four analytes using these conditions is shown in Fig. 2a. Better resolution of streptomycin and dihydrostreptomycin is achieved with this method than with methods using alkyl sulfonate pairing ions [3,8,33].

Contrary to the predicted behavior for ion-pair systems, an increase in retention was observed with decreasing pairing-ion concentration for the Spherisorb column, as shown in Fig. 2b and c [34]. Also, increased peak asymmetry is evident in Fig. 2c. For example, the peak asymmetry for hygromycin B increases from a value of 1.07 with 20 m*M* PFPA to 1.86 with 5 m*M* PFPA. The fact that neither an ultra-end-capped polysiloxane-based Inertsil ODS-2 column nor a polystyrene (PS)–divinylbenzene (DVB) column displayed this type of behavior suggests that the effect is due to adsorption to residual silanol sites. These sites may be more effectively masked by higher pairing-ion concentrations.

The elution behaviors with the Spherisorb and Inertsil columns are compared in the plots of capacity factor (k') as a function of PFPA concentration shown in Fig. 3a and b. The Inertsil ODS-2 column shows the expected increase in capacity factor as the pairing-ion concentration is increased from 0 to 20 m*M*. Both of these columns are able to separate the four analytes at concentrations of 10 and 20 m*M* PFPA. However, resolution is too low with 10 m*M* PFPA on the Inertsil column if window acquisition is to be used with the mass spectrometer, although the analysis time is shorter. The separation efficiency on the Inertsil column is slightly lower at 20 m*M* as compared with the Spherisorb column. The Spherisorb ODS-2 packing material is the only one of the three tested that is available as 3-μm diameter particles.

A concentration of PFPA as low as 5 m*M* gave poor results with the Spherisorb ODS-2 column, as shown in Fig. 2c. This low concentration is also not effective with the Inertsil or PS–DVB columns, from which the analytes were observed to elute only partially resolved with capacity factors of less than 2.5. With the Inertsil ODS-2 column it is possible to achieve baseline separation of the four analytes by decreasing the amount of ACN to 4%, but this eluent was found not to give greater mass spectrometric sensitivity than the others tested (see below).

After 5 months of use with these acidic eluents (pH 2), the efficiency of the 100 mm × 4.6 mm I.D. Spherisorb ODS-2 column decreased by *ca.* 20%. A decrease in octadecylsilane (ODS) column life-time when using these eluents has been reported previously [26]. For that reason, the pH stability of the PS–DVB columns makes them an attractive alternative. However, at concentrations higher than 5 m*M* PFPA, spectinomycin and hygromycin were found to co-elute on the PS-DVB column. Therefore, the Spherisorb ODS-2 column and an eluent of 8% ACN in 10 or 20 m*M* PFPA was used for most of this work.

Effect of pairing-ion concentration on ion spray mass spectrometry

As mentioned previously, the general approach to ion spray HPLC–MS includes minimization of eluent ionic strength, use of as much organic modifier as practical and avoidance of buffers, unless they facilitate ionization, because of competitive

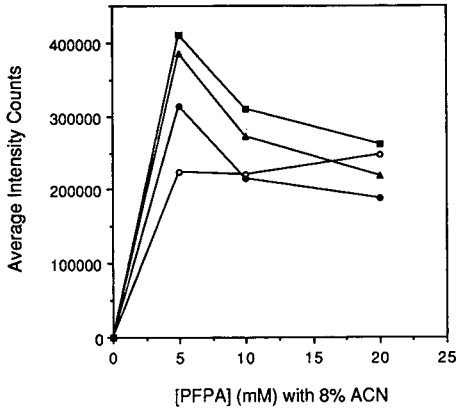

Fig. 3. Dependence of k' on the concentration of PFPA in 8% ACN–water for (a) Spherosorb ODS-2 column and (b) Inertsil ODS-2 ultra-end-capped column. With the Spherisorb column and no PFPA none of the analytes was observed to elute within 40 min. Data were obtained using PAD. ○ = Spectinomycin; ■ = hygromycin B; □ = streptomycin; ● = dihydrostreptomycin.

desorption and high chemical background caused by adducts extending to a fairly high mass-to-charge ratio (m/z). These considerations affect the choice of separation mode, especially for the aminoglycosides, which cannot be separated under typical reversed-phase conditions. We used FIA–ion spray MS experiments to assess the affect of pairing-ion concentration on sensitivity. Fig. 4 presents a plot of average MS peak intensity for three 20-ng injections of each of the four analytes at various concentrations of PFPA. Base-peak ions were monitored in the SIM mode. Related experiments in the full-scan acquisition mode showed that no significant mass spectral changes are caused by the different mobile phases tested, except that without a pairing ion present (neutral pH) no analyte signal is detected.

The observed signal is highest at 5 m*M* PFPA and decreases as the concentration is increased to 20 m*M* PFPA for each of the analytes except spectinomycin. The average response obtained with a mobile phase of 5 m*M* PFPA–4% ACN was the same as that for 10 m*M* PFPA–8% ACN. The latter eluent, however, provided better chromatographic resolution. For three of the analytes the response observed by FIA–ion spray MS is *ca.* 15–20% higher with 10 m*M* than with 20 m*M* PFPA. However, the peak heights measured on chromatograms obtained with PAD decrease by approximately the same amount when 10 m*M* is used instead of 20 m*M* PFPA owing to the longer retention. Hence concentrations of 10 and 20 m*M* PFPA may give comparable HPLC–MS results with the Spherisorb column. A concentration of 40 m*M* PFPA in the eluent resulted in a high voltage discharge between the interface and the mass spectrometer under the instrumental conditions used.

Effect of pairing-ion hydrophobicity

In reversed-phase ion-pair systems, the use of a more hydrophobic pairing ion will increase the analyte retention [35]. Therefore, HFBA was explored as a means of using a higher concentration of organic modifier in the eluent. The usefulness was tested by injecting a synthetic mixture of AGs under the two different HPLC conditions described in Fig. 5. Data were collected in both full-scan and SIM modes; only the full-scan results are shown here but the SIM results agreed well. For the same concentration of HFBA, the percentage of ACN may be doubled while still resolving the analytes. However, the longer retention times and concomitant band broadening appear to offset any increased sensitivity that might be associated with the higher concentration of organic solvent. Average peak intensity data obtained from three injections of this mixture indicate that only the spectinomycin response is significantly increased with the HFBA eluent. This is presumably because the retention time of this analyte remains approximately the same when the organic modifier concentration is increased. A more complex explanation is also possible. Inchauspé *et al.* [25] have reported variations in the number of theoretical plates with different pairing ions on an analyte-dependent basis. Ion spray phenomena may also vary by compound in the presence of different additives. In any case, HFBA did not offer a substantial improvement for the ion spray HPLC–MS analysis of this mixture of antibiotics.

In another attempt to increase the organic modifier concentration, the use of methanol was explored. Because methanol is a weaker reversed-phase eluent than acetonitrile, concentrations of *ca.* 20% (v/v) may be used to obtain similar retention. Although methanol cannot be used with PAD because it is electroactive at the potential used to oxidize the analytes, it was tested using HPLC–UV and HPLC–MS methods. In both instances broad, tailing peaks were observed for the carbonyl-containing compounds spectinomycin and streptomycin, owing to apparent hemiketal and hemiacetal formation, respectively, at this low pH. The hemiketal and hemiacetal products were identified in the ion spray mass spectra together with the ketone- and aldehyde-hydrate species normally observed so that the ion current is distributed among several ions for these analytes. However, the poor chromatographic peak shape alone precludes the use of methanol at this low pH.

Ion spray mass spectra

Full-scan mass spectra (165–600 dalton) were obtained by HPLC–MS in 8% ACN–20 m*M* PFPA from injection of 2 μg per component. Spectinomycin exists in solution as a ketone-hydrate [36] and yields a singly charged protonated molecule of this species $[M + H_2O + H]^+$ at m/z 351 as the base peak. A singly charged species corresponding to the

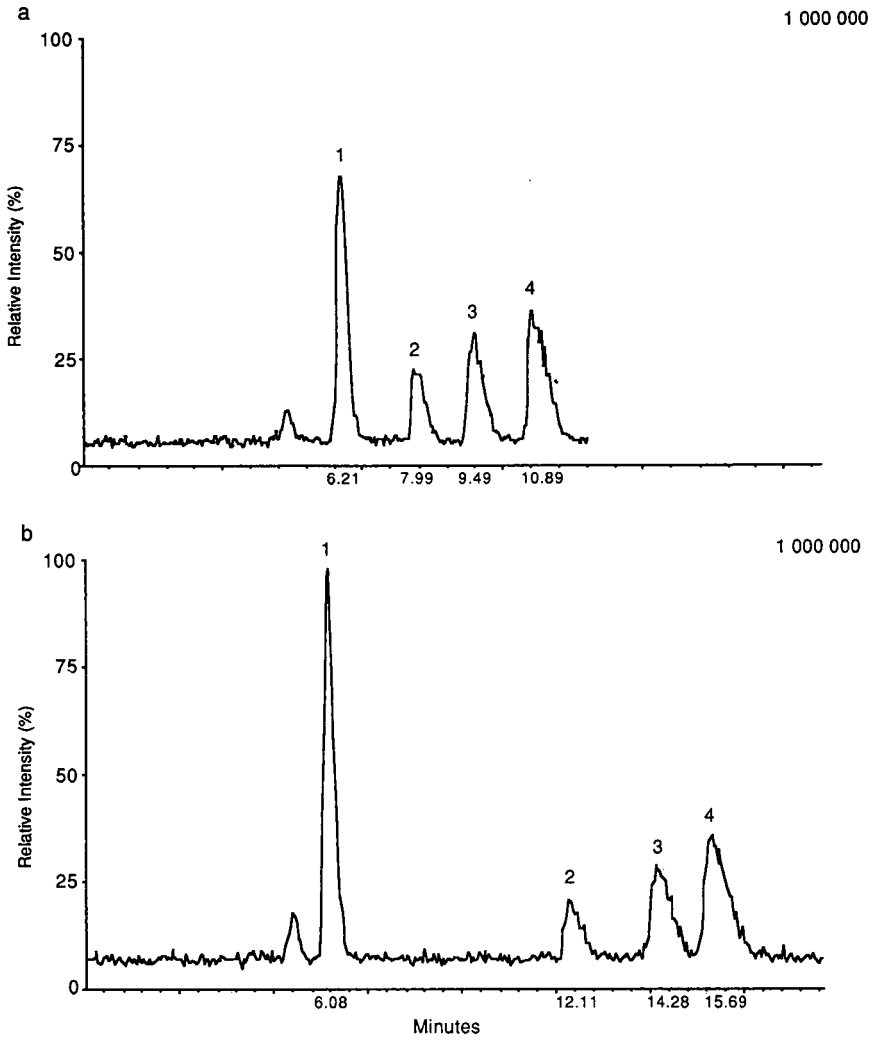

Fig. 5. Comparison of HPLC–MS ion spray elution profiles on the Spherisorb ODS-2 column using (a) 8% ACN–20 m*M* PFPA and (b) 16% ACN–20 m*M* HFBA. Data shown are reconstructed total ion current profiles from full-scan (260–400 dalton) acquisition data. Peaks: 1 = spectinomycin (400 ng); 2 = hygromycin B (550 ng); 3 = streptomycin (723 ng); 4 = dihydrostreptomycin (723 ng). Numbers at top right indicate ion counts.

non-hydrated or dehydrated molecule $[M + H]^+$ is observed at *m/z* 333 with a relative abundance of 8%. The predominant ions observed under these conditions for the other three analytes are doubly protonated, doubly charged species. For dihydrostreptomycin and hygromycin B the base peaks $[M + 2H]^{2+}$ are ions of *m/z* 293 and 265, respectively. In the mass spectrum of hygromycin B the singly charged protonated molecule $[M + H]^+$ at *m/z* 528 is observed with a relative abundance of 9%. Streptomycin appears to exist as an aldehyde-hydrate characterized by the base peak $[M + H_2O + 2H]^{2+}$ at *m/z* 301. The eluent pH is probably too low for streptomycin to exist in solution as the cyclic carbinolamine tautomer from reported [36]. Also observed is the non-hydrated or dehydrated form $[M + 2H]^{2+}$ at *m/z* 292 with a relative abundance of 21%. No significant fragmentation was observed at the declustering potential of 30 V used to obtain these spectra. Concentration of the ion current into one

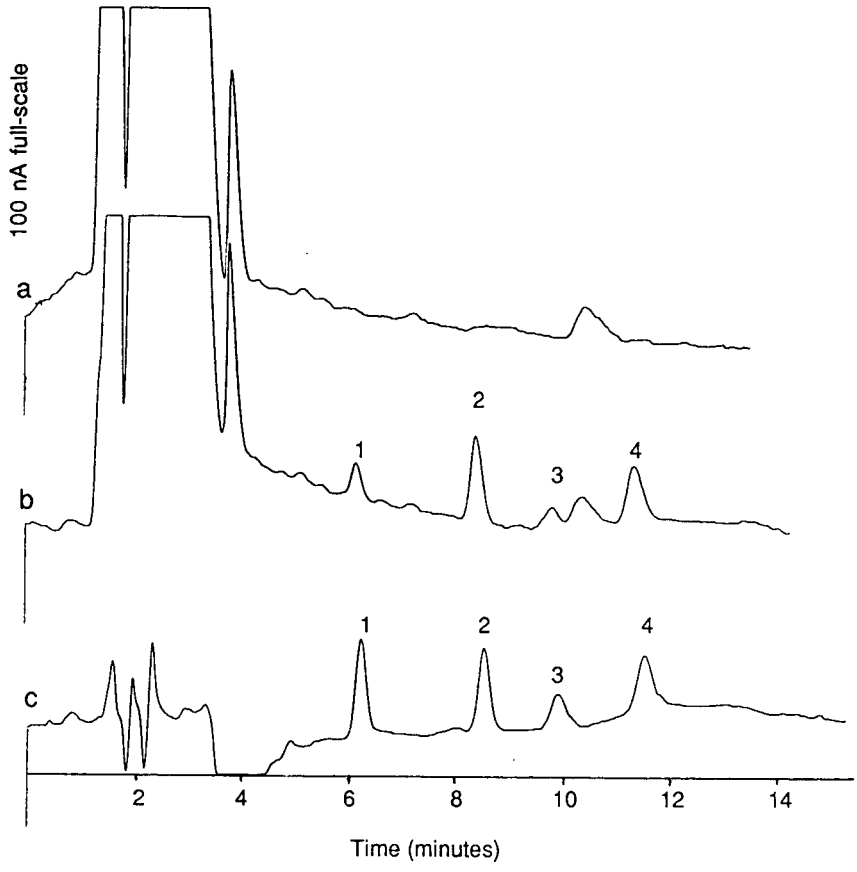

Fig. 6. HPLC–PAD of (a) MSPD extract of control bovine kidney, (b) MSPD extract of bovine kidney fortified at the 20 ppm level and (c) synthetic mixture of standards at levels of 15 ng per component injected, representative of 100% recovery. Peaks: 1 = spectinomycin; 2 = hygromycin B; 3 = streptomycin; 4 = dihydrostreptomycin.

principal species is ideal for subsequent SRM work although the lower m/z of the doubly charged species puts them in a region of higher chemical background. At a higher declustering potential of 70 V it is possible to obtain mass spectra having the corresponding singly charged species as the base peak. However, analyte signals observed for the singly charged species are much lower than those obtainable for the doubly charged species and may not be adequate for SRM work.

HPLC–PAD for aminoglycoside determination

The ion-pair system is compatible with PAD utilizing post-column addition of strong base. This HPLC–PAD system can detect *ca.* 5 ng of free base per component with signal-to-noise ratios (S/N) ranging from 4 for streptomycin to 14 for dihydrostreptomycin. These observations agree well with the detection limit of 2 ng (S/N = 3) reported for tobramycin using PAD with anion-exchange chromatography [5]. Fig. 6 shows the results for a bovine kidney sample fortified at 20 ppm of each of the analytes and extracted by MSPD together with a control kidney extract and a standard equivalent to 15 ng per component injected on-column, representative of 100% recovery. Further sample clean-up and increased recovery of spectinomycin would be necessary to reach lower concentrations with this method and to be competitive with fluorescence detection, which has been used to determine neomycin in bovine kidney at 2.5 ppm also using the MSPD technique for sample preparation [9]. It should be noted that PAD will not be limited to certain pairing-ion concentrations and non-volatile salts may

be used to improve peak shape. The only limitations we have encountered in this work are with electroactive species such as methanol and ammonium compounds, which produce an unstable baseline.

Ion spray HPLC–MS for aminoglycoside determination

Detection limits for these analytes using ion spray MS in the SIM mode are in the low nanogram range. For injection of between 4 and 7 ng of free base per component, corresponding to 12 pmol per component, S/N values range from 2 for streptomycin and hygromycin B to 6 for dihydrostreptomycin and 9 for spectinomycin. These results were obtained using the 8% ACN–20 mM PFPA eluent with the 100 mm × 2 mm I.D. Spherisorb ODS-2 column with a post-column split. The base-peak ion was monitored for each compound. Noise associated with background ion current coincident with the m/z of the hygromycin B and streptomycin ions increases the detection limits for these compounds.

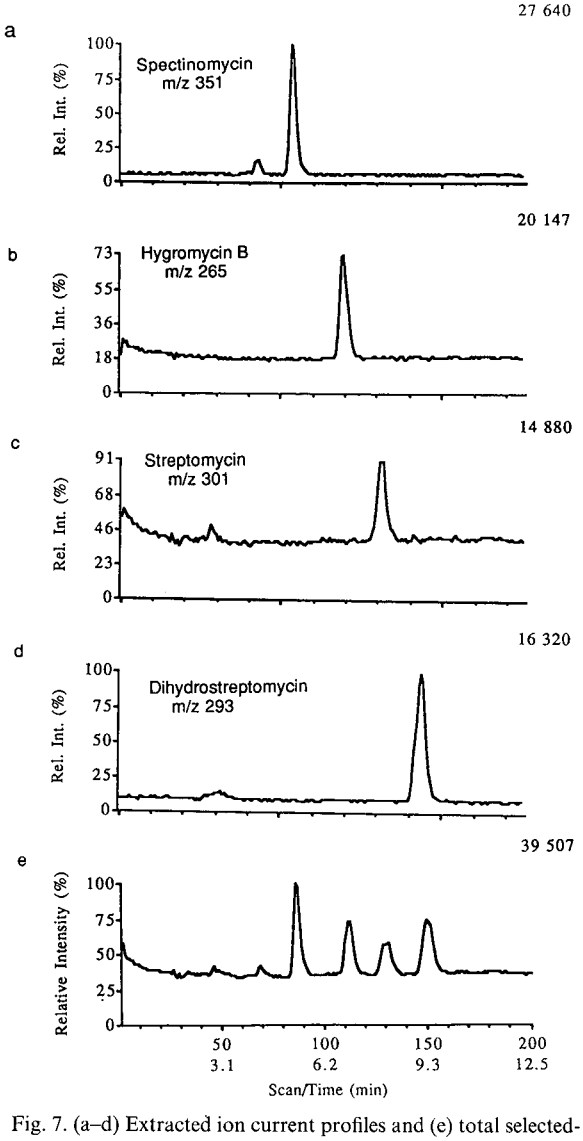

Fig. 7. (a–d) Extracted ion current profiles and (e) total selected-ion current profile of an ion spray HPLC–MS analysis of a synthetic mixture of the four analytes at the level of 40 ng per component injected, corresponding to 100% recovery from a 20 ppm sample. Numbers at top right indicate ion counts.

The determination in the SIM mode of a 40 ng per component synthetic mixture of the four analytes is shown in Fig. 7 together with an extract of bovine kidney fortified at 20 ppm of each of the analytes in Fig. 8. The decrease in ion current seen in Fig. 8c is caused by the competitive desorption of matrix components eluting prior to 3 min. The 40-ng level corresponds to 100% recovery from a 20 ppm sample. For this work, an aliquot of the 9-ml aqueous sample extract was concentrated by a factor of four and 10 μl were injected. No matrix interferences were observed in the analysis of a control kidney extract. Determination at the levels of regulatory interest using this method would require on-column detection of 44 pg of hygromycin B, 0.22 ng of spectinomycin and 1.1 ng of streptomycin and dihydrostreptomycin. These amounts are all below the instrumental detection limits discussed above. However, because only a small fraction of the sample extract was injected and no matrix interferences were observed, further concentration of the 9-ml solid phase dispersion eluate should allow the determination of all analytes, except possibly hygromycin B. If further concentration is not possible owing to solubility limitations or overloading of the HPLC column, an additional clean-up step will be necessary. Determination of hygromycin B may require extraction of a larger tissue sample.

Also, because the sensitivity of this method is adversely affected by the high water content of the eluent (92%) and the 10–20 mM concentration of PFPA necessary to effect separation, we shall continue to evaluate columns that would allow use of more compatible eluents. Use of microbore HPLC columns (1 mm I.D.) would increase the method sensitivity owing to peak-volume concentration and

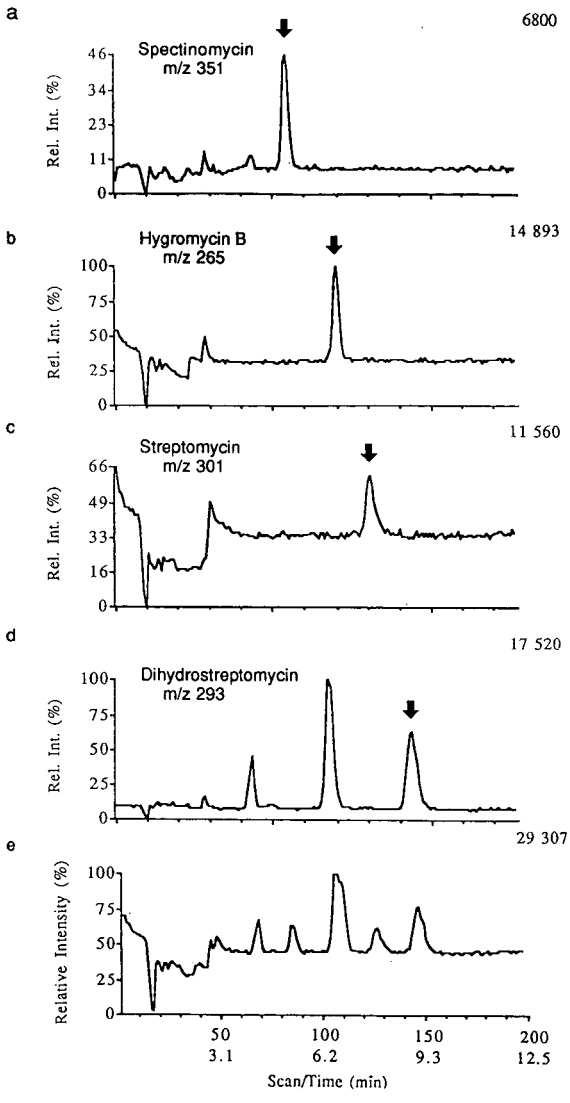

Fig. 8. (a–d) Extracted ion current profiles and (e) total selected-ion current profile of an ion spray HPLC–MS analysis of an MSPD extract of bovine kidney fortified at 20 ppm with each of the four analytes. Numbers at top right indicate ion counts.

the fact that at the lower flow-rates used with these columns no post-column split is required. However, because of their reduced loading capacity their applicability to these complex sample matrices remains to be demonstrated.

CONCLUSIONS

Although increasing concentrations of PFPA in the eluent were found to decrease the ion spray sensitivity for most of the compounds studied, a concentration of at least 10 m*M* was necessary for adequate chromatographic resolution on the columns tested. A concentration of 20 m*M* PFPA in 8% ACN provided the best separation efficiency and resolution on the Spherisorb ODS-2 column. PAD was useful for method development as it can detect as little as a few nanograms of underivatized aminoglycosides. Further clean-up will be needed if PAD is to be used for screening and quantification in the sub-ppm range in bovine kidney extracts. The detection limits of ion spray HPLC–MS in the SIM mode are also in the low nanogram range. Further concentration and possibly further clean-up of the bovine kidney extracts will be necessary to achieve determination at target levels. The even greater selectivity with respect to matrix interferences of the SRM mode to be used for eventual confirmation should allow injection of more concentrated extracts. Although sensitivity in the SRM mode remains to be optimized for confirmatory work, these results demonstrate the feasibility of this approach for determining aminoglycoside and aminocyclitol residues in bovine kidney. Future work will focus on the optimization of SRM parameters, improvement of analyte isolation and recovery from bovine kidney, evaluation of other chromatographic modes and application of the method to other aminoglycoside antibiotics and other biological matrices.

ACKNOWLEDGEMENTS

The authors thank the US FDA for funding this work under agreement No. FD-U-000577-02 and P. J. Kijak and F. J. Schenck for providing useful information. Dionex is gratefully acknowledged for the loan of the pulsed amperometric system, as are M. Mercer and J. Korpi for helpful discussions. Sciex is acknowledged for hardware and research support.

REFERENCES

1 *Fed. Regist.*, 42, No. 35 (1977) 10427.
2 G. Inchauspé and D. Samain, *J. Chromatogr.*, 303 (1984) 277.
3 T. J. Whall, *J. Chromatogr.*, 219 (1981) 89.
4 J. A. Polta, D. C. Johnson and K. E. Merkel, *J. Chromatogr.*, 324 (1985) 407.

5 J. A. Statler, *J. Chromatogr.*, 527 (1990) 244.
6 T. A. Getek, A. C. Haneke and G. B. Selzer, *J. Assoc. Off. Anal. Chem.*, 66 (1983) 172.
7 B. Shaikh and E. H. Allen, *J. Assoc. Off. Anal. Chem.*, 68 (1985) 1007.
8 B. Shaikh, E. H. Allen and J. C. Gridley, *J. Assoc. Off. Anal. Chem.*, 68 (1985) 29.
9 F. J. Schenck, *US FDA Laboratory Information Bulletin*, Vol. 7, Issue No. 4, No. 3559, US Food and Drug Administration, Rockville, MD, 1991.
10 B. Shaikh and J. Jackson, *J. Liq. Chromatogr.*, 12 (1989) 1497.
11 V. K. Agarwal, *J. Liq. Chromatogr.*, 13 (1990) 2475.
12 V. K. Agarwal, *J. Liq. Chromatogr.*, 12 (1989) 3265.
13 V. K. Agarwal, *J. Liq. Chromatogr.*, 12 (1989) 613.
14 G. Lachatre, G. Nicot, C. Gonnet, J. Tronchet, L. Merle, J. P. Valette and Y. Nouaille, *Analusis*, 11 (1983) 168.
15 A. Okayama, K. Yoshimi, Y. Aoki, S. Umesato, H. Ono, Y. Nishii and H. Kubo, *Bunseki Kagaku*, 37 (1988) 221; *C.A.*, 109 (1988) 36714.
16 D. E. Games, M. A. McDowall, K. Levsen, K. H. Schafer, P. Dobberstein and J. L. Gower, *Biomed. Mass Spectrom.*, 11 (1984) 87.
17 Y. Kato, S. Takahashi, H. Hirose, M. Sakairi and H. Kambara, *Biomed. Environ. Mass Spectrom.*, 16 (1988) 331.
18 M. Sakairi and H. Kambara, *Anal. Chem.*, 60 (1988) 774.
19 M. A. Moseley, L. J. Deterding, J. S. M. de Wit, K. B. Tomer, R. T. Kennedy, N. Bragg and J. W. Jorgenson, *Anal. Chem.*, 61 (1989) 1577.
20 T. A. Getek, M. L. Vestal and T. G. Alexander, *J. Chromatogr.*, 554 (1991) 191.
21 A. P. Bruins, T. R. Covey and J. D. Henion, *Anal. Chem.*, 59 (1987) 2642.
22 M. G. Ikonomou, A. T. Blades and P. Kebarle, *Anal. Chem.*, 62 (1990) 957.
23 G. Inchauspé, C. Deshaye and D. Samain, *J. Antibiot.*, 38 (1985) 1526.
24 E. C. Huang and J. D. Henion, *Anal. Chem.*, 63 (1991) 732.
25 G. Inchauspé, P. Delrieu, P. Dupin, M. Laurent and D. Samain, *J. Chromatogr.*, 404 (1987) 53.
26 I. De Miguel, E. Puech-Costes and D. Samain, *J. Chromatogr.*, 407 (1987) 109.
27 J. J. Conboy, J. D. Henion, M. W. Martin and J. A. Zweigenbaum, *Anal. Chem.*, 62 (1990) 800.
28 K. L. Rinehart, *J. Infect. Dis.*, 119 (1969) 345.
29 *Code of Federal Regulations*, 21, 556.200, 556.330, 556.600, 556.610 (1989).
30 P. J. Kijak, FDA, Beltsville, MD, personal communication.
31 J. P. Anhalt and S. D. Brown, *Clin. Chem.*, 24 (1978) 1940.
32 S. A. Barker, A. R. Long and C. R. Short, *J. Chromatogr.*, 475 (1989) 353.
33 N. Kurosawa, S. Kuribayashi, E. Owada, K. Ito, M. Nioka, M. Arakawa and R. Fukuda, *J. Chromatogr.*, 343 (1985) 379.
34 B. A. Bidlingmeyer, S. N. Deming, W. P. Price, Jr., B. Sachok and M. Petrusek, *J. Chromatogr.*, 186 (1979) 419.
35 B. A. Bidlingmeyer, *J. Chromatogr. Sci.*, 18 (1980) 525.
36 S. Umezawa, in S. Mitsuhashi (Editor), *Aminoglycoside Antibiotics*, University Park Press, Baltimore, 1975, pp. 3–43.

Journal of Chromatography, 591 (1992) 207–217
Elsevier Science Publishers B.V., Amsterdam

CHROM. 23 785

Optimization of a peak compression system for a remoxipride metabolite (FLA797) and its application to bioanalysis

Lars B. Nilsson

Bioanalysis, Astra Arcus AB, S-151 85 Södertälje (Sweden)

(First received April 24th, 1991; revised manuscript received September 18th, 1991)

ABSTRACT

A peak compression system is optimized for FLA797 (**I**), a phenolic tertiary amine and a metabolite to the antipsychotic drug remoxipride. An application is described where this effect is used to give a 6–7-fold improvement of the quantification limit in an assay of **I** in plasma. The liquid chromatographic system is constructed so that the injection of **I** dissolved in a solution of a competing amine gives a very high and narrow analyte peak with an apparent efficiency of $1.5 \cdot 10^6$ plates/m. When the levels of **I** in plasma are determined, an internal standard, giving a normal isocratic peak, is added to the plasma sample before the extraction. Concentrations of **I** down to 0.5–1.0 n*M* can be determined with reasonable precision. FLA908, another phenolic remoxipride metabolite and a regioisomer to **I**, eluting as a normal isocratic peak, can be determined simultaneously although only at concentrations higher than 10–15 n*M*.

INTRODUCTION

Peak compression was introduced some years ago as a possible way to improve the quantification limits in liquid chromatography [1]. Amines were used as analytes. The columns were packed with octadecylsilica stationary phases with residual silanols, giving the addition of a competing amine to the mobile phase a significant influence on the retention of the amine analyte. The compressed peak was a consequence of the co-elution of the analyte peak with a system peak originating from the UV-transparent amine modifier. The UV-absorbing amine analyte was injected dissolved in a solution of a lipophilic organic anion. This anion generated a system peak with an amine modifier deficit, *i.e.*, a zone where the amine analyte was more strongly retained compared with the bulk mobile phase. The resulting analyte peak was very narrow. The effects on other analytes not co-eluting with the zone were small. These principles were applied in an assay of FLA908 (**II**), a remoxipride metabolite, in urine [2]. At that time, however, the lipophilicity of the amine modifier and the variation of the concentration of organic anion in the injected solution were the only parameters known that could be used for the optimization of a peak compression system for a given analyte. Both approaches are useful but have their drawbacks. Varying the lipophilicity of the amine modifier gives system peaks with very different capacity factors. Peak compression is seen for amine analytes having about the same capacity factor as the amine modifier, but not for the amine analytes with a differing retention. By increasing the concentration of the anion in the injected solution, the amine modifier deficiency zone is made larger and more amine analytes will be affected by the zone. This gives possibilities of obtaining compressed peaks in the same system for several amine analytes but, as they will all elute at the same time, at the expense of a decrease in selectivity.

It would be desirable to find means to change the capacity factor of the system peak relative to the capacity factor of the analyte. Such means were reported recently [3], resulting in an optimization strategy where the first step always is to find an

0021-9673/92/$05.00

amine modifier with about the same retention as the analyte. Then an octadecylsilica column with a suitable amount of residual silanols is chosen. This can be achieved by mixing stationary phases with different amounts of silanols. The final fine regulation can be made by adjusting the ionic strength of the phosphate buffer in the mobile phase, as the capacity factor of the system peak was found to increase and the capacity factor of the amine analyte decreased with increasing ionic strength.

Effects on peak shape, both compression and deformation, in similar systems have been studied by Johansson and co-workers [4,5] and Fornstedt *et al.* [6,7]. Peak focusing effects in injection-generated ion-pair gradients have been reported by Šlais *et al.* [8] and recently peak compression of trace components in displacement chromatography was described [9,10].

Remoxipride is a new antipsychotic drug, acting as a selective dopamine-D_2 receptor antagonist [11,12]. Remoxipride levels in plasma and urine were determined by reversed-phase high-performance liquid chromatography (HPLC) [13]. The compound is metabolized to a great extent in both man and animals [14] and also the phenolic metabolites **I** and **II** have been shown to be active at the dopamine-D_2 receptor [15]. These metabolites are present in only minute amounts and highly sensitive methods for their determination in biological fluids are therefore of great interest. In this paper, the optimization of a peak compression system for **I** is described. By injecting the analyte in a solution of the amine modifier also present in the mobile phase, a zone with an excess of amine modifier was created which was able to compress the analyte peak. The optimized system was applied to the determination of low levels of **I** in plasma. A system such as this is as simple to use as a normal isocratic system but takes a longer time to develop. The benefit is the possibility of achieving 5–10-fold improvements of the limit of quantification (LOQ). Other advantages and disadvantages are discussed.

EXPERIMENTAL

Chemicals

N,N-Dimethyldecylamine (DMDA) and N,N-dimethylnonylamine (DMNA) was obtained from Ames Labs. (Millford, CT, USA). DMDA was distilled before use. N,N-Dimethyloctylamine (DMOA) was obtained from Heraeus (Karlsruhe, Germany) and N,N-dimethyldodecylamine (DMDoA) from Aldrich-Chemie (Steinheim, Germany). Other chemicals, of HPLC or analytical-reagent grade, were obtained from the usual commercial sources and used as received.

Compounds **I**, **II** and **III** (the internal standard) were prepared at CNS Research and Development, Astra Arcus (Södertälje, Sweden). Their syntheses have been described [15]. Also some other similar compounds from the same laboratory (raclopride, remoxipride, **IV** and **V**) were used as model compounds. The structures are shown in Fig. 1. Standard solutions of these compounds were made in phosphate buffer (pH 2). The solutions of the phenolic compounds are slightly light sensitive and were therefore kept in the dark and prepared freshly every third week.

Chromatography

The columns (100 × 4.6 mm I.D.) were packed with 5-μm Spherisorb ODS-1 (Phase Separations, Queensferry, UK) from different batches. The packing was performed at 400 bar with methyl isobutyl phases as slurry medium and hexane as the eluent.

The mobile phases were mixtures of acetonitrile and phosphate buffer (pH 2) of different ionic strengths and with the addition of amine modifiers such as DMDA. The injected samples were dissolved in either neat phosphate buffer (pH 2) or in a solution of amine modifier in phosphate buffer.

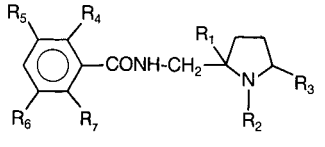

	R_1	R_2	R_3	R_4	R_5	R_6	R_7
I	H	C_2H_5	2H	OCH_3	H	Br	OH
II	H	C_2H_5	2H	OH	H	Br	OCH_3
III	H	C_2H_5	2H	OCH_3	H	H	OH
Remoxipride	H	C_2H_5	2H	OCH_3	H	Br	OCH_3
Raclopride	H	C_2H_5	2H	OCH_3	Cl	Cl	OH
IV	H	H	2H	OCH_3	H	Br	OCH_3
V	OH	C_2H_5	O	OCH_3	H	Br	OCH_3

Fig. 1. Structures of the remoxipride-related compounds.

The chromatographic system consisted of a Waters Assoc. (Milford, MA, USA) Model 590 pump, a Perkin-Elmer (Überlingen, Germany) ISS-100 autosampler, with an injection volume always of 200 μl, and a Waters Model 470 fluorescence detector with a 5- or 16-μl cell volume. The excitation wavelength was 316 nm, slit width 18 nm, and the emission wavelength was 465 nm, slit width 30 nm. The shortest available time constant, 0.5 s, was used. A Perkin-Elmer LC-95 UV detector was also used. This detector was operated at 212 nm, the cell volume was 1.4 μl and the time constant was 0.02 s. The system peaks were followed with a Waters Model 410 refractive index (RI) detector coupled in series with the UV detector. The fluorescence and UV signals were monitored with an SP 4270 integrator (Spectra-Physics, San Jose, CA, USA) using the shortest available PW (peak width) value. The RI detector signal was monitored with a standard recorder. To prolong the lifetime of the analytical column, a membrane pulse damper (SP-21; Scientific Systems, State College, PA, USA) and a guard column (100 × 4.6 mm I.D.) dry-packed with Corasil (37–50 μm) (Waters Assoc.) were placed between the pump and the autosampler.

The apparent efficiencies of the compressed peaks were calculated using the peak width at half-height. Peak asymmetry factors were calculated at 10% of the peak height.

*Determination of **I** and **II** in plasma*

Plasma samples (0.50–1.00 ml) were adjusted to pH 9–10 by the addition of an equal amount of 0.1 *M* carbonate buffer (pH 10). The appropriate amount (50–100 pmol) of internal standard (**III**) and 4 ml of 20% *n*-hexane in diethyl ether were added. The sample tubes were extracted in a rotary mixer for 5 min and then centrifuged for 2 × 10 min at 1500 *g* and 2°C. The organic phase was transferred into another tube and evaporated to dryness under a stream of nitrogen at 40°C. The residue was dissolved in 250 μl of 0.8 m*M* DMDA in 0.039 *M* phosphate buffer (pH 2) ($I = 0.015$) and 200 μl were injected.

The column was packed with Spherisorb ODS-1, batch 29/81. The mobile phase was 31% acetonitrile in 0.039 *M* phosphate buffer (pH 2) ($I = 0.015$) with the addition of 0.5 m*M* DMDA. Fluorescence detection was used.

The unknown concentrations of **I** and **II** were calculated from a linear calibration graph consisting of 6–8 spiked plasma samples. To study the absolute recoveries, extractions were performed using aliquots. The absolute recovery was calculated by dividing the slope of the concentration *versus* peak height graph by the slope of a calibration graph obtained from direct injection of aqueous standard solutions of the compounds. The precision and accuracy were studied by spiking a number of blank plasma samples with known amounts of **I** and **II**. Thereafter the samples were analysed as described above.

RESULTS AND DISCUSSION

Optimization of the chromatographic conditions

When a peak compression system is to be optimized for a specific analyte, the first step is the choice of an amine modifier with about the same retention as the analyte, *i.e.*, giving a capacity factor ratio as close to unity as possible. The second step is the choice of a column with the appropriate amount of residual silanols and the third step is to adjust the ionic strength of the phosphate buffer of the mobile phase to give a capacity factor ratio of 1.00 [3]. Other parameters, such as acetonitrile concentration, amine modifier concentration and pH, were found to have a minor or negligible influence on the capacity factor ratio for this kind of system [3].

When DMNA, DMDA and DMDoA were used as amine modifiers in otherwise similar mobile phases, their system peaks gave capacity factor ratios, relative to **I**, of 0.48, 1.04 and 4.38, respectively. DMDA was therefore the most appropriate amine modifier for **I** and it was used in a mobile phase concentration of 0.5 m*M*. A concentration of 31% acetonitrile in the mobile phase gave a practical retention time.

Then, ideally two octadecylsilica (ODS) materials with a large difference in the residual silanol content were mixed to give a suitable column. As a measure of the silanol content the ratio of the capacity factor for the system peak to the capacity factor for an amine analyte (remoxipride) was used. Earlier [3], Spherisorb ODS-1, having a ratio of 1.93, and ODS-2, with a ratio of 4.36, were used. As small variations in the ionic strength of the mobile phase might have a drastic effect on the capacity factor

ratio at low ionic strengths, it was proposed earlier that peak compression effects at high ionic strengths would possibly be more robust [3]. Preliminary tests with **I** showed that the ideal ODS-1 material should have a capacity factor ratio of about 2 in the experiment above, then a high ionic strength could be used. Unfortunately, the currently available ODS-1 batches gave higher ratios, between 2.6 and 3.4. Therefore, the ODS-1 batch with the lowest ratio (batch 29/81) was chosen, but had to be used unmixed and combined with a low ionic strength of the mobile phase buffer. As a consequence, part of the flexibility in the design of the peak compression system was lost.

The third step in the optimization strategy was to find a situation where the capacity factor of the system peak exactly equals the capacity factor of the analyte, and this is done by adjusting the ionic strength of the mobile phase buffer. A capacity factor ratio of unity was found at $I = 0.015$–0.020. No negative effects of using this low ionic strength were observed.

The results so far were obtained by the injection of **I** in neat buffer. By using this technique a small positive DMDA system peak, the height depending on the DMDA concentration in the mobile phase, was generated in agreement with, *e.g.*, ref. 16. Also, this small system peak gave a compressed peak for **I**, but with good apparent efficiency ($N_{app}/m > 10^6$) only when very small amounts were injected (linearity is discussed further below). A larger compressing zone can be generated in several ways, two of them being the injection of an anion more lipophilic than DMDA or by injection of DMDA itself. The first approach, used in earlier work [1,2,4–7], gives a zone with a DMDA deficit and with a higher capacity factor than the small positive peak. This negative peak can give efficient compression but often also split peaks and other deformations. Another disadvantage is that the peak containing the lipophilic anion must be eluted before the next injection is made. Hence the sample throughput becomes lower than with an isocratic system. The injection of DMDA supplements the DMDA excess generated by the injection of buffer and this larger excess also has a shorter retention then the system peak from a buffer injection. The retention depends on the DMDA concentration in the peak as the adsorption isotherm for DMDA is non-linear under the conditions described. The positive DMDA peak was found to be the best way to generate peak compression effects as it gives efficient compression and also gives a fast system without late-eluting anion peaks.

The optimization described so far has been focused on giving **I** and the system peak the same capacity factor, the prerequisite for peak compression effects. To optimize also the efficiency of the compressed peak, the influence of the amine modifier concentration in the injected solution must be studied. In Fig. 2 the influence of the DMDA concentration on the apparent efficiency for **I** is shown. Under these conditions an optimum was found at 1.5 m*M* DMDA, where the apparent efficiency (N_{app}/m) was about $1.75 \cdot 10^6$ plates.

In conclusion, in the optimized system a column with unmixed Spherisorb ODS-1, batch 29/81, was used together with a mobile phase consisting of 31% acetonitrile in phosphate buffer (pH 2, ionic strength 0.015) containing 0.5 m*M* DMDA. The sample was dissolved in a solution of 1.5 m*M* DMDA in phosphate buffer. The resulting chromatographic peaks for **I** and **II** are shown in Fig. 3. A high chart speed was used to demonstrate the peak shape.

Optimization of detectability

The width of a compressed peak in the discussed

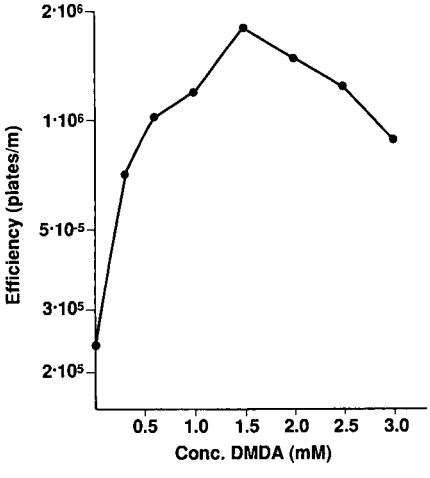

Fig. 2. Influence of DMDA concentration in the injected solution on the chromatographic efficiency for **I**. Mobile phase: 31% acetonitrile in phosphate buffer (pH 2, $I = 0.015$) containing 0.4 m*M* DMDA. Sample: **I** (1 μM) dissolved in 0–3 m*M* DMDA, 200 μl injected. UV detection. Flow-rate, 1.0 ml/min.

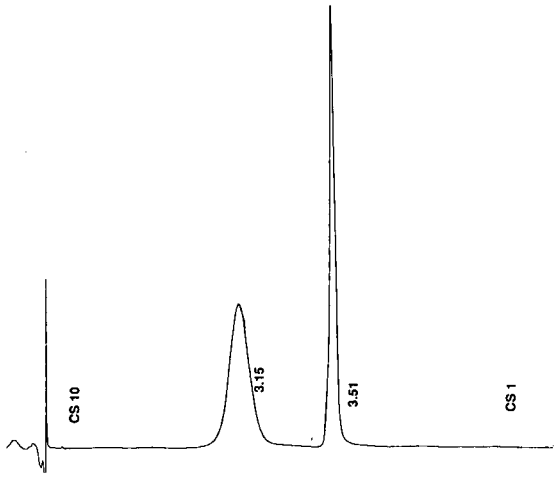

Fig. 3. Peak shapes for the isocratic compound **II** peak and for the compressed compound **I** peak. Sample: **II** (2 μM) and **I** (1 μM) dissolved in 1.5 mM DMDA. Other conditions as in Fig. 2. Programmed chart speed (CS): 0–2.5 min, 10 mm/min; 2.5–4.0 min, 100 mm/min; 4.0–6.0 min, 10 mm/min. Numbers at peaks indicate retention times in min.

systems is typically 10–20 μl and necessitates a detector with a small cell volume and a short time constant. In the optimization of the present system, UV detection with a detector cell volume of 1.4 μl and a time constant of 0.02 s was used, giving negligible loss in efficiency for most peaks. When attempts were made to use the peak compression system combined with UV detection at high sensitivity and for quantitative purposes, a large blank disturbance was seen when DMDA was injected. This peak had the same retention as **I** and the system peak. The peak height depended on the injected concentration of DMDA and was probably a result of a low UV absorbance of DMDA itself and/or an amine impurity. Distillation of DMDA did reduce, but not remove, the peak. Using the optimized system described above and a flow-rate of 1.0 ml/min, the peak height of the blank disturbance corresponded to an injected amount of 2 pmol of **I**. This blank disturbance was unacceptable.

The phenolic metabolites to remoxipride also have natural fluorescence, however, and the UV detector was replaced with a fluorescence detector with a standard 16-μl flow cell and the shortest time constant of 0.5 s. The blank disturbance was reduced, now corresponding to 200 fmol of **I** or about four times the noise level of the fluorescence signal. Obviously, this cell is much too large and the apparent efficiency for the **I** peak was reduced from $N_{app}/m = 1.75 \cdot 10^6$ (UV) to $0.64 \cdot 10^6$. At the same time, the peak asymmetry factor (Asf) increased from 1.5 to 2.4. Replacing the original cell with a 5-μl cell and connecting the column directly to the cell improved both the efficiency ($N_{app}/m = 0.8 \cdot 10^6$) and the symmetry ($Asf = 2.0$), but still about 50% of the efficiency was lost. As the asymmetry of the peak still was markedly higher than that of the peak from the UV detector, the flow characteristics of the cell were thought to be inadequate and the flow-rate was reduced to 0.5 ml/min, resulting in $N_{app}/m = 1.25 \cdot 10^6$ and $Asf = 1.8$. An interesting effect of the reduction in flow-rate was that the optimum efficiency was found at a lower amine modifier concentration, possibly owing to kinetic effects in the contributing equilibria. This is demonstrated in Fig. 4, where the apparent efficiency is plotted against the DMDA concentration in the injected solution. Using the fluorescence detector and a flow-rate of 0.5 ml/min, the optimum ($N_{app}/m = 1.45 \cdot 10^6$ with $Asf = 1.8$) was found at 0.8 mM DMDA. This can be compared with $N_{app}/m = 1.75 \cdot 10^6$ and $Asf = 1.5$ for the optimized UV system. The losses in efficiency and symmetry are due to the larger cell volume and the higher time constant of the fluorescence detector. The influence of cell

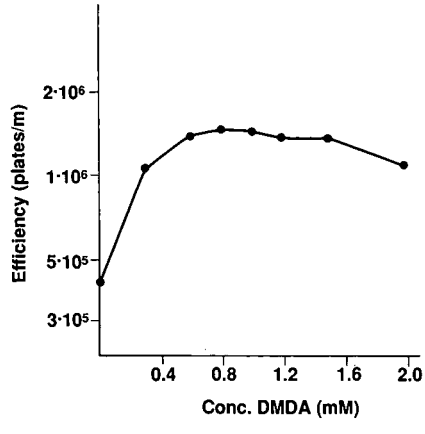

Fig. 4. Influence of DMDA concentration in the injected solution on the chromatographic efficiency for **I**. Mobile phase: 31% acetonitrile in phosphate buffer (pH 2, $I = 0.015$) containing 0.5 mM DMDA. Sample: **I** (1 μM) dissolved in 0–2 mM DMDA, 200 μl injected. Fluorescence detection. Flow-rate, 0.5 ml/min.

volume and time constant on the peak broadening can be calculated using the equations introduced by Martin *et al.* [17]. The 20% loss in efficiency found, corresponding to a peak broadening of about 10%, is considerably lower than the value calculated using these equations, partly owing to the overestimation of the plate number for asymmetric peaks. As the optimum efficiency was found at a lower injected concentration of DMDA, the blank disturbance was also lowered to the same extent, now corresponding to an injected amount of about 100 fmol of **I** or twice the noise level.

The total result of changing detection principle was a 20-fold reduction of the blank disturbance, but also a loss of about 20% in the number of theoretical plates and an increase asymmetry of the peak.

Selectivity in peak compression systems

An inherent disadvantage with peak compression systems is the loss of selectivity in the zone where the analyte peak is compressed. All injected amines, and probably also other compounds with an ability to interact with silanols, with capacity factors covered by the zone will elute in the same peak. Obviously, the zone should be kept as small as possible. The importance of keeping the zone small is demonstrated in Fig. 5, where the internal standard, **II**, **I** and the later eluting raclopride were injected dissolved in increasing concentrations of DMDA. The system peak co-eluted with **I** at all concentrations. Without DMDA in the injected solution all four peaks were well separated. At DMDA concentrations $\geqslant 2$ mM, **I** and raclopride eluted together in a compressed peak and at 4 mM also **II** was trapped in the DMDA zone. The chromatograms at 0.5 and 2.5 mM DMDA are shown in Fig. 6. The peak shape for the last-eluting compound at the low DMDA concentration can be noted. This analyte has about the same retention as the zone within the zone, but considerably slower retention in the bulk mobile phase. When the analyte molecules reach the mobile phase behind the zone they will start to move

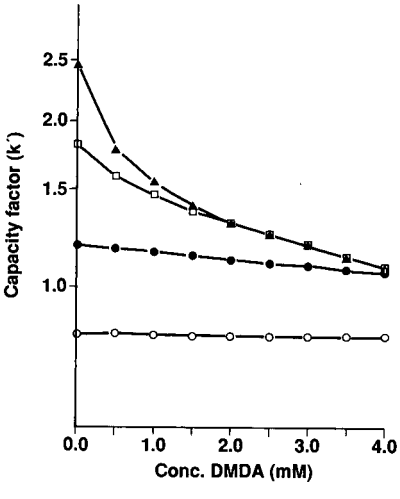

Fig. 5. Influence of DMDA concentration in the injected solution on the selectivity. Mobile phase, flow-rate and detection as in Fig. 4. Sample: (○) **III** (0.5 μM), (●) **II** (0.5 μM), (□) **I** (0.2 μM) and (▲) raclopride (0.5 μM) dissolved in 0–4 mM DMDA.

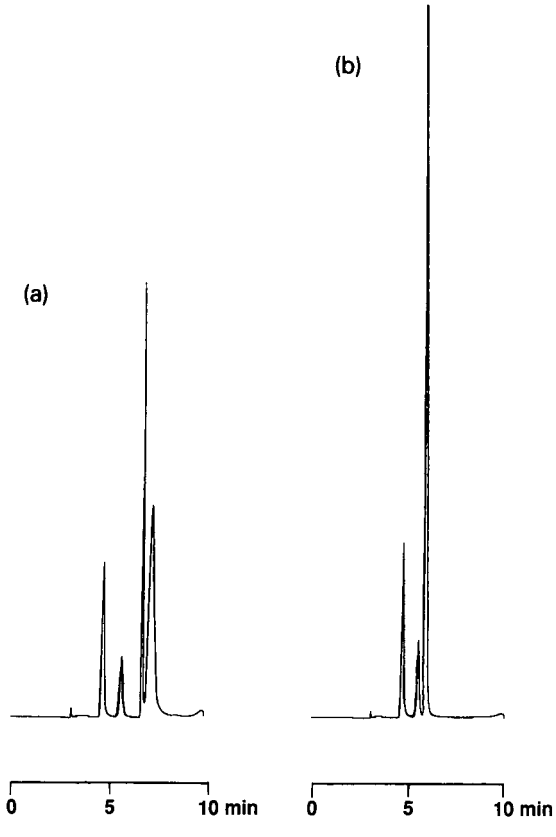

Fig. 6. Chromatograms demonstrating the change in selectivity with increase in the size of the compressing zone. Conditions and elution order as in Fig. 5. Sample dissolved in (a) 0.5 mM and (b) 2.5 mM DMDA.

more slowly than the zone and, consequently, peak broadening will occur.

Compounds with no ability to interact with silanols are not affected at all by the amine modifier zone, *i.e.*, neither the capacity factor nor peak shape is influenced. If the isocratic peak of such a compound elutes together with the compressed peak, the amine modifier concentration in the injected solution can be adjusted in order to make these peaks separate. This possibility of regulating the selectivity between amines and non-amines by varying the amine modifier concentration in the injected solution is demonstrated in a similar system where remoxipride and a lactam metabolite (**V**) eluted as one peak when dissolved in neat phosphate buffer (Fig. 7a). When the sample was dissolved in 2 m*M* DMOA the remoxipride peak instead was eluted as a compressed peak in front of the lactam (Fig. 7b). The retention of the lactam, and also that of the early eluting amine **IV**, were unchanged.

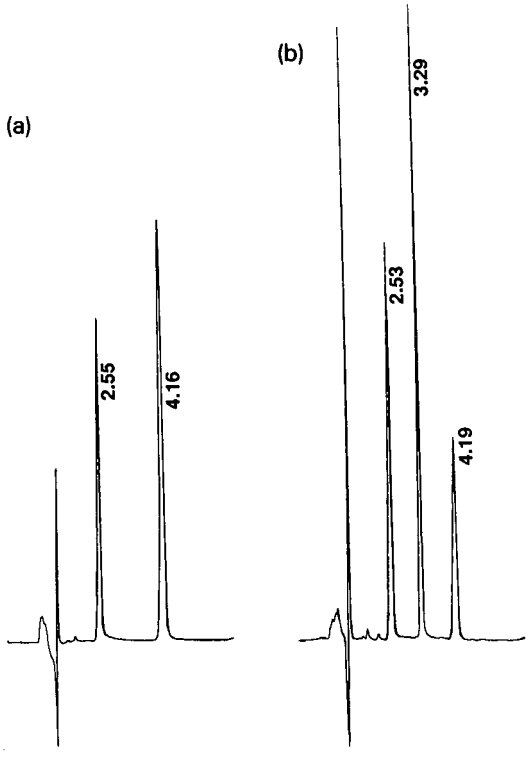

Fig. 7. Chromatograms showing the selectivity towards compounds not interacting with residual silanols. Column: Spherisorb ODS-1, batch 28/25. Mobile phase: 26% acetonitrile in phosphate buffer (pH 2, $I = 0.04$) containing 0.6 m*M* DMOA. Sample: **IV**, remoxipride and **V**, 1 μM each. (a) Sample dissolved in neat buffer; **IV** peak at 2.55 min and combined peak of remoxipride and **V** at 4.16 min. (b) Sample dissolved in 2 m*M* DMOA; **IV** peak at 2.53 min, remoxipride peak at 3.29 min and **V** peak at 4.19 min.

Compounds **I** and **II** are the two most lipophilic of the remoxipride metabolites and they are also considerably more retained than remoxipride itself. Therefore, when analysing samples from subjects treated with remoxipride, no remoxipride-related compounds will interfere with the **I** peak. The loss of selectivity in the present system was minimized as a concentration of only 0.8 m*M* DMDA was used to generate a compressed peak. Combining this with the selective fluorescence detection, the risk of false peaks for **I** must be considered to be very low.

Linearity

The linearity of the peak compression system was found to be limited and dependent on the concentration of the amine modifier in the injected solution. In Fig. 8, peak height for **I** is plotted against injected amount at three different amine modifier concentrations. When **I** was dissolved in 2 m*M* DMDA a straight line was obtained up to about 300 pmol of **I** injected. When dissolved in 1 and 0.3 m*M* DMDA, the plot was linear up to about 200 and 100 pmol, respectively. The non-linearity above these concen-

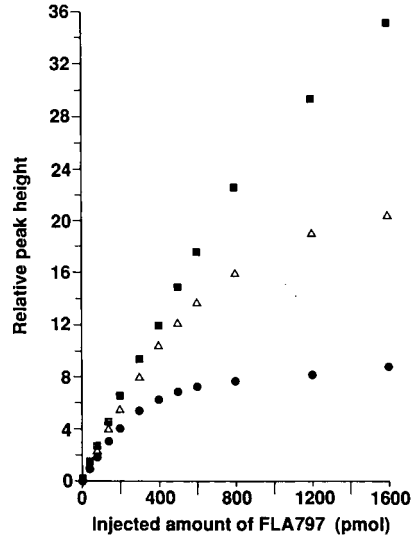

Fig. 8. Linearity in peak compression systems. Mobile phase as in Fig. 4, flow-rate 1.0 ml/min and UV detection. Sample: **I** (0–8 μM) dissolved in (●) 0.3, (△) 1.0 and (■) 2.0 m*M* DMDA.

trations was due to peak broadening. The mechanism behind the limited linear range is not understood but some additional experimental data can be given to describe the non-linearity. The height of the DMDA peak depends on both the injected amount and the DMDA concentration in the mobile phase. The linear range correlated well with the height of the DMDA peak, measured from the RI detector signal, which was 10.5 mm (0.3 m*M* DMDA), 19 mm (1.0 m*M* DMDA) and 31 mm (2.0 m*M* DMDA). The concentration at the peak maximum (C_{max}) can be calculated for both the system peak and the analyte peak using the equation

$$C_{max} = \frac{\sqrt{N_{app}}m}{\sqrt{2\pi}V_R} \quad (1)$$

where m is the injected amount and V_R the retention volume. If the found values for each parameter (N_{app} and V_R for the DMDA peak decreases with increasing injected amount of DMDA) were used, C_{max} in the DMDA peak was calculated to be 270, 490 and 790 μM, respectively, at the three injected DMDA concentrations. The corresponding peak maximum concentrations for the analyte peak were 3.9, 8.8 and 14.9 μM, when calculated on the highest concentration in the linear range. The results suggest that, for efficient peak compression to occur, the excess of amine modifier over the analyte must be >60. A lower ratio of the peak maximum concentrations results in peak broadening.

The linearity for the isocratic peak for **II** was also found to be limited, but this limitation was independent of the DMDA concentration. Injected amounts above 1200 pmol gave deviations from the straight line at all three DMDA concentrations. An experiment was also performed to establish whether high amounts of **II** influenced the linearity of **I**. No such influence could be seen.

It can be noted that if the sample is injected dissolved in a high concentration of the amine modifier, this will improve the linearity but decrease the selectivity and increase the blank disturbance. Consequently, the amine modifier concentration is always a compromise but normally the linearity will be sacrificed in favour of selectivity and sensitivity.

Optimization of the plasma extractions

Compounds **I** and **II** and also the internal standard (**III**) are both tertiary amines and phenols. The plasma extractions were performed at pH 9–10, where these groups are not ionized. Under these conditions, and using an organic phase of 20% *n*-hexane in diethyl ether, the absolute recovery was quantitative (>95%) for all three compounds. When the alkalinization was effected with sodium hydroxide, an addition to the blank disturbance described above was seen. This blank disturbance corresponded to an injected amount of 1 pmol of **I**. If the sodium hydroxide was replaced with carbonate buffer, the total blank disturbance was reduced to 200 fmol. These blank disturbances were equally large also when the aqueous phase in the extraction was water instead of plasma, indicating that plasma itself gave no contribution. As the blank disturbance was related to the amount of DMDA in the injected sample and the contribution from the carbonate buffer, two parameters that are easily controlled as they are the same for all samples in a set, the blank disturbance was found to be sufficiently reproducible not to hamper seriously the plasma determinations.

Repeatability and limit of quantification

To demonstrate the repeatability of the peak compression effect itself, an experiment was performed in which 32 consecutive injections of the same solution were made. This solution contained **I** (0.5 μM) and **II** (1 μM) dissolved in 1.5 m*M* DMDA. UV detection was used, the flow-rate was 1.0 ml/min and the heights for each peak were measured. When the relative standard deviations (R.S.D.) were calculated for the whole run, the R.S.D. for the peak height of the compressed peak was good (1.6%), although that for the isocratic peak was lower (0.7%). A trend for increasing peak heights during the run was observed for both compounds. This was probably due to evaporation of water as the autosampler vials were not capped. If the precision instead was calculated for ten consecutive injections, the mean R.S.D. was about 0.4% for the isocratic peak and 0.5% for the compressed peak. This appears to be as good as for normal isocratic systems when using the described autosampler.

The above results also showed, as both the compressed and the isocratic peak gave similar precision, that it would be possible to use another isocratic peak as internal standard for both com-

TABLE I

WITHIN-RUN PRECISION AND ACCURACY FOR PLASMA DETERMINATIONS OF I AND II

Spiked plasma samples were analysed as described under Experimental. The peak heights were measured by the integrator.

Compound	Accuracy		Precision, R.S.D. (%)	*n*
	Added concentration (n*M*)	Found concentration (n*M*)		
II	200	201	2.4	10
I	25.0	25.4	2.3	10
II	10.0	10.8	17	10
I	1.00	1.00	11	10
I[a]	1.00	1.08	5.2	10

[a] Manually measured peak heights.

pounds when determining their concentrations in plasma. In a peak compression system with an excess of amine modifier as compressing zone, an internal standard is preferably eluted before the compounds of interest because, as discussed above, amine peaks eluting closely after the system peak are broadened.

The phenolic compound **III**, similar to **I** and **II** but not a metabolite to remoxipride, had a suitable capacity factor and was chosen as the internal standard. The within-run precision and accuracy for spiked plasma samples, using the internal standard and extraction and analysis as described under Experimental, are presented in Table I. At the higher concentration the precision was about 2% for both compounds. At the low concentration, manual measurement of the peak heights for **I** gave a higher precision than using the peak heights reported by the integrator. For very small peaks it seemed easier to obtain a good measure of the distance between the peak apex and the average noise when they were measured manually. The results also showed that plasma extracts did not influence the chromatography. A calibration graph, ranging from 1 to 40 n*M* of **I**, is presented in Fig. 9, and Fig. 10 shows one of the chromatograms from that graph. A chromatogram for a real sample with a low concentration of **I**, 0.6 n*M*, and an unmeasurable concentration of **II** is shown in Fig. 11. In this chromatogram it can be noted that about one third of the peak height originated from the blank disturbance and also that

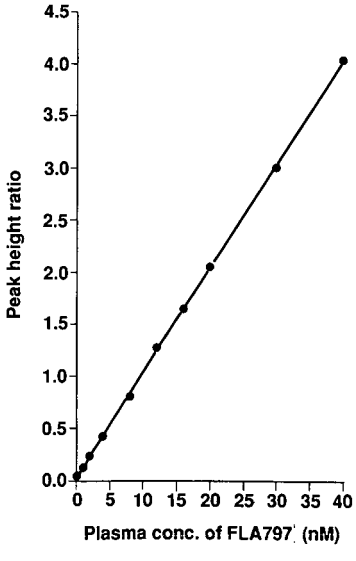

Fig. 9. Calibration graph for the determination of **I** in plasma. Sample work-up and chromatography as described under Experimental. Found intercept: −0.35 n*M*; correlation coefficient (R^2) = 0.9997.

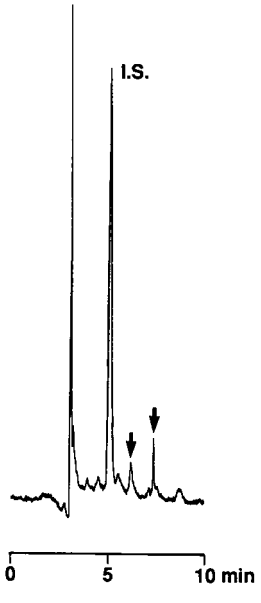

Fig. 10. Chromatogram of a standard sample. Sample work-up and chromatography as described under Experimental. Added concentrations: **II** = 5.0 n*M*, **I** = 1.0 n*M* and **III** (internal standard, I.S.) = 75 n*M*. The arrows indicate the positions of **II** (first arrow) and **I** (second arrow).

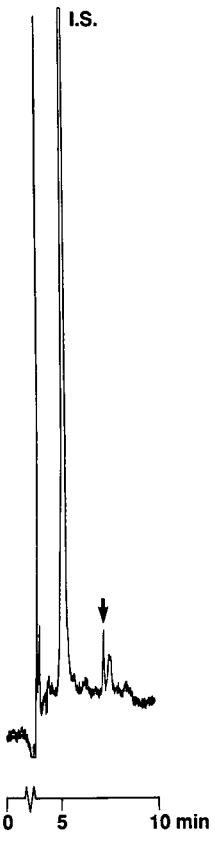

Fig. 11. Rat plasma chromatogram, sample taken 20 min after intraperitoneal administration of 40 μmol/kg of remoxipride. Sample work-up (plasma volume 635 μl) and chromatography as described under Experimental. The arrow indicates the position of **I**, found concentration 0.6 n*M*; internal standard (I.S.) concentration, 100 n*M*.

an isocratic endogenous peak eluted close to **I** without disturbing its peak height.

Based on the reported precision, it seemed possible to determine plasma concentrations of **I** down to 0.5–1.0 n*M* with reasonable precision while the LOQ for **II** was 10–15 n*M*. As **I** has a three times better fluorescence response than **II**, the peak compression effect can be estimated to give 6–7 times better sensitivity for **I** than an isocratic system with the same instrumental set-up.

Advantages and disadvantages of peak compression systems

Although more difficult to develop, this work shows that peak compression systems utilizing an excess of amine modifier as a compressing zone are equivalent to conventional isocratic systems in terms of reproducibility, sample capacity and simplicity. Using this kind of peak compression system, the only practical difference is that the sample is injected dissolved in a solution of the amine modifier and the only visible difference is that one peak is very narrow. Other compounds giving isocratic peaks can be determined simultaneously or added to the sample and used as an internal standard. The height of the compressed peak was shown to be as reliable and reproducible as the height of an isocratic peak, although the high efficiency of the compressed peak seemed to make it more sensitive to the condition of the column. This kind of system can also be compared with the displacement systems for peak compression [10]. In the displacement systems, the sample is injected into a column with a pure mobile phase and thereafter a mobile phase containing the displacer is introduced. The degree of compression seems to be about the same but the selectivity is low in the displacement system as a high concentration of a general displacer is used. On the other hand, the peak compression is not restricted to amines. The major drawback with the displacement systems is the need for regeneration of the column between each run, making these systems impractical for routine determinations of trace levels.

There are, however, two important limitations with the peak compression systems described in this paper: the requirement for a non-standard detector and the limited linearity. Although the linearity of a peak compression system is limited, the linear range for the described application is large enough (0.5–200 pmol) for the intended samples. If high concentrations (>200 n*M* of **I** in plasma) must be determined, the samples are simply diluted before injection or a normal isocratic system is used. In conventional HPLC, cell volumes of 8–15 μl and time constants of 1.0 s or more are used. The sharp peaks obtained with peak compression systems make it impossible to use these conditions. Although smaller cells are available, the optical system is usually not optimized for these cells, resulting in a larger decrease in signal-to-noise ratio than is expected from the difference in cell length/volume. Often also the stray light becomes higher when a smaller cell is used, leading to limitations in linearity. The peak compression effect improved the sensitivity for **I** by

6–7 times compared with an isocratic system with the same instruments. However, if the large 16-μl cell and a time constant of 1 s were used in the isocratic system, the signal-to-noise ratio would be improved, giving an LOQ almost comparable to that with the peak compression system. Until more optimum fluorescence detectors are commercially available, perhaps based on laser sources, the benefits of the described peak compression system regarding sensitivity enhancement cannot be fully utilized.

ACKNOWLEDGEMENTS

Phase Separations are acknowledged for their generous gifts of samples of stationary phases. Professor D. Westerlund and Dr. T. Nordgren are thanked for valuable criticisms of the manuscript.

REFERENCES

1 L. B. Nilsson and D. Westerlund, *Anal. Chem.*, 57 (1985) 1835.
2 L. B. Nilsson, M. Widman, B. Bryske and D. Westerlund, *Chromatographia*, 22 (1986) 283.
3 L. B. Nilsson, *J. Chromatogr.*, 506 (1990) 253.
4 M. Johansson and D. Westerlund, *J. Chromatogr.*, 452 (1988) 241.
5 M. Johansson, H. Forsmo-Bruce, A. Tufvesson-Alm and D. Westerlund, *J. Pharm. Biomed. Anal.*, 7 (1989) 1055.
6 T. Fornstedt, D. Westerlund and A. Sokolowski, *J. Liq. Chromatogr.*, 11 (1988) 2645.
7 T. Fornstedt, D. Westerlund and A. Sokolowski, *J. Chromatogr.*, 506 (1990) 61.
8 K. Šlais, M. Krejčí and D. Kouřilová, *J. Chromatogr.*, 352 (1986) 179.
9 J. Frenz, J. Bourell and W. S. Hancock, *J. Chromatogr.*, 512 (1990) 299.
10 R. Ramsey, A. M. Katti and G. Guiochon, *Anal. Chem.*, 62 (1990) 2557.
11 L. Florvall, M.-L. Persson and S.-O. Ögren, *Acta Pharm. Suec.*, 20 (1983) 365.
12 C. Köhler, H. Hall, O. Magnusson, T. Lewander and K. Gustafsson, *Acta Psychiatr. Scand.*, 82 (1990) 27.
13 L. B. Nilsson, *J. Chromatogr.*, 526 (1990) 139.
14 M. Widman, L. B. Nilsson, B. Bryske and J. Lundström, presented at the *12th European Workshop on Drug Metabolism, Basle, September 16–21, 1990.*
15 T. de Paulis, Y. Kumar, L. Johansson, S. Rämsby, L. Florvall, H. Hall, K. Ängeby-Möller and S.-O. Ögren, *J. Med. Chem.*, 28 (1985) 1263.
16 A. Sokolowski, T. Fornstedt and D. Westerlund, *J. Liq. Chromatogr.*, 10 (1987) 1629.
17 M. Martin, C. Eon and G. Guiochon, *J. Chromatogr.*, 108 (1975) 229.

Journal of Chromatography, 591 (1992) 219–224
Elsevier Science Publishers B.V., Amsterdam

CHROM. 23 803

UV spectrophotometric detection in the ion chromatographic analysis of alkali and alkaline earth metal and ammonium cations

P. Pastore* and A. Boaretto

Department of Inorganic, Metallorganic and Analytical Chemistry, University of Padova, via Marzolo 1, 35131 Padova (Italy)

I. Lavagnini

Institute of Industrial Chemistry, University of Padova, via Marzolo 9, 35131 Padova (Italy)

A. Diop

Department of Chemistry, Faculty of Sciences, University C. Anta Diop, Dakar (Sénègal)

(First received May 28th, 1991; revised manuscript received October 10th, 1991)

ABSTRACT

A spectrophotometric detection procedure for the high-performance ion chromatographic determination of alkali and alkaline earth metal and ammonium cations, after chemical suppression of the eluent, is proposed. Measurements at 200 nm revealed the presence of hydroxide ions, which bear a stoichiometric relationship with the eluted M^{n+} cations. The detection limits and sensitivities were similar to those obtained by the usual conductivity method. The suggested procedure, when tested in the analysis of samples of ammonium cations, gave responses dependent also on the pH of the suppressed solution and relative pK_a values. Fitting of the calibration graphs by means of a non-linear regression routine also allows the determination of the equilibrium constants of the cations.

INTRODUCTION

Ion chromatography (IC) can be a powerful analytical tool for the analysis of ionic and ionizable species [1] if the appropriate column, eluent composition and detector are selected. In analyses for alkali and akaline earth metal and ammonium cations, suppressed conductivity detection is generally adopted whereas a UV–VIS detector is the best choice for absorbing species. However, the demand for "universal" detectors, with a resolution set by the column, required an extension of the range of applicability of available detectors. As chromatographic measurements of akali metal ions using suppressed conductimetric and spectrophotometric detectors connected in series show correlated peaks, attention was devoted to verifying whether UV detection at 200 nm, with suppression of the usual hydrochloric acid eluent, would be a successful alternative for the detection of monovalent and divalent cations. The investigation was also based on the circumstance that the UV absorbance of an aqueous alkaline solution is higher than that of a neutral solution [2,3].

EXPERIMENTAL

Chemicals

All chemicals were of analytical-reagent grade. Demineralized water was passed through a Millipore GS (cartridge 0.22 μm) for final purification and deaerated with helium. Standard solutions of

0021-9673/92/$05.00

the different cations were prepared by dissolving weighed amounts of the corresponding chloride in water. An ammonium standard solution was prepared from the sulphate [4] and an *n*-propylammonium standard solution from a weighed amount of the corresponding amine. Tetrabutylammonium hydroxide (TBAOH) 30-hydrate (>99%) from Fluka and 40% aqueous TBAOH from Aldrich were used to prepare regenerating solutions.

Apparatus and procedure

A Waters ActIon Analyzer ion chromatograph equipped with a 20-μl sample loop was used. Chromatograms were recorded with a Hewlett-Packard Model 7090A digital plotter and a Spectra-Physics SP4270 integrator. The column, obtained from Dionex, was a CS3 (250 mm × 4 mm I.D.) in conjunction with a CG3 (50 mm × 4 mm I.D.) guard column. The suppression device was Dionex CMMS. A Knauer Model SP87 variable-wavelength UV–VIS detector was employed. Preliminary UV spectra were recorded with a Perkin-Elmer Model Lambda 5 spectrophotometer. In the chromatographic tests the eluent solutions were 25 m*M* HCl–0.25 m*M* diaminopropionic acid (DAP) aqueous solution for monovalent cations and 48 m*M* HCl–8 m*M* DAP aqueous solution for doubly charged cations. To regenerate the anion micromembrane suppressor 0.05 and 0.1 *M* TBAOH solutions for monovalent and divalent cations were used, respectively, at a flow-rate of 3 ml/min. For pH measurements a Metrohm Model 654 pH meter was used. The simplex algorithm, as a non-linear regression method, was written in FORTRAN 77 and run under the DOS 3.3 operating system on an IGS (CPU i80286) personal computer equipped with an i80287 numerical processor. All plots were made using an HP Model 7090A digital plotter.

RESULTS AND DISCUSSION

Basic considerations

Suppressed conductimetric detection is based on the fact that the cation micromembrane suppressor effects chemical elimination of eluent H^+ ions as the Cl^- counter ion is replaced with OH^-, which neutralizes H^+, whereas an M^{n+} cation only exchanges its counter ion and consequently passes through the detector as $M^{n+} + nOH^-$. This excess of OH^- is measured by the conductimetric detector [1].

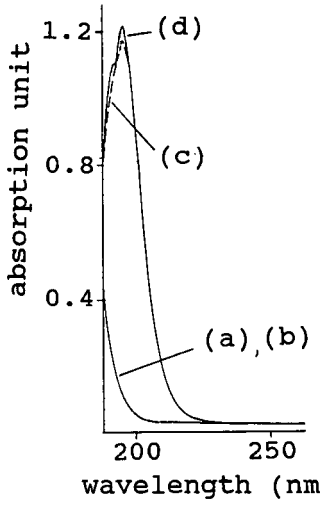

Fig. 1. UV spectra of (a) 10^{-3} *M* HCl, (b) 10^{-3} *M* KCl, (c) 10^{-3} *M* KOH and (d) 10^{-3} *M* KOH–10^{-3} *M* KCl.

The role of OH^- ions in also producing an absorption peak can be seen from the UV spectra for 10^{-3} *M* KCl, 10^{-3} *M* HCl, 10^{-3} *M* KOH and 10^{-3} *M* KCl–10^{-3} *M* KOH aqueous solutions reported in Fig. 1. The spectra of KCl and HCl solutions coincide with a low absorbance, because only the Cl^- ion weakly absorbs, whereas the absorbances of KOH and KOH–KCl solutions are higher owing to the presence of OH^- and are slightly different from each other because of the small contribution of the Cl^- ion. Also, the absorbances of equimolar solutions of monovalent cation hydroxides are identical whereas those of divalent ions are twice as high. These findings suggest the possibility of utilizing the spectrophotometric detector at 200 nm in place of the usual conductimetric detector for quantitative high-performance IC analyses.

As the highest signal for both the conductimetric and spectrophotometric detection modes is obtained when the excess of OH^- is a maximum, the suppression step must be optimized by varying the flow-rate of the regenerating solution. Two aspects of the suppressor device have to be taken into account: the finite rate of regeneration of the membrane suppressor and the permeation of the regenerating solution through the porous membrane. The regeneration is no longer quantitative when both the

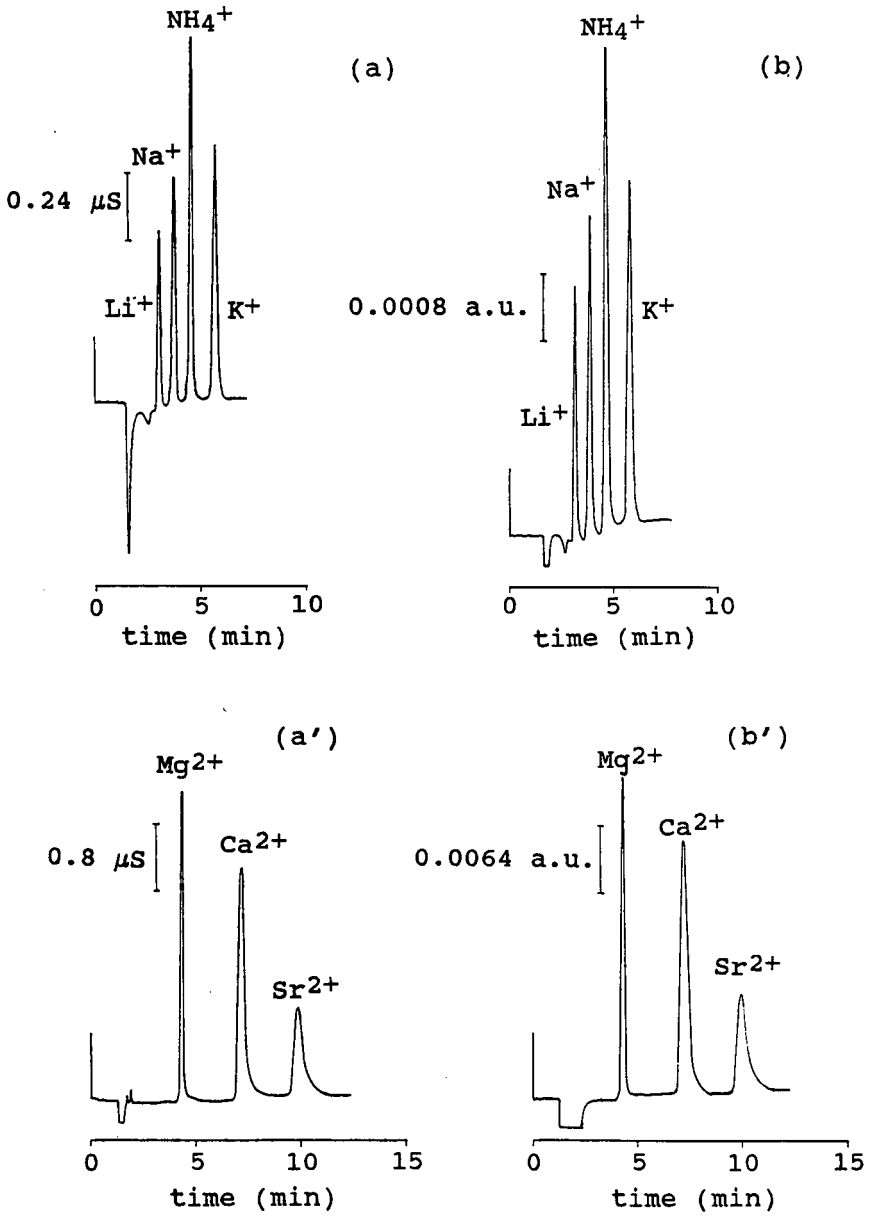

Fig. 2. IC responses of various monovalent and divalent cations with (a and a') the suppressed conductivity detection and (b and b') the suppressed spectrophotometric detection at 200 nm. Chromatographic conditions: flow-rate, 1 ml/min; sample loop, 20 μl; column, Dionex CS3 plus a CG3 guard column; mobile phase, (a) and (b) 25 m*M* HCl–0.25 m*M* DAP in water, (a') and (b'), 48 m*M* HCl–8 m*M* DAP in water. Cation concentrations: Li^+, 0.1; Na^+, 0.4; NH_4^+, 4; K^+, 1; Mg^{2+}, 2; Ca^{2+}, 4; Sr^{2+}, 6 mg/l.

flow-rate and concentration are too low, whereas permeation occurs when they are too high so that suitable values of concentration and flow-rate must be selected.

Alkali and alkaline earth metal cations

Fig. 2 shows the chromatograms of monovalent and divalent cations detected with the conductimetric detector (a,a') in comparison with those

TABLE I

DETECTION LIMITS CALCULATED AS PEAK HEIGHTS EQUAL TO THREE TIMES THE STANDARD DEVIATION OF THE BASELINE NOISE FOR DIFFERENT MONOVALENT AND DIVALENT CATIONS

Regenerating concentration, 0.05 and 0.1 *M* TBAOH for singly and doubly charged cations, respectively. Chromatographic conditions as in Fig. 2.

Ion	Detection limit (μg/l)	
	UV detection	Conductimetric detection
Li^+	0.97	0.94
Na^+	1.25	1.22
NH_4^+	2.1	2.0
$C_3H_{10}N^+$	5.4	6.0
K^+	6.81	6.12
Mg^{2+}	3.69	6.39
Ca^{2+}	9.99	16.89
Sr^{2+}	19.38	66.60

recorded with the spectrophotometric detector (b,b'). Table I reports the detection limits calculated as peak heights equal to three times the standard deviation of the baseline noise. Both monovalent and divalent cations, with the exception of ammonium ions, exhibit a linear range of response up to 10^{-3} *M*.

The fact that the detection process always involves the measurement of the excess of OH^- generated by the replacement of the counter ion makes it possible, in principle, to use a single calibration graph whatever the cation to be analysed. In this particular instance peak areas must be used in place of peak heights, as the peak height depends on the retention time of the eluted species, and the proper ratio M^{n+}/OH^- has to be taken into account.

Ammonium cations

In the determination of ammonium ions, even if a strict relationship between spectrophotometric and conductimetric detection holds, some drawbacks can arise owing to the weakness of the conjugated bases. The OH^- ions generated in the suppression step react with the ammonium ion to reach an equilibrium concentration, so generating a downward curvature of the calibration line. This curvature depends on the equilibrium constant of the weak base and on the pH of the eluent solution after the suppression in the absence of the analyte. The pH, in fact, assumes different values, higher than 7, depending on the purity of the regenerating agent used for the membrane suppressor as a consequence of the "slip" of the regenerating solution, aqueous TBAOH solution, through the membrane. Dedicated ion chromatographic analyses of collected eluent samples revealed the presence of Na^+ and K^+ impurities coming from the TBAOH. These impurities are responsible for the pH value higher than 7 as they pass through the micromembrane together with their OH^- counter ion. This drawback can be

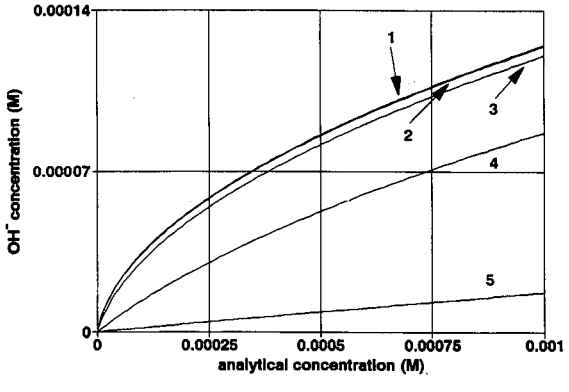

Fig. 3. Theoretical calibration graphs for a weak acid obtained with the model given by eqn. A5 in which $C_{max} = C^0$ for pK_a = 9.25 and $B = 10^{-7}$ (1), 10^{-6} (2), 10^{-5} (3), 10^{-4} (4) and 10^{-3} (5) *M* OH^-.

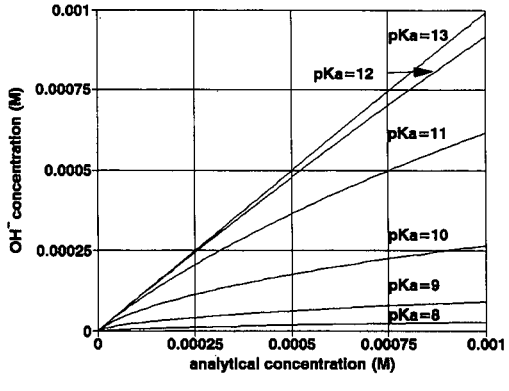

Fig. 4. Theoretical calibration graphs for a weak acid obtained with the model given by the eqn. A5 in which $C_{max} = C^0$ for $B = 10^{-5}$ *M* OH^- and pK_a = 13, 12, 11, 10, 9 and 8.

almost eliminated by using ultra-pure TBAOH solution free from alkali metals, so obtaining a final pH of the eluent solution after the suppression very near to 7 (7.2 in our case).

To clarify the influence of the pK_a values of the eluted species and of different background pH values, several plots of the excess of the OH^- ion *vs.* the analyte concentration were calculated (see Appendix). As the peak height and width depend on particular experimental situations (column, flow-rate, eluent strength), the calculations were carried out using eqn. A5 in which C_{max} was replaced by the analytical concentration C^0. The curves reported in Figs. 3 and 4 show that for a fixed pK_a value, the higher the background pH value the smaller is the curvature with a concomitant lower sensitivity, whereas for a fixed background pH analytes characterized by high pK_a values exhibit good linearity with a sensitivity approaching that of a strong base.

In agreement with the above considerations, the experimental curves in Fig. 5 show that NH_4^+ (pK_a = 9.25), $C_3H_7NH_3^+$ (pK_a = 10.71) and K^+ give progressively higher signals. Further, by using the simplex procedure [5] as a non-linear fitting approach we tried to extract from the experimental curve relative to the NH_4^+ ion the background pH value, the equilibrium constant and the molar absorptivity of OH^- ion (see eqn. A6). Fig. 6 shows the close fit between the calculated and the experimental absorbance values. The estimated parameter

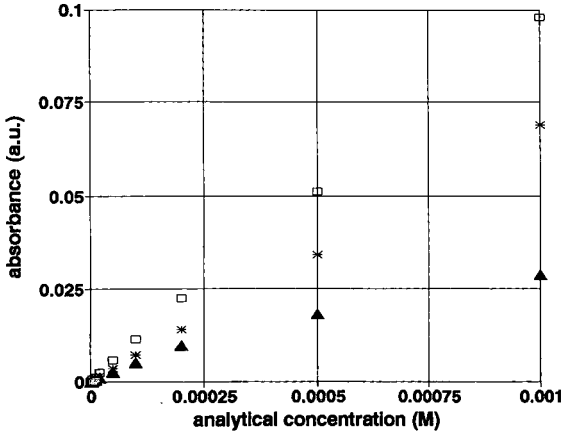

Fig. 5. Experimental calibration graphs for (▲) NH_4^+, (✳) $C_3H_7NH_3^+$ and (□) K^+. Chromatographic conditions as in Fig. 2 for singly charged cations.

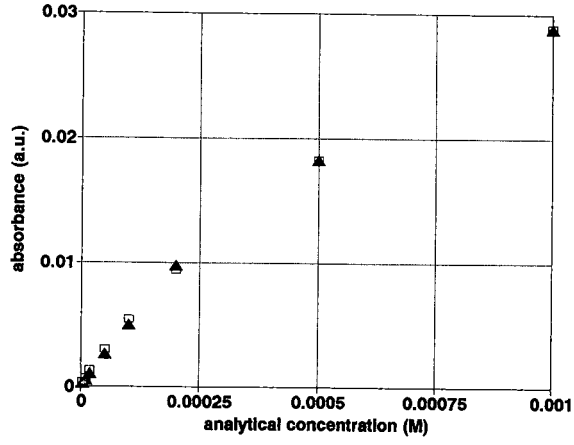

Fig 6. (▲) Experimental calibration graph for NH_4^+ and (□) calibration graph obtained by the simplex method. Values used in the fitting procedure: V_{inj} = sample loop, 20 μl, σ = 0.12 ml, b = 1 cm.

values are pH = 7.13, pK_a = 9.32 and ε_{200} = 1018, which are in excellent agreement with the expected values, namely $pH_{exp.}$ = 7.2, pK_a = 9.25 and ε_{200} = 900 (value obtained from our UV spectra). In this connection, it must be pointed out that in the calculation of the parameters some sources of error are undoubtedly present, namely the dynamic character of the measurements, generally not desirable when equilibrium constants are looked for, the inaccurate calculation of the dilution factor $V_{inj}/(\sigma\sqrt{2\pi})$ owing to the inaccuracy of the peak width, $W = 4\sigma$, and the imperfect reproducibility of the peak height. However, the results found demonstrate that at the peak maximum, where the concentration is almost uniform, the equilibrium is effectively reached for short time intervals even if the concentration profile does not follow strictly a Gaussian shape.

CONCLUSIONS

It has been demonstrated, both theoretically and experimentally, that in the chromatographic determination of cations the conductimetric detector can be replaced, without appreciable loss of sensitivity, with a spectrophotometric detector. The absorbance at 200 nm, even in the absence of a rounded maximum in the spectrum, reveals fairly well the presence of an excess of OH^- ions which are

associated with the analyte cations after the suppression step. Therefore, the procedure described can be a suitable way of working when the chromatographic analysis of different species requires the use of more than one detector connected in series or when an ion replacement procedure is adopted [6]. Finally, the fitting procedure for the calibration graph, in addition to confirming the general correctness of our reasoning, indicates an easy way of measuring the pK_a values of the eluted ammonium cations.

ACKNOWLEDGEMENTS

We acknowledge the financial support provided by the National Council of Research (CNR) and the Ministry of Public Education.

APPENDIX

Model for calculation of the theoretical calibration graph

Under the hypothesis that the chromatographic peak relative to a generic ammonium ion, NH^+, is Gaussian in shape, it holds that

$$C_{NH^+} = C_{max} \exp\left[-\frac{1}{2}\left(\frac{V_{max} - V}{\sigma}\right)^2\right]$$

where V_{max} is the retention volume and C_{max}, the concentration relative to the peak height, can be expressed as

$$C_{max} = C^0 V_{inj}/(\sigma \sqrt{2\pi})$$

as $C^0 V_{inj}$ is the amount of the analyte taken.

The passage through the membrane suppressor (where all the chloride counter ions are converted and a slight permeation of the regenerating solution can occur) generates OH^- ions with a concentration profile similar to that of NH^+ but modified by the attainment of the following acid–base equilibrium:

$$NH^+ + OH^- \overset{K}{\rightleftharpoons} N + H_2O$$

Among the peak concentrations of all the species involved, the following relationships hold:

$$|NH^+|_0 = C_{max};\ |NH^+| = C_{max} - x \quad (A1)$$

$$|OH^-|_0 = C_{max} + B;\ |OH^-| = C_{max} + B - x \quad (A2)$$

$$|N|_0 = 0;\ |N| = x \quad (A3)$$

The subscripts 0 indicate concentrations before the acid–base equilibrium, B is the concentration of hydroxide permeated (that is, the background) and x is the amount of NH^+ reacted with OH^- as determined by the equilibrium constant K:

$$K = \frac{|N|}{|NH^+||OH^-|} \quad (A4)$$

As the effective signal is given by the excess of OH^- in respect to the background B, namely $C_{max} - x$, insertion of eqns. A1–A3 in eqn. A4 gives

$$|OH^-|_{exc} = C_{max} - x = -\frac{KB + 1}{2K} + \frac{(K^2B^2 + 1 + 4KC_{max} + 2KB)^{\frac{1}{2}}}{2K} \quad (A5)$$

Combining the Lambert–Beer relationship, $A_{peak} = \varepsilon b|OH^-|_{exc}$, the molar absorptivity, ε, of OH^- and the optical path, b, the following equation can be derived:

$$A_{peak} = \varepsilon b\left[-\frac{KB + 1}{2K} + \frac{(K^2B^2 + 1 + 4KC_{max} + 2KB)^{\frac{1}{2}}}{2K}\right] \quad (A6)$$

The unknown parameters ε, B and K can be determined from the experimental measurements of the absorbance by using a non-linear regression algorithm. In particular, a Nelder and Mead four-vertices simplex algorithm, which compares experimental and calculated absorbances for different concentrations of NH^+ injected, was successfully used.

REFERENCES

1 J. Weiss, *Handbook of Ion Chromatography*, Dionex, Sunnyvale, CA, 1986.
2 P. Zuman and W. Szafranski, *Anal. Chem.*, 48 (1976) 2162.
3 M. Fox and R. McIntire, *Faraday Discuss. Chem. Soc.*, 64 (1977) 167.
4 ASTM Committee, *1982 Annual Books of Standards, Part 31*, American Society for Testing and Materials, Philadelphia, 1982, p. 273, designation D1426-79.
5 W. H. Press, B. P. Flannery, S. A. Teukolsky and W. T. Wetterling, *Numerical Recipes*, Cambridge University Press, Cambridge, 1987, Ch. 10 and 14.
6 P. R. Haddad and P. E. Jackson, *Ion Chromatography —Principles and Applications (Journal of Chromatography Library*, Vol. 46), Elsevier, Amsterdam, 1990, Ch. 12.

Journal of Chromatography, 591 (1992) 225–232
Elsevier Science Publishers B.V., Amsterdam

CHROMSYMP. 2482

High-performance liquid chromatographic–mass spectrometric analysis of oligosaccharides from enzymatic digestion of glycosaminoglycans

Application to human samples☆

L. Silvestro* and I. Viano

Istituto di Farmacologia e Terapia Sperimentale, Facoltà di Medicina, Università di Torino, Via P. Giuria 13, 10125 Turin (Italy)

A. Naggi and G. Torri

Istituto Scientifico di Chimica e Biochimica "G. Ronzoni", Via G. Colombo 81, Milan (Italy)

R. Da Col

Respharma Pharmacological Research srl, Via Belfiore 57, 10125 Turin (Italy)

C. Baiocchi

Dipartimento di Chimica Analitica, Università di Torino, Via P. Giuria 5, 10125 Turin (Italy)

(First received August 10th, 1991; revised manuscript received October 24th, 1991)

ABSTRACT

Glycosaminoglycan contents were evaluated in plasma and urine samples from volunteers treated intravenously with a mixture of dermatan sulphate and heparin, combining a novel liquid chromatographic–mass spectrometric technique for the determination of oligosaccharides from glycosaminoglycans with a classical technique for the extraction of glycosaminoglycans from biological samples (precipitation with cetylpyridinium chloride). In plasma samples dermatan sulphate and heparin can be measured for 2 h after treatment; urine excretion was detectable for 24 h. These results suggest that this novel approach is promising for future studies on the pharmacokinetics of glycosaminoglycans, although some technical aspects need further improvement, mainly regarding the procedures for sample clean-up; cetylpiridinium precipitation is a complex procedure and the recovery is limited.

INTRODUCTION

Sulphated glycosaminoglycans (GAGs) are a large family of heterogeneous polysaccharides playing important roles in all living organisms and sometimes having notable pharmacological activities [1]. Pharmacokinetic studies of these products have generally been carried out by evaluating biological effects (*e.g.*, coagulation) [2] or by means of radiolabelled derivatives [3]. Both approaches present problems. GAG derivatives sometimes present biological effects, such as antithrombotic activity,

☆ Presented at the *8th (Montreux) Symposium on Liquid Chromatography–Mass Spectrometry (LC–MS, SFC–MS, CE–MS, IC–MS), Ithaca, NY, July 17–19, 1991.*

0021-9673/92/$05.00

that cannot be evaluated easily *in vitro* [4]. The use of radiolabelled molecules involves ethical problems that reduce the applicability of this method. Few pharmacokinetic studies have been performed based on chemical analysis to detect GAGs in biological fluids (generally electrophoresis was used) [5,6].

Recently we developed a new technique for the determination of GAGs using high-performance liquid chromatography–mass spectrometry (HPLC–MS) [7], with a sensitivity and specificity suitable for its application to biological samples. This method is based on the degradation of GAGs present in real samples with specific lyases followed by determination of the disaccharides, typical of different GAGs, by HPLC–MS. An ionspray interface was adopted for effective ionization of such polar molecules. In this paper we describe the results obtained with this technique on blood and urine samples from healthy volunteers treated intravenously (i.v.) with a mixture of heparin (Hep) and dermatan sulphate (DeS). GAGs were precipitated from biological samples with cetylpyridinium chloride (CPC) as reported elsewhere [6,8,9].

EXPERIMENTAL

Chemicals

Hep, DeS, heparinase (Hep.ase), chondroitinase ABC (Ch.ase ABC) and pronase were purchased from Sigma. DeS of different average molecular weight (3300, 5000, 7100, 12 000 and 20 000 dalton) for gel permeation chromatographic (GPC) calibration were kindly provided by Ricerchimica (Milan, Italy). Acetonitrile (HPLC-grade) and all other chemicals, of the purest grade available, were obtained from Fluka. Ultrapure water was obtained with a Milli-Q system (Millipore). The internal standard, deuterium-labelled DeS, was prepared as described previously [7]. Briefly, an aliquot of DeS was treated at 105°C for 5 h with hydrazine to achieve partial (>50%) deacetylation then, after purification by dialysis and lyophilization, the sample was reacetylated with an excess of perdeuterated acetic anhydride. The content of deuterium in the internal standard, determined by HPLC–MS on enzymatic digestion samples, was 40%. The GAG mixture, for the treatment of volunteers, was obtained as vials for clinical use (Ateroid; Crinos, Villa Guardia–Como, Italy).

Standard solutions

Stock solutions of 1 mg/ml Hep and DeS were prepared in water and stored at −20°C; these solutions were prepared freshly each week. Solutions of deuterated DeS were also prepared with the same technique for use as an internal standard.

Extraction from plasma

A 2-ml volume of each plasma sample were treated for 12 h at 45°C with 6.0 mg of pronase to degrade the protein matrix, after addition of 0.4 ml of 50 m*M* Tris–acetate buffer (pH 8.0) containing the internal standard (10 μg of deuterium-labelled DeS). Then trichloroacetic acid (50%, w/w, in water) was added up to a final concentration of 5% and the samples were left for 1 h at 4°C. After centrifugation at 2000 *g* (Hermle BHG Z320K) for 10 min, the supernatants were collected and 4.0 *M* NaOH was added to obtain a final concentration of 0.5 *M*. After 24 h at 4°C, the samples were neutralized with 10.0 *M* HCl and dialysed for 48 h against distilled water with continuous recycling at room temperature using dialysis membranes with a molecular weight cut-off of 3500 (Spectra/Por molecular porous membrane tubing; Spectrum) prewashed in distilled water. After lyophilization (Univapo 15A H; Stepbio), the samples were dissolved in 0.2 ml of 20 m*M* NaCl and injected into the HPLC system to separate high-molecular-weight GAGs from low-molecular-weight degradation products by means of GPC.

Separations were carried out with the technique described below and for each sample the fraction eluting between 9.5 and 16.5 min was collected. GAGs were precipitated from the mobile phase by addition of CPC to a final concentration of 0.015% and overnight incubation at 4°C. Then the samples, after thawing at 20°C, were centrifuged for 20 min at 3000 *g* at room temperature. The precipitates obtained, after carefully removal of supernatants, were washed three times with 80% ethanol saturated with NaCl, three times with 80% ethanol in water, once with absolute ethanol and once with diethyl ether. Finally, the dried pellets obtained from precipitation were digested for 48 h at 37°C with 1.5 mU of Hep.ase and 80 mU of Ch.ase ABC dissolved in 0.5 ml of 50 m*M* ammonium acetate buffer (pH 7.0) containing 1 m*M* $CaCl_2$ as activator of the enzymatic reaction. Then enzymes were precipitated by

addition of three volumes of cold methanol, centrifugation (10 min at 5000 *g*) and the supernatants were lyophilized. Before HPLC–MS analysis the samples were dissolved in 50 μl of distilled water.

Sample volumes of 25 μl were injected into the RP-HPLC system connected to a mass spectrometer (PE-Sciex API III biomolecular mass analyser) equipped with an ionspray interface without splitting, and the traces corresponding to the molecular weights of the disaccharides from enzymatic digestion of Hep and chondroitin sulphate (ChS) are analysed.

Extraction from urine

Aliquots of urine samples (10.0 ml) spiked with 500 μg of deuterated internal standard, after centrifugation (15 min at 5000 *g*) to remove any particulates, were treated with CPC, at a final concentration of 1%, to precipitate GAGs. Then samples were treated as described for plasma.

Chromatographic separations

All the HPLC separations were performed using a Gilson HPLC system (Model 302 pump + Model 305 pump) equipped with a microbore dynamic mixer and a Rheodyne Model 7125 injection valve with a loop of 500 μl for GPC separations or a loop of 20 μl for HPLC–MS analysis with a microbore column. When needed, UV absorbance was monitored using a Pharmacia Model 2141 variable-wavelength UV–VIS detector and data were treated with a Varian 4270 computing integrator.

GPC separations were performed with a Pharmacia TSK G2000 SW column (300 mm × 7.5 mm I.D.) connected with a Supelco Progel TSK G3000 PWXL column (300 mm × 7.8 mm I.D.) under isocratic conditions with 0.1 *M* NaCl as mobile phase at a constant flow-rate of 1.0 ml/min; the signal was monitored at 210 nm.

Gradient RP-HPLC separations were obtained with a hexyl reversed-phase column (Phase Separations C_6, 5 μm, 150 mm × 1 mm I.D.). The mobile phase was composed of 3.3 m*M* tetrapropylammonium hydroxide (TPA) in water adjusted to pH 4 with formic acid (buffer A) and 3.3 m*M* TPA in water–acetonitrile (10:90) at the same pH (buffer B). The gradient elution conditions adopted consisted of 3 min isocratic at 100% buffer A, then a linear gradient to 40% buffer B in 17 min and a final isocratic step of 10 min at this composition. The flow-rate was 0.05 ml/min.

Mass spectrometry

The effluent from the HPLC microbore column, flow-rate 0.05 ml/min, was connected to a PE-Sciex API III triple quadrupole mass spectrometer (Sciex, Thornhill, Canada) equipped with an atmospheric pressure articulated ionspray source. Analyses were performed by selective ion monitoring for negative ions, with a dwell time of 150 ms, at *m/z* 458, 461 and 946. These values, according to our previous results, correspond respectively to the molecular ions of the disaccharide produced by the enzymatic digestion of DeS, the molecular ions of the disaccharide characteristic of the enzymatic digest of deuterated DeS (internal standard) and the ions formed by the adducts of trisulphated disaccharide, typical of Hep enzymatic digestion, with the ion-pair reagent (TPA).

Calibration and quantification

Blank plasma samples (2.0 ml) from a pool of plasma and blank urine samples (20.0 ml) were spiked with both Hep and DeS, using stock solutions, at concentrations of 1, 3, 30 and 100 μg/ml. Appropriate volumes of water were also added to ensure an equivalent total volume (*e.g.*, 0.2 ml for plasma and 2.0 ml for urine) in each instance. For quantification these samples were treated as unknown samples. Separate for calibration graphs for Hep and DeS were constructed of GAG concentrations *versus* the ratio of the peak areas of Hep or DeS to that of the Internal standard. Peak areas for DeS, Hep and the internal standard were evaluated for the peaks eluting at 13.8 min with *m/z* 458, 17.8 min with *m/z* 946 and 13.8 min with *m/z* 461, respectively. Calibration graphs for a new set of spiked samples were prepared after every 30 unknown samples to avoid quantification bias due to the complex extraction and degradation procedure.

Recovery and reproducibility

The percentage recovery of each GAG was determined by comparing the extraction from plasma or urine spiked with GAGs (1, 10 and 100 μg/ml of each GAG) with the equivalent concentration of standard solution dissolved in water, lyophilized and degraded with enzymes as real samples. In both

instances internal standard was added. The reproducibility of the method was determined from samples prepared as before and analysed in triplicate within the same series of analyses or in different set of samples.

Application to plasma and urine samples after i.v. treatment with a mixture of GAGs

Two normal female volunteers were treated intravenously with a single dose of a GAG mixture (DeS 30 mg + Hep 70 mg). Venous blood samples (10.0 ml) were taken before and then 10, 20, 30, 60, 240 and 360 min after the treatment. The blood samples were collected in tubes containing sodium citrate as anticoagulant and immediately centrifuged at 2000 *g* for 10 min at 4°C; 4 ml of each sample were stored at −80°C until analysed.

Urine samples were collected 24 h before and after drug treatment, divided into fractions of 6 h (0–6, 6–12, 12–18 and 18–24 h). After measuring the volume of the diuresis, 50 ml of each fraction were stored at −80°C until analysed.

RESULTS

Chromatographic separations

Using the GPC conditions described previously, standards of DeS, Hep and deuterated DeS eluted together with a retention time of 11 min; the peaks were large, from 9.5 to 17.5 min, owing to the heterogeneity of these molecules. The standard of low-molecular-weight DeS (3300 dalton) had a retention time of 16.7 min and the total elution time of the peak was between 14 and 18 min. Based on these results, a collection time between 9 and 16.5 min was chosen in prepartive GPC to isolate polymeric GAGs (moleculr weight > 3000 dalton) from oligosaccharides. Fig. 1 shows a chromatogram obtained under reversed-phase separation conditions with mass spectrometric detection for an enzymatic digestion of standard GAGs. As reported previously [7], the disaccharide characteristic of DeS degradation, at *m/z* 458, elutes between 13 and 14 min (13.31 min); the same oligosaccharide from the internal standard has the same retention time, as shown by the trace at *m/z* 461. The trisulphated disaccharide characteristic of Hep is more retained and is eluted between 17 and 18 min (17.41 min).

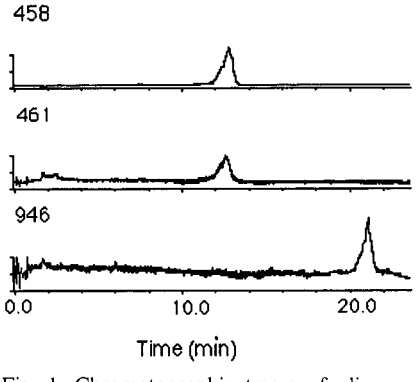

Fig. 1. Chromatographic traces of oligosaccharides from an enzymatic digestion of a standard containing DeS (*m/z* 458), deuterated DeS (*m/z* 461) and Hep (*m/z* 946). The amount injected corresponds to 1 μg of each substance.

Linearity

Good linear correlations were observed between concentrations and peak areas of standard DeS or Hep in water. Straight lines were also obtained by plotting peak-area ratios of DeS or Hep to the internal standard *versus* concentrations in plasma or urine (Fig. 2). For plasma and urine, the relationships were linear ($r > 0.995$) over the range of concentrations tested (1–100 μg/ml) for both DeS and Hep. For Hep the regression line intercept was not significantly different from zero whereas for DeS, especially in urine, the intercept was higher than zero, probably owing to the endogenous ChS and DeS [6,10].

Precision and accuracy

Standards in water of Hep and DeS at 1–10 and 100 μg/ml were analysed in triplicate, after enzyme digestion, to evaluate the variability of the methods without the extraction problems. The results were similar at different concentrations with both substances and the relative standard deviations were between 2.8 and 3.3%. Table I show the concentrations and standard deviations determined for spiked plasma and urine samples, at the same concentrations, extracted and analysed in triplicate within the same set of samples, using the same calibration graphs. Similar relative standard deviations, ranging from 3.3 to 4.5%, were observed with Hep and DeS at different concentrations in both plasma and urine. Table I also gives the results obtained with the same analytical technique and identical

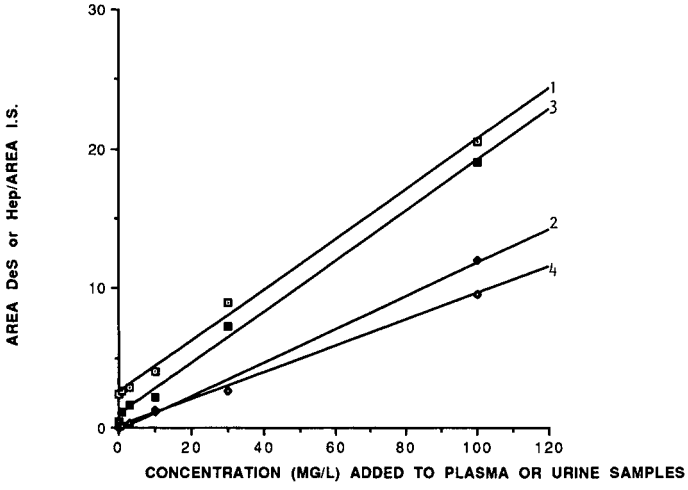

Fig. 2. Linear regressions between concentration of Hep or DeS added to samples of plasma or urine and ratio of peak area of Hep or DeS to that of deuterated DeS added as internal standard (I.S.). Lines: 1 (□) = urine + DeS, R^2 = 0.995; 2 (◆) = urine + Hep, R^2 = 0.995; 3 (■) = plasma + DeS, R^2 = 0.995; 4 (◇) = plasma + Hep, R^2 = 0.997.

range of concentrations from samples analysed in triplicate on different days then using different calibration graphs. The relative standard deviations are higher, between 4.3 and 5.6%, but still reasonable.

Extraction recoveries

Table II gives the results for experiments on the recovery of GAGs and internal standard in plasma and urine. The recoveries of DeS and Hep added to plasma were similar for both molecules, 27.7 ± 2.3

TABLE I

EVALUATION OF PRECISION AND ACCURACY FOR REPLICATE (n = 3) SPIKED SAMPLES OF PLASMA OR URINE ANALYSED ON THE SAME DAY OR ON DIFFERENT DAYS

Concentration added to sample (mg/l)	Concentration determined (mg/l)		Relative standard deviation (%)	
	Hep	DeS	Hep	DeS
Plasma samples analysed on the same day				
100	98.6	101.3	3.9	3.3
10	10.7	9.6	4.1	3.6
1	0.9	1.1	4.2	4.3
Plasma samples analysed on different days				
100	97.4	100.8	4.4	4.3
10	9.1	9.8	5.2	4.8
1	1.1	1.1	5.3	5.1
Urine samples analysed on the same day				
100	103.4	96.2	3.6	4.1
10	10.5	11.1	3.9	4.3
1	0.9	1	4.5	4.5
Urine samples analysed on different days				
100	96.8	102.1	4.3	3.9
10	9.7	10.6	4.5	4.6
1	0.9	1.1	5.6	5.1

TABLE II

EXTRACTION RECOVERIES AND RELATIVE STANDARD DEVIATIONS FOR REPLICATE STANDARDS (n = 3) EXTRACTED FROM SPIKED HUMAN PLASMA OR URINE

Samples	Concentration mg/l	Recovery (%)			Relative standard deviation (%)		
		DeS	Hep	Deuterated DeS	DeS	Hep	Deuterated DeS
Plasma	100	30.2	32.1	31.6	3.4	3.8	3.1
	10	27.3	28.9	30.5	4.4	3.6	3.9
	1	25.6	27.2	27.8	3.8	4.5	4.3
Urine	100	19.2	18.9	19.8	2.8	2.6	2.4
	10	17.3	18.3	3.1	3.5	2.8	
	1	17.1	16.8	17.8	3.1	3.9	3.3

and 29.4 ± 2.5%, respectively (mean ± standard devition at different concentrations tested), with small differences depending on the concentration tested. In urine samples a lower recovery was observed with both GAGs, 17.9 ± 1.2 and 17.8 ± 1.1%, respectively, at all concentrations. The recovery of the internal standard was of the same order as those of Hep and DeS.

Selectivity

No endogenous interfering peaks, except the possible physiological presence of the same substances, were visible in blank plasma or urine samples at the retention times and m/z values characteristic of disaccharides from enzymatic digestion of DeS and Hep.

Sensitivity

The detection limits in plasma samples, corresponding to a signal-to-noise ratio of 2, were 0.5 μg/ml for DeS and 1 μg/ml and Hep. In urine samples, under the same experimental conditions, the detection limits were 0.1 μg/ml for DeS and 0.2 μg/ml for Hep.

Pharmacokinetic study

Fig. 3 shows the chromatograms at m/z 458–946 of plasma samples withdrawn from a volunteer before and 10–120 min after treatment with the mixture of GAGs. The peak corresponding to the internal standard, m/z 461, was well characterized in all samples (chromatograms not reported). In the chromatogram at m/z 458 a peak with the character-

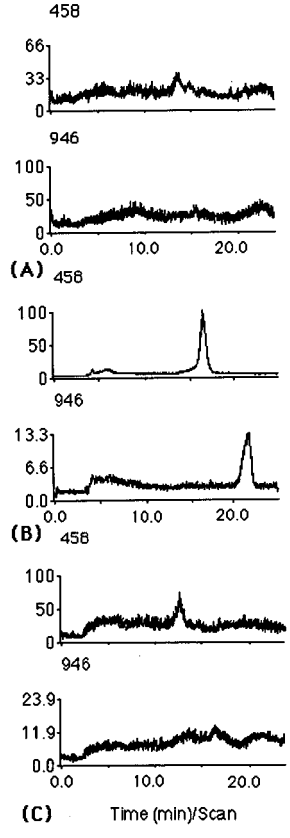

Fig. 3. Chromatographic profiles corresponding to oligosaccharides from DeS (m/z 458) or Hep (m/z 946) obtained from plasma samples of a volunteer (A) before and (B) 10 min and (C) 120 min after i.v. treatment with a mixture of GAGs.

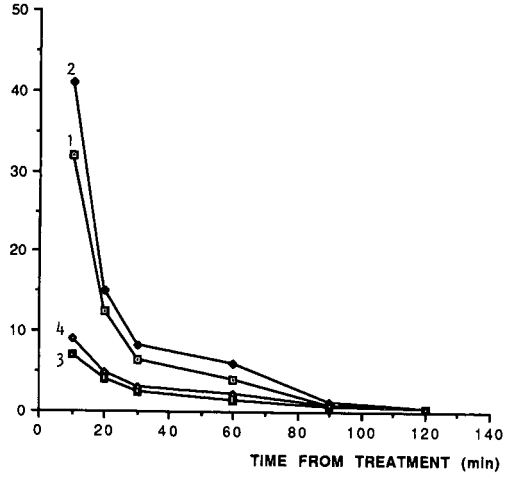

Fig. 4. Plot of DeS and Hep concentrations measured in plasma samples withdrawn from two volunteers at different times after i.v. treatment with a mixture of GAGs. Lines: 1 (□) = patient A, Hep; 2 (◆) = patient B, Hep; 3 (■) = patient A, DeS; 4 (◇) = patient B, DeS.

istic retention time of the digestion product of DeS or ChS is present in the sample before the treatment due to the endogenous content of these GAGs. As expected, its area increased in the samples after treatment. In contrast the peak corresponding to the digestion product of Hep (*m/z* 946, retention time 17.4 min) can be observed only after treatment; in fact a previous study did not show detectable levels of endogenous Hep in blood [6].

Fig. 4 shows graphically the plasma levels of DeS and Hep evaluated in volunteers after the treatment with GAGs. The concentrations of DeS reported were subtracted from the basal levels of DeS of 5.4 and 4.8 μg/ml in patients A and B, respectively. Detectable levels of both GAGs were measured for 2 h after the treatment, the plasma half-life being short, about 10 min.

Fig. 5 shows the chromatograms at *m/z* 458, 461 and 946 of urine samples collected before and 0–6 or 18–24 h after the treatment. DeS is present at high concentration also in the blank urine, but after intravenous treatment the concentrations are higher. Hep could not be measured before treatment but considerable amounts were present after drug administration.

Results for urine excretion are summarized in Table III (results for DeS were subtracted from the basal values). Considerable amounts of DeS and

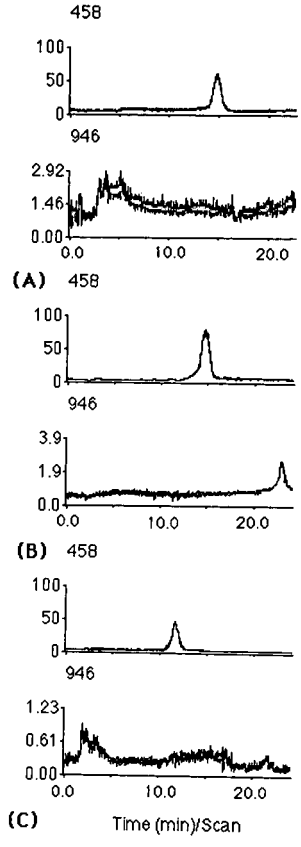

Fig. 5. Chromatographic profiles corresponding to oligosaccharides from DeS (*m/z* 458) or Hep (*m/z* 946) obtained for urine samples from a volunteer collected (A) before and (B) 0–6 h and (C) 18–24 h after i.v. treatment with a mixture of GAGs.

TABLE III

AMOUNTS OF DeS AND Hep EXCRETED IN URINE OF TWO VOLUNTEERS COLLECTED AT DIFFERENT TIMES AFTER I.V. TREATMENT WITH A MIXTURE OF GAGs

Treatment	Time after treatment (h)	Amount determined (mg excreted)	
		Patient A	Patient B
Hep	0–6	9.3	8.0
6–12	4.1	4.5	
	12–18	0.9	0.8
	18–24	0.0	0.0
DeS	0–6	4.4	3.9
	6–12	3.6	4.6
	12–18	1.2	1.5
	18–24	0.6	1.2

Hep are excreted in the 24 h after the treatment, about 35–40% of the injected dose. In the last fractions Hep is not present, suggesting a faster metabolism of this substance than DeS.

DISCUSSION

An effective technique has been developed for studying GAGs in biological samples with adequate sensitivity for pharmacokinetic studies. The technique is specific (no interference was observed in blank samples), is reproducible (reasonable inter- and intrassay variability) and quantification is linear over a wide range of concentrations. The results of recovery studies were not very good, although they were reproducible, and were far from the values reported for some studies using similar techniques [6,9]; moreover this technique is fairly complex. We consider that in future studies, other extraction techniques, *e.g.*, on ECTEOLA-cellulose [5] or Polybrene-Sepharose [3], should be tested in order to improve the recovery and the sensitivity of the technique. The use of degration of GAGs by specific lyases gave interesting results and is highly specific. The lack of activity, at least for Hep.ase [11], on desulphated products may be a limitation for future studies aimed also at the study of possible metabolites that seem to be desulphated [12]. The introduction of other degradation techniques such as with nitrous acid may be appropriate.

The present HPLC–MS approach is really promising in attempts to study GAG metabolites, mainly for the structural information obtainable. Moreover, the results obtained with deuterium-labelled GAGs as internal standard suggest the use of similar derivatives in healthy volunteers to study the pharmacokinetics without interferences from endogenous GAGs. With the improvements suggested above we consider that this technique should be effective also for more demanding pharmacokinetic studies on GAGs such as those after oral treatment or concerning drug metabolism.

REFERENCES

1 L. A. Fransson, in G. O. Aspinall (Editor), *Mammalian Glycosaminoglycans*, Academic Press, New York, 1985, Ch. 3, p. 337.
2 L. B. Jaques, *Pharmacol. Rev.*, 31 (1980) 99.
3 J. Dawes, C. V. Prowse and S. Pepper, *Thromb. Haemost.*, 54 (1985) 630.
4 L. B. Jaques, *Prog. Med. Chem.*, 5 (1967) 139.
5 L. B. Jaques, S. M. Wice and L. M. Hiebert, *J. Lab. Clin. Med.*, 115 (1990) 422.
6 F. Niebes and M. H. Schifflers, *Clin. Chim. Acta*, 62 (1975) 195.
7 L. Silvestro, A. Naggi, C. Baiocchi, R. Da Col, G. Torri and I. Viano, *Anal. Biochem.*, submitted for publication.
8 K. Murata, K. Nakazawa and A. Hamai, *Atherosclerosis*, 21 (1975) 93.
9 M. E. Tira, A. Calatroni, C. Balduini, G. Torri, R. Moretti and B. Casu, *Perspect. Inher. Metab. Dis.*, 2 (1979) 165.
10 I. Staprans, S. J. Garon, J. Hopper Jr. and J. M. Felts, *Biochim. Biophys. Acta*, 678 (1981) 414.
11 R. J. Linhardt, *Biochim. Biophys. Acta*, 702 (1982) 197.
12 J. Dawes and D. S. Pepper, *Thromb. Res.*, 14 (1979) 845.

Journal of Chromatography, 591 (1992) 233–243
Elsevier Science Publishers B.V., Amsterdam

CHROM. 23 782

Experimental determination of adsorption isotherm data for the study of the surface energy distribution of various solid surfaces by inverse gas–solid chromatography

Jeffry Roles and Georges Guiochon*

**Department of Chemistry, University of Tennessee, Knoxville, TN 37996-1501 and Division of Analytical Chemistry, Oak Ridge National Laboratory, Oak Ridge, TN 37831-6120 (USA)*

(First received June 14th, 1991; revised manuscript received September 30th, 1991)

ABSTRACT

Fine, solid ceramic particles were coated on the inner wall of an open-tubular quartz column. The tube was filled with a slurry of the particles under investigation in an appropriate solvent, closed at one end and introduced slowly into an oven where the solvent vaporized. After thermal conditioning of the column, adsorption isotherms were determined by the classical method of elution of characteristic points, using large-size samples of organic vapors (diethyl ether, chlorobutane). These isotherms were used to calculate the distribution of adsorption energy of the probe on the ceramic surface.

INTRODUCTION

As suggested originally by Smidsrod and Guillet [1,2], gas chromatography can be used for the study of the properties of any material which can serve as a stationary phase. Chromatographic data are determined for a group of properly selected probe solutes. These data give clues regarding the interactions between these known molecules and the material under investigation. Results obtained by inverse chromatography have been reviewed by Gilbert [3]. This method is particularly suited to the analysis of solid surfaces, the only requirement being that the specific surface area of the sample exceeds about 1 m^2 g^{-1}. Gas–solid interactions are strong and permit the use of small molecules as probe solutes, measurements being made at room or moderate temperatures. This is advantageous because, for nearly any type of interaction, it is possible to select a small molecule which embodies it almost exclusively.

Except for the determination of equilibrium isotherms, however, almost all the applications of inverse chromatography have been carried out under linear conditions [3]. For example, Guillet and co-workers have developed methods to measure the glass transitions of polymers [1], to study the temperature dependence of their crystallinity [4–6] and to determine the Flory interaction parameter [2, 4] and the Hildebrand–Scatchard solubility parameter [1,2]. Several studies have investigated various aspects of heterogeneous catalysis [7]. The fate of toxic solutes adsorbed on fly ash [8] and diesel particulate matter [9] has been studied. In all instances, except for the determination of isotherms, *e.g.*, with the elution by characteristic points (ECP) method, small amounts of the probe compounds are injected and the interactions at infinite dilution only are investigated. Although there have been many applications of the ECP method for the determination of single-component isotherms, the precision and accuracy of the results obtained have not been studied in great detail so far.

Gas–solid chromatography has been used for a long time to measure rapidly and conveniently the equilibrium isotherms of gases and vapors on the surface of adsorbents [10]. Several chromatographic methods have been developed. The most accurate is

0021-9673/92/$05.00

probably frontal analysis [11,12], but it is not very convenient to implement in gas chromatography where ECP is preferred [13]. The detailed study of the properties of equilibrium isotherms for a group of selected probe solutes is very informative regarding the properties of the surface considered [10]. This is especially true if the surface is heterogeneous.

Although the concept of energetic heterogeneity of surfaces was introduced long ago by Langmuir [14], interest in studying this property as a means of material characterization did not develop until the past 20 years. Even in chromatography, where peak tailing is systematically blamed on the occurrence of active sites on the surface of the adsorbent or of the support used in gas–liquid chromatography [15], few experimental investigations of the energetic heterogeneity of the surface of the material used have been made [16]. The basis of these studies is the calculation of the adsorption energy distribution function of a series of probe compounds from their adsorption isotherms [16]. These functions provide valuable qualitative information regarding the energetic heterogeneity of the surface. More importantly, it has been shown that thermodynamic quantities (*e.g.*, monolayer energies) may be calculated from the energy distributions obtained from inverse gas chromatographic experiments [17]. Thus, the surface energetics may be parameterized, and the information obtained may be much more useful for the characterization of the material than, for example, the retention times of the probe compounds, their retention indices or even their adsorption isotherm data. Considerable effort has been devoted recently to the calculation of physically meaningful energy distribution functions [16,18].

We are investigating the surface properties of ceramic powders used for the manufacturing of advanced ceramic materials. Lack of lot-to-lot reproducibility of the ceramic material properties has been blamed on differences between the chemistry of the particle surface [19]. The procedure we have developed involves the determination of the adsorption isotherm of probe solutes and the calculation of the adsorption energy distribution [18]. We have found that reproducible results can be obtained only if great care is taken to follow a carefully established procedure, minimizing the experimental errors. This paper describes the experimental procedure. A companion paper presents an analysis of the errors made in the determination of equilibrium isotherms by the ECP method [20]. In a separate paper we present results obtained when applying the method to a series of alumina samples [21]. The same procedure could be applied to the study of stationary phases for chromatography, especially in connection with the investigation of tailing problems.

THEORY

Derivation of the adsorption isotherm by ECP

The chromatograms of the probe solutes used with alumina (diethyl ether and 1-chlorobutane) have a very sharp front and a tailing rear. These band profiles correspond to a convex upwards isotherm [10]. The isotherm is derived by integrating the rear (*i.e.*, diffuse) profile [13]. The points on the adsorption isotherm, $q(P)$ (moles of adsorbate per unit mass of adsorbent), are given by a quadrature:

$$q(P) = \frac{1}{J_3^2 R T} \int_0^P V_N(P)\, dP \tag{1}$$

where P is the partial pressure of the probe, $V_N(P)$ is the specific retention volume corrected for the void volume, T is the column temperature, R is the universal gas constant and J_3^2 is the James and Martin correction factor [15]:

$$J_3^2 = \frac{3}{2} \cdot \frac{(P_i/P_0)^2 - 1}{(P_i/P_0)^3 - 1} \tag{2}$$

where P_i and P_0 are the inlet and outlet pressures of the carrier gas.

The essential measurement problem is the conversion of the chromatogram, a profile of detector signal *versus* time into a profile of probe partial pressure *versus* specific retention volume. Then the application of eqn. 1 is straightforward.

Determination of the distribution of adsorption energy

If we assume that the adsorbent surface is heterogeneous and that $f(E)$ is the distribution of the adsorption energy over a certain energy range, Ω, we need to calculate $f(E)$. $f(E)\, dE$ is the amount of probe component adsorbed per unit mass of the adsorbent studied, with an adsorption energy between E and $E + dE$ [22]. We measure the adsorption isotherm, which is the total amount of material adsorbed by the surface when in equilibrium with a

gas where the probe partial pressure is P. The global adsorption isotherm is

$$q(P) = \int_{\Omega} \Theta(E, P) f(E) \, dE \quad (3)$$

where $\Theta(E, P)$ is the local equilibrium isotherm of the adsorbate probe on the part of the surface which has an adsorption energy between E and $E + dE$. Only $q(E)$ is experimentally accessible, but we need to determine $f(E)$ and $\Theta(E, P)$. This problem is ill-posed and does not have a unique solution [23]. It has been extensively discussed in the literature [16,18] and it is not the purpose of this paper to discuss a new solution. The results reported here have been obtained in an attempt to implement the original solution described previously [18].

EXPERIMENTAL

The procedures have been elaborated carefully to achieve a high level of reproducibility of the data and good accuracy. For this reason, we have developed the instrumentation which permits easy detector calibration or other measurements (*e.g.*, volume flow-rates). When these measurements are easy, it is possible to repeat them often and make sure the instrument response is stable, and possible drifts can be corrected for.

Chromatograph

Chromatographic data were obtained on a Perkin-Elmer (Norwalk, CT, USA) Model 8500 gas chromatograph. The only instrumental modification required was to move the inlet pressure transducer to a position on the inlet carrier gas line which is closer to the injection port. The purpose of this modification was to reduce the pressure drop (to a negligible value at the flow-rates used) between the transducer and the column inlet. This gives a more accurate measure of the column inlet pressure. The analogue output from the flame ionization detector was digitized and recorded on an IBM PC. The computer was interfaced to the chromatograph by an I/O board (Data Translation, Marlborough, MA, USA) which used 12-bit A/D conversion and was controlled by in-house written software.

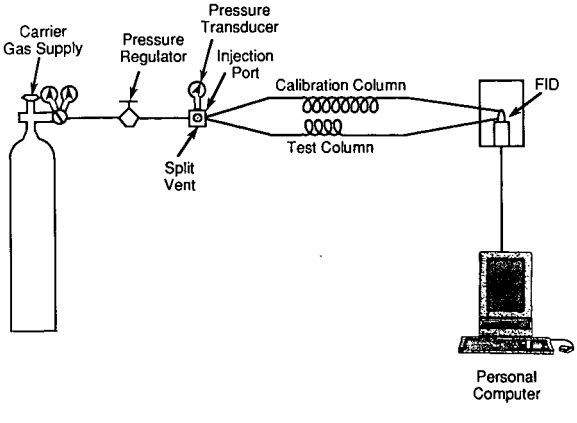

Fig. 1. Schematic diagram of the chromatographic system used to record overloaded elution band profiles.

To permit accurate calibration of the detector and quantitative analysis, two parallel columns were used, a calibration column on which the probe is retained without experiencing irreversible adsorption and the column made with the ceramic material studied. The flow scheme of the gas chromatograph is shown in Fig. 1. Both columns are connected directly to both the injector and the detector using a two-hole ferrule. No-hole 40% graphite–60% Vespel ferrules were purchased from Alltech (Deerfield, IL, USA) and drilled in-house. The inlet pressure was 5.0 p.s.i. and the dimensions of the two columns are such that the calibration column peak elutes after the test peak has returned to the baseline.

In the measurements performed here, contrary to analytical applications of chromatography, it is important to know the exact amount of sample injected into the column. Therefore, syringe injection volumes must be both accurate and precise. It is necessary that the syringes used be of the type in which the injection volume is contained entirely in the needle, so that one is certain that the entire desired injection volume is vaporized in the injection port. A 0–5-μl Hamilton syringe (Model 7105NCH, obtained from Alltech), equipped with a Chaney adapter and needle spacer was calibrated by weighing injection volumes of water on a Cahn 28 automatic electrobalance (Cahn Instruments, Cerritos, CA, USA).

Chemicals

Solvents. Dimethyl sulfoxide (DMSO) was of high-performance liquid chromatographic (HPLC) grade from Aldrich (Milwaukee, WI, USA). Methanol was of HPLC grade from Baker (Phillipsburg,

NJ, USA) and was dried over 3 Å molecular sieves.

Ceramic material. A typical alumina powder used for the preparation of alumina ceramics was used. High-purity α-alumina [product identification number RHPC-DBM (w/o MgO), lot number BM-2216] was obtained from Malakoff Industries (Malakoff, TX, USA). The powder had been dry bore milled by the manufacturer to an average particle diameter of 0.5–0.8 μm. The surface area measured by the BET method was 8–10 $m^2 g^{-1}$.

Probe solutes. HPLC-grade diethyl ether preserved with 0.1 ppm of 2,6-di-*tert.*-butyl-4-methylphenol (BHT) was obtained from Aldrich. Chloroform (HPLC grade) was obtained from Burdick & Jackson (Muskegon, MI, USA). 1-Chlorobutane and pyridine (both of HPLC grade) were obtained from Aldrich. Each of these solutes was used as received.

Column preparation

Ceramic materials are prepared by firing cast forms made from very fine, solid particle powders. Because such fine particles filling a column of reasonable length would yield a prohibitively high back-pressure, we decided to use porous-layer open-tubular (PLOT) columns instead. The PLOT column was fabricated using a dynamic method similar to that described by Halasz and Horvath [24] for making support-coated open-tubular (SCOT) columns.

Preparation of ceramic powder sample. A 500-mg sample of the alumina powder was dried for 24 h in a vacuum oven (150°C, 381 Torr vacuum gauge pressure). It was then suspended (1%, w/v) in DMSO by placing the volumetric flask containing the mixture in an ultrasonic bath for 30 min. Heating of the suspension while in the bath was prevented by periodically measuring the bath temperature and adding ice chips to the bath as needed. The slurry was poured into a 1/8-in. O.D. stainless-steel tube, similar to those used to prepare chromatographic columns, which was fitted with 1/8-in. O.D. glass tube ports to allow Swagelok connections to the quartz column and to the helium pressure regulator.

Preparation of column tubing. The silica tubing (16 m × 530 μm I.D.) (Alltech Europe, Nazareth, Belgium) was prepared by rinsing with *ca.* five volumes of dry methanol and conditioning in a gas chromatograph at 320°C for 72 h with a helium inlet pressure of 1.0 p.s.i. The tubing, already placed on a tared low-thermal-mass column cage, was then weighed on an analytical balance which was contained in a glove-bag (I^2R, Cheltenham, PA, USA) filled with dry helium. The length of the tubing was determined by measuring it with a meter stick.

After a dry weight had been obtained for the silica tubing, it was prepared by placing a drawing hook and a drag hook on the proximal and distal ends, respectively. Each hook was constructed by attaching a loop of narrow-gauge copper wire to the respective end of the silica tubing with shrinkable PTFE tubing (Alltech). The purpose of these hooks is to provide a convenient means to attach a line to each end of the tubing.

Finally, the distal end of the column must be closed to prevent leakage of the stationary phase slurry during the coating procedure. A plug was constructed as follows. A custom-fitted seat for the plug was provided by attaching a section of 0.06-in. I.D. shrinkable PTFE tubing to the distal end of the silica tubing so that a 1.5-in. long piece of shrinkable PTFE tubing extended out past the end of the silica tube. This "hole" was then shrunk around the plug, a stainless-steel sewing needle (size 7, betweens). The plug was withdrawn as the PTFE cooled (at the point when it turned from translucent to opaque) so that the lumen of the PTFE tubing was formed into the shape of the needle.

Coating apparatus. A schematic diagram is shown in Fig. 2. It consists of a mechanical convection oven (Gallenkamp, Loughborough, UK) which was modified in-house. A 1/8 rpm high-torque electric motor (Cramer, Old Saybrook, CT, USA) was provided to turn the upper hub. The thermal gradient was constructed by passing a length of 1/4-in. O.D. stainless-steel tubing through the floor of the oven (see Fig. 3). Heated nitrogen (10 p.s.i. at the gas cylinder) flowed into this tube from a tee just below the floor of the oven. The downward flow of hot gas caused the thermal gradient tube to be heated in an approximately linear fashion, room temperature at the bottom end and the temperature of the oven at the top end. This was confirmed by drawing a thermal transducer up the tube and measuring the temperature in the tube as a function of distance traveled up the tube. The upward flow of nitrogen aided the convection motor in purging the oven of the potentially explosive DMSO–air mixture. The

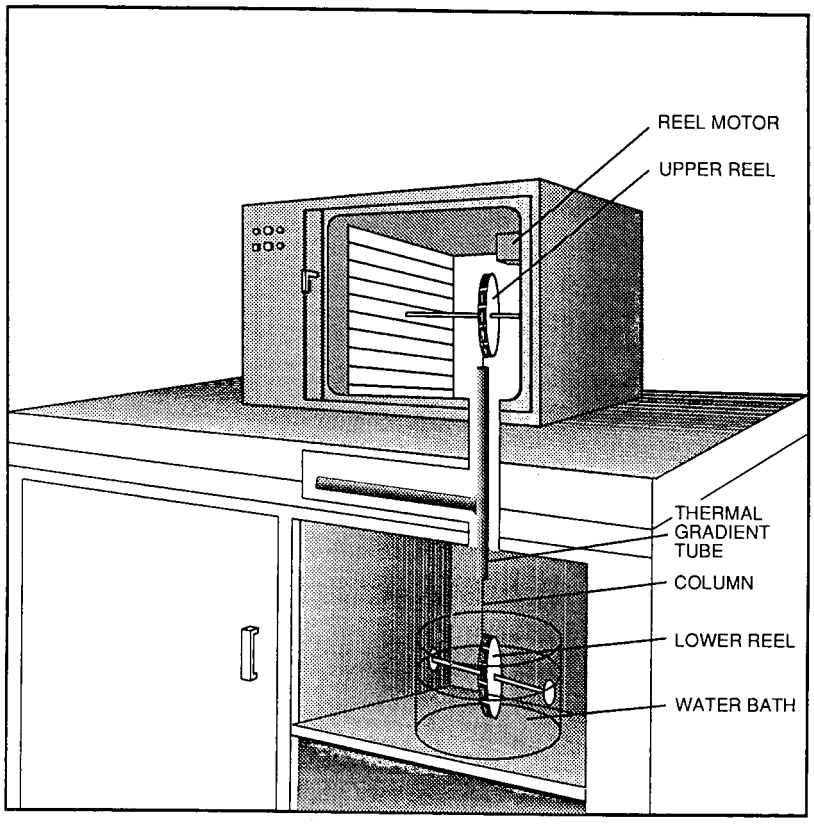

Fig. 2. Schematic diagram of the apparatus used to manufacture PLOT chromatographic columns.

oven was placed in a fume-hood and the thermal gradient tube traversed the floor of the hood.

Coating procedure. The suspension was pumped into the proximal end of the column from the chromatographic precolumn under 20 p.s.i. helium pressure. After the column had been filled and while the suspension was flowing from the distal end of the column, the hole was plugged. The integrity of the plug was insured by passing a piece of copper wire through the eye of the needle and through a pair of holes previously drilled in the wall of the PTFE tubing. This plugging method is adapted from the method suggested by Sandra and Verzele [25] but was found to bc much easier experimentally.

Because of the strong tendency of fused-silica tubing to straighten, great care must be exercised in winding it around the lower hub. Also, the proper tension must be maintained on the tubing as it is drawn off the lower hub, through the thermal gradient and on to the upper hub. For that purpose, a drawing line was attached to the drawing hook at the proximal column end. This line was passed through the thermal gradient tube and attached to the upper hub so that, when the upper hub turned, the proximal end was drawn into the oven. Similarly, a drag line was attached to the distal end. This line was attached to the lower hub so that, as the column was drawn into the oven, proper tension was maintained on the column by the resistance (to rotation) of the lower hub against the water in the bath.

The column, wound on the lower hub, was then placed in the room-temperature water-bath, drawn through the thermal gradient tube and coiled on the upper hub. Approximately 4 h were required for a 16-m column to be drawn into the 250°C oven. The velocity of the column was set so that the DMSO vaporized and its meniscus stabilized somewhere in

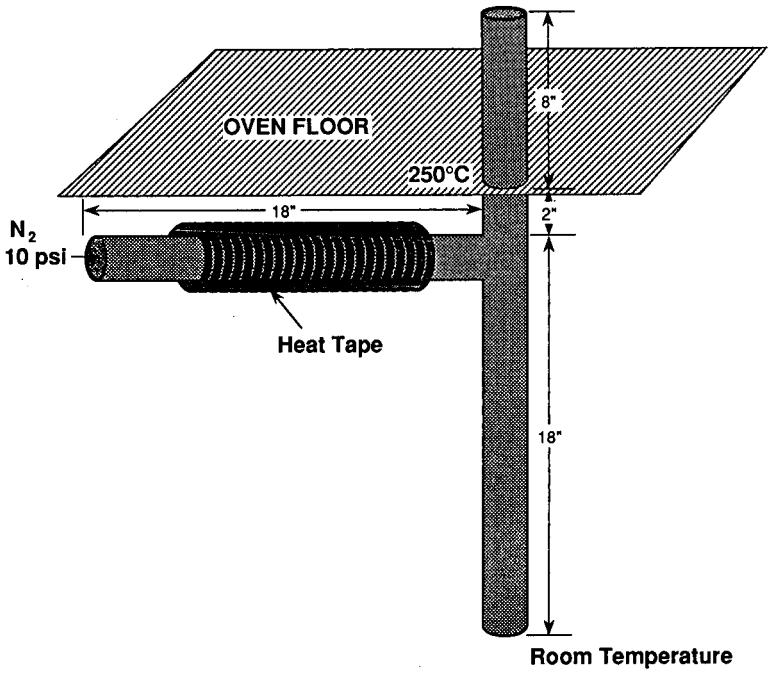

Fig. 3. Detailed schematic diagram of the thermal gradient tube.

the thermal gradient along the metal tube. When the entire length of the column was in the oven, it was cooled to room temperature. The column was placed on the column cage and 0.5 m of tubing were removed from each end. It was placed in the gas chromatograph and conditioned using 1.0 p.s.i. (inlet pressure) helium carrier gas and a slow temperature ramp followed by a 72-h period at 320°C.

Detector calibration

Detector calibration is needed to transform the profiles, which are initially recorded as detector signal *versus* retention time elution profiles, into solute partial pressure *versus* retention time elution profiles. Earlier experimental work with alumina and several other energetically microscopically heterogeneous ceramic powders (silica, nitrides and carbides), using a variety of probe solutes, revealed that, if the chromatogram is measured at a temperature where the probe is significantly retained, not all of the material injected elutes before the detector signal appears to have returned to the baseline. Because of this phenomenon of quasi-irreversible adsorption, the amount of solute injected into the column does not correspond to the area of the elution profile. Hence there is no simple way to perform the calibration. Further, this calibration has to be repeated often to determine the amount of probe compound unaccounted for by the detector signal and to control possible drifts of the detector.

Therefore, calibration is performed using a calibration column which is parallel to the measurement column. There is no irreversible adsorption on the calibration column and the probe solute elutes from it after the end of the tail of its band on the main column.

The detector response curve is a plot of the area (V min) of the calibration-column peak (which is Gaussian) *versus* the amount injected (mol). It is determined periodically and it has always been found to be linear. The slope of this straight line is designated S_1. It is calculated from the average of a number of points. Care was taken to insure that the range of peak heights in the calibration graph included the peak height of all the test peaks. The sensitivity, S_2 (solute partial pressure in atm over detector response in V) is determined by assuming

that (i) the outlet flow-rate is not perturbed by the passage of the band and (ii) that no solute is lost through irreversible adsorption in the calibration column. S_2 is given by

$$S_2 = \frac{R\,T}{(1 + S_{P,1})(1 + S_{P,2})\,S_1\,F_0} \tag{4}$$

where R is the universal gas constant (atm ml mol^{-1} K^{-1}), T the absolute column temperature (K), F_0 is the total outlet flow-rate of both columns and $S_{P,1}$ and $S_{P,2}$ are the splitting ratios corresponding to the inlet (injection) splitter and to the flow split between the two columns, respectively. The splitting ratios are determined by measuring the volumetric flow-rates out of the two columns and out of the inlet split vent using a soap-bubble flow meter. The measurement method is described in the next section.

Calibration column. A 60 m × 320 μm I.D. DB-5 column was obtained from J&W Scientific (Folsom, CA, USA). It was shortened to 40 m for this experiment, in order to balance properly its retention time and pneumatic resistance with that of the measurement columns.

Experimental procedure for isotherm determination

We have to measure the flow-rates and the splitting ratios, to estimate the amount of probe compound which is not eluted from the column after the signal has apparently returned to the baseline and to relate the partial pressure of the eluate to the detector response, which is done using the detector calibration (see above).

Flow-rate measurements. Because the PLOT columns are fragile, it is undesirable to disconnect them from the flame ionization detector each time data are collected in order to measure the outlet flow-rates. However, one must have an accurate knowledge of the flow-rates and the two splitting ratios in order to perform the physico-chemical calculations and these parameters change in response to changing experimental conditions. Therefore, the following procedure is used.

After a stable weight is obtained for the column, it is installed in the chromatograph along with the parallel calibration column and conditioned for an additional 24 h at 320°C with an inlet pressure of 5.0 p.s.i. The outlet flow-rates of both columns are measured while the columns are held at constant temperature. This is accomplished by connecting each column in turn to the thermal conductivity detector and attaching the flow meter to the flow output port of the detector. The two volumetric outlet flow-rates, $F_{0,T}$ and $F_{0,C}$ for the test (PLOT) column and the calibration column, respectively, are corrected for the temperature differential between the column and the flow meter and for the vapor pressure of water, using the equation given by Karger *et al.* [26]. The corrected outlet volumetric flow-rate from the test column is then

$$F_{0,T} = F_{M,T} \cdot \frac{T}{T_M} \cdot \frac{P_M - P_W}{P_M} \tag{5}$$

where $F_{M,T}$ is the flow-rate measured at the flow meter whose pressure and temperature are P_M and T_M, respectively, P_W is the vapor pressure of water at temperature T_M and T is the column temperature.

These outlet flow-rate measurements are made only once, before the two columns are connected to the flame ionization detector. Subsequent flow-rates are calculated, based on their proportionality to the void times (measured accurately on the chromatograms) and to the outlet flow-rates initially measured.

Void volume determination. The column void volume, $V_{M,T}$, is calculated from the measured outlet flow-rate. For the test column this is given by

$$V_{M,T} = F_{0,T}\,t_{0,T}\,J_3^2 \tag{6}$$

where J_3^2 is the James–Martin correction factor (eqn. 2) and $t_{0,T}$ is the void time for the test column measured immediately after measuring the outlet flow-rates. The void volume for the calibration column, $V_{M,C}$, is calculated similarly. The molar flow-rate is then calculated on subsequent days (or when experimental conditions change) by assuming an ideal mobile phase. For the test column, the molar flow-rate $\dot{F}_T$ is given by

$$\dot{F}_T = P_M\,V_{M,T}/R\,T\,J_3^2\,t_{0,T} \tag{7}$$

The molar flow-rate for the calibration column, $\dot{F}_C$, is calculated similarly. The corrected molar flow-rate from the inlet splitter port is calculated from daily measurements:

$$\dot{F}_{SV} = F_{SV}(P_M - P_W)/RT_M \tag{8}$$

where F_{SV} is the volumetric flow-rate measured at the flow meter.

Determination of splitting ratios. The splitting ratios may then be calculated by

$$S_{P,2} = \dot{F}_C/\dot{F}_T \quad (9)$$

and

$$S_{P,1} = (\dot{F}_T + \dot{F}_C)/\dot{F}_{SV} \quad (10)$$

The validity of the assumption that the void volumes remain constant is tested daily, by calculating the ratio of the void times of the two columns and comparing the result with the value derived on the day the columns were installed in the chromatograph. Once, after a column had been left to condition for 1 week, the deviation between the initial void time ratio and a subsequent ratio exceeded 1% (relative). The two columns were carefully disconnected from the flame ionization detector and their outlet flow-rates measured again, as described above.

Even methane is slightly retained on alumina at the column temperatures used. Measurements of the retention times of methane and nitrogen performed with a thermal conductivity detector indicate a retention factor of 0.025 for methane at 60°C. This would result in a 2.5% systematic error on the void volume at 60°C. As the correction remains small, an attempt was made to calculate the void times from the retention times of a homologous series of linear alkanes, methane, ethane and propane [27]:

$$t_{0,T} = -\frac{t_{R,2}^2 - t_{R,1}t_{R,3}}{t_{R,1} + t_{R,3} - 2t_{R,2}} \quad (11)$$

where $t_{R,1}$, $t_{R,2}$ and $t_{R,3}$ are the retention times of methane, ethane and propane, respectively, determined by calculating the first statistical moment of each peak. The method is not accurate, however, and we chose to measure the methane retention time and to correct it for the retention of methane, using the measured figure given above ($k' = 0.025$).

Probe mass balance. With each of the adsorbent–adsorbate pairs we have studied, a broadened second peak was recorded when the column was thermally conditioned between runs by heating on a 20°C min^{-1} ramp to 320°C and maintaining the column at the high temperature for 5 min. A typical example chromatogram is shown in Fig. 4. Considerable attention was paid to this phenomenon because the occurrence of irreversible or slowly reversible adsorption in studies such as ours is highly undesirable [20]. In the former instance, the solid surface is chemically altered and the isotherm data would be inaccurate. Material which is irreversibly adsorbed may be detected by making two successive injections of the same amount of probe compound at short intervals and thermally conditioning the column between the two runs. If the area of the second peak is greater than the first, one may suspect that irreversible adsorption is occurring. No evidence of irreversible adsorption was observed with any of the probe compounds used in this study. Calculations made on the basis of the isotherm derived from the band profile (Figs. 5 and 6) show that the second peak in the chromatogram shown in Fig. 4 is entirely accounted for by this isotherm. The initial slope is very steep, corresponding to very long retention times (*ca.* 40 min), and the apparent return to the baseline is deceptive [20].

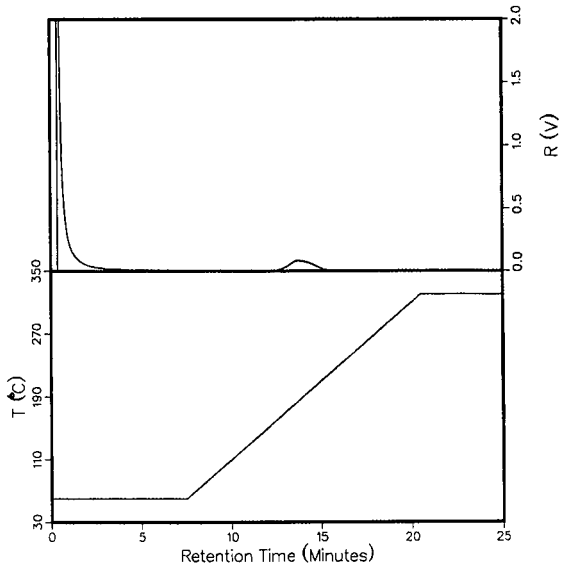

Fig. 4. Top: chromatogram obtained with an alumina column, showing the presence of a diffuse peak which elutes during column conditioning, between measurement runs. Experimental conditions: probe solute, diethyl ether; column temperature, 60°C; inlet pressure, 1.34 atm; t_0 = 22.7 s; outlet pressure, 1.0 atm; carrier gas, helium; column, 15 m × 0.53 mm I.D.; mass of stationary phase in the column, 44 mg. Peak areas (V min): large non-linear peak, 0.911; small diffuse peak, 0.087. Bottom: temperature program used to condition the column between runs.

It appears, therefore, that the material injected on to the column is physically adsorbed and either is entirely eluted before the detector signal returns to the baseline or, when it desorbs too slowly, does so

because of a very steep isotherm and not because of slow kinetics and can be desorbed entirely at a higher temperature, *e.g.*, by temperature programming [20].

Data acquisition and handling

The detector signal of the chromatograph was acquired with an IBM PC at a sampling rate of 10 Hz and stored as an ASCII file. A dedicated Fortran program written in-house and run on the PC, was used to perform several tasks on each successive file: (i) the chromatogram was baseline corrected, if the baseline was not 0 V; (ii) the peaks corresponding to both the test column (referred to later as the test peak) and the calibration column were integrated using a trapezoidal rule; (iii) the tail portion of the test peak was smoothed using five-point quadratic smoothing [28]; (iv) the test peak was written out into a separate ASCII file, recording only every fifth point, so that the final file has two data points per second of retention time.

The records for a complete experiment leading to the determination of an isotherm include (i) a set of chromatograms (usually six) used to generate a detector calibration graph [29]; (ii) a set of elution peaks, corresponding to a broad range of column loading factors; after plotting these peaks on the same graph to insure that their diffuse rear boundaries lie on the same curve as the rear boundary of the largest peak, this largest peak of the set only is used to calculate the isotherm; (iii) a duplicate elution peak corresponding to the same amount injected as the peak used for isotherm determination, to permit accuracy and precision estimation; and (iv) as ASCII file containing the following parameters: the detector sensitivity, S_2 (atm V^{-1}), determined as described earlier; the void time, $t_{0,T}$ (min); the void volume, $V_{M,T}$ (ml); the column inlet pressure, P_{IN} (atm); the column outlet pressure, P_{OUT} (atm); the mass of adsorbent in the column, M_S (g); the peak area A_P (V min); the column temperature, T (K); the vapor pressure of the probe solute at the column temperature, P_S (atm); and the heat of vaporization of the probe solute, E_V (kcal mol^{-1}); these last two parameters are obtained from the literature [30].

If the data set obtained meets the minimum quality control criteria discussed in the companion paper [20], the test peak file is transferred to the mainframe computer. Subsequent calculations, involving the determination of the adsorption isotherm and the adsorption energy distribution, are performed by a single computer program.

The content of the test peak file is read into the program. The response factor is derived from the calibration chromatograms and the peak voltages are converted into partial pressures. Then, the data corresponding to the tail portion of the test chromatogram are sorted into a file of increasing P. This partial pressure *versus* retention time profile is interpolated using the Akima cubic spline [31] and evaluated at 1000 values of the pressure which lie within the range of the pressures measured and which have equal logarithmic spacing [18]. The spacing is chosen to weight more heavily the low-pressure region where the isotherm curvature is greater. Retention times are converted to specific corrected retention volumes and the integration (eqn. 1) is performed using a trapezoidal rule. The actual equation calculated is

$$q(P) = \frac{V_{M,T}}{J_3^2 \, R \, T \, M_S \, t_{0,T}} \int_0^P (t_{R,T}(P) - t_{0,T}) \, dP \quad (12)$$

The adsorption isotherm is stored and printed, then the program pursues the calculation of the adsorption energy distribution [18].

RESULTS AND DISCUSSION

As an example of the experimental results which are discussed elsewhere [20,21], we show in Fig. 5 the band profile (solid line) recorded for a sample of diethyl ether on an open-tubular column prepared with the sample of RHCP alumina used for the development of our method. The band profile has a nearly vertical front and a long tailing rear, typical of convex upwards isotherms [32]. The front is eluted very early (the retention factor of the front is 0.17), indicating a high degree of column overload. The isotherm derived from the rear of the profile is given in Fig. 6. As expected, it is strongly curved in the region 0–3 mbar.

From the isotherm in Fig. 6, and using the equilibrium dispersive model [32] adapted to gas chromatography [33], it is possible to calculate numerically the elution profile of the sample considered, assuming for the column an efficiency of 8000 plates, close to that determined for the column

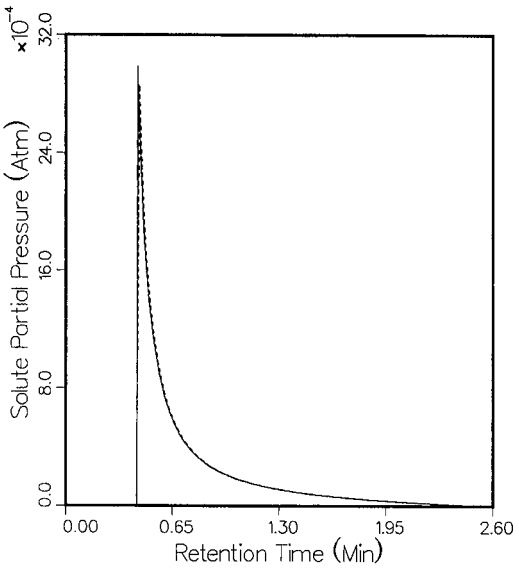

Fig. 5. Comparison between an experimental elution profile (solid line) and a calculated profile (dashed line). The calculated profile was obtained using the semi-ideal model of chromatography and the isotherm derived from the experimental profile through the ECP method. Diethyl ether on RHCP alumina at 60°C. Experimental conditions as in Fig. 4. Sample size, 0.47 μg; peak area, $4.85 \cdot 10^{-4}$ atm min; number of theoretical plates, 8000.

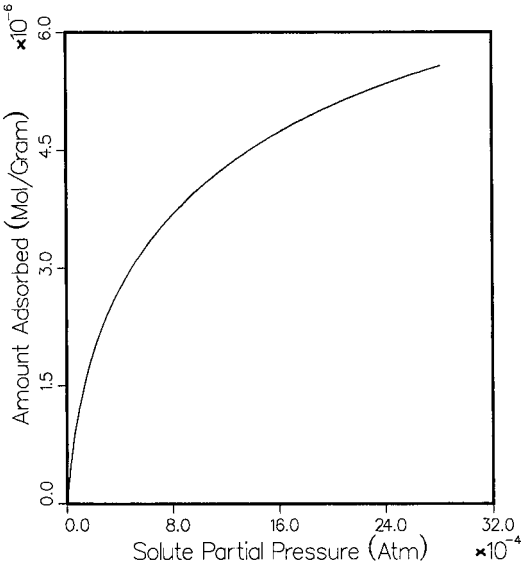

Fig. 6. Adsorption isotherm of diethyl ether on RHCP alumina at 60°C. The isotherm is derived from the elution profile shown in Fig. 5 (solid line).

under linear conditions [20]. The calculated band profile is shown in Fig. 5 (dashed line). It is very difficult to distinguish it from the experimental profile recorded. The ECP method uses the analytical solution of the ideal model of chromatography to derive the isotherm from the diffuse part of the band profile, while the equilibrium dispersive model uses the differential mass balances of the probe and of the carrier gas and calculates numerical solutions of this partial differential equation. The agreement between the two profiles in Fig. 5 shows that the calculation procedure accounts well for the influence on the band profile of the column efficiency and the gas-phase compressibility.

ACKNOWLEDGEMENTS

This work was supported in part by Grant DE-FG05-88ER13859 from the US Department of Energy, Office of Basic Energy Research, and by the cooperative agreement between the University of Tennessee and the Oak Ridge National Laboratory.

REFERENCES

1 O. Smidsrod and J. E. Guillet, *Macromolecules*, 2 (1969) 443.
2 J. E. Guillet, *J. Macromol. Sci. Chem.*, A4 (1970) 1669.
3 J. E. Gilbert, *Adv. Chromatogr.*, 23 (1984) 199.
4 A. N. Stein and J. E. Guillet, *Macromolecules*, 3 (1970) 102.
5 D. G. Gray and J. E. Guillet, *Macromolecules*, 4 (1971) 129.
6 A. N. Stein, D. G. Gray and J. E. Guillet, *Br. Polym. J.*, 3 (1971) 175.
7 T. Paryjczak, *Gas Chromatography in Adsorption and Catalysis*, Wiley, Chichester, New York, 1986.
8 G. A. Eiceman and V. J. Vandiver, *Atmos. Environ.*, 17 (1983) 461.
9 M. M. Ross, S. S. Risby, S. S. Lettz and R. E. Yasbin, *Environ. Sci. Technol.*, 16 (1982) 75.
10 A. V. Kiselev and Ya. I. Yashin, *Gas Adsorption Chromatography*, Plenum Press, New York, 1969.
11 G. Schay and G. Szekely, *Acta Chim. Hung.*, 5 (1954) 167.
12 D. H. James and C. S. G. Phillips, *J. Chem. Soc.*, (1954) 1066.
13 E. Cremer and J. F. K. Huber, *Angew. Chem.*, 73 (1961) 461.
14 I. Langmuir, *J. Am. Chem. Soc.*, 40 (1981) 1361.
15 G. Guiochon and C. Guillemin, *Quantitative Gas Chromatography*, Elsevier, Amsterdam, 1988.
16 M. Jaroniec and R. Madey, *Physical Adsorption on Heterogeneous Solids*, Elsevier, Amsterdam, 1988.
17 S. P. Boudreau and W. T. Cooper, *Anal. Chem.*, 59 (1987) 353.
18 J. Roles and G. Guiochon, *J. Phys. Chem.*, 95 (1991) 4098.
19 D. R. Johnson, M. A. Janney and R. W. McLung, in A. Vary and J. Snyder (Editors), *Proceedings of the Joint Conference on Nondestructive Testing of High Performance Ceramics*, American Ceramic Society, Columbus, OH, 1987, p. 19.

20 J. Roles and G. Guiochon, *J. Chromatogr.*, 591 (1992) 245.
21 J. Roles and G. Guiochon, *Anal. Chem.*, in press.
22 R. Sips, *J. Chem. Phys.*, 16 (1949) 490.
23 A. W. Adamson, I. Ling, L. M. Dormant and M. Oren, *J. Colloid Interface Sci.*, 21 (1966) 445.
24 I. Halasz and Cs. Horváth, *Nature (London)*, 197 (1963) 72.
25 P. Sandra and M. Verzele, *Chromatographia*, 11 (1978) 102.
26 B. L. Karger, L. R. Snyder and Cs. Horváth, *An Introduction to Separation Science*, Wiley, New York, 1973, p. 215.
27 Cs. Horváth, in L. S. Ettre and A. Zlatkis (Editors), *The Practice of Chromatography*, Wiley, New York, 1967, Ch. 4.
28 A. Savitzky and M. J. E. Golay, *Anal. Chem.*, 36 (1964) 1627.
29 E. V. Dose and G. Guiochon, *Anal. Chem.*, 62 (1990) 816.
30 *Selected Values of Properties of Chemical Compounds*, Thermodynamics Research Center, Texas A&M University, College Station, TX, 1963.
31 H. Akima, *J. Am. Ceram. Soc.*, 17 (1970) 589.
32 G. Guiochon, S. Golshan-Shirazi and A. Jaulmes, *Anal. Chem.*, 60 (1988) 1856.
33 P. Rouchon, M. Schonauer, P. Valentin, C. Vidal-Madjar and G. Guiochon, *J. Phys. Chem.*, 89 (1985) 2076.

Journal of Chromatography, 591 (1992) 245–265
Elsevier Science Publishers B.V., Amsterdam

CHROM. 23 783

Precision and accuracy of the gas–solid adsorption isotherms derived by the elution-by-characteristic-points method

Jeffry Roles and Georges Guiochon*

**Department of Chemistry, University of Tennessee, Knoxville, TN 37996-1501 and Division of Analytical Chemistry, Oak Ridge National Laboratory, Oak Ridge, TN 37831-6120 (USA)*

(First received June 14th, 1991; revised manuscript received September 30th, 1991)

ABSTRACT

The influence of the fluctuations of the experimental parameters on the reproducibility of the overloaded band profiles used to determine the isotherms by the elution-by-characteristic-points (ECP) method was investigated using two new tools. A parameter measuring the difference between two similar curves, such as overloaded elution profiles or adsorption isotherms, was defined. The band profiles measured were compared with those calculated from the derived isotherm, using models from the theory of non-linear chromatography. The agreement between both profiles was defined as a distance lower than twice the average distance between two profiles measured on the same day on the same column. The degree of validity of the various assumptions made in the ECP method was assessed.

INTRODUCTION

In a companion paper [1], we described the procedure used for the acquisition of the experimental data needed for the accurate determination of equilibrium isotherms using the classical elution-by-characteristic-points (ECP) method [2–4]. In this paper, we discuss the sources of errors encountered in this determination and the procedures used to eliminate or reduce these errors and to validate the data obtained. In a further paper [5] we shall discuss the similar problems in the derivation of the adsorption energy distribution from the isotherm data. The aim of this work was the development of a procedure for the study of the solid surfaces encountered in a number of applications (*e.g.*, the manufacture of advanced ceramic materials, the production of fillers and pigments and the preparation of adsorbents for chromatography).

It is important for us to assess the precision and accuracy of the isotherm data because the experimental isotherm will be used to derive the adsorption energy distribution. This distribution is not accessible otherwise than by using a theoretical model [6,7] and applying it to the experimental data. For reasons of experimental convenience [1], we have used the ECP method to derive the isotherm from the band profile acquired. It is important, therefore, to test carefully each step of the computation proving the validity of the model and to make sure that experimental errors are kept low enough and cannot generate significant artefacts. The situation is complicated by the fact that two models must be validated successively: the chromatographic model used to calculate the isotherm from the elution profile (ECP model [2–4]) and the Langmuir model of localized adsorption which is used to relate the adsorption energy distribution to the parameters of the experimental isotherm.

Although the determination of equilibrium isotherms using chromatographic methods has been discussed and reviewed abundantly and in detail [8,9], too little attention has been devoted to the precision and accuracy of the data obtained. In addition to the general lack of interest of most chromatographers in the study of accuracy, this apparent neglect stems from the difficulty of the problem. It is much more difficult to quantify

0021-9673/92/$05.00

uncertainties in non-linear than in linear chromatography. For example, in the latter method the retention time is used to calculate the slope of the linear isotherm. The reproducibility of retention times is measured by a simple standard deviation. In contrast, in non-linear chromatography, one must measure the reproducibility of a whole chromatogram, consisting of a set of retention times as a function of peak heights. In order to quantify the uncertainty, various figures of merit can be chosen, *e.g.*, the distance, Δ, between two curves obtained by distribution function analysis [10,11]. The mere fact that several figures of merit are deemed necessary to describe and quantify the reproducibility is in itself an indication of the difficulty involved in this endeavor.

THEORY

As we are studying the properties of heterogeneous surfaces by determining the adsorption isotherms of probe components, we are only interested here in the band profiles of samples of single, pure compounds. This work is based on the use of the equilibrium-dispersive model of non-linear chromatography, which relates the elution profile of high-concentration bands, the equilibrium isotherm of the component between the two phases of the chromatographic system and the column efficiency [12]. We use the model in both directions. In the direct problem, we calculate the elution profile knowing the isotherm, the column efficiency and the sample size. In the inverse problem, we derive the isotherm from the recorded elution profile of a known amount.

From a purely mathematical point of view, the direct problem is well posed and its solution is straightforward, even if it is difficult or even impossible to derive a closed-form solution. The numerical calculation of solutions raises no difficulty of principle [13]. The inverse problem is still poorly understood by mathematicians and few fundamental results are available with which the physical chemist can work. As a consequence, it is investigated using only very simple boundary conditions, *e.g.*, frontal analysis. Although more complex in principle, ECP proves the point: it is based on the use of one of the few analytical solutions of the direct problem, in the case of the ideal model. ECP is widely used in gas chromatography for its simplicity. A brief discussion of the direct and inverse problems of chromatography is useful.

Calculation of chromatographic band profiles from the adsorption isotherms

The elution profiles of single-component bands are obtained as solutions of the system of mass-balance equation for the component considered and for the mobile phase [12,14,17]:

$$\frac{\partial PuX}{\partial z} + P \cdot \frac{\partial X}{\partial t} + \frac{RTm_g}{V_g} \cdot \frac{\partial q}{\partial t} = D \cdot \frac{\partial^2 X}{\partial z^2} \tag{1a}$$

$$\frac{\partial Pu(1-X)}{\partial z} - P \cdot \frac{\partial X}{\partial t} = -D \cdot \frac{\partial^2 X}{\partial z^2} \tag{1b}$$

where $p = XP$ is the partial pressure of the probe, P the pressure of the mobile phase, X the mole fraction of the probe, q its concentration in the stationary phase, z and t the abscissa and time coordinates, respectively, u the local mobile phase velocity, R the universal gas constant, T the column absolute temperature, m_g the mass of stationary phase per unit column length, V_g the void volume per unit column length and D the apparent dispersion coefficient.

These two partial differential equations are completed by the equilibrium isotherm [$q = f(p)$], the apparent dispersion coefficient, D, related to the column efficiency, and the Darcy equation relating the mobile phase velocity and the pressure gradient [13–15]. In most instances, it is convenient to assume that the passage of the high-concentration band does not modify the pressure profile along the column [14]. The pressure profile remains the steady-state profile observed when pure carrier gas flows through the column:

$$P(z) = P_o \sqrt{\left(\frac{P_i}{P_o}\right)^2 - \frac{z}{L}\left[\left(\frac{P_i}{P_o}\right)^2 - 1\right]} \tag{2}$$

where P_i and P_o are the inlet and outlet column pressures, and L is the column length.

It is not possible to derive analytical solutions of the system of equations of either the ideal or the equilibrium-dispersive model in gas chromatography [12–15]. On the other hand, numerical solutions can be easily derived, using a variety of calculation schemes [13,14,16]. As we discuss elsewhere, the band profiles supplied by such calculations are

in excellent agreement with experimental results [13,16,17]. Obviously, the agreement between the experimental band profile and the profile calculated as a numerical solution of the equilibrium-dispersive model of chromatography is a useful test of the validity of the model used to derive the isotherm from the experimental data and of the self-consistency of the approach used to interpret these experimental results.

Derivation of the adsorption isotherm from the profile of high-concentration bands

Several methods have been used to derive equilibrium isotherms from chromatographic data pertaining to pure compounds [9]. Among them, the ECP method is the most popular in gas chromatography because of the simplicity of its implementation [2–4]. It has been used in this work to derive adsorption isotherms from the profile of high-concentration bands of the probe components.

If we neglect the influence of the apparent dispersion on the band profile, assume the axial dispersion to be negligible and the rate of the mass-transfer kinetics to be infinite, we have a column with an infinite efficiency (*i.e.*, $D = 0$ in eqn. 1). In this case, it is easy to show that a velocity is associated with each concentration and that the band profile derives directly from the combination of these velocities [12,18]. In the case of a convex upwards isotherm, the velocity associated with a concentration increases with increasing concentrations. As high concentrations cannot pass low ones, the profile has a front shock and a diffuse rear [12,19]. The equation of the band rear [3,12,20] is

$$t = t_p + t_0\left(1 + F \cdot \frac{dq}{dc}\right) \qquad (3)$$

where t_p is the width of the rectangular injection plug, t_0 is the hold-up time, F a phase ratio and $q(c)$ is the equilibrium isotherm. The position of the shock is also easy to calculate [21], but is not useful in the present application. Eqn. 3 gives the band rear when the isotherm is convex upward, *i.e.*, when $d^2q/dc^2 < 0$, the band front in the other case. It is valid only in liquid chromatography, as it neglects the compressibility of the mobile phase and the difference in partial molar volumes of the component in the gas and the stationary phases. We discuss first the influence of the finite column efficiency, then that of the mobile phase compressibility and density.

Influence of a finite column efficiency. The ECP method is directly derived from eqn. 3. In our case, it is applied to the rear of the profile. Unfortunately, the column has a finite efficiency and the rear profile is broadened by dispersion.

Golay has derived equations which yield the elution profile of a band in linear chromatography, with an open-tubular column, either with a liquid-coated wall [22] or with a porous layer along the wall [23]. These equations take effectively into account the influence of the axial dispersion and of the finite kinetics of mass transfers in the column. However, they are not applicable in non-linear chromatography. In this instance, the influence of the thermodynamics and the mass-transfer kinetics on the band profile cannot be separated. The problem has no exact analytical solution. Several approaches have been suggested.

Haarhoff and Van der Linde [24] and Conder and Purnell [15] studied the elution band profile in the case of a finite column efficiency and with a parabolic isotherm (*i.e.*, a two-term expansion of the isotherm). Neglecting the gas-phase compressibility, which was taken into account by Conder and Purnell, Haarhoff and Van der Linde derived an approximate equation which gives satisfactory results at moderate concentrations [9,20]. This solution, however, is not generally applicable for the determination of equilibrium isotherms, as it assumes that they are parabolic.

The calculation of numerical solutions of the differential mass-balance equation of the probe solute in a slice of the column (*i.e.*, eqns. 1) has been developed [13,16,25]. The algorithms for these numerical calculations are written on the assumptions that the column efficiency is high enough, the stationary phase is always almost in equilibrium with the mobile phase and the effect of a finite column efficiency can be accounted for by using an apparent dispersion term in place of the axial dispersion term in the mass-balance equation. These numerical solutions permit an accurate prediction of the band profile when the isotherm is known [26,27], provided that the rates of the mass-transfer kinetics and of the kinetics of adsorption–desorption are large enough and the column efficiency exceeds a few hundred theoretical plates.

In the adsorption of light vapors, such as diethyl ether (molecular weight, MW = 74 dalton, b.p. 34.5°C) or 1-chlorobutane (MW 92 dalton, b.p. 78.4°C), adsorbed on solid alumina particles, the mass-transfer kinetics have to be fast: the thickness of the porous layer coated on the column wall is of the order of 1 μm [1]. As long as the adsorption energy is not very high, the kinetics of adsorption–desorption are also fast, so we can expect the column efficiency to be high enough to warrant the use of the equilibrium-dispersive model for the calculation of band profiles in the case studied here. Chemisorption of ethers on alumina is a distinct possibility. However, chemisorbed molecules will not be eluted to a significant extent during the time of an experiment. The extent to which chemisorption is involved will be seen if a mass balance of the probe solute can be measured.

Gas-phase compressibility and density. If we take into account these effects, but still assume that the column efficiency is infinite (*i.e.*, $D = 0$ in eqn. 1), and consider the migration of a given partial pressure, we obtain an equation which can be integrated into [2–5,15]

$$V_g = J_3^2 RT(\mathrm{d}q/\mathrm{d}p) \tag{4}$$

where V_g is the specific retention volume of the partial pressure p and J_3^2 is the James and Martin correction factor [28]. (Assumptions made in the derivation of eqn. 4 are given in the Appendix.) Slightly different forms of this equation, which is the basis of the ECP method, have been published by Cremer and Huber [2–4], Chueh and Ziegler [29], Peterson and Helfferich [30] and Conder [31].

Eqn. 4 assumes that the mobile phase is an ideal gas. Conder and Purnell [15] derived an equation similar to eqn. 4, which relates the retention volume of a concentration, the gas compressibility factor, the non-ideal behavior of the carrier gas and the slope of the isotherm:

$$V_N = V_s(1 - ajy_o)\left(\frac{\partial q}{\partial C}\right)_{P=P_m} \tag{5}$$

where V_N is the net retention volume $[j(V_R - V_m)]$, V_s is the amount of adsorbent in the column, y_o is the mole fraction of the characteristic point when it reaches the column outlet (note that a characteristic point in gas chromatography has a constant concentration, C, hence a rising mole fraction in the gas phase as the pressure falls along the column), j is the actual pressure gradient correction factor (different from the James and Martin factor which assumes ideal gas behavior), the pressure P_m is an average pressure given by

$$P_m = P_o J_3^4 = \frac{3P_o}{4} \cdot \frac{\left(\frac{P_i}{P_o}\right)^4 - 1}{\left(\frac{P_i}{P_o}\right)^3 - 1} \tag{6}$$

and the other parameters are

$$a = \frac{b_2^1}{b_3^2}\left[1 + \frac{2y_o P_o B_{11}}{RT}(1 - y_o J_2^1)\right] \tag{7a}$$

$$b_n^m = 1 + k(1 - J_n^m y_o) \tag{7b}$$

$$j = J_3^2\left[1 + \frac{y_o^2 P_o B_{11}}{RT}(J_3^2 - 1)\right] \tag{7c}$$

$$J_n^m = \frac{n}{m}\left[\frac{(P_i/P_o)^m - 1}{(P_i/P_o)^n - 1}\right] \tag{7d}$$

where k is the mass distribution coefficient, $qV_s/(CV_M^0)$ and B_{11} is the second virial coefficient of the pure solute vapor. It is often possible to simplify these equations and write $a = 1$ and $j = J_3^2$. Hence, under the experimental conditions used in our work (see below, *e.g.*, Fig. 5), the maximum outlet partial pressure of the probe is $3 \cdot 10^{-3}$ atm, thus y_o is 0.003; under our conditions, $J_3^2 = 0.849$; the second virial coefficient for diethyl ether at 60°C derived from the equation of Guggenheim and McGlashan [32] is -826 cm^3 mol^{-1}; hence, from eqn. 7c, $j = 1.000001 J_3^2$ and $a = 0.9998$. Thus,

$$V_N = V_s(1 - J_3^2 y_o)\left(\frac{\partial q}{\partial C}\right)_{P=P_o J_3^4} \tag{8}$$

The compressibility correction term J_3^2 is 0.849, so the correction term in eqn. 8 is $1.2 \cdot 10^{-3}$, which can be neglected. Then, eqn. 8 is equivalent to eqn. 4, as $V_g = V_N/V_s$ and $C = n/V = p/RT$. The point of the isotherm derived from a mole fraction y_o is referred to the partial pressure $y_o P_o J_3^4 = 1.186p$, which requires a significant correction on the isotherm, but one which is simple, corresponding to a mere expansion of the pressure scale.

EXPERIMENTAL

The equipment and the experimental procedures used have been described in sufficient detail in the companion paper [1]. A porous-layer open-tubular column was prepared with the powder under study, alumina in the present instance. A 0.53 mm I.D. quartz tube was filled with a slurry of the powder in a suitable solvent (dimethyl sulfoxide) in which it does not settle. One end of the tube was closed and the tube was slowly coiled by the other end inside an oven placed under a hood. As it entered the oven, the solvent vaporized and was vented out, leaving a regular layer of powder on the column wall. The column was then fitted within the oven of a Perkin-Elmer (Norwalk, CT, USA) Model 8500 gas chromatograph operated isothermally. Large samples of the probe compounds (diethyl ether and 1-chlorobutane) were injected and the elution band profiles recorded using an IBM PC interfaced with a Data Translation (Marlboro, MA, USA) I/O Board. The equilibrium isotherm was derived from the elution profile using the ECP method [2–4]. From this isotherm, it was possible to derive the distribution of the adsorption energy of the probe [7].

We discuss in this section the sources of errors encountered in the measurement of the experimental parameters needed for an accurate determination of the equilibrium isotherm.

Reproducibility of the primary parameters

We discuss in the next few sections the problems associated with the accurate determination of the primary parameters involved in the measurement of equilibrium isotherms by the ECP method and with their reproducibility. These parameters are the void volume of the column and the hold-up time, the volumetric flow-rate of the carrier gas, the splitting ratios, the peak areas, the sample size, the response factor of the detector, the column length and the mass of stationary phase that it contains. Our estimates of the reproducibility of the measurement of each of these parameters are summarized in Table I, which contains the confidence intervals at the 95% confidence levels.

Reproducibility of the hold-up time

This is an important parameter, which has to be subtracted from the retention times in order to calculate the corrected retention times and hence the specific retention volume. Small errors in the hold-up time may have an important effect on the precision of the measurements because at high partial pressures the retention of the probe compounds decreases and may become very small. The corresponding retention time tends towards the hold-up time.

The experimental factors which influence the precision of the hold-up time are (i) the fluctuations of the oven temperature, resulting in variations of the carrier gas viscosity; (ii) the fluctuations of the column inlet and outlet pressures caused by a drift of the inlet pressure controller and by variations of the atmospheric pressure, respectively; (iii) possible fluctuations of the column permeability; (iv) errors made in the measurement of the actual injection time; and (v) errors in the time measurement.

The precision on the hold-up time was estimated by determining the reproducibility of ten replicate measurements. The determination of the uncertainty on the hold-up time was made over the time period necessary to complete a routine experiment. With the parallel columns in place, one void time measurement was made for each column every 30 min, allowing a total of 5 h for the complete experiment. The data sets were not skewed, demonstrating that the uncertainty is dominated by random errors. It should be noted that on some days ambient conditions (especially the atmospheric pressure) may change rapidly so that greater uncertainty may be observed on some days, especially during stormy weather. The estimated uncertainties on the void times of both columns are reported in Table I.

Reproducibility of the volumetric flow-rate

The same factors which affect the uncertainty of the void time also affect the uncertainty of the flow-rate. Several additional factors must be mentioned. First, a systematic error due to a leak in the chromatograph or in the connection between the column end and the flow meter is always a possibility. Second, the correction for the vapor pressure of water in the flow-rate measurements made with a soap-bubble flow meter introduces some error. Given the design of soap-bubble flow meters, the partial pressure of water in the gas may be slightly less than its vapor pressure; the temperature of the soap solution fluctuates; the leakage rate of helium through the bubble is unknown.

An experiment similar to that carried out for the

determination of the error of measurement of the void time was performed. Two flow-rates were measured, the split vent flow-rate and the combined outlet flow-rate of the two columns. The two parallel columns were connected to the two branches of the thermal conductivity detector and the flow-rate of the combined streams was measured. The precisions of both flow-rate measurements are reported in the Table I.

Reproducibility of the splitting ratios

The uncertainty of the flow-rate determination dominates the uncertainties of the values derived for the void volumes, the molar flow-rates and the splitting ratios. Therefore, the uncertainty of the splitting ratios was calculated from the error made on the flow-rate results. The variance of the splitting ratio was taken as twice the variance of the flow-rate.

Reproducibility of the peak areas

We do not measure the area of the peak used in the ECP method, except to determine the mass balance of the probe and the fraction that is not eluted at the end of the experiment (see below, *Assumption VIII*). The accuracy of this determination is not critical.

The peak area of importance in this work is the area of the elution band of the fraction of the sample which is injected into the calibration column. This area is used to compute the response factor of the detector. The data set used to determine the reproducibility of this peak area was obtained by making a 5.00-μl injection of pure diethyl ether on six successive days. The peaks recorded were corrected for a possible baseline shift, but were not smoothed. At least 175 data points per peak were used in the trapezoidal rule integration.

It is interesting that the relative standard deviation of the area of the peaks recorded at the exit of the test column was twice that for the calibration peaks. The poorer reproducibility was due to the difficulty encountered in the integration of the highly skewed elution profiles obtained. The time at which the integration was ended fluctuated widely. Note that on the days when the ambient temperature is high (*e.g.*, 28°C), the reproducibility of the peak area of diethyl ether is significantly reduced.

Reproducibility of the sample size

It is necessary that the syringes used be of the type in which the sample injected is contained entirely in the needle, so that one is certain that the entire desired injection volume is vaporized in the injection port. A 0–5-μl Hamilton syringe, Model 7105NCH, obtained from Alltech (Deerfield, IL, USA), equipped with a Chaney adapter and a needle spacer was calibrated by weighing volumes of water on a Cahn (Cerritos, CA, USA) Model 28 automatic electrobalance. The standard deviation of the water injection volume, determined from the reproducibility of the weighings, was 10 nl. However, the weighing experiment fails to take into account either the variation in the splitting ratio over time or the sample losses resulting from the relatively high volatility of diethyl ether. As the peak-area reproducibility for diethyl ether was much worse than the reproducibility of the weighings, the uncertainty in the sample size was revised to the same relative standard deviation as that of the peak areas.

Reproducibility of the detector response factor

The reproducibility of the detector response factor was determined by collecting data over six consecutive days, on the same column, using diethyl ether as the probe. The precision observed is better than one would predict from an error analysis based

TABLE I

ESTIMATED UNCERTAINTY OF THE EXPERIMENTAL PARAMETERS

Parameter	Uncertainty (%)	Parameter	Uncertainty (%)
Void time ($t_{0,2}$)	1.0	Peak area	1.0
Void time ($t_{0,1}$)	0.9	Sample size	1.0
Flow-rate (column)	1.0	Response factor	3.0
Flow-rate (split vent)	0.8	Column length	0.1
Splitting ratio	2.0	Mass of stationary phase	6.5

on the contributions of the uncertainties of the peak area, the splitting ratio and the sample size, all parameters which are used in the calculation of the response factor. This may be explained by the fact that the estimated errors on some of these factors are related, so their contributions cancel out in part.

Reproducibility of the column length

The length of the column was measured by repeatedly marking off 1-m lengths, measured by a meter stick. This method is fairly accurate as the silica tubing tends to lie along a straight line. As sixteen successive measurements are necessary to obtain the length of a *ca.* 16-m column, and the estimated uncertainty for each measurement was 1 mm, the sum of the individual uncertainties was taken as the total uncertainty.

Reproducibility of the mass of stationary phase in the column

Because the ends of the column are cut off at the end of the preparation process, the gravimetric procedure for determining the mass of stationary phase is accurate only as long as the density of the silica tubing, or mass of the silica tubing per unit length, remains constant. This was confirmed experimentally. Nine columns were cut from the same continuous section of tubing. The relative standard deviation for the weight of these nine sections of empty dry tubing was 0.03%. Error analysis reveals, however, that this error propagates to produce a much greater relative uncertainty on the weight (*ca.* 40 mg) of the stationary phase in the column, because this amount is small compared with the column weight.

RESULTS AND DISCUSSION

Reproducibility of the retention data

In this section, we discuss the reproducibility of the set of retention data acquired in an experiment. The characterization of this reproducibility is not straightforward, as we are not collecting repetitive estimates of a single number, *e.g.*, a retention time, a retention factor or a peak area for which the determination of a standard deviation suffices. The result of a single experiment, *i.e.*, the record of a band profile, gives an entire section of the isotherm. This is the major advantage of the ECP method over frontal analysis [4]. We summarize first the method used for assessing the reproducibility of these experimental results and the various calculations performed to supply estimates of the uncertainty of the retention data at the different stages in the process of calculating the isotherm.

We then report the results obtained. A three-step reproducibility experiment was performed. First, reproducibility was determined on the same column, on the same day. Six band profiles were measured and the same experimental parameters were used in the six calculations. Second, the same data were measured on the same column, but on different days, over a period of time. The experimental parameters (*e.g.*, the void time and the detector response factor) used for the processing of each of the six measurements were determined at the time of the measurements. Finally, a complete set of measurements was performed for three different columns. The protocol for determining the uncertainty for each step of the study is as follows. Each set of retention data is compared with all of the other sets obtained during the particular step considered. For example, for the same day and the same column step, six sets of data were collected and fifteen comparisons were made. The results are reported as the mean and the standard deviation of each of the comparison parameters for each step.

Distribution function analysis of the band profiles. The reproducibility of the thermodynamic parameters calculated from the retention data is closely related to the reproducibility of the band profiles used to calculate the isotherm. Recognizing the inadequacy of the classical parameters (*e.g.*, statistical moments) used to characterize chromatographic band profiles when they are applied to strongly skewed peaks, Rix [10] and later Excoffier *et al.* [11] used distribution function analysis (DFA) to detect small differences between the shapes of two similar peaks. In this method, the difference between the shape of two profiles is parameterized by the numerical calculation of a shape difference parameter, δ, defined below.

First, we emphasize that it is possible to compare only the rear portions of the elution profiles which cover the same range of signal, *i.e.*, for which the probe partial pressure is between zero and the lower of the two peak maxima. Of the two peaks to be compared, it is determined first which peak maxi-

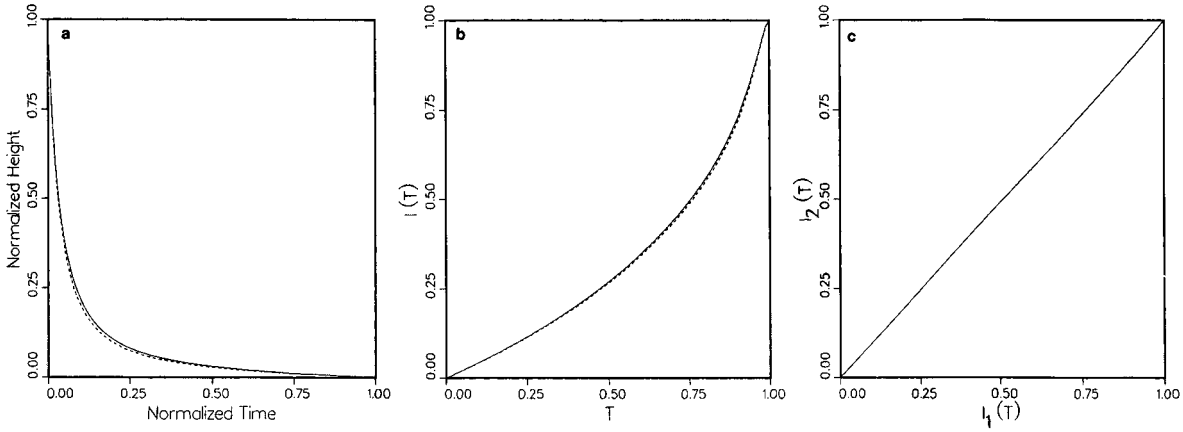

Fig. 1. Comparison between two normalized elution profile tails. Diethyl ether on RHCP alumina at 60°C, helium carrier gas. (a) Elution profiles, measured on the same day, with the same column. (b) Distribution function corresponding to the elution profiles in (a). The solid line corresponds to the normalized tail represented by a solid line in (a). (c) Plot of the distribution function I_2 represented by the dashed line in (b) *versus* the distribution function I_1 represented by the solid line. This particular curve is designated by $\Phi(I_2, I_1)$.

mum is the smaller and only the proper part of the other peak is considered. Similarly, the two profiles have to be stopped at some arbitrary set time, when the signal is too small to be significantly different from the baseline. As the band profiles are very similar, there is no difficulty in stopping them at the same time. We then need to digitize both profiles consistently. To that effect, both rear profiles, below the lower peak maximum, are fitted to a cubic spline. The range of peak height (between zero and the lower maximum) is divided into 500 evenly spaced points and, for each peak, the retention times corresponding to each of these 500 values of the peak height are evaluated from the spline. Each of these curves is then normalized in both dimensions. Each peak height is divided by the maximum peak height, producing a normalized peak height, Π_N. A normalized time, τ, is then computed:

$$\tau = (t - t_1)/(t_2 - t_1) \tag{9}$$

In eqn. 9, the times t_1 and t_2 correspond to the maximum and the minimum peak heights of the profile considered, respectively; t_2 is the time when the chromatograms evaluated are ended. Two such normalized elution profiles, obtained the same day and on the same column are shown in Fig. 1a for illustration. These profiles are similar. To compare them quantitatively, the distribution function, $I(\tau)$, is calculated for each normalized profile:

$$I(\tau) = \int_0^\tau \Pi_N(\tau)\mathrm{d}\tau \tag{10}$$

The distribution functions corresponding to the normalized profiles shown in Fig. 1a, obtained the same day and on the same column, are shown in Fig. 1b. A numerical comparison between the two distribution functions is made by plotting one distribution as a function of the other one, *i.e.*, I_2 as a function of I_1, τ now being the parameter of the point on the new curve. Such a plot is shown in Fig. 1c. The resulting curve is the diagonal line of the square defined by the origin of coordinates and the point (1,1), if the two distribution functions are identical. If they are not, the area of the surface between the curve and the coordinate bisector is taken as a measure of their difference. For symmetry reasons, the shape distance parameter, δ, is defined as

$$\delta = \frac{1}{2}\left\{\sum_{i=1}^{n}[\Phi(I_2, I_1, i) - \Phi(I_1, I_2, i)]^2 + \sum_{i=1}^{n}[\Phi(I_1, I_2, i) - \Phi(I_2, I_1, i)]^2\right\} \tag{11}$$

where $\Phi(I_2, I_1, i)$ is the curve obtained when I_2 is plotted as a function of I_1 and i is the rank, 0 to n, of the point considered. To reduce computation times, the distance, δ, is computed by considering only every fifth point (*i.e.*, n in eqn. 11 is 100). The two-dimensional sum of squares is performed to give the parameter the mathematical properties of a distance [11].

Parameters characterizing the reproducibility of the elution profiles. In addition to the distances, δ, between the profiles, their average and standard deviation for a series of determinations performed under the same set of experimental conditions, three parameters are used to assess the reproducibility of the retention data, a figure of the error on the retention times, a figure of the error on the retention factors and a figure of the error on the amount adsorbed at equilibrium with a partial pressure P.

t_{RMS} is the root-mean-square relative error between the retention times corresponding to two elution profiles. It is calculated by summing the squares of the differences between the elution times of the same concentration on the two profiles for all the 500 concentrations measured, dividing by 500 and taking the square root. This parameter is calculated in the same time as the DFA data, from the retention times which were evaluated from the spline.

k_{RMS} is the root-mean-square relative error between the values of the retention factor, $k' = (t_R - t_0)/t_0$, where t_R is the retention time of a concentration and t_0 is the hold-up time, for the two peaks. k' is calculated directly from the retention times (evaluated from the spline, as described in the previous sub-section) and is a function of the peak height.

q_{RMS} is the root-mean-square relative error between the isotherm points. As with the previously described parameters, it can be evaluated only for the portion of the data which overlap in the probe partial pressure range. Both isotherms were fitted to a spline and evaluated at equally spaced values of the partial pressure, within the common range of partial pressure. The deviation between the resulting isotherms were then compared.

For each difference parameter, an upper confidence limit was computed for each step of the reproducibility study (*i.e.*, same column, same day, same column, different days and different columns, different days). This upper confidence limit was taken as the mean of the difference parameter plus twice the standard deviation.

Results of the study of the retention data. These results are given in Tables II (reproducibility) and III (confidence limits). Several trends may be observed. As expected, the reproducibility of the retention factors was better than the reproducibility of the retention times. This was especially true for the data obtained on different days, with different columns, demonstrating the importance of comparing relative retention rather than absolute retentions.

As the value calculated for the amount adsorbed, q, at equilibrium with a vapor pressure P depends on both the flow-rate and the detector response factor, it is not surprising that the degradation of the reproducibility when going from k' to q is much worse in the second step (measures made on different days with the same column) than in the first one (measures made the same day), as the flow-rates and the response factor drift and have to be measured every day. The poor reproducibility of the absolute data (retention time and amount adsorbed at equilibrium) measured for different columns (compared with measures made with the same column, on

TABLE II

REPRODUCIBILITY OF RETENTION DATA

Mean value of the parameter (%) and relative standard deviation (%) in parentheses.

Comparison basis	Mean t_{TMS} (%)	Mean k'_{RMS} (%)	Mean q_{RMS} (%)	Mean Δ (%)
Same day, same column	1.1 (0.7)	0.9 (0.4)	4.0 (1.2)	8.1 (3.1)
Different day, same column	1.4 (0.6)	0.9 (0.3)	6.0 (1.1)	10. (3)
Different day, different column	4.3 (1.5)	1.1 (0.4)	10. (2)	12. (3)

TABLE III

CONFIDENCE LIMIT (CL) INTERVALS (%) FOR THE RETENTION DIFFERENCE PARAMETERS

Comparison basis	CL t_{TMS} (%)	CL k'_{RMS} (%)	CL q_{RMS} (%)	CL Δ (%)
Same day, same column	1.8	1.3	5.2	11.
Different day, same column	2.0	1.2	7.1	13
Different day, different column	5.8	1.5	12	15

different days) can be explained by the error made on the determination of the mass of stationary phase in the column.

Reproducibility of the calculated parameters

Energy distribution functions were calculated for each set of retention data described in the previous section. Thus, we can compare the reproducibility of the calculated parameters determined in the three steps of the study, and corresponding to measures performed (i) on the same day, with the same column, (ii) on different days, with the same column and (iii) on different days, with different columns. The reproducibility results regarding the parameters of the adsorption energy distribution are given in Table IV. The reproducibilities given correspond to twice the relative standard deviation (R.S.D., %) of the mean.

As the energy distribution of the alumina studied has two peaks (both approximated by a Gaussian function), the data given here are those corresponding to the peak with the worse reproducibility for each given parameter. For example, for the first step (data measured the same day, on the same column), the relative standard deviations of the monolayer capacities were 1% and 2% for the low and high-energy peaks. The worst of the two values, 2%, was reported in Table IV.

TABLE IV

REPRODUCIBILITY OF THE CALCULATED PARAMETERS

Confidence intervals of the parameter (%).

Comparison basis	q_m (%)	E_{AVG} (%)	σ^2 (%)
Same day, same column	4.0	1.0	100
Different day, same column	6.4	1.0	126
Different day, different column	12	1.6	130

The reproducibility of the calculated values of the parameters of the adsorption energy distribution may be entirely explained by the retention data reproducibility itself. The increase in the relative standard deviation of the monolayer capacity when going from one step of the study to the next follows the same trend as q_{RMS}. In fact, it is nearly equal. It is remarkable that the average value of the adsorption energy is highly reproducible (R.S.D. = 1%). This is explained by the fact that it is a normalized quantity. It follows the same trend as the retention factor, k'. The variance of the peaks of the energy distribution should be a function of the shape of the normalized elution peak and therefore its reproducibility should be a function of the reproducibility of δ. This seems to be the case.

Assessment of the validity of the assumptions made in the model relating the isotherm to the primary chromatographic data

The classical theory of analytical chromatography [33,34] assumes that the solute is infinitely dilute in the carrier gas. Because of this assumption, a number of effects can be neglected. The retention time of the band is determined by the column capacity factor or retention factor, k', proportional to the initial slope of the isotherm, that is, by the thermodynamics of the phase equilibrium. On the other hand, the band shape is determined by the kinetics of mass transfers in the chromatographic column. The peak is Gaussian, provided that the mass-transfer kinetics are fast. This profile is independent of the sample size. Further, there is no

coupling between the thermodynamics and the kinetics of retention.

In contrast, non-linear chromatographic band profiles change shape with increasing sample concentration. The elution profile broadens and becomes unsymmetrical. Coupling between thermodynamics and kinetics of retention takes place [35]. In order to model the migration of high-concentration bands, the relative effect of the non-linear (*i.e.*, concentration dependent) factors must be assessed, so they can either be neglected or taken into account, depending on their significance. As the ECP method is based on a result derived from the ideal model (eqn. 4), we also need to assess the importance of the deviation from ideal behavior.

The assumptions which are made or implied in the derivation of eqn. 4 are listed in the Appendix. In this section, we address these assumptions and their degree of validity. To validate the method that we have developed for the determination of the adsorption energy distribution, it is necessary that quality control protocols be established and applied to insure that the data (*i,e.*, the experimental band profiles) are not significantly influenced by the effects of some non-ideal behavior. The validity of the model must be demonstrated for each set of data.

One of the simplest and most direct methods to ascertain the accuracy of the isotherm derived for a chromatographic system is to compare the recorded band profile for a large size sample with the profile calculated using a general model. Simulations are very important to this type of validity testing as they may allow the validity of each assumption to be tested independently. This practice is usually impossible experimentally. We have largely used this powerful tool which we have developed in the recent past. Details of the implementation of the program, together with an investigation of the influence of the column permeability on the actual band profile, are reported elsewhere [5].

Assumption I. The column is homogeneous. The column is filled with a homogeneous slurry, prepared by sonication. The rate at which the particles settle in the slurry is very low (only after 24–36 h is it possible to notice that they have settled to a significant extent) and the time needed to vaporize the solvent and to coil the column in the oven is *ca.* 4 h. After the column has been taken from the oven in which it has been coiled, the column is always kept horizontal. Thus, all efforts are made to obtain and conserve a homogeneous column.

Assumption II. The column is isothermal. The range of temperature fluctuations experienced in a fixed point of the oven, under isothermal conditions, is of the order of ± 0.1°C. The temperature gradient in the oven is more important. The detector and injector are set at temperatures higher than the oven. Significant gradients may exist in the proximity of the heating elements. In the center of the oven, where the column is placed, the gradient is estimated to be of the order of 0.1°C cm^{-1}. The metallic cage holding the column may contribute to relax these gradients.

As discussed previously [36], the effect of these fluctuations of the temperature of the band on the retention data obtained with a coiled column will be small compared with that of the other sources of errors. At most they will contribute to a slight shift in the energy distribution, which has a negligible effect on the comparison made between different columns, as all the columns are carefully positioned at the same place in the oven.

Assumption III. The heat balance can be neglected. Gas–solid adsorption is an exothermic process. When the probe vapor is adsorbed at the band front, some heat is generated. Only part of this heat is conducted away, axially and radially. When the solute is desorbed on the band tail, heat is adsorbed in the process. Thus, the band front moves in a warm zone and tends to migrate faster than in an isothermal column. The rear of the profile is moving along a column zone whose temperature decreases and it tends to move more slowly than in an isothermal column. The band is broadened. The consequences of this effect are usually neglected. There is no evidence to suggest that this practice causes a significant error [14,16].

Assumption IV. The mobile phase viscosity is constant. Most organic vapors have a lower viscosity than helium. If the local probe partial pressure is high enough, this may alter the local viscosity of the mobile phase and hence its local velocity. The effect of a changing viscosity of the mobile phase as a band passes a point on the column has been discussed previously [14,37]. The viscosity change causes the pressure to deviate non-uniformly over the column and alters the pressure and the velocity profiles. Taking into account the viscosity effect in a chroma-

tographic model would be very difficult, however, and this has never been done before.

Fortunately, this effect may be neglected as long as the column is radially homogeneous [38,39]. In our study of the adsorption energy distribution on alumina particles, we determine the adsorption isotherm of diethyl ether and 1-chlorobutane in the range of partial pressure from 0 to less than $5 \cdot 10^{-3}$ atm, while the average column pressure is less than 1.2 atm. Although the partial pressure of the probe at the beginning of the column certainly exceeds 0.4% of the inlet pressure, the effect can be only minimal.

Assumption V. The mobile phase behaves as an ideal gas. In the Theory section, we have discussed the equation derived by Conder and Young [9] to take into account the deviation of the mobile phase behavior from that of an ideal gas. We have shown that, in the range of partial pressures of the probe at which the measurements are carried out, the corrections for non-ideal behavior that were introduced remain negligible.

Another, entirely different, approach leads to the same conclusion. We have seen above that the average column pressure is $J_4^3 P_o$ [15]. In order to estimate the magnitude of the effect due to the deviation of the behavior of the carrier gas from ideal, we can calculate the pressure, P', under which the same amount of a real gas would be, if stored in the same column volume. The calculation uses the Beattie–Bridgeman equation [40,41], an empirical equation of state valid over the range of temperature and pressure of interest here. The value obtained is compared with the pressure calculated by the ideal gas equation.

Our experiments were conducted at an inlet pressure, P_i, of 1.340 atm and an outlet pressure, P_o, of 1.000 atm. The average pressure, $P_{4,3}$ is thus 1.186 atm. For the temperature of 333 K and a column volume of 3.29 ml, the number of moles of an ideal gas contained in the column is $1.428 \cdot 10^{-4}$ (molar volume $2.304 \cdot 10^4$ ml mol^{-1}). The Beattie–Bridgeman equation is written as [40]

$$P = RT \cdot \frac{1 - \dfrac{c_{BB}}{V_{BB} T^3}}{V_{BB}^2} (V_{BB} + B_{BB}) - \frac{A_{BB}}{V_{BB}^2} \qquad (12)$$

where V_{BB} is the molar volume of the gas, and the coefficients are

$$A_{BB} = A_{0,BB}\left(1 - \frac{a_{BB}}{V_{BB}}\right) \qquad (13a)$$

$$B_{BB} = B_{0,BB}\left(1 - \frac{b_{BB}}{V_{BB}}\right) \qquad (13b)$$

The empirical constants for helium are [41]

$A_{0,BB} = 2.16 \cdot 10^4$ atm cm^6 mol^{-2}

$a_{BB} = 59.84$ cm^3 mol^{-2}

$B_{0,BB} = 14.00$ cm^3 mol^{-1}

$b_{BB} = 0.0$ cm^3 mol^{-1}

$c_{BB} = 4.0 \cdot 10^4$ cm^3 K^3 mol^{-1}

The value of the pressure calculated from the Beattie–Bridgeman equation is 1.187 atm. This agrees with the pressure of an ideal gas (relative error = 0.08%). The mobile phase (helium) may be assumed to behave as an ideal gas under the experimental conditions used in this work.

Assumption VI. The carrier gas is not retained. Helium is not significantly adsorbed on alumina at 60°C. The retention time of methane was compared with that of nitrogen on a 10-m column containing 60 mg of alumina. The retention factor of methane, assuming that nitrogen is not sorbed, was found to be 0.05. The columns we use for the determination of the adsorption energy distribution on alumina contain *ca.* 44 mg of alumina in a 15-m column. The phase ratio is thus twice as small and the retention factor becomes 0.025. A correction is made to the retention volume of methane when determining the void volume of a new column.

Assumption VII. Adsorption of the probe takes place only on the stationary phase. In order to check this assumption, elution profiles of the probe compounds were recorded on a blank column, made with a piece of clean, uncoated quartz tube, under the same experimental conditions as for the regular measurements of adsorption isotherms. The amount of solute injected was sufficient to cause the eluted peak to be as high as the peaks used for the ECP measurements. The elution profiles obtained with the two probes are shown in Fig. 2. Both peaks eluted at the void time and neither of them is skewed. The column plate number was computed numerically for each peak using the Foley–Dorsey equation [42]. In each instance it was 10 200 theoretical plates.

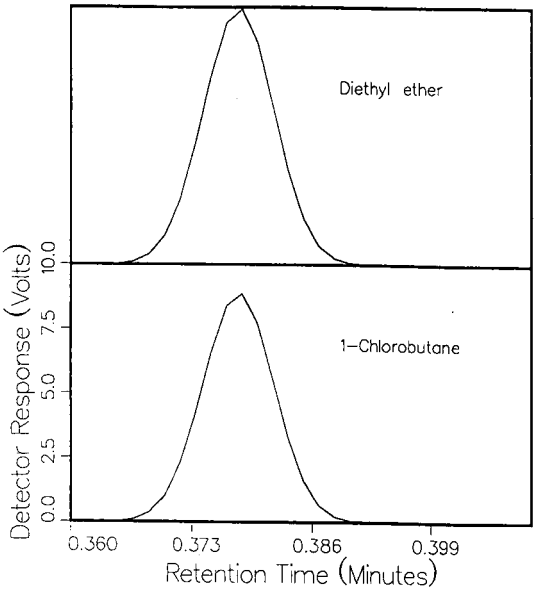

Fig. 2. Elution profiles of the probes obtained on a blank column. Chromatographic conditions: carrier gas: helium, pressure drop, 0.34 atm; outlet velocity, 56 cm^{-1}; column, 15 m × 0.53 mm I.D.; hold-up time, 22.7 s in both instances; temperature, top 60°C, bottom 40°C.

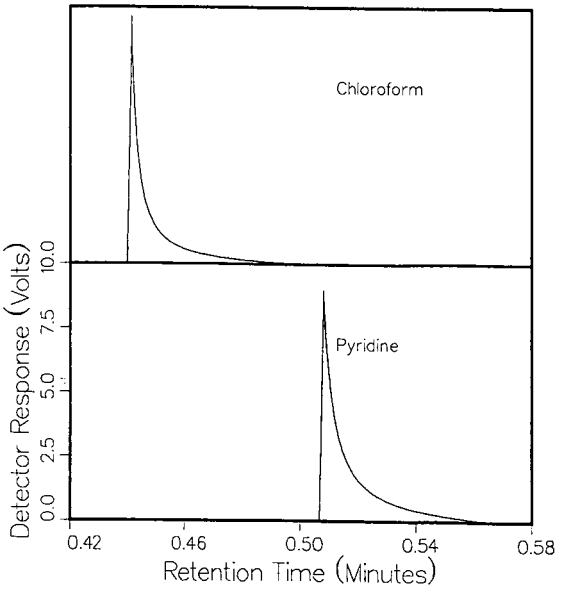

Fig. 3. Elution profiles of some vapors obtained on a blank column. Chromatographic conditions as in Fig. 2, except top chromatogram, chloroform, 100°C, hold-up time 28.4 s and bottom chromatogram, pyridine, 150°C, hold-up time 30.1 s.

It is interesting to compare this efficiency with that predicted by the Golay equation [22,23]. For a non-retained compound ($k' = 0$), this equation becomes

$$H = \frac{2D_g}{u} + \frac{d_c^2 u}{96 D_g} \tag{14}$$

where H is the column HETP and d_c its inner diameter. The molecular diffusion coefficient of the probe, D_g, can be derived from the Fuller–Giddings equation [43]:

$$D_g = \frac{1.0 \cdot 10^{-3} T^{1.75}}{P\left[\left(\sum \varepsilon_i\right)_A^{1/3} + \left(\sum \varepsilon_i\right)_B^{1/3}\right]} \left(\frac{1}{M_A} + \frac{1}{M_B}\right)^{1/2} \tag{15}$$

where the subscripts A and B refer to the probe vapor and the carrier gas, respectively, P is the pressure in atm and ε_i is an atomic contribution to the diffusion volume of the molecule, found in a table [43]. For diethyl ether and helium, the volumes $\left(\sum \varepsilon_i\right)_A$ and $\left(\sum \varepsilon_i\right)_B$ are 91.3 and 5.4, respectively. The diffusion coefficient of diethyl ether in helium at 60°C under atmospheric pressure is 2.1 $cm^2\ s^{-1}$. Hence, with a carrier gas outlet velocity of 66 cm s^{-1}, $H = 0.066$ cm ($N = 22\,700$ theoretical plates). The 50% loss of efficiency probably comes from extra-column contributions. As shown by the Golay equation, however, the band width increases very rapidly with increasing retention and the extra-column contribution becomes negligible for retained components.

For some other solutes, however, adsorption does occur on sites located on the column wall. Fig. 3 shows the elution profiles on the blank column for two compounds which were considered as potential probes, chloroform eluted at 100°C and pyridine at 150°C. These peaks are highly unsymmetrical, denoting the presence of some high-energy adsorption sites in the system. Because of the increase in the carrier gas viscosity with increasing temperature, the hold-up times at constant inlet pressure are 26.4 s at 60°C and 30.1 s at 150°C. Hence the band fronts are eluted nearly at the hold-up time. The retention of these two compounds on the blank column is probably only barely significant, however.

For example, for pyridine, the retention time

corresponding to the minimum detectable voltage (5 mV) is only 34 s, corresponding to $k' = 0.13$. When the elution profile of pyridine is recorded on an actual alumina column, the retention factor corresponding to the minimum detectable voltage is of the order of 7. Based on the upper confidence limit (Table III) for k'_{RMS}, one may assign a confidence interval of $\pm 1.3\%$ (*i.e.*, 7 ± 0.1) to this measurement. As a correction could be made, the additional shift is virtually negligible, even for pyridine.

Assumption VIII. The entire amount of the probe compound injected is eluted. We have observed for diethyl ether, but not for 1-chlorobutane, that not all the amount injected into the column elutes before the detector response returns to the baseline [1]. Some of the sample, always less than 10% of the amount injected, elutes later. This elution can be observed, for example, during temperature programming of the column [1]. Such a thermal conditioning of the column is always performed between two successive experiments with a column. It is important to understand the reason for this phenomenon, which could be due to a slow desorption kinetics.

We can demonstrate that no measurable amount of diethyl ether remains chemisorbed on the column by making two successive large injections of the same amount of diethyl ether, separated by a thermal conditioning of the column, and comparing the peak areas. They are identical, and it is highly improbable that the same amount of sample would be absorbed irreversibly each time. The most probable explanation is that the tail of an isothermal elution profile is extremely long and is far from completely eluted when the detector signal appears to return to the baseline. In order to investigate this possibility, the following analysis was performed.

For diethyl ether on alumina, the area corresponding to the injected band profile was 0.91 V min. If we assume that 10% of the material injected remains on the column after the detector response decays to 5 mV, the peak area lost is 0.09 V min. If we approximate the portion of the tail of the elution profile below 5 mV by a right triangle, the time required to decay from 5 to 0 mV is given by

$$t_w = (2 \cdot 0.09)/(5 \cdot 10^{-3}) = 36 \text{ min}$$

If we assume instead an exponential decay, $y = y_0 e^{-kt}$, for the detector signal, beyond the time t_f when we usually end the recording, with a time constant k, the area under the exponential is

$$A = \int_{t_f}^{\infty} y dt = \frac{y_0}{k} [-e^{-kt}]_{t_f}^{\infty} = \frac{y_0}{k}$$

With a value $y_0 = 5$ mV for the detector signal and an area of 0.09 mV min for the residual amount, we find a time constant of 18 min. After two time constants, the area has decreased by a factor of 7.4. An experiment was performed with an extended isothermal period of 7.5 + 36 = 43.5 min, instead of the normal 7.5 min, prior to undergoing the regular thermal conditioning. This time, no peak was observed during temperature programming of the column. This experiment shows that the observation of residual amount of diethyl ether is due to the limited time window used for data acquisition of this profile.

Further evidence was provided by fitting the adsorption isotherm to a multi-Langmuir equation and extrapolating to infinite dilution. A bi-Langmuir equation was used in this case:

$$q(P) = \frac{a_1 P}{1 + b_1 P} + \frac{a_2 P}{1 + b_2 P} \tag{16}$$

Taking the first derivative and extrapolating to $P = 0$ gives a limit of dq/dP equal to $a_1 + a_2$. The retention time of the end of the profile predicted by the ideal model is

$$t_R = t_0 \left[1 + \frac{jRTm_s}{V_m} (a_1 + a_2) \right] \tag{17}$$

For diethyl ether on RHCP alumina at 60°C, the best-fit bi-Langmuir coefficients were $a_1 = 0.145$ and $a_2 = 0.0229$. The other parameters in eqn. 17 are $j = 0.846$, $V_m = 3.29$ ml, $m_s = 44$ mg and $t_0 = 0.372$ min. Using these values in eqn. 11 yields $t_R = 19.7$ min. While the three analyses yield values of the retention times at infinite dilution which appear to be in poor agreement, 19.7 min, 43.5 min and infinity, they all yield retention times which are significantly greater than the time at which the sensitivity of the detector mandates the end of the experiment. The only consequence of this loss, however, is a slight decrease in the accuracy of the isotherm measured at very low partial pressures.

Assumption IX. The shape and width of the injection profile have no influence on the elution profile. That the shape of the injection profile does not influence the profile of the elution bands may be concluded by studying the profiles of the peaks eluted from the blank column. These peaks are Gaussian and exhibit no or negligible tailing (Fig. 2). The width of these peaks is negligible compared with the width of the peaks used for the determination of adsorption isotherms using the ECP method.

Because the amount injected in the blank column, on which there is no retention and hence little dilution, is much lower than the amount injected for the determination of the elution profiles used for isotherm calculations, the effect of the sample width or volume on the elution profile must be assessed in the case of large injections. First, the band profile is calculated with the semi-equilibrium model of chromatography, as explained elsewhere [5,13,17,25], using the narrowest possible profile. Next, the calculation is repeated, assuming a rectangular profile with a height equal to P_{MAX}, the height of the elution profile at the detector. The width is nearly 10 s. Based on the results described in the last section, the plate number used for both simulations is 8000. The two injection profiles are shown in Fig. 4. The two calculated band profiles are compared with the experimental band profile in Fig. 5. Although the band height can only decrease during an isothermal elution, the dramatic increase in the injection width of the second calculated band has very little effect on its elution profile. We conclude that, as long as the injection profile does not tail badly, the effect of its profile on the determination of the isotherm is negligible. This result is in agreement with the findings of Knox and Pyper [44], who have shown that the sample volume does not affect the band profile up to a fairly large value.

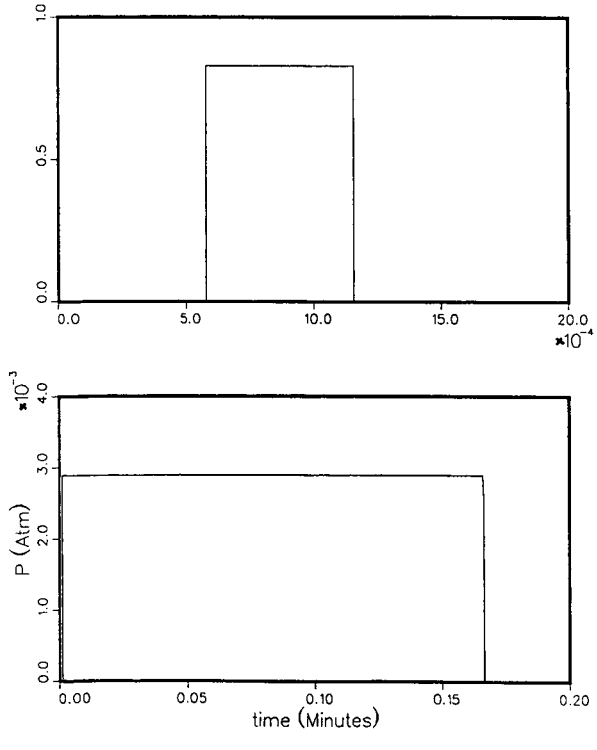

Fig. 4. Injection profiles used for the simulation of the elution profile of diethyl ether on RHCP alumina at 60°C. Experimental conditions as in Fig. 2. Peak area, $4.80 \cdot 10^{-4}$ atm min; number of theoretical plates, 8000.

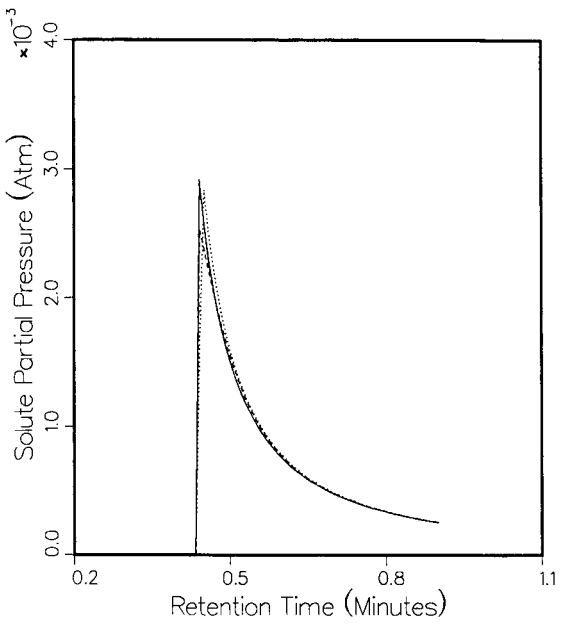

Fig. 5. Comparison between an experimental elution profile (solid line) and the profiles calculated with the semi-ideal model of chromatography, using the experimental isotherm and the injection profiles shown in Fig. 4. Dotted line, profile calculated with the narrow injection profile; dashed line, profile calculated with the wide injection profile. Experimental conditions as in Fig. 4. Number of theoretical plates, 8000.

Assumption X. The influence of the finite efficiency of the column is negligible. In order to insure that the effects of the non-ideal behavior of the column on

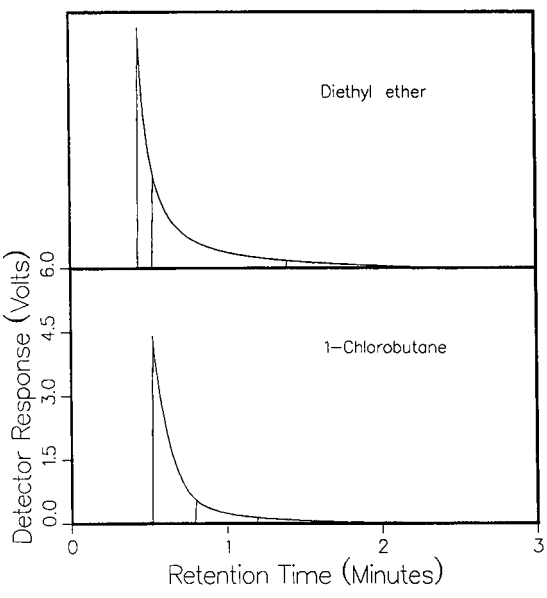

Fig. 6. Good coincidence of the tails of elution profiles corresponding to different amounts injected. Experimental conditions as in Fig. 2. Stationary phase, RHCP alumina; mass of stationary phase, m_s, 44 mg. Top chromatograms: diethyl ether; temperature, 60°C; hold-up, 22.7 s; sample sizes, large peak 0.460 μg (area 0.911 V min), medium peak 0.30 μg, small peak 0.035 μg. Bottom chromatogram: 1-chlorobutane; temperature, 40°C; hold-up time, 21.5 s; sample sizes, 0.18, 0.034 and 0.016 μg; large peak area, 0.678 V min.

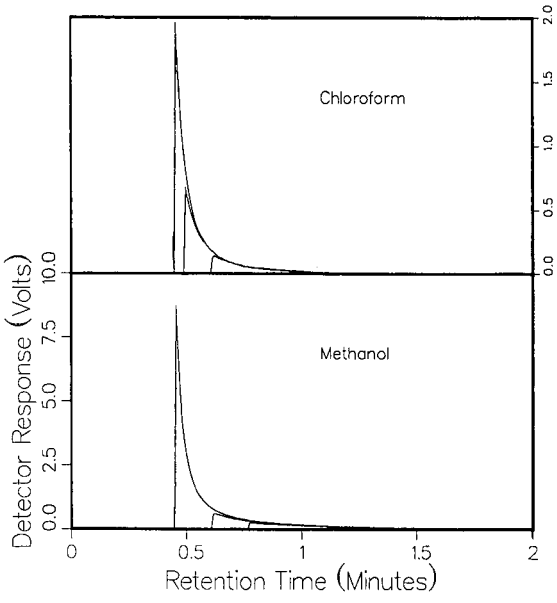

Fig. 7. Poor coincidence of the tails of elution profiles corresponding to different amounts injected. Experimental conditions as in Fig. 2. Top chromatogram: chloroform; temperature, 40°C; hold-up time, 21.6 s; sample sizes, 0.24, 0.10 and 0.06 μg; large peak area, 0.331 V min. Bottom chromatogram: methanol; temperature, 80°C; hold-up time, 25.9 s; sample sizes, 0.36, 0.12 and 0.05 μg; large peak area, 0.611 V min.

the probe band profile may be neglected, the method first suggested by Huber and Keulemans [45] is used. Several elution profiles corresponding to increasing amounts of the probe are recorded. These chromatograms are superimposed and it is determined whether or not their tails lie on the same curve. Huber and Keulemans [45] stated that, if the tails do coincide, then one may safely conclude that the effects of the apparent axial dispersion may be neglected. Although it is true that this condition is necessary to obtain isotherms which are independent of the concentration (a minimum requirement), a significant efficiency is also necessary to minimize the contribution of band spreading on the ECP balance at low concentrations. In Fig. 6, we show the coincidence of the tails for three sample sizes of the two probe compounds (diethyl ether and 1-chlorobutane) used to characterize the alumina. In Fig. 7, two similar sets of data are shown, for chloroform at 40°C and methanol at 80°C. In this instance, the band tails of increasing size samples do not coincide. This phenomenon is probably related to the concentration-dependent nature of the non-equilibrium effects [45]. Similar results (not shown) were also observed for benzene and pyridine.

The non-equilibrium behavior manifested by chloroform and methanol may be due to slow kinetics of adsorption–desorption. We expect that methanol chemisorbs to some extent as those alcohols which are structurally capable of losing a water molecule dehydrate rapidly in contact with alumina. However, the deviation of the tails from one another in Fig. 7 is small and this phenomenon deserves a more detailed study.

In order to simulate the effect of the finite column efficiency on the profiles of the bands of probe compounds recorded, a series of simulations were performed [13,17,25]. Using the adsorption isotherm for diethyl ether on RHCP alumina at 60°C, the band profiles predicted by the equilibrium-diffusive model on three hypothetical columns having efficiencies of 6000, 8000 and 20 000 theoretical plates,

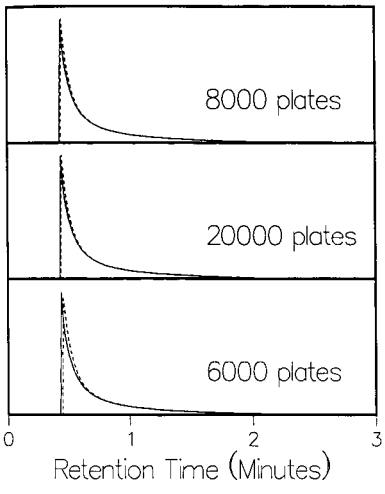

Fig. 8. Comparison between the experimental chromatogram of diethyl ether on RHCP alumina at 60°C (solid line) and the elution profiles calculated with the semi-ideal model, the adsorption isotherm derived by the ECP method and using different column efficiencies. Dashed line: simulated chromatogram with a column efficiency of 8000 theoretical plates (top), 20 000 plates (middle) and 6000 plates (bottom). Experimental conditions as in Fig. 2.

respectively, were calculated (note that the real column used has 10 000 plates under the usual experimental conditions). The details of the calculations involved will be published elsewhere [5]. The numerical solutions obtained were compared with the actual band profiles. The results are shown in Fig. 8.

We see in Fig. 8 that there are no significant differences between the experimental profiles and the profiles calculated for columns having 8000 and 20 000. The nearly perfect coincidence between the experimental profile and the two numerical solutions validates the whole calculation process and the experimental isotherm. A systematic deviation between calculated and experimental profiles appears for an efficiency of 6000 plates and would increase for lower efficiencies. In practice, the efficiency of a porous-layer open-tubular column appears necessary for accurate determinations of isotherm data by the ECP method.

Assumption XI. There are no sources of extra-column band broadening. Extra-column volumes, whether swept or dead, contribute to band broadening. The injector and the detector both behave as mixing chambers. In contrast with analytical chromatography, these contributions cannot be dealt with simply using the rule of the additivity of the contributions to the band variance. It is easy to show that, in non-linear chromatography, the extra-column contributions have the effect of a shift-variant convolution [46]. The variances contributed by the band broadening sources which are upstream of the column are no longer additive. However, the variances contributed by the sources placed downstream remain additive.

It is as imperative as in analytical applications to keep to a minimum the extra-column contributions to band broadening. A well designed splitting device is needed to ensure a narrow, rectangular injection plug. As shown above, the equipment contributes significantly to the broadening of non-retained component bands under linear conditions, but this contribution is small enough to become negligible with retained components. Further, the extra-column band broadening contributions become less important in non-linear chromatography because the band profile is more controlled by thermodynamics than by kinetics.

Assumption XII. The sorption effect has negligible effect. The sorption effect, a dependence of the local mobile phase velocity on the local solute partial pressure, is due to the large difference between the partial molar volumes of the solute in the stationary and the mobile phases and to the fact that the carrier gas flow-rate is held constant at the column inlet. This has been pointed out and studied by Bosanquet and Morgan [47]. As the front of a finite concentration band passes a point in the column, sorption of the probe vapor occurs and the mobile phase is partially depleted. Because of this depletion, the mobile phase flow-rate downstream of the band is slower than at the band front. Similarly, at the rear of the band, the local mobile phase velocity is lower upstream of the band than in the band itself. The effect of this flow-rate profile on the probe concentration profile in the band is similar to the effect caused by a Langmuir isotherm [14,47]. The front boundary of the band is self-sharpening and the rear boundary is diffuse.

For a given amount of the probe compound, the magnitude of the sorption effect is related to the magnitude of the column pressure drop (or rather to the average column pressure). If the pressure drop is high, the carrier gas density is high and the mole fraction of the probe solute is relatively low

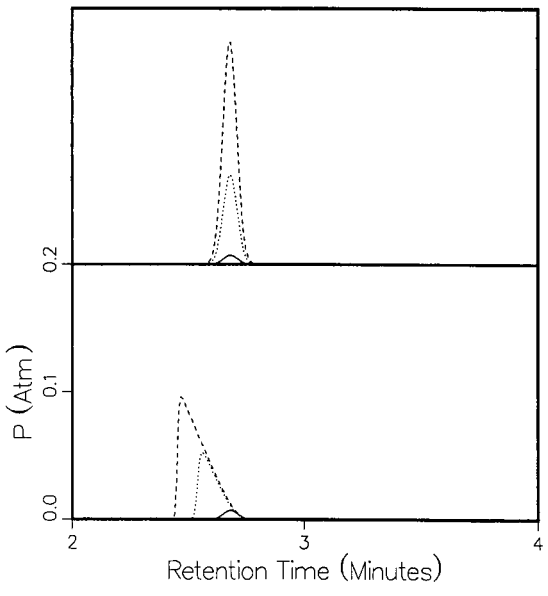

Fig. 9. Theoretical study of the sorption effect. Comparison between calculated elution profiles for different size samples. Experimental conditions as in Fig. 4 (top), except linear isotherm with a slope of 0.02 mol g^{-1} atm^{-1}. Column efficiency, 8000 theoretical plates. Top chromatograms: profiles calculated without sorption effect. Bottom chromatograms: profiles calculated with a program including the carrier gas mass balance and the sorption effect. Sample sizes, 0.51, 5.1 and 12.6 μg; peak area, solid line $0.53 \cdot 10^{-3}$, dotted line $5.3 \cdot 10^{-3}$, dashed line $13.2 \cdot 10^{-3}$ atm min.

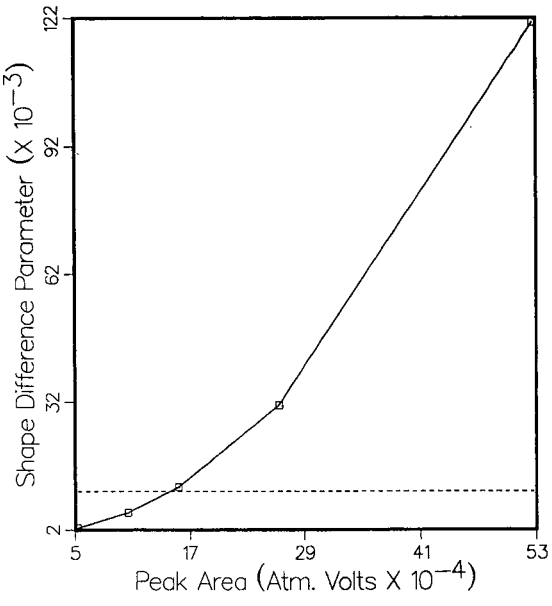

Fig. 10. Theoretical study of the sorption effect. Plot of shape difference parameter *versus* peak area for the comparison between the band profiles calculated with and without taking the sorption effect into account. Experimental conditions as in Fig. 9. Dashed line, upper confidence limit for the reproducibility of the shape parameter, for measurements made on the same day and with the same column.

over most of the column length. The mobile phase flow-rate is less perturbed by the passage of the band. It would be possible to decrease the intensity of the sorption effect by increasing the average column pressure. In fact, one can even decrease the magnitude of the sorption effect by increasing both the inlet and the outlet column pressures, and hence the average column pressure, without increasing the pressure drop [13,14,38,19]. On the other hand, the sorption effect is important at low column pressure drops, which is almost always the condition under which wide-bore open-tubular columns are operated.

In order to estimate the degree of column overloading at which the sorption effect begins to be noticeable, simulations were carried out. Elution band profiles were calculated using the equilibrium-dispersive model, a linear isotherm and two computer programs. One of these programs ignores the sorption effect and the other takes it into account. The results are compared for three different sample sizes in Fig. 9. The smallest of the three peaks corresponds approximately to the amount injected in the determinations of the adsorption isotherms of the probes on the alumina samples. It is essentially the same in both parts of Fig. 9. No significant degree of column overloading is achieved with this small sample and non-linear behavior of the elution profiles is not observed. In contrast, such non-linear effects are important with the other two sample sizes. The shapes of the simulated band profiles were compared by calculating the shape difference parameter, δ, for each peak. A plot of the shape difference *versus* the peak area is shown in Fig. 10. This plot demonstrates that, under our experimental conditions, the shape difference caused by the sorption effect is insignificant unless the peak area exceeds $15 \cdot 10^{-4}$ atm V. Our measurements use sample sizes corresponding to peak areas between 0.5 and $1 \cdot 10^{-3}$ atm V.

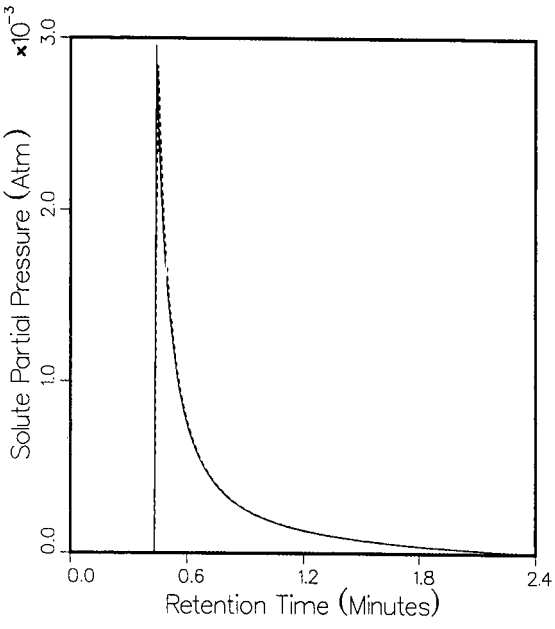

Fig. 11. Theoretical study of the sorption effect. Comparison between an experimental elution profile and the band profile calculated with the program taking the sorption effect into account. Experimental conditions as in Fig. 4 (top). The shape difference parameter, δ, is $1.1 \cdot 10^{-3}$.

Finally, we compare in Fig. 11 the elution band profile recorded for diethyl ether on RHCP alumina at 60°C and that calculated with the program taking the sorption effect into account. The narrow injection profile (Fig. 4) and a column efficiency of 8000 theoretical plates were used for this calculation. The value of the shape difference parameter between these two elution profiles is well below the confidence limit for profiles recorded on the same day and with the same column. This result completes the demonstration that the sorption effect and the pressure drop effect may be neglected under the experimental conditions used here.

These results also validate the use of our conventional liquid chromatography program [25] for the calculations reported in Fig. 8. Although the more complex program [5] taking the carrier gas mass balance (and hence the sorption effect) into account should have been used, it was not because it requires significantly more CPU time than the former program.

CONCLUSIONS

Many of the assumptions whose validity was assessed in this investigation remain valid from experiment to experiment as long as the experimental conditions and the instrument used are not significantly changed. These assumptions, however, must be tested each time a new powder sample is studied. They are (i) that adsorption occurs only on the stationary phase (*i.e.*, that the number of adsorption sites on the wall of the fused-silica tubing and on the extra-column surfaces is negligible); and (ii) that the effect of the finite column efficiency on the equilibrium isotherm derived by the ECP method may be neglected. The procedures for testing the validity of these assumptions have been described. These procedures are the quality control (QC) protocols which are necessary to test the models.

Before proceeding further with the use of the adsorption isotherms determined from elution profiles by the ECP method, it is necessary to test the reproducibility at the experimental data, *i.e.*, the band profiles, as the results of this test determine directly the reproducibility of the calculated isotherm data. The QC protocol for the reproducibility of elution profiles is as follows.

Detector response factor

If a probe is used for the first time, the response factor must be determined on two different days. The reproducibility of this factor may then be compared with the reproducibility data given in Table I. If the solute has been used before, and the response factor does not agree with earlier data, it is measured again on another day. Response factors are rejected even without different day reproducibility checks if the statistical data regarding the calibration graph are poor or if the peak-area reproducibility is not satisfactory.

Elution profile

Each elution profile used to calculate an energy distribution function is measured in duplicate. The shape difference parameter for these two measurements is calculated. If this parameter exceeds the value corresponding to the confidence limit for the reproducibility of the band shape on the same day and with the same column (see Table III), the data set should be rejected.

Accuracy of the data set

The accuracy of each data set is assessed by back-calculating the elution profile and comparing the values of the parameters t_{RMS} and δ for the simulated and the experimental band profiles with the upper confidence limits for values obtained on the same day and with the same column. If either of these parameters is greater than the corresponding upper confidence limit, the data set should be rejected.

Finally, our results demonstrate that high quality data in inverse chromatography may be obtained on an essentially unmodified, commercially available gas chromatograph. Specially designed and custom-built equipment does not seem as necessary now as it was 20 years ago [48,49]. The reproducibility of the parameters which can be calculated from the band profiles is determined almost entirely by the experimental reproducibility of these measurements. The general validity of most of the assumptions made in the derivation of the adsorption isotherm by the ECP method has been demonstrated. Only a few of the assumptions must be tested for each new set of experimental data.

ACKNOWLEDGEMENTS

This work was supported in part by Grant DE-FG05-88ER13859 from the US Department of Energy, Office of Basic Energy Research, and by the cooperative agreement between the University of Tennessee and the Oak Ridge National Laboratory. We acknowledge support of our computational effort by the University of Tennessee Computing Center.

APPENDIX

Assumptions made in the derivation of eqn. 4

Assumption I. The stationary phase is distributed evenly along the length of the column.

Assumption II. The column is isothermal.

Assumption III. The thermal effect may be neglected.

Assumption IV. The viscosity effect may be neglected.

Assumption V. The mobile phase behaves as an ideal gas.

Assumption VI. The carrier gas is not sorbed by the stationary phase.

Assumption VII. Adsorption occurs only on the stationary phase, *i.e.*, the number of adsorption sites on the wall of the fused-silica tubing and on the extra-column surfaces is negligible.

Assumption VIII. The entire sample amount injected is eluted.

Assumption IX. The influence of the shape and finite width of the injection profile on the elution profile of the probe is negligible.

Assumption X. The effects of the axial dispersion and the mass-transfer kinetics on the band profile (*i.e.*, of the finite column efficiency) may be neglected.

Assumption XI. There are no extra-column sources of band broadening.

Assumption XII. The influence of the sorption effect and the pressure drop along the column on the elution profile are negligible.

REFERENCES

1 J. Roles and G. Guiochon, *J. Chromatogr.*, 591 (1992) 233.
2 E. Cremer, *Monatsh. Chem.*, 92 (1961) 112.
3 E. Cremer and J. F. K. Huber, *Angew. Chem.*, 73 (1961) 461.
4 E. Cremer and J. F. K. Huber, in N. Brenner, J. E. Callen and M. D. Weiss (Editors), *Proceedings of the Third International Symposium on Chromatography*, Academic Press, New York, 1962, p. 169.
5 J. Roles and G. Guiochon, *J. Chromatogr.*, 591 (1992) 267.
6 M. Jaroniec and R. Madey, *Physical Adsorption on Heterogeneous Solids*, Elsevier, Amsterdam, 1988.
7 J. Roles and G. Guiochon, *J. Phys. Chem.*, 95 (1991) 4098.
8 J. F. K. Huber and R. G. Gerritse, *J. Chromatogr.*, 58 (1971) 137.
9 J. R. Conder and C. L. Young, *Physicochemical Measurements by Gas Chromatography*, Wiley, New York, 1979.
10 H. Rix, *J. Chromatogr.*, 204 (1981) 163.
11 J. Excoffier, A. Jaulmes, C. Vidal-Madjar and G. Guiochon, *Anal. Chem.*, 54 (1982) 1941.
12 R. Aris and N. R. Amundson, *Mathematical Methods in Chemical Engineering*, Vol. 2, Prentice Hall, Englewood Cliffs, NJ, 1973.
13 P. Rouchon, M. Schonauer, P. Valentin and G. Guiochon, *Sep. Sci. Technol.*, 22 (1987) 1793.
14 G. Guiochon and L. Jacob, *Chromatogr. Rev.*, 14 (1971) 77.
15 J. R. Conder and J. H. Purnell, *Trans. Faraday Soc.*, 64 (1968) 3100.
16 P. Rouchon, M. Schonauer, P. Valentin, C. Vidal-Madjar and G. Guiochon, *J. Phys. Chem.*, 89 (1985) 2076.
17 J. Roles and G. Guiochon, *J. Chromatogr.*, 589 (1992) 223.
18 J. N. Wilson, *J. Am. Chem. Soc.*, 62 (1940) 1583.
19 B. C. Lin, S. Golshan-Shirazi, Z. Ma and G. Guiochon, *Anal. Chem.*, 60 (1988) 2647.
20 S. Golshan-Shirazi and G. Guiochon, *J. Chromatogr.*, 506 (1990) 495.
21 S. Golshan-Shirazi and G. Guiochon, *J. Phys. Chem.*, 94 (1990) 495.

22 M. J. E. Golay, in D. H. Desty (Editors), *Gas Chromatography 1958*, Butterworths, London, 1958, p. 36.
23 M. J. E. Golay, *Nature (London)*, 199 (1963) 370.
24 P. C. Haarhoff and H. J. Van der Linde, *Anal. Chem.*, 38 (1966) 573.
25 G. Guiochon, S. Golshan-Shirazi and A. Jaulmes, *Anal. Chem.*, 60 (1988) 1856.
26 S. Golshan-Shirazi and G. Guiochon, *Anal. Chem.*, 60 (1988) 2634.
27 S. Jacobson, S. Golshan-Shirazi and G. Guiochon, *AIChE. J.*, 37 (1991) 836.
28 A. T. James and A. J. P. Martin, *Biochem.*, 50 (1952) 679.
29 C. F. Chueh and W. T. Ziegler, *AIChE. J.*, 11 (1965) 508.
30 D. L. Peterson and F. Helfferich, *J. Phys. Chem.*, 69 (1965) 1283.
31 J. R. Conder, *Chromatographia*, 7 (1974) 387.
32 E. A. Guggenheim and M. L. McGlashan, *Proc. R. Soc., London, Ser. A*, 206 (1951) 448.
33 A. J. P. Martin and R. L. M. Synge, *Biochem. J.*, 35 (1941) 1358.
34 J. C. Giddings, *The Dynamics of Chromatography*, Marcel Dekker, New York, 1966.
35 B. C. Lin, S. Golshan-Shirazi and G. Guiochon, *J. Phys. Chem.*, 93 (1989) 3363.
36 M. Goedert and G. Guiochon, *Anal. Chem.*, 45 (1973) 1180.
37 C. J. Chen and J. F. Parcher, *Anal. Chem.*, 43 (1971) 1738.
38 P. Valentin and G. Guiochon, *Sep. Sci.*, 10 (1975) 245.
39 P. Valentin and G. Guiochon, *Sep. Sci.*, 10 (1975) 289.
40 J. A. Beattie and O. C. Bridgeman, *J. Am. Chem. Soc.*, 50 (1927) 3133.
41 J. A. Beattie and O. C. Bridgeman, *Proc. Am. Acad. Arts Sci.*, 63 (1928) 229.
42 J. P. Foley and J. G. Dorsey, *Anal. Chem.*, 55 (1983) 730.
43 E. N. Fuller, P. D. Schettler and J. C. Giddings, *Ind. Eng. Chem.*, 58 (1966) 19.
44 J. H. Knox and H. M. Pyper, *J. Chromatogr.*, 363 (1986) 1.
45 J. F. K. Huber and A. I. M. Keulemans, in M. Van Swaay (Editor), *Gas Chromatography 1962*, Butterworths, London, 1962, p. 26.
46 E. Dose and G. Guiochon, *Anal. Chem.*, 61 (1990) 1723.
47 C. Bosanquet and G. D. Morgan, in D. H. Desty (Editor), *Vapour Phase Chromatography*, Butterworths, London, 1957, p. 35.
48 J. E. Oberholtzer and L. B. Rogers, *Anal. Chem.*, 41 (1969) 1234.
49 M. Goedert and G. Guiochon, *Anal. Chem.*, 42 (1970) 962.

Journal of Chromatography, 591 (1992) 267–272
Elsevier Science Publishers B.V., Amsterdam

CHROM. 23 784

Validity of the model used to relate the energy distribution and the adsorption isotherm

Jeffry Roles and Georges Guiochon*

**Department of Chemistry, University of Tennessee, Knoxville, TN 37996-1501 and Division of Analytical Chemistry, Oak Ridge National Laboratory, Oak Ridge, TN 37831-6120 (USA)*

(First received June 19th, 1991; revised manuscript received September 30th, 1991)

ABSTRACT

The reproducibility and accuracy of the determination of the adsorption energy distribution for a probe compound on a solid surface is discussed. This distribution can be calculated from the adsorption isotherm, itself derived from the chromatographic profiles of high concentration bands, using the elution by characteristic points method. Distributions derived from experimental data acquired under different experimental conditions agree well within the limits of the reproducibility of these data. Band profiles calculated from the adsorption energy distribution are also in excellent agreement with those recorded.

INTRODUCTION

In a separate paper [1], we examined the validity of the model used to derive an equilibrium isotherm from the elution profiles of high-concentration chromatographic bands using the elution by characteristic points (ECP) method. The sources of experimental errors, the accuracy and the precision were discussed. Using comparisons between the experimental elution profiles and the band profiles calculated from the general model of non-linear gas chromatography, we have demonstrated the lack of significant systematic errors.

Adsorption isotherms can be used to understand various aspects of the interactions of the adsorbate molecules with themselves or with the surface of the adsorbent. Currently, we are using the adsorption isotherms of various selected probes to investigate the degree of heterogeneity of a solid surface [2,3]. The adsorption energy distribution of a probe compound on a surface can be calculated by solving a Fredholm integral equation [2]. The complexity of the theoretical problem and of the numerical solution which is needed makes all the more desirable a systematic investigation of the accuracy and reproducibility of the energy distribution derived from the determination of the adsorption isotherm using the ECP method.

We discuss here the problems associated with the derivation of the energy distribution of diethyl ether on the surface of the fine, solid particles used as raw material for the preparation of alumina ceramics [4]. Systematic results obtained with various samples of alumina are reported separately [3].

THEORY

The apparent or observed adsorption isotherm, $q(P)$, is related to the local isotherm, $\Theta(E,P)$, and the energy distribution, $f(E)$, by the linear, first-kind Fredholm equation [5]:

$$q(P) = \int_{\Omega} \Theta(E,P)\, f(E)\, dE \qquad (1)$$

where E is the adsorption energy, Ω the energy range considered, $f(E)$ the fraction of the surface on which the adsorption energy of the probe is between E and $E + dE$ and $\Theta(E,P)$ the local adsorption isotherm of the probe on the fraction of the surface on which the adsorption energy is between E and

0021-9673/92/$05.00

$E + dE$. Eqn. 1 has no analytical solution; in fact, it has an infinite number of oscillatory solutions [6], and restrictions must be imposed to obtain a solution which has a physical sense.

We have shown [2] how a robust numerical solution can be obtained, by replacing in a first stage the experimental isotherm by a smooth function:

$$q(P) = \sum_k \frac{a_k P}{1 + b_k P} \quad (2)$$

and deriving the values of the numerical coefficients a_k and b_k by fitting the experimental data to eqn. 2. Usually, a bi-Langmuir isotherm equation is sufficient. In some instances [2,3], a tri-Langmuir equation becomes necessary. A numerical procedure using the iterative improvement scheme of Adamson and Ling [7] and an algorithm adapted from House and Jaycock [8] has been developed. This procedure usually reveals a multi-modal energy distribution. The minimization of the distance between the experimental isotherm and the isotherm calculated by integration of eqn. 1 is improved in a second stage of optimization in which the experimental isotherm is used and each mode of the energy distribution is represented by a Gaussian distribution if the mode appears symmetrical, by an exponentially modified Gaussian if is moderately unsymmetrical and by a gamma function it is strongly unsymmetrical [2]. A simplex routine [9] is used as explained by Adamson and Ling [7]. Convergence is rapid and the method is robust.

Assuming that the exact adsorption isotherm has been determined, four fundamental assumptions made during the derivation of the model of adsorption energy distribution must be discussed and have to be validated for each new application. These assumptions are: (i) the portion of the adsorption isotherm which has been determined experimentally represents accurately the entire sub-monolayer isotherm; (ii) the Langmuir constant, K, serves to define adequately the thermodynamic reference point; (iii) the intermolecular attractive forces between adsorbate molecules are negligible; and (iv) the adsorbed phase is not mobile (*i.e.*, mass transfer occurs only between the adsorbed phase and the gas phase, not from sites to sites in the adsorbed phase).

The degree of validity of these assumptions may best be assessed by a qualitative description of the phenomena which take place when adsorption occurs at increasingly high concentrations on heterogeneous surface. The adsorbate molecules do not form a simple, regular monolayer on the surface. High-energy sites are covered first, and local multilayer coverage of these sites may even take place before total monolayer coverage of the surface occurs [10]. The model of heterogeneous surface we have developed allows for the fact that adsorption is more likely to occur on high-energy than on low-energy sites and that, accordingly, a higher fraction of these sites are covered at any value of the coverage ratio [2]. However, our model does not allow for the possibility of local multi-layer coverage. On the one hand, our model implies that capillary condensation occurs at the point of monolayer capacity, but on the other it fails to take into account any positive (*i.e.*, convex downward) isotherm curvature in the region just below the monolayer capacity. Hence the model implies a discontinuity in the isotherm at the point of monolayer capacity. Clearly, this implication of the assumptions listed above is not realistic and these assumptions are not valid. It can be shown, however, that the error they induce is not significant.

We discuss here the precision and accuracy of the energy distribution obtained following our procedure. The precision was studied by determining the influence of the fluctuations of the experimental conditions on the distance between the energy distributions calculated [1]. The accuracy was studied by comparing the experimental isotherm with the isotherm calculated as a direct solution of eqn. 1.

EXPERIMENTAL

We have described previously [4] the experimental procedures followed. A quartz open-tubular column (15 m × 0.53 mm I.D.) was filled with a thin slurry of the particles suspended in a solvent where these particles settle very slowly. After closing one of its ends, the column was coiled inside an oven, through a long, heated metal tube. The solvent vaporized into the oven and was vented, while a thin layer of particles coated the inside wall of the column. The column was then fixed to a Perkin-Elmer (Norwalk, CT, USA) Model 8500 gas chromatograph with a flame ionization detector. After thermal conditioning, large-size samples of the probes

used were introduced into the column and the elution band was recorded. The detector signal was digitized and collected as a computer file. It was transformed into a partial pressure *versus* time elution profile using the detector response factor. The equilibrium isotherm was determined from this profile, using the ECP method [11].

The material studied was RCHP alumina, a high-purity grade of α-alumina for ceramics manufactured by Malakoff Industries (Malakoff, TX, USA). The dry-ball-milled powder particles had an average diameter of 0.5–0.8 μm and a specific surface area of 8–10 $m^2\ g^{-1}$, for a geometrical surface area of *ca.* 1.5 $m^2\ g^{-1}$.

RESULTS AND DISCUSSION

First, as the BET equation does take into account the upward curvature of the isotherm at monolayer capacity, it is instructive to compare the BET surface area with the surface area derived from our model. The total monolayer capacity determined for diethyl ether on RCHP alumina [1] at 60°C was $7.89 \cdot 10^{-6}$ mol g^{-1}. Based on the adsorption area model proposed by Jovanovic [12], and on an assumed molecular diameter of 4 Å for diethyl ether, we calculated the surface area occupied by one molecule of adsorbed diethyl ether to be $25 \cdot 10^{-20}$ m^2. Hence the specific surface area of the alumina sample should be 1.2 $m^2\ g^{-1}$. The BET surface area measured for this sample was 8–10 $m^2\ g^{-1}$, *i.e.*, 7–8 times larger. It is difficult to expect a better agreement because of the approximations made, including the estimate of the surface area occupied by a molecule of adsorbed diethyl ether, and because as all surfaces have a fractal dimension their specific surface area decrease with increasing molecular size of the adsorbate.

Second, one should consider the self-consistent agreement between the adsorption isotherm derived from the recorded band profiles, using the ECP method, and the isotherm calculated from the energy distribution, as explained above and in ref. 2. This agreement parallels that observed between the profiles recorded during the experiments and those calculated with the semi-ideal model of chromatography, from the isotherm measured by ECP [1]. It shows that the complex calculation procedure is consistent and does converge toward the solution of eqn. 1. In a previous paper, and in agreement with previous results [13], we have shown that the width of the injection profile had no effect on the simulated chromatogram, as long as it was sufficiently narrow. Nevertheless, calculations were made using the narrowest possible injection. The use of a highly concentrated injection maximizes the influence of the high-surface-coverage portion of the isotherm on the calculated band profile. Hence the magnitude of the error which would be induced by a disagreement between the model and reality is reflected by the magnitude of the error between the calculated and the experimental band profiles.

An example of the degree of agreement obtained between experimental and calculated band profiles is shown in Fig. 1. Application of the retention data difference program [1] to compute the difference parameters for the two bands yields: $t_{RMS} = 1.1\%$ and $\Delta = 8.8 \cdot 10^{-5}$, where t_{RMS} is a measure of the repro-

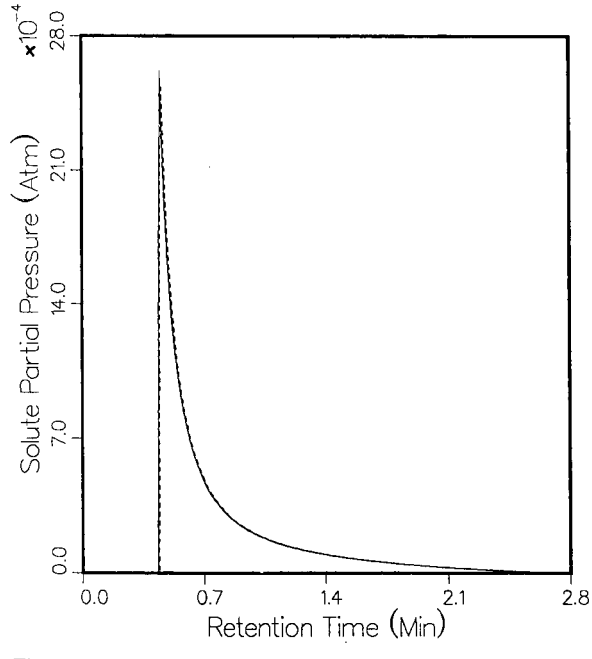

Fig. 1. Comparison between (solid line) the experimental profile obtained for a high-concentration band and (dashed line) the profile calculated from the adsorption isotherm. Diethyl ether on RCHP alumina at 60°C. Experimental conditions: column dimensions, 15 m × 0.53 mm I.D.; mass of alumina, 44 mg; carrier gas, helium; column inlet pressure, 1.34 atm; outlet pressure, 1.0 atm; column efficiency, 8000 theoretical plate; sample size, 0.45 μg.

TABLE I

CHANGE IN THE ELUTION BAND PROFILE AS A FUNCTION OF THE SAMPLE SIZE

Sample size (μg)	Peak area (V min)	Shape difference Parameter, $\Delta \times 10^3$
0.50	1.0	2.4
1.0	2.0	6.0
1.5	3.0	12.0
2.5	5.0	31.2
5.0	10.0	121
10.0	20.0	481
15.0	30.0	1080
25.0	50.0	3010

ducibility of the retention time profile [1] and Δ is the distance between these two profiles [1]. Both of these difference parameters are much smaller than the corresponding confidence limits for the reproducibility of experimental data acquired the same day and with the same column. This result indicates that the extrapolation of the measured isotherm, and the failure of the model to take into account the possible upward curvature of the isotherm at high concentrations, cause an error which is smaller than the experimental uncertainty.

As a test of the model which relates the adsorption isotherm and the adsorption energy distribution, further calculations were performed using data regarding the adsorption of diethyl ether on RCHP alumina obtained at column temperatures of 60 and 72°C. Ideally, the adsorption energy distribution and the thermodynamic parameters derived from this distribution should be identical whether they are derived from the isotherms determined at one or the other temperatures. The data were obtained with the same column on different days, and only small differences, which were not statistically significant, were observed. The results are summarized in Table II. The elution profiles recorded at the two temperatures are compared in Fig. 2, the adsorption isotherms in Fig. 3 and the resulting adsorption energy distributions in Fig. 4.

As expected, the retention time is lower at the higher temperature and the tail much shorter. The higher temperature isotherm has a smaller initial slope, but nearly the same saturation capacity. The differences between the thermodynamic parameters

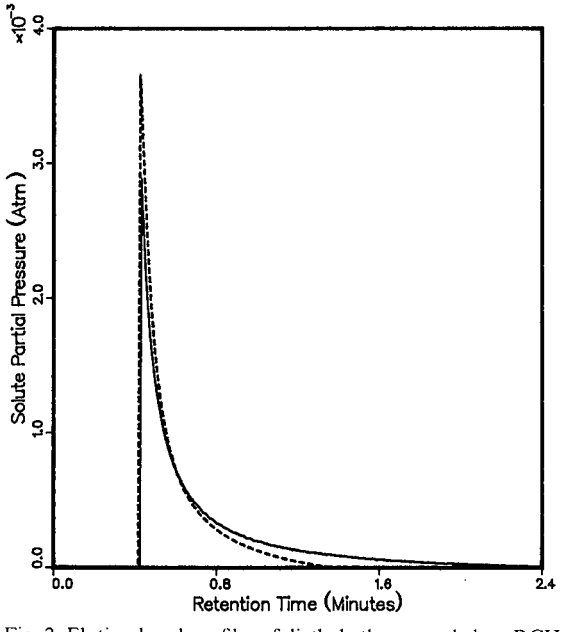

Fig. 2. Elution band profiles of diethyl ether recorded on RCHP alumina at two different temperatures. Experimental conditions as in Fig. 1. Solid line: column temperature, 60°C; peak area, 0.911 V min; t_0, 22.7 s. Dashed line: column temperature, 72°C; peak area, 0.883 V min; t_0, 23.0 s.

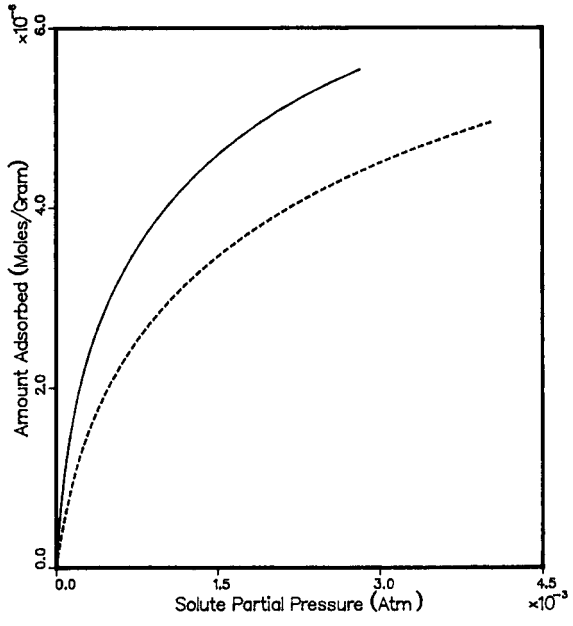

Fig. 3. Adsorption isotherms of diethyl ether on RCHP alumina derived from the band profiles recorded at two different temperatures (profiles in Fig. 2). Solid line, 60°C; dashed line, 72°C.

TABLE II

CHARACTERISTICS OF THE ADSORPTION ENERGY DISTRIBUTION AT TWO DIFFERENT TEMPERATURES

Parameter[a]	60°C	72°C	Relative difference (%)
$q_{s,1}$ (μmol g^{-1})	5.36	5.2	−3.0
$E_{AVG,1}$ (kcal mol^{-1})	11.04	10.9	−1.0
σ_1^2	17	11	−34
$q_{s,2}$ (μmol g^{-1})	2.53	92.64	4.3
$E_{AVG,2}$ (kcal mol^{-1})	12.68	12.54	−1.0
σ_2^2	1.0	1.0	2.3

[a] $q_{s,1}$, $q_{s,2}$: specific saturation capacity of the two modes of the adsorption energy distribution.
$E_{AVG,1}$, $E_{AVG,2}$: average energy of the two modes of the adsorption energy distribution.
σ_1^2, σ_2^2: variance of the two modes of the adsorption energy distribution; in 10^{-6} kcal^2 mol^{-2}.

calculated from the two adsorption energy distributions are smaller than the differences expected for parameters derived from experimental data obtained with the same column on different days (see Table II). The fact that there are two modes in Fig. 4 is not a consequence of the use of a bi-Langmuir isotherm during the first stage of the calculation procedure. This isotherm is used to enable the numerical solution of a less ill-condition problem [2]. Details of the procedure used to determine which analytical isotherm should be used in the first stage of a particular optimization have been presented [3]. The experimental isotherm is used in the second stage of the optimization, so the number of modes is not an artefact of the calculation procedure. Trimodal energy distributions have been measured with some samples [3].

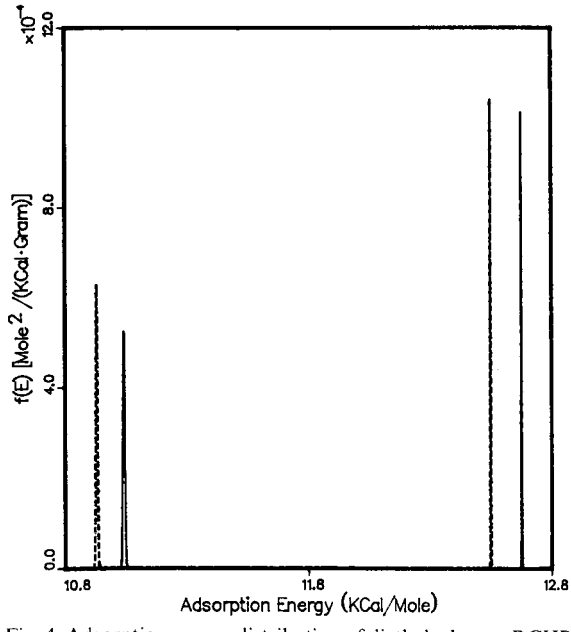

Fig. 4. Adsorption energy distribution of diethyl ether on RCHP alumina determined at two different temperatures (isotherms in Fig. 3). Solid line, 60°C; dashed line, 72°C.

Finally, earlier studies [6,14,15] have compared the results of the calculations of adsorption energy distributions made using the Langmuir model of localized adsorption with the results of more sophisticated models which take into account intermolecular interactions between sorbed molecules and/or the mobility of the adsorbed phase on the solid surface. These studies have shown that the only difference is a constant shift in energy for the entire distribution.

There are several good reasons for using a simple model of adsorption energy distribution, as we did. First, the aim of the whole study is to compare different adsorbates. For this purpose, it does not really matter what thermodynamic reference point is used, as long as the series of results are self-consistent [3]. Second, a more sophisticated model may increase the complexity of the problem, and especially of its numerical analysis, to a point of intractability. Finally, a thermodynamic reference point which is based on physically measurable quantities (*i.e.*, on the physicochemical properties of the solute) is more desirable than a thermodynamic reference point which is based either on some property of the isotherm, which is subject to experimental error, or on factors which have to be calculated through quantum mechanics and which depend on assumptions which are difficult to prove or validate.

CONCLUSIONS

This work shows that highly reproducible data regarding the adsorption energy distribution of probes on solid surfaces can be derived from chromatographic data which are easy to obtain using

conventional, commercial equipment and simple experimental procedures. These data are also self-consistent, as the band profiles can be calculated from adsorption isotherms which, in turn, can be derived from the adsorption energy distribution.

The features of the adsorption energy distribution, such as the mean energy of a mode of this distribution, may, to some extent, be relative and not absolute quantities. This mean adsorption energy may be shifted with respect to the value derived from the conventional thermodynamic reference point. Nevertheless, these data are extremely useful as they permit an easy and detailed characterization of solid surfaces [3].

This work has demonstrated the potential usefulness of the systematic determination of adsorption energy distribution for series of selected probes in order to characterize solid surfaces and investigate material properties which are related to the chemistry of the gas–solid surface.

ACKNOWLEDGEMENTS

This work was supported in part by Grant DE-FG05-88ER13859 of the US Department of Energy, Office of Basic Energy Research, and by the cooperative agreement between the University of Tennessee and the Oak Ridge National Laboratory. We acknowledge support of our computational effort by the University of Tennessee Computing Center.

REFERENCES

1 J. Roles and G. Guiochon, *J. Chromatogr.*, 591 (1992) 245.
2 J. Roles and G. Guiochon, *J. Phys. Chem.*, 95 (1991) 4098.
3 J. Roles and G. Guiochon, *Anal. Chem.*, in press.
4 J. Roles and G. Guiochon, *J. Chromatogr.*, 591 (1992) 233.
5 M. Jaroniec and R. Madey, *Physical Adsorption on Heterogeneous Solids*, Elsevier, Amsterdam, 1988.
6 A. W. Adamson, I. Ling, L. M. Dormant and M. Oren, *J. Colloid Interface Sci.*, 21 (1966) 445.
7 A. W. Adamson and I. Ling, *Adv. Chem. Ser.*, 33 (1961) 51.
8 W. A. House and M. J. Jaycock, *Colloid Polym. Sci.*, 256 (1978) 52.
9 E. Dose, *Anal. Chem.*, 59 (1987) 2420.
10 S. P. Boudreau and W. T. Cooper, *Anal. Chem.*, 59 (1987) 353.
11 E. Cremer and J. F. K. Huber, *Angew. Chem.*, 73 (1961) 461.
12 D. S. Jovanovic, *Kolloid Z. Z. Polym.*, 235 (1969) 1203.
13 G. Guiochon, S. Golshan-Shirazi and A. Jaulmes, *Anal. Chem.*, 60 (1988) 1856.
14 J. B. Sorrell and R. Rowan, *Anal. Chem.*, 42 (1970) 1712.
15 R. Braüer, W. A. House and M. Jaroniec, *Thin Solid Films*, 97 (1982) 369.

Journal of Chromatography, 591 (1992) 273–286
Elsevier Science Publishers B.V., Amsterdam

CHROM. 23 805

Theory of linear non-equilibrium chromatography with beds of a finite length

Jindřich Stárek

J. Heyrovský Institute of Physical Chemistry and Electrochemistry, Czechoslovak Academy of Sciences, Dolejškova 3, 182 23 Prague 8 (Czechoslovakia)

(First received July 8th, 1991; revised manuscript received October 15th, 1991)

ABSTRACT

The phenomenological model of linear non-equilibrium chromatography in an isothermal column (adsorber) with constant cross-section was solved for finite, static and statistically homogeneous and isotropic sorption layers. The model applies the linear adsorption isotherm and accounts for contributions from convection, axial dispersion, external mass transfer and internal diffusion and the adsorption rate. The Laplace inversion of the solutions was obtained and the statistical moments up to the fourth order were calculated on this basis. Analysis of the moments obtained confirmed the negative influence of the dead volume of the column and of boundary effects on the component separation in chromatographic analysis. Comparison of the relationships for the first normal and second central moments, obtained by solving the models of infinite, semi-infinite and finite sorption layers, demonstrated that the choice of the theoretical model for experimental data processing is not critical.

INTRODUCTION

The models and theories of gas chromatography (GC) and of the closely connected dynamics of adsorption have undergone intense development in the last 35 years and have been used to analyse chromatographic processes from various points of view, *e.g.*, the shape of the adsorption isotherm, axial dispersion, external and internal mass transfer and adsorption rate. The solution of these models and theories has been based on a number of different theoretical approaches; most often, the phenomenological model, following from a set of mass balance partial differential equations, has been employed. The largest group of these theories consists of the phenomenological theories of linear non-equilibrium chromatography that, especially after the introduction by Kubín [1] and Kučera [2] of their moment analysis method and its further development [3–10], contributed greatly to progress with the theoretical principles of chromatography and its application in the study of transport processes [11] in adsorption and catalysis [12]. However, the transport of the adsorbate in finite layers and the effects of the boundary conditions at their edges has not yet been systematically analysed. These effects have been stated or assumed with little or no discussion, mainly in applications of chromatographic methods.

Boundary effects have been studied only with respect to the experimental determination of the axial dispersion coefficient for chemical engineering calculations on reactors. Analysis has been carried out for empty tubes with various locations of injection and measurement points inside [13–16] or outside [16] the test section. The effect of various initial and boundary conditions on the dispersion of the tracer in columns with finite and non-adsorbing packing was analysed in refs. 16–18. Brenner [17] studied the dispersion model for non-adsorbing layers of finite length and obtained equations for the dimensionless breakthrough curve and the average adsorbate concentration in the layer. Carleton *et al.* [18] appear to be the only workers to have studied the transport of the adsorbate in a finite sorption layer, obtaining the first normal statistical moment of the eluted peaks for a non-isobaric layer. How-

ever, they did not consider dispersion of the adsorbate outside the layer and limited their analysis to the original Danckwerts boundary conditions [19].

This work is an attempt to solve the problem of linear chromatography with a finite sorption layer under the conditions of axial dispersion and with slow establishment of equilibrium between the mobile and stationary phases, utilizing the above-mentioned moment method of Kubín [1] and Kučera [2]. On the basis of the statistical moments obtained, the influence of the dead volume of the column and effects at the packing boundary on the GC separation are discussed.

THEORETICAL

Definition of the problem

Consider an infinite column (adsorber) with constant cross-section S_L, in a section of which, $z \in \langle 0, z_L \rangle$ is located a static, statistically homogeneous and isotropic sorption layer with finite length L and external porosity α (Fig. 1). Hypothetical indication sensors are located at points A and B, while injection takes place at point O. An "incompressible" carrier medium flows along the z-axis with a volumetric flow-rate F_v. The linear flow-rates at intervals $z \in (-\infty, 0)$, $z \in \langle 0, z_L \rangle$ and $z \in (z_L, +\infty)$ are denoted as ${}^{A}u$, u and ${}^{B}u$, respectively. It follows from the restriction of constant cross-section of the column, for a linear flow-rate that

$$ {}^{A}u = {}^{B}u = \frac{F_v}{S_L} \tag{1a} $$

and

$$ u = \frac{F_v}{\alpha S_L} \tag{1b} $$

and thus also that

$$ {}^{A}D_p({}^{A}u) = {}^{B}D_p({}^{B}u) \tag{2} $$

where the superscripts A and B characterize the quantities related to the entrance and exit sections, respectively.

It is further assumed that:

(1) The column is isothermal and of the fixed-bed type.

(2) The mobile phase flows through the column in the axial direction, is incompressible (and hence has a constant density) and consists of a mixture of inert carrier medium and n adsorbates with low concentrations that do not interact.

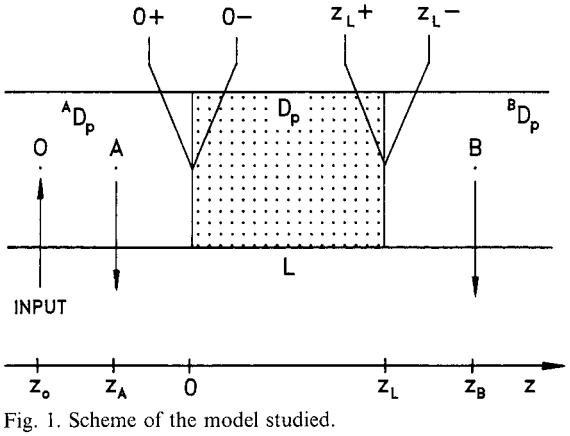

Fig. 1. Scheme of the model studied.

(3) The vector field of the mobile phase velocities is quasi-stationary.

(4) The sorption layer, consisting of porous granules is statistically homogeneous and isotropic and can be considered as a coherent continuum [20–22].

(5) The granules of adsorbent (with uniform size and with statistically homogeneous and isotropic porous structure) have the shape of spheres, "infinite" cylinders or "infinite" plates, and can also be considered as a continuum. Adsorption on the external surface and the contact regions between the grains can be neglected.

(6) The resistance of the phase boundary to mass transfer is zero.

(7) Radial effects can be neglected in the column.

(8) Adsorption is governed by a linear isotherm.

(9) The source of adsorbates is located only in the front of sorption layer.

The transport process of any arbitrary adsorbate in the column can then be represented by the following set of equations:

$$\frac{\partial\, {}^{A}c(z,t)}{\partial t} + {}^{A}u \cdot \frac{\partial\, {}^{A}c}{\partial z} - {}^{A}D_{p} \cdot \frac{\partial^2\, {}^{A}c}{\partial z^2} = {}^{A}Q_{z}(z,t) \qquad (\text{for } z < 0) \tag{3}$$

$$\frac{\partial c(z,t)}{\partial t} + u \cdot \frac{\partial c}{\partial z} - D_{p} \cdot \frac{\partial^2 c}{\partial z^2} = Q_{c}(z,t) \qquad (\text{for } 0 \leqslant z \leqslant z_{L}) \tag{4}$$

$$\frac{\partial\, {}^{B}c(z,t)}{\partial t} + {}^{A}u \cdot \frac{\partial\, {}^{B}c}{\partial z} - {}^{A}D_{p} \cdot \frac{\partial^2\, {}^{B}c}{\partial z^2} = 0 \qquad (\text{for } z > z_{L}) \tag{5}$$

$$\frac{\partial C(z,r,t)}{\partial t} - D_{r}\left(\frac{\nu - 1}{r} \cdot \frac{\partial C}{\partial r} + \frac{\partial^2 C}{\partial r^2}\right) = Q_{n}(z,r,t) \tag{6}$$

$$Q_{c} = -\frac{H\, S_{v}}{\alpha}\left[c - C|_{r=R}\right] \tag{7}$$

$$Q_{n} = -\frac{\partial n(z,r,t)}{\partial t} = -H_{n}(K_{n}C - n) \tag{8}$$

with boundary conditions for:

(a) equality of the flows at the adsorbent grain boundary,

$$Q_{c} = -D_{r} \cdot \frac{P_{v}}{\alpha} \cdot \left.\frac{\partial C}{\partial r}\right|_{r=R} \tag{9}$$

(b) symmetry in the centre of the adsorbent grain,

$$0 = \left.\frac{\partial C}{\partial r}\right|_{r=0} \tag{10}$$

The Danckwerts conditions [19] in the extended form of Wehner and Wilhelm [23] are considered to be valid at the boundary of the sorption layer; these conditions are based on the intuitive assumptions for:

(a) continuity of the concentrations,

$${}^{A}c(0^{-}) = c(0^{+}) \tag{11a}$$

$$c(z_{L}^{-}) = {}^{B}c(z_{L}^{+}) \tag{11b}$$

(b) equality of the flows,

$${}^{A}u(0^{-})\,{}^{A}c(0^{-}) - {}^{A}D_{p} \cdot \frac{\partial\, {}^{A}c(0^{-})}{\partial z} = \alpha\left[u(0^{+})c(0^{+}) - D_{p} \cdot \frac{\partial c(0^{+})}{\partial z}\right] \tag{12a}$$

$$\alpha\left[u(z_{L}^{-})c(z_{L}^{-}) - D_{p} \cdot \frac{\partial c(z_{L}^{-})}{\partial z}\right] = {}^{B}u(z_{L}^{+})\,{}^{B}c(z_{L}^{+}) - {}^{A}D_{p} \cdot \frac{\partial\, {}^{B}c(z_{L}^{+})}{\partial z} \tag{12b}$$

Combination of conditions 11 and 12, assuming that ${}^{A}u(0^-) = \alpha\, u(0^+) = \alpha\, u(z_L^-) = {}^{B}u(z_L^+)$ (see eqn. 1), permits us to write

$${}^{A}D_p \cdot \frac{\partial\, {}^{A}c(0^-)}{\partial z} = \alpha\, D_p \cdot \frac{\partial c(0^+)}{\partial z} \tag{13a}$$

$${}^{A}D_p \cdot \frac{\partial\, {}^{B}c(z_L^+)}{\partial z} = \alpha\, D_p \cdot \frac{\partial c(z_L^-)}{\partial z} \tag{13b}$$

In eqns. 3–13, t is time, z is the axial coordinate in the column, r is the radial coordinate in the adsorbent grain, Q_z is the rate of increase of the adsorbate concentration from the source, K_n is the slope of the Henry adsorption isotherm and v is a shape factor with values of 1, 2 or 3 for prismatic, cylindrical or spherical particles of adsorbent, respectively, with characteristic dimension R.

The local concentration of adsorbate in the fluid phase, c, the linear flow-rate of the fluid phase, u, the axial dispersion coefficient, D_p, the rate of change in concentration c through adsorbate transport into the adsorbent grains, Q_c, the Shilov *et al.* [24] and Mecklenburg [25] external mass transfer coefficient, H, related to unit intergranular free volume, the external porosity, α, the external specific surface of the adsorbent grains $S_v = v(1 - \alpha)/R$, related to unit volume of the layer, and the mean area of the boundary between the pores and the external free volume, $P_v = \beta S_v$ (also related to unit volume of the layer), are all quantities averaged throughout a physically infinitesimal volume element [20–22] of the *sorption layer*.

Similarly, the local adsorbate concentration in the pores, C, the local concentration of the adsorbed compound, n, related to unit pore volume, the effective coefficient of internal diffusion, D_r, the rate of change of concentration C through adsorption, Q_n, the coefficient of the adsorbate transfer from the volume towards the internal surface of the pores, H_n, and the internal porosity of the adsorbent granules, β, are all quantities averaged throughout a physically infinitesimal volume element [20–22] of the *adsorbent grain*.

Various types of chromatography or dynamics of adsorption can be characterized by the following initial and boundary conditions:

Case $t < 0$:

$$\begin{aligned}
&{}^{A}c(z,t) = 0 && \text{for } -\infty < z < 0\\
&c(z,t) = 0 && \text{for } 0 \leqslant z \leqslant z_L\\
&{}^{B}c(z,t) = 0 && \text{for } z_L < z < +\infty\\
&C(z,r,t) = n(z,r,t) = 0 && \text{for } 0 \leqslant r \leqslant R \quad \text{and} \quad 0 \leqslant z \leqslant z_L
\end{aligned}$$

Case $t = 0$:

$$\begin{aligned}
&{}^{A}c(z,t) = {}^{A}c_i(z) && \text{for } -\infty < z < 0\\
&c(z,t) = c_i(z) && \text{for } 0 \leqslant z \leqslant z_L\\
&{}^{B}c(z,t) = {}^{B}c_i(z) && \text{for } z_L < z < +\infty\\
&C(z,r,t) = C_i(z) \\ &n(z,r,t) = n_i(z) && \text{for } 0 \leqslant r \leqslant R \quad \text{and} \quad 0 \leqslant z \leqslant z_L
\end{aligned} \tag{14}$$

Case $t > 0$:

$$\begin{aligned}
&{}^{A}c(z,t) = \text{finite} && \text{for } z \to -\infty\\
&{}^{B}c(z,t) = \text{finite} && \text{for } z \to +\infty
\end{aligned}$$

where ${}^{A}c_i(z)$, $c_i(z)$, ${}^{B}c(z)$ and $C_i(z)$ are the initial distributions of the corresponding concentrations and z_L is the positional coordinate of the end of sorption layer.

Solution of the model

The solution of the set of eqns. 3–8 with initial and boundary conditions 9–11, 13 and 14 can be considerably simplified using the Laplace integral transformation:

$$L\{f(t)\} \equiv \tilde{f}(s) = \int_0^{+\infty} f(t)\, e^{-st}\, dt \tag{15}$$

where s is a complex parameter. Solution [26] of the new set of transformed equations then leads to the following relationships for the transformed adsorbate concentrations in the different parts of the column (adsorber):

(A) The region in front of the sorption layer [$z \in (-\infty,0)$]:

$$^{A}\tilde{c}(z,s) = \frac{1 - \frac{^{A}\lambda_2}{^{A}\lambda_1}}{W_{11}(s)} \cdot e^{^{A}\lambda_1 z} \int_{-\infty}^{0} {}^{A}X(\xi,s)\, e^{-^{A}\lambda_2 \xi}\, d\xi - e^{^{A}\lambda_1 z} \int_{-\infty}^{0} {}^{A}X(\xi,s)(e^{-^{A}\lambda_2 \xi} - e^{-^{A}\lambda_1 \xi})\, d\xi +$$

$$\int_{-\infty}^{z} {}^{A}X(\xi,s)[e^{^{A}\lambda_2(z-\xi)} - e^{^{A}\lambda_1(z-\xi)}]\, d\xi - \frac{\lambda_2 - \lambda_1}{^{A}\lambda_1} \cdot \frac{\alpha\, D_p}{^{A}D_p} \cdot \frac{U(s)}{T(s)} \cdot e^{^{A}\lambda_1 z} \tag{16a}$$

(B) The section of the sorption layer ($z \in \langle 0, z_L \rangle$):

$$\tilde{c}(z,s) = \frac{1 - \frac{^{A}\lambda_2}{^{A}\lambda_1}}{W_{11}(s)} \cdot e^{^{A}\lambda_1 z} \int_{-\infty}^{0} {}^{A}X(\xi,s)\, e^{-^{A}\lambda_2 \xi}\, d\xi + \int_{0}^{z} X(\xi,s)[e^{\lambda_2(z-\xi)} - e^{\lambda_1(z-\xi)}]\, d\xi -$$

$$[W_{11}(s)\, e^{\lambda_2 z} - W_{21}(s)\, e^{\lambda_1 z}] \frac{U(s)}{T(s)} \tag{16b}$$

(C) The region after the sorption layer [$z \in (z_L, +\infty)$]:

$$^{B}\tilde{c}(z,s) = \frac{1 - \frac{^{A}\lambda_2}{^{A}\lambda_1}}{W_{11}(s)} \cdot e^{(\lambda_1 - ^{A}\lambda_2)z_L} \int_{-\infty}^{0} {}^{A}X(\xi,s)\, e^{^{A}\lambda_2(z-\xi)}\, d\xi + e^{^{A}\lambda_2(z-z_L)} \int_{0}^{z_L} X(\xi,s)[e^{\lambda_2(z_L-\xi)} - e^{\lambda_1(z_L-\xi)}]\, d\xi -$$

$$e^{^{A}\lambda_2(z-z_L)} \int_{z_L}^{+\infty} {}^{B}X(\xi,s)\, e^{^{A}\lambda_1(z_L-\xi)}\, d\xi + \int_{z_L}^{z} {}^{B}X(\xi,s)\, e^{^{A}\lambda_2(z-\xi)}\, d\xi + \int_{z}^{+\infty} {}^{B}X(\xi,s)\, e^{^{A}\lambda_1(z-\xi)}\, d\xi -$$

$$\{W_{11}(s)\, e^{[(\lambda_2 - ^{A}\lambda_2)z_L + ^{A}\lambda_2 z]} - W_{21}(s)\, e^{[(\lambda_1 - ^{A}\lambda_2)z_L + ^{A}\lambda_2 z]}\} \frac{U(s)}{T(s)} \tag{16c}$$

It holds for the auxiliary functions that

$$\lambda_{1,2} = \frac{u}{2D_p} \pm \sqrt{\left(\frac{u}{2D_p}\right)^2 + \frac{\sigma_v}{D_p}} \tag{17a}$$

$$^{A}\lambda_{1,2} = \frac{^{A}u}{2\,^{A}D_p} \pm \sqrt{\left(\frac{^{A}u}{2\,^{A}D_p}\right)^2 + \frac{s}{^{A}D_p}} \tag{17b}$$

$$^{(A,B)}X(z,s) = \frac{^{(A,B)}\gamma_v(z,s)}{^{(A)}D_p[^{(A)}\lambda_1 - {}^{(A)}\lambda_2]} \tag{17c}$$

$$W_{ij}(s) = 1 - \frac{\alpha\, D_p}{^{A}D_p} \cdot \frac{\lambda_i}{^{A}\lambda_j} \qquad (\text{for } i = 1,2 \quad \text{and} \quad j = 1,2) \tag{17d}$$

$$T(s) = W_{11} W_{22}\, e^{\lambda_2 z_L} - W_{12} W_{21}\, e^{\lambda_1 z_L} \tag{17e}$$

$$U(s) = \frac{W_{12}}{W_{11}}\left(1 - \frac{{}^{A}\lambda_2}{{}^{A}\lambda_1}\right) e^{\lambda_1 z_L} \int_{-\infty}^{0} {}^{A}X(\xi,s)\, e^{-{}^{A}\lambda_2 \xi}\, d\xi - W_{12} \int_{0}^{z_L} X(\xi,s)\, e^{\lambda_1(z_L-\xi)}\, d\xi +$$

$$W_{22} \int_{0}^{z_L} X(\xi,s)\, e^{\lambda_2(z_L-\xi)}\, d\xi - \left(1 - \frac{{}^{A}\lambda_1}{{}^{A}\lambda_2}\right) \int_{z_L}^{+\infty} {}^{B}X(\xi,s)\, e^{{}^{A}\lambda_1(z_L-\xi)}\, d\xi \quad (17f)$$

where

$$\sigma_v(s) = s + \frac{H\, S_v}{\alpha\, A(s)} \quad (18a)$$

$$A(s) = 1 + \frac{H}{\beta} \cdot \frac{R}{D_r} \cdot \frac{\psi_v(\rho)}{\rho\, \psi'_v(\rho)} \quad (18b)$$

$${}^{A}\gamma_v(z,s) = \tilde{Q}_z(z,s) + {}^{A}c_i\,(z) \quad (18c)$$

$$\gamma_v(z,s) = c_i\,(z) + \frac{H\, S_v\, \gamma(z,s)}{\alpha\, A(s)\, \sigma(s)} \quad (18d)$$

$${}^{B}\gamma_v(z,s) = {}^{B}c_i\,(z) \quad (18e)$$

The functions $\gamma(z,s)$, $\sigma(s)$, $\psi_v(\rho)$ and ρ are defined by the expression

$$\gamma(z,s) = c_i\,(z) + \frac{n_i\,(z)\, H_n}{s + H_n} \quad (19a)$$

$$\sigma(s) = s\left(1 + \frac{K_n\, H_n}{s + H_n}\right) \quad (19b)$$

$$\psi_v(\rho) = \sum_{k=0}^{+\infty} \frac{\rho^{2k}}{2^k\, k!\, v(v+2) \ldots [v + 2(k-1)]} = \begin{cases} ch(\rho) & (v = 1) \\ I_0\,(\rho) & (v = 2) \\ \dfrac{sh(\rho)}{\rho} & (v = 3) \end{cases} \quad (19c)$$

$$\rho = R\sqrt{(\sigma/D_r)} \quad (19d)$$

Solution for basic types of sampling

Inversion 16c describes an arbitrary type of dynamic adsorption or desorption from the point of view both the initial distributions of concentrations in the layer and the course of the input adsorbate concentration. Consequently, both common special cases, elution and frontal, can be obtained.

First consider general sampling of the adsorbate at point $z_0 \in (-\infty,0)$ prior to the sorption layer determined by the function $c_0\,(t)$. For the usual assumption of zero initial ($t = 0$) distributions of the adsorbate concentrations ${}^{A}c_i\,(z) = c_i\,(z) = {}^{B}c_i\,(z) = C_i\,(z) = n_i\,(z) = 0$, it follows from eqns. 18d and 18e that

$$\gamma_v(z,s) = {}^{B}\gamma_v(z,s) = 0 \quad (20)$$

The adsorbate sampling can be described by the source function:

$$Q_z(z,t) = u\, c_0\,(t)\, \delta(z,z_0) \quad (21)$$

and it therefore holds according to eqn. 18c that

$${}^{A}\gamma_v(z,s) = \tilde{Q}_z(z,s) = u\, \tilde{c}_0\,(s)\, \delta(z,z_0) \quad (22)$$

Substitution and rearrangement of inversion 16c yields the following relationship for the transformed elution curve:

$$^{B}\tilde{c}(z,s) = \tilde{c}_0\,(s) \cdot \frac{u}{\alpha\, D_p} \cdot \frac{\lambda\, e^{-(z-z_L-z_0)\tau}}{\left(\lambda + \frac{^{A}D_p}{\alpha\, D_p} \cdot \tau\right)^2 e^{\lambda z_L} - \left(\lambda - \frac{^{A}D_p}{\alpha\, D_p} \cdot \tau\right)^2 e^{-\lambda z_L}} \tag{23}$$

where it holds for the auxiliary functions λ and τ that

$$\tau(s) = \sqrt{\left(\frac{^{A}u}{2^{A}D_p}\right)^2 + \frac{s}{^{A}D_p}} \tag{24a}$$

$$\lambda[\sigma_v(s)] = \sqrt{\left(\frac{^{A}u}{2\alpha D_p}\right)^2 + \frac{\sigma_v(s)}{D_p}} \tag{24b}$$

It follows from the definition of the Dirac δ-function that [27]

$$\int_a^b f(\tau)\, \delta(\tau,\tau_0)\, d\tau = \begin{cases} 0 & \text{for } \tau_0 \notin (a,b) \\ f(\tau_0) & \text{for } \tau_0 \in (a,b) \end{cases} \tag{25}$$

Laplace inversion of the solution for general sampling of the adsorbate readily yields the inversion for both basic types of sampling.

The elution case, the most common approach to chromatographic analysis, usually carried out by injection with a syringe, can be successfully modelled by the impulse Dirac δ-function. Then

$$c_0\,(t) = \frac{M_A}{u\, S_L} \cdot \delta(t,t_0) \tag{26}$$

where M_A is the total injected amount of the adsorbate. Supposing that the start of time measurement is given by the moment of the sampling ($t_0 = 0$), then $L\{\delta(t,0)\} = 1$, and the term $\tilde{c}_0\,(s)$ in eqn. 23 describing the inversion of the elution curve in this case is given by

$$\tilde{c}_0\,(s) = \frac{M_A}{u\, S_L} \tag{27}$$

The frontal case, employed primarily in separation processes, utilizes a second basic type of sampling, where a constant concentration, $c_0\,(t) = c_0 =$ constant, is maintained at the injection point during the separation. The initial adsorbate concentration in the adsorber is zero. This type can be described by the step function. Subsequently, eqn. 23 with the term

$$\tilde{c}_0\,(s) = c_0/s \tag{28}$$

describes the inversion of the breakthrough curve.

Comparison of the Laplace images of the solutions for the elution and frontal cases of adsorbate sampling with $uc_0 = M_A/S_L$ yields the following relationship between the eluted peaks and breakthrough curves:

$$[^{B}c(z,t)]_{elution} = \left[\frac{\partial\, ^{B}c(z,t)}{\partial\, t}\right]_{frontal} \tag{29}$$

It holds in general that

$$L\left\{\frac{\partial\, ^{B}c(z,t)}{\partial\, t}\right\} = s\, ^{B}\tilde{c}(z,s) - {}^{B}c_i\,(z) = s\, ^{B}\tilde{c}(z,s) \tag{30}$$

as it is assumed that $^{B}c_i\,(z) = 0$.

Statistical moments of the elution curves

An attempt to carry out the inverse transformation of the obtained Laplace images was not successful. Consequently, the statistical moments of the elution curves will be employed to characterize adsorbate transport in a column with a finite sorption layer. The normal statistical moments μ'_k and the central moments μ_k can be derived [1,2] from the relationships

$$\mu'_k = (-1)^k \lim_{s \to 0+} \frac{\frac{\mathrm{d}^k \tilde{f}(s)}{\mathrm{d}s^k}}{\tilde{f}(s)} \tag{31a}$$

and

$$\mu_k = \sum_{i=0}^{k} \binom{k}{i} (-\mu'_k)^i \mu'_{k-i} \tag{31b}$$

where $\tilde{f}(s)$ is the known Laplace inversion.

As the breakthrough curve resulting in the frontal case of adsorbate injection, in contrast to the eluted peak, does not have the character of a frequency function [it does not fulfil the condition $\lim_{t \to +\infty} {}^{\mathrm{B}}c(z,t) = 0$], there are no statistical moments of this curve. However, there are the moments of the derivative $\partial {}^{\mathrm{B}}c(z,t)/\partial t$ that, with respect to eqns. 29 and 31, will correspond with the moments of the eluted peak, independently of the amount of adsorbate injected.

After tedious calculations, the following equations for the normal and central statistical moments of the elution curves are obtained from the respective inversions (eqns. 23 and 27, or 23, 28 and 30) with respect to eqn. 31:

$$\mu'_0(z) = 1 \tag{32a}$$

$$\mu'_1(z) = \frac{z_{\mathrm{L}}}{u}\left[(\chi_v)_1 + \left(x_{\mathrm{E}} + 2 \cdot \frac{x_{\mathrm{D}}}{Pe}\right)\right] \tag{32b}$$

$$\mu_0(z) = 1 \tag{33a}$$

$$\mu_1(z) = 0 \tag{33b}$$

$$\mu_2(z) = 2 \cdot \frac{z_{\mathrm{L}}^2}{u^2}\left\{\frac{1}{Pe^2}[Pe - (1 - \mathrm{e}^{-Pe})](\chi_v)_1^2 + 2 \cdot \frac{x_{\mathrm{D}}}{Pe^2}(1 - \mathrm{e}^{-Pe})(\chi_v)_1 + \varepsilon(x_v)_2 + \frac{x_{\mathrm{D}}}{Pe}\left[x_{\mathrm{E}} + \frac{x_{\mathrm{D}}}{Pe}(3 + \mathrm{e}^{-Pe})\right]\right\} \tag{33c}$$

$$\mu_3(z) = 2 \cdot \frac{z_{\mathrm{L}}^3}{u^3}\left\{\frac{6}{Pe^3}[Pe(1 + \mathrm{e}^{-Pe}) - 2(1 - \mathrm{e}^{-Pe})](\chi_v)_1^3 - 12 \cdot \frac{x_{\mathrm{D}}}{Pe^3}[Pe\,\mathrm{e}^{-Pe} - (1 - \mathrm{e}^{-Pe})](\chi_v)_1^2 + 6 \cdot \frac{x_{\mathrm{D}}^2}{Pe^3}[Pe\,\mathrm{e}^{-Pe} + 2(1 - \mathrm{e}^{-Pe})](\chi_v)_1 + 6 \cdot \frac{1}{Pe^2}\varepsilon[Pe - (1 - \mathrm{e}^{-Pe})](\chi_v)_1(x_v)_2 + 6 \cdot \frac{x_{\mathrm{D}}}{Pe^2}\varepsilon(1 - \mathrm{e}^{-Pe})(x_v)_2 + 3\varepsilon(x_v)_3 + 2 \cdot \frac{x_{\mathrm{D}}^2}{Pe^2}\left[3x_{\mathrm{E}} + 2 \cdot \frac{x_{\mathrm{D}}}{Pe}(5 + 3\mathrm{e}^{-Pe})\right]\right\} \tag{33d}$$

$$\mu_4(z) = 4 \cdot \frac{z_{\mathrm{L}}^4}{u^4}\left\{\frac{3}{Pe^4}[Pe^2(1 + 4\mathrm{e}^{-Pe}) + 2Pe(4 + 11\mathrm{e}^{-Pe}) - 2(1 - \mathrm{e}^{-Pe})(14 + \mathrm{e}^{-Pe})](\chi_v)_1^4 - 12 \cdot \frac{x_{\mathrm{D}}}{Pe^4}[2Pe^2\,\mathrm{e}^{-Pe} - Pe(1 - 7\mathrm{e}^{-Pe}) - 2(1 - \mathrm{e}^{-Pe})(2 + \mathrm{e}^{-Pe})](\chi_v)_1^3 + 6 \cdot \frac{x_{\mathrm{D}}^2}{Pe^4}[2Pe^2\,\mathrm{e}^{-Pe} +$$

$$Pe(3 - 5e^{-Pe}) + 2(4 - 7e^{-Pe} + 3e^{-2Pe})](\chi_v)_1^2 + 24 \cdot \frac{x_D^3}{Pe^4}[2Pe\, e^{-Pe} + (1 - e^{-Pe})(4 + e^{-Pe})](\chi_v)_1 +$$

$$6 \cdot \frac{x_D}{Pe^3} \cdot x_E[Pe - (1 - e^{-Pe})](\chi_v)_1^2 + 12 \cdot \frac{x_D^2}{Pe^3} \cdot x_E(1 - e^{-Pe})(\chi_v)_1 + 6 \cdot \frac{1}{Pe^3}\varepsilon[Pe^2 + Pe(5 + 7e^{-Pe}) -$$

$$12(1 - e^{-Pe})](\chi_v)_1^2(x_v)_2 + 12 \cdot \frac{x_D}{Pe^3}\varepsilon[Pe(1 - 5e^{-Pe}) + 4(1 - e^{-Pe})](\chi_v)_1(x_v)_2 +$$

$$6 \cdot \frac{x_D^2}{Pe^3}\varepsilon[3Pe(1 + e^{-Pe}) + 4(1 - e^{-Pe})](x_v)_2 + 3 \cdot \frac{1}{Pe^2}\varepsilon^2[Pe^2 + 2Pe - 2(1 - e^{-Pe})](x_v)_2^2 +$$

$$6 \cdot \frac{x_D}{Pe} \cdot x_E\varepsilon(x_v)_2 + 12 \cdot \frac{1}{Pe^2}\varepsilon[Pe - (1 - e^{-Pe})](\chi_v)_1(x_v)_3 + 12 \cdot \frac{x_D}{Pe^2}\varepsilon(1 - e^{-Pe})(x_v)_3 +$$

$$6\varepsilon(x_v)_4 + 3 \cdot \frac{x_D^2}{Pe^2}\left[x_E^2 + 2 \cdot \frac{x_D}{Pe} \cdot x_E(8 + e^{-Pe}) + 2 \cdot \frac{x_D^2}{Pe^2}(22 + 17e^{-Pe} + e^{-2Pe})\right]\Bigg\} \quad (33e)$$

where the dimensionless complexes Pe, x_E, x_D and $(x_v)_k$ are defined by the relationships

$$Pe = z_L \cdot \frac{u}{D_p} \quad (34)$$

$$x_E = \frac{z - z_L - z_0}{\alpha z_L} \quad (35a)$$

$$x_D = \frac{{}^A D_p}{\alpha^2 D_p} \quad (35b)$$

$$(x_v)_k = \left(\frac{u}{z_L}\right)^{k-1}(\chi_v)_k \quad (\text{for } k = 2,3,4) \quad (36)$$

For the parameters $(\chi_v)_k$, characterizing transport of the adsorbate into the adsorbent grain, we have

$$(\chi_v)_1 = 1 + \varepsilon(1 + K_n) \quad (37a)$$

$$(\chi_v)_2 = \frac{R^2}{D_r} \cdot \frac{(1 + K_n)^2}{\nu(\nu + 2)} + \frac{\beta R(1 + K_n)^2}{\nu H} + \frac{K_n}{H_n} \quad (37b)$$

$$(\chi_v)_3 = \left(\frac{R^2}{D_r}\right)^2 \cdot \frac{2(1 + K_n)^3}{\nu^2(\nu + 2)(\nu + 4)} + \frac{R^2}{D_r} \cdot \frac{2(1 + K_n)}{\nu(\nu + 2)}\left[\frac{\beta R(1 + K_n)^2}{\nu H} + \frac{K_n}{H_n}\right] + \frac{\beta^2 R^2(1 + K_n)^3}{\nu^2 H^2} +$$

$$\frac{2\beta R(1 + K_n)K_n}{\nu H_n H} + \frac{K_n}{H_n^2} \quad (37c)$$

$$(\chi_v)_4 = \left(\frac{R^2}{D_r}\right)^3 \cdot \frac{(5\nu + 12)(1 + K_n)^4}{\nu^3(\nu + 2)^2(\nu + 4)(\nu + 6)} + \left(\frac{R^2}{D_r}\right)^2 \cdot \frac{(1 + K_n)^2}{\nu^2(\nu + 2)^2(\nu + 4)} \cdot \left[\frac{\beta R(5\nu + 12)(1 + K_n)^2}{\nu H} + \right.$$

$$\left. \frac{(6\nu + 12)K_n}{H_n}\right] + \frac{R^2}{D_r} \cdot \frac{1}{\nu(\nu + 2)}\left[\frac{3\beta^2 R^2(1 + K_n)^4}{\nu^2 H^2} + \frac{6\beta R(1 + K_n)^2 K_n}{\nu H_n H} + \frac{(2 + 3K_n)K_n}{H_n^2}\right] +$$

$$\frac{\beta^3 R^3(1 + K_n)^4}{\nu^3 H^3} + \frac{3\beta^2 R^2(1 + K_n)^2 K_n}{\nu^2 H^2 H_n} + \frac{\beta R(2 + 3K_n)K_n}{\nu H_n^2 H} + \frac{K_n}{H_n^3} \quad (37d)$$

where ε is the porosity function defined by

$$\varepsilon = \beta(1 - \alpha)/\alpha \quad (38)$$

DISCUSSION

The terms in the relationships for the moments containing parameters x_E or x_D describe the contribution of the dead section of the column or effects on the boundaries of the sorption layer on adsorbate transport. The moments are independent of the absolute position of the injection and detection points, and are determined only by the total of their distances from the boundaries of the layer.

Let us analyse the influence of the dead volume and of the boundary effects on the separation of two components a and b in a chromatographic analysis. Its efficiency is usually characterized by the resolution:

$$R_s = 2d/(W_a + W_b) \tag{39}$$

where d is the distance between the peak maxima and W_a and W_b are the individual base peak widths. The peaks are "perfectly" separated for $R_s \geqslant 1$. It holds for a Gaussian shape of the peaks that $d = (\mu_1')_b - (\mu_1')_a$ and $W_{a,b} = 4(\mu_2)^{\frac{1}{2}}_{a,b}$. The new resolution, defined by the following expression, will be utilized as a test criterion:

$$R_s^* = \frac{(\mu_1')_b - (\mu_1')_a}{2[(\mu_2)^{\frac{1}{2}}_a + (\mu_2)^{\frac{1}{2}}_b]} \tag{40}$$

Let us assume that the axial dispersion coefficients of these components are not well distinguished. After substitution of eqns. 32a and 33c and their limiting cases for $x_E \to 0$ (neglecting the dead volume) and $x_D \to 0$ (neglecting the boundary effects) in eqn. 40, we obtain the following relationships:

$$R_s^* < (R_s^*)_{x_E \to 0} \text{ and } R_s^* < (R_s^*)_{x_D \to 0} \tag{41a,b}$$

Consequently, the dead volume and the effects at the boundaries of the sorption layer decrease the separation efficiency, in agreement with experimental results.

For the semi-quantitative determination of these dependences, numerical analysis was applied. The results of the computer simulation are given in Figs. 2 and 3. As the starting point of computation, the retention times of methane (3 min) and carbon dioxide (5 min), found in GC tables [28] for isothermal GC separation on a 35 cm × 0.4 cm I.D. column of activated charcoal (75–100 mesh; 40°C; nitrogen carrier gas at 20 ml/min; thermal conductivity detector), and results of the dynamic adsorption of methane on activated carbon [26] (250–315 μm; 40°C; nitrogen carrier gas; Henry constant of methane $K_n = 28$) was used. In a first approximation, identity of diffusivities was assumed for both separated components; $D_r = 8 \cdot 10^{-2}$ mm²/s, $H = 1.8$ mm/s and $H_n = 10^3$ s^{-1}. The values of the axial

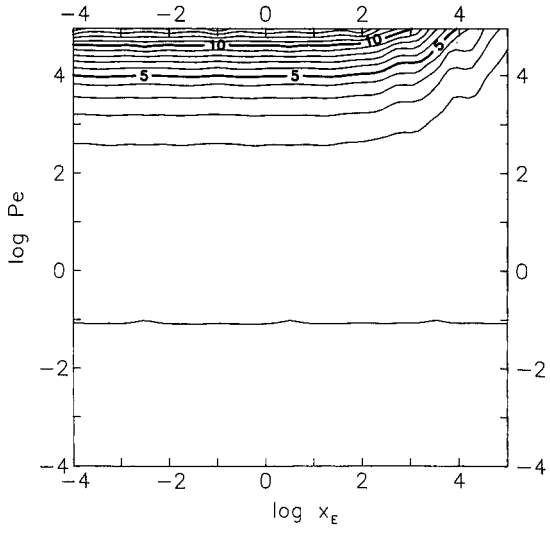

Fig. 2. Contour map of the computer-simulated dependence of resolution, R_s^*, on x_E and Pe (for methane) for the GC separation of methane and carbon dioxide.

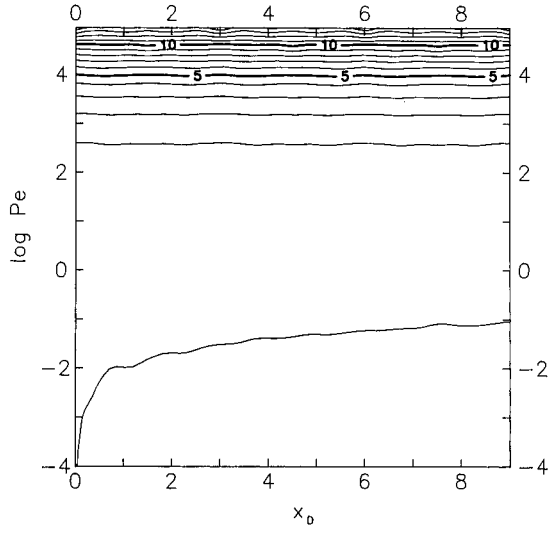

Fig. 3. Contour map of the computer-simulated dependence of resolution, R_s^*, on x_D and Pe (for methane) at a constant level $x_E = 0$ for the GC separation of methane and carbon dioxide.

dispersion coefficients of carbon dioxide ($^{A}D_p$ = 0.216 cm^2/s; D_p = 0.264 cm^2/s) and methane ($^{A}D_p$ = 0.26 cm^2/s; D_p = 0.297 cm^2/s) were calculated from Aris's [29] theoretical expression for these coefficients in a straight empty tube with laminar flow and a parabolic distribution of fluid phase velocities in its cross-section:

$$D_p = D_g + \frac{r_t^2 u_m^2}{48 D_g} \tag{42}$$

where D_g is the coefficient of molecular diffusion, r_t is the radius of tube and u_m is the mean linear flow velocity. The tabulated values [30] 0.184 and 0.235 cm^2/s (after conversion to 40°C) were used for the coefficients of molecular diffusion, D_g, of carbon dioxide and methane, respectively. On the basis of these results and estimates, the other parameters (Henry constant of carbon dioxide K_n = 48.5, u = 66 mm/s, α = 0.4, β = 0.7, ε = 1.0, R = 9 · 10^{-2} mm, R^2/D_r = 10^{-1} s, R/H = 5 · 10^{-2} s, D_p/u^2 = 6.006 · 10^{-3} and 6.757 · 10^{-3} s, x_D = 5.114 and 5.471 and Pe = 879 and 781 for carbon dioxide and methane, respectively) were calculated.

Fig. 2 shows the contour map of the dependence of resolution, R_s^*, on the dimensionless parameters x_E and Pe (for methane) for the above-mentioned model example. From the plot it is evident that the peaks are perfectly separated ($R_s^* \geqslant 1$) for log x_E < 1.3 and log Pe > 2.6, *i.e.*, *ca.* x_E < 20 and Pe > 400. In other words, the length of the dead part of column can be up to eight times greater (2.8 m) than the length of sorption layer without a more substantial change in the separation. For the topical value of Pe = 781 in the sorption layer, $R_s^* \geqslant 1$ even for log x_E < 3.2. Generally, the influence of dead volume, characterized by the parameter x_E, decreases with increasing Pe. In agreement with eqn. 41a, for a given value of the Pe, the resolution increases with decreasing dead volume (x_E).

Fig. 3 shows the contour map of the dependence of resolution, R_s^*, on the dimensionless parameters x_D and Pe (for methane) for a constant level x_E = 0. The dependence has the same shape as this plot, with minimal difference, also for non-zero values of x_E (verified up to x_E = 200). The resolution $R_s^* \geqslant 1$ for log Pe > 2.6 (*ca.* Pe > 400) in the whole analysed interval $x_D \in \langle 0,9 \rangle$. The increase in resolution with decreasing boundary effects (see eqn. 42b) at a given Pe is very small, and this is evident only from numerical values.

Further, we restrict ourselves only to the first two non-trivial statistical moments having the fundamental meaning in chromatography: the first normal moment μ_1', characterizing the time coordinate of the centre (of gravity) of the eluted peak (retention time), and the second central moment μ_2, connected with its width. Table I summarizes expressions for moments μ_1' and μ_2, calculated on the basis of models of infinite [2,26,31,32], semi-infinite [26,33] and finite sorption layers.

It is evident from comparison of the expressions in Table I that the choice of a theoretical model can essentially affect the treatment and interpretation of chromatographic and dynamic sorption measure-

TABLE I

STATISTICAL MOMENTS FOR MODELS OF AN (A) INFINITE, (B) SEMI-INFINITE AND (C) FINITE SORPTION LAYER

Model	μ_1'	μ_2
A	$\frac{z_L}{u} \cdot \frac{1}{Pe}(2 + Pe)(\chi_v)_1$	$2 \cdot \frac{z_L^2}{u^2} \cdot \frac{1}{Pe}\left[\frac{1}{Pe}(4 + Pe)(\chi_v)_1^2 + \varepsilon(2 + Pe)(x_v)_2\right]$
B	$\frac{z_L}{u}(\chi_v)_1$	$2 \cdot \frac{z_L^2}{u^2}\left[\frac{1}{Pe}(\chi_v)_1^2 + \varepsilon(x_v)_2\right]$
C	$\frac{z_L}{u}\left[(\chi_v)_1 + \left(x_E + 2 \cdot \frac{x_D}{Pe}\right)\right]$	$2 \cdot \frac{z_L^2}{u^2}\left\{\frac{1}{Pe^2}[Pe - (1 - e^{-Pe})](\chi_v)_1^2 + 2 \cdot \frac{x_D}{Pe^2}(1 - e^{-Pe})(\chi_v)_1 + \varepsilon(x_v)_2 + \frac{x_D}{Pe}\left[x_E + \frac{x_D}{Pe}(3 + e^{-Pe})\right]\right\}$

TABLE II

LIMITING EXPRESSIONS OF THE STATISTICAL MOMENTS FOR MODELS OF AN (A) INFINITE, (B) SEMI-INFINITE AND (C) FINITE SORPTION LAYER

Pe	Model	μ_1'	μ_2
$<10^{-2}$	A	$\frac{z_L}{u} \cdot \frac{2}{Pe} (\chi_v)_1$	$4 \cdot \frac{z_L^2}{u^2} \cdot \frac{1}{Pe} \left[\frac{2}{Pe} (\chi_v)_1^2 + \varepsilon(x_v)_2 \right]$
	B	$\frac{z_L}{u} (\chi_v)_1$	$2 \cdot \frac{z_L^2}{u^2} \left[\frac{1}{Pe} (\chi_v)_1^2 + \varepsilon(x_v)_2 \right]$
	C	$\frac{z_L}{u} \left[(\chi_v)_1 + \left(x_E + 2 \cdot \frac{x_D}{Pe} \right) \right]$	$2 \cdot \frac{z_L^2}{u^2} \left[\frac{1}{Pe} (\chi_v)_1^2 + \varepsilon(x_v)_2 + \frac{x_D}{Pe} \left(x_E + 4 \cdot \frac{x_D}{Pe} \right) \right]$
>400	A	$\frac{z_L}{u} (\chi_v)_1$	$2 \cdot \frac{z_L^2}{u^2} \left[\frac{1}{Pe} (\chi_v)_1^2 + \varepsilon(x_v)_2 \right]$
	B	$\frac{z_L}{u} (\chi_v)_1$	$2 \cdot \frac{z_L^2}{u^2} \left[\frac{1}{Pe} (\chi_v)_1^2 + \varepsilon(x_v)_2 \right]$
	C	$\frac{z_L}{u} \left[(\chi_v)_1 + \left(x_E + 2 \cdot \frac{x_D}{Pe} \right) \right]$	$2 \cdot \frac{z_L^2}{u^2} \left[\frac{1}{Pe} (\chi_v)_1^2 + 2 \cdot \frac{x_D}{Pe^2} (\chi_v)_1 + \varepsilon(x_v)_2 + \frac{x_D}{Pe} \left(x_E + 3 \cdot \frac{x_D}{Pe} \right) \right]$

ments. In the methodological basis used, the model of a finite layer is probably the most exact from a physical point of view.

Let us consider the limiting cases for very small or very large values of Pe, defined by eqn. 34. For $Pe \to 0$, adsorbate is transported through the column almost exclusively by diffusion. In the second limiting case, $Pe \to +\infty$, on the other hand, transport is controlled by convection. The simpler limiting expressions given in Table II, valid with an error of less than 1%, can be obtained for the moments in these limiting cases. Namely, the term $\exp(-Pe) \approx 1$ (for $Pe < 10^{-2}$) or $\exp(-Pe) \approx 0$ (for $Pe > 5$), and also terms $(n + Pe) \approx Pe$ ($n = 1, \ldots, 4$, see Table I) for $Pe > 100n$, are valid with the same error. The resultant condition $Pe > 400$ is usually achieved for normal chromatographic conditions.

It follows from Table II for very small values of Pe that there is a fundamental difference among the statistical moments for various models of the sorption layer. In the more frequent case of large Pe values, the corresponding moments reduce to the same expressions, and this process is faster for the model of a finite sorption layer (neglecting the dead volume of the column, *i.e.*, $x_E \to 0$) as the influence of boundary effects (and axial dispersion outside the sorption layer) decreases and as the value of Pe increases. These qualitative conclusions have following practical consequences: (i) it is preferable to work in the region of small Peclet numbers for experimental verification of various theoretical models; (ii) otherwise, the largest possible Pe values should be used, which can be attained by a suitable choice of experimental conditions. This limits the influence of boundary effects, decreases the dependence on the choice of the theoretical model and simultaneously simplifies the numerical treatment of the experimental data.

CONCLUSIONS

The solution of the phenomenological model of linear non-equilibrium chromatography for beds of a finite length in Laplace domain has been obtained. The statistical moments of the elution peak up to the fourth order have been calculated. By the theoretical and numerical analysis of moments, the negative influence of the dead volume and boundary effects on GC separations has been confirmed. However, these dependences are not excessively important for the usual experimental conditions. The selection of the expressions for the first normal and second central moment, calculated on the basis of the

models of an infinite, semi-infinite or finite sorption layer, is not decisive for data analysis of current chromatographic measurements.

SYMBOLS

$A(s)$	function defined by eqn. 18b
c	local concentration of adsorbate in the fluid phase
c_0	input adsorbate concentration
C	local adsorbate concentration in the pores of adsorbent particles
d	distance between two peak maxima
D_g	coefficient of molecular diffusion
D_p	axial dispersion coefficient
D_r	effective coefficient of internal diffusion
F_v	volumetric flow-rate of the fluid phase
H	external mass transfer coefficient
H_n	coefficient of the adsorbate transfer from the volume towards the internal surface of the pores
K_n	slope of the Henry adsorption isotherm
L	length of the sorption layer
$L\{f(t)\}$	operator of the Laplace transform
M_A	total injected amount of the adsorbate
n	local concentration of the adsorbed compound
Pe	Peclet number defined by eqn. 34 (dimensionless)
P_v	mean area of the boundary between the pores and the external free volume, βS_v
Q_c	rate of change in adsorbate concentration through transport into the adsorbent grains
Q_n	rate of change of concentration C through adsorption
Q_z	rate of increase of the adsorbate concentration from the source
r	radial coordinate in the adsorbent grain
r_t	radius of the straight empty tube
R	characteristic dimension of the adsorbent particle
R_s	resolution between two consecutive peaks defined by eqn. 39
R_s^*	resolution defined by means of statistical moments; eqn. 40
s	complex parameter of the Laplace transform
S_L	total cross-sectional area of the column
S_v	external specific surface of the adsorbent grains, $v(1 - \alpha)/R$
t	time
$T(s)$	function defined by eqn. 17e
u	linear flow-rate of the fluid phase
u_m	mean linear flow velocity
$U(s)$	function defined by eqn. 17f
W	base peak width
$W_{ij}(s)$	functions defined by eqn. 17d
x_D	dimensionless parameter defined by eqn. 35b
x_E	dimensionless parameter defined by eqn. 35a
$(x_v)_k$	dimensionless complexes defined by eqn. 36
$X(z,s)$	functions defined by eqn. 17c
z	axial coordinate in the column
z_0	positional coordinate of the adsorbate sampling
z_L	positional coordinate of the end of sorption layer

Greek symbols

α	external porosity of the sorption layer
β	internal porosity of the adsorbent granules
$\gamma(z,s)$	function defined by eqn. 19a
$\gamma_v(z,s)$	functions defined by eqn. 18
δ	Dirac delta function
ε	porosity function, $\beta(1 - \alpha)/\alpha$
$\lambda[\sigma_v(s)]$	function defined by eqn. 24b
$\lambda_{1,2}$	roots of the characteristic equation, defined by eqn. 17a
${}^A\lambda_{1,2}$	roots of the characteristic equation, defined by eqn. 17b
μ_k	kth normal statistical moment
μ'_k	kth central statistical moment
ν	shape factor of the adsorbent grain
ρ	function defined by eqn. 19d
$\sigma(s)$	function defined by eqn. 19b
$\sigma_v(s)$	function defined by eqn. 18a
$\tau(s)$	function defined by eqn. 24a
$\psi_v(\rho)$	function defined by eqn. 19c
$(\chi_v)_k$	parameters defined by eqn. 37

Subscripts

i	refers to the initial distribution of the adsorbate concentration
k	refers to the moment order

ν refers to the shape factor of the adsorbent grain

Superscripts

A pertaining to entrance section of the column

B pertaining to exit section of the column

$\sim$ refers to the Laplace transform

REFERENCES

1 M. Kubín, *Collect. Czech. Chem. Commun.*, 30 (1965) 1104, 2900.
2 E. Kučera, *J. Chromatogr.*, 19 (1965) 237.
3 O. Grubner, *Adv. Chromatogr.*, 6 (1968) 173.
4 O. Grubner and D. W. Underhill, *Sep. Sci.*, 5 (1970) 555.
5 O. Grubner, *Anal. Chem.*, 43 (1971) 1934.
6 P. Schneider and J. M. Smith, *AIChE J.*, 14 (1968) 762, 886.
7 G. Padberg and J. M. Smith, *J. Catal.*, 12 (1968) 172.
8 J. C. Adrian and J. M. Smith, *J. Catal.*, 18 (1970) 57.
9 N. Hashimota and J. M. Smith, *Ind. Eng. Chem., Fundam.*, 12 (1973) 353.
10 M. A. Galan, M. Suzuki and J. M. Smith, *Ind. Eng. Chem., Fundam.*, 14 (1975) 273.
11 V. R. Choudhary, *J. Chromatogr.*, 98 (1974) 491.
12 V. R. Choudhary and L. K. Doriaswamy, *Ind. Eng. Chem., Prod. Res. Dev.*, 10 (1971) 218.
13 E. T. van der Laan, *Chem. Eng. Sci.*, 7 (1958) 187.
14 R. Aris, *Chem. Eng. Sci.*, 9 (1959) 266.
15 K. B. Bischoff, *Chem. Eng. Sci.*, 12 (1960) 69.
16 K. B. Bischoff and O. Levenspiel, *Chem. Eng. Sci.*, 17 (1962) 245, 257.
17 H. Brenner, *Chem. Eng. Sci.*, 17 (1962) 229.
18 F. B. Carleton, L. S. Kerstenbaum and W. A. Wakeham, *Chem. Eng. Sci.*, 33 (1978) 1239.
19 P. V. Danckwerts, *Chem. Eng. Sci.*, 2 (1953) 1.
20 P. P. Zolotarev and L. V. Radushkevich, *Dokl. Akad. Nauk SSSR*, 182 (1968) 126.
21 P. P. Zolotarev and L. V. Radushkevich, *Zh. Fiz. Khim.*, 44 (1970) 1071.
22 P. P. Zolotarev and M. M. Dubinin, *Dokl. Akad. Nauk SSSR*, 210 (1973) 136.
23 J. F. Wehner and R. H. Wilhelm, *Chem. Eng. Sci.*, 6 (1956) 89.
24 N. A. Shilov, L. K. Lepin and S. A. Voznesenskii, *Zh. Russ. Khim. Ova.*, 51 (1929) 1107.
25 W. Mecklenburg, *Kolloid. Z.*, 52 (1930) 88.
26 J. Stárek, *Thesis*, J. Heyrovský Institute of Physical Chemistry and Electrochemistry, Czechoslovak Academy of Sciences, Prague, 1984.
27 A. Kneschke, *Používanie diferenciálnych rovníc v praxi (The Use of Differential Equations in Practice)*, Alfa, Bratislava, 1969.
28 C. Hamel, in G. Zweig and J. Sherma (Editors), *Handbook of Chromatography*, Vol. I, CRC Press, Cleveland, OH, 1972, p. 130.
29 R. Aris, *Proc. R. Soc. London, Ser. A*, 235 (1959) 67.
30 Landolt-Börnstein, *Zahlenwerte und Funktionen aus Physik, Chemie, Astronomie, Geophysik und Technik*, Band II, Teil 5, Springer, Berlin, Heidelberg, New York, 1969, p. 549.
31 C. Vidal-Madjar and G. Guiochon, *J. Chromatogr.*, 142 (1977) 61.
32 J. Stárek, M. Kočiřík and A. Zukal, *Collect. Czech. Chem. Commun.*, 48 (1983) 1390.
33 M. Kočiřík and J. Hálová, *Collect. Czech. Chem. Commun.*, 47 (1982) 1931.

Journal of Chromatography, 591 (1992) 287–295
Elsevier Science Publishers B.V., Amsterdam

CHROM. 23 775

Polynuclear aromatic hydrocarbon retention indices on SE-54 stationary phase of the volatile components of a coal tar pitch

Relationships between chromatographic retention and thermal reactivity

M. D. Guillén*, M. J. Iglesias, A. Dominguez and C. G. Blanco

Instituto Nacional del Carbón, CSIC, Ap. 73, 33080 Oviedo (Spain)

(First received July 4th, 1991; revised manuscript received September 27th, 1991)

ABSTRACT

The components of the volatile fraction of a coal tar pitch were studied by capillary gas chromatography and combined gas chromatography–mass spectrometry using the stationary phase SE-54 in both instances. The molecular weight and the retention indices of each identified compound are given. These values are compared with those determined on the stationary phase OV-1701. Relationships between information from the gas chromatography study and from the thermal reactivity of coal tar pitch components are discussed.

INTRODUCTION

Coal tar pitches are very complex mixtures of polynuclear aromatic hydrocarbons (PAHs) and heterocyclic compounds [1] and they behave as eutectic mixtures. Their chemical compositions, physical properties and structures are not known with any degree of certainty. However, it is obvious that their behaviour, reactivity and properties are governed by their composition, and it is generally accepted that the search for relationships between composition, properties and behaviour in the study of carbonaceous materials constitutes the key for a more rational use of these materials [2].

However, the study of their composition is very difficult. Sample fractionations and subsequent characterization of the fractions obtained may be an adequate approach [3–5]. Another possible approach is the characterization of the volatile fraction and the search for relationships between the composition and properties of the entire coal tar pitch. Whatever the approach used, the reproducibility of the fractionation or extraction experiment should always be taken into account. Our experience with coal tar pitch extractions has shown a reproducibility of experiments with some solvents [6], which hinders the correct qualitative and quantitative characterization of coal tar pitches.

Capillary gas chromatography (GC) and gas chromatography–mass spectrometry (GC–MS) [7, 8] are two of the most powerful techniques for the study of mixtures of polynuclear aromatic compounds. In our efforts to study in depth the volatile fraction of a coal tar pitch, we have reported the retention indices of the possible components of this complex mixture [9] on OV-1701 stationary phase (86% methyl, 7% phenyl, 7% cyanopropyl). In this paper GC and GC–MS studies of the volatile

0021-9673/92/$05.00

fraction of the same coal tar pitch using SE-54 stationary phase (94% methyl, 5% phenyl, 1% vinyl) are reported. The retention indices and the masses of all the peaks obtained are given. These values are compared with those determined on OV-1701. Relationships between information from the GC study and the thermal reactivity of coal tar pitch components are discussed.

EXPERIMENTAL

The sample was the fraction of a coal tar pitch obtained by extraction in an ultrasonic bath using toluene as solvent. The characteristics of the coal tar pitch and the extraction procedure have been described in detail elsewhere [6].

Retention times were determined with a Model 8320 gas chromatograph (Perkin-Elmer, Beaconsfield, UK) with flame ionization detection (FID). Separation was carried out on a fused-silica capillary column (25 m × 0.22 mm I.D.) (Chrompack) coated with SE-54 stationary phase with hydrogen as the carrier gas at a flow-rate of 1.8 ml/min (measured at the working temperature). The splitting ratio was 1:120. The detector and injector temperatures were 300°C and the column temperature was programmed from 50 to 300°C at 4°C/min.

The PAH retention indices (I) [10,11] were calculated as follows:

$$I = 100\left[n + \frac{t_r(compound) - t_r(n)}{t_r(n+1) - t_r(n)}\right] \quad (1)$$

where n is the number of rings in the hydrocarbon standard that elutes prior to the substance being measured, t_r(compound) is the retention time of the analyte compound and $t_r(n)$ and $t_r(n+1)$ are the retention times of the PAH standard that elutes just before and after the analyte compound. The standards used were naphthalene, phenanthrene, chrysene and picene. Some retention indices after picene were calculated from an extension of the chrysene–picene interval. The number of determinations was more than 10.

Mass spectral data were obtained with a Hewlett-Packard combined Model 5880A gas chromatograph–Model 5987A mass spectrometer. The same capillary column as used in GC coated with SE-54 was connected directly to the ion source. The instrument was calibrated with perfluorotributylamine and electron impact mass spectra were recorded at an ionization energy of 70 eV. Peaks in the mass spectra were identified through comparison with other spectra in the literature [12]. Further, for the identification of the compounds, previous knowledge of the chromatographic behaviour (on stationary phases of different polarity) of a large group of compounds belonging to the different families of compounds present in coal tar pitches was used [13,14].

RESULTS AND DISCUSSION

Fig. 1 shows the chromatogram of the volatile fraction of Al coal tar pitch on SE-54 stationary phase. Table I gives the retention indices, the mass and the compound assigned to each peak in Fig. 1. The retention indices of some of the coal tar pitch components obtained on SE-54 are fairly close to those obtained on SE-52 for standard compounds [10,11].

In agreement with previous results [9], the fraction examined is composed basically of polynuclear aromatic *cata-* and *peri*-condensed hydrocarbons, and among the latter there are alternant and non-alternant systems[a], acenaphtene and fluorene and their benzo derivatives, some partially hydrogenated PAHs, benzo derivatives of quinoline, carbazole, dibenzo[*b,d*]thiophene and dibenzofuran, alkyl derivatives of all the above-mentioned compounds and PAHs supporting phenyl or naphthyl radicals.

Table II shows some components of the different families together with the differences in their retention indices on SE-54 (non-polar) and OV-1701 (moderately polar) stationary phases. The data on OV-1701 were taken from a previous paper [9]. For the comparison of some incompletely identified compounds such as methyl, phenyl or naphthyl derivatives, the first isomer eluted was taken into account. It was observed that the unsubstituted PAHs show the same elution order with both stationary phases, and in general they show a smaller retention index on SE-54 than on OV-1701 (with some exceptions). However, the latter stationary phase is able to separate benz[*a*]anthracene,

[a] Alternant systems contain only six-membered rings; non-alternant systems have at least one five-membered ring.

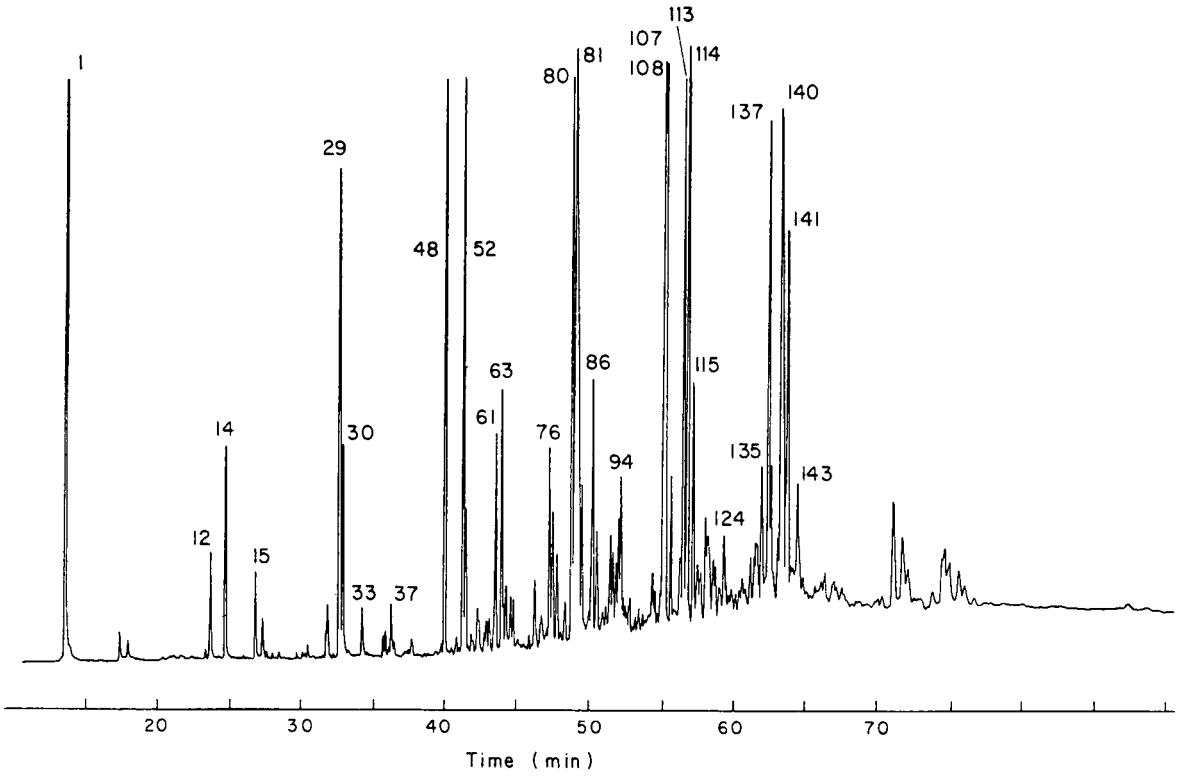

Fig. 1. Capillary gas chromatogram of the volatile fraction of a coal tar pitch on SE-54 stationary phase. For peaks, see Table I.

chrysene and triphenylene (see Fig. 2), like Poly-179 polyphenyl ether sulphone [15] and mixtures of BBBT liquid crystal and SE-52 silicone gum [16]. Acenaphthene, fluorene its benzo derivatives and partially hydrogenated PAHs elute in a similar order on both stationary phases, always before the corresponding hydrocarbons. However, they show higher retentions on SE-54 than on OV-1701, apart from some benzo derivatives of fluorene. The alkylated benzo derivatives elute in the same order on both stationary phases, but in all instances (except for the methyl derivatives of carbazole) their retention is higher on SE-54 than on OV-1701. Other groups of compounds such as phenyl and naphthyl derivatives are also more retained on SE-54 than on OV-1701.

The oxygen benzo derivatives are more retained on SE-54 than on OV-1701. The benzo derivatives of dibenzo[*b,d*]thiophene show a similar retention and elution order on both stationary phases, and there is no general trend. The pyrrole and pyridine benzo derivatives are retained much more on OV-1701 than on SE-54, especially the pyrrole derivatives, which change their elution order. As shown in Figs. 1 and 2, the characterization of benzo derivatives of carbazole can be achieved much better on OV-1701 because on this stationary phase these compounds elute in a zone free from other compounds, whereas on SE-54 these compounds elute in the chrysene–methylchrysene range. For this reason, the quantification of these compounds in coal tar pitches using the non-polar stationary phase is much more difficult, if not impossible. It is concluded that although non-polar stationary phases such as SE-52 and SE-54 have often been used for the chromatographic study of PAHs in general, OV-1701 has advantages for the characterization of the volatile components of coal tar pitches.

The reactivity of a compound is governed by its ability to establish interactions with other molecules. In the chromatographic process the solute–stationary phase interactions also control solute retention. In a chromatographic run the stationary

TABLE I

PAH RETENTION INDICES (I) ON SE-54 STATIONARY PHASE AND MOLECULAR WEIGHTS OF THE COMPONENTS IDENTIFIED IN THE VOLATILE FRACTION OF A COAL TAR PITCH

Peak No. (Fig. 1)	I^{SE-54}	Molecular weight	Possible compound
1	200.00	128	Naphthalene
2	201.44	134	Benzo[*b*]thiophene
3	210.17	129	Quinoline
4	220.06	142	2-Methylnaphthalene
5	223.06	142	1-Methylnaphthalene
6	235.51	154	Biphenyl
7	237.74	156	2-Ethylnaphthalene
8	239.81	156	Dimethylnaphthalene
9	242.13	156	Dimethylnaphthalene
10	243.01	156	Dimethylnaphthalene
11	248.85	168	Methylbiphenyl
12	253.15	154	Acenaphthene
13	255.85	153	Naphtonitrile or azaacenaphthylene
14	258.53	168	Dibenzofuran
15	269.22	166	Fluorene
16	271.08	168	Methylacenaphthene
17	271.91	168	Methylacenaphthene
18	273.32	168	Methylacenaphthene
19	275.32	182	Methyldibenzofuran
20	277.60	182	Methyldibenzofuran
21	284.15	180	9,10-Dihydroanthracene
22	286.22	180	9,10-Dihydrophenanthrene
23	287.24	180	Methylfluorene
24	288.31	180	Methylfluorene
25	289.85	180	Methylfluorene
26	293.48	180	Methylfluorene
27	294.67	182	1,2,3,4-Tetrahydroanthracene
28	295.24	184	Dibenzo[*b,d*]thiophene
29	300.00	178	Phenanthrene
30	301.05	178	Anthracene
31	302.98	179	Acridine
32	307.03	179	Phenanthridine
33	309.02	167	Carbazole
34	317.68	192	Methylphenanthrene, -anthracene
35	318.53	192	Methylphenanthrene, -anthracene
36	320.04	192	Methylphenanthrene, -anthracene
37	321.05	190	4*H*-Cyclopenta[*def*]phenanthrene
38	322.38	192	Methylphenanthrene, -anthracene
39	325.81	192	Methylphenanthrene, -anthracene
79	391.46	232	Tetrahydrochrysene or isomer
80	393.17	234	Benzo[*a*]naphtho[2,3-*d*]thiophene
81	396.46	228	Benz[*a*]anthracene
82a	400.00	228	Chrysene
82b		217	11*H*-Benzo[*a*]carbazole
83a	401.28	228	Naphthacene
83b		248	Methylbenzonaphthothiophene
84	404.38		
85a	405.34	242	Methylbenz[*a*]anthracene or isomer
85b		258	Tetramethylfluoranthene or isomer
86a	406.26	217	7*H*-Benzo[*c*]carbazole
86b		242	Methylbenz[*a*]anthracene or isomer
86c		258	Tetramethylfluoranthene or isomer
87a	407.54	217	5*H*-Benzo[*b*]carbazole
87b		243	Methylbenzophenanthridine or isomer
88a	411.20	219	Dimethylbenzo[*cd,f*]carbazole
88b		242	Methylchrysene or isomer
89	412.71	242	Methylchrysene or isomer
90a	414.26	242	Methylbenz[*a*]anthracene or isomer
90b		256	Dimethylbenz[*a*]anthracene or isomer
91a	415.66	242	Methylbenz[*a*]anthracene or isomer
91b		256	Dimethylbenz[*a*]anthracene or isomer
92a	417.16	240	11*H*-Benz[*bc*]aceanthrylene or isomer
92b		242	Methylbenz[*a*]anthracene or isomer
93a	418.55	240	4*H*-Cyclopenta[*def*]chrysene or isomer
93b		242	Methylbenz(a)anthracene or isomer
93c		254	Binaphthalene or isomer
94	419.67	240	4*H*-Cyclopenta[*def*]triphenylene or isomer
95a	420.56	256	Dimethylbenz[*a*]anthracene or isomer
95b		242	Methylbenz[*a*]anthracene or isomer
96	421.56	254	Binaphthalene or isomer
97a	422.44	256	Dimethylbenz[*a*]anthracene or isomer
97b		242	Methylbenz[*a*]anthracene or isomer
98	423.92	254	Binaphthalene or isomer
99	425.67		
100	426.96		
101	428.36	254	Phenylphenanthrene or isomer
102	430.42		

40	326.84	181	Methylcarbazole
41	328.57	181	Methylcarbazole
42	329.78	204	2-Phenylnaphthalene
43	332.07		
44	334.82		
45	336.17		
46	339.44		
47	341.63	204	Dihydropyrene or isomer
48	343.24	202	Fluoranthene
49	345.73	203	Azafluoranthene, -pyrene
50	347.89	208	Phenanthro[4,5-*bcd*]thiophene
51	348.68	203	Azafluoranthene, -pyrene
52	350.83	202	Pyrene
53a	351.66	218	Benzonaphthofuran
53b		204	Benzacenaphthene or isomer
54	352.60	204	Benzacenaphthene or isomer
55	354.31	218	Benzonaphthofuran
56	356.50	218	Benzonaphthofuran
57	356.93	203	Benzo[*lmn*]phenanthridine
58	359.77	218	Benzo[*kl*]xanthene
59	360.61	216	Methylfluoranthene, -pyrene
60a	361.51	191	4*H*-Benzo[*def*]carbazole
60b		203	Azafluoranthene, -pyrene
61	364.80	216	Benzo[*a*]fluorene
62	365.48	216	Methylfluoranthene, -pyrene
63	367.20	216	Benzo[*b*]fluorene
64	367.62	216	Benzo[*c*]fluorene or isomer
65a	368.61	218	Methylbenzacenaphthene or isomer
65b		232	Methylbenzonaphthofuran or isomer
66	370.22	216	Methylpyrene or isomer
67	371.72	216	Methylpyrene or isomer
68	373.73	232	Methylbenzonaphthofuran or isomer
69	376.32	232	Methylbenzonaphthofuran or isomer
70a	377.16	217	Methylazapyrene or isomer
70b		232	Methylbenzonaphthofuran or isomer
71	378.52	230	Methylbenzofluorene
72	379.39		
73	380.62	230	Dihydrochrysene or isomer
74a	383.09	230	Dimethylfluoranthene, -pyrene
74b		244	Trimethylfluoranthene, -pyrene
75	383.96	230	Dimethylfluoranthene, -pyrene
76	387.08	234	Benzo[*b*]naphtho[2,1-*d*]thiophene
77a	388.58	228	Benzo[*c*]phenanthrene
77b		226	Benzo[*ghi*]fluoranthene
77c		246	Dimethylbenzonaphthofuran
78a	390.33	234	Benzo[*b*]naphtho[1,2-*d*]thiophene
78b		229	Dibenzoquinoline or isomer
103	431.68	254	Dihydrobenzofluoranthene or isomer
103a		256	Dimethylchrysene or isomer
104a	434.97	253	Dibenzophenanthridine or isomer
104b		256	Biquinoline
105	436.51	256	Biquinoline
106	437.41		
107a	440.92	252	Benzo[*j*]fluoranthene
107b		254	Dihydrobenzofluoranthene or isomer
108a	441.63	252	Benzo[*b*]fluoranthene
108b		254	Dihydrobenzofluoranthene or isomer
109a	444.43	252	Benzo[*k*]fluoranthene
109b		268	Dibenzonaphthofuran or isomer
109c		254	Dihydrobenzofluoranthene or isomer
110a	445.61	256	Dimethylchrysene or isomer
110b		253	Azabenzopyrene or isomer
111	446.28		
112a	448.67	268	Dibenzonaphthofuran or isomer
112b		258	Benzophenanthrothiophene
112c		253	Azabenzopyrene or isomer
113a	450.75	252	Benzo[*e*]pyrene
113b		268	Dibenzonaphthofuran or isomer
114a	452.95	252	Benzo[*a*]pyrene
114b		268	Dibenzonaphthofuran or isomer
115a	455.59	252	Perylene
115b		268	Dibenzonaphthofuran or isomer
115c		266	Methylbenzofluoranthene or isomer
116a	457.84	266	Methylbenzofluoranthene or isomer
116b		253	Azabenzopyrene or isomer
117a	459.33	241	4*H*-Naphtho[1,2,3,4-*def*]carbazole or isomer
117b		266	Methylbenzofluoranthene or isomer
118a	461.52	266	Dibenzofluorene or isomer
118b		278	Dihydroindenopyrene or isomer
119	462.33	266	Dibenzofluorene or isomer
120	462.92	266	Dibenzofluorene or isomer
121a	465.39	266	Methylbenzopyrene or isomer
121b		278	Dibenzo[*c,g*]phenanthrene or isomer
121c		282	Dimethyldibenzonaphthofuran or isomer
122	466.29	266	Methylbenzopyrene or isomer
123	468.38	266	Methylbenzopyrene or isomer
124a	470.53	264	11*H*-Cyclopenta[*ghi*]perylene or isomer
124b		266	Methylbenzopyrene or isomer
124c		280	Dimethylbenzopyrene or isomer
125	471.41	266	Methylbenzopyrene or isomer
126a	473.15	266	Methylbenzopyrene or isomer
126b		280	Dimethylbenzopyrene or isomer
127a	474.21	264	11*H*-Indeno[2,1,7-*cde*]pyrene or isomer
127b		280	Dimethylbenzopyrene or isomer

(*Continued on p. 292*)

TABLE I (*continued*)

Peak No. (Fig. 1)	I^{SE-54}	Molecular weight	Possible compound	Peak No. (Fig. 1)	I^{SE-54}	Molecular weight	Possible compound
128	476.15			135c		282	Dimethyldibenzonaphthofuran
129a	478.30	284	Dinaphthothiophene	135d		292	Methyldibenzophenanthrene, -anthracene
129b		280	Dimethylbenzopyrene or isomer	136a	492.60	276	Indenopyrene or isomer
129c		279	Dibenzophenanthridine or isomer	136b		272	Methylbenzophenanthrothiophene
130a	479.38	284	Dibenzonaphthothiophene	137a	493.39	278	Dibenz[*a,c*]anthracene
130b		280	Dimethylbenzopyrene or isomer	137b		292	Methyldibenzophenanthrene, -anthracene
131a	480.58	267	Dibenzocarbazole	137c		280	Dimethylbenzofluoranthene or isomer
131b		280	Dimethylbenzopyrene or isomer	138a	494.19	278	Dibenz[*a,h*]anthracene
131c		278	Dibenzo[*b,g*]phenanthrene or isomer	138b		294	Trimethylbenzofluoranthene or isomer
132a	483.25	278	Benzo[*g*]chrysene or isomer	138c		292	Dimethyldibenzophenanthrene, -anthracene
132b		284	Dinaphthothiophene	139a	496.65	278	Benzo[*b*]chrysene
132c		280	Dimethylbenzofluoranthene or isomer	139b		282	Dimethyldibenzonaphthofuran
133a	485.20	279	Dibenzoacridine or isomer	140a	500.00	278	Picene
133b		284	Dinaphthothiophene	140b		280	Dimethylbenzopyrene or isomer
134a	486.20	284	Dinaphthothiophene	140c		282	Dimethyldibenzonaphtofuran
134b		278	Benzo[*c*]chrysene or isomer	141	501.90	276	Benzo[*ghi*]perylene
134c		267	Dibenzocarbazole	142a	503.80	278	Benzo[*a*]naphthacene or pentacene
134d		280	Dimethylbenzofluoranthene or isomer	142b		282	Dimethyldibenzonaphthofuran
135a	488.81	278	Dibenz[*a,j*]anthracene	143a	506.49	276	Anthanthrene
135b		276	Indenopyrene or isomer	143b		290	Methyl derivative of indenopyrene or isomer

TABLE II

DIFFERENCES IN THE PAH RETENTION INDICES OF SOME COMPOUNDS OF SEVERAL FAMILIES ON SE-54 AND OV-1701 STATIONARY PHASES

Compound	$I^{SE-54} - I^{OV-1701}$	Compound	$I^{SE-54} - I^{OV-1701}$
Anthracene	+0.3	Dimethylnaphthalene	+1.8
Fluoranthene	−1.0	Methylacenaphthene	+3.4
Pyrene	−0.4	Methyldibenzofuran	+3.4
Benzo[*c*]phenanthrene	0.0	Methylfluorene	+4.0
Benzo[*ghi*]fluoranthene	−1.1	Methylphenanthrene, -anthracene	+1.9
Benzo[*a*]anthracene	−1.4	Methylcarbazole	−14.9
Triphenylene	+0.3	Methyl 4*H*-cyclopenta[*def*]phenanthrene	+7.0
Naphthacene	−1.1	Methylfluoranthene, -pyrene	+2.3
Benzo[*j*]fluoranthene	−2.4	Methylbenzonaphthofuran	+3.0
Benzo[*b*]fluoranthene	−2.7	Dimethylbenzonaphthofuran	+4.7
Benzo[*k*]fluoranthene	−2.5	Methylbenz[*a*]anthracene	+1.9
Benzo[*e*]pyrene	−2.5		
Benzo[*a*]pyrene	−2.0	Biphenyl	+3.0
Perylene	−2.5	2-Phenylnaphthalene	+2.1
Dibenz[*a,j*]anthracene	−3.2	Binaphthalene	+3.5
Dibenz[*a,c*]anthracene	−1.4	Phenylphenanthrene	+5.5
Dibenz[*a,h*]anthracene	−1.9		
Benzo[*ghi*]perylene	−0.6	Benzo[*b*]thiophene	−0.2
Benzo[*a*]naphthacene	−1.0	Dibenzo[*b,d*]thiophene	+0.4
Anthanthrene	+1.7	Phenanthro[4,5-*bcd*]thiophene	+0.1
		Benzonaphtho[2,1-*d*]thiophene	−0.4
Acenaphthene	+2.6	Benzonaphtho[1,2-*d*]thiophene	−0.3
Fluorene	+2.5	Benzonaphtho[2,3-*d*]thiophene	−1.3
9,10-Dihydroanthracene	+2.6	Benzophenanthrothiophene	+0.3
9,10-Dihydrophenanthrene	+3.7		
1,2,3,4-Tetrahydroanthracene	+4.1	Dibenzofuran	+1.9
4*H*-Cyclopenta[*def*]phenanthrene	+1.5	Benzonaphthofuran	+1.2
Benzo[*a*]fluorene	+0.5	Benzo[*kl*]xanthene	+1.8
Benzo[*b*]fluorene	−0.0		
Benzo[*c*]fluorene	−0.6	Quinoline	−3.3
11*H*-Benz[*bc*]aceanthrylene	−0.9	Azafluoranthene	−3.7
4*H*-Cyclopenta[*def*]chrysene	−1.1	Dibenzoquinoline	−1.2
4*H*-Cyclopent[*def*]triphenylene	−1.0		
		Carbazole	−19.2
2-Methylnaphthalene	+2.2	4*H*-Benzo[*def*]carbazole	−18.5
1-Methylnaphthalene	+2.2	11*H*-Benzo[*a*]carbazole	−22.9
2-Ethylnaphthalene	+5.6	7*H*-Benzo[*c*]carbazole	−20.0
		5*H*-Benzo[*b*]carbazole	−24.0
		4*H*-Naphtho[1,2,3,4-*def*]carbazole	−18.7
		Dibenzocarbazole	−15.6

phase is the same for all components of the sample to be chromatographed. For this reason, the difference in the retentions of the several compounds in a mixture on two stationary phases of different polarity could be related to the reactivity of the compounds.

In carbonaceous mixtures, such as coal tar pitches, thermal reactivity is the factor controlling their behaviour in the pyrolysis process, and for this reason it has been studied experimentally for many polynuclear aromatic compounds [17]. Although it is very difficult to establish a reactivity scale among the different polynuclear aromatic compounds, it is generally accepted, on an experimental basis, that among the unsubstituted PAHs the most thermally reactive are those having an anthracene configuration; the alkyl-substituted PAHs are more reactive than the unsubstituted PAHs, the effect being more

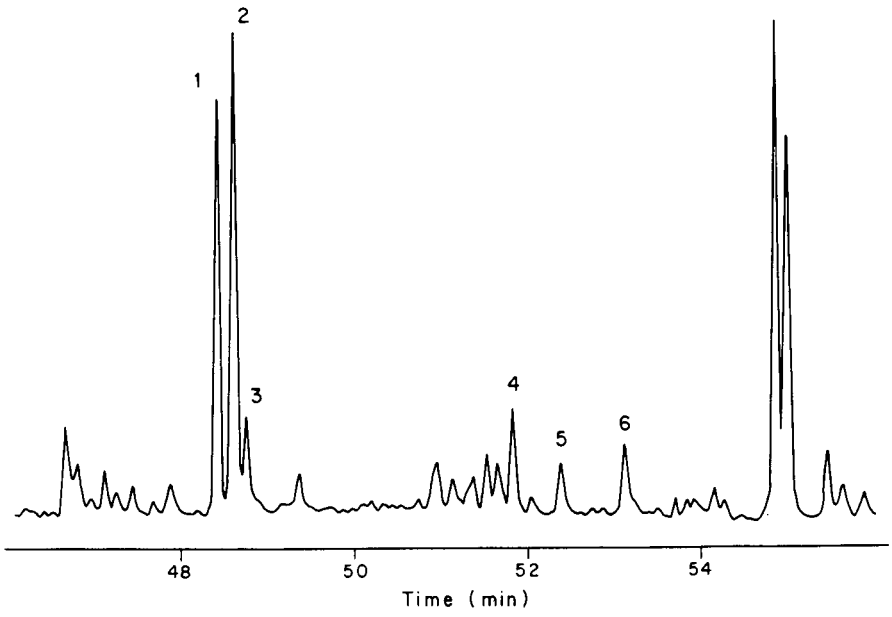

Fig. 2. Extension of a part of the capillary gas chromatogram of the volatile fraction of the coal tar pitch on OV-1701 stationary phase. Peaks: 1 = Benzo[*a*]anthracene; 2 = chrysene; 3 = triphenylene; 4 = 11*H*-benzo[*a*]carbazole; 5 = 7*H*-benzo[*c*]carbazole; 6 = 5*H*-benzo[*b*]carbazole.

pronounced the greater the number and length of the alkyl groups. Further, some workers [18] have identified as thermally reactive compounds 1-phenylnaphthalene and 9,10-dihydroanthracene and aromatics which have methylene bridges, such as 1,2-diphenylethane. However, the thermal stability of aromatics such as dibenzofuran [19] and dibenzo[*b,d*]thiophene [19,20] is thought to be high, and quinoline, isoquinoline and carbazole are considered to be very stable compounds [19].

From a careful study of Table II, it can be concluded, with some exceptions, that the compounds more retained on SE-54 than on OV-1701 are in general those considered to be more reactive in thermal processes, whereas the compounds more retained on OV-1701 than on SE-54 stationary phase are in general those considered to be more thermally stable.

It is known that solute–non-polar stationary phase interactions are governed basically by dispersive interactions expressed by the molar refraction or molecular polarizability of each solute [21–23]. In addition, it is generally accepted that in solute–polar stationary phase interactions, in addition to the dispersive interactions there are also others that take place due to the polarity [24,25]. From what has been said, it might be considered that the thermal reactivity of polynuclear aromatic compounds is more closely related to the molecular polarizability than to the polarity of the compound.

Studies directed towards the search for relationships between the concentration of some families of compounds in the volatile fraction of several pitches and their thermal behaviour are in progress.

ACKNOWLEDGEMENTS

This work was supported by the DGICYT, Project No. PB88-0002. M. J. Iglesias thanks the Consejo Superior de Investigaciones Cientificas for a postdoctoral fellowship.

REFERENCES

1 M. Zander, *Fuel*, 66 (1987) 1536.
2 M. H. Wagner, H. Jäger, J. Letizia and G. Wilhelmi, *Fuel*, 67 (1988) 792.
3 G.-P. Blümer, H. W. Kleffner, W. Lücke and M. Zander, *Fuel*, 59 (1980) 600.
4 W. Boenigk, M. W. Haenel and M. Zander, *Fuel*, 69 (1990) 1226.

5 K. D. Bartle, *Rev. Pure Appl. Chem.*, 22 (1972) 79.
6 M. D. Guillén, J. Blanco, J. S. Canga and C. G. Blanco, *Energy Fuels*, 5 (1991) 188.
7 A. Bjorseth (Editor), *Handbook of Polycyclic Aromatic Hydrocarbons*, Marcel Dekker, New York, Basle, 1983.
8 A. Bjorseth and T. Randall (Editors), *Handbook of Polycyclic Aromatic Hydrocarbons*, Vol. 2, Marcel Dekker, New York, Basle, 1985.
9 C. G. Blanco, J. Blanco, P. Bernad and M. D. Guillén, *J. Chromatogr.*, 539 (1991) 157.
10 M. L. Lee, D. L. Vassilaros, C. M. White and M. V. Novotny, *Anal. Chem.*, 51 (1979) 768.
11 M. L. Lee, M. V. Novotny, K. D. Bartle, *Analytical Chemistry of Polycyclic Aromatic Compounds*, Academic Press, New York, London, Toronto, 1981.
12 S. R. Heller and G. W. A. Milne, *EPA NIH Mass Spectral Data Base*, National Technical Information Service, US Department of Commerce, Washington, DC, 1978.
13 C. G. Blanco, J. Blanco, J. Bermejo and M. D. Guillén, *J. Chromatogr.*, 465 (1989) 378.
14 M. D. Guillén, J. Blanco, J. Bermejo and C. G. Blanco, *J. High Resolut. Chromatogr.*, 12 (1989) 552.
15 H. Borwitzky and G. Schomburg, *J. Chromatogr.*, 170 (1979) 99.
16 R. J. Laub, W. L. Roberts and C. A. Smith, *J. High Resolut. Chromatogr. Chromatogr. Commun.*, 7 (1980) 355.
17 E. Fitzer, H. Mueller and W. Schaefer, in P. L. Walker, Jr. (Editor), *Chemistry and Physics of Carbon*, Vol. 7, Marcel Dekker, New York, 1971, p. 287.
18 A. G. Sharkey, J. L. Schultz and R. A. Frieder, *Carbon*, 4 (1966) 365.
19 J. J. Madison and R. M. Roberts, *Ind. Eng. Chem.*, 50 (1958) 237.
20 G.-P. Blümer and M. Zander, *DGMK Compendium, Suppl. to Erdöl Kohle Erdgas Petrochem.*, (1977/78) 235.
21 J. Bermejo and M. D. Guillén, *Chromatographia*, 17 (1983) 664.
22 J. Bermejo and M. D. Guillén, *J. High Resolut. Chromatogr. Chromatogr. Commun.*, 7 (1984) 191.
23 J. Bermejo and M. D. Guillén, *Int. J. Environ. Anal. Chem.*, 23 (1985) 77.
24 J. Bermejo and M. D. Guillén, *J. Chromatogr.*, 318 (1985) 187.
25 J. Bermejo and M. D. Guillén, *Anal. Chem.*, 59 (1987) 94.

Journal of Chromatography, 591 (1992) 297–301
Elsevier Science Publishers B.V., Amsterdam

CHROM. 23 774

Gas chromatography of Titan's atmosphere

III. Analysis of low-molecular-weight hydrocarbons and nitriles with a CP-Sil-5 CB WCOT capillary column

L. Do and F. Raulin*

Laboratoire de Physico-Chimie de l'Environnement, Université Paris XII, 94010 Creteil Cedex (France)

(First received June 21st, 1991; revised manuscript received September 27th, 1991)

ABSTRACT

The systematic calibration of a CP-Sil-5 CB wall-coated open-tubular capillary column (0.15 mm I.D., 2 μm film) with a chemically bonded stationary phase (dimethyl polysiloxane) is reported for the separation of C_1–C_6 hydrocarbons and C_1–C_4 nitriles, at temperatures ranging from 20 to 80°C. Retention indices are given for these solutes at 20°C. Van Deemter curves are also plotted for propionitrile, *n*-hexane and benzene at 20 and 50°C. The column provides good efficiency and resolution, suitable for the conditions required by a flight instrument aboard a Titan probe, such as the gas chromatography–mass spectrometry experiment on the Huygens probe of the Cassini mission.

INTRODUCTION

In the frame of the development of a gas chromatographic–mass spectrometric (GC–MS) instrument [1] for the Titan Huygens probe in the Cassini mission, we are currently studying GC columns which could provide the best conditions for analysing the atmosphere of Titan (a satellite of Saturn) within the constraints of space instrumentation. In previous papers in the series [2,3], we reported the behaviour of porous-layer open-tubular (PLOT) capillary columns in the separation of C_1–C_8 hydrocarbons and C_1–C_4 nitriles. However, in spite of their attractive chromatographic behaviour, recent mechanical tests [4] suggested that such columns do not fulfil all the requirements of space instrumentation: their mechanical strength appears too weak, so far, to resist the severe conditions of a flight instrument, in particular the acceleration and vibration during the launch. The main problem seems to be the degradation of the coating when the column is exposed to such intense vibrations. In this respect, wall-coated open-tubular (WCOT) capillary columns with a chemically bonded stationary phase may be a better choice. In such columns, by means of a chemical reaction, the molecules of the stationary phase are linked among themselves and to the inner wall of the fused-silica tubing [5]. Consequently, transformation of the liquid phase structure into a three-dimensional association system occurs. It gives not only better mechanical resistance but also high thermal stability, decreasing markedly the bleeding of the column [6].

A WCOT capillary column coated with dimethyl polysiloxane such as the CP-Sil-5 CB column (Chrompack, Middelburg, Netherlands) has already shown good behaviour for the simultaneous determination of polar and non-polar low-molecular-weight compounds [7], but there are no data on the behaviour of this type of column relative to nitriles. We report here the results of a detailed chromatographic study of a CP-Sil-5 CB fused-silica capillary column, including the simultaneous separation of mixtures of hydrocarbons and nitriles

0021-9673/92/$05.00

and the Van Deemter curves for some of these compounds.

EXPERIMENTAL

The CP-SIL-5 CB WCOT column (Chrompack) was a 25 m × 0.15 mm I.D. WCOT fused-silica capillary coated with a 2-μm thick film of 100% dimethyl polysiloxane. It was installed in the split mode (splitting ratio generally 305:1) on the same gas chromatograph as described in Part I [2]. The injector and detector temperatures were 100°C. The carrier gas was hydrogen.

Sampling techniques, most of the reagents and the method of determination of the Van Deemter curves were the same as described in Part I [2]. The additional solutes, cyclopropane and 1,3-butadiene, were obtained from Alphagaz–L'Air Liquid (Bois d'Arcy, France) and Aldrich (Strasbourg, France), respectively. Butadiyne was prepared by dehydrochlorination of 1,4-dichloro-2-butyne (Aldrich) with potassium hydroxide in water–dioxane solution [8].

RESULTS AND DISCUSSION

To determine the efficiency of the column and the optimum flow-rate for a gas mixture of hydrocarbons and nitriles, we measured the HETP (H) as a function of the mean linear gas velocity (u) at different temperatures. To plot Van Deemter curves we injected a gas mixture of propionitrile, n-hexane, benzene and methane in constant amounts (7–12 nmol in the injector of the gas chromatograph) at 20 and 50°C.

The curves for propionitrile are shown in Fig. 1A. The minimum values of H are 0.5 mm at 20°C and 0.74 mm at 50°C. The linear part of the H *vs.* u curve for this polar compound rises slowly at high velocities of the carrier gas. Fig. 1B shows the curves relating to n-hexane. The minimum values of H are 0.42 mm at 20°C and 0.58 mm at 50°C.

The curves obtained with benzene (Fig. 2) exhibit a relatively flat minimum. It is observed at linear velocities of the carrier gas of *ca.* 30 cm/s. The minimum values of H are 0.31 mm at 20°C, corresponding to 3265 theoretical plates/m and 0.43 mm at 50°C. With the three components stated above, we observed that the column efficiency decreases slightly when the temperature is increased in the range tested. In addition, the efficiency of the column for the selected solutes appears very high according to the observed minimum values of H and the theoretical plate number.

To calibrate the column with a mixture of C_1–C_6 hydrocarbons and C_1–C_4 nitriles, we chose 0.6 ml/min for the outlet flow-rate of the carrier gas. Fig. 3 shows a chromatogram of such a mixture at 20°C.

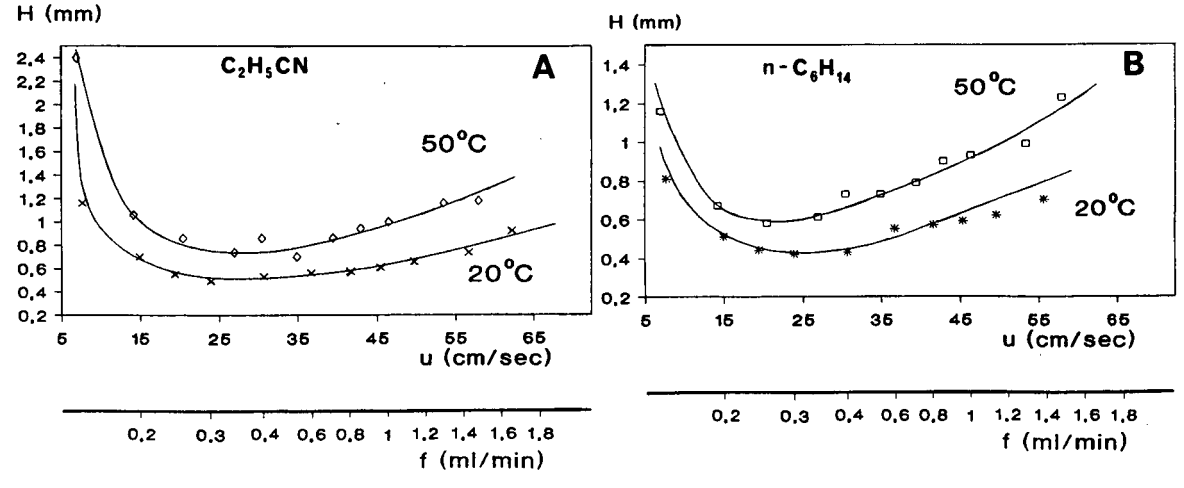

Fig. 1. (A) Propionitrile and (B) n-hexane: variation of the height equivalent to a theoretical plate (H) with the mean linear velocity (u) and outlet flow-rate (f) of the carrier gas (hydrogen) at 20 and 50°C on a 0.15 mm I.D. fused-silica CP-Sil-5 CB WCOT column (2-μm thick coating). Total amounts injected: propionitrile 12 nmol, n-hexane 7 nmol; split mode (305:1).

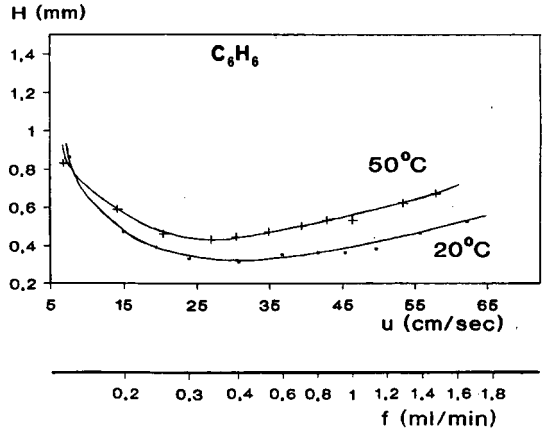

Fig. 2. Benzene: variation of H with u and f as in Fig. 1. Total amount injected: 10 nmol.

With this isothermal condition, several solutes are co-eluted. Ethene is co-eluted with ethyne, 1-butene with isobutene and *trans*- or *cis*-crotononitrile with benzene. Apart from these compounds, all the selected solutes are well separated. Further, the profile of most peaks is sharp and symmetrical. However, the peaks of the non-volatile nitriles show a very slight tailing compared with those of hydrocarbons. This could be due to strong adsorption of nitriles on the stationary phase and slow kinetics of mass transfer between the gas and liquid phases [9]. The elution of all injected solutes is completed in 35 min. The nature of the films of ParaPLOT Q and CP-Sil-5 CB is almost apolar. However, for several hydrocarbons relative to neighbouring nitriles, there are peak inversions between the two columns, as shown in Table I. Apolar or almost apolar hydrocarbons are eluted before the nitrile (*e.g.*, 1-pentene and acrylonitrile, 3-methylpentane and isobutyronitrile) with the CP-Sil-5 CB column but after the nitrile with the PoraPLOT Q column. Hence the stationary phase in the CP-Sil-5 CB column could be slightly less apolar than the adsorbent film in the PoraPLOT Q column.

To improve the separation of solutes and to shorten the analysis time, we programmed the column temperature as a function of time. For the analysis of the same gaseous mixture, we introduced a column temperature programme from 20°C (isothermal for 4 min) at 20°C/min to 80°C (Fig. 4). The separation of all solutes was accomplished in

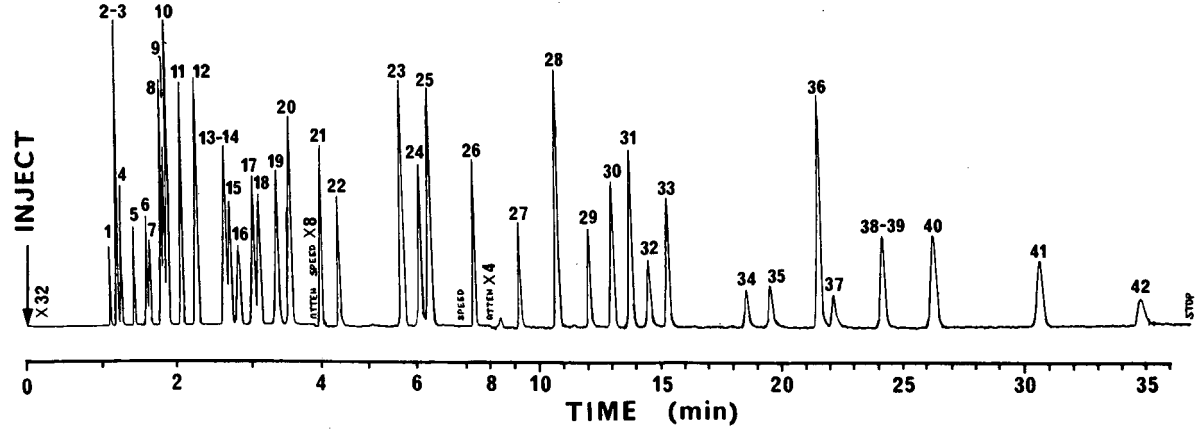

Fig. 3. Gas chromatogram of a gaseous mixture of C_1–C_6 hydrocarbons and C_1–C_4 nitriles on a 25 m × 0.15 mm I.D. CP-Sil 5 CB (2-μm thick coating) fused-silica WCOT column at 20°C. Carrier gas, hydrogen; outlet flow-rate, 0.6 ml/min; amount injected, 1–5 nmol of each constituent; split mode (305:1); flame ionization detector. Peaks: 1 = methane; 2 = ethene; 3 = ethyne; 4 = ethane; 5 = cyanogen; 6 = propene; 7 = propane; 8 = hydrocyanic acid; 9 = propyne; 10 = allene; 11 = cyclopropane; 12 = isobutane; 13 = 1-butene; 14 = isobutene; 15 = 1,3-butadiene; 16 = butane; 17 = *trans*-2-butene; 18 = 1-butyne; 19 = *cis*-2-butene; 20 = butadiyne; 21 = cyanoacetylene; 22 = acetonitrile; 23 = 1-pentene; 24 = acrylonitrile; 25 = *n*-pentane; 26 = 2-methyl-2-butene; 27 = propionitrile; 28 = cyclopentane; 29 = methacrylonitrile; 30 = 3-methylpentane; 31 = 1-hexene; 32 = isobutyronitrile; 33 = *n*-hexane; 34 = *cis*- or *trans*-crotononitrile; 35 = 3-butenenitrile; 36 = 2-butynenitrile; 37 = butyronitrile; 38 = *trans*- or *cis*-crotononitrile; 39 = benzene; 40 = cyclohexane; 41 = cyclohexene; 42 = cyclopropanecarbonitrile.

TABLE I

RETENTION INDICES OF HYDROCARBONS AND NITRILES ON A CP-SIL-5 CB WCOT COLUMN AT 20°C AND (FOR COMPARISON) ON A PORAPLOT Q COLUMN [2] AT 100°C

Reference alkanes are listed in parentheses.

Solute	Retention index	
	CP-Sil-5 CB (20°C)	PoraPLOT Q (100°C)
(Ethane)	200	
Cyanogen	259.2	
Propene	294	
(Propane)	300	300
Hydrogen cyanide	319.9	291.9
Propyne	323.6	
Allene	329.5	
Cyclopropane	348.8	
Isobutane	366	
1-Butane	391	
Isobutene	391	
1,3-Butadiene	394.3	
(Butane)	400	
trans-2-Butene	410.2	
1-Butyne	414	
cis-2-Butene	425	
Butadiyne	431	
Cyanoacetylene	447.6	
Acetonitrile	456.9	
1-Pentene	488.8	489.2
Acrylonitrile	496.4	475.6
(*n*-Pentane)	500	500
2-Methyl-2-butene	520.1	
Propionitrile	545.3	523.3
Cyclopentane	562.6	516.1
Methacrylonitrile	574.9	
3-Methylpentane	583	592.2 (2)[a]
1-Hexene	588.9	592.2 (3)[a]
Isobutyronitrile	594.4	592.2 (1)[a]
(*n*-Hexane)	600	600
cis- or *trans*-crotononitrile	619.8	596.5
3-butenenitrile	625.2	
Cyanopropyne	637.9	
Butyronitrile	638.1	
trans- or *cis*-crotononitrile	647.2	
Benzene	647.2	
Cyclohexane	655.7	
Cyclohexene	671	
Cyclopropyl cyanide	684	
(*n*-Heptane)	700	

[a] Order of appearance of peaks.

less than 16 min, and *cis*- or *trans*-crotononitrile and benzene were separated. The entire analysis time is much reduced, but a drift of the baseline was observed with increasing column temperature. This is due to "bleeding" of the stationary phase, the thickness of which is relatively large (2 μm).

We also measured the retention indices $I(i)$, of the compounds studied in order to obtain a more general view of the behaviour of the column in relation to these solutes. The retention indices are determined from the classical equation

$$I(i) = 100 \cdot \frac{\log t'_{R(i)} - \log t'_{R(P_z)}}{\log t'_{R(P_{z+1})} - \log t'_{R(P_z)}} + 100Z$$

where t'_R is the relative retention time, P_z and P_{z+1} correspond to the paraffins with z and $z+1$ carbon atoms, respectively, and i correspond to a solute, the retention time of which is between that of P_z and P_{z+1}. These retention indices at 20°C (Table I) vary linearly with the carbon number of the solute for a given chemical family. It must be pointed out that these experimental values appeared to be highly reproducible for most of all solutes, the relative error being less than 0.8%.

Under isothermal conditions (20°C), the detection limit (signal twice the baseline noise) corresponds to an absolute amount of solute in the column of less than about 10^{-12}–10^{-13} mol for C_2–C_3 hydrocarbons, HCN and cyanoacetylene. This limit comes mainly from the detection sensitivity (flame ionization detector) and not from the column. For the same organics, the amounts that will be injected into the GC–MS instrument are expected to be in this range or even higher. Therefore, this column should be compatible with the GC–MS analysis on the Huygens probe, at least in terms of sensitivity.

The results demonstrate that a 25 m × 0.15 mm I.D. fused-silica CP-Sil-5 CB (film thickness 2 μm) WCOT column is efficient for the separation of C_1–C_6 hydrocarbons and C_1–C_4 nitriles at low temperature. Moreover, faster analysis was achieved by temperature programming; however, the bleeding of the stationary phase may decrease significantly the signal-to-noise ratio of the GC–MS instrument of the Huygens probe. To reduce the analysis time under isothermal conditions, the column length could be shortened while the thickness of the film is decreased in order to reduce the bleeding of the stationary phase during temperature programming. If the column is so modified, it can be used for faster

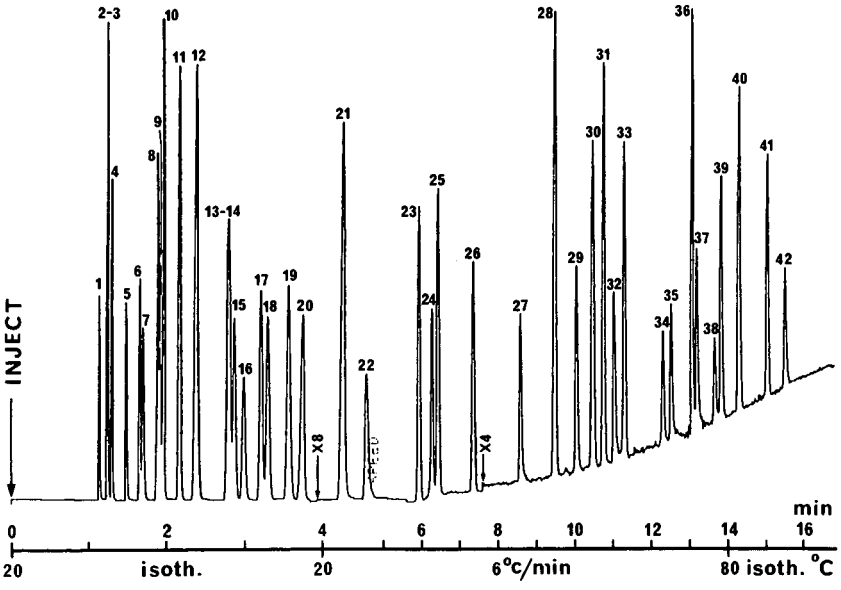

Fig. 4. Chromatogram obtained under the same conditions as in Fig. 3, but with temperature programming of the column: isothermal for 4 min at 20°C, then increased at 6°C/min to 80°C. Peak numbers as in Fig. 3.

analysis and with a lower inlet pressure of the carrier gas.

ACKNOWLEDGEMENTS

We thank Dr. G. Gaspar and J. de Zeeuw for their help with this work. This study was supported by a grant from the Centre National d'Etudes Spatiales.

REFERENCES

1 H. Niemann, *Proposal to ESA Cassini Mission: Huygens Probe*, NASA–Goddard Space Flight Center, Greenbelt, MD, (1990).
2 L. Do and F. Raulin, *J. Chromatogr.*, 481 (1989) 45.
3 L. Do and F. Raulin, *J. Chromatogr.*, 514 (1990) 65.
4 H. Niemann, personal communication.
5 *Chrompack News, No. 13*, Chrompack, Middelburg, 1986, p. 1.
6 *Chrompack News, No. 12*, Chrompack, Middelburg, 1986, p. 3.
7 *Chrompack News, No. 12*, Chrompack, Middelburg, 1985, p. 4.
8 K. K. Georgieff and Y. Richard, *Can. J. Chem.*, 36 (1958) 1280.
9 G. Guiochon and C. L. Guillemin, *Quantitative Gas Chromatography*, Elsevier, Amsterdam, 1988.

Journal of Chromatography, 591 (1992) 303–311
Elsevier Science Publishers B.V., Amsterdam

CHROM. 23 773

Comparative study of clean-up and fractionation methods for the determination of organochlorine pesticides in lipids by gas chromatography

Jesús Eduardo Quintanilla-López, Rosa Lebrón-Aguilar and Luis María Polo-Díez*

Departamento de Química Analítica, Facultad de Ciencias Químicas, Universidad Complutense de Madrid, 28040 Madrid (Spain)

(First received June 17th, 1991; revised manuscript received September 26th, 1991)

ABSTRACT

Three of the methods most often used for the clean-up and fractionation of organochlorine pesticides in lipid residue analysis by gas chromatography with electron-capture detection were compared. The overall recoveries of twenty pesticides from spiked samples were higher than 88%, the relative standard deviation being in the range 3–11% ($n = 6$) at the 36–80 ppb (10^9) level. The three methods were compared by analysis of variance, with no differences in precision at the 0.05 significance level. Differences in recoveries appeared in only two instances. None of the three methods seems to be significantly better than the others for the determination of the pesticides studied.

INTRODUCTION

The well known persistence of organochlorine pesticides due to their low biodegradability, together with their biosolubility in lipid tissues and high toxicity, require the analysis of this kind of sample in routine pollution studies [1]. Owing to the complexity of these lipid samples and their low pesticide concentrations, the analytical technique most often used is gas chromatography (GC) with electron-capture detection (ECD) after extraction of the pesticides in organic solvents. In order to prevent deterioration of the detector, extracts must be clean, particularly regarding the absence of fatty matter; consequently, clean-up is necessary. Fractionation of pesticides in groups by differential elution should simplify chromatograms and signal processing.

Extracts containing lipid residues may be purified by both chemical or physical methods. The main reagents used for purification include concentrated sulphuric acid, chromium trioxide and potassium hydroxide in ethanol [2–8]; however, the organochlorine pesticides are decomposed in different ways. Hence physical purification is preferred; this involves the use of adsorption columns containing silica gel [9], alumina [1,10] or Florisil [11–15]. The use of these adsorbents involves particular problems. Thus, silica contains large amounts of impurities, which are extremely difficult to remove [16], and the fractionation ability of alumina is limited [17]. The main problem with Florisil is the repeatability, but the standardization proposed by Mills [18] seems to have overcome this problem, and the use of Florisil has become well accepted [19]. However, some disagreement still remains regarding the fractionation of pesticides when different eluents are used.

This paper reports the results of a comparative study of the three elution systems most often used with Florisil to purify extracts from lipid samples for the determination of organochlorine pesticide residues.

0021-9673/92/$05.00

EXPERIMENTAL

Apparatus

A Hewlett-Packard Model 5890A gas chromatograph equipped with a packed-column injection port, a Hewlett-Packard cross-linked 5% phenylmethylsilicone (2.65 μm film thickness) fused-silica capillary column (30 m × 0.53 mm I.D.) and an electron-capture detector (^{63}Ni) was used. Data from the detector were processed using an HP Vectra ES/12 computer and were reported with an HP 3365 ChemStation system. The injection port and detector temperatures were 230 and 300°C, respectively. The oven temperature was programmed with an initial hold for 6 min at 180°C, followed by an increase at 7°C/min to 220°C, a hold for 6 min, then an increase at 10°C/min to 260°C, with a final hold for 3 min. Nitrogen flow-rates were carrier gas 10 ml/min and make-up gas 50 ml/min.

Soxhlet extractors (125 ml) were used, equipped with extraction cartridges with No. 1 fritted plate bottoms. A Heidolph VV 2000 rotary evaporator, a P-Selecta hot water-bath and a Waring blender were employed. Chromatographic columns with a borosilicate stopcock and a coarse fritted plate (No. 0), 40 × 1.6 cm I.D., were used. Volumetric glassware of Class A was used, all glassware being washed with soapy water, rinsed with tap water, immersed in chromic acid mixture for about 5 h, rinsed with distilled water and acetone and stored with openings covered with aluminium foil previously heated at 350°C for 12 h.

Reagents and standards

The solvents benzene, *n*-hexane, light petroleum (b.p. 40–60°C), diethyl ether, dichloromethane, acetonitrile and acetone were of pesticide grade from Carlo Erba. Lauric acid and absolute ethanol (analytical-reagent grade) were obtained from Merck and phenolphthalein (PRS) and sodium hydroxide (PRS, 97%) from Panreac. Anhydrous sodium sulfate (analytical-reagent grade) from Merck was used as a drying agent.

Florisil (60–100 mesh) was purchased from Carlo Erba (RS) and was activated at 676°C and stored in the dark in a glass container with a glass stopper or foil-lined screw-cap. The amount of Florisil used in each column was calculated by standardization [18]. Before use, each portion was activated overnight at 130°C in a foil-covered glass container and cooled in a desiccator at room temperature. The three elution procedures compared use a glass chromatographic column loaded with 8.5 g of Florisil, determined from the lauric acid value and column inside diameter. The column was topped with glass-wool, 2 cm of anhydrous sodium sulphate and finally glass-wool.

Pesticide standards were obtained from Riedel-de Häen: aldrin, captan, chlorfenson, *p,p'*-DDD, *o,p'*-DDE, *p,p'*-DDE, *o,p'*-DDT, *p,p'*-DDT, dicofol, dieldrin, endosulfan-I, endosulfan-II, endrin, hexachlorobenzene (HCB), heptachlor, heptachlor epoxide, lindane, methoxychlor, mirex, tetradifon and trifluralin. Stock solutions containing 80–150 ppm were prepared by dissolving the analytical reference standards in benzene and diluting to 50 ml in a volumetric flask. These solutions were stored in glass bottles under refrigeration (0°C). Suitable dilutions were made to obtain more dilute standard solutions and mixtures in *n*-hexane.

Sample

About 1.1 kg of bonito fish (*Thynnus pelamys*) sample, taken as recomended by Aminot and Chaussepied [20], was cut, blended and spiked with pesticides as indicated in Table I. Subsequently the sample was freeze dried.

Extraction

A 5-g amount of sample was weighed and extracted in a Soxhlet extractor with 150 ml of *n*-hex-

TABLE I

FORTIFICATION LEVELS IN UNLYOPHILIZED SAMPLE

Pesticide	ppb[a] (w/w)	Pesticide	ppb (w/w)
Captan	37	Endosulfan-II	42
Chlorfenson	49	Endrin	51
p,p'-DDD	64	HCB	42
o,p'-DDE	53	Heptachlor	36
p,p'-DDE	56	Heptachlor epoxide	42
o,p'-DDT	60	Lindane	43
p,p'-DDT	56	Methoxychlor	57
Dicofol	80	Mirex	52
Dieldrin	49	Tetradifon	69
Endosulfan-I	51	Trifluralin	42

[a] Throughout this article, the American billion (10^9) is meant.

ane for 4 h. The extract was concentrated to 10 ml in the rotary evaporator under vacuum.

Clean-up and fractionation

The elution volumes were 100 ml as required by the use of columns of 1.6 cm I.D. The three procedures are given in the form of instructions.

Standard procedure [19]. Pre-elute the column with 25–30 ml of light petroleum. Discard the eluted solutions until just before the sodium sulphate layer is exposed to air; quantitatively transfer 3 ml of sample extract into the column by careful decantation and subsequently wash with light petroleum ether (2 ml maximum). Adjust the elution rate to about 5 ml/min. Collect three fractions in 125-ml flasks using the following eluents: first, diethyl ether–light petroleum (6:94, v/v); second, diethyl ether–light petroleum (15:85, v/v); and third, diethyl ether–light petroleum (50:50, v/v). Alternatively, separate polychlorinated biphenyls (PCBs) by eluting first with 100 ml of light petroleum.

Stimac procedure [21]. This is a modification of the previous procedure. Pre-wash the column with 50 ml of diethyl ether–light petroleum (30:70, v/v) followed by 25 ml of light petroleum. Let the light petroleum elute down to 1–2 mm above the packing. Transfer 3.0 ml of the sample extract to the column. Rinse the walls of the column with 1 ml of light petroleum and elute at *ca.* 5 ml/min with 100 ml of diethyl ether–light petroleum (6:94, v/v).

Mills et al. procedure [22]. Pre-wet column with 40–50 ml of *n*-hexane. Transfer 3 ml of the sample extract solution to the column, allowing it to pass through at *ca.* 5 ml/min. Rinse the walls of the column with 1 ml of *n*-hexane. Elute the column with 100 ml of each of the following solvent mixtures: first, eluent A, dichloromethane–*n*-hexane (20:80, v/v), second, eluent B, dichloromethane–*n*-hexane (50:50, v/v) containing 0.35% (v/v) of acetonitrile; and third, eluent C, dichloromethane–*n*-hexane (50:50, v/v) containing 1.5% (v/v) of acetonitrile.

In all procedures, the sample extract must be dry and free from polar solvents when placed in the column.

Determination

Each eluted sample was evaporated to dryness in a rotary evaporator at 40°C under vacuum. The residue was dissolved in 1–2 ml of *n*-hexane, 40 ppb of aldrin as internal standard were added and the volume was made up to 5 ml with *n*-hexane. A 1-μl volume of this solution was injected into a gas chromatograph. The chromatographic peaks were identified by comparing their relative retention times with respect to the aldrin peak with those of the respective pesticide standards. Quantification was by internal standard calibration, measuring peak heights.

RESULTS AND DISCUSSION

Studies on standard mixtures

First, the experimental chromatographic conditions, mainly regarding the oven temperature programme, were optimized to separate the twenty pesticides studied in the 45–95 ppb range. The best results were given by the temperature programme specified under Experimental. The resulting chromatogram is shown in Fig. 1. It shows that the three pairs dieldrin–*p,p'*-DDE, *p,p'*-DDD–*o,p'*-DDT and dicofol–methoxychlor completely overlap (the first pair can be separated by changing chromatographic conditions, but not the other two pairs) and that the pair heptachlor epoxide–captan does not permit more than 98% separation; however, the other pesticides are clearly separated (>98%); the criterion used to judge this was a resolution higher than 1. Individual determination of the above overlapping pairs requires previous fractionation by one of the three procedures specified under Experimental.

The analytical characteristics obtained by injecting pesticide standard mixtures in which no peak overlap appeared are shown in Table II. Internal calibration graphs were prepared in all instances using 1.8 ppm of aldrin; this concentration was useful for relative comparison purposes over the whole pesticide concentration range studied. The detection limit was defined as $2N/S$ [23], where S is the slope of the calibration graph and N is the noise; it was determined for low attenuation and then the software was used to convert it into the attenuation employed in the above expression. Under these conditions, the detection limits ranged between 24 and 80 ppt (10^{12}). The calibration graphs were linear over five orders of magnitude. The relative standard deviations for eight determinations at a concentration level of about 40 ppb, using 40 ppb of aldrin as internal standard, were 0.8–2.2%. The pesticides

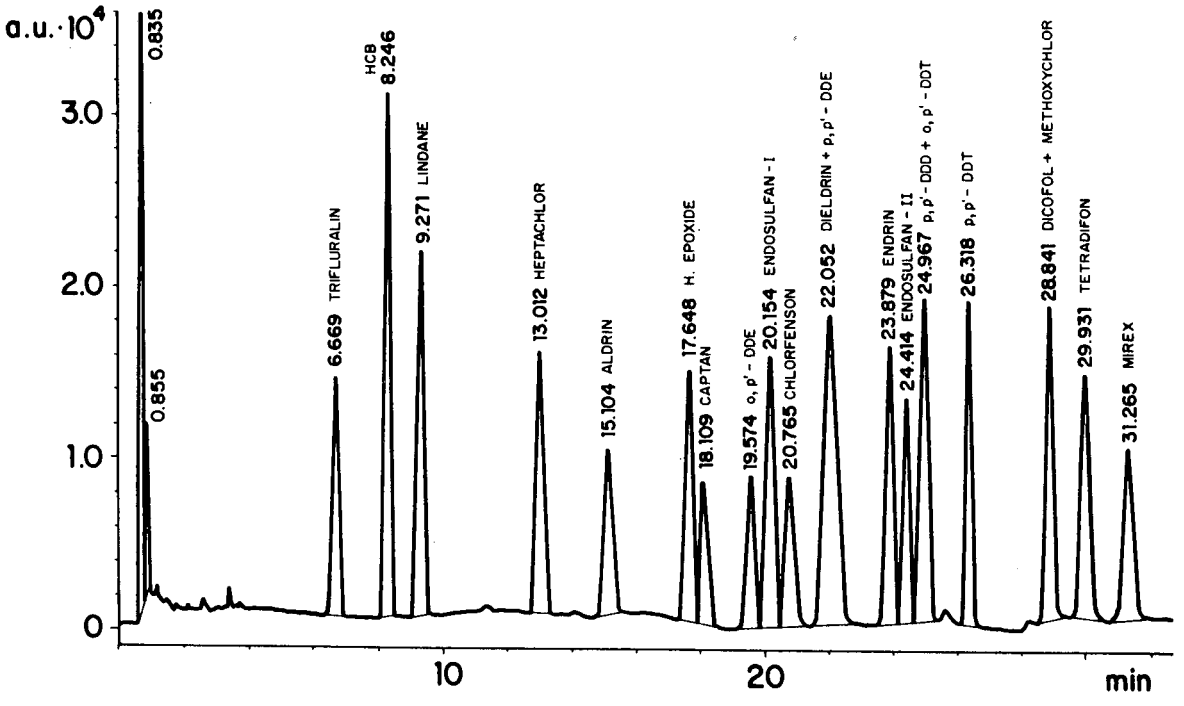

Fig. 1. Gas chromatogram of pesticides. For conditions of analysis, see Experimental.

TABLE II

ANALYTICAL CHARACTERISTICS

Conditions as in Results and Discussion section. S = sensitivity; D.L. = detection limit ($2N/S$); Detn.L. = determination limit ($10N/S$); L.U.L. = linear upper limit; R.S.D. = Relative standard deviation for eight determinations.

Pesticide	S [μV (ppb)$^{-1}$]	D.L. (ppb)	Detn.L. (ppb)	L.U.L. (ppb × 10^4)	R.S.D. (%)
Captan	85	0.025	0.126	1.22	1.69
Chlorfenson	33	0.064	0.322	3.11	0.85
p,p'-DDD	41	0.053	0.263	2.54	1.62
o,p'-DDE	33	0.065	0.325	2.91	1.87
p,p'-DDE	47	0.046	0.230	2.10	2.20
o,p'-DDT	27	0.080	0.401	3.84	1.24
p,p'-DDT	40	0.053	0.267	2.56	2.17
Dicofol	44	0.049	0.243	2.59	1.93
Dieldrin	51	0.042	0.212	2.01	1.32
Endolfulfan-I	61	0.035	0.177	1.67	1.30
Endosulfan-II	55	0.039	0.197	1.91	2.17
Endrin	54	0.040	0.198	1.87	1.18
HCB	67	0.032	0.161	1.50	0.79
Heptachlor	71	0.031	0.153	1.43	0.93
Heptachlor epoxide	85	0.025	0.126	1.14	1.53
Lindane	91	0.024	0.118	1.14	1.58
Methoxychlor	28	0.076	0.380	3.60	2.21
Mirex	39	0.055	0.276	2.63	1.98
Tetradifon	35	0.061	0.305	2.15	2.11
Trifluralin	27	0.081	0.404	1.84	1.67

TABLE III

RETENTION TIMES

Conditions as in Experimental. t_R = absolute retention time; RRT = relative retention time with respect to aldrin as internal standard.

Pesticide	t_R (min)	RRT
Trifluralin	6.669	0.442
HCB	8.246	0.546
Lindane	9.271	0.614
Heptachlor	13.012	0.862
Aldrin	15.104	1.000
Heptachlor epoxide	17.648	1.168
Captan	18.109	1.199
o,p'-DDE	19.574	1.296
Endosulfan-I	20.154	1.334
Chlorfenson	20.765	1.375
p,p'-DDE	22.052	1.460
Dieldrin	22.052	1.460
Endrin	23.879	1.581
Endosulfan-II	24.414	1.616
p,p'-DDD	24.967	1.653
o,p'-DDT	24.967	1.653
p,p'-DDT	26.318	1.742
Dicofol	28.841	1.909
Methoxychlor	28.841	1.909
Tetradifon	29.931	1.982
Mirex	31.265	2.070

were identified by comparing their retention times with those of aldrin. The results are given in Table III.

Studies on spiked lipid samples

Clean-up. The *n*-hexane extracts obtained from spiked lipid samples were fractionated by following the three procedures specified under Experimental; the non-spiked sample did not give significant peaks. Regarding the removal of lipids from the extracts, which is necessary for the use of ECD, the blanks obtained from the three procedures (first-eluted fraction) are shown in Fig. 2. The standard and Stimac procedures gave similar, fairly clean chromatograms with no significant peaks at the retention times at which pesticides are eluted. This was also so with the Mills *et al.* procedure, although the noise in the blank was clearly higher; in fact, the eluted fractions showed slight turbidity.

Fractionation and recoveries. The results of fractionation, after passing the extracts through the Florisil column and eluting as detailed under Experimental, are given in Tables IV–VI. Recoveries were calculated from internal calibration graphs. Different standard pesticide mixtures in the concentration range 5–140 ppb, also containing 40 ppb of aldrin as internal standard, were used to prepare these calibration graphs. In the standard procedure, no pes-

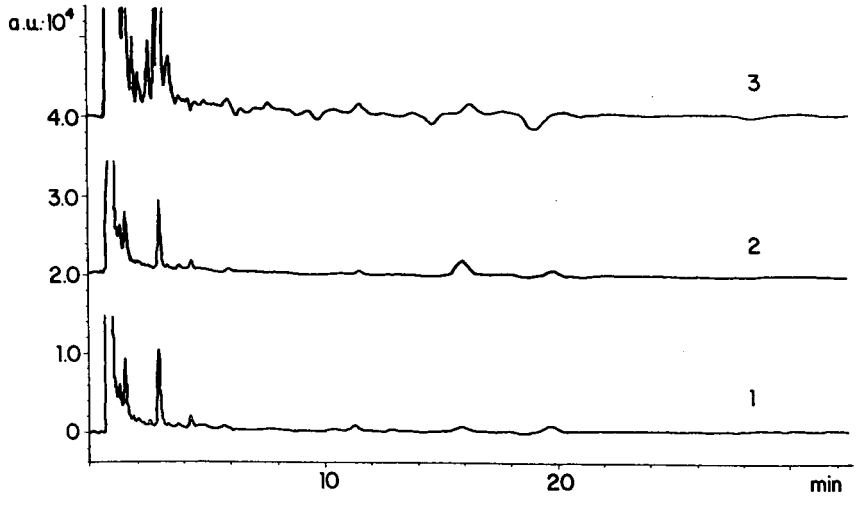

Fig. 2. Gas chromatograms from unfortified sample extracts. For conditions of analysis, see Experimental. Procedures: 1 = standard [19]; 2 = Stimac [21]; 3 = Mills *et al.* [22].

TABLE IV

STANDARD PROCEDURE [19]: FRACTIONATION AND RECOVERIES

Conditions as in Experimental. DE–LP = diethyl ether–light petroleum; Rec. = recovery and R.S.D. = relative standard deviation for six determinations.

Pesticide	Eluent					
	DE–LP (6:94, v/v)		DE–LP (15:85, v/v)		DE–LP (50:50, v/v)	
	Rec. (%)	R.S.D. (%)	Rec. (%)	R.S.D. (%)	Rec. (%)	R.S.D. (%)
Captan	–		–		90.2	5.12
Chlorfenson	–		101.3	8.07	–	
p,p'-DDD	93.5	6.98	–		–	
o,p'-DDE	94.8	6.97	–		–	
p,p'-DDE	95.3	5.74	–		–	
o,p'-DDT	99.2	7.25	–		–	
p,p'-DDT	100.5	9.20	–		–	
Dicofol	87.8	6.58	–		–	
Dieldrin	–		92.8	9.35	–	
Endosulfan-I	–		91.7	5.80	–	
Endosulfan-II	–		–		99.7	8.83
Endrin	–		89.8	7.26	–	
HCB	98.2	7.16	–		–	
Heptachlor	99.7	7.14	–		–	
Heptachlor epoxide	92.7	4.99	–		–	
Lindane	96.5	6.93	–		–	
Methoxychlor	98.2	6.22	–		–	
Mirex	99.3	10.06	–		–	
Tetradifon	–		–		97.0	6.71
Trifluralin	90.8	4.54	–		–	

ticide appeared in significant amounts in more than one eluted fraction. Further, no disagreements appeared with respect to the data from the literature.

The Stimac procedure involves partial Florisil deactivation by running 50 ml of diethyl ether–light petroleum (30:70, v/v) before the sample; this may explain differences from the standard procedure, although both of them use diethyl ether–light petroleum (6:94, v/v) as the first eluent. When the Stimac procedure was used, two pesticides, dieldrin and endrin, were distributed over two eluted fractions, which was not in agreement with the literature. The reproducibility, expressed as the relative standard deviation, confirmed these results. An eluent consisting of diethyl ether-light petroleum (35:65, v/v) was necessary to elute these pesticides completely in addition to captan, chlorfenson, endosulfan-II and tetradifon.

When the Mills *et al.* procedure was used, only heptachlor epoxide was distributed over two eluted fractions, and dicofol was limited to eluted fraction B; these results are in disagreement with those reported in the original paper by Mills *et al.* [22]. According to Mills *et al.* [22], heptachlor epoxide should appear in eluted fraction B and dicofol should be distributed over eluted fractions A and B. This disagreement was also found using hexane pesticide standard solutions, so it cannot be attributed to the polarity of the sample. No explanation has been found.

The results obtained and the relative standard deviations are given in Tables IV–VI. They show that total recoveries are close to 100%. It must be emphasized that the relative standard deviations are usually lower than 10–11% except for those pesticides which are distributed over two eluted fractions such as dieldrin and endrin in the Stimac procedure. These results are compared in Table VII

TABLE V

STIMAC PROCEDURE [21]: FRACTIONATION AND RECOVERIES

Conditions as in Experimental. Abbreviations as in Table IV.

Pesticide	Eluent			
	DE–LP (6:94, v/v)		DE–LP (35:65, v/v)[a]	
	Rec. (%)	R.S.D. (%)	Rec. (%)	R.S.D. (%)
Captan	–		88.8	6.66
Chlorfenson	–		99.5	8.45
p,p'-DDD	94.5	4.95	–	
o,p'-DDE	94.7	4.80	–	
p,p'-DDE	96.5	4.76	–	
o,p'-DDT	97.3	4.89	–	
p,p'-DDT	101.2	7.51	–	
Dicofol	88.7	5.28	–	
Dieldrin	22.3	44.98	78.0	10.09
Endosulfan-I	107.7	5.17	–	
Endosulfan-II	–		97.8	3.00
Endrin	14.5	24.97	77.7	10.09
HCB	98.2	7.16	–	
Heptachlor	102.8	8.81	–	
Heptachlor epoxide	94.2	5.94	–	
Lindane	96.0	9.61	–	
Methoxychlor	101.2	7.19	–	
Mirex	102.0	7.86	–	
Tetradifon	–		94.7	5.33
Trifluralin	88.5	7.56	–	

[a] This fraction was not used in the original Stimac method.

and Fig. 3, in which these aspects are apparent. For pesticides distributed over two eluted fractions the total percentage was used for calculation purposes.

Precision and accuracy. The precision and accuracy of the three methods were compared by analysis of variance (ANOVA) [24,25]. The relative standard deviations were not different at the 0.05 significance level. Regarding accuracy, significant differences at the 0.05 significance level were observed only for dicofol and captan. For these compounds, the best procedure seems to be that proposed by Mills *et al.* [22], as its precision is similar to that of the other procedures studied but its recoveries are closer to 100%.

CONCLUSIONS

We conclude that the three methods studied give good and similar results for the determination of eighteen of the twenty organochlorine pesticides studied. However, the method of Mills *et al.* [22] seems to be superior for the determination of dicofol and captan because its precision is similar to that of the other two methods but the recoveries are closer to 100%; the standard method seems the most suitable with regard to lipid removal from the *n*-hexane extracts and pesticide distribution in a single eluted fraction.

TABLE VI

MILLS *et al.* PROCEDURE [22]: FRACTIONATION AND RECOVERIES

Conditions as in Experimental. For eluents A, B and C, see procedure; Rec. and R.S.D. as in Table IV.

Pesticide	Eluent					
	A		B		C	
	Rec. (%)	R.S.D. (%)	Rec. (%)	R.S.D. (%)	Rec. (%)	R.S.D. (%)
Captan	–		–		105.8	5.46
Chlorfenson	–		106.3	6.11	–	
p,p'-DDD	88.7	4.60	–		–	
o,p'-DDE	92.0	3.76	–		–	
p,p'-DDE	95.3	6.00	–		–	
o,p'-DDT	96.7	5.31	–		–	
p,p'-DDT	99.7	3.57	–		–	
Dicofol	–		106.8	3.31	–	
Dieldrin	–		96.7	3.68	–	
Endosulfan-I	–		98.3	3.26	–	
Endosulfan-II	–		101.7	5.48	–	
Endrin	–		96.0	4.97	–	
HCB	91.3	6.27	–		–	
Heptachlor	95.7	4.61	–		–	
Heptachlor epoxide	13.8	11.59	87.3	4.08	–	
Lindane	91.3	10.77	–		–	
Methoxychlor	–		99.2	3.22	–	
Mirex	95.8	5.34	–		–	
Tetradifon	–		98.2	4.88	–	
Trifluralin	–		95.0	10.32	–	

TABLE VII

TOTAL RECOVERIES OF PESTICIDES BY THE THREE METHODS STUDIED

No.	Pesticide	Recovery (%)		
		Standard [19]	Stimac [21]	Mills *et al.* [22]
1	Captan	90.2	88.8	105.8
2	Chlorfenson	101.3	99.5	106.3
3	*p,p'*-DDD	93.5	94.5	88.7
4	*o,p'*-DDE	94.8	94.7	92.0
5	*p,p'*-DDE	95.3	96.5	95.3
6	*o,p'*-DDT	99.2	97.3	96.7
7	*p,p'*-DDT	100.5	101.2	99.7
8	Dicofol	87.8	88.7	106.8
9	Dieldrin	92.8	100.3	96.7
10	Endosulfan-I	91.7	107.7	98.3
11	Endosulfan-II	99.7	97.8	101.7
12	Endrin	89.8	92.2	96.0
13	HCB	98.2	100.2	91.3
14	Heptachlor	99.7	102.8	95.7
15	Heptachlor epoxide	92.7	94.2	101.2
16	Lindane	96.5	96.0	91.3
17	Methoxychlor	98.2	101.2	99.2
18	Mirex	99.3	102.0	95.8
19	Tetradifon	97.0	94.7	98.2
20	Trifluralin	90.8	88.5	95.0

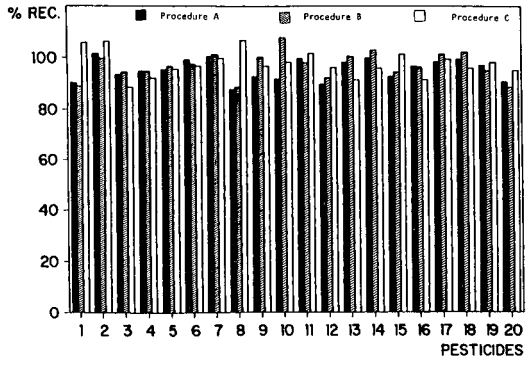

Fig. 3. Comparison of recoveries. Procedures: A = standard [19]; B = Stimac [21]; C = Mills *et al.* [22]. Compound numbers as in Table VII.

ACKNOWLEDGEMENT

The financial support of the Spanish DGICYT, Project PB89-0109, is gratefully acknowledged.

REFERENCES

1 J. Satsmadjis and B. Iatridis, *Centro*, 2 (1985) 57.
2 M. Marchand, D. Vas and E. K. Duursma, *Mar. Pollut. Bull.*, 7 (1976) 65.
3 O. Basturk, M. Dogan, I. Salihoglu and T. Y. Balkas, *Mar. Pollut. Bull.*, 11 (1980) 191.
4 R. Dubrawski and J. Falandysz, *Mar. Pollut. Bull.*, 11 (1980) 15.
5 A. H. Knap and T. D. Jickels, *Mar. Pollut. Bull.*, 14 (1983) 217.
6 J. A. García-Regueiro, I. Díaz and J. M. Monfort, *Rev. Agroquím. Tecnol. Aliment.*, 27 (1987) 405.
7 M. L. Ribeiro, J. L. Monfardini and A. Del'Acqua, *Ecletica Quim.*, 13 (1988) 81.
8 M. Camps, J. Planas, J. Gómez-Catalán, M. Sabroso, J. To-Figueras and J. Corbella, *Bull. Environ. Contam. Toxicol.*, 42 (1989) 195.
9 V. Contardi, R. Capelli, G. Zanicchi and M. Drago, *Analyst (London)*, 108 (1983) 510.
10 Q. Zhang, *Yankuang Ceshi*, 8 (1989) 122.
11 A. Venant, S. Borrel and L. Richou-Bac, *Analusis*, 10 (1982) 333.
12 L. K. Marble and J. J. Delfino, *Am. Lab.*, 20 (1988) 23.
13 A. R. Erney, *J. Assoc. Off. Anal. Chem.*, 66 (1983) 969.
14 Y. Tonagai, Y. Hasegawa, Y. Nakamura, S. Fujimo and Y. Ito, *Food Protect*, 52 (1989) 92.
15 A. D. Viveros, L. A. Albert and D. Namihira, *Rev. Toxicol.*, 6 (1989) 209.
16 J. Satsmadjis, E. Georgakopoulos-Gregoriades and F. Voutsinou-Taliadouri, *J. Chromatogr.*, 437 (1988) 254.
17 A. V. Holden and K. Marsden, *J. Chromatogr.*, 44 (1969) 481.
18 P. A. Mills, *J. Assoc. Off. Anal. Chem.*, 51 (1968) 29.
19 American Public Health Association, *Standard Methods for the Examination of Water and Wastewater*, Joint Editorial Board, Washington, DC, 12th ed., 1980.
20 A. Aminot and M. Chaussepied, *Manuel des Analyses Chimiques en Milieu Marin*, Centre National pour l'Exploitation des Océans, Paris, 1983.
21 R. M. Stimac, *J. Assoc. Off. Anal. Chem.*, 62 (1979) 85.
22 P. A. Mills, B. A. Bong, L. R. Kamps and J. A. Burke, *J. Assoc. Off. Anal. Chem.*, 55 (1972) 39.
23 L. Gascó, *Teoria y Prática de la Cromatografia en Fase Gaseosa*, J.E.N., Madrid, 1969.
24 J. Hilman and G. V. Glass, *J. Educ. Meas.*, 4 (1967) 41.
25 W. G. Cochran and G. M. Cox, *Diseños Experimentales*, Trillas, Madrid, 1974.

Journal of Chromatography, 591 (1992) 313–323
Elsevier Science Publishers B.V., Amsterdam

CHROM. 23 799

Comparison of commercially available atomic emission and chemiluminescence detectors for sulfur-selective gas chromatographic detection

Sally E. Eckert-Tilotta, Steven B. Hawthorne* and David J. Miller

Energy and Environmental Research Center, P.O. Box 8213, University Station, University of North Dakota, Grand Forks, ND 58202 (USA)

(Received August 13th, 1991)

ABSTRACT

The determination of sulfur with sulfur chemiluminescence detection (SCD) and microwave-induced plasma atomic emission spectroscopic detection (AED) was compared for ten aliphatic and aromatic sulfur-containing organic compounds. Each detector was shown to be a sensitive and specific detector for sulfur present in different molecular forms. The linear dynamic range (LDR) for AED was independent of sulfur species at 10^5, whereas the LDR for the SCD was generally 10^4. The detection limit for both detectors was *ca.* 6–10 pg injected sulfur. Under conditions which optimized the SCD response for sulfur, the LDR for hydrocarbons using flame ionization detection (FID) (required for SCD operation) was similar to the 193-nm carbon emission line for the AED, but the sensitivities and reproducibilities with FID–SCD were poorer. The results of this study demonstrate that the selection of AED or SCD for sulfur detection is dependent on cost and whether the need is for a sulfur-only detector or a multi-element detector.

INTRODUCTION

The qualitative and quantitative determination of sulfur species in complex samples is becoming increasingly important to understand the sources of sulfur contamination and develop methods for removing them from the matrices of interest. For example, organic sulfur species are oxidized and released to the environment during combustion of fuels. These species are thought to exist in fuels as a mixture of thiols, sulfides, disulfides and thiophenes [1]. In addition to contributing to air pollution, many of these species are known to be mutagenic [2], affect the storage stability of petroleum products [3] and be detrimental to the catalysts used in processing hydrocarbon fuels [4].

One of the most frequently chosen methods for organic sulfur determination involves high-resolution gas chromatography (GC) with flame photometric detection (FPD). Although FPD is inexpensive and selective and sensitive to sulfur, it has several disadvantages. The response is dependent on the environment of the sulfur atom and is subject to quenching by co-eluting hydrocarbons and water [5,6]. Two other sulfur-selective detection methods have recently become commercially available. Sulfur chemiluminescence detection (SCD) takes advantage of the fact that SO is produced during flame ionization detection (FID) when organic sulfur species are introduced by gas chromatography [4,7,8]. When SO reacts with ozone, a strong blue chemiluminescence signal is emitted by the resulting excited SO_2*. The signal is isolated from other radiation from the reaction chamber and detected by a photomultiplier tube [4]. Whereas SCD is specific for sulfur, atomic emission spectrometric detection (AED) is a multi-element method capable of detecting elements with atomic emission lines in the vacuum-UV, UV, visible and near-IR portions of the electromagnetic spectrum [9,10]. Radiation from the microwave-induced plasma is dispersed on a diode array spectrometer to monitor several ele-

0021-9673/92/$05.00

ments at one time, including (but not limited to) C, H, S, N, O, P, halogens and many metals. The data are collected and manipulated by a computer.

Selectivity and sensitivity are minimum requirements for a useful sulfur detector for real, complex samples. Ideally, the detector will have a constant response per unit mass of sulfur regardless of the chemical form of the sulfur species that elutes from the gas chromatographic (GC) column. In addition, as sulfur components in real samples often co-elute with hydrocarbons present in much larger amounts (*e.g.*, fuels), a useful sulfur detector should not show a change in sulfur response regardless of the presence of co-eluting hydrocarbons.

The aim of this work was to compare SCD and AED for a variety of sulfur-containing organics. In addition, the carbon response with AED is compared with the hydrocarbon response obtained with FID–SCD. The detectors were characterized using laboratory-prepared sulfur standards and chromatograms of real samples.

EXPERIMENTAL

Apparatus

The Model 350 sulfur chemiluminescence detector for SCD was provided by Sievers Research (Boulder, CO, USA). This detector was coupled in accordance with the manufacturer's specifications directly to a Hewlett-Packard (Avondale, PA, USA) Model 5890 gas chromatograph through a probe assembly attached to the FID flame ionization detector. The probe assembly was placed at a height of 6.0 mm above the flame of the flame ionization detector. The flow-rates of the hydrogen and oxygen in the flame ionization detector were measured to be 348 and 185 ml/min, respectively, for all analyses. The air pressure to the ozone generator in the sulfur chemiluminescence detector was maintained at 8 p.s.i. The flame ionization detector temperature was 350°C. The sulfur chemiluminescence detector allows smoothing of the millivolt output by an operator-selected integration time. An integration constant of 0.12 s was chosen to maximize the sulfur signal. The output was directed to a Hewlett-Packard Model 3393A integrator equipped with a Hewlett-Packard Model 9122 disk drive for data storage.

Detector gas flow-rates and probe placement for the SCD instrument were optimized by maximizing the sulfur signal from 1-μl injections of a 50 pg/μl solution of methyl ethyl sulfide in benzene. Interference from carbon signals can be seen on the SCD output when the hydrogen-to-air ratio is adjusted incorrectly, resulting in negative peaks when the flame ionization detector flame is hydrogen poor and positive peaks when the flame is hydrogen rich. The conditions were considered to be optimum when the maximum sulfur signal occurred with no response to carbon.

The AED system was a Hewlett-Packard Model 5921A microwave plasma emission detector coupled with a Hewlett-Packard Model 5890 series II gas chromatograph. Data acquisition and manipulation were performed through a ChemStation, a computer and software package provided by Hewlett-Packard. The instrumental design and data manipulation techniques are described elsewhere [9,10]. Sulfur and carbon were monitored on the AED system at the vacuum-UV wavelengths of 181.037 and 193.030 nm, respectively, using the manufacturer's recommended conditions. Helium supply gas for the plasma was maintained at 30 p.s.i. and the cavity pressure was 1.5 p.s.i. Unless noted otherwise, solvent was vented for the first 3.2 min of each chromatographic run to protect the plasma discharge tube from soot build-up.

The chromatographic conditions used with each detector were as identical as possible. All standard analyses were performed with 1-μl splitless injections (1 min) using an HP 7673 autosampler. The same DB-5 (30 m × 320 μm I.D., film thickness 1.0 μm) capillary column (J&W Scientific) was used for all SCD and AED standard analyses. The GC temperature programs for the sulfur standards were 60°C initially for 1 min with an increase at 8°C/min to 330°C. Both injection ports were at 300°C.

Preparation of standards and samples

Standard solutions were prepared using analytical-reagent grade chemicals (purity $\geqslant$ 95%) as received. Approximately 0.2 g of each sulfur compound was dissolved in 100 ml of benzene to prepare a stock solution. Appropriate dilutions in benzene were made to obtain 22 standards with concentrations ranging from 5 pg to 0.9 μg/μl of sulfur, corrected for the purity of the sulfur standard component. Each sulfur standard dilution was injected

on three different days using each detector system. This procedure was used to yield "worst case" results, as both detector systems were set up each day to run the series of standards.

RESULTS AND DISCUSSION

Sulfur response and reproducibility

Representative standard chromatograms obtained with SCD and AED are shown in Fig. 1. In general, the peak shapes are comparable in each detector system, indicating no loss in chromatographic resolution due to the detectors. The cause of randomly occurring negative peaks on the SCD trace is unclear, but this interference has since been removed by installing a heated transfer line (now standard on this instrument) between the probe and detector. A comparison of methyl ethyl sulfide for each detector could not be made as this compound elutes near the solvent peak, and the solvent was

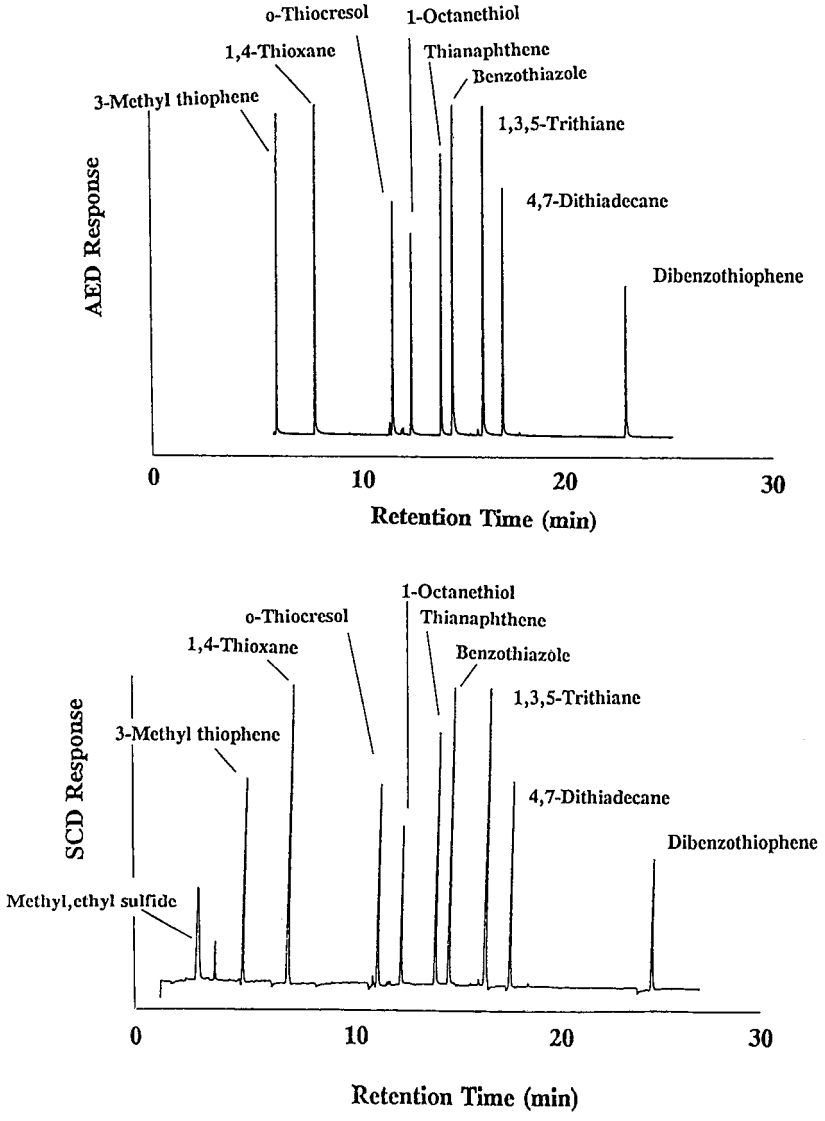

Fig. 1. Representative chromatograms for sulfur standards obtained using (top) AED and (bottom) SCD. Chromatographic oven program for both: 60°C for 1 min, increased at 8°C/min to 330°C.

TABLE I

SIGNAL-TO-NOISE RATIOS (*S/N*) FOR LOW-CONCENTRATION SULFUR STANDARDS

Component	Sulfur (*pg*)[a]	*S/N*[b]		Sulfur (pg)	*S/N*	
		SCD	AED		SCD	AED
Methyl ethyl sulfide	9.2	1.0	ND[c]	27.6	4.1	ND
3-Methylthiophene	6.7	3.9	5.1	20.1	7.6	23.0
1,4-Thioxane	9.1	2.1	5.4	27.4	10.7	8.9
o-Thiocresol	6.8	1.2	3.0	20.4	5.3	8.4
1-Octanethiol	4.9	1.0	2.4	14.7	3.5	14.8
Thianaphthene	5.9	1.2	3.5	17.6	7.3	27.8
Benzothiazole	8.9	2.8	11.0	26.7	8.9	35.1
1,3,5-Trithiane	14.1	2.5	10.0	42.2	12.7	12.7
4,7-Dithiadecane	5.7	1.3	3.2	17.1	6.1	9.0
Dibenzothiophene	3.7	1.1	3.0	11.0	4.3	14.8

[a] Amount of S present for each species in the 1-μl splitless injections.
[b] Values are averages of three injections.
[c] ND = Not determined. This species eluted during the solvent vent step using AED.

vented from the AED system to prevent soot build-up on the quartz emission tube.

Both detectors have sulfur detection limits in the low picogram range. Table I lists the signal-to-noise ratio (*S/N*) for the samples containing the two lowest concentrations of each sulfur-containing organic standard. The amount of sulfur injected was calculated from the mass of each standard in the 1-μl splitless injections. Noise was determined as peak-to-peak baseline measurements collected over 60 s. As shown in Table I, the lowest standard used was at or below the detection limit for SCD, if the minimum detection limit for each sulfur component is defined as $S/N \geqslant 3$. Six of the ten sulfur responses are statistically indistinguishable from the noise. As can be seen from Table I, the *S/N* of these components from a more concentrated solution (sulfur amounts equaling three times those in the most dilute sample) range from 3.5 to 12.7, all above the detection limit. While the sensitivity of AED is slightly better, the *S/N* is generally less than four times that of SCD, indicating similar sensitivities for both detectors.

Because the standard dilutions were run as a set, and each set was run on a different day, each instrument was essentially set up on three separate occasions. Thianaphthene was arbitrarily chosen as the internal standard (sulfur response factor = 1.000), and response factors for the remaining sulfur compounds were calculated as peak areas per picogram of sulfur injected relative to thianaphthene (also corrected for the mass of sulfur). Both detectors show a relatively constant chromatographic mass response despite the different molecular forms of sulfur. Table II lists response factors for sulfur for four representative standard dilutions ranging from *ca.* 50 to *ca.* $4 \cdot 10^5$ pg/μl of sulfur injected. Peak areas are averages of the three replicate injections of the sulfur standard performed on three different days as described earlier. The sulfur response (determined chromatographically) increased with increasing retention time for both detectors (opposite from the trend expected from splitter discrimination). Similar changes in response with run time are also seen from the AED carbon response. The response factors for *o*-thiocresol and 1-octanethiol (species with weakly acidic hydrogens) are possibly low because of integration errors caused by chromatographic peak tailing associated with acids. The response factors for 1,3,5-trithiane determined with SCD were also low, whereas the AED response for this compound followed the trend of increased response with increasing retention time. The low SCD response may be due to inefficient SO production for this compound.

Table III lists the relative standard deviations (R.S.D.s) for both the raw peak areas (not relative to the internal standard) and the peak areas of each

TABLE II

RESPONSE FACTORS (RRF) PER UNIT MASS OF SULFUR RELATIVE TO THIANAPHTHENE FOR REPRESENTATIVE SULFUR STANDARDS

Component	Sulfur injected (pg)[a]	RRF[b]		Sulfur injected (pg)	RRF		Sulfur injected (pg)	RRF		Sulfur injected (ng)	RRF	
		SCD	AED		SCD	AED		SCD	AED		SCD	AED
Methyl ethyl sulfide	64.4	0.725	ND[c]	828	0.596	ND	8280	0.614	ND	449	0.973	ND
3-Methylthiophene	47.0	0.653	0.781	604	0.662	0.792	6040	0.702	0.755	365	0.683	0.768
1,4-Thioxane	63.8	0.928	0.876	820	0.806	0.931	8210	0.759	0.891	474	0.649	0.823
o-Thiocresol	47.5	0.614	0.557	611	0.659	0.634	6110	0.783	0.792	326	0.896	0.904
1-Octanethiol	34.3	0.645	0.731	442	0.679	0.783	4420	0.789	0.827	264	1.034	0.945
Benzothiazole	62.3	0.927	0.882	802	0.810	0.923	8020	0.804	0.855	432	0.750	0.912
1,3,5-Trithiane	98.5	0.671	0.999	1270	0.789	1.005	12 700	0.630	0.939	721	0.535	0.934
4,7-Dithiadecane	39.9	0.790	0.885	513	0.966	0.914	5130	0.938	0.915	310	0.957	1.124
Dibenzothiophene	25.8	0.990	0.996	332	0.914	1.013	3320	0.980	1.013	185	1.211	1.231

[a] Amount of S present for each species in the 1-μl splitless injections.
[b] RRF = Relative response factor. Values are averages of three runs performed on three days.
[c] ND = Not determined.

component relative to the thianaphthene internal standard for the same four standard dilutions shown in Table II. The R.S.D.s for raw peak areas for injections on three different days were higher (typically 5–15%) with SCD than with AED (typically 5%, with a few values as high as 15%). The R.S.D.s for injections on three different days relative to the internal standard were similar for both detectors, with nearly all the standards showing acceptable day-to-day reproducibility (< 5% R.S.D.).

The linear dynamic range (LDR) with AED is less compound dependent than that with SCD, and it consistently remains approximately one decade greater than that for the corresponding component determined with SCD. Typical calibration graphs [ln (peak area) *vs.* ln (mass of sulfur)] are shown in Fig. 2 for 1,3,5-trithiane and dibenzothiophene. The calibration graphs for the remaining sulfur standards are very similar to those shown. As shown in Fig. 2, the AED calibration graphs for each species appear to be linear over the entire concentration range studied, but the SCD plots curve downward between the points corresponding to 10^3 and 10^4 pg of sulfur. Based on visual inspection, linear regression correlation coefficients (r^2) were calculated for each detector from their detection limits to be *ca.* $3 \cdot 10^4$ pg of sulfur injected (all but the highest three standard concentrations) and from detection limits to be *ca.* $6 \cdot 10^5$ pg of sulfur injected (all standards) for each of the organic sulfur species. As can be seen in Table IV, all but 1,4-thioxane and 1,3,5-trithiane determined with SCD show $r^2 \geqslant 0.990$ at 10^4 pg of sulfur injected, but significantly lower correlation coefficients were obtained with SCD for each species calculated over the entire concentration range. In contrast, AED showed correlation coefficients > 0.990 for all of the test species over the entire concentration range. The LDRs determined are consistent with previously published data for both AED [9] and SCD [4]. The consistent LDRs for AED indicate that the compounds are stable over the chromatography portion of the analysis; hence the differences in LDRs are probably due to the detectors.

Hydrocarbon interference on sulfur response

To test the ability of SCD to determine sulfur in the presence of large amounts of co-eluting hydrocarbons, dilutions of 3-methylthiophene in toluene were injected into the SCD system at an oven temperature of 90°C so that the 3-methylthiophene eluted under the toluene solvent peak. A plot of picograms of sulfur, calculated as the mass of sulfur injected in a 1-μl injection, *versus* the average peak areas for duplicate injections is shown in Fig. 3. The lowest amount of sulfur shown is *ca.* 8 pg, and this amount is easily integrated. As previously seen in Table I, the S/N for 6.7 pg of sulfur was 3.9; hence

TABLE III

REPRODUCIBILITIES OF RAW PEAK AREAS AND PEAK AREAS RELATIVE TO INTERNAL STANDARD FOR DETERMINATIONS OF THREE DIFFERENT DAYS

Component	Sulfur (pg)[a]	R.S.D. (%)				Sulfur (pg)	R.S.D. (%)				Sulfur (pg)	R.S.D. (%)				Sulfur (ng)	R.S.D. (%)			
		Raw[b]		Relative[c]			Raw		Relative			Raw		Relative			Raw		Relative	
		SCD	AED	SCD	AED		SCD	AED	SCD	AED		SCD	AED	SCD	AED		SCD	AED	SCD	AED
Methyl ethyl sulfide	64.4	3.4	ND[d]	3.1	ND	828	14.8	ND	5.0	ND	8280	9.4	ND	4.8	ND	449	12.6	ND	4.2	ND
3-Methylthiophene	47.0	4.2	9.1	1.4	1.9	604	13.8	14.7	7.1	1.3	6040	14.5	3.5	3.5	0.6	365	5.4	4.5	3.5	0.9
1,4-Thioxane	63.8	8.3	3.7	1.9	1.3	820	13.1	5.2	4.1	3.7	8210	7.7	3.6	5.2	0.5	474	10.6	4.4	2.6	0.8
o-Thiocresol	47.5	1.6	5.4	0.5	2.7	611	2.9	7.5	2.0	6.4	6110	11.5	3.7	3.6	0.3	326	10.4	4.5	2.7	1.1
1-Octanethiol	34.3	12.3	9.9	2.2	1.8	442	9.1	4.7	5.3	2.1	4420	16.1	1.0	3.6	0.1	264	4.9	4.4	0.9	0.3
Benzothiazole	62.3	5.8	13.9	3.6	4.1	802	18.3	4.6	7.5	0.6	8020	11.6	2.1	4.7	0.5	432	3.8	4.0	1.1	0.5
1,3,5-Trithiane	98.5	18.7	2.9	1.8	0.8	1270	15.3	4.6	4.0	0.9	12 700	15.5	4.5	5.2	0.4	721	3.0	4.2	0.9	0.2
4,7-Dithiadecane	39.9	9.8	9.9	2.7	2.9	513	9.1	4.0	3.0	3.9	5130	10.5	5.5	5.1	0.2	310	10.8	4.2	1.5	0.6
Dibenzothiophene	25.8	19.0	5.2	3.7	3.4	332	15.8	2.6	5.4	1.7	3320	9.5	3.9	3.6	0.1	185	10.9	4.4	0.5	3.1

[a] Amount of S present for each species in the 1-μl splitless injections.
[b] R.S.D. in raw area counts for injections on three different days.
[c] R.S.D. in area counts relative to the internal standard for injections on three different days.
[d] ND = Not determined.

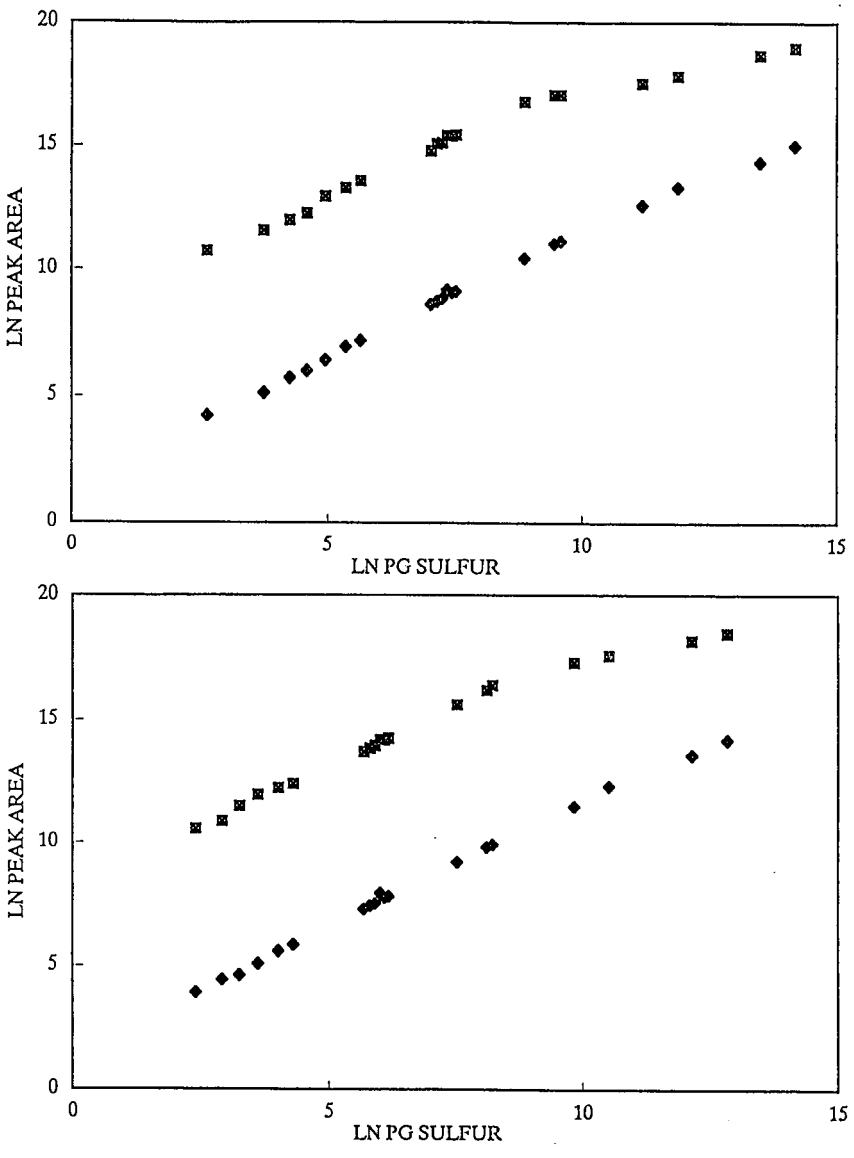

Fig. 2. Calibration graphs [ln (peak area) *vs.* (mass of sulfur)] for (top) 1,3,5-trithiane and (bottom) dibenzothiophene, determined using (◆) AED and (■) SCD.

one would not expect difficulty in integrating peaks at the 8-pg level if there were no interference from the large solvent peak. An additional sample containing *ca.* 0.8 pg of sulfur was injected but was not detected, as one would expect as this amount of sulfur is below the detection limit even without coelution of the toluene solvent peak. In addition, there was no detectable effect of toluene on a sample containing *ca.* 24 pg sulfur when compared with the sample injected at an oven temperature of 60°C, a temperature where 3-methylthiophene was resolved from the solvent. The calibration graph shown in Fig. 3 also shows good linearity (r^2 = 0.999) for the 3-methylthiophene, despite the coeluting toluene solvent peak.

Determining sulfur under a solvent peak as a

TABLE IV

LINEAR CORRELATION COEFFICIENTS (r^2) FOR SULFUR COMPONENT CALIBRATION GRAPHS

Component	r^2			
	SCD		AED	
	10–10^5 pg S[a]	10–10^4 pg S	10–10^5 pg S	10–10^4 pg S
Methyl ethyl sulfide	0.968	0.995	ND[b]	ND
3-Methylthiophene	0.952	0.991	0.993	0.998
1,4-Thioxane	0.942	0.984	0.992	0.997
o-Thiocresol	0.945	0.993	0.993	0.997
1-Octanethiol	0.952	0.994	0.995	0.998
Thianaphthene	0.953	0.994	0.994	0.998
Benzothiazole	0.942	0.990	0.993	0.998
1,3,5-Trithiane	0.953	0.985	0.994	0.997
4,7-Dithiadecane	0.938	0.992	0.994	0.998
Dibenzothiophene	0.971	0.997	0.996	0.997

[a] Approximate amount of sulfur injected. See Table I for the exact amounts for the detection limits and Table III for the highest amount injected (*ca.* 10^5 pg). The amount 10^4 pg represents a 1:10 dilution of the highest concentration.
[b] ND = Not determined.

strategy for detecting sulfur with large amounts of co-eluting hydrocarbon was not attempted with AED, because the solvent peak should be vented to reduce soot build-up and erosion of the discharge tube. However, the selectivity of one channel over another (*i.e.*, sulfur over carbon) for the AED instrument can be determined by measuring the ratio of the peak response per mole of sulfur *versus* the peak response per mole of carbon for interfering signals [9–11]. Eicosane, used as a carbon source,

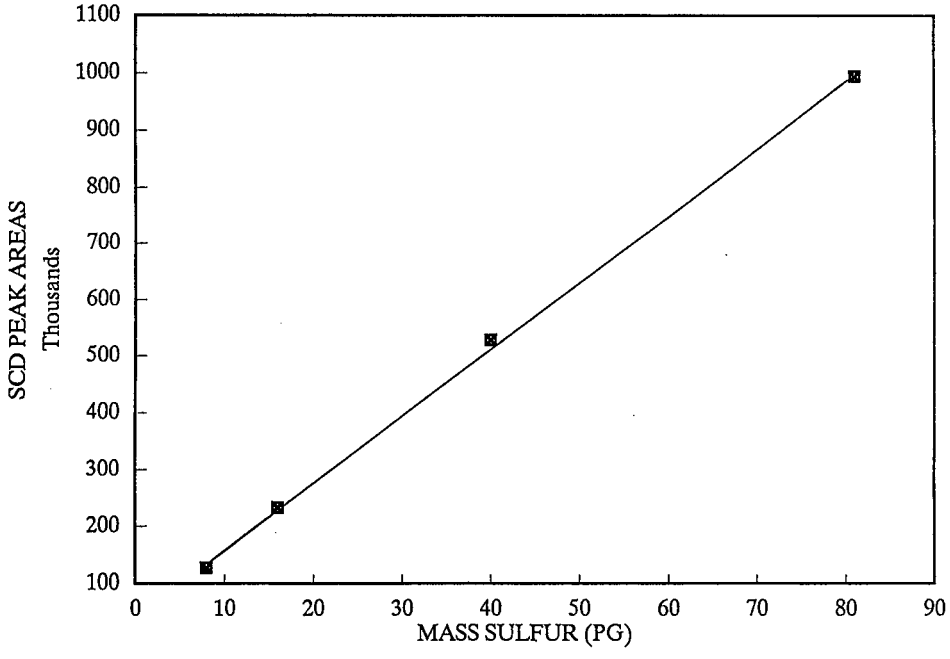

Fig. 3. Plot of SCD peak area *versus* mass of sulfur injected for 3-methylthiophene co-eluting with a toluene solvent peak.

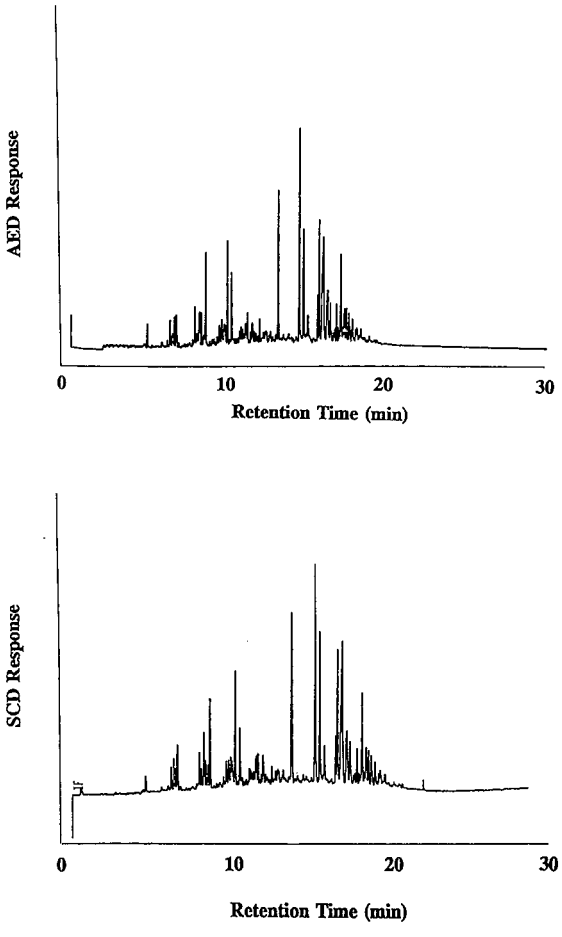

Fig. 4. Chromatograms for NIST 1624b standard for sulfur in diesel fuel obtained using (top) AED and (bottom) SCD. Injections of 1 μl were made on an HP-5 capillary column (25 m × 320 μm I.D., film thickness 0.17 μm) (Hewlett-Packard) in the split mode (*ca.* 1:20). Chromatographic oven program for both: 70°C for 1 min, increased at 8°C/min to 320°C.

was injected in the splitless mode and the 181-nm sulfur signal was monitored. Using the peak-to-peak noise as the sulfur signal (per mole), the selectivity for sulfur over carbon was calculated to be $> 10^4$. This is consistent with previous published reports of selectivity equalling $1.5 \cdot 10^5$ [9].

Fig. 4 shows sulfur responses from each of the detectors for a sample of diesel fuel (NIST 1624B standard reference materials for sulfur in diesel fuel). The chromatographic conditions were as identical as possible between the two detectors. The NIST standard, at *ca.* 0.33 wt.% total sulfur, was injected neat as a 1-μl volume split *ca.* 1:20. As seen in Fig. 4, chromatograms with AED and SCD for the NIST standard agree fairly closely. Neither baseline exhibits drifting, despite the large amounts of hydrocarbons that are co-eluting with the sulfur species, and good resolution is evident within groups of closely-eluting sulfur species.

Carbon and hydrocarbon response

The sulfur chemiluminescence detector utilizes SO produced from sulfur-containing species in the flame ionization detector to determine sulfur. To prevent carbon species from interfering, the flame ionization detector gases are set at a level that produces a reducing flame, a condition not optimum for detecting hydrocarbons. To determine if the flame ionization detector (with the sulfur chemiluminescence detector probe attached) is useful for determining hydrocarbons, the former detector signals for the sulfur standards were recorded in tandem with the sulfur signals from the latter detector. The results were compared with those collected using AED with the same samples by simultaneously measuring the 181-nm sulfur line and the 193-nm carbon signal. Data acquisition and manipulation for each element were accomplished by using the appropriate "recipes" provided by the manufacturer, and no modifications were made to optimize AED further. The following data treatment for carbon (AED) and hydrocarbon (FID–SCD) was performed similarly to the data treatment for sulfur as discussed in the previous section.

Table V gives the S/N values for samples with the corresponding masses of carbon for the lowest concentration standards detected by each detector. The mass of carbon was calculated similarly to that previously described for sulfur, *i.e.*, the amount of carbon in a 1-μl injection using the splitless mode. Although both detection methods are partly compound dependent, the FID–SCD system is clearly less sensitive than the AED system for all the compounds. As reported previously [4], some reduction in sensitivity would be expected as the flame ionization detector was not optimized for hydrocarbon response. However, the FID–SCD method is still useful for hydrocarbon detection in many applications, as nanogram amounts were detected for each component.

Detector response reproducibilities were deter-

TABLE V

SIGNAL-TO-NOISE RATIOS (*S/N*) FOR CARBON (AED) AND HYDROCARBON (FID–SCD) RESPONSES

Component	FID–SCD		AED	
	Carbon *(pg)*[a]	*S/N*[b]	Carbon (pg)	*S/N*
3-Methylthiophene	1110	10.4	139	30.1
1,4-Thioxane	1850	8.2	144	12.7
o-Thiocresol	1760	10.8	137	31.9
1-Octanethiol	1750	8.4	175	17.4
Thianaphthene	1510	13.6	132	14.4
Benzothiazole	2300	16.0	143	13.0
1,3,5-Trithiane	3120	8.9	44	15.8
4,7-Dithiadecane	1130	6.4	103	31.3
Dibenzothiophene	1410	8.2	176	10.9

[a] Amount of C present for each species in the 1-μl splitless injections.
[b] Values are averages of three injections.

mined in the same manner as that described for sulfur using thianaphthene as the internal standard, and the R.S.D.s and the relative responses (corrected by mass of carbon) of the other components were determined relative to thianaphthene. Again, the triplicate sample runs were designed to test a "worst case", with three runs performed on three separate days. The R.S.D.s for the FID–SCD peak areas are generally higher than the corresponding R.S.D.s for AED, and the R.S.D.s for raw peak areas and for peak areas relative to the internal standard were essentially identical with those in Table II for sulfur. The mass response for both detectors (listed in Table VI) also remained relatively constant, and both detectors showed an increase in chromatographic response with increasing retention time, similar to the trend seen for the sulfur signals. With the exception of 1,3,5-trithiane, both detectors showed good linearity ($r^2 > 0.990$) from their detection limits reported in Table V to the highest concentration tested (*ca.* 2 μg of carbon injected). The LDR for 1,3,5-trithiane was only *ca.* 10^2 with FID–SCD and 10^4 with AED.

CONCLUSIONS

Both the AED and the SCD instruments are sensitive, selective detectors for organic sulfur and respond on a relatively constant mass basis independent of the source of the sulfur. The sulfur linear dynamic ranges and the detection limits with AED were slightly better than those with SCD, but these differences are small enough that they may not be significant for most applications. Both detectors were reliable during the course of this study and required only minimum routine maintenance by the operator. AED has the advantage of being a multi-

TABLE VI

RESPONSE FACTORS PER UNIT MASS OF CARBON RELATIVE TO THIANAPHTHENE FOR REPRESENTATIVE CARBON STANDARDS

Component	Carbon injected (pg)[a]	RRF[b]		Carbon injected (pg)	RRF		Carbon injected (ng)	RRF		Carbon injected (ng)	RRF	
		FID–SCD	AED		FID–SCD	AED		FID–SCD	AED		FID–SCD	AED
3-Methylthiophene	139	ND[c]	0.620	1530	0.685	0.587	12.5	0.725	0.702	75.5	0.802	0.756
1,4-Thioxane	206	ND	0.633	2260	0.558	0.590	18.5	0.502	0.645	107	0.494	0.668
o-Thiocresol	195	ND	0.857	2150	0.749	0.794	17.6	0.817	0.838	93.9	0.914	0.960
1-Octanethiol	175	ND	0.731	1920	0.821	0.750	15.7	0.718	0.772	94.1	0.832	0.947
Benzothiazole	287	ND	0.822	3160	0.850	0.776	25.8	0.751	0.773	139	0.823	0.845
1,3,5-Trithiane	62.3	ND	0.891	686	ND	0.820	5.61	0.831	0.896	31.9	0.950	1.322
4,7-Dithiadecane	103	ND	0.803	1130	0.928	0.845	9.27	0.854	0.862	56	0.899	1.128
Dibenzothiophene	176	ND	1.010	1940	0.898	1.004	15.8	1.035	1.035	88.5	1.099	1.180

[a] Amount of C present for each species in the 1-μl splitless injections.
[b] Carbon response factor relative to internal standard. Values are averages of three runs performed on three days.
[c] Hydrocarbon amounts were below the detection limit.

element detection method, allowing the detection of many different elements (although only a few combinations of elements can be obtained simultaneously), while SCD can only be used for sulfur and for hydrocarbon detection. However, AED instrumentation is more expensive (*ca.* four times) and requires more laboratory space than SCD instrumentation.

ACKNOWLEDGEMENTS

Funding for this research was provided by the Department of Energy (Contract No. DE-FC21-86MC10637). We express our gratitude to Sievers Research for the loan of the sulfur chemiluminescence detector and to Marianne Novelli (Sievers Research) for many helpful discussions.

REFERENCES

1 R. C. Eliot (Editor), *Coal Desulfurization Prior to Combustion*, Noyes Data, Park Ridge, NJ, 1978, p. 33.
2 D. A. Eastmond, G. M. Booth and M. L. Lee, *Arch. Environ. Contam. Toxicol.*, 13 (1984) 105–111.
3 R. J. Skelton, Jr., H.-C. K. Chang, P. B. Farnsworth, K. E. Markides and M. L. Lee, *Anal. Chem.*, 61 (1989) 2292–2298.
4 R. L. Shearer, D. L. O'Neal, R. Rios and M. D. Baker, *J. Chromatogr. Sci.*, 28 (1990) 24–28.
5 S. Farwell and C. Barinaga, *J. Chromatogr. Sci.*, 24 (1986) 483–494.
6 J. N. Driscoll and A. W. Berger, *J. Chromatogr.*, 468 (1989) 303–308.
7 R. S. Hutte, R. E. Sievers and J. W. Birks, *J. Chromatogr. Sci.*, 24 (1986) 499–505.
8 R. L. Benner and D. H. Stedman, *Anal. Chem.*, 61 (1989) 1268–1271.
9 B. D. Quimby and J. J. Sullivan, *Anal. Chem.*, 62 (1990) 1027–1034.
10 J. J. Sullivan and B. D. Quimby, *Anal. Chem.*, 62 (1990) 1034–1043.
11 K. Tanabe, H. Haraguchi and K. Fuwa, *Spectrochim. Acta Part B*, 36 (1981) 633–639.

Journal of Chromatography, 591 (1992) 325–339
Elsevier Science Publishers B.V., Amsterdam

CHROMSYMP. 2470

Comparison of liquid-junction and coaxial interfaces for capillary electrophoresis–mass spectrometry with application to compounds of concern to the aquaculture industry☆,☆☆

S. Pleasance*,☆☆☆, P. Thibault and J. Kelly☆☆☆

**Institute for Marine Biosciences, National Research Council of Canada, 1411 Oxford Street, Halifax, Nova Scotia B3H 3Z1 (Canada)*

(First received July 17th, 1991; revised manuscript received October 12th, 1991)

ABSTRACT

The application of capillary electrophoresis–mass spectrometry (CE–MS) to the analysis of compounds of concern to the aquaculture industry is reported. Two different approaches to coupling the CE column to an IonSpray atmospheric pressure ionization (API) interface, *viz.*, a liquid-junction and a coaxial arrangement, are described and compared with regard to ruggedness, ease of use, sensitivity and electrophoretic performance. The different injection modes used in three commercial capillary electrophoresis systems were also evaluated for their applicability to CE–MS. The use of CE–MS for the analysis of a variety of classes of antibiotics used in the fish aquaculture industry, such as the sulfonamides and their potentiators (*e.g.*, trimethoprim), is demonstrated and was used to confirm the presence of these components in shellfish extracts at the low ppm level. CE–MS was also applied to the analysis of marine toxins such as saxitoxin and its analogues which are associated with paralytic shellfish poisoning, and also to the toxins responsible for amnesic and diarrhetic shellfish poisoning. Tandem mass spectrometry (MS–MS) was used to provide structural information on these analytes, and the ability to distinguish isomeric compounds based on their different migration and fragmentation characteristics using CE–MS–MS is demonstrated.

INTRODUCTION

The last decade has seen a dramatic rise in aquaculture operations in Canadian coastal waters. As in terrestrial agriculture, intensive farming techniques have resulted in the increasing use of antibiotics to control disease. A major concern with the use of these compounds is that residues may be present in food products if proper withdrawal times for treated animals have not been strictly observed. The tolerance levels established by regulatory agencies (typically 0.1 ppm) demand the development of highly sensitive and selective confirmatory methods for these compounds in marine species and other food products.

As well as coping with the problems of man-made chemicals, there are other natural hazards to the particularly fragile shellfish industry. Toxic algal blooms occur all over the world and appear to be increasing in number and diversity [1]. Of major concern are the species of phytoplankton whose metabolites can cause human illness ranging from mild discomfort to paralysis, and even death, following the ingestion of shellfish which have been feeding on the toxic algae. The most notorious hazard in North America is paralytic shellfish poisoning (PSP), caused by a group of highly potent neu-

☆ Presented at the *8th (Montreux) Symposium on Liquid Chromatography–Mass Spectrometry (LC–MS, SFC–MS, CE–MS, IC–MS), Ithaca, NY, July 17–19, 1991.*

☆☆ NRCC 32994.

☆☆☆ Under contract from SCIEX, 55 Glen Cameron Road, Thornhill, Ontario, L3T 1P2, Canada.

rotoxins produced by the "red-tide" dinoflagellates, *Alexandrium* spp. [2]. Other toxins of concern to the Canadian shellfish industry include those responsible for amnesic shellfish poisoning (ASP, [3]) and diarrhetic shellfish poisoning (DSP, [4]).

Although high-performance liquid chromatography (HPLC) is currently the most commonly used instrumental technique for the analysis of both antibiotics [5,6] and marine toxins [7–9], capillary electrophoresis (CE), initially described by Jorgenson and Lukacs in 1981 [10], is rapidly becoming an important analytical tool, complementary to HPLC [11]. The technique exploits differences in electrophoretic mobilities of charged compounds under an applied electric field, and is characterized by extremely high separation efficiencies. Both HPLC and CE, however, are often frustrated by the lack of a sensitive, universal detector. The most common detection systems used with CE thus far have been ultraviolet (UV) and fluorescence spectrophotometry [12], although electrochemical detection has also been reported [13]. In view of the potential of coupling high-resolution separation techniques with mass spectrometry as the ideal confirmatory method, we have undertaken to develop such methods for the analysis of compounds of concern to the aquaculture industry. We have previously demonstrated the capability of LC–mass spectrometry (LC–MS) and LC–tandem MS (LC–MS–MS) to provide confirmatory analysis of both antibiotics in fin-fish [14] and marine toxins in phytoplankton [15].

Other workers have reported the successful coupling of CE to MS using either atmospheric pressure ionization (API) techniques such as electrospray (ES) [16–19] and ionspray (ISP) [20,21], or fast atom bombardment ionization (FAB) using a continuous-flow (CF-FAB) interface [22–25]. With both ionization techniques, two approaches to interfacing CE to mass spectrometry have emerged. The first uses what is termed a "liquid-junction" [20–22,25], in which the CE column is connected, via a tee-junction, to a transfer line which is in turn coupled to the ion source of the mass spectrometer. A make-up flow of a suitable buffer (containing a matrix such as glycerol in the case of CF-FAB) is added at the liquid junction. The other approach employs a "coaxial" capillary arrangement [16–19,23,24] with the CE column inside a sheath capillary through which the make-up buffer is added concentrically. In this configuration the CE column terminates at the ion source. Both approaches have succesfully demonstrated the potential of CE–MS for the analysis of drugs [25], amines [18], sulfonated azo dyes [21], quaternary phosphonium [18] and ammonium salts [16,17] and peptides and proteins [19,20,22–25]. More recently, a CE method with UV detection for the determination of underivatized PSP toxins was reported [26], in which a preliminary CE–MS interface was used to confirm UV peak identities.

In this paper we describe the design and application of two robust, interchangeable interfaces for CE–MS utilizing ISP on a triple quadrupole mass spectrometer. The practical details of their construction and use are discussed, together with the advantages and disadvantages of the various injection modes employed on commercial capillary electrophoresis systems. We have developed CE methods for a variety of classes of antibiotics used in aquaculture, including the sulfonamides and their potentiators (*e.g.*, trimethoprim), tetracyclines and macrolide antibiotics such as erythromycin, as well as for the analysis of saxitoxin and other PSP toxins in phytoplankton and shellfish extracts. MS–MS has been used to differentiate isomeric compounds and provide confirmatory analysis using selected reaction monitoring. The application of CE–MS to other types of marine toxins, such as those responsible for amnesic (ASP) and diarrhetic shellfish poisoning (DSP), is also reported.

EXPERIMENTAL

Chemicals

All of the antibiotics used were obtained from Sigma (St. Louis, MO, USA). Domoic acid is supplied as an instrument calibration solution (DACS-1) from this laboratory through the Marine Analytical Chemistry Standards Program. Sodium hydroxide (AnalaR grade) was obtained from BDH (Toronto, Canada). Acetonitrile was Fisher Scientific OPTIMA grade, and HPLC-grade water was generated from glass-distilled water using a Millipore Milli-Q Reagent Water System. Trisma buffer (pH 7.2) was prepared by appropriate additions of Trisma HCl (*ca.* 0.7 g) and Trisma base (*ca.* 0.07 g) in 100 ml of distilled water. Cyclohexylaminopropyl

sulfate (CAPS) buffer (pH 11) was obtained from Applied Biosystems (ABI, San Jose, CA, USA).

Biological extracts

Shellfish (oyster) tissue fortified with known levels of antibiotics was extracted using procedures described previously [14]. Saxitoxin (STX) and other PSP toxins were isolated from a toxic strain of *Alexandrium excavatum* dinoflagellates as described previously [26]. Okadaic acid was isolated from a culture of *Prorocentrum lima* using a combination of column chromatography and preparative HPLC [27].

Capillary electrophoresis

Three commercially available capillary electrophoresis systems were used: a ISCO (Lincoln, NE, USA) Model 3850, a P/ACE System 2100 (Beckman Canada, Mississauga, Canada) and an Applied Biosystems (ABI) Model 270A. All three systems were equipped with variable-wavelength UV detectors using through-column optics. Both the ISCO and ABI systems were interfaced, via a Hewlett-Packard Model 3396A integrator, to an MS-DOS computer based on a 80286 processor using Chromperfect software (Justice Innovations, Palo Alto, CA, USA). The Beckman system was interfaced directly to an MS-DOS computer (80386 processor) using a Beckman System Gold dedicated software package. The ISCO system was equipped with a manual split-flow injector, which utilizes PEEK tubing of various lengths and/or I.D. as a restrictor to vary the splitting ratio. The ABI and Beckman systems both employ software-controlled hydrodynamic injection techniques in which either a vacuum is applied at the detector end reservoir (ABI), or pressure is applied at the injection end reservoir (Beckman). All three systems are also capable of electrokinetic injections, although the ISCO system had to be modified in-house to make this possible. The advantages and disadvantages of the various injection modes, with regard to coupling the electropherographs to atmospheric pressure ionization mass spectrometry (API-MS), will be discussed later. All untreated fused-silica capillaries were obtained from Polymicro Technologies (Phoenix, AZ, USA) and CE separations were achieved on columns of 50 μm I.D. and between 75 and 90 cm in length.

Mass spectrometry

All combined CE–MS and CE–MS–MS experiments were performed on a SCIEX (Thornhill, Canada) API III triple quadrupole mass spectrometer equipped with an API source. A Macintosh IIx computer was used for instrument control, data acquisition and data processing. The two CE–MS interface configurations used were both constructed from a commercial fully-articulated IonSpray (ISP) interface (SCIEX) (Fig. 1). Details of the modifications are described below. Aqueous formic acid (0.2%) was used as the make-up flow in both configurations for positive ion analyses. In the liquid-junction configuration the make-up reservoir consisted of a 1-ml syringe mounted on the ISP interface flange, whereas in the coaxial design the make-up was delivered at 3–8 μl/min by a Microgradient LC syringe pump (ABI) via a submicroliter injection valve (Valco) with a 60-nl loop. This injector was used to optimize the interface and for all flow-injection experiments. The voltage on the ISP interface was maintained at *ca.* 5.6 kV, *i.e.*, providing an effective 24.4 kV across the CE column when

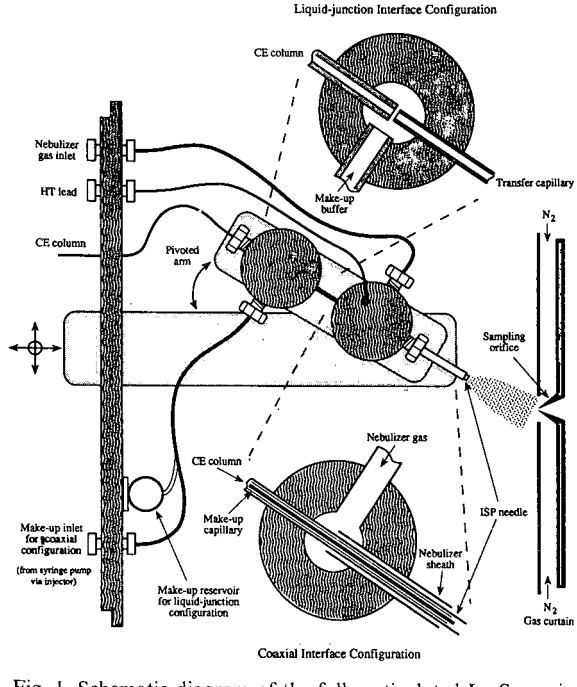

Fig. 1. Schematic diagram of the fully-articulated IonSpray interface showing the liquid-junction and coaxial configurations for CE–MS.

operating in the positive ion mode with 30 kV applied at the cathode. High-purity air was used as the nebulizing gas. Dwell times of 5 and 200 ms per dalton were used for full-scan and selected ion monitoring LC–MS experiments, respectively. MS–MS measurements were based on collision-induced dissociation (CID) of protonated molecules in the RF-only quadrupole using a collision energy of 20–35 eV and a target gas thickness (argon) of $3.0 \cdot 10^{14}$ molecules cm^{-2}.

Capillary electrophoresis–mass spectrometry

Although a detailed description of capillary electrophoresis (CE) is not within the scope of this paper, it is necessary to describe the basic elements of the CE experiment in order to appreciate the problems associated with coupling the technique to mass spectrometry. CE is performed in lengths of flexible capillary tubing filled with an appropriate buffer solution, similar to the buffers used in conventional electrophoresis. A small volume of sample (typically $<2\%$ of the column volume) is introduced into the capillary, across which an electric potential (*ca.* 20–30 kV) is then applied. Charged species inside the capillary exhibit different electrophoretic mobilities, and are thereby separated. Other components of a CE system include a high-voltage power supply, buffer reservoirs and electrodes, an injection system and a suitable detector.

Unlike HPLC, CE does not involve a mobile phase *per se*, which may be used to sweep known volumes of analyte solution onto the column from an injection valve. There are, however, several injection techniques available in CE, including hydrostatic, hydrodynamic (pressure or vacuum), split-flow and electrokinetic methods. A brief description of the injection methods evaluated during this study will be given later. It should be noted that, except for the electrokinetic injection mode, the method of sample injection is also the means by which the capillary is filled with the running buffer. When using untreated fused-silica capillary columns, in order to maintain reproducible migration times and electrophoretic performance, it is necessary to flush the column with several column volumnes (*ca.* 10 μl) of the running buffer after each analysis. In addition, it is also common practice to wash the column regularly with a weak base (typically a 0.1 *M* solution of sodium hydroxide) to remove adsorbed material from the walls of the capillary. Most of the available commercial systems have motorized carousels allowing wash–fill–inject–run sequences to be programmed into a method file.

Detection in CE is usually achieved by spectrophotometric methods; an optical window is typically created in the column itself by burning off a portion of the polyimide coating of the fused-silica capillary. As mass spectrometry is a destructive technique, however, the exit of the CE column must be physically connected or *interfaced* to the ion source of the mass spectrometer. The methods used to achieve this are described below.

Both the liquid-junction and coaxial approaches to achieving CE–MS were evaluated. Both approaches utilized a modified commercial fully-articulated IonSpray interface and the different configurations are shown schematically in Fig. 1. The fully-articulated interface is a development of the original ISP probe and has been designed for ease of optimization and greater flexibility in the coupling of chromatographic and electrophoretic systems. The commercial interface consists of two zero dead volume tee-junctions mounted on an articulated arm attached to the clear plastic source flange by a system of vernier micrometers. The first tee is used for the introduction of the ISP nebulizing gas, and the second may be used as a post-column splitter in HPLC or for CE coupling (described below). The micrometers provide movement of the arm in the axial and both lateral directions (x, y, z), and allow precise positioning of the ISP needle relative to the sampling orifice. The arm itself is pivoted, allowing the ISP needle to be moved at an angle (ϕ) to the sampling orifice. This additional degree of freedom was included as it has been found that, under certain conditions, a significant reduction in background cluster ions can be obtained by sampling the spray at an oblique angle to the interface plate and sampling orifice.

Coaxial interface. Based on previous experience with a coaxial arrangement of fused-silica capillaries for the coupling of packed capillary columns with continuous-flow FAB-MS [28], a preliminary coaxial CE–MS interface was used to confirm peak identities in the recent development of a CE–UV method for PSP toxins [26]. The principal difference between this preliminary interface and the current design is that the length of the coaxial sheath capil-

lary is greatly reduced in the latter, thereby lowering the back-pressure generated so that an inexpensive syringe pump may be used to deliver the make-up flow. The design also makes it much easier to change the CE column. The zero dead volume tee nearest the orifice was replaced with one drilled-out to accommodate a larger ISP needle through which the sheath capillary, containing the CE column, was fed (Fig. 1).

The important parameters in the construction of this particular configuration are the tight fits of the various concentric capillaries inside one another and their relative positioning at the probe tip. The I.D. of the in-house manufactured metal nebulizer sheath was drilled to accommodate the ISP needle (20-gauge stainless-steel tubing) with a snug fit, as the interspacial gap provides the restriction to the nebulizer gas against which its flow is controlled. The ISP needle protrudes *ca.* 0.5 mm from the nebulizer sheath to provide a focused spray of charged droplets. In later designs we hope to dispense with the fused-silica sheath capillary by extending the metal ISP needle to the second tee. The exit of the CE column (360 μm O.D., 50 μm I.D.) is held 0.5 mm inside that of the ISP needle, and the sheath capillary (500 μm O.D., 390 μm I.D.) a further 0.5 mm back from the CE column. This arrangement ensures good mixing of the effluents from the sheath capillary and column, minimizes the dead volume and maintains good electrical contact between the combined effluent and the ISP needle.

The make-up buffer for the sheath capillary is delivered to the back tee by a syringe pump, via a submicroliter injector (60-nl loop), at 3–8 μl/min. Formic acid (0.2%) was found to be the most suitable make-up buffer for positive ion analyses. At higher concentrations, the increased conductivity led to high CE currents (tripping the safety interlock on the CE systems) and instability in the ISP ion current. The injector provides a rapid means of optimizing the interface by flow-injection analysis (FIA). Another advantage of this injector was that it was found to provide a means of independently determining the amount of material injected on the CE column by injecting a suitable standard after the CE–MS experiment.

Liquid-junction interface. In this configuration the back zero dead volume tee (Fig. 1) is replaced by a modified tee which has one side replaced with a glass window to allow accurate alignment of the CE column and a transfer line (140 μm O.D., 75 μm I.D.) attached to opposite sides of the tee. The distance between the two capillaries is critical to the performance of this configuration. If it is too large the analyte, on exiting the CE column, can diffuse into the junction, leading to a loss in electrophoretic performance, whereas if the capillaries are too close, insufficient make-up buffer may be drawn into the flow into the transfer line to maintain a stable ion current. Thus, a gap of *ca.* 10–20 μm was found to be optimum. The make-up reservoir (a 1-ml syringe) is mounted on the interface flange, 3–5 cm above the ISP needle. The make-up buffer enters the transfer capillary via a combination of gravity and the venturi vacuum generated by the escaping nebulizing gas at the end of the ISP needle. In operation, a flow-rate of 2–3 μl/min was measured by observing the loss from the reservoir over a period of time.

The two configurations are readily interchangeable; with experience it was found to be possible to change from one to the other in a few minutes, although obtaining the correct gap in the liquid-junction configuration often required several attempts.

RESULTS AND DISCUSSION

Evaluation of injection techniques for CE–MS

The coaxial CE–MS interface was used for all of these experiments, as it was possible to perform flow-injection analysis (FIA) via the make-up flow and thereby independently obtain quantification of electrophoretic peaks. While the hydrostatic (or siphon) injection technique, in which either the sample end of the capillary is raised or the detector end (*i.e.*, the mass spectrometer) is lowered, has been used successfully for CE–MS by other workers [20], in our hands the technique was found to be impractical, and was not used during this investigation. However, it was important to keep the ends of the capillary at the same level to prevent siphoning. Similarly, it has not so far been possible to envisage a simple apparatus which applies a vacuum at the end of the capillary (similar to that used in the ABI system) once it was positioned within the CE–MS interface; unlike conventional mass spectrometers there is no vacuum in the API ion source which may be utilized for injection.

Pressure injection (Beckman). In this approach,

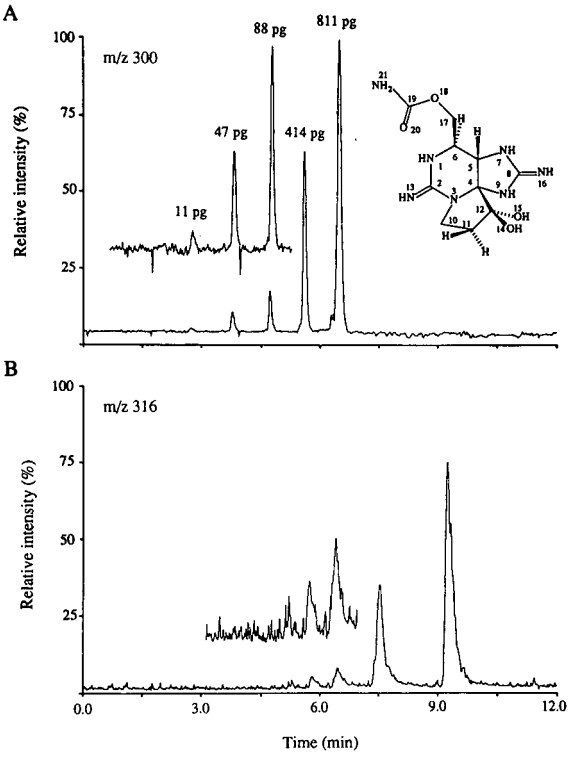

Fig. 2. Separation of the PSP toxins (A) saxitoxin and (B) neosaxitoxin by CE–MS using selected ion monitoring of MH^+ ions. Conditions; consecutive 10-s pressure injections of serial dilutions (1:1, 1:2, 1:10, 1:20 and 1:100) of a 500 μg/ml (each) solution, Trisma buffer (pH 7.2), voltage 24.4 kV (effective), coaxial CE–MS interface using make-up of 0.2% formic acid at 8 μl/min. Column, 90 cm × 50 μm I.D.

the sample end of the capillary and the electrode are inserted through gas-tight septa of individual sample and/or buffer vials. To inject, the sample vial is pressurized (*ca.* 0.5 p.s.i.) for a set time, forcing a small volume of the solution into the CE column. The amount injected is obviously dependent on the dimensions of the column, and on the viscosity of the solution. One of the criteria used to compare the injection methods was linearity of response, and Fig. 2 shows the CE–MS response obtained by consecutive 10-s pressure injections of various dilutions of a mixture of the PSP toxin saxitoxin (STX) and its N_1-hydroxylated analogue, neosaxitoxin (NEO), using selected ion monitoring (SIM) of their respective protonated molecules (MH^+). The electrophoretic process was stopped for each injection (made at 1-min intervals) by turning off the CE voltage, and it can be seen that the peak widths increase with the order of injection due to diffusion of the analytes while the electrophoresis was stopped and the next pressure injection performed. Comparison of the two ion electropherograms shows that each corresponding pair of the two toxins is well resolved, with neosaxitoxin migrating after saxitoxin. Peak-area measurements for saxitoxin were compared with those of standard solutions obtained by FIA following the electrophoresis experiment to give the amounts indicated in Fig. 2. From these amounts and the known concentrations it was estimated that *ca.* 1.8 nl was injected on to the CE column. It can be seen that the detection limit of saxitoxin is *ca.* 10 pg with a signal-to-noise ratio of 2. Even though this approach was used simply to illustrate the flexibility of the injection system and would not be the method used to generate a calibration graph, the CE–MS response for both toxins was found to be linear over two orders of magnitude (5–500 μg/ml).

Split-flow injection (ISCO). This method of injection is similar in principle to the split injection technique in gas chromatography (GC), in which only a portion of the analyte solution injected is introduced on to the column. An HPLC syringe (10 μl) is used to inject the sample into one port of a three-way injection block [29]. The tip of the CE column seats into the top port by means of a septum seal and the third (split-vent) port, opposite the syringe port, is plumbed with capillary tubing of varying lengths (3–5 cm) and/or I.D., (0.005–0.020 in.) which provides the splitting ratio.

The selected ion electropherogram (SIE) obtained from the CE–MS analysis of a mixture of five antibiotics used in the aquaculture industry using a 1-μl split-flow injection is shown in Fig. 3B. Only four peaks are observed as erythromycin (ETH) comigrates with ometoprim (OMP). The separation was performed at 24.4 kV (effective) using Trisma buffer (pH 7.2). One of the advantages of using the coaxial design with this injection technique is that the splitting ratio can be accurately calculated by comparison of the electrophoretic response with the FIA response obtained after the electrophoretic experiment is complete. Using a standard solution of trimethoprim (TMP), a split ratio of 1:60 was calculated for this analysis, indicating an injection volume of the order of 16 nl, which represents 116 pg on-column of each component (7.1 μg/ml) except

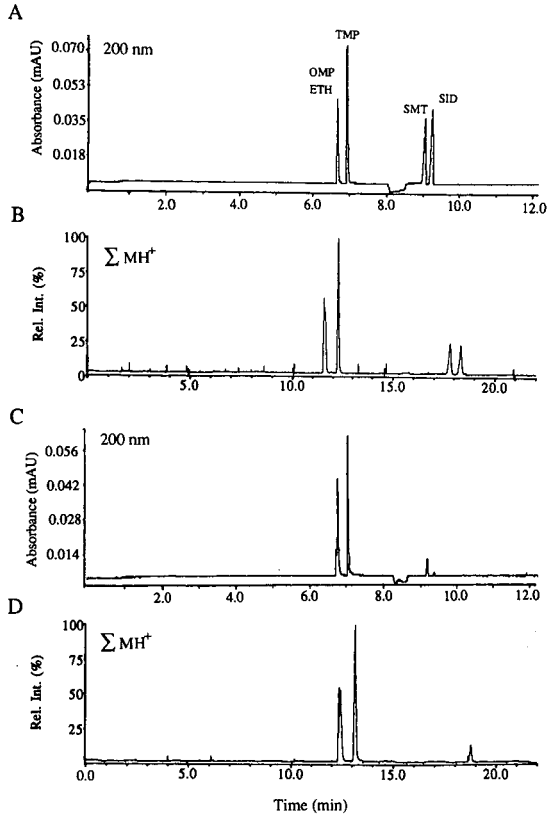

Fig. 3. Separation of antibacterial drugs used in the aquaculture industry by (A and C) CE–UV (200 nm) and (B and D) CE–MS (SIM). Conditions as in Fig. 2 except injection for (A) 3-s vacuum, (B) 1-μl split-flow (1:60) and (C and D) 10-s electrokinetic (5 kV).

erythromycin, which at 71.4 μg/ml represents 1.16 ng on-column.

The CE–MS SIE compares favorably with the CE–UV trace shown in Fig. 3A, which was obtained using vacuum injection (ABI) and 24 kV. The difference in migration times between the CE–UV electropherogram and the CE–MS SIE is due to the fact that UV detection occurs 22 cm before the end of the capillary. In order to compare the electrophoretic performance of the CE–MS interface with that obtained using the UV detector, the plate numbers were calculated for the single component peaks. The plate numbers (and peak width at half-height) for the trimethoprim peak by CE–UV and CE–MS were 225 000 (2.1 s) and 181 500 (4.1 s), respectively. Although the latter represents a 20% loss in electrophoretic efficiency over the CE–UV analyses, it should be recalled that mass spectral detection occurs 22 cm after the UV and diffusion of the analyte during migration over this additional length of capillary would account for a significant portion of the observed loss in efficiency. Unfortunately, the physical dimensions of the electropherograph and mass spectrometer are such that they could not be brought closer together, although a smaller CE system has been constructed in this laboratory, which will allow much shorter columns to be used. These and similar comparisons indicate that the coaxial interface can maintain both chromatographic integrity and the high separation efficiencies available with CE. These comparisons also confirm the effectiveness of the split-flow method for sample introduction in CE–MS. The quantitative performance of the split-flow injection method, however, was not so encouraging. Although reproducibility was obviously dependent on the accurate dispensing of 1-μl volumes, obtaining and maintaining the correct splitting ratio were found in practice to be the major problems associated with this injection technique. Using replicate injections it was found that peak areas could vary by as much as $\pm$ 10%. Partial blocking of the split-vent tubing by a build-up of salts was found to be a major source of irreproducibility.

Electrokinetic injection (all three CE systems). This mode of injection, in which the analyte migrates into the column under an applied field, is perhaps the easiest to accomplish in that no special vials, seals or plumbing of gas/vacuum lines are required. Typically, a voltage of 5 kV is applied for a fixed time (*ca.* 1–30 s) before the capillary is returned to the running buffer and the analysis started. Despite its simplicity, there is a problem due to electrophoretic discrimination associated with this injection mode, in that the amount of a particular analyte injected will be proportional to its electrophoretic mobility. This is illustrated in Fig. 3D, which shows the SIE of the mixture of five antibiotics using a 10-s electrokinetic injection (it should be noted that the ISP voltage is turned off during the electrokinetic injection). Comparison with the corresponding SIE in Fig. 3A reveals that the late-migrating isomeric sulfonamides, sulfamethazine (SMT) and sulfaisomidine (SID), both show extensive discrimination. The corresponding CE–UV trace obtained using an electrokinetic in-

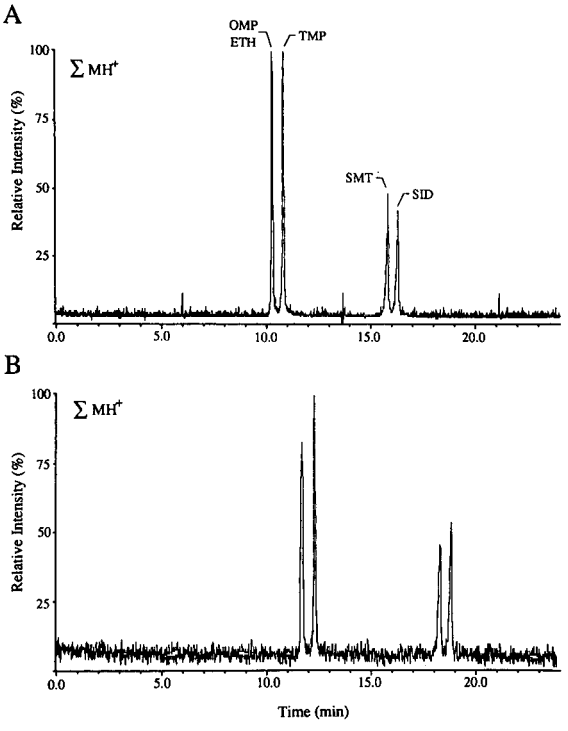

Fig. 4. Separation of antibacterial drugs by CE–MS using (A) coaxial and (B) liquid-junction interface configurations. Conditions as in Fig. 3B.

jection is presented in Fig. 3C, and confirms that the discrimination is not merely an artifact of the CE–MS interface. Indeed, the two UV electropherograms (Fig. 3A and C) were run consecutively on the same CE system. A second disadvantage of the electrokinetic injection method is that the amount of sample injected is also a function of the sample buffer composition. This can cause problems in the analysis of complex extracts containing high levels of salts.

Comparison of CE–MS interface configurations

The CE–MS SIEs of the five antibiotics, using the coaxial and liquid-junction configurations, are shown in Fig. 4A and B, respectively. The analyses were performed on the same day, under indentical CE conditions using a 1-μl split-flow injection. The most obvious difference between the two CE–MS separations is the migration time. Although the analyses were conducted on the same column, the migration times are longer in the case of the liquid junction. These differences were initially believed to be due simply to the additional length of transfer capillary (8 cm) used in the latter configuration. However, the 2 μl/min flow-rate through the transfer capillary (as determined by the observed loss of make-up buffer from the reservoir with time) is higher than that through the column, and thus the residence time is at most 30 s and does not account for the 1–1.5 min difference in migration times. In considering a possible explanation for the observed differences, a potential disadvantage of the liquid junction was revealed. It was noted that the current recorded with the liquid junction was *ca.* 10–12 μA higher than that during the coaxial analysis, and this was believed to result from a difference in the buffer composition at the interface. When filling and washing the capillary between runs with the liquid-junction, it was found that the effluent does not exit into the ion source, as in the coaxial configuration, but takes the path of least resistance and flows into the make-up reservoir line. To minimize this problem, the column was re-filled and washed with minimum volumes of buffer solutions (2–5 μl), and the interface was left for 10 min prior to injection in order for sufficient make-up buffer to wash through the junction. The possible influence of this changing composition on the sensitivity of the ISP process is discussed below.

Closer examination of the individual traces reveals a further loss of electrophoretic performance with the liquid-junction interface, in addition to that already described in the comparison between the CE–UV and CE–MS (coaxial) electropherograms (Fig. 3). The calculated plate numbers for trimethoprim, with the coaxial and liquid-junction configurations, were 169 800 and 101 500, respectively. This represents a 1.67-fold difference for the two interfaces. Similar improvements in calculated plate numbers were found for the other antibiotics with the coaxial relative to the liquid-junction configuration: ometoprim (2.29), erythromycin (1.21), sulfamethazine (2.43) and sulfaisomidine (3.59). Consideration of the expected additional band broadening with the inclusion of the liquid-junction transfer capillary does not account for all of the observed loss in plate number, and this is attributed to the junction itself. This is supported by other workers [25] who, using fluorescence detection, reported a tenfold decrease in plate number with the inclusion of a similar liquid-junction.

The other notable difference is the higher noise level in the liquid-junction SIE (which actually comes predominantly from only one ion, *m/z* 279). This is believed to be due, in part, to the lower flow-rate of make-up buffer (0.2% formic acid), which results in an increased contribution of the CE buffer (Trisma) to the background. Peak-area measurements showed that the responses for ometoprim, trimethoprim, sulfamethazine and sulfaisomidine were 47, 44, 49 and 31% higher, respectively, with the coaxial than with the liquid-junction arrangement, although interestingly the response for the higher molecular weight erythromycin was 28% higher with the latter. It is possible that the splitting ratio is different in the two configurations, with the liquid-junction generating a higher back-pressure

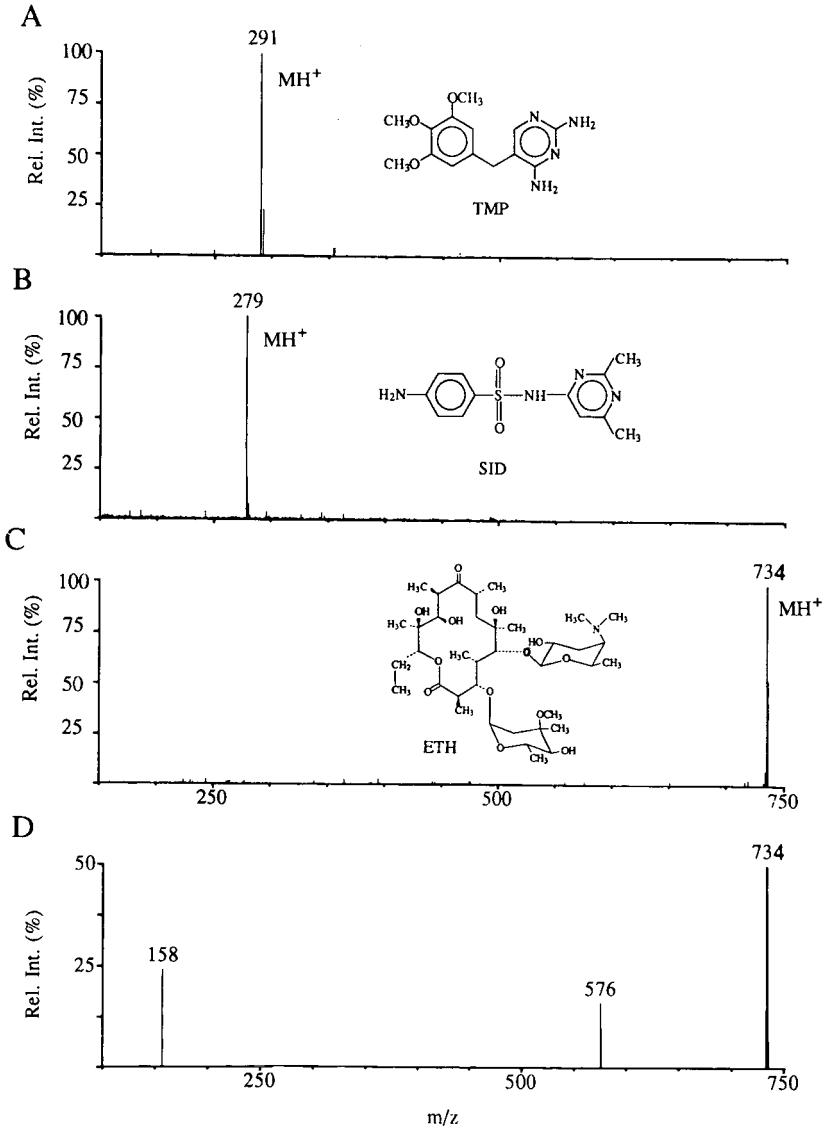

Fig. 5. Background-subtracted CE mass spectra of (A) trimethoprim (TMP), (B) sulfaisomidine (SID) and (C) erythromycin (ETH). CE conditions as in Fig. 3. Mass range, 150–750 dalton. (D) MS–MS of erythromycin by flow-injection analysis. Collision energy (laboratory frame), 35 eV; target gas (argon) thickness, $3.5 \cdot 10^{14}$ cm^{-2}.

than the coaxial configuration, resulting in less sample being injected in the former interface. This is thought to be unlikely as the make-up flow to the junction is through wide-bore Teflon tubing. It is also possible that the changing composition of the make-up buffer in the liquid junction may affect the ISP response. Without the ability to use FIA with this interface it is not possible to substantiate these arguments.

Full-scan analyses were also performed with this mixture of antibiotics, and the full-scan (150–750 dalton) CE–MS mass spectra of trimethoprim, sulfaisomidine and erythromycin are shown in Fig. 5A, B and C, respectively. These spectra are typical of those obtained by the mild ISP process, consisting of simply the protonated molecule and little or no fragmentation. The spectra of ometoprim, trimethoprim and sulfaisomidine are identical with those recently obtained by LC–MS [14]. Full-scan CE–MS detection limits for the antibiotics were not as good as expected from the excellent SIM results. It is pertinent at this time to mention a limitation of scanning mass spectrometers as detectors for CE. As discussed above, the high-efficiency separations currently achieved in CE–MS result in peak widths of the order of 3–5 s. The problem is a more extreme version of the well known dilemma in capillary GC–MS, where the chromatographic peak widths require a mass spectrometer scan cycle of no more than *ca.* 1 s in order to avoid serious distortions of the mass spectra. In addition, sample loadings are smaller in CE, so that the question of the signal-to-noise ratio in the mass spectra is even more pressing than in GC–MS. The volume of analyte solution can be no more than *ca.* 1% of the column volume if optimum CE performance is to be maintained; this implies a maximum injection volume of *ca.* 20 nl, a factor of 50–100 smaller than the typical injection volumes in capillary GC–MS. Therefore, a compromise must be found for individual CE–MS experiments, in which mass spectral quality (signal-to-noise ratio and freedom from distortion) is traded off against mass scan-range and speed, and also against CE peak width via injection volume. Based on experience with a range of analytes with molecular weights in the range of a few hundred daltons, *ca.* 1 ng of sample injected on-column is required if a mass spectrum of adequate signal-to-noise ratio is to be acquired at a scan rate of *ca.* 250 dalton/s

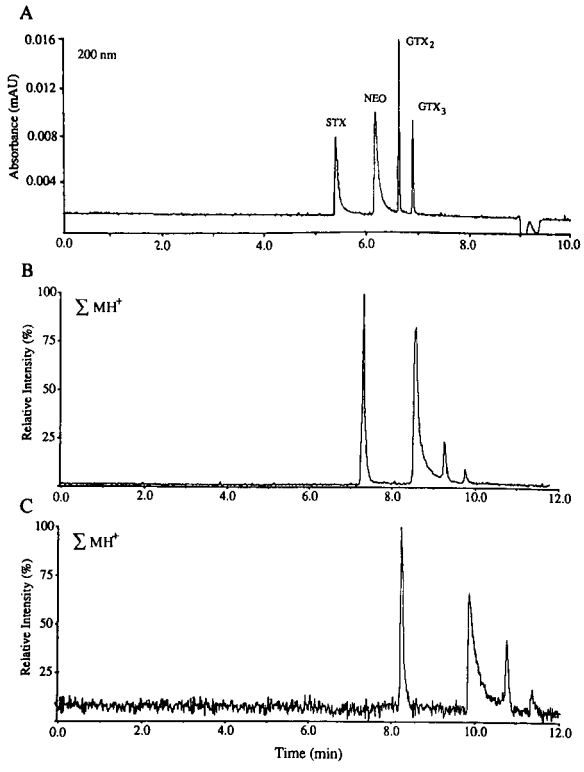

Fig. 6. Separation of PSP toxins isolated from a culture of the dinoflagette spp. *Alexandrium excavatum* by (A) CE–UV (200 nm) and by CE–MS using (B) coaxial and (C) liquid-junction interface configurations. Conditions as in Fig. 3B.

using ISP CE–MS. These constraints can be removed if a non-scanning mass spectrometer is used, either a focal-plane instrument with a channel electron multiplier array detector [30] or an ion trap permitting ion storage over the duration of the CE peak.

The electrophoretic separation of saxitoxin, neosaxitoxin and the C_{11}-sulfated gonyautoxins (GTX-2 and GTX-3), performed at 24 kV using UV detection at 200 nm, is presented in Fig. 6A. The toxins, isolated from a strain of *Alexandrium excavatum* dinoflagellates, are well resolved although the neosaxitoxin peak shows significant tailing owing to interaction of the hydroxyl group with the capillary walls. The corresponding CE–MS separation using the coaxial and liquid-junction interfaces are shown in Fig. 6B and C, respectively. The SIEs consist of the respective MH^+ ions (*m/z* 300, 316 and 396) and compare favorably with the UV trace,

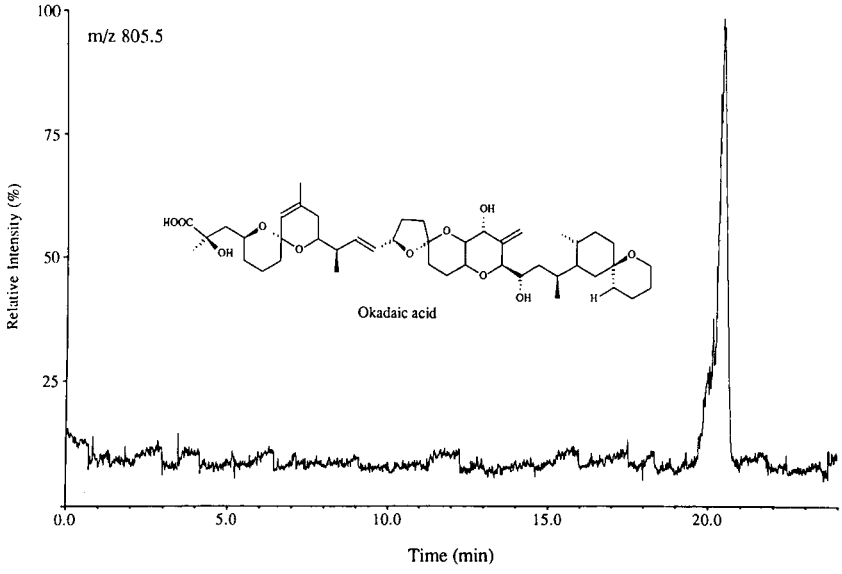

Fig. 7. CE–MS SIM response for 16 ng of the DSP toxin okadaic acid (*m/z* 805.5). Conditions as in Fig. 4A.

providing unambiguous confirmation of UV peak identities. The relative abundances of the peaks corresponding to the gonyautoxins were found to be higher in the CE–UV electropherogram. This is due to the fragmentation of the labile sulfated analogues under ISP ionization [26], via loss of the sulfate (80 dalton) to give the charged species $[M+H-SO_3]^+$ at *m/z* 316, which coincidently is the same mass as the protonated molecule of neosaxitoxin. The differences between the two SIEs are similar to those discussed above, with the migration times being slightly longer with the liquid-junction interface.

CE–MS was also applied to other marine toxins of concern to the Canadian aquaculture industry. Fig. 7 shows the SIE obtained from the CE–MS analysis of okadaic acid, the principal toxin associated with DSP [4], using the coaxial interface. Under the electrophoretic conditions used (Trisma, pH 7.2), the lipid-soluble polyether toxin migrates in its anionic form, as evidenced by the characteristic (fronting) electrophoretic profile. Quantification of the peak by FIA after the electrophoretic experiment indicated 16 ng of the toxin was injected on-column. In this case, significant improvements in sensitivity will have to be made in order for CE–MS to offer an alternative to the ISP LC–MS method for DSP toxins recently described [15]. The application of the CE to the analysis of domoic acid, the neurotoxin responsible for amnesic shellfish poisoning [3], has been recently reported [31]. Fig. 8A shows the reconstructed ion electropherogram of the MH^+ (*m/z* 312) from the full-scan (150–350 dalton) CE–MS analysis (CAPS, pH 11) of the instrument calibration solution of the toxin (DACS-1, 80 μg/ml) available from this laboratory under the Marine Analytical Chemistry Standards Program. The CE mass spectrum taken at the top of the electrophoretic peak is presented in Fig. 8B, and resulted from the introduction of 1.6 ng of the toxin.

Capillary electrophoresis with tandem mass spectrometry (CE–MS–MS)

The use of MS–MS with ISP-MS to provide structural information on sulfonamides and their potentiators has been described recently [14]. The product ion spectra of protonated trimetoprim, ometoprim, and the isomeric sulfonamides, obtained by CE–MS–MS, were identical with those obtained previously by LC–MS–MS [14]. The CID product ion spectrum of protonated erythromycin obtained by FIA (via the coaxial make-up buffer inlet) is shown in Fig. 5D, and compares favorably with that reported during a recent investigation of

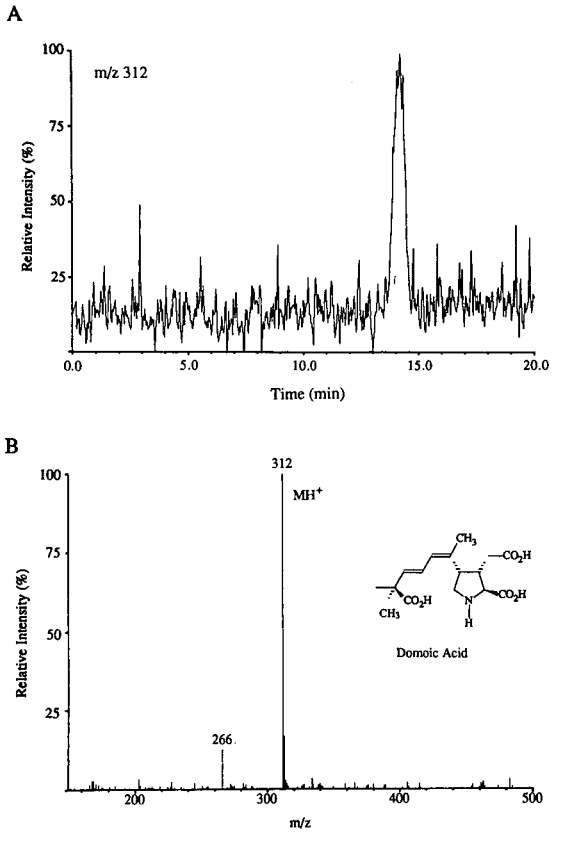

Fig. 8. Full-scan analysis of the neurotoxin domoic acid by CE–MS. (A) Reconstructed ion electropherogram of MH^+ (*m/z* 312) and (B) background-subtracted mass spectrum. Conditions: CAPS buffer (pH 11), voltage 24.6 kV (effective), mass range 150–500 dalton.

the MS–MS of erythromycin and other macrolide antibiotics using FAB ionization on a tandem sector instrument [32]. Two major product ions are observed at *m/z* 576 and 158. These ions are indicative of bond cleavage accompanied by hydrogen rearrangement at the site of the glycosidic oxygen. As a result, the non-amino sugar is lost as a neutral fragment (156 dalton) to give the product ion at *m/z* 576, but the amino sugar is observed as a charged species (*m/z* 158).

Product ions of antibiotics thus identified by MS–MS may be used in CE–MS–MS methodologies, either to provide increased selectivity by using selected reaction monotoring (SRM) or to aid in the identification of related species by using precursor scans of common product ions. The former technique is illustrated in Fig. 9, which shows the SRM electropherograms obtained from CE–MS–MS analysis of the mixture of the five antibiotics under conditions identical with those described above, monitoring the dissociation of MH^+ ions to characteristic product ions. For the isomeric sulfonamides two reactions were monitored, *viz*, *m/z* 279 > 156 (Fig. 9C) and *m/z* 279 > 213 (Fig. 9B). The latter ion is assigned to the loss of (H_2, SO_2), and it can be seen that sulfamethazine selectively shows this fragmentation, thus providing both electrophoretic and mass spectrometric confirmation of this isomer.

The application of CE–MS and CE–MS–MS to the analysis of a shellfish extract fortified with sulfadimethoxine (SDM) at the 1 ppm level is demonstrated in Fig. 10A and B, respectively. The CE–MS SIM electropherogram of the MH^+ ion of sulfadimethoxine (*m/z* 311) shows a peak close to the migration time observed for the standard and well re-

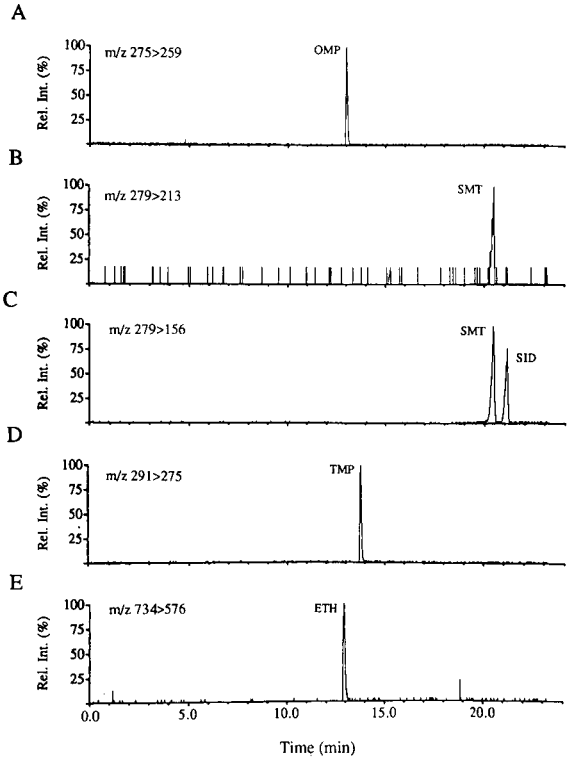

Fig. 9. Separation of antibacterials by CE–MS–MS using selected reaction monitoring. CE conditions as in Fig. 4A and MS–MS conditions as in Fig. 5.

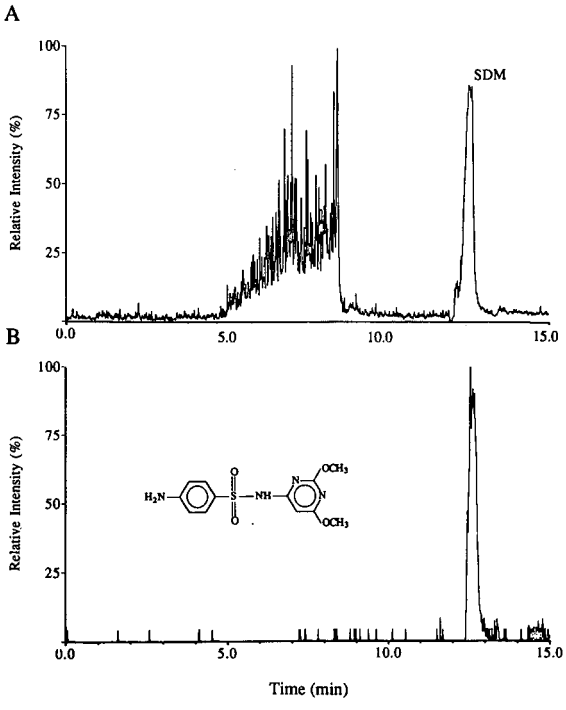

Fig. 10. Analysis of shellfish extract fortified with sulfadimethoxine (1 ppm) by (A) CE–MS using SIM (*m/z* 311) and (B) CE–MS–MS using SRM (*m/z* 311 > 156). CE conditions as in Fig. 4A and MS–MS conditions as in Fig. 5.

solved from a significant degree of interference in the early part of the electropherogram. The observed CE–MS peak width for sulfadimethoxine is significantly larger than those observed for standard sulfonamides, and is assigned to the effect of high salt concentrations in the extract. The corresponding CE–MS–MS SRM electropherogram (Fig. 10B), monitoring the dissociation of the MH^+ ion to *m/z* 156 (a common product ion of the sulfonamides [14]), demonstrates the increased selectivity obtained via the significant reduction in chemical noise.

CONCLUSIONS

Although both interface designs have been shown to be capable of providing efficient coupling of CE to API-MS, it is felt that the coaxial configuration provides a more robust and reproducible interface. The major advantage of the coaxial over the liquid-junction interface is that the make-up flow is delivered independently of the CE column effluent. This provides greater flexibility in the type of CE buffer that may be used, and offers the potential for FIA and even LC–MS of other samples via the make-up capillary without dismantling the CE interface. The use of FIA also provides an independent means of quantification, and this can also be used to determine accurately the splitting ratio when using a split-flow injection system. One other advantage of the coaxial configuration was more recently realized during the analysis of high-molecular-weight proteins by CE–MS. The FIA of a calibrant just prior to a CE–MS analysis permits mass accuracies, similar to those obtained by infusion, to be achieved. The application of these CE–MS interfaces to the analysis of proteins will be reported separately.

All three CE instruments performed well in the present CE–MS experiments. The only feature which differentiated significantly amongst them in this regard was the technique used for sample injection. Of the different injection modes evaluated for CE–MS, pressure injection seems to offer the best means of introducing the sample and associated buffer solutions into the CE column, without disturbing the interface. Compared with the electrokinetic injection technique, pressure injection shows no discrimination amongst analytes on the basis of electrophoretic mobility.

It has been shown that CE–MS and CE–MS–MS can be used to analyze a variety of compounds of concern to the aquaculture industry. There are some additional concerns, however. One drawback of CE is that migration times and separation efficiency are dependent on the composition of the analyte solution, and for regulatory work the use of suitable migration markers and internal standards would be a necessity. Another general problem arises as a consequence of the low sample volumes (1–30 nl) which can be injected without degradation of electrophoretic separation. The implications of this restraint can be appreciated most easily by considering an contaminant with a regulatory limit of 1 μg per gram of fish tissue (1 ppm). The extract from 1 g of tissue would most likely be made up to a total volume of 1 ml, in order to keep the total concentration of co-extracted salts and other endogenous material down to manageable levels. A 10–20-nl injection of such a solution contains 10–20 pg of the

target analyte. A useful analytical technique should be capable of operating below the regulatory limit by at least a factor of ten, *i.e.*, for CE methods the detection limit must be of the order of 1–2 pg (for a 1 ppm limit). This detection limit may be improved by either improved clean-up procedures, preconcentration of the sample or larger injection volumes, although the last two options are both undertaken at the cost of degradation in electrophoretic efficiency.

Nevertheless, using a combination of selected ion and selected reaction monitoring, CE–MS is currently capable of confirming the presence of antibiotics at the low ppm level in complex matrices. Improvements in the CE analysis of real extracts, which should bring the CE–MS detection limits for these compounds below the regulatory limit (0.1 ppm), and in line with those available by ISP LC–MS [15], are currently under investigation.

With regard to the marine toxins examined, the results obtained for the PSP toxins are particularly encouraging. Considering the challenge that these labile toxins present to the analytical chemist, CE offers a real alternative to the HPLC–fluorescence detection method currently used for the regulatory monitoring of shellfish, with regard to both sensitivity and ease of use. Full details of the application of CE–MS for the analysis of PSP toxins in biological extracts will be reported elsewhere [33]. The CE–MS instrumental detection limit for okadaic acid is sufficiently high that it seems highly unlikely that this technique will ever form the basis of a routine analytical method for underivatized DSP toxins. The case of domoic acid is slighly more promising, but it is felt that at present the CE methodology cannot successfully compete with LC–MS.

ACKNOWLEDGEMENTS

The authors thank Dr. R. K. Boyd for useful discussions regarding the manuscript and J. F. Anacleto for help with the artwork. They are grateful to Dr. B. Thomson (SCIEX) for technical assistance and to J. Chapman (Beckman) for providing the P/ACE CE system. Thanks are also due to Dr. M. Little of Syndel Laboratories (Vancouver, Canada) for providing the shellfish extracts. This research was supported in part by the Defence Research Establishment Suffield, Department of National Defence (Medicine Hat, Canada) and by the Bureau of Veterinary Drugs, Health and Welfare Canada (Ottawa, Canada).

REFERENCES

1 D. C. Gordon (Editor), *Proceedings of the 2nd Canadian Workshop on Harmful Marine Algae, Bedford Institute of Oceanography, Dartmouth, N.S., October 2–4 1990; Can. Tech. Rep. Fish. Aquat. Sci.*, No. 1799 (1991).
2 Y. Shimizu, in A. T. Tu (Editor), *Handbook of Natural Toxins, Vol. 3, Marine Toxins and Venoms*, Marcel Dekker, New York, 1988, p. 63.
3 M. A. Quilliam and J. L. C. Wrigth, *Anal. Chem.*, 61 (1989) 1053A.
4 T. Yasumoto, M. Murata, Y. Oshima, G. L. Matsumoto and J. Clardy, in E. Ragelis (Editor), *Seafood Toxins (ACS Symposium Series*, Vol. 262), American Chemical Society, Washington, DC, 1984, p. 207.
5 W. A. Moats, *J. Assoc. Off. Anal. Chem.*, 73 (1990) 343.
6 R. F. Cross, *J. Chromatogr.*, 478 (1989) 42.
7 J. J. Sullivan and W. T. Iwaoka, *J. Assoc. Off. Anal. Chem.*, 66 (1983) 297.
8 J. S. Lee, T. Yanagi, R. Kenma and T. Yaumoto, *Agric. Biol. Chem.*, 51 (1987) 877.
9 M. A. Quilliam, P. G. Sim, A. W. McCulloch and A. G. McInnes, *Int. J. Environ. Anal. Chem.*, 36 (1989) 139.
10 J. W. Jorgenson and K. D. Lukacs, *J. Chromatogr.*, 218 (1981) 209.
11 A. Wainwright, *J. Microcol. Sep.*, 2 (1990) 167.
12 Y. Walbroehl and W. Jorgenson, *J. Chromatogr.*, 315 (1984) 135.
13 R. A. Wallingford and A. G. Ewing, *Anal. Chem.*, 59 (1987) 1762.
14 S. Pleasance, P. Blay, M. A. Quilliam and G. O'Hara, *J. Chromatogr.*, 558 (1991) 155.
15 S. Pleasance, M. A. Quilliam, A. S. W. deFreitas, J. C. Marr and A. D. Cembella, *Rapid Commun. Mass Spectrom.*, 4 (1990) 204.
16 J. A. Olivares, H. T. Nguyen, C. R. Yonker and R. D. Smith, *Anal. Chem.*, 59 (1987) 1230.
17 R. D. Smith, J. A. Olivares, N. Nguyen and H. R. Udseth, *Anal. Chem.*, 60 (1988) 436.
18 R. D. Smith, C. J. Barinaga and H. R. Udseth, *Anal. Chem.*, 60 (1988) 1948.
19 J. A. Loo, H. R. Udseth and R. D. Smith, *Anal. Biochem.*, 179 (1989) 404.
20 E. D. Lee, W. Muck, J. D. Henion and T. R. Covey, *J. Chromatogr.*, 458 (1989) 313.
21 E. D. Lee, W. Much, J. D. Henion and T. R. Covey, *Biomed. Environ. Mass Spectrom.*, 18 (1989) 253.
22 R. D. Minard, D. Chin-Fatt, P. Curry and A. G. Ewing, in *Proceedings of the 36th ASMS Conference on Mass Spectrometry and Allied Topics, San Francisco, CA, June 5–10, 1988*, American Society for Mass Spectrometry, East Lansing, MI, 1988, p. 950.
23 J. S. M. deWit, L. J. Deterding, M. A. Mosely, K. B. Tomer and J. W. Jorgenson, *Rapid Commun. Mass Spectrom.*, 2 (1988) 100.

24 M. A. Mosely, L. J. Deterding, K. B. Tomer and J. W. Jorgenson, *Rapid Commun. Mass Spectrom.*, 3 (1989) 87.
25 N. J. Reinhoud, W. M. A. Niessen, U. R. Tjaden, L. G. Gramberg, E. R. Verheij and J. van der Greef, *Rapid Commun. Mass Spectrom.*, 3 (1989) 87.
26 P. Thibault, S. Plesance and M. V. Laycock, *J. Chromatogr.*, 542 (1991) 483.
27 T. Hu, A. S. W. deFreitas, J. Marr, S. Pleasance and J. L. C. Wright, unpublished results.
28 J. Tehrani, R. Macomber and L. Day, *J. High Resolut. Chromatogr.*, 14 (1991) 10.
29 S. Pleasance, P. Thibault, M. A. Mosely, L. J. Deterding, K. B. Tomer and J. W. Jorgenson, *J. Am. Soc. Mass Spectrom.*, 1 (1990) 312.
30 N. J. Reinhoud, E. Schröder, U. R. Tjaden, W. M. A. Niessen, M. C. Ten Noever de Brauw and J. van der Greef, *J. Chromatogr.*, 516 (1990) 147.
31 S. W. Ayer, J. C. Marr, S. Pleasance, M. A. Quilliam, P. G. Sim and P. Thibault, in E. G. Bligh (Editor), *Seafood Science and Technology, Proceedings of the SEAFOOD 2000 Conference, Halifax, NS, May 13–16, 1990*, Blackwell Scientific Publications, Oxford, 1991, in press.
32 D. K. MacMillan, M. L. Gross, B. N. Pramanik and A. K. Mallams, in *Proceedings of the 39th ASMS Conference on Mass Spectrometry and Allied Topics, Nashville, TN, May 20–24, 1991*, American Society for Mass Spectrometry, East Lansing, MI, 1991, p. 124.
33 P. Thibault and S. Pleasance, in preparation.

Journal of Chromatography, 591 (1992) 341–349
Elsevier Science Publishers B.V., Amsterdam

CHROM. 23 809

Analyte focusing in capillary electrophoresis using on-line isotachophoresis

D. S. Stegehuis, U. R. Tjaden* and J. van der Greef

Division of Analytical Chemistry, Center for Bio-Pharmaceutical Sciences, Leiden University, P.O. Box 9502, 2300 RA Leiden (Netherlands)

(First received June 26th, 1991; revised manuscript received October 21st, 1991)

ABSTRACT

The on-line coupling of isotachophoresis with capillary electrophoresis as presented earlier was improved with respect to recovery, reproducibility and ease of operation by developing a new system. Owing to the isotachophoretic sample pretreatment resulting in analyte focusing, the corresponding determination limits in capillary electrophoresis could be enhanced by three orders of magnitude. It is shown that both the reproducibility and selectivity are improved considerably owing to the two-dimensional electrophoretic approach. The potential of one-line coupled isotachophoresis–electrophoresis was demonstrated using a fluorescein isothiocyanate derivative of the peptide angiotensin III as test compound.

INTRODUCTION

In the last year, a number of papers [1–7] have been published dealing with sample pretreatment methods which are compatible with a highly efficient, miniaturized technique such as capillary electrophoresis (CE). Major goals are the improvement of both the loadability of the CE system and the applicability of CE in bioanalysis. The combination of two orthogonal separation methods such as high-performance liquid chromatography (HPLC) and CE has already been applied in various configurations [8,9]. The major advantage of this combination is an enhanced resolution and peak capacity, although the effective loadability is still limited.

Another approach is to use preconcentrating sample pretreatment techniques [10]. Similarly to the use of precolumns in HPLC, they can be applied in combination with CE. Micro-scale precolumns can be installed in series with the CE capillary. A disadvantage of these systems is that they are very easily plugged by particles or denaturating macromolecular compounds, making this method less suitable for routine analysis of biological samples. A similar method with promising results is the use of conventional HPLC off-line precolumn cartridges (1–0.1 ml), which are commercially available and can be used instead of micro-scale columns. This method led to an increased detectability by a factor of 15 [11].

The application of coating of the fused-silica wall capable of binding the analyte has also been described [12,13]. Micellar electrokinetic capillary chromatography (MECC) is an example combining the mechanisms of electrophoresis and chromatography, making CE more suitable for the analysis of biological fluids [14]. These electrochromatographic techniques increase the selectivity of the electrophoretic system but give little or no improvement in the loadability.

Instead of combining a chromatographic method with CE for a two-dimensional separation, it is also possible to couple two electrophoretic methods. Similarly to two-dimensional chromatography, two-dimensional electrophoresis can be applied using different electrophoretic separation mechanisms to increase the loadability and selectivity. The most common example of such an approach is in fact the injection of diluted samples, which induces a higher field strength than the electrophoresis buffer in the

0021-9673/92/$05.00

CE system. This principle is also called sample stacking [15–17]. In this instance a discontinuous electrophoresis system is created, resulting in isotachophoretic zone sharpening and concentration. Sample stacking has been used successfully in gel electrophoresis but can also be used in free solution electrophoresis [18]. However, in free solution electrophoresis the isotachophoretic effect may be decreased by the electroosmotic flow (EOF). This EOF can be reduced by using capillaries that are deactivated by a special coating minimizing the zeta potential. Such capillaries are already supplied by various manufacturers. Concentration factors of about 25 can be obtained by applying these isotachophoretic phenomena in capillary electrophoresis [12]. Everaerts and co-workers [19–21] reported the use of ITP and CE effects in both ITP and CE, demonstrating the good compatibility of both electrophoretic methods.

Recently several papers have been published that describe the use of a complete isotachophoretic system coupled on-line to a capillary electrophoresis system. Kaniansky and Marak [22] used an isotachophoretic system with a sample preconcentration part. Both the ITP and CE parts of their system had an I.D. of 300 μm. Dolnik *et al.* [23] developed an ITP system consisting of compartments with decreasing diameters, permitting the introduction of larger volumes. Stegehuis and co-workers [1,24–26] presented a system in which a separate ITP system was coupled to a separate CE system. The ITP system had an I.D. of 500 μm and the CE an I.D. of 50 μm. The dimensions were chosen to ensure that both systems could operate at maximum performance. An increase in detectability by a factor of 100 was shown. Foret *et al.* [27] described a similar system using dyes to determine the moment of injection from ITP to CE.

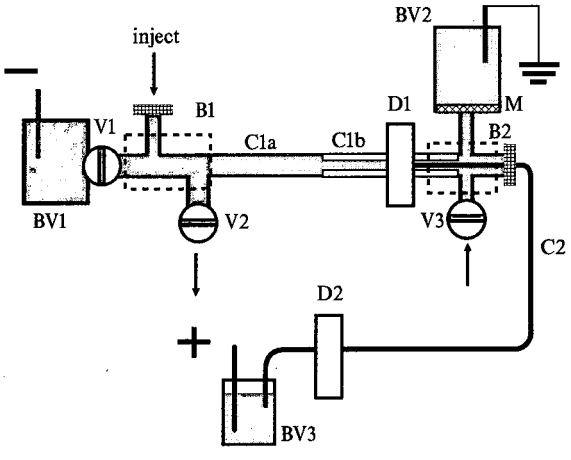

Fig. 1. Schematic diagram of complete ITP–CE system. V1 = valve 1; V2 = valve 2; V3 = valve 3; D1 = ITP UV detector; D2 = CE LIF detector; M = membrane; BV1 = terminating buffer vial; BV2 = leading buffer vial; BV3 = electrophoresis buffer vial; B1 = injection block; B2 = ITP–CE interface block; C1a = separation part of the ITP capillary; C1b = detection part of the ITP capillary; C2 = CE capillary.

This paper describes an improved ITP–CE system derived from the system presented earlier [1]. With the developed system improvements were achieved with respect to recovery, reproducibility and ease of operation. The detectability was improved by three orders of magnitude compared with off-line CE. A fluorescein isothiocyanate derivative of angiotensin III was used as a test compound.

EXPERIMENTAL

Materials

Hydrochloric acid (HCl) and acetonitrile (ACN) was purchased from Baker Chemicals (Deventer, Netherlands), tris(hydroxymethyl)aminomethane (Tris), barium hydroxide and sodium borate from Merck (Darmstadt, Germany), hydroxypropylmethylcellulose (HPMC) from Sigma (St. Louis, MO, USA), β-alanine (β-ala) and fluorescein isothiocyanate (FITC) from Aldrich (Steinheim, Germany) and angiotensin III (A III) from Bachem Feinchemicalien (Bubendorf, Switzerland).

The leading buffer (LB) was 0.01 *M* HCl adjusted to pH 9.2 with 0.5 *M* Tris containing 0.05% (w/w) HPMC. After preparation the buffer can be used for about 2 weeks. The same buffer was used for CE. The terminating buffer (TB) was 0.01 *M* β-ala adjusted to pH 10.4 with a saturated solution of $Ba(OH)_2$. This buffer was prepared freshly every day. The borate buffer used for the FITC derivatization reaction was 0.2 *M* sodium borate. Demineralized water was used throughout.

Equipment

Isotachophoresis. A schematic diagram of the coupled ITP–CE system is given in Fig. 1. The buffer vials and the injection block were laboratory-

made and constructed from Plexiglas. The injection block of the ITP system was constructed as described [28]. The leading buffer vial and the capillary were connected by a Plexiglas block which also formed the interface to the CE system. Between this interface block and the leading buffer compartment a semi-permeable membrane was placed in order to prevent the LB from the buffer vial from flowing into the capillary either electrokinetically or hydrodynamically. The ITP capillary consisted of two parts, a separation part made of PTFE (250 mm × 450 μm I.D. × 700 μm O.D.) and a detection part made of fused silica (50 mm × 320 μm I.D. × 450 μm O.D.). A few millimetres of coating were burned off for on-column detection, for which a modified liquid chromatographic UV detector was used (Model 440, Waters Assoc., Milford, MA, USA). The conventional flow cell was replaced with a messing block positioning the capillary in-line with a 300-μm pinhole through which light was guided. The signal in the reference channel was reduced to the same extent.

Injection into the ITP system was done with a 100-μl syringe. For the ITP system a power supply with reversible polarity (Model RR 100-1.5R Gamma, High Voltage Research, Coimex, Hattem, Netherlands) was used in the negative mode.

Capillary electrophoresis

The CE system was a modular laboratory-made system using capillaries of 50 μm I.D. and 220 μm O.D. (SGE, North Melbourne, Australia). The total length of the capillary was *ca.* 500 mm with a length of *ca.* 300 mm to the detector. In order to obtain a reproducible performance, the dynamic coating with HPMC in the CE capillary was renewed and saturated between every run by flushing it with LB for 10–15 min.

Detection was based on laser-induced fluorescence (LIF) using an air-cooled argon ion laser (Model 161 C, Spectra-Physics, San Jose, CA, USA) lasing at 488 nm. On-capillary detection was performed by focusing the laser beam on the capillary, from which the coating on a small part had been removed, placed in a laboratory-made holder.

The fluorescence was detected with a blue–green-sensitive photomultiplier tube (PMT) (Model 635B, Thorn EMI, Ruislip, Middlesex, UK) operating at 600 V generated by a high-voltage power supply (Model 244, Keithley Instruments, Cleveland, OH, USA). The signal was processed by a current amplifier (Model 427, Keithley Instruments). For CE a 40-kV positive high-voltage power supply (Model RR 40-1.5P Gamma) was used. Electropherograms of both ITP and CE were registered on a flat-bed recorder (Model 40, Kipp & Zonen, Delft, Netherlands).

Coupled isotachophoresis–capillary electrophoresis. To couple the ITP and the CE system the CE capillary was inserted into the ITP capillary through the Plexiglas interface block (Fig. 1). The CE capillary was positioned just "downstream" of the location where UV detection takes place on the ITP capillary. The exact position of the capillary was determined by inserting the CE capillary just before blocking the light beam of the UV source. The levels of the terminating buffer vial and the buffer vial at the outlet of the CE capillary were adjusted carefully to prevent hydrodynamic flow.

Procedures

Derivatization of angiotensin III. To 50 μl of a 1 m*M* A-III solution (1 mg/ml), 50 μl of 2.5 m*M* FITC solution in borate buffer (0.2 *M*, pH 9.5) were added. The derivatization mixture was heated at 60°C for 30 min in order to complete the reaction. The samples for the calibration graphs were prepared by appropriate dilutions of A-III–FITC in demineralized water.

Pretreatment of plasma samples. Before injection into the ITP system, the plasma samples were deproteinated by adding 2 ml of ACN, vortexing for 10 s and centrifugating for 10 min at 2000 *g*. To the decanted supernatant either FITC (blank plasma samples) or A-III + FITC (spiked plasma samples) was added.

RESULTS AND DISCUSSION

In order to make optimum use of the focusing effect of the ITP system and the efficiency of the CE system, the coupled system was developed such that the mutual influence of the two systems was minimal. Further, the system was optimized with respect to reproducibility and ease of operation.

Isotachophoresis

In the system used, the leading and terminating

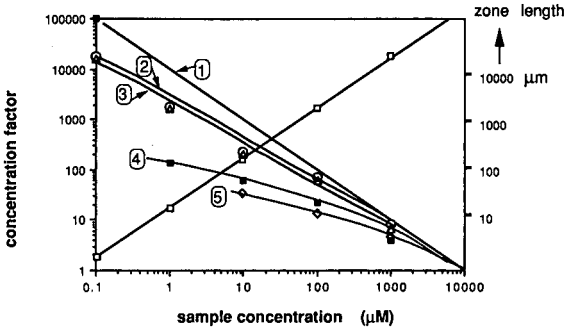

Fig. 2. Concentrating capacity of the ITP system as a function of the sample concentrations at different percentages of HPMC in the leading buffer. 1 = Theoretical concentration factor; 2 = 0.1% HPMC; 3 = 0.05% HPMC; 4 = 0.025% HPMC; 5 = 0.01% HPMC. On the right-hand ordinate the zone length (□) at different concentrations is given at a concentration of 0.05% HPMC in the leading buffer.

buffers have relatively high pH values, resulting in a very high EOF. Usually in ITP the effect of EOF can be limited but not eliminated by using PTFE capillaries and using a membrane between the leading electrolyte buffer vial and the capillary. However, in the developed system a piece of fused silica was installed in order to perform on-capillary detection. At pH 9.2 this piece of fused silica induces such a high EOF that the ITP process is extremely hampered. The EOF can be decreased by adding a non-ionic surfactant such as HPMC [29–31]. This non-ionic surfactant increases the viscosity of the buffer and forms a dynamic coating on the capillary wall. Fig. 2 shows the influence of different percentages of HPMC on the concentrating capacity of the ITP system. Without HPMC an EOF exists in the direction of the terminating buffer vial, while the ITP process takes place in the opposite direction. In this way the concentrating capacity and the zone-sharpening effect are almost completely destroyed. By adding HPMC the ITP process functions again according to Kohlrausch's law [32], implying that the sample zone will acquire a concentration related to that of the leading buffer and the respective mobilities. Despite the addition of HPMC it must be noted that below a certain zone length the observed signal starts to deviate from the theoretical value. This can be explained by the fact that below a critical zone length the sample zone starts to become shorter than the size of the detection window (300 μm). Consequently, the intensity of the signal is no longer representative of the concentration factor.

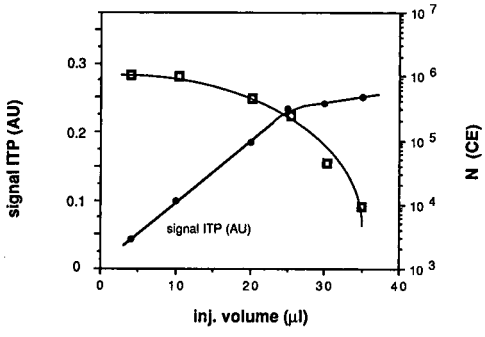

Fig. 3. Influence of injection volume on the detector signal measured in the ITP system [left-hand ordinate (●)] and the performance of the CE system [right-hand ordinate (□)].

The optimum concentration of HPMC was 0.05% w/w, this being a compromise between reduction of the EOF and an unacceptable increase in viscosity. At HPMC concentrations of 0.1% (w/w) and higher, flushing of the 50-μm I.D. CE capillary became a major problem and blockage of the CE capillary repeatedly occurred.

Injection into the ITP system took place using a 100-μl injection syringe. Possible memory effects can be avoided by flushing the needle between injections with a buffer solution containing HPMC. Fig. 3 shows the performance of the ITP system using different injection volumes. Injection volumes above 20 μl resulted in a decreased signal and reproducibility. The internal volume of the Plexiglas block in which the sample is injected is about 50 μl, whereas the internal volume of the capillary is only 35 μl. The capacity of the ITP system is related to the volume of the ITP capillary. Consequently, the capacity can be increased by using longer capillaries, but doubling the length would raise the loadability only by a factor of two but would increase the analysis time considerably. Taking into consideration that by using the concentration capacity of the ITP system an improvement in detection limit of three orders of magnitude can be obtained, the factor of two resulting from doubling the length of the capillary can be neglected.

Capillary electrophoresis

The leading buffer of the ITP system containing HPMC was also used as the electrophoresis buffer in the CE system. The addition of HPMC to the CE system had major consequences for the EOF. Although the EOF was not completely stopped it was

lowered considerably. The EOF was slowed so much that the negatively charged FITC derivatives migrated in the direction of the anode. As a consequence of this strongly reduced EOF, relatively short capillaries (300 mm to the detector) could be used for CE separation.

Coupled isotachophoresis–capillary electrophoresis

Injection into the CE system is possible electrokinetically, hydrodynamically or as a combination of the two. Because the CE capillary is exactly positioned "downstream" of the UV detector in the ITP system, it should be possible to time the moment of injection accurately. This injection method leads to the highest selectivity because a perfect heart cut could be made out of a large number of zones. Nevertheless, making a reproducible electrokinetic injection of a zone a few micrometres in length, migrating with a velocity of *ca.* 250 μm/s, would still be very difficult.

A less selective but more reproducible injection strategy would be to choose ITP conditions so that as little as possible of the zones comigrate with the analyte zone, and all zones migrating between the leading and terminating buffers are injected hydrodynamically into the CE system. Such a hydrodynamic injection has to be performed very carefully in order not to disturb either the ITP or CE process, which can be done by syphoning in the direction of the CE capillary during the ITP process. Because of the large differences in dimensions between the ITP and CE systems, this can be achieved by applying a small difference in level (*ca.* 4 cm) between the terminating buffer vial and the electrophoresis buffer vial, generating a small hydrodynamic flow. After starting the CE process, valve 1 (Fig. 1) is closed and valves 2 and 3 are opened. Now all vessels are on the same level and the CE process will take place without disturbance caused by hydrodynamic flow. During the hydrodynamic injection a radial split with a ratio of 1:10 is made. This means that 10% of the analyte ions injected into the ITP system are introduced into the CE system.

The injection into the CE system was optimized with respect to the moment of stopping the ITP process and starting the CE process, and the time between starting the CE and flushing the ITP system. The optimum moment of injection can be determined by plotting the signal obtained in CE *versus* the moment of injection. The moment of injection can be defined by t_i, the time between the appearance of the signal in the ITP system and actually stopping the ITP process. A negative value of t_i means that the ITP is stopped before appearance of the signal. The results are shown in Fig. 4. Although in principle a recovery of 100% can be obtained, the reproducibility is very poor and the efficiency is also affected. In that case not only an axial but also a radial migration is needed, leading to considerable entrance functions. The poor reproducibility is caused by the fact that the moment of injection is very critical, as discussed above. A recovery of 100% can only be obtained if the zone is exactly and completely in front of the capillary. At the moment the high voltage is switched on the zones are injected electrokinetically. Zones with a length in the micrometres or even nanometres range are therefore difficult to inject. Also, matrix compounds that migrate in front of the analyte zone might influence the retention time of the analyte, making reproducible time-based injection with 100% recovery impossible.

After $t_i \geqslant 2$ min (Fig. 4), a very reproducible split of 1:10 is made. This injection is exclusively made by hydrodynamic flow and not electrokinetically. Although only a recovery of 10% is obtained in this way, this moment of injection is preferred because of the high reproducibility and the possibility of time-based injection. Within a time window of at least 5 min the injections can still be performed with a relative standard deviation (R.S.D.) of $\leqslant 5\%$.

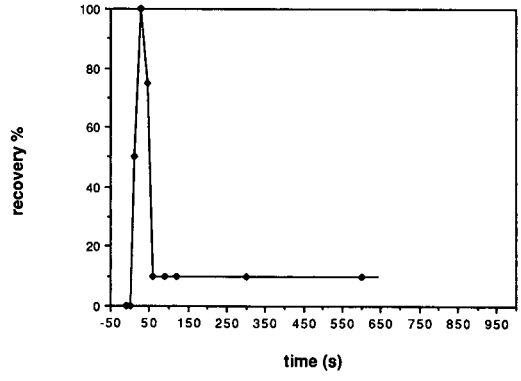

Fig. 4. Recovery in the CE system as a function of the moment of injection from the ITP into the CE system ($t = 0$ is the time that the signal has been detected in the ITP detector).

This gives the ITP process sufficient space for retention time variations caused by differences in sample composition.

After the CE process has been started, the ITP system must be backflushed, which is done after closing valve 1 (Fig. 1) and opening valves 2 and 3, in order to prevent the terminating buffer from entering the CE system and disturbing the continuous buffer system. The time between starting the CE system and flushing the ITP system is only critical if injections are made at $t_i \leqslant 2$ min. In these situations the analyte is still at the initial part of the CE capillary. The hydrodynamic velocity in the CE capillary is much smaller than the migration velocity during electrophoresis, so with the sample still being at the initial part of the CE capillary the possibility exists that the sample is flushed partly or completely out of the CE capillary during the backflushing of the ITP system, which can cause irregularities. If $t_i \geqslant 2$ min and the time before flushing is between 5 and 10 s, no sample will be flushed out and the TB will not influence the CE process.

Quantitative aspects

In order to investigate the quantitative potential of the combined ITP–CE system, calibration graphs of an FITC derivative of the peptide angiotensin III were made. For comparison with CE also some graphs for this derivative were obtained with off-line CE, using the optimized conditions as given in Table I. The results for both systems are given in Table II.

From these results from Fig. 5a and b (representing an injection of a 5 μl/ml and a 5 ng/ml solution in an off-line CE and an ITP-CE system, respectively) it can be seen that a factor of 1000 in detectability has been achieved. The absolute minimum detectable amount is the same in both configurations because detection takes place in both systems in the same CE-LIF combination. The minimum detectable concentration could be lowered a factor of 1000 by applying analyte focusing using a two-dimensional electrophoresis system. The precision of CE determinations can also be improved from an R.S.D. of the peak area of 9–7% to 5–3% by coupling it on-line to an ITP pretreatment unit.

Influence of biological matrix

To establish whether this two-dimensional electrophoretic system also results in an increase in selectivity, some experiments were done with plasma samples. Plasma was spiked with FITC-derivatized A-III. There was no intention of determining endogenous A-III because the derivatization procedure was not optimized for this application. These experiments were carried out only to observe the performance of the ITP-CE system when plasma samples were injected repeatedly. In off-line CE often a rapid decrease in performance is observed with repeated injections of biological samples. Fig. 6a shows plasma samples containing blank deprotei-

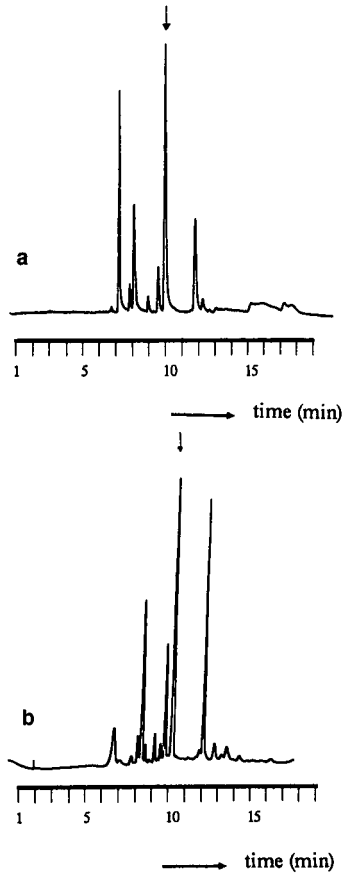

Fig. 5. (a) Electropherogram of off-line CE. An equivalent of about 1 nl of a solution of A-III–FITC derivative with a concentration of 5 μg/ml was injected hydrostatically. For other conditions, see Table I. The arrow indicates the A-III–FITC derivative peak. (b) Electropherogram of on-line ITP-CE. 10 μl of a solution of A-III–FITC derivative with a concentration of 5 ng/ml were injected into the ITP system. For other conditions, see Table I. The arrow indicates the A-III–FITC derivative peak.

TABLE I

OPTIMIZED CONDITIONS FOR THE ITP AND CE SYSTEMS

Parameter	ITP	CE
Buffers	0.01 *M* β-ala	
TB	pH = 10.4	
	$Ba(OH)_2$	
LB	0.01 *M* Cl^-–Tris	0.01 *M* Cl^-–Tris
	pH = 9.2	pH = 9.2
HPMC	0.05% (w/w)	0.05% (w/w)
Voltage (kV)	5	25
Capillary:		
Total length (cm)	25	50
Length to detector (cm)	22.5	30
Material	20 cm PTFE + 5 cm fused silica	50 cm fused silica
Detection	UV (254 nm) on-capillary	LIF ($\lambda_{ex}/\lambda_{em}$ 488/514 nm) on-capillary
Injection	10 μl (syringe)	10% equivalent of ITP injection

TABLE II

VALIDATION AND COMPARISON OF THE PERFORMANCE OF THE CE SYSTEM AND THE COUPLED ITP–CE SYSTEM

Conditions as in Table I.

Parameter	CE		ITP–CE	
	A-III–FITC concentration (μg/ml)	R.S.D. (%)	A-III–FITC concentration (ng/ml)	R.S.D. (%)
	1	8.5	0.5	3.7
	5	7.0	5	2.9
	20	7.0	10	4.5
Day to day ($n = 3$)	5	7.7	5	3.5
Calibration graph	$y = (0.51 \pm 0.02)x + (0.1 \pm 0.4)$		$y = (1.43 \pm 0.01)x + (0.04 \pm 0.04)$	
Correlation coefficient	0.9982		0.999	
Minimum detectable concentration (signal-to-noise = 3)	100 ng/ml		100 pg/ml	
	100 nmol/l		100 pmol/l	
Absolute detection limit	100 fg		100 fg	
	100 amol		100 amol	

nized plasma spiked with an overload of FITC and Fig. 6b shows a deproteinized plasma sample spiked with A-III and an overload of FITC. Even with such complex samples reproducible results are obtained on applying ITP–CE, making CE suitable for the routine analysis of biological samples. About 10% of the whole zone that migrates in the ITP system is injected into the CE system. Therefore, the selectivity has to be tuned by the choice of the combination of LB and TB. If this buffer system forms a very small mobility window around the analyte of interest, the selectivity will be high. If several components have to be monitored by CE, a relatively large mobility window can be chosen in the ITP buffer system, making a more universal analysis method possible.

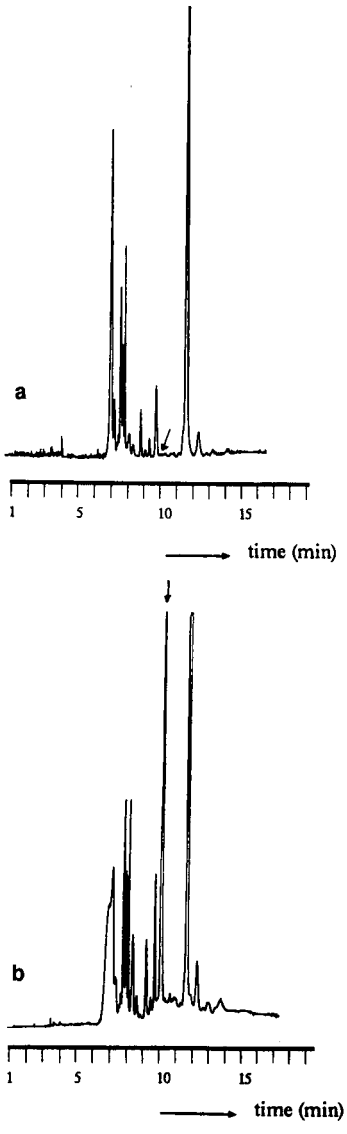

Fig. 6. (a) Electropherogram of deproteinized plasma derivatized with FITC. 10 μl were injected into the ITP system. For other conditions, see Table I. The arrow indicates the time at which the A-III–FITC derivative would migrate. (b) Electropherogram of deproteinated plasma derivatized with FITC and spiked with A-III–FITC (50 ng/ml). A 10-μl sample was injected into the ITP system. For other conditions, see Table I. The arrow indicates the A-III–FITC derivative peak.

CONCLUSIONS

Analyte focusing in CE using on-line ITP has been performed in a two-dimensional electrophoresis system which has been developed and optimized. Analogously to multi-dimensional chromatography, this resulted in increases in detectability, selectivity and reproducibility. In comparison with CE an improvement in the minimum detectable concentration of a factor of 1000 is achieved. The reproducibility of the peak area is improved from R.S.D. *ca.* 7% to *ca.* 3.5% without the use of an automated system. The ease of operation is improved in comparison with off-line CE because injection can be performed by syringe.

REFERENCES

1 D. S. Stegehuis, H. Irth, U. R. Tjaden and J. van der Greef, *J. Chromatogr.*, 538 (1991) 393.
2 W. G. Kuhr, *Anal. Chem.*, 62 (1990) 403.
3 D. M. Goodall, D. K. Lloyd and S. J. Williams, *LC · GC Int.*, 3, No. 7 (1990) 28.
4 S. Terabe, *Anal. Chem.*, 62 (1990) 10.
5 J. H. Knox and K. A. McCormack, *J. Liq. Chromatogr.*, 12 (1990) 2435.
6 P. G. Righetti, *J. Chromatogr.*, 516 (1990) 3.
7 T. Hanai, H. Hatano, N. Nimura and T. Kinoshita, *J. High. Resolut. Chromatogr.*, 13 (1990) 624.
8 W. Th. Kok, K. P. Hupe and R. W. Frei, *J. Chromatogr.*, 436 (1988) 421.
9 M. M. Bushey and J. W. Jorgenson, *Anal. Chem.*, 62 (1990) 978-984.
10 J. P. Larmann and J. W. Jorgenson, paper presented at the *Third International Symposium on High Performance Capillary Electrophoresis, San Diego, CA, February 3–6, 1991*, Abstract No. PM-13.
11 H. Haataja and M. Novotny, paper presented at the *Third International Symposium on High Performance Capillary Electrophoresis, San Diego, CA, February 3–6, 1991*, Abstract No. PT-45.
12 Z. El Rassi and J. Cai, paper presented at the *Third International Symposium on High Performance Capillary Electrophoresis, San Diego, CA, February 3–6, 1991*, Abstract No. PM-51.
13 G. J. M. Bruin, P. P. H. Tock, J. C. Kraak and H. Poppe, *J. Chromatogr.*, 517 (1990) 557.
14 S. Terabe, Y. Miyashita, O. Shibata, E. R. Barnhart, L. R. Alexander, D. G. Patterson, B. L. Karger, K. Hosaya and N. Tanaka, *J. Chromatogr.*, 516 (1990) 23.
15 R. Aebersold and H. D. Morrison, *J. Chromatogr.*, 516 (1990) 79.
16 A. Vinther, F. M. Everaerts and H. Soeberg, *J. High Resolut. Chromatogr.*, 13 (1990) 639.
17 X. Huang and J. I. Ohms, *J. Chromatogr.*, 516 (1990) 233.
18 V. Dolnik, K. A. Cobb and M. Novotny, *J. Microcolumn Sep.*, 3 (1990) 127.
19 Th. P. E. M. Verheggen, A. C. Schoots and F. M. Everaerts, *J. Chromatogr.*, 503 (1990) 245.
20 J. L. Beckers and F. M. Everaerts, *J. Chromatogr.*, 508 (1990) 3.

21 J. L. Beckers and F. M. Everaerts, *J. Chromatogr.*, 508 (1990) 19.
22 D. Kaniansky and J. Marak, *J. Chromatogr.*, 498 (1990) 191.
23 V. Dolnik, M. Deml and P. Bocek, *J. Chromatogr.*, 320 (1985) 89.
24 D. S. Stegehuis, U. R. Tjaden and J. van der Greef, paper presented at *The 14th International Symposium on Column Liquid Chromatography, Boston, MA, May 20–25, 1990*, P415.
25 U. R. Tjaden, D. S. Stegehuis and J. van der Greef, paper presented at the *Second international Symposium on Microcolumn Separation Methods*, Balsta, Sweden, August 19–22, 1990.
26 D. S. Stegehuis, U. R. Tjaden and J. van der Greef, paper presented at the *18th International Symposium on Chromatography, Amsterdam, September 23—28, 1990*, Abstract No. P013.
27 F. Foret, V. Sustacek and P. Bocek, *J. Microcolumn Sep.*, 5 (1990) 229.
28 F. M. Everaerts, J. L. Beckers and Th. P. E. M. Verheggen, *Isotachophoresis— Theory, Instrumentation and Application*, Elsevier, Amsterdam, 1976.
29 S. Hjerten, L. Valtcheva, K. Elinbring and D. Eaker, *J. Liq. Chromatogr.*, 12 (1989) 2471.
30 P. Oefner, R. Hafele, G. Bartschand and G. Bonn, *J. Chromatogr.*, 516 (1990) 251.
31 D. Josic, K. Zeilinger, W. Reutter, A. Bottcher and G. Schmitz, *J. Chromatogr.*, 516 (1990) 89.
32 F. Kohlrausch, *Ann. Phys. Chem.*, 62 (1987) 209.

Journal of Chromatography, 591 (1992) 351–357
Elsevier Science Publishers B.V., Amsterdam

CHROM. 23 793

Thin-layer electrophoresis of hydroxyethyl starches on a modified silica gel support

D. Haidacher and G. K. Bonn

Institute of Radiochemistry, University of Innsbruck, Innrain 52a, A-6020 Innsbruck (Austria)

H. Scherz*

Deutsche Forschungsanstalt für Lebensmittelchemie, Lichtenbergstrasse 4, W-8046 Garching (Germany)

E. Nitsch and R. Wutka

Laevosan-GmbH, Estermannstrasse 17, A-4021 Linz (Austria)

(First received May 31st, 1991; revised manuscript received October 7th, 1991)

ABSTRACT

The recent developed thin-layer electrophoresis on modified silanized silica gel was applied to the separation of hydroxyethyl starches (HES) and glycogen and of HES with different degrees of substitution. This method permits a rapid qualitative and semi-quantitative determination of HES in animal tissues such as liver, lung, heart and kidney after their disintegration with alkali and precipitation with ethanol.

INTRODUCTION

Hydroxyethyl starch (HES) is produced by hydroxyethylation of starch [1] and is applied increasingly as a blood plasma expander instead of the dextrans used so far [2]. To obtain information about its distribution and degradation in bodies it is important to determine HES concentrations in individual tissues.

Previous methods for the determination of HES are based on two principles: (a) conversion of the hydroxyethyl group attached to the starch molecules into ethyl iodide by heating the sample with concentrated hydriodic acid and determination of the ethyl iodide either by reaction with silver nitrate and bromine in acetic acid [3] or by gas chromatography [4,5]; (b) hydrolysis of the HES with acid and determination of the substituted and non-substituted glucose units by gas chromatography after derivatization either to O-trimethylsilyl ether [6,7] or to alditol acetates [8]. These methods have the disadvantage, that only the total amount of hydroxyethyl groups can be determined. In the present application, where the samples consist of a mixture of HES and glycogen, it is not possible to determine the real concentration of HES with these methods and a prior separation of the individual components has to be carried out.

Recently, a thin-layer electrophoretic method was developed for the separation of polysaccharides using silanized silica gel, the surface of which is covered with a thin film of 1-octanol [9–11]. With this stationary phase, better separations of the polysaccharides could be achieved than on chromatographic paper or cellulose acetate sheets. A further advantage lies in the possibility of revealing the separated polysaccharides with specific and sensitive sulphuric acid- and phosphoric acid-containing car-

0021-9673/92/$05.00

bohydrate reagents, which was not possible on the previously used supports such as cellulose or acetylcellulose owing to the formation of intense background coloration. This paper describes the application of this method to the separation of HES and glycogen and of HES with different degrees of substitution and its detection and determination in animal tissues.

EXPERIMENTAL

Materials

The experiments were carried out with a Bio-Rad electrophoretic cell (Type 1405) for 150 × 200 mm plates and a Bio-Rad power supply (Bio-Rad Labs., Richmond, CA, USA); thin-layer plates were prepared with equipment from Desaga (Heidelberg, Germany). The quantitative evaluation of the separated zones was carried out by the thin-layer scanner (Shimadzu, Tokyo, Japan).

Silanized silica gel for thin-layer chromatography and 1-octanol were purchased from Merck (Darmstadt, Germany), Whatman GF/C glass-fibre paper from Whatman (Maidstone, UK), 1,3-dihydroxynaphthalene (naphthoresorcinol) from Serva (Heidelberg, Germany) and polyvinylpyrrolidone K-90 (relative molecular mass M_r = 360 000 dalton) from Fluka (Buchs, Switzerland). Hydroxyethyl starches with different degrees of substitution and relative molecular mass (*e.g.*, HES 450/0.7, M_r = 450 000 dalton, degree of substitution = 0.7), non-substituted starch (degraded amylopectin) and glycogen were supplied by Laevosan (Linz, Austria).

Isolation of hydroxyethyl starches from animal tissues

The procedure is based on the method of Grossfeld [12] for the determination of starches in meat products and which was adapted for the analysis of thickening agents in the same materials by Bauer and Vali [13]. The organs were placed in 35% potassium hydroxyde solution and heated for 3 h under reflux in a boiling water-bath. The proteins and lipid compounds are degraded whereas the polysaccharides, especially the 1,4-glycans, remain unaltered by this treatment. After cooling, a sixfold excess of ethanol was added to precipitate the polysaccharides. After standing at 0–4°C overnight, the precipitate was centrifuged at 0°C and 8000 *g*. The supernatant was removed and the residue was washed three times with absolute ethanol and dissolved in 2.0 ml of the analyte buffer. An aliquot of 2–5 μl was used for electrophoresis.

For the test with albumin, a 5% aqueous solution was diluted with 0.3 *M* borate buffer (1:1, v/v) and 1.5 mg of HES 450/0.7 and 1.5 mg of glycogen were dissolved in 1 ml of this solution. With blood plasma the pure product was diluted with 0.3 *M* borate buffer (1:1, v/v) and 1.5 mg of HES 450/0.7 and 1.5 mg of HES 70/0.3 were dissolved in 1 ml.

For the determination of HES in animal tissues, rabbits had been treated with HES injections and killed after certain periods of time. Their organs were kept at −70°C until analysis. After thawing and weighing the organs, the polysaccharide were isolated according to the procedure described above.

Electrophoresis on the silanized silica gel–1-octanol support

The idea for this system was to develop a support for electrophoretic separations on which the adsorption and molecular sieve effect and the electroendoosmosis are minimal and on which the separated substances can be revealed with agressive reagents (*e.g.*, those containing sulphuric or phosphoric acid) as on normal thin-layer chromatograms. This was achieved with silanized silica gel, the surface of which was covered with a thin film of 1-octanol [9]. The latter compound can be removed from the plate after the run by evaporation and the separated substances can be detected on the dry silica gel layer as usual by spraying with the respective detection reagent and additional heating if necessary.

For its preparation, silanized silica gel is suspended in a low-boiling organic solvent (*e.g.*, methyl acetate, dichloromethane) containing 1-octanol. After stirring for *ca.* 30 min to obtain a uniform impregnation of the particles with the solution, the solvent is evaporated *in vacuo* until a lump-free powder is obtained. For impregnation with buffer, the dry powder is placed in a mortar and the buffer solution used for electrophoresis is added stepwise under vigorous stirring with the pestle. A small separate part of this buffer contains 2% of polyvinylpyrrolidone as binding agent for the dry layer ready for detection after the electrophoresis. The particles are

wetted and the homogeneous slurry obtained is spread on 200 × 200 mm glass plates (layer thickness 0.3 mm). Immediately after coating, the plates are transferred to a desiccator with a humid atmosphere. They can be used after a storage time of 3 h; this times should not exceed 48 h because after that period the loss of water from the layer becomes too high.

The silanized silica gel–1-octanol system prepared in this manner has a structure like a very weak gel. The 1-octanol liquid phase is attached strongly to the surface of the silanized silica gel particles even after their suspension in the aqueous buffer and no leaching out into the surrounding aqueous phase was observed. It is possible that this weak gel structure is formed by hydrogen bonds between the OH groups of the 1-octanol and the water molecules while the strong adsorption of 1-octanol itself is due to a hydrophobic interaction between the hydrocarbon part of the latter molecules with the hydrophobic groups on the surface of the silanized silica gel. The electroendoosmosis is also strongly diminished (see the low mobility of ω-hydroxymethylfurfurol in the present electropherograms) and this effect can be explained by coverage of the charges on the silica gel surface by the 1-octanol phase.

Conversely, when normal unsilanized silica gel is used for the preparation of this system, the 1-octanol is detached from the surface of the particles immediately after wetting with the aqueous buffer with the formation of an organic phase in the liquid. The adhesion forces between 1-octanol and the silica gel surface are too low in that event to maintain further adsorption.

The electrophoresis has to be carried out under very moist conditions and substantial evaporation of water from the surface of the layer diminishes the electrophoretic mobilities of the samples.

For the run, 10–15 mm long groves are made with a tip of the needle in the layer and the samples, dissolved in the running buffer, are deposited in the groves. After the electrophoresis the plate is dried at 90°C for 30 min to evaporate the 1-octanol and water. The remaining dry, inert silica gel layer can then be treated with detection reagents is the same way as a normal thin-layer plate.

The exact procedures for preparing the support to be spread on glass plates, electrophoresis and detection were described in detail in previous papers [9–11].

In subsequent experiments the electrophoretic runs were performed under the following conditions: buffer, 0.3 *M* borate (pH 10); current 200 V; time, 120–240 min; temperature, 22–28°C; detection reagent, naphthoresorcinol–sulphuric acid according to Scherz [9].

RESULTS AND DISCUSSION

Separation of standard compounds

Fig. 1 shows the electropherogram of HES with different degrees of substitution but equal average relative molecular mass (M_r = 70 000 dalton) together with unsubstituted starch (M_r = 70 000 dalton) and glycogen. The results from the electrophoretic runs with HES compounds with the same degree of substitution but different relative molecular masses show no significant differences in their mobilities. These results demonstrate that only the degree of substitution is important for the electrophoretic mobilities of these starches on this stationary phase. The higher the degree of substitution, the lower is the formation of charged complexes with

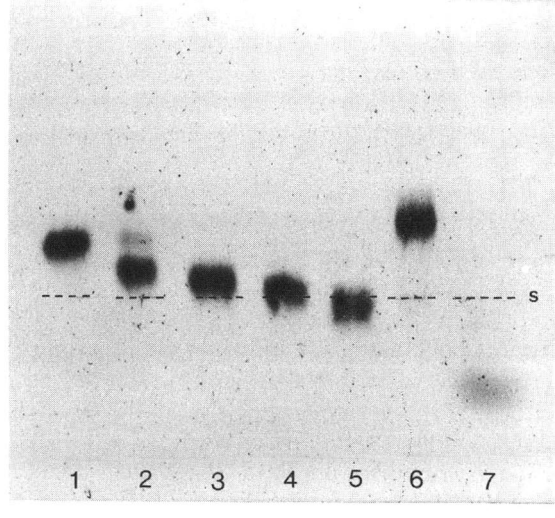

Fig. 1. Electropherogram of hydroxyethyl starches, unsubstituted starch and glycogen. Electrophoresis: 0.3 *M* borate (pH 10.0); 220 V; 240 min; 22°C. 1 = unsubstituted starch; 2 = HES 70/0.3; 3 = HES 70/0.4; 4 = HES 70/0.5; 5 = HES 70/0.7; 6 = glycogen; 7 = ω-hydroxymethylfurfurol. 1–7 dissolved in 0.3 *M* borate buffer (5 mg/ml).

borate ions, which are responsible for the movement in the electric field. The relative molecular mass has no significant influence, *i.e.*, with this material the molecular sieve effect does not occur, in contrast to other materials such as polyacrylamide gel.

Effect of temperature on thin-layer electrophoresis of HES

The temperature of the thin-layer plates exerts a significant influence on the thin-layer electrophoretic separation. By enhancement of the temperature, zone sharpening occurs with a decrease in the individual mobilities and the electroendosmosis is markedly reduced. The optimum temperature was found to be 25–26°C, which was used in subsequent experiments. Fig. 2 shows an optimized separation of the individual components of a mixture of glycogen and HES with of different degrees of substitution.

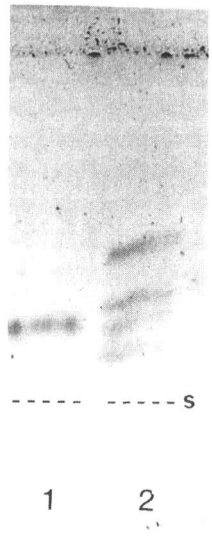

Fig. 2. Effect of temperature of the thin-layer electrophoresis of HES; electropherogram at the optimum temperature for separation. Electrophoresis: 0.3 *M* borate buffer (pH 10); 220 V; 240 min; 26°C. 1 = HES 200/0.5 (1 mg/ml); 2 = HES 70/0.3, HES 200/0.5, HES 450/0.7 and glycogen (0.35 mg/ml each). 1 and 2 dissolved in 0.3 *M* borate buffer.

Quantitative evaluation of thin-layer electropherograms

Solutions of HES 200/0.5 in 0.3 *M* borate buffer were prepared with different concentrations. The

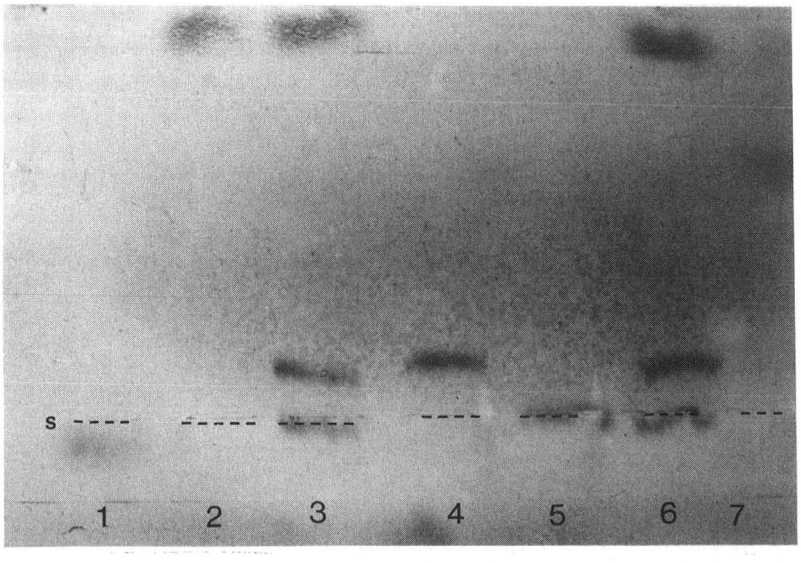

Fig. 3. Detection of HES in human albumin. Electrophoresis: 0.3 *M* borate buffer (pH 10); 180 V; 180 min; 28°C. 1 = ω-hydroxymethylfurfurol; 2 = 5% aqueous solution of human albumin–0.3 *M* borate buffer (pH 10) (1:1, v/v); 3 = HES 450/0.7 (1.5 mg/ml) and glycogen (1.5 mg/ml) dissolved in 5% aqueous solution of human albumin–0.3 *M* borate buffer (pH 10) (1:1, v/v); 4 = glycogen (1.5 mg/ml); 5 = HES 450/0.7 (1.5 mg/ml); 6 = 3; 7 = 3-hydroxyethylglucose (6 mg/ml). 1, 4, 5 and 7 dissolved in 0.3 *M* borate buffer.

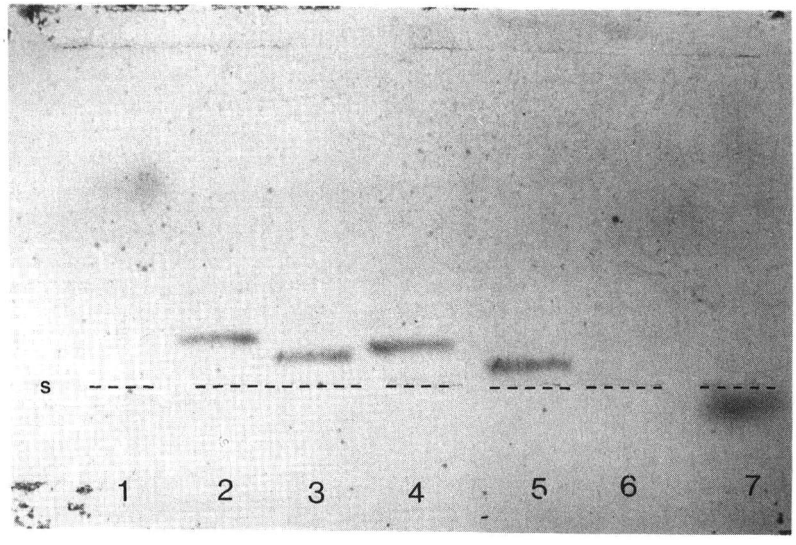

Fig. 4. Detection of HES in blood plasma. Electrophoresis: 0.3 *M* borate buffer (pH 10); 220 V; 120 min; 26°C. 1 = 3-hydroxyethylglucose (6 mg/ml); 2 = HES 70/0.3 (1.5 mg/ml); 3 = HES 450/0.7 (1.5 mg/ml); 4 = HES 70/0.3 dissolved in blood plasma–0.3 *M* borate buffer (pH 10) (1:1, v/v) (1.5 mg/ml); 5 = HES 450/0.7 (1.5 mg/ml) dissolved in blood plasma–0.3 *M* borate buffer (pH 10) (1:1, v/v); 6 = blood plasma–0.3 *M* borate buffer (pH 10) 1:1, v/v); 7 = ω-hydroxymethylfurfurol. 1, 2, 3 and 7 dissolved in 0.3 *M* borate buffer.

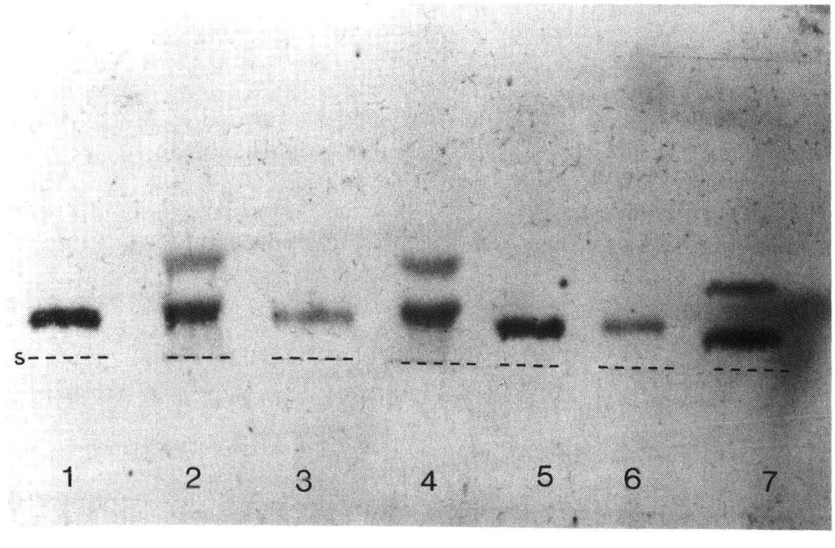

Fig. 5. Detection of HES in rabbit heart. Electrophoresis: 0.3 *M* borate buffer (pH 10.0); 180 V; 120 min; 25°C. 1 = HES 450/0.7 (3 mg/ml); 2 = HES isolated from rabbit heart; 3 = HES 450/0.7 (0.5 mg/ml); 4 = 2; 5 = 1; 6 = 3; 7 = HES 450/0.7 (3 mg/ml) and glycogen (0.5 mg/ml). 1–7 dissolved in 0.3 *M* borate buffer.

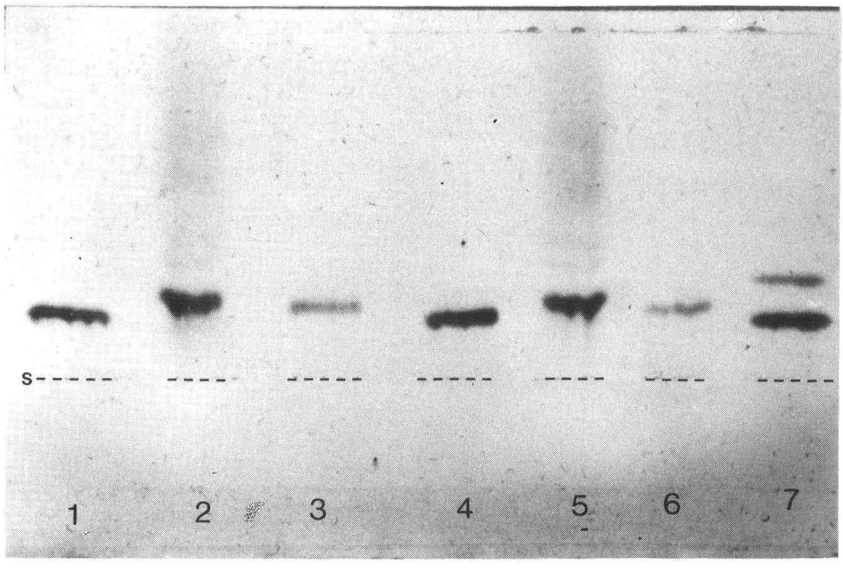

Fig. 6. Detection of HES in rabbit lung. Electrophoresis: 0.3 *M* borate buffer (pH 10); 180 V; 120 min; 25°C. 1 = HES 450/0.7 (3 mg/ml); 2 = HES isolated from rabbit lung; 3 = HES (0.5 mg/ml); 4 = 1; 5 = 2; 6 = 3; 7 = HES 450/0.7 (3.0 mg/ml) and glycogen (0.5 mg/ml). 1–7 dissolved in 0.3 *M* borate buffer.

scanning of their detected zones on the electropherograms with a thin-layer scanner with a linearization program showed a good linear correlation between concentrations and integration values in the range 0.25–3.0 mg/ml HES.

Application of the method to physiological samples

HES–albumin and HES–blood plasma. The electropherograms in Figs. 3 and 4 show that in all instances the HES compounds appear as sharp zones. The large excess of proteins in the albumin and blood plasma samples does not influence either the shape of the zones or the colour intensities in comparison with the pure compounds. Additionally, the albumin electropherograms show in the upper region deep blue zones of D-glucose, which was present as a stabilizing agent in the albumin solution.

Animal tissues. To demonstrate the usefulness of this method for the determination of HES in animal tissues, a weighed amount of HES was added to an HES-free pig liver sample and the isolation was carried out as described. Simultaneously, the same amount of HES without liver tissue was treated in the same way. The isolated polysaccharides were dissolved in 0.3 *M* borate buffer and the electrophoresis was carried out with aliquots of the solutions. The detected sample zones and those of pure HES (two different concentrations) on the electropherograms were scanned and the HES concentrations were calculated from the corresponding calibration graphs. For the amount of HES in the liver sample a recovery of 87.5% relative to the liver-free sample was obtained.

The method was also applied to several tissue samples from rabbits that had been treated with HES, such as the spleen, kidney, heart and lungs. Figs. 5 and 6 show the electropherograms of a heart and a lung sample. The concentrations of HES in

TABLE I

AMOUNTS OF HES IN DIFFERENT RABBIT ORGANS

Mean values of two different determinations.

Organ	Fresh weight of organ (g)	HES per organ (mg)
Lung	6.66	1.7
Heart	5.12	0.55
Kidney	12.7	0.95
Spleen	2.3	0.41

the organs were determined by scanning the detected zones. The results of a few determinations are given in Table I.

REFERENCES

1 W. Banks, C. T. Greenwood and D. D. Muir, *Stärke/Starch*, 24 (1972) 181–212.
2 E. Mutschler, *Arzneimittelwirkungen (Lehrbuch der Pharmakologie und Toxikologie)*, Wissenschaftliche Verlagsgesellschaft, Stuttgart, 1986, pp. 392–395.
3 H. J. Lortz, *Anal. Chem.*, 28 (1956) 892–895.
4 K. L. Hodges, E. W. Kester, D. L. Wiederrich and A. J. Grover, *Anal. Chem.*, 51 (1979) 2172–2176.
5 Y.-C. Lee, D. M. Baaske and J. E. Carter, *Anal. Chem.*, 55 (1983) 334–338.
6 C. Y. Sum, K. Mai, S. Kam, C. Lai, A. Yacobi and T. F. Kalhorn, *J. Chromatogr.*, 254 (1983) 187.
7 J. W. Mourits, H. G. Merkus and L. de Galan, *Anal. Chem.*, 48 (1976) 1557–1561.
8 S. Ukai, A. Honda, K. Nagai and T. Tsuchiya, *J. Chromatogr.*, 435 (1988) 374–379.
9 H. Scherz, *Z. Lebensm.-Unters.-Forsch.*, 181 (1985) 40–44.
10 G. Bonn, M. Grünwald, H. Scherz and O. Bobleter, *J. Chromatogr.*, 370 (1986) 485–493.
11 H. Scherz, *Electrophoresis*, 11 (1990) 18–22.
12 J. Grossfeld, *Z. Unters. Nahr.-Genussm. Gebrauchsgegenstände*, 42 (1921) 29–31.
13 F. Bauer and S. Vali, *Z. Lebensm.-Unters.-Forsch.*, 187 (1988) 354–358.

Journal of Chromatography, 591 (1992) 358–361
Elsevier Science Publishers B.V., Amsterdam

CHROM. 23 842

Short Communication

Photoionization assessment of C_3–C_5 alkadienes and alkenes in urban air

Lars Löfgren and Göran Petersson*

Department of Chemical Environmental Science, Chalmers University of Technology, S-412 96 Gothenburg (Sweden)

(First received August 15th, 1991; revised manuscript received October 28th, 1991)

ABSTRACT

Hydrocarbons from samples of traffic-polluted urban air were separated by gas chromatography on an aluminium oxide column and assessed simultaneously by photoionization detection (PID) and flame ionization detection (FID) after effluent splitting. The 10.2 eV photoionization detector selectively detects alkadienes and alkenes but not alkanes and alkynes in the C_3–C_5 region. The maximum PID/FID response ratio for alkadienes and alkenes is also obtained in this region. The analytical system as a whole is particularly favourable for the C_3–C_5 alkenes. Analytical data are given for propadiene, 1,3-butadiene, propene, butenes and pentenes.

INTRODUCTION

In the complex hydrocarbon mixture of urban air, volatile arenes and alkenes are of particular interest with respect to impact on health as well as the environment. It was early recognized that photoionization detection (PID) offers a high selectivity for these hydrocarbons as compared with alkanes [1], because of the lower ionization potential of unsaturated hydrocarbons. Techniques based on the simultaneous use of PID and flame ionization detection (FID) in parallel [2] or in series [3] have been developed with applications to urban air in mind. These techniques have also been described in a review of multiple detection in gas chromatography [4].

The purpose of the present study is to demonstrate the advantages of the dual detector technique for assessing C_3–C_5 hydrocarbons in urban air. Applications are based on a recently described system for adsorption sampling and gas chromatographic separation [5]. This system is particularly advantageous for the C_3–C_5 alkenes, permitting the full capability of the selective detection to be utilized.

EXPERIMENTAL

Samples of urban air (0.2–2 l) were passed through triple-layer adsorbent cartridges with Tenax TA in the front end followed by Carbotrap and Carbosieve S-III. In the laboratory, the hydrocarbons were thermally desorbed and analysed using temperature-programmed gas chromatography. The column (Chrompack) was a 50 m × 0.32 mm I.D. porous-layer open tubular capillary with aluminium oxide treated with 5% potassium chloride as the stationary phase. The temperature sequence was 0–110°C (10°C/min), 110°C (14 min) and 110–200°C (4°C/min). Further analytical data are given in a recent methodological report focused on alkenes recorded by FID [5].

0021-9673/92/$05.00

The column effluent (helium, 2 ml/min) was split with *ca.* 55% to the flame ionization detector and *ca.* 45% to an optional 10.2 eV photoionization detector (HNU, Model PI-52) which was kept at *ca.* 200°C. The splitting device and detector arrangement were similar to those reported in a basic study of the use of parallel FID and PID [2]. Make-up gas (helium, 10 ml/min) was used for PID.

RESULTS AND DISCUSSION

The chromatograms in Fig. 1 illustrate the excellent selectivity of the photoionization detector for the environmentally critical C_3–C_5 alkadienes and alkenes. The alkynes and the predominant alkanes recorded by flame ionization are virtually absent in the PID chromatogram. Relevant data for the alkadienes and alkenes are given in Table I.

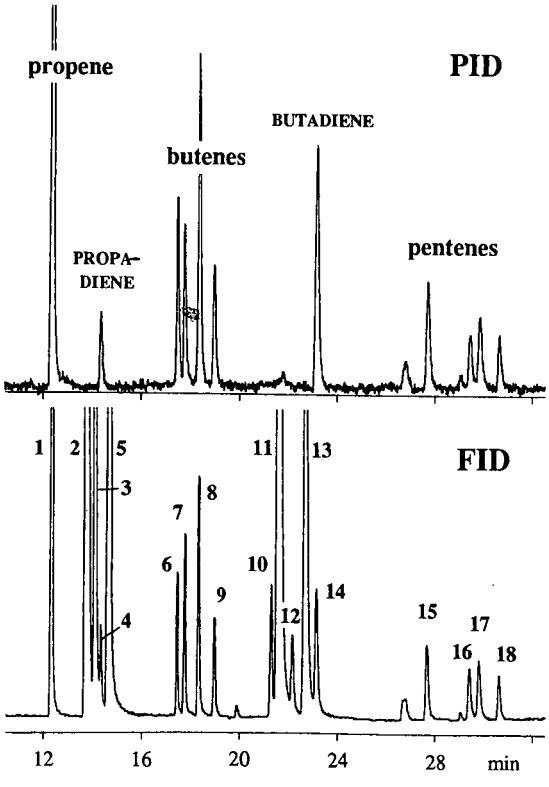

Fig. 1. Simultaneous photoionization and flame ionization records of chromatograms of hydrocarbons from traffic-polluted urban air. Peaks: 1 = propene; 2 = ethyne; 3 = methylpropane; 4 = propadiene; 5 = butane; 6 = *trans*-2-butene; 7 = 1-butene; 8 = methylpropene; 9 = *cis*-2-butene; 10 = cyclopentane; 11 = methylbutane; 12 = propyne; 13 = pentane; 14 = 1,3-butadiene; 15 = *trans*-2-pentene; 16 = 1-pentene; 17 = 2-methyl-1-butene; 18 = *cis*-2-pentene.

Response ratios

From Fig. 1, the high PID/FID response ratio for alkadienes and alkenes is evident. This ratio depends strongly on a number of instrumental parameters, and few data have been given [2]. Normalized PID/FID response ratios are more widely valid and therefore preferred. Among the C_3–C_5 alkenes and alkadienes, propene was chosen as the reference hydrocarbon because it is frequently determined and reported. In Table I, PID/FID ratios normalized to propene are given for the sample corresponding to Fig. 1 and for a duplicate sample. These two high-concentration samples offer a more complete and reliable set of data than samples corresponding to normal urban air pollution levels. The PID selectivity is highest for the conjugated alkadiene 1,3-butadiene. For alkenes, the ratio tends to be lower for 1-alkenes than for 2-alkenes, to increase with branching, and to decrease with molecular weight.

The propene-normalized PID/FID ratios for benzene and toluene were found to be 1.5 and 1.4, respectively, permitting comparisons with data normalized to these hydrocarbons which are favourably recorded by PID. For a 10.0 eV PID, toluene-normalized PID/FID ratios have been reported for many hydrocarbons, including alkenes and alkadienes [2]. The PID/FID ratios given in Table I agree closely for the hydrocarbons included in both sets of data.

For C_7–C_{22} hydrocarbons, the PID selectivity at 10.2 eV for alkenes compared with alkanes decreases rapidly with molecular weight [6]. Consequently, PID detection offers by far the best selectivity in the C_3–C_5 region.

Alkadienes

Propadiene and 1,3-butadiene were the two prominent alkadienes assessed. They are seldom reported in studies of urban air because they elute close to, and are masked by, alkanes on non-polar columns. As illustrated in Fig. 1, they may be well enough separated on the aluminium oxide column for FID assessment, but PID offers superior selectivity and response. It should be noted that propadiene and

TABLE I

NORMALIZED PID/FID RESPONSE, URBAN CONCENTRATIONS AND PHYSICAL DATA OF VOLATILE ALKADIENES AND ALKENES

The concentrations given reflect a high exposure level of pedestrians to vehicle-polluted urban air (Gothenburg, November 30th, 1989, street intersection, 0°C, winter inversion). The proportions of the hydrocarbons are expressed as a percentage of total hydrocarbons except methane, and retention data are given relative to *n*-alkanes in methylene units (MU). Columns 1, 3, 4 and 5 give data for the sample corresponding to Fig. 1.

	PID/FID (propene: 1.00) duplicate samples		Conc. ($\mu g/m^3$)	CH_x Fraction (%)	Rel. retention (MU)	Boiling point (°C)
Alkadienes						
Propadiene	1.03	1.06	2.0	0.2	3.95	−35
1,3-Butadiene	1.56	1.51	6.1	0.5	5.03	−4
Alkenes						
Propene	1.00	1.00	26	2.0	3.57	−47
trans-2-Butene	1.28	1.30	3.7	0.3	4.35	1
1-Butene	0.81	0.83	5.2	0.4	4.39	−6
Methylpropene	1.24	1.28	7.7	0.6	4.46	−7
cis-2-Butene	1.13	1.15	3.2	0.3	4.54	4
trans-2-Pentene	1.19	1.18	3.6	0.3	5.36	36
1-Pentene	0.81	0.78	2.4	0.2	5.48	30
2-Methyl-1-butene	0.92	0.93	2.9	0.2	5.51	31
cis-2-Pentene	0.98	1.03	1.9	0.2	5.57	37

1,3-butadiene were not separated from adjacent alkanes when certain different temperature programs were used. Actually, the two C_4 alkanes (methylpropane and *n*-butane) have been reported to elute both before propadiene [7] and after propadiene [8] on aluminium oxide–potassium chloride columns.

The results of a number of urban air samples from different vehicle-polluted locations indicated almost the same proportions between the two alkadienes. The concentration of 1,3-butadiene was about three times higher than that of propadiene. It is concluded that propadiene as well as propene and 1,3-butadiene are combustion products. The concentration of the carcinogenic 1,3-butadiene is typically 20–25% of the concentration of propene [9] which is frequently reported.

Evidently, the presence of anthropogenic alkadienes in outdoor urban air, as reported in Table I, is predominantly due to vehicle exhaust. For smokers and passive smokers, tobacco smoke is a major source of 1,3-butadiene [10].

Alkenes

The aluminium oxide–potassium chloride column is well suited to the assessment of alkenes in urban air with FID [5], but PID offers increased selectivity and confirmation of alkene identity. Because of its high ionization potential, ethene is not detected by PID. In addition to ethene and propene, the major portion of the butenes originates from engine combustion in traffic-polluted urban air [9]. The pentenes and part of the butenes originate from tailpipe emissions of unburnt petrol and from petrol vapour [5]. In Table I, the alkenes are characterized with respect to abundance in urban air, relative retentions and boiling points.

The pentenes, particularly 2-methyl-2-butene, are the most reactive of the C_3–C_5 alkenes and alkadienes and may be partially lost during adsorbent sampling by reaction with ozone and other agents in urban air. In Fig. 1, the pentenes are recorded in the expected proportions [5] except for the deviating small peak of 2-methyl-2-butene in front of 1-pentene. The loss of 2-methyl-2-butene illustrates the danger of relying on good chromatographic results without controlling the quality of sampling. It was found that sampling losses could be avoided by treating the front end of the adsorbent layer with antioxidative thiosulphate before sampling. This technique was recently described in more detail for

the sampling of easily oxidized monoterpenes on Tenax cartridges [11].

CONCLUSIONS

The results demonstrate that dual PID/FID assessment is particularly favourable for C_3–C_5 alkadienes and alkenes with respect to sensitivity as well as selectivity. The greatest advantages are obtained for the majority of samples containing much larger amounts of volatile alkanes. The applied methods for sampling from air and gas chromatographic separation [5] are also especially favourable for C_3–C_5 alkenes in contrast to several conventional methods. It is concluded that the reported analytical approach is a powerful aid for meeting the increasing interest in these genotoxic and efficiently photooxidant-forming hydrocarbons.

REFERENCES

1 J. N. Driscoll, J. Ford, L. F. Jaramillo and E. T. Gruber, *J. Chromatogr.*, 158 (1978) 171.
2 R. D. Cox and R. F. Earp, *Anal. Chem.*, 54 (1982) 2265.
3 W. Nutmagul, D. R. Cronn and H. H. Hill, *Anal. Chem.*, 55 (1983) 2160.
4 I. S. Krull, M. Swartz and J. N. Driscoll, in J. C. Giddings, E. Grushka, J. Cazes and P. R. Brown (Editors), *Advances in Chromatography*, Marcel Dekker, New York, Vol. 24, 1984, Ch. 8, p. 247.
5 L. Löfgren, P. M. Berglund, R. Nordlinder, G. Petersson and O. Ramnäs, *Int. J. Environ. Anal. Chem.*, 45 (1991) 39.
6 M. L. Langhorst, *J. Chromatogr. Sci.*, 19 (1981) 98.
7 H. Tani and M. Furuno, *J. High Resolut. Chromatogr. Chromatogr. Commun.*, 9 (1986) 712.
8 R. Snel, *Chromatographia*, 21 (1986) 265.
9 L. Löfgren and G. Petersson, *Sci. Total Environ.*, in press.
10 G. Löfroth, R. M. Burton, L. Forehand, S. K. Hammond, R. L. Seila, R. B. Zweidinger and J. Lewtas, *Environ. Sci. Technol.*, 23 (1989) 610.
11 A.-M. Strömvall and G. Petersson, *J. Chromatogr.*, 589 (1992) 385.

Journal of Chromatography, 591 (1992) 362–366
Elsevier Science Publishers B.V., Amsterdam

CHROM. 23 879

Short Communication

Decomposition of two methylbenzothiophene sulphoxides in a commercial gas chromatography injection port liner

Phillip M. Fedorak*

Department of Microbiology, University of Alberta, Edmonton, Alberta T6G 2E9 (Canada)

Jan T. Andersson☆

Department of Analytical and Environmental Chemistry, University of Ulm, Postfach 4066, D-7900 Ulm (Germany)

(First received August 13th, 1991; revised manuscript received November 1st, 1991)

ABSTRACT

2-Methylbenzothiophene sulphoxide and 3-methylbenzothiophene sulphoxide were produced as metabolites by an aromatic hydrocarbon-degrading bacterial culture. Because dibenzothiophene sulphoxide is know to decompose in gas chromatography injectors, the two bacterial products were tested for their stability in a gas chromatography injection port containing a standard Jennings/cup mixing chamber. The two methylbenzothiophene sulphoxides were purified by silica gel chromatography and reversed-phase high-performance liquid chromatography. These sulphoxides decomposed in the injection port giving the corresponding methylbenzothiophene as the major product and the corresponding sulphone as a minor product. The proportions of decomposition products were quite variable and the amount of decomposition was greatest in an injection port liner that had been soiled by the routine analyses of dozens of petroleum samples.

INTRODUCTION

Benzothiophene and alkylbenzothiophenes are found in crude oils [1], shale oils [2,3] and coal tar [4]. Some of these compounds have been shown to be "biodegradable" in laboratory studies [5–7] and petroleum reservoir investigations [8]. However, little is known about the identities of the metabolites of these biotransformations or about the fates of the metabolites in laboratory cultures and in the environment [9]. Recent investigations showed that bacterial cometabolism of 3-methylbenzothiophene (3-MBT) [10] and 2-methylbenzothiophene (2-MBT) [11] yielded the sulphoxides and sulphones of these two compounds.

Dibenzothiophene (DBT) has been used extensively as a model compound to study the metabolism of organosulphur compounds found in petroleum [9]. DBT sulphoxide has been observed as a metabolite in bacterial [12,13] and mammalian [14] systems. Upon gas chromatographic (GC) analysis, DBT-sulphoxide has been shown to decompose in hot injection ports to DBT [15,16] and DBT sulphone [15]. The stabilities of benzothiophene sulphoxides to analysis by GC have not been addressed.

☆ Present address: Analytical Chemistry Department, University of Münster, Wilhelm-Klemm-Strasse 8, D-4400 Münster, Germany.

0021-9673/92/$05.00

Many chemical reactions that oxidize the sulphur atom in benzothiophenes do not stop at the sulphoxide, but they continue and produce the sulphone. Although the bacterial culture that we are studying produces trace amounts of sulphones from 3-MBT and 2-MBT, the more abundant oxidation products are the corresponding sulphoxides [10,11]. Surprisingly, this culture will not form the sulphoxides or sulphones of benzothiophene or some other isomers of methylbenzothiophene. This bacterial culture was used to produce the sulphoxides of 3-MBT and 2-MBT and these were isolated by high-performance liquid chromatography (HPLC) to determine whether they would decompose in a commercial GC injection port.

EXPERIMENTAL

Microbial production of the sulphoxides and sulphones of 3-MBT and 2-MBT

Pseudomonas strain BT1 was grown under shake-flask conditions at 28°C in 200 ml of mineral medium supplemented with trace metals [10]. To provide sufficient amounts of metabolites, seven replicate cultures were incubated simultaneously. For metabolite production from 3-MBT, each culture contained 50 μl of 1-methylnaphthalene, which served as the growth substrate, and approximately 10 μl of 3-MBT. To produce the metabolites from 2-MBT, each culture contained 250 mg of glucose/l, which served as the growth substrate, and approximately 10 mg of 2-MBT. After 14 days of incubation, the cultures were acidified to below pH 2 with HCl and extracted with methylene chloride (5 times 15 ml). The extracts were dried over anhydrous sodium sulphate and replicate extracts were combined and concentrated prior to column chromatography. The sulphoxides were identified by GC–mass spectrometry (MS) and GC–Fourier transform infrared spectroscopy (FTIR) [10,11] whereas the sulphones were identified by comparisons of the GC–FTIR spectra from the culture extracts with those of authentic standards.

Isolation of the sulphoxides and sulphones of 3-MBT and 2-MBT

The polar metabolites were isolated by silica gel column chromatography using a 30 cm × 1.1 cm I.D. glass column. A slurry of 7 g of silica gel (Fisher Scientific, 100–200 mesh, Type 150A, Grade 644, activated at 125°C for 24 h) in methylene chloride was poured into the column and the solvent was displaced with 50 ml of *n*-pentane. The methylene chloride extract from the culture was adsorbed to 0.2 g of silica gel, the solvent was removed under a stream of nitrogen gas, and the sample was loaded onto the column which was then developed with 5 ml of *n*-pentane, 5 ml methylene chloride–*n*-pentane (20:80), 25 ml of methylene chloride–*n*-pentane (50:50) and 30 ml methanol–benzene (50:50). The first 50 ml of the column effluent were discarded and the last 12 ml from the column contained the polar metabolites.

HPLC method and fraction collection

The solvent was evaporated from samples of culture extracts and the residues were dissolved in acetonitrile for HPLC analysis using a Hewlett-Packard series 1050 instrument with a reversed-phase LiChrospher 100 RP-18 column (5 μm, 125 mm × 4 mm I.D., Hewlett-Packard). Two mobile phases were used. For routine analysis, acetonitrile–water (50:50) (solvent 1) was used. To obtain baseline separation for the manual collection of the fractions containing the sulphoxides and sulphones, acetonitrile–water (25:75) (solvent 2) was used. In both cases, the flow-rate was 1.0 ml/min and the effluent was monitored at 280 nm.

GC analysis of the sulphoxides and sulphones of 3-MBT and 2-MBT

Culture extracts and collected fractions were analyzed by capillary GC using a 30 m × 0.25 mm O.D. (0.25 μm film thickness) DB-5 column (J & W Scientific) housed in a Hewlett-Packard (Model 5890) GC system equipped with flame ionization detection (FID) and flame photometric detection (FPD). The column effluent was split so that the sample was analyzed simultaneously by the two detection systems [5]. The decomposition products were identified on the basis of their retention times on the GC–FPD chromatogram which matched those of authentic standards. The injector temperature was 250°C and the oven temperature program used for all GC analyses was; 90°C for 2 min, 4°C/min to 250°C which was held for 16 min. All other operating conditions were as previously reported [5]. The injection split ratio was approximately 1:20 and the

injector contained a standard Hewlett-Packard Jennings/cup mixing chamber (part No. 18740-80190) injection port liner packed with 10% OV-1 on 80–100 mesh Chromosorb W HP as suggested by Hewlett-Packard.

Chemicals

3-MBT was purchased from Lancaster Synthesis (Windham, NH, USA) and its sulphone was synthesized by the method for benzothiophene sulphone synthesis [16]. 2-MBT and its sulphone were synthesized as outlined by Andersson [17].

Pesticide-grade solvents were used for extractions and column chromatography and HPLC-grade acetonitrile was used. Water for HPLC work was purified by passage through a Milli-Q apparatus (Millipore).

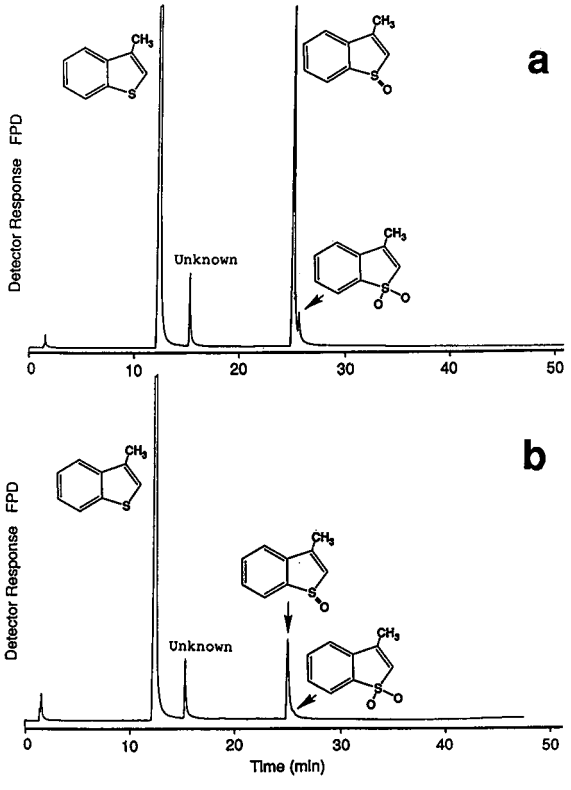

Fig. 1. GC analyses of (a) the polar fraction of extracts from cultures grown in the presence of 3-MBT and (b) the 3-MBT sulphoxide-containing fraction (the shaded portion in Fig. 2a) obtained by HPLC purification.

RESULTS AND DISCUSSION

Fig. 1a shows a GC–FPD chromatogram of the extract of *Pseudomonas* sp. BT1 grown on 1-methylnaphthalene in the presence of 3-MBT. Typically we observed the parent compound 3-MBT in these chromatograms and we assumed that the bacterial cometabolism left some of this compound unoxidized. However, after silica gel column chromatography was used to separate the polar sulphoxide and sulphone from the 3-MBT, GC analysis of the polar fraction gave a chromatogram that was essentially the same as Fig. 1a suggesting that sulphoxide was decomposing to 3-MBT.

This polar fraction was analyzed by HPLC and the resulting chromatogram is shown in Fig. 2a. Decomposition of the sulphoxide and the sulphone would not occur during HPLC analysis [18]. Authentic 3-MBT eluted at 28.18 min under these chromatographic conditions. Although there is a very small peak at 27.82 min, we have been unable to ascertain whether or not this was a trace amount of 3-MBT.

Using solvent 2, fractions of the effluent from the HPLC column containing 3-MBT sulphoxide and 3-MBT sulphone were collected individually and analyzed by GC. The fraction that contained only the 3-MBT sulphoxide gave the GC chromatogram shown in Fig. 1b, in which 3-MBT and, to a lesser extent, its sulphoxide were observed because of decomposition of the sulphoxide in the injection port. Analysis of the sulphoxide-containing fraction by HPLC showed only the presence of 3-MBT sulphoxide (Fig. 2b).

GC analysis of the HPLC fraction containing the 3-MBT sulphone showed only one peak which corresponded to the sulphone. This is consistent with previous observations that the sulphones of alkylbenzothiophenes and DBT do not decompose during GC analysis [15].

Similarly, HPLC was used to obtain the 2-MBT sulphoxide-containing fraction from the polar fraction of the methylene chloride extract of cultures grown in the presence of 2-MBT. HPLC analysis of the 2-MBT sulphoxide-containing fraction showed no other peaks. However, when this fraction was analyzed by GC, 2-MBT and a trace amount of 2-MBT sulphone were observed. These results demonstrated that 2-MBT sulphoxide was also suscepti-

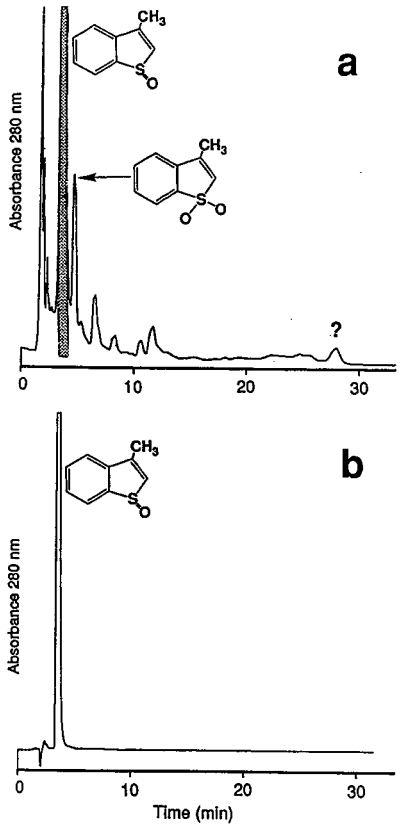

Fig. 2. HPLC analyses of (a) the polar fraction of extracts from cultures grown in the presence of 3-MBT and (b) the 3-MBT sulphoxide-containing fraction (the shaded portion in Fig. 2a) obtained by HPLC purification. Analyses done using solvent 1.

ble to decomposition in the GC injection port.

The GC analyses described above were interspersed among routine analyses of petroleum and petroleum fractions from biodegradation studies. Thus no special consideration was given to the condition of the commercial injection port liner. To assess the effects of the condition of the injection port liner, samples of the polar fraction from a culture grown in the presence of 3-MBT were analyzed and the ratios of 3-MBT/3-MBT sulphoxide and 3-MBT sulphone/3-MBT sulphoxide were calculated based on the FID response (Table I). Injections into a liner that had been used for the analyses of dozens of petroleum samples yielded the largest ratios indicating that the greatest amount of decomposition occurred under these conditions. The ratios were much smaller when a clean liner, with or without packing material was used. The ratios from duplicate injections showed that decomposition of 3-MBT sulphoxide was quite variable, especially when the soiled injection port liner was used. With the cleaned injection port liner, the relative standard deviations of the replicate injections were much smaller, most being $< 10\%$.

These investigations demonstrated that GC methods using this commercially available injection port liner led to the decomposition of the two methylbenzothiophene sulphoxides studied. Indeed, the cleanliness of the liner determined the extent and reproducibility of the decomposition. Therefore we suggest that the use of this commercially available injection port liner is not appropriate for the determinations of the amounts of 3-MBT and 2-MBT biotransformed or the amounts of their sulphoxides produced in biodegradation studies. In addition, sulphones detected by the GC analysis of extracts from cultures grown in the presence of these methyl-

TABLE I

RELATIVE PROPORTIONS OF 3-MBT AND ITS OXIDES IN THE POLAR FRACTION OF EXTRACTS FROM CULTURES GROWN IN THE PRESENCE OF 3-MBT

Ratios determined from FID responses of duplicate GC analyses using a commercially available injection port liner under various conditions. R.S.D. = Relative standard deviation.

Liner condition	3-MBT/sulphoxide			Sulphone/sulphoxide		
	Injection 1	Injection 2	R.S.D.	Injection 1	Injection 2	R.S.D.
Packed[a] and soiled by dozens of injections of petroleum samples	22.8	10.8	51%	3.8	1.9	47%
Freshly cleaned and empty	0.10	0.11	8%	0.25	0.27	6%
Freshly cleaned and packed[a]	0.20	0.16	13%	0.28	0.26	4%

[a] With 10% OV-1 on 80–100 mesh Chromosorb W HP.

benzothiophenes may be due to the decomposition of the corresponding sulphoxide in the injection port. Thus HPLC analysis should be used to verify the biologically-mediated formation of these sulphones.

ACKNOWLEDGEMENTS

This work was supported by Canada Centre for Mineral and Energy Technology, Energy Mines and Resources Canada contract No. 23440-0-9163/01-SS and by the Natural Sciences and Research Council of Canada. We thank D. Coy for technical assistance.

REFERENCES

1 H. T. Rall, C. J. Thompson, H. J. Coleman and R. L. Hopkins, *Sulfur Compounds in Crude Oil, Bulletin 659*, US Department of the Interior, Bureau of Mines, Washington, DC, 1972.
2 C. Willey, M. Iwao, R. N. Castle and M. L. Lee, *Anal. Chem.* 53 (1981) 400.
3 M. Nishioka, J. S. Bradshaw, M. L. Lee, Y. Tominaga, M. Tedjamulia and R. M. Castle, *Anal. Chem.* 57 (1985) 309.
4 P. Burchill, A. A. Herod and E. Pritchard, *J. Chromatogr.*, 242 (1982) 51.
5 P. M. Fedorak and D. W. S. Westlake, *Can. J. Microbiol.*, 29 (1983) 291.
6 P. M. Fedorak and D. W. S. Westlake, *Wat. Air Soil Pollut.*, 21 (1984) 225.
7 J. M. Foght and D. W. S. Westlake, *Can. J. Microbiol.*, 34 (1988) 1135.
8 J. A. Williams, M. Bjorøy, D. L. Dolcater and J. C. Winters, *Org. Geochem.*, 10 (1986) 451.
9 P. M. Fedorak, in W. L. Orr and C. M. White (Editors), *Geochemistry of Sulfur in Fossil Fuels*, American Chemical Society, Washington, DC, 1990, Ch. 6, p. 93.
10 P. M. Fedorak and D. Grbić-Galić, *Appl. Environ. Microbiol.*, 57 (1991) 932.
11 S. Saftić, J. T. Andersson and P. M. Fedorak, in preparation.
12 K. Kodama, S. Nakatani, K. Umehara, K. Shimizu, Y. Minoda and K. Yamada, *Biol. Chem.* 34 (1970) 1320.
13 A. L. Laborde and D. T. Gibson, *Appl. Environ. Microbiol.*, 34 (1977) 738.
14 V. Vignier, F. Berthou, Y. Dreano and H. H. Floch, *Xenobiotica*, 15 (1985) 991.
15 J. T. Andersson, *J. High Resolut. Chromatogr. Chromatogr. Commun.*, 7 (1984) 334.
16 F. G. Bordwell, B. B. Lampert and W. H. McKellin, *J. Am. Chem. Soc.*, 71 (1949) 1702.
17 J. T. Andersson, *J. Chromatogr.*, 354 (1986) 83.
18 V. Vignier, F. Berthou and D. Picart, *J. High Resolut. Chromatogr. Chromatogr. Commun.*, 6 (1983) 661.

Journal of Chromatography, 591 (1992) 367–370
Elsevier Science Publishers B.V., Amsterdam

CHROM. 23 845

Short Communication

R_M values of some colchicines and colchiceinamides determined by reversed-phase thin-layer chromatography

Damjan Glavač

Faculty of Science and Technology, University of Ljubljana, Ljubljana (Yugoslavia)

(First received March 20th, 1991; revised manuscript received October 10th, 1991)

ABSTRACT

The R_M values of twelve colchicines and eight colchiceinamides were measured using reversed-phase thin-layer chromatography. The R_M values were calculated by extrapolation from the linear range of a plot of R_M values *versus* the composition of the mobile phase. The results showed that in the colchicine series substitution at the nitrogen in position C_7 decreases the lipophilicity, whereas in the colchiceinamide series substitution at the nitrogen in position C_{10} increases lipophilicity. The influence of other substituent groups on the R_M values are considered.

INTRODUCTION

The usefulness of partition coefficients and R_M values [$R_M = \log(1/R_F - 1)$] as an expression of the lipophilic character of the molecule in quantitative structure–activity relationship studies has been shown for several series of biologically active compounds such as penicillins [1], steroids [2], benzodiazepins [3] and nucleosides [4]. Colchicine and many of its derivatives are powerful mitotic poisons, anti-inflammatory agents and inhibitors of tubulin, but their effects were only observed at near toxic levels [5]. The relationship between the physicochemical properties and biological activity of some colchicinoids was studied by Quinn and co-workers [6,7], who showed that there is a parabolic dependence of the antitumour potency on the partition coefficient [6].

The purpose of the work reported here was to study a larger number of natural colchicines and their synthetic analogues to compare their lipophilic characters. The colchicinoids given in Table I were either isolated from natural sources [8,9] or synthesized in this laboratory [10].

EXPERIMENTAL

The R_M values were measured using a reversed-phase thin-layer chromatography technique which allowed the partitioning of colchicinoids between the polar mobile phase and the non-polar stationary phase. The mobile phase consisted of a phosphate buffer (pH 7.4) in various mixtures with acetone. The stationary phase was obtained by impregnating precoated silica gel 60 F_{254} plates (0.25 mm, Merck) with 5% (v/v) liquid paraffin (Merck) in diethyl ether. The method of impregnating the plates and other details of the chromatographic technique have been described elsewhere [1–3]. The plates were left in the chamber for 12 h, that is, for several hours after the paraffin solution had reached the top of the plates.

0021-9673/92/$05.00

TABLE I

STRUCTURES AND R_M VALUES OF COLCHICINES AND COLCHICEINAMIDES

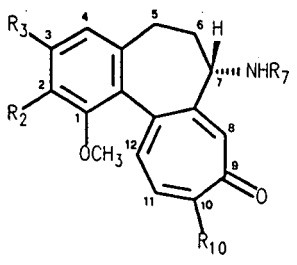

β-lumicolchicine

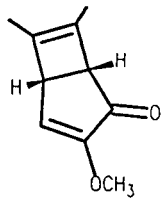

Compound		R_2	R_3	R_7	R_{10}	R_M	Log P^c
No.	Name						
1	Colchicine	OCH_3	OCH_3	$COCH_3$	OCH_3	0.87	1.03
2	N-Deacetylcolchicine[a]	OCH_3	OCH_3	H	OCH_3	1.21	1.10
3	N-Acetoacetylcolchicine	OCH_3	OCH_3	$COCH_2COCH_3$	OCH_3	0.92	
4	Colchifoline	OCH_3	OCH_3	$COCH_2OH$	OCH_3	0.68	
5	N-Formylcolchicine	OCH_3	OCH_3	CHO	OCH_3	0.76	1.02
6	2-Demethylcolchicine	OH	OCH_3	$COCH_3$	OCH_3	0.61	
7	3-Demethylcolchicine	OCH_3	OH	$COCH_3$	OCH_3	0.57	0.93
8	Demecolcine	OCH_3	OCH_3	CH_3	OCH_3	1.29	1.53
9	2-Demethyldemecolcine	OH	OCH_3	CH_3	OCH_3	0.78	
10	3-Demethyldemecolcine	OCH_3	OH	CH_3	OCH_3	0.73	
11	β-Lumicolchicine	OCH_3	OCH_3	$COCH_3$	OCH_3	1.57	
12	Colchicoside	OCH_3	gluc.[b]	$COCH_3$	OCH_3	0.36	
13	Colchiceinamide (CA)[a]	OCH_3	OCH_3	$COCH_3$	NH_2	0.82	
14	Formyl-CA[a]	OCH_3	OCH_3	$COCH_3$	NHCHO	1.16	
15	Acetyl-CA[a]	OCH_3	OCH_3	$COCH_3$	$NHCOCH_3$	1.25	
16	Glycolyl-CA[a]	OCH_3	OCH_3	$COCH_3$	$NHCOCH_2OH$	1.07	
17	Acetoacetyl-CA[a]	OCH_3	OCH_3	$COCH_3$	$NHCOCH_2COCH_3$	1.34	
18	N-Deacetyl-CA[a]	OCH_3	OCH_3	H	NH_2	0.97	
19	2-Demethyl-CA[a]	OH	OCH_3	$COCH_3$	NH_2	0.54	
20	O-Acetyl-glycolyl-CA[a]	OCH_3	OCH_3	$COCH_3$	$NHCOCH_2OCOCH_3$	1.52	

[a] Synthesized as in Glavač *et al.* [10].
[b] β-D-glucosyl.
[c] Taken from Quinn and Beisler [6]; P = *n*-octanol–water partition coefficient.

The colchicinoids were dissolved in acetone (5 mg/ml) and 1 μl of the solution was spotted onto the plates in random allocations to avoid any systematic error. A migration of 10 cm was obtained on all plates by cutting the layer at 12 cm and spotting the compounds on a line 2 cm from the lower edge of the plate. The mobile phase, saturated with liquid paraffin, was an aqueous buffer (pH 7.4 phosphate buffer) mixed with the following amounts of acetone: 4, 6, 8, 10, 12, 14, 16, 18 and 20% (v/v). The developed plates were dried, and the compounds were detected in UV light at 250 nm, then sprayed with a saturated solution of iron(III) chloride in water and treated with gaseous hydrogen chloride. Sprayed plates were heated at 120°C. Dark green spots appeared after a few minutes on a brown background. The R_M values were calculated by the formula: $R_M = \log(1/R_F - 1)$.

RESULTS AND DISCUSSION

The chromatographic separation showed that in the system with the paraffin–phosphate buffer the test compounds did not migrate when the mobile

phase contained only phosphate buffer. The addition of acetone was necessary to obtain acceptable R_F values. The transformation of R_F into R_M values gives a series of positive and negative R_M values which were plotted *versus* the acetone concentrations. The plots are shown in Fig. 1. The test compounds could be divided into several groups on the basis of the acetone concentrations necessary to obtain a suitable range of R_M values. For each compound there was a linear relationship between the R_M values and the composition of the mobile phase. The straight lines were calculated by regression equations with the R_M values in the linearity region between 4 and 20% acetone concentration. For compound **12** (see Table I) there were few available points because with higher acetone concentrations in the mobile phase it migrated with the solvent front. The R_M values indicated in Table I are theoretical R_M values corresponding to a 0% acetone concentration in the mobile phase.

The reported R_M values allow the influence of substituent groups on the partitioning of natural

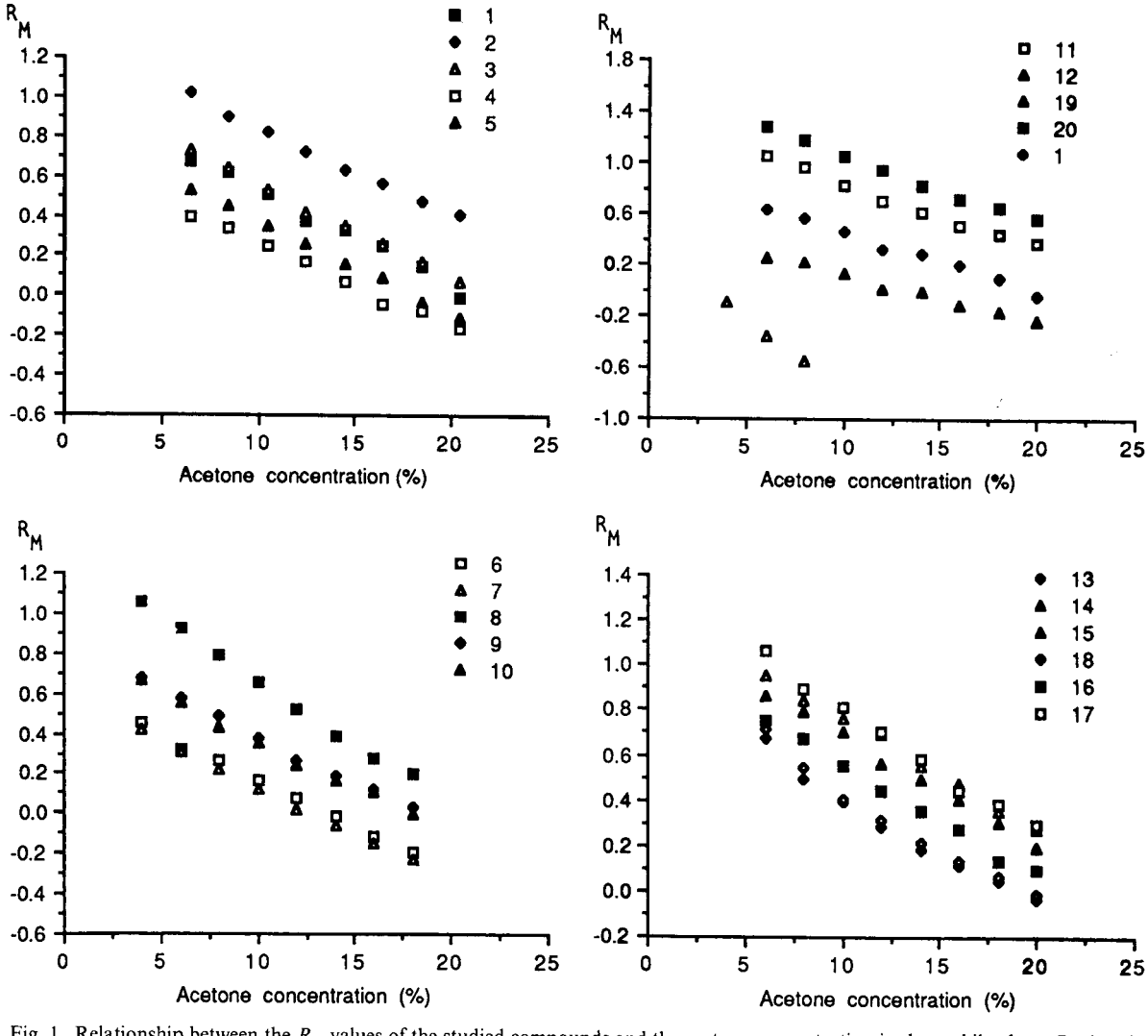

Fig. 1. Relationship between the R_M values of the studied compounds and the acetone concentration in the mobile phase. Each point represents the mean of five determinations. The compounds are numbered as in Table I.

colchicines and colchiceinamides derivatives to be studied. Higher R_M values indicate compounds more lipophilic than those represented by lower R_M values. In a series of natural colchicines the most lipophilic compounds are **2**, **8** and **11**, with $R_M > 1$, and the most hydrophilic is compound **12**, with $R_M = 0.36$.

The ΔR_M values are calculated as the difference between the R_M value of the unsubstituted compound and the R_M value of a compound bearing a certain substituent. ΔR_M values allow an evaluation of the contribution of functional groups to the lipophilicity of the whole molecule. Especially interesting in this respect is the substitution at the amino side-chain in **2** in the colchicine series and **13** in colchiceinamide series. In the colchicine series a substitution of the amino group decreases the lipophilicity in the following order: $-COCH_2COCH_3$ ($\Delta R_M = -0.29$), $-COCH_3$ ($\Delta R_M = -0.34$), $-CHO$ ($\Delta R_M = -0.45$), $-COCH_2OH$ ($\Delta R_M = -0.53$). Therefore **4** is the most hydrophilic compound in this series. The introduction of a methyl group into **8** slightly increases the R_M value ($\Delta R_M = 0.08$). The cleavage of the ether groups in ring A in general decreases the R_M value. The cleavage of a methoxy group in position C_2 has slightly less influence on the lipophilicity ($\Delta R_M = -0.26$) of the whole molecule than in position C_3 ($\Delta R_M = -0.30$). The same influence was observed in the demecolcine series. The transformation of the tropolone ring in **11** increases the lipophilicity more than the introduction of a glucose moiety ($\Delta R_M = -0.51$) into ring A in **12** ($\Delta R_M = 0.70$) decreases the lipophilicity.

The log P values of five colchicinoids, determined by Quinn and Beisler [6] in an octanol–water system (for **1** and **2**) and calculated using constant π and/or fragment values for the substituent (for **5**, **7** and **8**) are reported in Table I. They are, in general, in the same decreasing order as the corresponding R_M values determined in a system.

In the series of N-acylcolchiceinamides the hydrophilic character decreases with the substitution on the nitrogen: $-COCH_2OH$ ($\Delta R_M = 0.25$), $-CHO$ ($\Delta R_M = 0.34$), $-COCH_3$ ($\Delta R_M = 0.43$), $-COCH_2COCH_3$ ($\Delta R_M = 0.52$) and $-COCH_2OCOCH_3$ ($\Delta R_M = 0.70$). Therefore, the O-acetylated compound **20** is the most lipophilic. Deacetylation on the nitrogen in position C_7 has less influence on lipophilicity of the whole molecule in **13** ($\Delta R_M = 0.15$), than in **1** ($\Delta R_M = 0.34$).

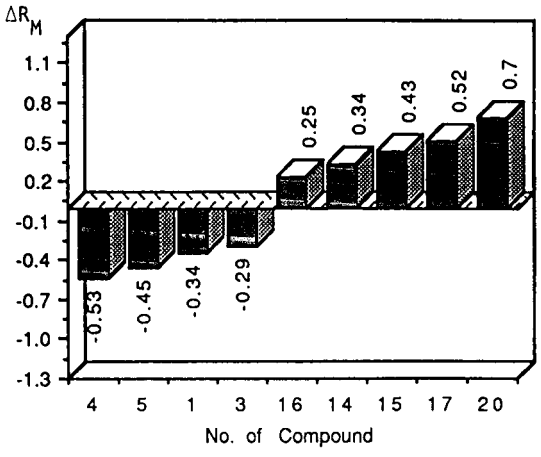

Fig. 2. Comparison of ΔR_M values of amino-substituted C_7 colchicines and amino-substituted C_{10} colchiceinamides.

In Fig. 2, ΔR_M values are given for those colchicines and colchiceinamides which are substituted by the same group in positions C_7 and C_{10}, respectively. In the colchicine series these groups decrease the lipophilicity and are on the negative scale of the plot, whereas in the colchiceinamide series the difference between the R_M value of colchiceinamide and its amino-substituted derivative give a positive ΔR_M value. This could be attributable to the ability of this group to increase the lipophilicity; colchiceinamide is the most hydrophilic in this series.

REFERENCES

1 G. L. Biagi, A. M. Barbaro, M. F. Gamba and M. C. Guerra, *J. Chromatogr.*, 41 (1969) 371.
2 G. L. Biagi, A. M. Barbaro, O. Gandolfi, M. C. Guerra and G. Cantelli-Forti, *J. Med. Chem.*, 18 (1975) 873.
3 G. L. Biagi, A. M. Barbaro, M. C. Guerra, M. Babbini, M. G. Gaiardi and M. Bartoletti, *J. Med. Chem.*, 23 (1980) 193.
4 A. P. Cheung and D. Kenney, *J. Chromatogr.*, 506 (1990) 119.
5 A. Brossi, H. J. C. Yeh, M. Chrzanowska, J. Wolff, E. Hamel, C. M. Lin, F. Quin, M. Suffness and J. Silverton, *Med. Res. Rev.*, 8 (1988) 77.
6 F. R. Quinn and J. A. Beisler, *J. Med. Chem.*, 24 (1981) 251.
7 F. R. Quinn, Z. Neiman and J. A. Beisler, *J. Med. Chem.*, 24 (1981) 636.
8 D. Glavač, A. Kornhauser and M. Ravnik-Glavač, *Bull. Slov. Chem. Soc.*, 31 (1984) 11.
9 D. Glavač and M. Ravnik-Glavač, *Acta. Pharm. Jugosl.*, 41 (1991) 237.
10 D. Glavač and M. Ravnik-Glavač, *Acta. Pharm. Jugosl.*, submitted for publication.

Author Index

Journal of Chromatography

Request for Manuscripts

M. Mills and E.M. Thurman will edit a special, thematic issue of the *Journal of Chromatography* entitled "**Principles and Applications of Solid Phase Extraction**". Both reviews and research articles will be included.

Topics such as the following will be covered:

- Surface Chemistry of Bonded Phases
- Analyte and Solvent Interaction with the Solid Phase
- Mechanisms of Isolation on Solid Phase Resins
- Automation of Solid Phase Extraction
- Innovative New Bonded Phases
- Innovative Applications of Solid Phase Extraction to Clinical and Environmental Chemistry

The deadline for receipt of submissions is **April 13th, 1992.** Five copies of the manuscript should be submitted to M. Mills, US Geological Survey, 4821 Quail Crest Place, Lawrence, Kansas 66049, USA. Tel.: (913) 842-9909; Fax: (913) 832-3500. All manuscripts will be reviewed and acceptance will be based on the usual criteria and suitability for the thematic issue, for publishing in the *Journal of Chromatography*. Potential authors of reviews should contact M. Mills prior to any submission.

PUBLICATION SCHEDULE FOR 1992

Journal of Chromatography and *Journal of Chromatography, Biomedical Applications*

MONTH	O 1991	N 1991	D 1991	J	F	M	
Journal of Chromatography	585/1	585/2 586/1 586/2 587/1	587/2 588/1+2	589/1+2 590/1 590/2	591/1+2 592/1+2 593/1+2	594/1+2 595/1+2	The publication schedule for further issues will be published later
Cumulative Indexes, Vols. 551–600							
Bibliography Section						610/1	
Biomedical Applications				573/1 573/2 574/1	574/2	575/1 575/2	

INFORMATION FOR AUTHORS

(Detailed *Instructions to Authors* were published in Vol. 558, pp. 469–472. A free reprint can be obtained by application to the publisher, Elsevier Science Publishers B.V., P.O. Box 330, 1000 AH Amsterdam, Netherlands.)

Types of Contributions. The following types of papers are published in the *Journal of Chromatography* and the section on *Biomedical Applications:* Regular research papers (Full-length papers), Review articles and Short Communications. Short Communications are usually descriptions of short investigations, or they can report minor technical improvements of previously published procedures; they reflect the same quality of research as Full-length papers, but should preferably not exceed five printed pages. For Review articles, see inside front cover under Submission of Papers.

Submission. Every paper must be accompanied by a letter from the senior author, stating that he/she is submitting the paper for publication in the *Journal of Chromatography*.

Manuscripts. Manuscripts should be typed in double spacing on consecutively numbered pages of uniform size. The manuscript should be preceded by a sheet of manuscript paper carrying the title of the paper and the name and full postal address of the person to whom the proofs are to be sent. As a rule, papers should be divided into sections, headed by a caption (*e.g.*, Abstract, Introduction, Experimental, Results, Discussion, etc.). All illustrations, photographs, tables, etc., should be on separate sheets.

Introduction. Every paper must have a concise introduction mentioning what has been done before on the topic described, and stating clearly what is new in the paper now submitted.

Abstract. All articles should have an abstract of 50–100 words which clearly and briefly indicates what is new, different and significant.

Illustrations. The figures should be submitted in a form suitable for reproduction, drawn in Indian ink on drawing or tracing paper. Each illustration should have a legend, all the *legends* being typed (with double spacing) together on a *separate sheet*. If structures are given in the text, the original drawings should be supplied. Coloured illustrations are reproduced at the author's expense, the cost being determined by the number of pages and by the number of colours needed. The written permission of the author and publisher must be obtained for the use of any figure already published. Its source must be indicated in the legend.

References. References should be numbered in the order in which they are cited in the text, and listed in numerical sequence on a separate sheet at the end of the article. Please check a recent issue for the layout of the reference list. Abbreviations for the titles of journals should follow the system used by *Chemical Abstracts*. Articles not yet published should be given as "in press" (journal should be specified), "submitted for publication" (journal should be specified), "in preparation" or "personal communication".

Dispatch. Before sending the manuscript to the Editor please check that the envelope contains four copies of the paper complete with references, legends and figures. One of the sets of figures must be the originals suitable for direct reproduction. Please also ensure that permission to publish has been obtained from your institute.

Proofs. One set of proofs will be sent to the author to be carefully checked for printer's errors. Corrections must be restricted to instances in which the proof is at variance with the manuscript. "Extra corrections" will be inserted at the author's expense.

Reprints. Fifty reprints of Full-length papers and Short Communications will be supplied free of charge. Additional reprints can be ordered by the authors. An order form containing price quotations will be sent to the authors together with the proofs of their article.

For Superior Chiral Separation From Analytical To Preparative.

The finest from DAICEL·····

Why look beyond DAICEL? We have developed the finest CHIRALCEL, CHIRALPAK and CROWNPAK with up to 17 types of HPLC columns, all providing superior resolution of racemic compounds.

NEW CHIRALPAK AS

● CHIRALPAK AS

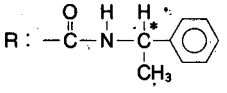

for β-Lactam antibiotics

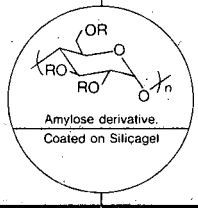

NEW CHIRALPAK AD

● CHIRALPAK AD

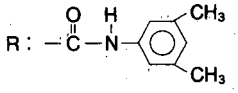

4-Acetoxy-2-azetidine

Eluent : Hexane/Ethanol = 8/2
Flow rate : 1.0mℓ/min
Temperature : r.t.
Detection : UV254nm

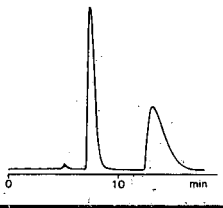

Oxyphencyclimine

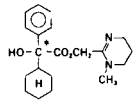

Eluent : Hexane/2-Propanol = 9/1
Flow rate : 1.0mℓ/min
Temperature : r.t.
Detection : UV254nm

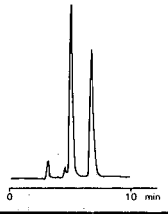

Ofloxacine methyl ester

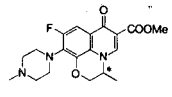

Eluent : Hexane/EtOH = 8/2
Flow rate : 1.2mℓ/min
Temperature : 40°C
Detection : UV254nm

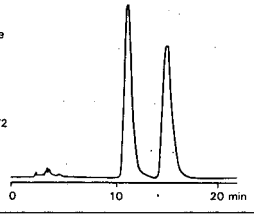

Verapamil

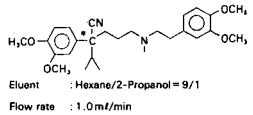

Eluent : Hexane/2-Propanol = 9/1
Flow rate : 1.0mℓ/min
Temperature : r.t.
Detection : UV254nm

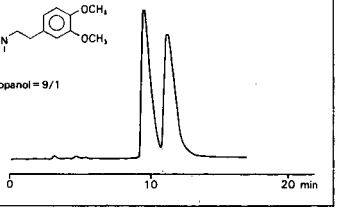

Analytical column 0.46cm × 25cm(10μm)

CHIRALCEL OA
OB
OC
OD
OJ
OF
OG
OK

CHIRALPAK AS
AD

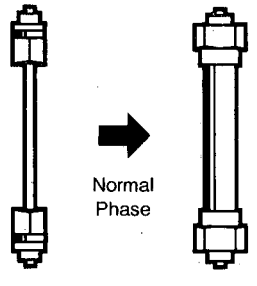

Semi-preparative column 2cm × 25cm(10μm)

You can have Pure enantiomer quickly!!

Separation Service

- A pure enantiomer separation in the amount of 100g~10kg is now available.
- Please contact us for additional information regarding the manner of use and application of our chiral columns and how to procure our separation service.

DAICEL CHEMICAL INDUSTRIES, LTD.

chiral chemicals division.
8-1, Kasumigaseki 3-chome, Chiyoda-ku, Tokyo 100, Japan Phone: 03 (507) 3151 FAX: 03 (507) 3193

DAICEL(U.S.A.), INC.
Fort Lee Executive Park
Two Executive Drive, Fort Lee,
New Jersey 07024
Phone: (201) 461-4466
FAX: (201) 461-2776

DAICEL(U.S.A.), INC.
23456 Hawthorne Blvd.
Bldg. 5, Suit 130
Torrance, CA 90505
Phone: (213) 791-2030
FAX: (213) 791-2031

DAICEL(EUROPA)GmbH
Oststr. 22
4000 Düsseldorf 1, F.R. Germany
Phone: (211) 369848
Telex: (41) 8588042 DCEL D
FAX: (211) 364429

DAICEL CHEMICAL(ASIA)PTE. LTD.
65 Chulia Street #40-07
OCBC Centre, Singapore 0104
Phone: 5332511
FAX: 5326454